ACQUISITION OF STUDY REPORTS FOR LITERATURE REVIEW OF HORIZONTAL WELLS AND MODELS FOR HORIZONTAL WELL INJECTORS AND PRODUCERS.

[Part of Energy, Mines and Resources Cost-Shared Energy Conversion Program and part of the Federal Panel on Energy P&D (PERD)]

Work on the project was conducted under the auspices of the Canada Center for Mineral and Energy Technology CANMET; Energy, Mines and Resources Canada.

Contract File No.:	23440-8-9231/02-SQ
CANMENT SCIENTIFIC AUTHORITY:	Dr. A.E. George
DATE:	April 1991

474 pp

PART 5

MICROMEDIA

3531

91-06120/

ALBERTA OIL SANDS
INFORMATION CENTRE

70

OIL FIELD PRODUCTION USING HORIZONTAL AND MULTIPLE-DEVIATION WELLS

Y. P. Borisov

Moskva, "Nedra", pp. 56-59, 80-93, 132-152 (1964)

Russian into French

J. Combe, Institut Français Du Pétrole
France

French into English

Translation: Jeanne Strauss

Technical Editing: S. D. Joshi

PHILLIPS PETROLEUM COMPANY

Bartlesville, Ok. 74004

U.S.A.

3531

INFORMATION AND DOCUMENTATION BOARD
Documentation Center

TA 65-83 JHS 86-83

AOSTRA OIL SANDS
INFORMATION CENTRE

BORISOV (Y. P.)

OIL FIELD PRODUCTION USING HORIZONTAL AND MULTIPLE-DEVIATION WELLS

Moskva, "Nedra", 1964. - 56-59, 80-93, 132-152.

French Petroleum Institute Translation

(Revised by J. Combe)

Russian No. 1200

AUGUST 1980

Institut Français du Petrole
Report No 28 363

OIL FIELD DEVELOPMENT AND PRODUCTION
USING HORIZONTAL AND MULTIPLE-DEVIATION WELLS

9. CALCULATION OF INTERFERENCE OF CLUSTERS OF MULTIPLE-DEVIATION INCLINED WELLS IN A BEDDED CIRCULAR RESERVOIR

Stating the problem

The purpose of this paragraph is to find approximate formulas that are simple and more convenient for computation while ensuring at the same time the necessary accuracy for an isolated well in an infinite reservoir as well as for well configurations.

Let us assume that a reservoir of finite thickness h is being developed by inclined or n multiple well deviations. The holes intersect the reservoir over an entire thickness from top to bottom. The vertical permeability is equal to zero, and the horizontal permeability is constant and equal to k.

In the reservoir each inclined hole appears in each stratum (or bed) as an elliptical well, but their position differs depending on the various strata, and the total flow rate of the inclined well or of any grouping of deviated holes is determined by the sum total of the flows in the different strata.

In a number of cases this sum is difficult to determine. If one succeeds in totaling the flow rates, rather complex calculation formulas are obtained.

It is known that a small change in well location, where wells are interfering with each other, has a small influence on their cumulative oil production.

This makes it possible to assume for all the beds an identical position of deviated hole sections, corresponding to the effective position of these sections in a given bed.

It is always possible to find a stratum with a mean flow rate that varies with the thickness of the bed. It will be shown further on that if an average stratum is taken as a base and located at equal distance from the top and the bottom, the formulas obtained in this manner will be entirely adequate for practical calcultions.

Fluid flow to the group of deviated wells

For a circular group of deviated wells, the fluid flow equation, based on the above assumption, can be written as follows:

$$Q = \frac{2 \pi kh (p_k - p_c)}{\mu \left(\text{Log} \frac{2R_k}{r_1+r_2} + \frac{1}{m} \text{Log} \frac{r_1+r_2}{2nr_o}\right)} \qquad (9.1)$$

where r_1 and r_2 are the radii of the cluster at the bottom and top level of the bed;

$\frac{r_1+r_2}{2}$ - radius at the mean stratum level;

r_o - radius of the circular well equivalent by its flow rate to an elliptical well;

$$r_o = \frac{r_c(1 + \cos \alpha)}{2 \cos \alpha} \quad . \qquad (9.2)$$

Here r_c is the effective radius of the well.

Table 2 shows the results of flow rate calculations for a group of deviated wells, such as obtained by formula (9.1) and by the specific formula (9.1) established at § 7 of this chapter.

TABLE 2

r_1, m	r_2, m	Group flow obtained by formula (9.1) m^3/day	Group flow obtained by formula (9.3) m^3/day	% relative, % error
300	400	72,57	72,68	0,12
500	600	98,56	99,10	0,54
700	800	130,32	131,28	0,73
800	900	148,97	150,81	1,22

$$Q = \frac{2\pi\ khnR_k(P_k - P_c)}{\mu(n-1)\ (r_2 - r_1)} \sqrt[n-1]{\frac{R_k}{nr_o}\left(Ei(t_1) - Ei(t_2)\right)}, \qquad (9.3)$$

where

$$t_1 = -\frac{1}{n-1} \text{Log} \frac{R_k}{nr_o} \left(\frac{R_k}{r_1}\right)^{n-1}$$

$$t_2 = -\frac{1}{n-1} \text{Log} \frac{R_k}{nr_o} \left(\frac{R_k}{r_2}\right)^{n-1}$$

It has been assumed here that $R_k = 1{,}000$ m; $k = 0.1$ darcys; $h = 30$m; $\Delta p = p_k - p_c = 30$ kgf/cm^2; $n = 10$; $\mu = 5$ cP; $r_c = 0.1$m.

Fluid flow in a multiple-deviation well

By taking in formula (9.1) $r_2 = 0$, we obtain the formula to calculate the fluid flow in a multiple-deviation well with m deviations (holes) regularly positioned on the surface of a cone:

$$q = \frac{2\pi kh\,(p_k - p_c)}{\mu\,(\mathrm{Log}\,\frac{2R_k}{r_1} + \frac{1}{m}\,\mathrm{Log}\,\frac{r_1}{2mr_0})} \qquad (9.4)$$

where r_1: projection length of a hole on the top or bottom of the bed.

If the deviated holes are initiated above the top of the bed, $r_2 \neq 0$, formula (9.1) can be used because in this case the cluster is not different from a circular group of deviated wells.

TABLE 3

m	r_1, m	Flow according to precise formula rm^3/day	Flow according to formula (9.4) m^3/day	relative error %
2	26	10.02	10.40	2.03
	85	12.21	12.49	2.30
3	26	11.71	11.80	0.77
	85	15.15	15.32	0.11
4	26	12.64	12.70	0.48
	85	16.82	16.98	0.97

Table 3 gives the result of the flow calculation according to formula (9.4) and by the precise formula established in § 3 of this chapter. Here, taking

$R_k = 500$ m; $k = 0.1$ darcys; $h = 15$ m; $\Delta p = p_k - p_c = 30$ kgf/cm^2; $\mu = 5$ cp; $r_c = 0.1$ m; $r_1 = 26$ m (for $\alpha = 60^\circ$) and $r_1 = 85$ m (for $\alpha = 80^\circ$).

Fluid flow in a group of well clusters

For a circular group of well clusters, by replacing each cluster by a vertical well with a radius r_e' (r_3), the following can be written:

$$\frac{\mu Q}{2\pi\ kh\ (p_k - p_c)} = \mathrm{Log}\,\frac{R_k}{r_b} + \frac{1}{n}\ln\frac{r_b}{nr_e'}\,, \qquad (9.5)$$

where r_b is the radius of the circle that passes through the centers of the clusters.

The value of r_e can easily be obtained by presenting formula (9.4) in this manner:

$$q = \frac{2\pi\ kh\ (p_k - p_c)}{\mu\ \mathrm{Log}\ \frac{Rk}{r}} \qquad (9.6)$$

and by equalizing one with the other the straight parts of (9.4) and (9.6).

$$\mathrm{Log}\ r_e' = \mathrm{Log}\ \frac{r_1}{2} - \frac{1}{m}\ \mathrm{Log}\ \frac{r_1}{2mr_0} \qquad (9.7)$$

We extract then from (9.5) and (9.7)

$$\frac{\mu Q}{2\pi\ kh\ (p_k - p_c)} = \mathrm{Log}\ \frac{R_k}{r_b} + \frac{1}{n}\ \mathrm{Log}\ \frac{2r_b}{nr_1} + \frac{1}{mn}\ \mathrm{Log}\ \frac{r_1}{2mr_0} \qquad (9.8)$$

Obviously, the calculation errors of interaction of the clusters with formula (9.8) will be smaller than those for clusters taken in isolation by using (9.4). It is also easy to transcribe formulas of the (9.1) and (9.8) type for rectilinear groups in a linear deposit (or reservoir).

Interaction of groups and general conclusions

It is easy to conclude, when analyzing the formulas obtained, that the interaction of groups of deviated wells in a stratified bed can be calculated with known formulas for the interaction of vertical wells. One must then take the radius of wells equal to the reduced radius r_0 determined by formula (9.2), and compute the position of the groups (circular or rectilinear) at the level of the average stratum located at equal distance from the top and the bottom of the bed.

The interaction of groups of well clusters can also be calculated by using formulas utilized for the interaction of groups of vertical wells (1). The clusters are replaced here by vertical wells located at the center of the clusters and having a (reduced) equivalent radius determined by formula (9.7).

In all the cases contemplated, the wells are supposed to penetrate the bed completely. We substitute then r_c, the effective radius of the well, in the calculation formula of r_o. If the wells are cased with liner strings and, consequently, perforated (drilled), the value of radius r_c in the calculation formula of r_o must be considered while taking into account the partial nature of the penetration.

r_c shall then be a function of the number of performations per meter, of their diameter, of the depth of penetration of (sealing) balls in the rock, etc... The value of r_c can be determined based on the studies of V. I. SHCHUROV.

In conclusion we shall supply the formulas to calculate the total internal resistance of groups:

1. Deviated wells in a circular reservoir:

$$\frac{2\pi\ kh}{\mu}\,\omega = \frac{1}{n}\,\text{Log}\ \frac{(r_1 + r_2)\cos\alpha}{nr_c\ (1+\cos\alpha)}\ . \tag{9.9}$$

2. Deviated wells in a linear deposit (or reservoir):

$$\frac{khb}{\mu}\,\omega = \frac{\sigma}{\pi}\,\text{Log}\ \frac{2\sigma\ \cos\alpha}{\pi r_c(1+\cos\alpha)}\ , \tag{9.10}$$

where b - length of the group;

2 σ - average distance between the wells in the group.

3. Well clusters in a circular reservoir:

$$\frac{2\pi\ kh}{\mu}\ \omega = \frac{1}{n}\ \mathrm{Log}\ \frac{2r_b}{nr_1} + \frac{1}{mn}\ \mathrm{Log}\ \frac{4_1\ \cos\ \alpha}{mr_c\ (1+\cos\ \alpha)} \qquad (9.11)$$

4. Clusters in a linear deposit (or reservoir):

$$\frac{khb}{\mu}\ \omega = \frac{\sigma}{\pi}\ \mathrm{Log}\ \frac{2\sigma}{\pi r_1} + \frac{\sigma}{\pi m}\ \mathrm{Log}\ \frac{r_1\ \cos\ \alpha}{mr_c\ (1+\cos\ \alpha)} \qquad (9.12)$$

where 2 σ - distance between well clusters in the group.

BIBLIOGRAPHY

1. BORISOV (Ju. P.)

   Flow determination of the wells when working jointly several rows of wells.

   Trudy MNI, vyp. 11, Gostoptekhizdat, 1951.

2. MERKULOV (V.P.), SURGUCHEV (M.L.)

   Determination of the flow and of the efficiency of deviated wells.

   Neft. khoz., 1960, No. 2.

3. PILATOVSKIJ (V.P.)

   Production problems of oval-shaped oil deposits. Determination of flows and pressures at bottom of the elliptical groups of wells.

4. PILATOVSKIJ (V.P.)

   Some general ideas concerning uniform flow. Scientific and technical collection on oil production, No. 4.

   Gostopekhizdat, 1959.

5. SHCHELKACHEV (V.N.)

   Stating the problem and studying some rules of water production rate of a well in the simplest conditions geological and production problems of oil and gas deposits (or reservoirs).

   Trudy MNI, vyp. 14, Gostoptekhizdat, 1955.

6. SHCHELKACHEV (V.N.), LAPUK (E.B.)
Underground hydraulics.
Gostoptekhizdat, 1949.

7. ROEMERSHAUSER (A.E.), HAWKINS, (M.F.)
The effect of slant hold, drain hole and lateral hole drilling on well productivity.
J. Petrol. Technol., 1955, vol. 7, No. 2, II.

6. APPROXIMATE SOLUTION OF THE PROBLEM OF OIL FLOW TOWARD HORIZONTAL AND DEVIATED WELLS IN A HOMOGENEOUS BED

Stating the problem

Precise analytical solutions of fluid flow problems in horizontal wells, inclined or multiple-deviation wells, in certain condiions, result in rather complicated, complex and sometimes inconvenient calculations. The results of electrolytic simulation of oil flow toward these wells can only be used when supplemented by diagrams and tables.

The purpose of this paragraph is to provide approximate formulas which are simple and easier to calculate and which will ensure the necessary accuracy for all practical purposes. The following comparison to be made between the formulas obtained and the results of electrolytic simulation shows tht their accuracy is entirely satisfactory. The method of flow resistances proposed by Ju. P. BORISOV [1] is used for solution.

The isolated horizontal well

Let us consider first a horizontal well of lenght ℓ, r_c radius, located at the center of a homogeneous isotropic bed with drainage radius R_k and reervoir pressure is P_k (fig. 45). The pressure at the bottom of the well is p_c. It is assumed that the bed and the fluid it contains are incompressible.

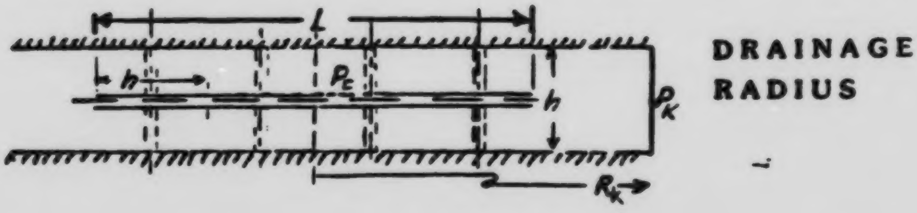

Fig. 45 - Horizontal well.

Total resistance to flow can be represented by the sum of two resistances: external resistance, of the feed contour to the rectilinear vertical tier (or series) coinciding with the projections of the horizontal well on the top (or bottom) of the bed, and internal resistance due to the fact that we have in reality a well and not a tier.

We determine the external resistance, based on § 6 of chapter II, as follows:

$$\Omega = \frac{\mu}{2\pi kh} \text{Log} \frac{4R}{\ell} . \tag{6.1}$$

We determine the internal resistance in the same manner as for a vertical well in a group, assuming that the thickness of the reservoir under consideration corresponds to the distance between the wells, and that the length of the vertical well hole is equal to the thickness in the case of a vertical well. We then have:

$$\omega = \frac{\mu}{2\pi kh} \text{Log} \frac{h}{2\pi r_c} . \tag{6.2}$$

This formula can be obtained by imagining the horizontal well being cut into segments of a length equal to the thickness of bed h, and by replacing each one of them in a vertical position. We shall thereby have a group of vertical wells, the distance between these being equal to h, and their number equal to $\frac{l}{h}$.

The sum total of these resistances will give us the ratio of the difference in pressure to the flow of the horizontal well:

$$\frac{P_k - P_c}{q} = \frac{\mu}{2\pi kh} \left(\text{Log} \frac{4R_k}{\ell} + \frac{h}{\ell} \text{Log} \frac{h}{2\pi r_c}\right) \tag{6.3}$$

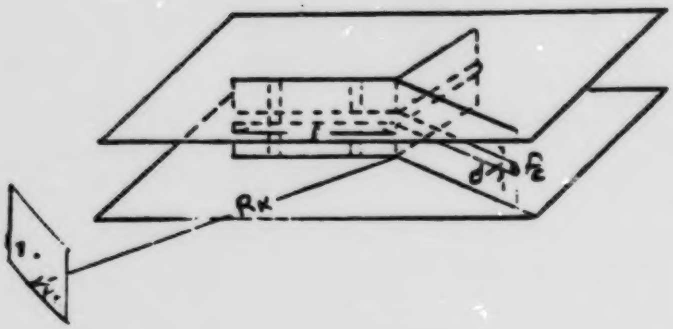

Fig. 46 - Diagram of a multiple-deviation well with horizontal holes.

1. Feed contour

we shall obtained, based on § 6 of chapter II and on the same notions concerning internal resistance, the following calculation formula:

$$\frac{P_k - P_c}{q} = \frac{\mu}{2\pi kh} \left(\text{Log} \frac{\eta R_k}{\ell} + \frac{h}{n\ell} \text{Log} \frac{h}{2\pi r_c} \right) \qquad (6.4)$$

where ℓ - length of a hole taken in isolation;

$\eta = \eta(n)$ - determined according to table 4.

TABLE 4

n	1	2	3	4
η(n)	4	2	1.86	1.78

From (6.4) we shall deduce (6.3) as a particular case for n = 1.

The isolated deviated well or the cluster of deviated wells

If one considers a deviated well (fig. 47), the fracture will pass through the axis of the well and shall be equal to the value of $\ell \sin \alpha$ (α - dip angle of the well in relation to the straight line). In order to determine internal resistance, it is also possible to "cut-out" the deviated well into segments of length h and to place them vertically, namely to utilize the diagram we have adopted for fluid flow toward such a well. The distance between the wells shall then be $h\sin\alpha$. The calculation formula for a cluster of deviated holes shall then be expressed as follows:

$$\frac{P_k - P_c}{q} = \frac{\mu}{2\pi kh} \left(\mathrm{Log}\,\frac{\eta R_k}{\ell \sin\alpha} + \frac{h}{n\ell}\,\mathrm{Log}\,\frac{h\sin\alpha}{2\pi\, r_c}\right) \qquad (6.5)$$

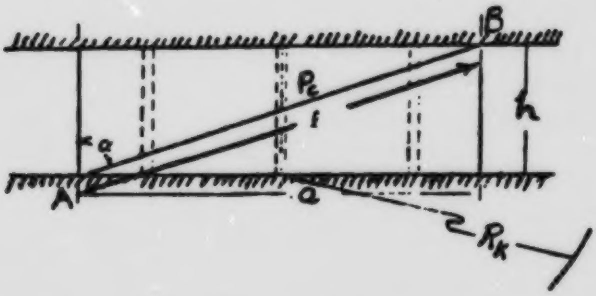

Fig. 47. - Deviated well in a homogeneous bed.

The particular case of the single deviated well can be inferred from (6.5) by posing $n = 1$ and $\eta = 4$. On the other hand, by taking $\alpha - 90^\circ$, we shall obtain the formulas for horizontal wells (6.4) and (6.3).

Thus, formula (6.5) can be considered as common to the isolated clusters or the deviated horizontal and isolated wells.

The formula to calculate the flow of a well with two holes, when one hole has been drilled straight down and the second hole in deviation, can be obtained in a manner similar to the preceding case.

In § 6 of chapter II the formula has been given to calculate the flow of a fracture with length a located at the center of a circular reservoir.

In the case under consideration, the vertical hole is at the center of the deposit and the deviated hole is off center; this is why the a lenght fracture must be arranged eccentrically in the circular reservoir.

After reasonings similar to those used in § 6 of chapter II, we shall obtain the searched for fracture flow:

$$q_g = \frac{2\pi \; kh \; (p_k - p_c)}{\mu \; \text{Log} \; \frac{4.48 \; R_k}{a}} \qquad (6.6)$$

Within the fracture not only n, but n+1 wells will be located. For a two hole well, the ratio between flows, geometric parameters and hydromechanical parameters can be written in this manner:

$$\frac{2\pi \; kh \; (p_k - p_c)}{\mu q_2} = \text{Log} \; \frac{4.48 \; R_k}{a} + \frac{1}{n+1} \; \text{Log} \; \frac{\sigma}{\pi r_c} \qquad (6.7)$$

but:

$$n+1 = \frac{1 + \cos \alpha}{\cos \alpha} \; , \; \sigma = \frac{a}{2(n+1)} + \frac{h}{2} \; \text{tg} \; \frac{\alpha}{2}$$

By substituting then the value of n+1 and of σ in the formula q_2, we obtain the following expression:

$$q_2 = \frac{2\pi \; kh \; (p_k - p_c)}{(\text{Log} \; \frac{4.48 \; R_k}{a} + \frac{\cos \alpha}{1+\cos \alpha} \; \text{Log} \; \frac{h \; \text{tg} \; \frac{\alpha}{2}}{2\pi \; r_c})} \qquad (6.8)$$

Here, as in the previous chapter, the wells are assumed to be of total penetration (r_c: real radius of horizontal wells, equal to the radius of vertical wells). If the wells are cased with a column and drilled, meaning that they are of partial penetration, instead of r_c it becomes necessary to take for the calculations using formula (6.8) the reduced radius of the wells which is defined, according to the works of V. I. SHCHUROV, as a function of the number of perforations per meter, of the diameter of the perforations, of the depth of penetration of the sealing balls in the rock, etc....

Interaction of deviated, horizontal and multiple deviation wells

The contemplated cluster or single well can be replaced for the purpose of calculations by a vertical well located on that same site and with an equivalent radius. We shall find the value of this radius from the equivalence condition of flow resistances in formula (6.5) and in the usual DUPOUY formula:

$$\frac{P_k - P_c}{q} = \frac{\mu}{2\pi\ kh} \text{Log} \frac{R_k}{r'_{ce}} \qquad (6.9)$$

we then have:

$$\text{Log}\ r'_{ce} = \text{Log} \frac{\ell \sin \alpha}{\eta} - \frac{h}{\ell n} \text{Log} \frac{h \sin \alpha}{2\pi\ r_c} \qquad (6.10)$$

By using formula (6.10) it is possible to find all specific cases by substituting the appropriate dimensions.

Formula (6.10) makes it possible to carry out the calculations to determine the flow or pressure differences for any plan (or layout diagram) of the deviated, horizontal or multiple deviation well groups for which the interaction formulas of vertical wells were given. The formulas or equations must then be written for the vertical wells whose location coincides with the central position of the deviated, horizontal or multiple deviation wells, and replace in these formulas of Log r_c (r_c - reduced radius or real radius of the vertical well) the magnitude Log r'_{ce} of formula (6.10).

Evaluation of the accuracy of the proposed formulas

In order to evaluate their accuracy, we shall compare the calculation results arrived at with the proposed formulas with those of electrolytic simulation. V.I. SHCHUROV has prepared the charts of correction C for a certain number of contemplated cases. He gives the outflow formula as follows:

$$q = \frac{2\pi\ kh\ (P_k - P_c)}{\mu\ (\mathrm{Log}\ \frac{R_k}{r_c} - C)} \qquad (6.11)$$

By comparing (6.9) and (6.11), we find:

$$C = \mathrm{Log}\ r'_{ce} - \mathrm{Log}\ r_c \qquad (6.12)$$

By utilizing (6.12) and (6.10), it is easy to obtain correction value C for any given case.

Table 5 indicates, for a formation (or bed) with $h = 7.5$ m, $d_{wells} = 0.2$ m and different ℓ lengths, the values of C as obtained with formulas (6.10) and (6.12), with the results of V.I. SHCHUROV such as he established them in 1952 at the VNII, and in accordance with the works of V.O. MERKULOV (4) for an isolated horizontal well.

Table 6 proposes a similar comparison for a well with four deviations and horizontal holes.

Analysis of Tables 5 and 6 shows that the deviation between the values of correction C obtained with the suggested formulas and that with the assistance of the model is contained within the accuracy limits of the

TABLE 5

ℓ	According to formulas (6.10) and (6.12)	According to data of V.I. SHCHUROV	According to data of V.P. MERKULOV	Difference between column (2) and (3) %	Difference between column (2) and (4), %
1	2	3	4	5	6
12.5	1.95	1.92	2.00	-1.43	+3.95
25.0	3.39	3.35	3.42	-1.21	+2.27
50.0	4.45	4.38	4.51	-1.57	+1.21
75.0	4.98	4.95	4.99	-0.56	+1.20
100.0	5.33	5.30	5.34	-0.65	+0.16
125.0	5.59	5.56	5.61	-0.59	+0.32

TABLE 6

ℓ	According to Formulas (6.10) and (6.12)	According to data of V.I. SHCHUROV	Error, %
12.5	3.8	3.74	-1.12
25.0	5.10	5.00	-2.01
37.7	5.70	5.59	-1.95
50.0	6.08	5.97	-1.76

simulation. (For a horizontal well the calculated values are comprised between the results obtained by V.I. SHCHUROV and those obtained by V.P. MERKULOV).

For a deviated well the values of correction C obtained by using formulas (6.10) and (6.12) are higher than the results obtained by V.I. SHCHUROV and V.P. MERKULOV, but there too they are within the accuracy limits of the simulation (Table 7).

In case of interaction between the different groups of wells mentioned previously, the flow errors and pressure differences will be even smaller.

TABLE 7

Inclination angle in degrees	C According to formulas (6.10) and (6.12)	 According to data of V. P. MERKULOV	% deviation between (2) and (3)
75	3.83	3.76	-1.86
60	2.45	2.42	-1.24
45	1.43	1.46	+2.06
30	0.85	0.83	-2.41
15	0.56	0.48	--

7. ESTIMATING THE FLOW RATE OF A MULTIPLE LEVEL WELL IN A HOMOGENEOUS AND VERY THICK FORMATION

The productive formations are very thick (300 m and more) in a number of oil fields of Bachkiria. Some of them are developed by using multiple deviation wells with numerous holes (from 2 to 11). In most cases, the holes are regularly drilled into a plane surface [or level] close to the bottom of the stratum. It appears that this arrangement must be efficient for formations with gravity drainage. When water drive is used to induce production, this arrangement is obviously not recommended.

Let us consider the following problem. A homogeneous, very thick formation H, with a k permeability, is saturated by a homogeneous incompressible fluid of μ viscosity. The fluid circulation in the formation is achieved under conditions of constant presure water-drive.

The bed is developed by a multiple deviation well with several levels (fig. 48), located in the center of the circular reservoir. The draining contour of radius R_k is subject to a p_k pressure. We consider the well bottomhole pressure (reduced to one plane) in all the holes as constant and equal to P_c. The holes have an r_c radius.

The purpose of this paragraph is to bring out the theoretical formulas and to demonstrate the connections between the necessary number of m levels; n, the number of holes in each level, and the length ℓ of a single hole.

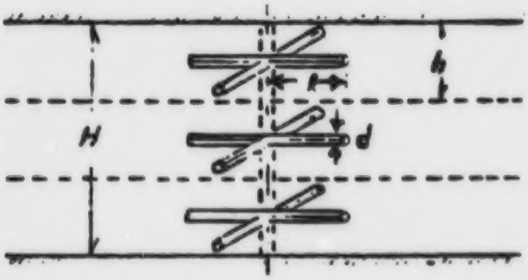

Fig. 48 -

SCHEME OF A WELL WITH MULTIPLE LEVELS

Let us assume that there is no fluid inflow through the vertical well and that it only is a discharge channel. Let us further suppose that the levels are located at identical distances from each other and that the distance of the bottom set from the reservoir bottom and that of the top set from the reservoir top are equal to one-half the distance between the levels.

By symmetry, the flux can be divided into m flows toward the various clusters of horizontal wells. Thickness h of the bed corresponds to one level. The radius of an equivalent vertical well will be determined by the flow to the cluster of horizontal wells using equation (6.10):

$$\text{Log } r_e' = \text{Log } \frac{\ell}{\eta} - \frac{h}{\ell n} \text{ Log } \frac{h}{2\pi \; r_c} \qquad (7.1)$$

where η is determined by Table 4.

We shall find the flow of a level in the form of:

$$q = \frac{2\pi \; kh \; (p_k - p_c)}{\mu \; (\text{Log } \frac{R_k \cdot \eta}{\ell} + \frac{h}{\ell n} \text{ Log } \frac{h}{2\pi \; r_c})} \qquad (7.2)$$

Taking into account that $H = hm$, we shall obtain the total flow rate of the multiple level well:

$$Q = qm = \frac{2\pi h \, \frac{k}{\mu} \, (p_k - p_c)}{\text{Log } \frac{R_k \cdot \eta}{\ell} + \frac{H}{\ell mn} \text{ Log } \frac{H}{2\pi \; r_c m}} \qquad (7.3)$$

Starting with (7.3), the radius of a vertical well with a flow rate equivalent to the multiple level well is calculated in the following manner:

$$\text{Log } r_{en}' = \text{Log } \frac{\ell}{\eta} - \frac{H}{mn\ell} \text{ Log } \frac{H}{2\pi \; r_c m} \qquad (7.4)$$

Therefore, in the presence of several multiple level wells, the formulas and equations of the interaction of vertical wells can be used, by replacing in these formulas the radius of the well by the equivalent radius determined with the assistance of formula (7.4).

It is important to ascertain which combination of values of m, n and ℓ is the most appropriate. It is possible, for example, to contemplate the problem of m, n and ℓ values which are best suited for a given total footage in the formation, namely:

$$m\ell = L = \text{const.} \tag{7.5}$$

If one tries, however, to find directly the extreme of equation (7.3), taking into account (7.5) by the LAGRANGE method, no solution can be found. The extremum is evidently not located within the area, but at the boundary line. Assuming that m is known, one has then $Q = Q_{max}$ when

$$\text{Log} = \frac{R_k\eta}{\ell} \rightarrow \text{min.}$$

As in this case $n = \frac{L}{m} = \text{const}$, we then find, by substituting the values of η of Table 4, that Log $\frac{R_k\eta}{\ell} \rightarrow$ min. when n = 1 or n = 2, namely when drilling one hole or two holes in directly opposite directions (which really amounts to the same thing from the hydrodynamic point of view). A similar conclusion can be reached starting with formula (7.2).

By substituting n = 1 and $\eta = 4$ in formula (7.3) and by expressing ℓ in function of m with the help of (7.5) we obtain:

$$Q = \frac{2\pi \frac{k}{\mu} H (p_k - p_c)}{\text{Log}\frac{4R_k m}{L} + \frac{H}{L}\text{Log}\frac{H}{2\pi r_c m}} = \frac{2\pi \frac{k}{\mu} H (p_k - p_c)}{\text{Log}\frac{4R_k}{L} + \frac{H}{L}\text{Log}\frac{H}{2\pi r_c} + (1-\frac{H}{L})\text{Log } m} \tag{7.6}$$

It appears from (7.6) that:

1. When L > H, Q → max for m = 1;
2. When L < H, Q → max when m → max.

The accuracy of the above is confirmed by the graphs of figures 49 and 50.

In the graphs the main values are given in a non-dimensional form, which are defined in equation (7.7).

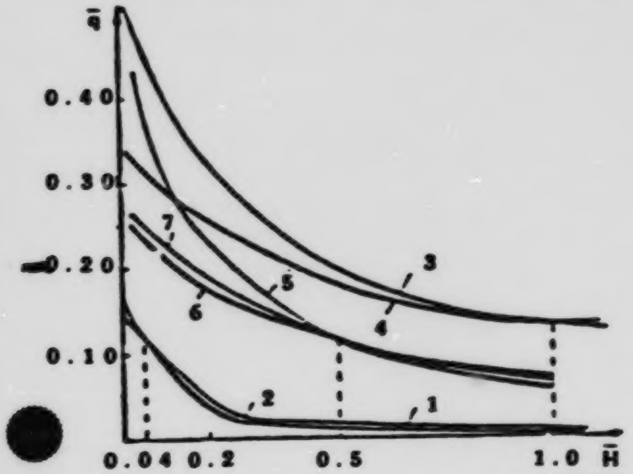

Curve Number	$\bar{l}$	m	n	$\bar{l}mn$
1	0.05	1	1	0.05
2	0.01	5	1	0.05
3	0.50	2	1	1
4	0.20	5	1	1
5	0.50	1	1	0.5
6	0.05	10	1	0.5
7	0.05	5	2	0.5

Fig. 49

RELATION BETWEEN $\bar{q}$ & H

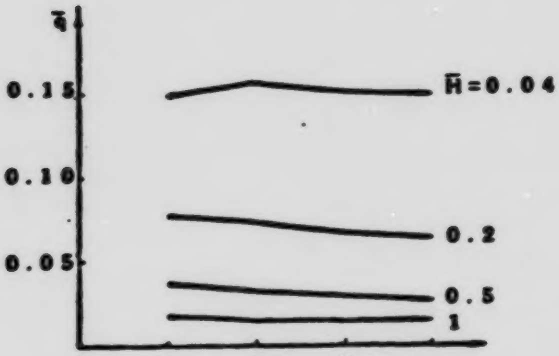

Curve Number	n	m	$\bar{l}$	$\bar{l}mn$
1	1	10	0.01	0.1
2	2	5	0.01	0.1
3	3	3	0.011	0.1
4	4	2	0.0125	0.1

Fig. 50

RELATION BETWEEN q & n WHEN $\bar{l}mn$ ARE CONSTANT

Figure 49 shows that, when values of ℓmn are identical, the curves overlap for values H equal to ℓmn, namely equal to the footage (drilling) in the formation.

$$\bar{q} = \frac{Q\mu}{2\pi\ kH\ (p_k - P_c)};\ \bar{H} = \frac{H}{R_k};\ \bar{\ell} = \frac{\ell}{R_k};\ \bar{r}_c = \frac{r_c}{R_k}\ . \qquad (7.7)$$

It can be seen on fig. 50 that for $n \geq 2$ the flow rates decrease when n increases, independently from the H/ℓ ratio. For $n = 1$, and $n = 2$, it is not the value of n that influences the flow rate (as $n = 1$ and $n = 2$ have the same meaning from the physical point of view), but the number of levels, which is twice as high for $n = 1$. This increment in the number of levels for a constant value of n involves an increase in flow rate when $H > L$ (the three lower curves) and a flow rate reduction when $H < L$ (upper curve).

For practice, the most interesting case is that where $L > H$, because when $L < H$ drilling horizontal holes becomes senseless.

Thus, for a given value of footage drilled in the formation, it is preferable, in an isotropic bed, to drill a single horizontal hole that is long in the center of the formation rather than several levels of a multiple deviation well. It should be noted that, in practice on site, it often happens that heterogeneous beds are encountered. The beds are divided into separate horizons by tight or almost impermeable barriers. In those cases, drilling multiple level wells, with a level for each horizon, can ensure the most rational drilling through the formation.

At the VNII, it has been calculated on an "Ural-1" computer: the flow rate without q dimension for the following parameters: $n = 1, 2, 3, 4$; $m = 1, 2, 3..., 10$; $H = 1.5, 0.2, 0.04$; $\ell = 0.01, 0.05, 0.2, 0.5$; $\bar{r}_c = 10^{-4}$.

The results of the computation have been carried over on the tables which have been used to establish the charts (18). The graphs clearly show that the length of the holes is a main factor in flow increase of the multiple level well. No direct proportionality has been observed, however. When the length of the hole is multiplied by 4, this entails a flow rate increase of approximately twice for $m = 10$ and $H = 0.5$, and of less than 1.5 times for $H = 0.04$. The influence of the number of levels varies in accordance with the different values of H. The smaller the dimensionless thickness of the bed, the higher is the dimensionless flow for an equal amount of levels and an equal dimensionless length of the holes.

An examination of the charts also leads to the conclusion that for values of H most often encountered, it is not necessary to drill more than three to four holes at each level.

If the length of hole that can be reached in practice is known, in order to select the necessary number of levels and holes at each level, a series of curves similar to those appearing on figure 51 must be constructed. When the number of levels is increased, the flow increases, but a close connection to direct proportionality has only been observed for values of $\bar{H}$ close to the unit and for small values of n and $\bar{L}$.

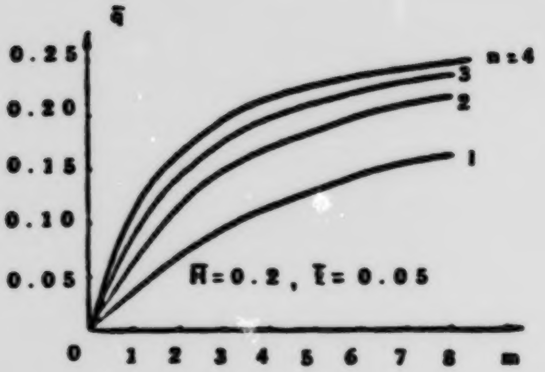

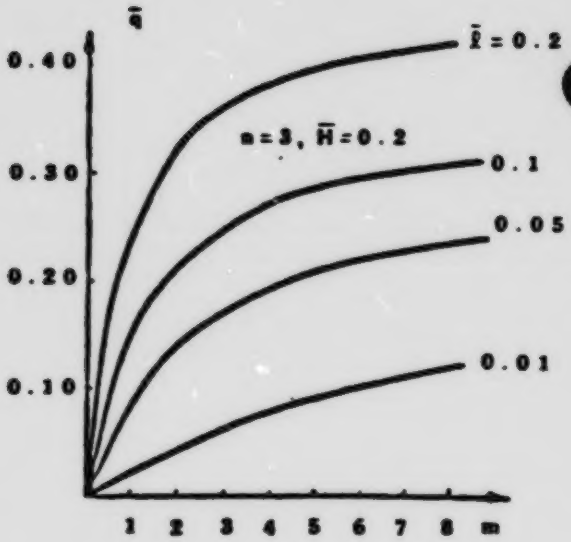

Fig. 51 DEPENDENCE OF $\bar{q}$ on m & n FOR CONSTANT $\bar{\ell}$ & $\bar{H}$

Fig. 52. DEPENDENCE OF $\bar{q}$ on m & $\bar{\ell}$ FOR CONSTANT n & $\bar{H}$

If we have set for ourselves a specific number of holes per level, in order to determine the necessary number of levels for different thicknesses and different hole lengths, it is necessary to construct flow charts similar to those of figure 52.

By using subsequently the expression (7.7), one can calculate dimensional sizes (or magnitudes).

In conclusion, let us note that in order to determine the base parameters of the multiple-level well (m, n and ℓ) one should not only take as a basis maximum production, but also consider that the set production level be reached with the minimum financial cost, and by producing the maximum of reserves.

8. THE PERMANENT FLUID FLOW TOWARD HORIZONTAL WELLS DEVELOPING GAS AND OIL PRODUCTION

Horizontal wells in oil and gas deposits with aquifer

Figure 53 shows diagrammatically such an oil and gas reservoir with an active aquifer. In the presence of an active aquifer and of a gas cap, the energy of the reservoir is distributed regularly over the surface of the productive formation.

Generally, the reservoirs of this type are developed by vertical wells regularly distributed over the field. When the pressure gets lower in the oil layer of the deposit, the gas of the gas cap and the water of the lower water table push the oil toward the drilled holes interval. To avoid water and gas coning the perforated (or drilled) interval must represent only a part of the thickness of the oil-saturated stratum and must be located at a predetermined place to ensure the simultaneous arrival of gas and water at the drilling interval.

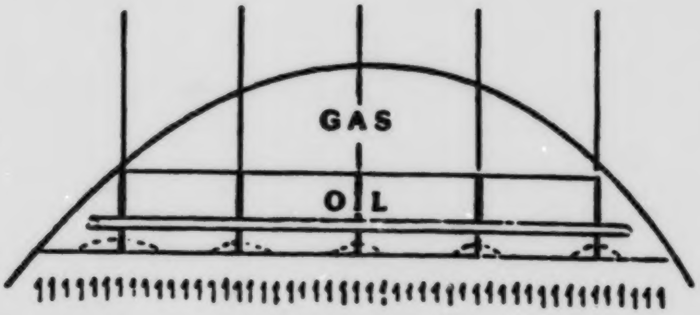

WATER ZONE

Fig. 53

VERTICAL CROSS-SECTION OF A RESERVOIR

A horizontal drain should pass through the center of the perforating intervals of the vertical wells. Even without carrying out calculations, it appears that the conditions of oil production of the deposit are thus largely improved. In the case of a homogeneous formation, more regular and complete drainage of oil by gas and water [drive] is obtained.

If a system of horizontal wells (channels) crosses the entire reservoir and if they are located at equal distances from each other (fig. 54), it is possible, on account of the symmetry of the entire (out)flow, to bring out a distinct element that is shaped like a prism. A horizontal well is at work in this prism. The boundaries between these prisms can be considered as tight (impermeable) barriers.

Fluid flow toward the horizontal well is ensured by the bilateral pressure originating from the water and the gas. Let us consider the flow toward a horizontal well of non-limited length under these conditions. By reason of the symmetry of the fluid flow within that same prism, we shall study the flow toward a unit of length of the horizontal well.

Let us assume that the pressure values on lines AB, gas-oil interface plane, is p_g and CD, water-oil interface plane is p_e (fig. 55).

Under real conditions the pressure in the gas cap can be taken to measure pressure. The well bottom pressure is p_c. Let us consider that the distance from the well to the gas-oil interface (h_1) and to the water-oil interface (h_2) is known.

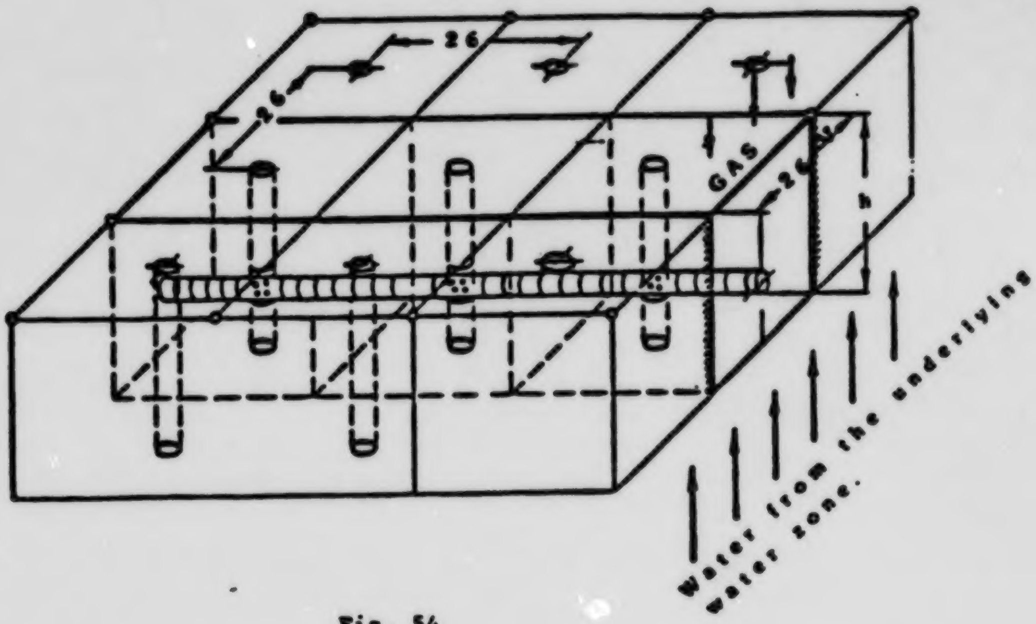
26
26
GAS
26
h
Water from the underlying water zone.

Fig. 54

SCHEMATIC REPRESENTATION OF A SEPARATE HORIZONTAL WELL

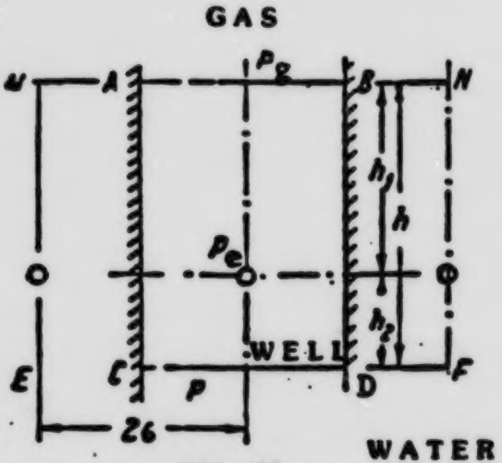
GAS
M
A
P_g
B
N
h_1
h
P_e
h_2
WELL
E
C
P
D
F
26
WATER

Fig. 55

VERTICAL CROSS-SECTION OF A RESERVOIR

The thickness of the oil formation is h. The distance between the horizontal wells is 2σ. The radius of the well is r. It is assumed that the oil and the water are homogeneous fluids of various colors.

In these conditions the expression for the calculation of a unit of length flow of the horizontal well will be:

$$q = \frac{2\pi \frac{k}{\mu} \frac{h_1}{h} Pe + \frac{h_2}{h} Pg - Pc}{\frac{\pi h_1 h_2}{\sigma h} + \text{Log} \frac{\sigma}{\pi r}} \qquad (8.1)$$

By multiplying (8.1) by ℓ (length of the well), we obtain the approximate formula to calculate the flow of the horizontal well:

Example:

Let $h = 22$ m; $h_1 = 8$ m;
$h_2 = 14$ m; $k = 0.106$ darcys
$\mu = 2.4$ cp;
$2\sigma = 300$ m; $\gamma_h = 0.908$ t/m^3;
$P_k - P_c = 1.2$ atm.

These data are close to the conditions of horizon IV of the Troicko-Anastasievskoe reservoir. Under these conditions the real flows of the vertical wells drilled in the productive formation over 2.4m, are about 40 t/day.

Assuming that $p_g = p_k$ and $p_e + h_h$, we draw from formula (8.1) the flow values for the different lengths of the horizontal wells.

The results of the computation are as follows:

ℓ, m	1	2.4	13.7	20	50	100
Q, t/day	2.91	7.00	40	58.2	145.5	291

By comparing the flow of the horizontal well with that of the vertical well, the following can be observed:

1. The flow of the unit of length (1 m) of the vertical well is much higher than that of the unit of length of the horizontal well (respectively 16.6 and 2.91 t/day). For a horizontal well length equal to the hole height of the formation in the vertical well, the flow of the horizontal well is lower than that of the vertical well (respectively 7.00 and 40 t/day).

2. With a horizontal well of 13.7 m in length, it is possible to obtain the same flow as in the vertical well (40 t/day).

3. With horizontal wells of 100 m in length a flow that is 7 times greater than that of the vertical well can be obtained. It should be noted here that in practice the petroleum industry has experimented already with horizontal wells of 100 m and beyond.

The longest horizontal hole has been drilled in limestones (or chalk stones) of average hardness over 260 m in length, at about 500 m depth in the Kartashovskoe reservoir.

4. Taking into account the fact that in order to calculate the flow of a finite length horizontal well the formula used for an unlimited horizontal well was applied, the results obtained must be considered as approximate, and formula (8.1) can be utilized for initial evaluation.

In the next chapter, we shall study in detail the present state of this question and we shall examine very interesting solutions of other problems closer to real conditions.

BIBLIOGRAPHY

1. BORISOV (Ju. P.)

   Flow determination of the wells when working jointly several rows of wells.

   Trudy MNI im. I.M. Gubkina, vyp. 11, 1951.

2. GREJ (Z.), METJUZ (G.B.), GRAY (Z), MATHEWS (G.B.)

   Bessel functions and their applications in physics and in mechanics.

   IL, 1953.

3. MERKULOV (V.P)

   Flow toward a horizontal well of finite length in a formation of finite thickness.

   Izv. MVO SSSR, Ser. Neftj i gaz, 1958, No. 1, No. 3.

4. MERKULOV (V.P.)

   The flow of deviated and horizontal wells.

   Neft. khoz., 1958, No. 6.

5. MERKULOV (V.P.), SURGUCHEV (M.L.)

   Determination of the flow and efficiency of deviated wells.

   Neft. khoz., 1960, No. 2.

6. MERKULOV (V.P.)

   Calculation of fluid inflow toward a cluster of wells with horizontal deviations.

   Trudy Kujbyshev NII, vyp. 2, 1960.

7. PILATOVSKIJ (V.P.)

Study of some problems concerning fluid flow toward horizontal wells and cracks in place draining a horizontal formation.

Trudy VNII, vyp. 32, 1961.

8. PILATOVSKIJ (V.P.)

Application of some contour integrals to the flow problems by pressure of an incompressible fluid toward the wells.

DAN SSSR, 1966, T. 110, No. 5.

9. PILATOVSKIJ (V.P.)

Approximate calculation of the values of the given function by Laplace representation.

DAN SSSR, T. 82, 1952, No. 2.

10. PILATOVSKIJ (V.P.)

Production problem of oval-shaped petroleum reservoirs. Determination of flows and pressures of the bottom of elliptical well groups.

Trudy VNII, 1958, No. 6.

11. PILATOVSKIJ (V.P.)

Establishment of the complete system of equations of hydrodynamic interaction of the parallel rows of wells draining a rectangular section of a formation.

NTS po dobyche nefti, VNII, 1959, No. 4.

CHAPTER V

TECHNICAL AND ECONOMIC EFFICIENCY OF DRILLING PRODUCTIVE OIL-BEARING STRATA USING HORIZONTAL AND MULTI-DEVIATION WELLS.

DEVELOPMENT CHARACTERISTICS OF MULTI-DEVIATION WELLS.

I. PRELIMINARY REMARKS

The problems concerning the economical efficiency of drilling productive formations using horizontal and multi-deviation wells are extremely important.

It is rather difficult to show this efficiency in accordance with the data gathered in the field. Even two neighboring wells drilling according to an identical program, generally differ in their productivity due to the fact of the natural heterogeneity of the formation. It is all the more difficult to analyze the productivity of wells producing by liberation of dissolved gases, especially those which have been put into production at different times, as the formation has been drilled in a different manner and the holes do not have the same length inside the productive layer.

The safest and most accurate method to determine the efficiency of the multi-deviation well would be to compare its yield with that of a vertical well located on the site of a multi-deviation well, by drilling the formation in the same manner and developing it under identical conditions. One might then consider that the ratio of yields of these two wells is truly the effect of the scope of the well, of its gradient, etc. Observation of these conditions and practice is, on the whole, feasible, but in most cases, we do not have data of this kind available. This is why comparison of the yield of multi-deviation wells and vertical wells in accordance with work site results does not permit us to draw specific conclusions with regard to the efficiency of drilling the productive formation using multiple holes, and the data obtained can only be considered as approximate.

We shall give hereafter an estimate of the economic efficiency of multi-deviation wells according to concrete examples of circular and linear reservoirs.

The following variables shall be taken into account in order to determine the economic efficiency of multi-deviation wells:

1. The oil production increase obtained by drilling horizontal multi-deviation wells located on the work-site of vertical wells and by drilling the formation in the same manner;
2. The amount of various multiple deviation wells by the number and length of deviation holes, necessary to obtain the same production as a given number of vertical wells;
3. The specific investments per ton of oil produced and the cost price of a ton of oil produced in the multiple deviation wells.

2. LINEAR RESERVOIR

Let us examine the efficiency of developing a linear reservoir by multi-deviation wells. By arranging on the deposits various numbers of rows of horizontal and multi-deviation wells, we shall determine the influence of the following parameters:

1. Number of deviation in the cluster;
2. Length of the holes;
3. Distance between the clusters and the draining contour.

We understand horizontal wells and multiple deviation wells to mean those having one, two, three or four deviations, the horizontal or deviation holes being arranged in a regular fashion.

Comparison for a Given Amount of Wells

It has been shown in paragraph 6 of Chapter II that it is possible to calculate the interaction of well clusters by using known formulas of interaction of vertical wells by replacing the radius of the wells by an equivalent radius of the cluster:

$$\mathrm{Log}\ r'_e = \mathrm{Log}\ \frac{\ell}{\eta(n)} - \frac{h}{\ell n}\ \mathrm{Log}\ \frac{h}{2\pi\ r_c} \qquad (2.1)$$

Where

ℓ - length of the hole;
n - number of deviations of holes;
h - formation thickness;
$\eta(n)$ - coefficient determined from Table No. 4.

We shall take the lengths of holes and the distance between the first row and the draining contour L in a non-dimensional manner, as the ratio of the two lengths in question to the thickness of the formation.

The yield increase of the straight line row of multiple deviation wells in relation to the yield of a similar row of vertical wells located on the site of multiple deviation wells, under otherwise equal conditions, can be defined as follows:

$$\phi = \frac{Q_{mdw}}{Q_v} = \frac{L + \frac{\sigma_v}{\pi} \text{Log} \frac{\sigma_v}{\pi r_c}}{L + \frac{\sigma}{\pi} \text{Log} \frac{\sigma}{\pi r'_e}} \qquad (2.2)$$

Table 8 lists of values of coefficient ϕ for different values of n, $\bar{\ell}$ and $\bar{L}$. Here $\bar{L} = \frac{L}{h}$ and $\bar{\ell} = \frac{\ell}{h}$

TABLE 8

$\bar{L}$	$\bar{L}_1 = 10$				$\bar{L}_1 = 20$			
n	1	2	3	4	1	2	3	4
1.335	1.21	1.63	1.79	1.95	1.15	1.41	1.50	1.59
2	1.44	1.90	2.05	2.15	1.31	1.56	1.64	1.69
3	1.70	2.20	2.36	2.45	1.46	1.71	1.78	1.82

$\bar{L}$	$\bar{L}_1 = 66.7$				$\bar{L}_1 = 266$			
n	1	2	3	4	1	2	3	4
1.335	1.07	1.16	1.19	1.21	1.02	1.04	1.05	1.06
2	1.12	1.21	1.23	1.24	1.04	1.05	1.06	1.065
3	1.17	1.24	1.26	1.27	1.05	1.08	1.07	1.075

For calculations the distance between well clusters, constant and equal to:

$$2\bar{\sigma} = \frac{2\sigma}{h} = 20 \qquad (2.3)$$

was used.

Specifically, the values obtained may correspond to the following data: $h = 30$ m; $2\sigma = 600$ m; $L_1 = 300, 600, 2000$ and 8000 m and $\ell = 40, 60, 90$ m.

It can be seen on Table 8 that the value of ϕ increases at the same time that the number of deviation holes in the cluster and the length of the holes increase. No direct proportionality has been observed in any of the two cases. By increasing the number of holes from 1 to 4 or $\bar{\ell} = 1.335$ and $\bar{L} = 10$, ϕ increased by 1.61 times, whereas the increase in lengths of the holes is 1.335 to 3, for $n = 1$, entailing an increase of ϕ by 1.42 times.

By analyzing the relationship between ϕ and $\bar{L}$, it may be noted that for the higher values of L we have practically no flow increase of the multiple deviation well in relation to vertical wells; this can be explained due to the fact that the external resistances to flow are much higher in this case than the internal resistances.

The maximum value of ϕ is 2.45. It must be observed that, in practice, the various horizontal holes have length of 250 meters and more.

The given lengths of holes in Table 8 are taken as examples of values occurring most frequently in industrial practice.

It can also be stated that the maximum value ϕ equal 2.45 has been obtained by a total drilling or headway within the productive formation of 360 meters, and for a thickness of the formation of 30 meters. A 12-fold increase in the lengths of holes thus equals a flow increase of only 2.45 times, and that only when the draining contour is close at hand.

On a certain number of work-sites, with similar length, the flow of multiple deviation wells has been increased tenfold and more in relation to the flow of vertical wells. This can be explained by the large heterogeneity or the high degree of fracturing of the reservoirs. A homogeneous formation has been taken for the calculations.

It can be seen on Table 8 that ϕ is higher than 2 only when the distance of the first row to the draining contour is small, when the length of the holes is considerable and their number is high. This may lead to the impression that multiple deviation wells are efficient only when all these conditions are met. This is not the case, however.

With constant differences in pressure, the same increase in oil production can be obtained by increasing considerably the number of vertical wells. Let us therefore, evaluate the additional amount of vertical wells making it possible to attain the same oil production increase as with multiple deviation wells. Let us consider magnitudes

$\phi = Q_{mdw}/Q_v$ and $\psi = Nv/N_{mdw}$ and in the case where $2\bar{\sigma} = 2\sigma/h = 20$ and $\frac{1}{r_c} = \frac{h}{r} = 300$ (in a specific case it can be the following values: h = 30m, 2σ = 600 m; r_c = 0.1 m). Here N_{mdw} and Nv are the number of multiple deviation wells and vertical wells required to give same production. The calculation sequence shall be given below. Results are shown in Table 9.

TABLE 9

	n				Remarks
	1	2	3	4	
$\psi = \frac{N_v}{N_{mdw}}$	1.97	2.52	3.06	3.23	Does not depend on $\bar{L}_1$
ϕ_1	1.70	2.20	2.35	2.45	$\bar{L}_1 = 10$
ϕ_2	1.17	1.24	1.25	1.27	$\bar{L}_1 = 66.7$
ϕ_3	1.05	1.06	1.07	1.075	$\bar{L}_1 = 265$

It can be seen in Table 9 that comparison of ψ is difficult because of the variation in ϕ and $\bar{L}$. It may be noted, however, that coefficient ψ is in all cases is more than ϕ. Thus, with a 3-deviation well, an oil production increase equal to 7% for $\bar{L}_1 = 265$ corresponding to an increase in the number of vertical wells of 3.06 times, whereas when $\bar{L}_1 = 10$, the flow can be increased 2.35 times by increasing by the same coefficient the number of vertical wells.

When $\bar{L}_1 = 66.7$, an increase from 1 to 4 in the number of holes in the cluster shall entail a flow increase of 1.085 times. And in this case, the amount of vertical wells necessary to ensure a similar flow increase is incremented to 1.64.

Similar calculations have been effected for a 2-row system. It has been shown that the flow of the second row of clusters is in all cases lower than that of the second row of vertical wells, and that it decreases when an n and Σ increase. If the flow ratio of the first row to the flow of the second row is equal to 1.61 for vertical wells, it is always higher for clusters of wells, ranging from 1.82 to 5.56. Therefore, the first row of well clusters has a definite barrier effect, which in the above mentioned conditions markedly reduces the flow of the second row.

Determination of The Needed Amount of Well Clusters
For a Given Level of Oil Production.

This amounts to determining the number of well clusters necessary to obtain the same flow as a given number of vertical wells. Such a comparison is more obvious, simpler and more convincing. It appears from the preceding that the flow of well clusters depends to a large extent on the distance to the draining contour. The smaller this distance, the greater the flow increase of the wells, and the more difficult it is to show their efficiency. By taking an identical level of oil production, with otherwise equal conditions, we shall make the comparison based on the amount of wells or on the ratio of the necessary number of vertical wells to the number of multiple deviation wells.

We shall first show that this ratio does not depend on the distance of the first row of wells to the draining contour.

For a straight line row of vertical wells of s lengths, one may write:

$$Q = \frac{2 \frac{kh}{\mu} (P_k - P_c)}{L + \frac{\sigma_v}{\pi} \text{Log} \frac{\sigma_v}{\pi r_c}} \qquad (2.4)$$

the corresponding formula for horizontal and multiple deviation wells is in the form of:

$$Q = \frac{2 \frac{kh}{\pi} (p_k - p_c)}{L + \frac{\sigma}{\pi} \operatorname{Log} \frac{\sigma}{\pi r_e'}} \tag{2.5}$$

where Log r_e' is determined by equation (2.1).

It can be observed that the results of Equation (2.4) and (2.5) shall be equal when their denominators are equal. By substituting magnitude r_e', we draw from equation (2.1) the following equivalents:

$$\bar{\sigma}_v \operatorname{Log} \frac{\bar{\sigma}_v}{\pi \bar{r}_c} = \bar{\sigma} \ \operatorname{Log} \frac{\bar{\sigma} \ \eta(n)}{\pi \bar{\ell}} + \frac{1}{\bar{\ell} n} \operatorname{Log} \frac{1}{2\pi \bar{r}_c} \tag{2.6}$$

where

$$\bar{\sigma}_v = \frac{\sigma_v}{h} \ ; \ \bar{r}_c = \frac{r_c}{h} \ ; \ \bar{\ell} = \frac{\ell}{h} \ ; \ \sigma = \frac{\sigma}{h}$$

By transforming equation (2.6) we obtain equation (2.6), to determine the ratio $\frac{\sigma}{\sigma_v}$ or $\frac{N_v}{N}$ as follows

$$\xi = \frac{\sigma}{\sigma_v} = \frac{\operatorname{Log} \frac{\sigma_v}{\pi \ \bar{r}_c}}{\operatorname{Log} \frac{\sigma}{\sigma_v} + \operatorname{Log} \frac{\bar{\sigma}_v \eta(n)}{\pi \bar{\ell}} + \frac{1}{\bar{\ell} n} \operatorname{Log} \frac{1}{2\pi \ \bar{r}_c}} \tag{2.7}$$

where n is the number of wells in the cluster and $\eta(n)$ is determined from Table 4.

We show in Table 10 and Figure 67 the results of computations for 4 cases which distinguish the main types of reservoirs.

TABLE 10

Number of Different Reservoirs

	I				II			
	n							
	1	2	3	4	1	2	3	4
1	1.05	1.42	1.54	1.63	1.07	2.06	2.60	3.14
2	1.42	1.82	1.93	2.00	2.06	3.95	4.80	5.44
3	1.65	2.08	2.20	2.25	3.00	5.61	6.90	7.50
4	1.82	2.27	2.41	2.45	3.95	7.5	8.80	9.40
6	2.08	2.45	2.71	2.76	5.61	10.7	12.1	13.6
8	2.27	2.83	2.95	3.02	7.5	14.1	15.6	17.6
12	2.45	--	--	--	10.7	--	--	--

Number of Different Reservoirs

	III				IV			
	n							
	1	2	3	4	1	2	3	4
1	1.05	1.70	2.04	2.30	1.055	1.62	1.88	2.05
2	1.70	2.61	3.00	3.23	1.62	2.34	2.61	2.78
3	2.17	3.32	3.72	3.98	2.02	2.86	3.13	3.30
4	2.61	3.91	4.34	4.61	2.34	3.29	3.55	3.74
6	3.37	4.95	5.42	5.74	2.86	3.99	4.26	4.47
8	3.91	5.91	6.40	6.70	3.28	4.58	4.89	5.10
12	4.90	--	--	--	3.99	--	--	--

I. $\frac{h}{r_c} = 100$; $2\ \bar{\sigma}_v = \frac{2\ \sigma_v}{h} = 100.$

Specific case: $h = 10$ m, $2\ \sigma = 1000$ m; $r_c = 0.1$ m.

These values are typical of Tatarian oil deposits.

II. $\frac{h}{r_c} = 1000$; $2\ \bar{\sigma}_v = \frac{2\ \sigma_v}{h} = 2.$

Specific case: $h = 150$ m, $2\ \sigma = 300$ m; $r_c = 0.15$ m.

These values are typical of reservoirs of the Ishimbaev (Bashkiria).

III. $\frac{h}{r_c} = 500$; $2\ \bar{\sigma}_v = \frac{2\ \sigma_v}{h} = 10.$

In particular: $h = 50$ m, $2\ \sigma = 500$ m; $r_c = 0.1$ m.

Certain deposits of reservoirs of the Kujbyshev area have characteristics that are close to these data.

IV. $\frac{h}{r_c} = 400$; $2\ \bar{\sigma}_v = 20.$

In particular: $h = 30$ m, $2\ \sigma = 600$ m; $r_c = 0.075$ m.

This case can be considered as characteristic of numerous oil deposits of the Ural-Volga Province, developed by using small diameter wells.

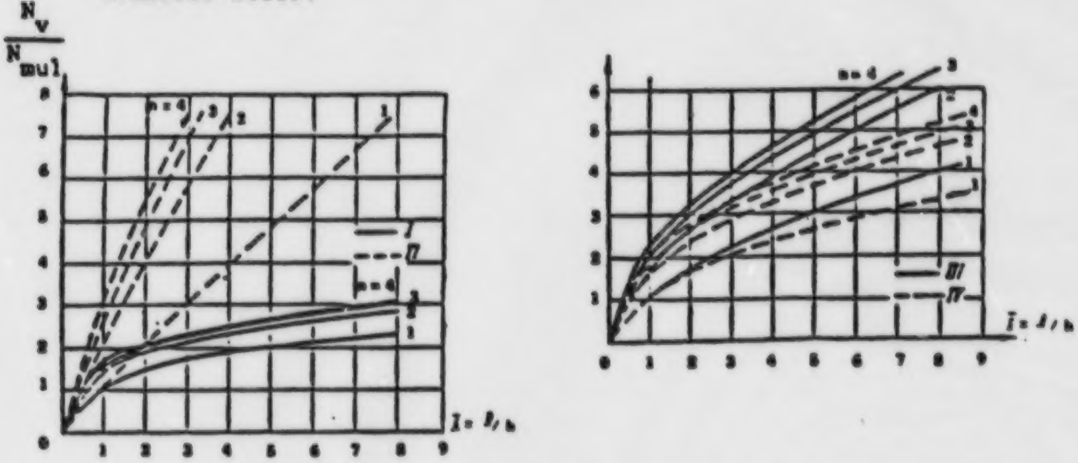

Fig. 67 - Relationship between $\frac{N_v}{N_{mdw}}$ and $\bar{I}$, n, $\bar{r}_c$, 2 σ, for equal values of cumulative production.

I $\frac{1}{\bar{r}_c} = \frac{h}{r_c} = 100$; $2\bar{\sigma}_v = \frac{2\sigma_v}{h} = 100$;

II $\frac{1}{\bar{r}_c} = \frac{h}{r_c} = 1000$; $2\bar{\sigma}_v = \frac{2\sigma_v}{h} = 2$;

III $\frac{1}{\bar{r}_c} = \frac{h}{r_c} = 500$; $2\bar{\sigma}_v = \frac{2\sigma_v}{h} = 10$;

IV $\frac{1}{\bar{r}_c} = \frac{h}{r_c} = 400$; $2\bar{\sigma}_v = \frac{2\sigma_v}{h} = 20$;

For the reservoirs of type I, the maximum value of N_v/N_{mdw} is about 3 when $n = 4$ and $\bar{l} = 8$. This corresponds to hole lengths equal to 80 meters for $h = 10$ meter. Holes of this length in formations of similar thickness have been recorded many times in a certain number of deposits. The fact that the number of wells is reduced by 3 times while the cost increase of multiple deviation wells is 1.5 to 2 times, shows the efficiency of the latter.

It should also be noted that when $h = 10$ meters and the lengths of the holes are equal to 120 meters, 2.45 times less horizontal wells are needed. Therefore, expenses are also reduced by 2.45 times for drilling and casing off vertical holes (the top of the producing bed).

The comparison made with equal values of n and $\bar{l}$ shows that the ψ coefficient increases as function of $\bar{l}$ without being directly proportional. The 12 fold increase in length only involved an increase of 2.23 times the value of ψ.

An increase from 1 to 4 of the number of holes for $\bar{l} = 3$, entails an increase of 1.36 times ψ.

It can be observed that, when $\bar{l}$ increases from 1 to 8, this ratio decreases from 1.55 to 1.33. In other words, the effect of the increase in the number of holes in the cluster is greater when the lengths are small and smaller when the lengths are greater.

When increasing the number of holes from 1 to 4, the ψ coefficient increases from 1.05 to 1.63, and when the non-dimensional length increases from 1 to 3, ψ increases from 1.05 to 1.65. It can be concluded, therefore, that a horizontal well of $\bar{L} = 3$ lengths is more efficient than multideviation horizontal wells with 4 holes of $\bar{L} = 1$. Taking into account the fact that drilling a branched well is more complex than that of a horizontal well, and taking into account also the difficulty of positioning the tool in each one of the holes when it is necessary during production, it can be stated that, for a given length of drilling within the productive formation, horizontal wells shall be more efficient.

The reservoirs of the second type are distinguished by high ψ coefficients for identical values of $\bar{L}$ and n in relation to those of the first case. The four hole well with each one having a non-dimensional length equal to 8, replaces 17 vertical wells with regard to flow. And when the length of the horizontal well is increased, its flow is incremented by 10 times. Nevetheless, for the specific case mentioned ($h = 150$ meters; $2\sigma = 300$ meters; $r_c = 0.15$) we have, in practice, $\bar{L}$ is equal to 3-4 maximum, but even with such length the ψ coefficient increases up to 7.5 to 9.5. For a horizontal well of $\bar{L} = 4$ lengths, the ψ coefficient is 1.26 times higher than was a 4 deviation well ($\bar{L} = 1$) for the same penetration length in the productive portion of the formation. This confirms once more the observation made above with regard to the greater efficiency of the horizontal well for the same total penetration of the reservoir. The computations indicate that multiple deviation wells can have a greater efficiency in the deposits developed by a dense network of wells.

The reservoirs of the second type are distinguished by a considerable thickness of the productive beds. For such formations, it will be efficient in many cases to drill multiple deviation wells (Paragraph 7 of Chapter III).

The deposits of the third and fourth type had intermediate features between the first and second type. The reservoirs of the third type have greater thicknesses and smaller distances between wells. In these conditions, the maximum number of multiple deviation wells capable of guaranteeing the same flow as a given number of vertical wells is being reduced from 5 to 7 times. A horizontal well of $\mathcal{L}$ = 8 lengths (for the fourth type) can, under the conditions stated, replace from 4 to 5 vertical wells.

It is interesting to effect a similar comparison for multiple deviation wells and vertical wells of regular and smaller diameter, under otherwise equal conditions. Table 11 shows the value of the coefficients calculated by using formula (8.7), for the following cases:

I. $h = 30$ m, $2\sigma = 600$ m; $r_c = 0{,}075$.

II. $h = 30$ m, $2\sigma = 600$ m; $r_c = 0.1$.

TABLE 11

Number of Variables	n			
	1	2	3	4
I	2.02	2.986	3.13	3.30
II	1.97	2.52	3.06	3.23

It is clear that multiple deviation wells of small diameter replace, for identical total flows, a larger number of vertical wells of small diameter than corresponding wells of large diameter. In the example given, this increment is small. With a number of deviations in the cluster equal to 3 or 4, this increase is on the order of 2%.

Calculations have shown that the value of the ratio of the number of vertical injection wells to the number of multiple deviation injection wells able to ensure an identical total injection flow, can likewise be calculated by formula (2.7). Table 10 shall be universal to a certain extent. In all cases, the use of multiple deviation horizontal wells as injector wells will make possible an important decrease (particularly for the reservoirs of the second type) in the number of wells while at the same time preserving an identical total flow of water injection in the formation.

Utilization of horizontal and double wells with deviation holes parallel to the contour of the productive area must ensure a regular displacement of the water - oil interface, if completion has been well done and if the reservoir is sufficiently homogenous.

All the conclusions drawn for a linear reservoir remain valid for a circular deposit.

III. EVALUATION OF THE ECONOMIC EFFICIENCY OF MULTIPLE AND HORIZONTAL WELLS

The evaluation of the economic efficiency of the new techniques and drilling methods of productive beds presupposes that the technical -

economical advantages of the new drilling method have been determined to be superior to the existing methods of well drilling.

The economic efficiency of the new high yield drilling method of productive beds involving the use of multiple deviation wells, can be calculated by comparing the technical - economic variables of this drilling method with the respective variables of vertical drilling.

The specific investments per ton of oil produced and the cost price of producing a ton of oil can be taken as variables to characterize the efficiency of multiple deviation wells for the development and production of oil reservoirs.

The main advantage of developing oil fields with the aid of multiple deviation wells is the possibility of obtaining a given level of oil production with a smaller number of wells of this type as would be the case with vertical wells, due to the fact that they provide a more extended flow surface. The utilization of multiple deviation -horizontal wells as injector wells make it possible to reduce their number considerably in relation to vertical wells, while at the same time, preserving the same flow of water injection in the formation. Let us study with a conventional example the economic efficiency of multiple deviation producing wells.

In a reservoir of the Kujbyshev area type, and for an annual production of 850,000 tons of oil, it is necessary to drill 50 producing vertical wells.

The amount of horizontal and multiple deviation wells necessary to achieve this production of 850,000 tons has been calculated with the above mentioned formulas, tables and charts.

The economic efficiency of horizontal and multiple deviation wells to develop an oilfield, in relation to vertical wells, is evaluated as stated above, by comparing the specific investments per ton of oil produced in one year, and the production costs of a ton of oil.

The total volume of investment necessary to develop the conventional oilfield is determined by drilling and fitting up expenses of the wells. The cost of multiple deviation wells is calculated based on the data obtained by drilling test wells in different regions.

Table 12 indicates the volume of investments needed to develop an ordinary field, by using both vertical wells and multiple deviation wells.

The results of Table 12 show that the cost of multiple deviation wells is much higher than that of vertical wells (on Figure 68, the cost of a vertical well is shown by an asterisk). And the cost of the wells increases as the number of deviation holes and their length increases (refer to Figure 68). If one takes into consideration the compared flow of multiple deviation wells and that of vertical wells, it has been found that this flow increases with the number of holes (Figure 69).

TABLE 12

Description of indices	Vertical wells	Horizontal wells			Double wells			Triple wells			4-deviation wells		
		Length of holes, m											
		150	200	250	150	200	250	150	200	250	150	200	250
Number of wells	50	22	18	17	15	12	11	14	11	10	13	10	9
Cost of drilling a well, thousands of roubles	23.5	35	36.5	38	42	45	48	49	53.5	58	58	62	68
Cost of drilling all wells, thousands of roubles	1175	770	657	646	630	540	528	686	588.5	580	728	620	612
Oil production per well and per year, thousands of tons	17.0	38.6	47.2	50	57	71	77	61	77	85	65	85	94
Total oil production, thousands of tons	850	850	850	850	850	850	850	850	850	850	850	850	850
Cost of equipment for a well, thousands of roubles	15.0	18	19	19	20	21	22	20	22	23	21	23	23
Cost of equipment for all wells, thousands of roubles	750	396	342	323	300	252	242	280	242	230	273	230	207
Specific investments per ton of oil produced, thousands of roubles	1925	1166	999	969	930	792	770	966	830.5	810	1001	850	829
Investment savings due to use of horizontal and multiple-deviation wells, thousands of roubles	2.27	1.37	1.17	1.14	1.1	0.93	0.91	1.14	0.98	0.95	1.18	1.0	0.9
Total investments, thousands of roubles	--	759	926	956	995	1133	1155	959	1094	1115	924	1075	1096

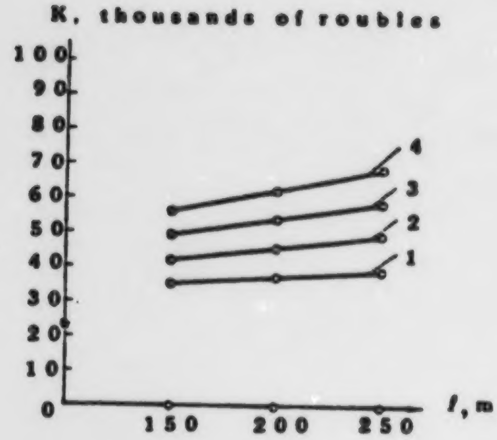

Fig. 68 Relationship between well cost k, number of wells n and well length ℓ.

1. horizontal well;
2. two wells
3. three wells;
4. four wells

If one compares the evolution dynamics of the cost of wells with those of flow increases, it is clear that the flow of wells increases in a more intensive manner than their cost. This is why, in spite of the fact that drilling cost of horizontal and multiple deviation wells is higher than that of vertical wells, the specific investments per ton of oil produced are much smaller with horizontal and multiple deviation wells.

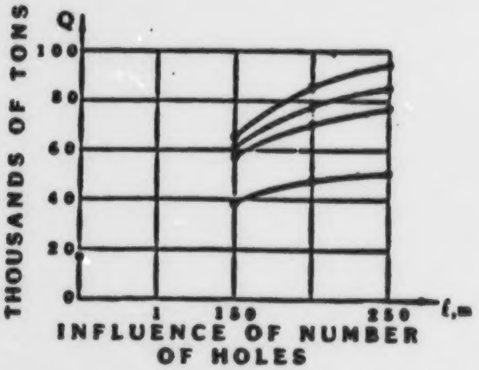

Fig. 69 Relationship between Q, the oil production per well per year, number of holes n and length of each hole.

1. horizontal well;
2. two wells
3. three wells;
4. four wells

as shown in Figure 68.

The smallest investment needed is for drilling 2-hole wells measuring 250 meters in length. The investment saving achieved by drilling double wells and holes of 250 meters in lengths, instead of vertical wells, amounts to $1155 billion Rubles (1,925,000 Rubles - 770,000 Rubles).

The most important index of economical efficiency of multiple deviation wells, aside from specific investments, is the production cost of a ton of oil.

Table 13 indicates the production cost of a ton of oil in a conventional field developed, either by vertical wells, or by multiple deviation wells. The production cost of the oil has been determined in accordance with the rules utilized for petroleum deposit development and production projects in (4).

TABLE 13

WELL CATEGORIES	Length of horizontal holes, m 0	150	200	250
	Cost, roubles-kopecks			
Vertical	1-52	--	--	--
Horizontal	--	1-20	1-23	1-18
Double	--	1-18	1-14	1-14
Triple	--	1-18	1-14	1-14
With 4 deviations	--	1-18	1-14	1-14

Based on the results shown at Table 13, it appears that the lowest cost for a ton of oil corresponds to wells with 2, 3 and 4 deviations of 200 and 250 meters in length. This proves the efficiency of the multiple deviation wells. This is why, for example, production costs saving for a conventional oil deposit, developed by triple wells and producing 850,000 tons of oil per year, amounts to 32,000 Rubles per year.

IV. COMPLETION OF MULTIPLE DEVIATION WELLS.

Completion of Producing Wells.

The aim of well completion is to clean the surface at the bottom of the well and of the channels through which fluid flow occurs, and to create the best conditions for the oil flow in the well over the entire cleared flow surface. It is well known that in well completions the final step consists of removing drilling mud from these wells to promote oil flow from the formation.

Completion of multiple deviation wells is of capital importance because the size of the holes inside the productive bed is important. As stated above, drilling formations with multiple deviations is used in a certain number of deposits of Bashkiria. Completion, however, has not been given special attention in any of them.

If one analyzes the balance sheet of the time spent in completion of multiple deviation wells, it appears that less than one-quarter of the time has been spent in productive work. The rest of the time has been divided between various idle times (absence of surface equipment, drilling cable, wenches, due to single team and testing work, etc.).

The special characteristics of this type of well are often overlooked at the time of completion of multiple deviation wells. Due to the fact that drilling of the productive bed is done by multiple deviations with ordinary drilling mud injection, cleaning all the holes up to the stage of clear water is an indispensable condition of completion. In order to facilitate completion and development, the auxiliary holes must be started as deep as possible. The practice of developing multiple deviation wells shows that the holes in which drilling mud has been left in, do not contribute to oil production after starting the operations.

In low pressure deposits, the drilling mud which remains in the holes partially infiltrates the formation and creates impermeable plugs at the bottom of the wells. Productivity of the well diminishes. The remaining drilling mud promotes, in certain holes, plugging of the deep well pump. The completion of a multiple deviation well must proceed in the following manner:

Washing all deviations with water in order to eliminate mud, mudcake and drill cuttings.

In case of direct washing, there is sometimes a spillage of mud in the already washed holes. This is why, after having washed the main well, the complementary holes must be washed in reverse circulation. It is desirable to use oil-based mud with surfactants.

After drilling the first multiple deviation wells, it has been established that at the time of initiating a new hole no plugs have formed in the preceding holes, and that in most cases, it is not necessary to wash again the holes. In a place where the production string has been lowered after drilling all the deviations, a prior careful cleaning is necessary. It has also been established that if one carries out a water cleaning after having lowered the oil string, no considerable overflow of mud occurs in the already cleaned holes. No complications have been noticed either by washing the sites of deviations, where the well dimensions have been notably increased. If one uses reverse circulation, probability of drilling mud overflows in the already washed holes becomes minimal.

II. ACID WASHING OF MULTIPLE DEVIATION WELLS.

It is carried out by the usual method. The amount of acid is calculated by taking into account the length of the holes inside the productive formation.

III. HYDRAULIC FRACTURING OF A FORMATION.

For ordinary vertical wells, hydraulic fracturing of the reservoir is an important factor of completion. It can be assumed that in multiple deviation wells also, it proves to be a useful measure, because in this case all the holes (or a part of them) are connected to each other.

It is in Well 617 of the Jablonovskoe field that for the first time, in January 1958, hydraulic fracturing of the formation has been carried out with hydrochloric acid. The lengths of the hole inside the formation was 145 meters. Approximately 200 cubic meters of hydrochloric acid were used as fracturing fluid. Fracturing has caused the flow to increase from 7 to 40 tons a day and has kept it stable for an extended period of time.

COMPLETION OF HORIZONTAL INJECTOR WELLS.

We have stated at the beginning of this chapter that it was possible to utilize successfully horizontal wells in place of vertical wells in order to inject the displacement fluid in the formation. In this manner, a more regular displacement of the water front (or of a gas front) can be ensured. The amount of injector wells for a total given volume of injection is thereby reduced.

Up to now there have been no horizontal injection well completion tests, because there was no drilling carried out for this purpose, neither in the USSR nor abroad. It is only possible to give some directions and to make use of the experience of vertical injection well completion.

As it was mentioned in another book (3), three completion methods of peripheral wells are presently utilized in Tataria:

1. Drilling the formations;
2. Temporary increase of pressure at the wellhead;
3. Hydraulic fracturing of the formation.

Good results have been obtained in a certain number of wells in Tataria by using electrical bottomhole pumps. If for some reason, lowering pump downhole should be impossible, well can be cleaned by swabbing.

In order to temporarily increase pressure at the injection wellhead, the method applied in Tataria can be utilized. The electrical bottomhole pump is placed horizontally immediately next to the well, a branch circuit of the main water pipe is connected to the inlet of the pump, and the discharge is connected on the wellhead. On the work sites of Romashkino and Minnibaev pressure has thus been increased from 30-35 to 100-110 kgf/cm^2.

Just a few words with regard to hydraulic fracturing of the formation. Until now there is practically no experience in the use of hydraulic fracturing of the formation in horizontal wells. It could be interesting to try directional hydraulic fracturing. Creation of cracks in a selected spot would make it possible to increase the productivity of the wells and to solve certain impermeable zone problems.

For completion of central horizontal injection wells, the methods applied in vertical wells could be utilized:

1. Maximum samplings of oil;
2. Reverse circulation of hot petroleum;
3. Injection of ordinary water with the highest possible startup pressure.

V. SOME SPECIAL FEATURES OF PRODUCTION AND OVERHAUL OF MUTLIPLE DEVIATION WELLS.

Development and production of multiple deviation wells, drilled in a formation where pressure ensures spontaneous flow does not at all differ from that of vertical wells.

But the production period by its spontaneous flow is followed, in general, by a production period using bottomhole pumping. Moreover, most of the multiple deviation wells presently drilled belong to older, low-pressure reservoirs intended for secondary recovery. Their development and production was achieved by using bottomhole pumps with rods.

When drilling multiple deviation wells it is always possible to drill holes with a slight deviation angle down to the determined depth to which the pump is lowered. This does not create new problems with regard to operating conditions of bottomhole pumps.

In order to extend to the maximum the active life of the additional holes, they must be deviated with the maximum possible intensity in keeping with the decreasing pressure of the reservoir.

The given possibility of suddenly deviating the holes with small curve radiuses makes it possible to keep up oil flow in the main well when reservoir pressures are reduced, which in turn, makes it possible to utilize to the maximum the simplest pumps with pipes or rods.

Oil production is considerably increased by maintaining the reservoir pressure up to the levels ensuring the passage of oil from the additional holes into the main well.

The conditions of use of bottomhole pumps and the useful life of the equipment in deviated wells have not been sufficiently studied.

The present report does not have this objective. Let us only mention that V.F. Troickij and A.N. Anodin (1) have studied the bottomhole equipment in deviated wells of the oil worksite called "26 Commissars of Bakou". They have reached the following conclusions:

1. Under identical geological and mineralogic conditions, the service life of tubing and bracket of rods is 2 to 4 times shorter in deviated wells than in vertical wells.

2. The operating period between maintenance and repair work in deviated wells is 1.2 to 2 times shorter depending on curvature (deviation of the hole) than in work vertical wells.

3. Power consumption is from 20 to 25% higher. Coefficient of utilization of the underground portion of the pumping facility is lower.

All of this shows that the main hole of the multiple deviation well must be as close as possible to the vertical, at least until reaching the depths of a bottomhole pump.

In cases where the main hole has a slight slanting angle, it is possible to reduce wear of pump rods, tubing and production string by using protective sleeves made of textolite, semitextolite or laminated wood. Such devices increase, no doubt, production costs. They are rather widely used in the Republic of Romania (5).

In exceptional cases where it is indispensable to position the pump in a part of the hole where the deviation angles are higher than 40 - 50 degree, pumps without pipes or rods must be used.

For production of the multiple deviation wells of the "Chernomorneftj" oilfield, considerable volumes of viscous oil had to be pumped.

The oil of the Miocene reservoirs is heavy (specific weight 0.950-0.980), resinous, non-paraffinic, very viscous; this had a bearing on the choice of bottomhole pumping equipment. For the production string, a tubing of 5 inches has been used in which a NGN-2 pump with a 95 millimeter barrel diameter has been lowered. Due to the high oil viscosity, the volumetric yield of the pump was low at first. This defect has been eliminated by the increase in the flow area of the inlet valve and elimination of the second discharge valve of the pump. In addition they also employed backflow of reservoir water or light oil in the annular space of the well.

Experience with maintenance and repair work of multiple deviation wells is still at an early stage. At the petroleum site of Ishinbajneftj, after extended production, a well workover has been attempted in Yard 64/65. Tests have shown that it was entirely possible to reach the well, without error in any deviated hole.

After lowering the production string in Well 154 of the Gorodeckoe reservoir, there was no cement plug in Interval 613-618 meters. And the string was not lowered down to the bottom. Entrance to the horizontal hole was filled with cement. The lower part of the hole was treated with a hydrochloric acid solution and hydrofluoric acid also. Then a swabbing tool was used to clean the rock affected by acid and then an attempt was made to reach the part of the hole that was opened by drilling. These operations did not succeed in penetrating the obstructed part of the well, and it was necessary to redrill a new hole while keeping the determined azimuths.

With regard to the repair and maintenance of this type of well, the following distinctive characteristics must be considered:

1. The need to install on the well in the process of maintenance a mobile light unit with equipment to direct the pipes.

2. The limited possibilities of using bailers and other tools that can be lowered by cable.

3. The limited possibilities of drilling compact plugs by rotary process and the need to use small size turbo drills.

Maintenance of an adequate production rate of multiple deviation wells, in accordance with rational development of the entire reservoir, requires systematic control and monitoring. This entire aspect should be carefully studied.

Besides the problems that vertical wells and multiple deviation wells have in common, it is necessary, in the latter, to measure the productivity of each hole; it is also necessary to take bottomhole samples from each hole and so on.

CONCLUSION

The main conclusions that can be drawn from the studies made are the following:

1. The multiple deviation wells make it possible to increase the flow of oil wells, the injectivity of injection wells in order to work on formations under various geological conditions. Wells of this type expand considerably the production possibilities of oil deposits with a low permeability and a very viscous oil, in which development of ordinary wells is not very profitable; they also increase considerably the profitability of reservoirs distinguished by a very irregular permeability of the rocks.

   The multiple deviation wells and the mine shafts with horizontal flow channels make it possible to increase appreciably water production of the aquifers. There is interest in using the multiple deviation wells to lower the water level when digging mine shafts, in order to carry off gas in coal mining, to accelerate prospecting operations and to reduce their cost, etc.

2. The survey we have provided of hydrodynamic studies on fluid flow toward multiple deviation wells shows that Soviet and foreign researchers have devoted to this question a large number of experimental and analytical works. Up to now, however, it has not been possible to establish simple, sufficiently accurate and convenient formulas for routine calculations to compute fluid flow to that type of wells.

Most oil deposits of the Oural-Volga region are distinguished by a wide surface area for a relatively thin oil zone and higly fractured productive formation. In addition deposits of some other areas are characterized by a high degree of stratification. Therefore, it was helpful to study the two-dimensional flow problems. Due to this fact, for a stratified formation, when vertical permeability equals zero and horizontal permeability is constant one obtains, for a constant pressure water-drive system, analytical relationships to calculate the fluid flow to isolated deviated wells, to multiple deviation double wells and to complex configuration wells in circular reservoirs and in linear deposits.

We have studied the interaction problems of well clusters (multiple deviation horizontal wells). We have shown that the interaction of clusters from a same group and of several groups of clusters can be calculated with the help of formulas pertaining to the interaction of vertical well clusters. To do this, the clusters are replaced by vertical wells located at the center of the clusters and having an equivalent radius, for whose calculation a method and respective formulas were provided.

3. We have studied the permanent flow problems of an incompressible fluid in a homogeneous formation of finite thickness, in the direction of horizontal wells, deviated, broken line, multiple deviations and multiple level wells.

The formulas thus obtained make it possible to calculate the flows and pressure differences for any plot plan of deviated well groups, horizontal, multiple deviation and multiple level groups.

The formulas to calculate flow resistances in deviated or isolated multiple deviation wells and in groups of wells of this type can be utilized in certain cases to calculate the production methods of the oil deposits producing by expansion or liberation of dissolved gases.

4. The new results of the study on fluid flow to horizontal wells draining a thin oil-bearing stratum with a lower water table, under conditions of stabilized or non-stabilized heterogeneous flow, as well as the results of the study on displacement stability of the water-oil interface, are of practical interest and must be taken into account in the respective calculations made by engineers.

5. The formulas presented in this report and the various ratios between magnitudes describing a given process make it possible to carry out hydrodynamic computations to study the projects concerning oil reservoir production systems.

6. The calculations carried out show that the flow of a multiple-deviation well, in otherwise identical conditions, is superior to that of a vertical well, and the closer the drainage contour the more applicable this is. When the length and the number of deviation holes is increased, the flow increases, but not in proportion to the increase in length and number of holes. In order to obtain same cumulative

oil production from a given field, many more vertical wells are needed than multiple deviation wells. The latter are needed all the less with greater length and a larger number of holes. It has been ascertained that horizontal injection wells are more efficient than vertical wells, because they have a greater absorption capacity than the vertical wells and can ensure a more regular displacement of the productive area contour.

7. Production experience with multiple deviation wells and calculations made show that in most cases increasing the length and the number of holes will not make it possible to multiply well flows in the same proportions. Some isolated cases can be explained by the considerable heterogeneity of the reservoirs. The main argument in favor of drilling multiple deviation wells must be the effort to create more favorable drainage conditions for the heterogeneous formations by increasing, to some extent, regular production. The more regular the drainage of all the various, separate areas of the formation, the better the conditions will be to achieve high oil production. It is possible to increase the efficiency and the economic profitability of oil production from deposits where the source rocks exhibit a great variety of facies. Production delays for a certain number of oil reservoirs can be reduced with multiple deviation wells. It is possible to utilize less dense well networks.

8. Analysis of the operation of multiple deviation wells shows that their exploitation (or production) does not involve any special complications, besides the difficulty of reaching rapidly and without error a

given hole, at will. Basically, development of multiple-deviation wells does not differ from that of vertical wells. The effect obtained by hydraulic fracturing, acid treatments and torpedoing is more important in multiple-deviation wells than in simple wells (from the point of view of absolute flow increase).

R&D 159

DEVELOPMENT OF OIL RESERVOIRS USING HORIZONTAL AND MULTIPLE DEVIATION WELLS

From: INSTITUT FRANCAIS DU PETROLE

By BORISOV (ju.P.) Moskva, "Nedra", 1964.

Translation into French by J. Combe of IFP, August, 1980

At the end of Chapter V (pp. 2851) there appears (translated here)

BIBLIOGRAPHY

1. ANODIN (A.N.), TROICKIJ (V.F.)
   Wear of deviated well equipment.
   Neftjanik, 1957, No. 12.

2. BRONZOV (A.S.), SMIRNOV (A.P.)
   Drilling deviated wells.
   Gostoptekhizdat, 1948.

3. ERONIN (V.A.), KRINARK (A.I.)
   The experience of oil well completion in Tatarian Republic (USSR)
   kazanj, Tatknigoizdat, 1959.

4. KRYLOV (A.P.) et al
   Study of petroleum reservoir development.
   Gostoptekhizdat, 1962.

5. Utilization of protective covers (or caps) in deviated wells.
   Neftjanik, 1958, No. 2.

1768 E

Alberta OIL SANDS
INFORMATION CENTRE

Alberta

UBLIC WORKS, SUPPLY & SERVICES

TRANSLATION SERVICES

403/427-9693
Telex 037-2065
Edmonton, Alberta, Canada
T5J 0K5

FRENCH-ENGLISH

(71)

ORIGINAL TRANSLATION

ALBERTA PUBLIC WORKS SUPPLY & SERVICES
CERTIFIED
Translation Service
TRUE TRANSLATION

TRANSLATED BY: MARY BOURNE
REVISED BY: ISABEL MILNE

1768 E

Alberta OIL SANDS
INFORMATION CENTRE

THEORETICAL EVALUATION OF EFFECT OF WATER CRESTING ON PRODUCTION BY HORIZONTAL WELLS [1]

361 [2]

F. Giger
Institut Français du Pétrole
1 et 4 avenue de Bois-Préau, BP311
92506 Rueil-Malmaison Cedex, France

*Water coning is a frequently-encountered phenomenon whose appearance, during production from an oil field having an oil-water contact surface near the wells, creates constraints that may be determinant concerning the rate at which the field is produced.

As part of research on motivations for horizontal drilling from the standpoint of reservoir engineering, at the same time as computer simulations using numerical models, it appeared interesting to evaluate what effect a water cresting would have and to determine the critical flow rate by an analytic method. This article takes up the hodograph method already applied to the problem by D.A. Efros. It investigates the shape of the crest when approaching the critical regime. A method is proposed for the practical solution of such problems by charts.*[1]

REVUE DE L'INSTITUT FRANÇAIS DU PÉTROLE [3]
VOL. 38, NO. 3, MAY-JUNE 1983

Translator's notes:

[1] Sections between asterisks are provided in English in the original text.

[2] Numbers shown in the margin indicate the page numbers of the original text.

[3] Approximate English equivalent: Journal of the French Petroleum Institute.

NOTATIONS

a : abscissa of point F in plane f

b : abscissa of point F in plane γ; parameter of the shape of oil/water surfaces

c_1 : constant

f : inverse of the reduced velocity

F : function of the Schwartz-Christoffel conformal transformation of γ on f

g : gravity acceleration

h : distance from the well to the peak of the water crest

H : opposite of the ordinate of point P on the oil/water surface

k : porosity of reservoir rock

k_H : horizontal porosity; k_V: vertical porosity

L : abscissa of point P on the oil/water surface

Log : Napierian logarithm

P : pressure

q' : dimensionless flow rate of the well drawing from below only

Q : flow rate per unit length of the well drawing from below only

Q_{cr} : flow rate per unit length of the well drawing from below

t, t' : (silent) variables of integration

u : reduced velocity of oil filtration

V : filtration velocity

w : reduced complex potential

x : reduced abscissa

y : reduced ordinate

z : reduced complex coordinate

Z : function of the Schwartz-Christoffel conformal transformation of γ on ζ

α : angle between the slope of the oil/water surface and the horizontal

β : maximum angle between the slope of the oil/water boundary and the horizontal

δ : auxiliary variable

Δl: distance travelled by the oil

$\Delta \rho$: difference between the densities of water and oil

ζ : auxiliary complex coordinate for which the domain of oil flow is a strip

η : ordinate of the physical plane

θ : abscissa of the auxiliary complex variable ζ [sic] [4]

χ : abscissa of the auxiliary complex coordinate [sic] [4]

μ : viscosity of the oil

ν : ordinate of the auxiliary complex variable [sic] [4]

ρ : density

Υ : auxiliary complex variable

ξ : abscissa of the physical plane

ω : ordinate of the auxiliary complex variable ζ [sic] [4]

363 INTRODUCTION

Whatever method is considered today for extracting oil from a reservoir having an oil/water or oil/gas contact near the wells, a so-called "critical flow" exists which cannot be exceeded without the rapid influx of water or gas into the drainage system. In the case of a vertical producing well, this is known as water-coning, a frequently encountered phenomenon which plays a decisive role in regard to the rate of production from the field.

According to physical theory, this phenomenon of deformation of the oil/water contact is due to the drop in pressure resulting from the dynamic flow of oil toward the drainage system. The greater the convergence of stream lines and the greater the differences in pressure, the more noticeable the effect.

For a vertical well with a radial-circular type flow as an initial approximation, substantial changes in pressure appear in the vicinity of

---

Translator's note:

[4] There appears to be some confusion between the "auxiliary complex variable" and the "auxiliary complex coordinate".

the well (represented as a single point on the horizontal plane) and cause the water to rise in the well's immediate surroundings, as explained above. The reference to the horizontal plane is justified by the fact that it extends, following the largest dimensions of the reservoir, parallel to the initial oil/water plane.

This observation enables us to expect that a horizontal well, open along its entire length and shown as a straight line segment on the horizontal plane, will result in a much more favourable flow with respect to both water influxes (insofar as the gradients are lower) and sweep efficiency (through removal of the single points representing vertical well production).

The purpose of this article is to propose an analytical solution which describes the shape of the water crest created by a horizontal well used to extract oil from a reservoir bounded by an impermeable horizontal roof and an oil/water interface. The well is located in the roof of the reservoir.

The calculations lead to an evaluation of the critical flow rate. They are presented in section III, in the form of charts for industrial use, to enable reservoir engineers to calculate the critical flow in an extremely simple manner. The first section may be omitted by the reader who is interested only in practical results.

I. CALCULATION METHOD

This article uses the hodograph method (Ref. 1, p. 300) applied to this problem by D.A. Efros (Ref. 2, pp. 31-61). A hodograph is the representation of a dynamic system in the domain of velocities; the coordinates of a point in the system are the components of its velocity vector. This method of solving problems in fluid mechanics has been applied to a similar case by R.E. Kidder (Ref. 3, p. 867 or Ref. 4, p.350).

A. Diagrams

The situation studied concerns the formation of a water crest when oil contained in the reservoir stratum is produced by an infinite well located at B in the horizontal roof (Fig. 1). An approximation of the flows is shown by a piston-type flow pattern. Capillary action is not taken into account.

The problem is such that it can be dealt with on the plane perpendicular to the well axis. It therefore involves the steady two-dimensional flow of an incompressible fluid through a porous medium. The velocity field is thus derived from a scalar potential for which the Laplace equation holds. This makes it possible to use an analytical method based on complex variable theory (Ref. 5, p. 74).

B. Equations

The equilibrium of pressures on either side of the oil/water surface is expressed by Darcy's equation (1) in order to take into account the dynamic pressure created by the oil flow, and the difference in the hydrostatic pressures in the oil and the water, resulting from the difference in their densities.(1)

$$\Delta P = -u\frac{\mu}{K}\Delta l \qquad (1)$$

$$\Delta P = -\Delta\rho g \Delta h \qquad (2)$$

364 By introducing angle α formed between a point on the oil/water surfac- and the horizontal we can express the local equation for the latter as follows:

$$V = \frac{K\Delta\rho g}{\mu}\sin\alpha \qquad (3)$$

---

(1) A geometric transformation is said to be conformal if, and only if, the angles are preserved.

On the hodograph (Fig. 2), the oil/water surface appears as a portion of a circle twice travelled by the image of moving point M.

C. Solution

The purpose of the calculations is to determine the shape of the oil/water surface; that is, the boundary of the fluid flow given in equation (3). This is done by performing a series of conformal transformations(2) that make it possible to go from an initial flow which is exactly known, particularly the boundaries, to that shown in Figure 1 which we are attempting to define.

By introducing a complex potential "w" after the variables have been made dimensionless, we can express the inverse f of the velocity using "w" on the one hand and equation (3) on the other:

$$f = \frac{dz}{dw} \qquad (4)$$

$$f = \frac{1}{\sin \alpha} \qquad (5)$$

The latter is a simplified expression of the boundary of the flow
365 under study, as shown by Figure 3, drawn in the plane of the variable f.
The image of point M, which in Figure 1 describes the oil/water boundary,
in Figure 3 describes portions of the straight line $\mathrm{Im}(z) = +i$, an image of
the portions of the circle in Figure 2 created by inverting centre E.

The initial flow chosen is that of an infinite horizontal well located at the top of a reservoir stratum containing only oil and bounded by two adjacent horizontal beds.

Figure 4 shows a reservoir cross-section perpendicular to the well axis. The stream lines which run parallel to the adjacent beds some distance from the well converge as they approach the well at B.

---

(2) A geometric transformation is said to be conformal if, and only if, the angles are preserved.

In this plane, perpendicular to the axis of the well, the flow is represented by equation (6) (Ref. 6, p. 18):

$$\frac{dw}{d\zeta} = -c_1 \cot\left(\frac{\pi i \zeta}{2}\right) \qquad (6)$$

D. Calculations

Given the symmetry in Figures 2 and 3 in relation to the vertical axis, only one side of the figures need be considered.

It is useful to introduce an intermediate variable τ defined in a quarter plane as shown in Figure 5.

Two conformal transformations from the quarter plane τ in Figure 5 to planes f and ζ shown in Figures 3 and 4 respectively will be specified. For a description of the Schwartz-Christoffel method used, the reader may consult Ref. 5, p. 108 or Ref. 7, p. 159. Composition of these transformations according to the diagram below will yield a transformation from plane ζ to plane f:

$$\begin{tikzcd} & \tau \arrow[dl, dash, "Z"'] \arrow[dr, dash, "F"] & \\ \zeta \arrow[rr, "F \circ Z^{-1}"] & & f \end{tikzcd}$$

$$Z(\tau) = i\left[\frac{\operatorname{arctg}\left[(\tau - 1)^{1/2}\right]}{\pi/2} - 1\right]$$

$$F(\tau) = -\frac{2}{\pi}\left(\frac{1}{b} - 1\right) i \operatorname{tg}\left(i\frac{\pi\zeta}{2}\right) - \zeta \qquad (8)$$

The composition of F and of the inverse of Z gives the transformation from plane ζ (Fig. 4) to plane $f =$ dz/dw (Fig. 3). Integration makes it possible to arrive at physical space and we obtain, taking into account boundary conditions:

$$z = \frac{\left(\frac{1}{b} - 1\right)\zeta + \frac{\pi}{2}\int_0^{\zeta} it \cot\left(\frac{\pi i t}{2}\right) dt}{\frac{1}{b} + \operatorname{Log} 2 - 1} \qquad (9)$$

where z is the dimensionless complex space variable of the plane perpendicular to the axis of the well in relation to which we are studying water cresting. The conformal transformation given in (9) solves the problem at the mathematical level, for it establishes a correspondence between the physical planes of a known flow (shown in Figure 4) and of the flow above the water crest, now also known.

II. RESULTS

A. Shape of the water crest

Formula (9) enables us to obtain a parametric expression of the oil/water surface which is shown in Figure 4 as the horizontal straight line passing through F.

$$x = -\frac{\left(\frac{1}{b}-1\right)\theta + \frac{\pi}{2}\int_0^\theta t' \,\mathrm{th}\left(\frac{\pi t'}{2}\right) dt'}{\frac{1}{b} + \mathrm{Log}\, 2 - 1} \qquad (10)$$

$$y = -1 - \frac{\mathrm{Log}\left[\mathrm{ch}\left(\frac{\pi}{2}\theta\right)\right]}{\frac{1}{b} + \mathrm{Log}\, 2 - 1} \qquad (11)$$

x and y are the dimensionless abscissa and the dimensionless ordinate of a moving point describing the boundary of the water crest. We will now study the shape of the crest which depends on parameter b -the abscissa of point F in plane τ , related to the value of angle β formed by the oil/water boundary and the horizontal at the point of inflexion (Ref. 8, p. 13) in Figure 1- and analyze the conclusions which may be drawn from it concerning the physics of this phenomenon.

1. Shape of the oil/water surface at its peak E

A development, limited to the vicinity of peak E, with only the first terms retained, enables us to obtain a local equation for the oil/water surface (Ref. 8, p. 21). Two cases arise, depending on the value of parameter b, for which the scope of variation is [0, 1]:

- where b ≠ 1:

$$y = \frac{\pi^2}{8} \frac{\frac{1}{b} + \mathrm{Log}\,2 - 1}{\left(\frac{1}{b} - 1\right)^2} x^2 - 1 \qquad (12)$$

These values of b correspond to values of angle β in Figure 1 which are strictly less than 90°.

The oil/water surface allows a horizontal tangent at point E and locally has the shape of a parabola (Fig. 6).

- where b = 1:

$$(y + 1)^3 = -\frac{9\pi^2}{8\,\mathrm{Log}\,2} x^2 \qquad (13)$$

In this case, angle β has reached 90°. Points D and F from Figure 1 have come together with point E.

The oil-water boundary line has a cusp at E with a vertical tangent (Fig. 7).

367 The latter figure illustrates the phenomenon of instability which leads to the influx of water when the critical flow rate is reached.

2. Shape of the oil/water surface some distance from the well

An adequate development in series (Ref. 8, p. 27), using only the first terms, gives an expression for x which is exact to within 10^{-3} degrees of relative error where $y < -8$:

$$x = \frac{-\left[y\left(\frac{1}{b} + \mathrm{Log}\,2 - 1\right)\right]^2 + \left(\frac{1}{b} - 1\right)^2 + \frac{\pi^2}{6}}{\left(\frac{1}{b} + \mathrm{Log}\,2 - 1\right)\pi} \qquad (14)$$

Equation (14) defines a half-parabola with a horizontal axis. It enables us to calculate the distance "h" from the peak of the water crest to the top of the stratum when we know, on the one hand, the coordinates L and H of any point "P" on the oil/water surface that is relatively far from the well, and, on the other hand, the type of flow defined by the single parameter "b":

$$h = \left(\frac{1}{b} - 1 + \mathrm{Log}\,2\right) H\,\delta\left(b, \frac{L}{H}\right) \qquad (15)$$

where:

$$\delta\left(b, \frac{L}{H}\right) = \frac{1}{\left(\frac{1}{b} - 1\right)^2 + \frac{\pi^2}{6}}$$

$$\left[\left(\frac{\pi^2}{6} + \left(\frac{1}{b} - 1\right)^2 + \frac{\pi^2}{4}\frac{L^2}{H^2}\right)^{1/2} - \frac{\pi}{2}\frac{L}{H}\right] \qquad (16)$$

We note, from expressions (15) and (16), that the family of curves representing the oil/water surfaces passing through a point P which is far from the well, in fact depends only on parameter b. These curves are shown in Figure 8. They have been moved upward so that all pass through the point defined by the coordinates (0, -1).

B. Produced rate

The production rate per unit length is expressed as follows:

$$Q = \frac{k \Delta\rho g}{\mu} H q' \qquad (17)$$

where the dimensionless flow rate "q'" is:

$$q' = \pi\,\delta\left(b, \frac{L}{H}\right) \qquad (18)$$

This dimensionless flow rate has been shown on the chart in Figure 9. Each curve has been drawn for a given value of the ratio H/L. If we wish to study a problem when the ratio H/L does not correspond to any of the proposed curves, it will suffice to draw the necessary curve between the two nearest curves by linear interpolation. The values of the H/L ratio which are greater than 1 have not been drawn on a curve as they are too large to correspond to present industrial needs. By referring to Figure 8 we can determine the shape of the oil/water boundary using the values of b.

Each curve in Figure 9 allows for a horizontal asymptote. Its ordinate gives the dimensionless critical flow rate. The very flat shape of the curves on the right side of the figure shows, using Figure 8, that a very slight variation in the production rate as it approaches the critical flow rate will bring about a major change in the shape of the oil/water boundary. This clearly illustrates the instability of the oil/water boundary.

As we have seen in subsection II.A.1, the critical flow rate per unit length is obtained where b = 1. Once L is large in relation to H, we have:

$$Q_{cr} = \frac{k \Delta \rho g}{\mu} \frac{H^2}{L} \left[1 - \frac{1}{6} \left(\frac{H}{L} \right)^2 \right] \qquad (19)$$

(where b = 1)

If we wish to use this formula with practical units, the multiplier 0.837×10^{-3} must be introduced into the right-hand term.

This critical flow rate per unit length depends only on the position of point P and the physical characteristics of the rock, water and oil. In practice, point P may be the oil/water contact in an observation well. Its position may also be determined hypothetically using a lateral feed mechanism diagrammed on a reservoir boundary.

III. SOLUTION USING CHARTS FOR INDUSTRIAL APPLICATIONS

A. Determination of the critical flow rate when the coordinates of a point P situated on the oil/water boundary are known.

The chart in Figure 9 provides the dimensionless critical flow rate q' for b = 1 on each curve drawn for a value of the ratio H/L. If necessary, linear interpolation must be used between two curves. The critical flow rate per unit length Q_{cr} is obtained by using equation (17) and multiplying q' by the term $\frac{K \Delta \rho g H}{\mu}$.

Let us consider the following example:

$H = 30\text{m}$
$L = 100\text{m}$
$k_V = k_H$ 100mD
$\Delta \rho = 0.1$ kg/litre
$\mu = 50$ cP
$g = 9.81$ N/kg

Multiplier in practical units: 0.837×10^{-3}

$$\frac{H}{L} = \frac{30}{100} = 0.3$$

(369 In Figure 9, where b = 1, the curve $\frac{H}{L} = 0.3$ yields: $q' = 0.294$

$$Q_{cr} = 0.837 \times 10^{-3} \times 0.294 \times \frac{100 \times 0.1 \times 9.81 \times 30}{50}$$
$$= 1.5 \times 10^{-2} \text{ m}^3/\text{day/m}$$

The same method enables us to choose the boundary shape we wish to obtain (using Figure 8) and to transfer the value of b to Figure 9 in order to determine the corresponding flow rates, dimensionless and per unit length.

B. Determining the extent of the zone in which the water level changes as a result of production by the well.

We know the initial height H of the oil zone, the distance h from the peak of the water crest to the top of the reservoir, and the flow rate per unit length Q produced by the well. It is necessary to determine the shape of the oil/water boundary and the lateral extent L of the zone where the boundary has been raised from its initial position.

Firstly, it is necessary to calculate the dimensionless flow rate q' by dividing the flow rate per unit length Q by the term $\frac{K\Delta\rho gH}{\mu}$ and to transfer it as an ordinate, drawing a horizontal line on the chart in Figure 9. Secondly, the factor $\frac{h}{Hq'}$ is to be calculated (by dividing the ratio $\frac{h}{H}$ by the dimensionless flow rate q') and the result transferred as an ordinate on to the curve shown in Figure 10. The value of b is given as the abscissa, which enables the shape of the oil/water boundary to be determined using Figure 8. By transferring this value of b as the abscissa to the horizontal straight line previously drawn on the chart in Figure 9, point N is obtained, making it possible to determine the value of the ratio H/L by interpolation. The extent L, which we wish to determine, is obtained by dividing H by the ratio H/L.

Let us consider the following example:

$H = 61\text{m}$
$h = 28\text{m}$
$Q = 2 \times 10^{-2}\ \text{m}^3/\text{day/m}$
$k = 200\text{mD}$
$\Delta\rho = 0.1$ kg/litre
$\mu = 100$ cP
$g = 9.81$ N/kg

Multiplier in practical units: 0.837×10^{-3}

$$q' = 2{,}10^{-3} / \left(\frac{0{,}837 \times 10^{-3} \times 200 \times 0{,}1 \times 9{,}81 \times 61}{100}\right) = 0{,}20$$

$$\frac{h}{Hq'} = \frac{28}{61 \times 0{,}20} = 2{,}3$$

Using the chart in Figure 10, with 2.3 [sic] as ordinate, we obtain:

$$b = 0.125$$

370 Taking this value into account, we obtain from Figure 8 some idea of the shape of the water crest.

By transferring the values of q' and b to the chart in Figure 9, we can locate point N and assess the value of H/L; that is:

$$H/L = 0.26$$

The lateral extent of the water crest is $L = 230$m on either side of the horizontal well.

The author wishes to thank Messrs. J. Combe of the Institut Français du Pétrole and D. Codreanu of Franlab, who provided him with a translation of the chapter of the hydraulics treatise by P.A. Efros (Ref. 2) on which this article is based, as well as M.C. Marle of the IFP for all his advice.

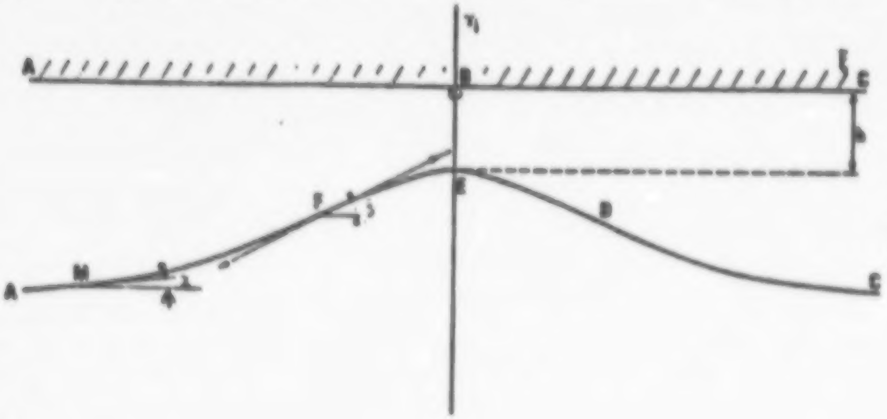
η
A
B
C
O
ξ
h
E
F
D
M
λ
A
C

Figure 1

Formation d'une arête d'eau dans le plan ξ, η vertical et perpendiculaire à l'axe du drain.

Water cresting in plane ξ, η, vertical and perpendicular to the axis of the well.

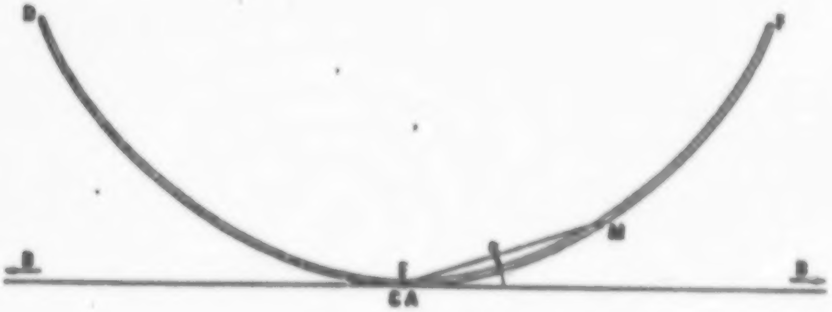

Figure 2

Hodographe, plan u.

Hodograph, plane u.

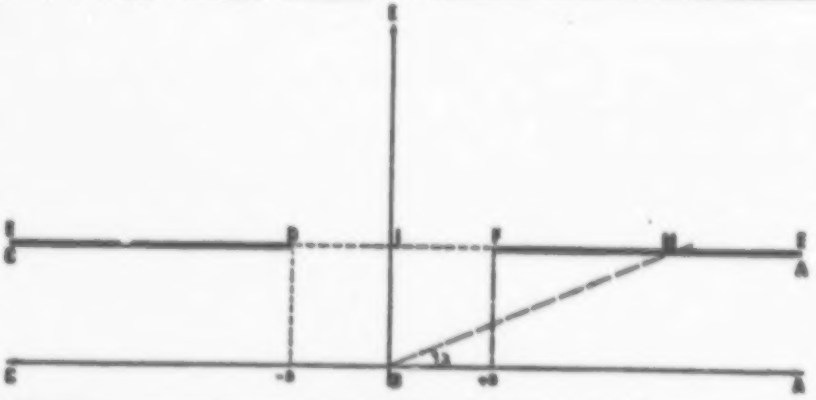
E
E
C
D
I
F
M
E
A
λ
E
-a
B
+a
A

Figure 3

Demi-plan $f = \frac{dz}{dw}$.

Semiplane $f = \frac{dz}{dw}$.

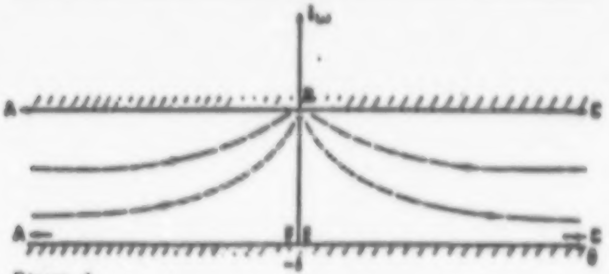

Figure 4

Ecoulement monophasique dans une bande du plan $\zeta = \theta + i\omega$.

Single-phase flow in a strip of plane $\zeta = \theta + i\omega$.

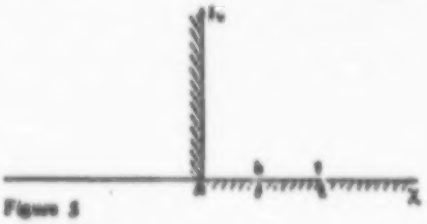

Figure 5

Quart de plan v.

Quarter plane v.

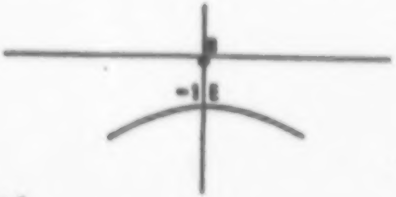

Figure 6

Sommet de la surface de séparation huile-eau pour un écoulement non critique.

Peak of oil-water separation area for a noncritical flow.

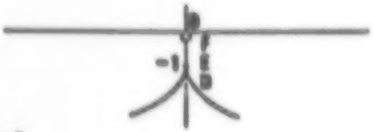

Figure 7

Sommet de la surface de séparation pour un écoulement critique.

Peak of the separation area for a critical flow.

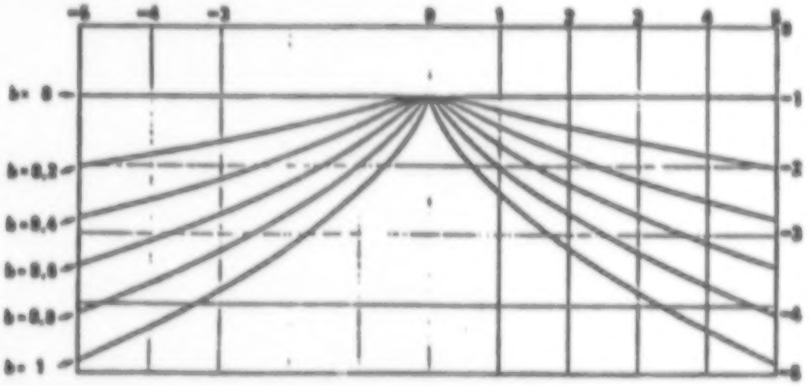

Figure 8

Famille des courbes représentant les surfaces de séparation eau-huile.

Family of curves representing the water-oil separation areas.

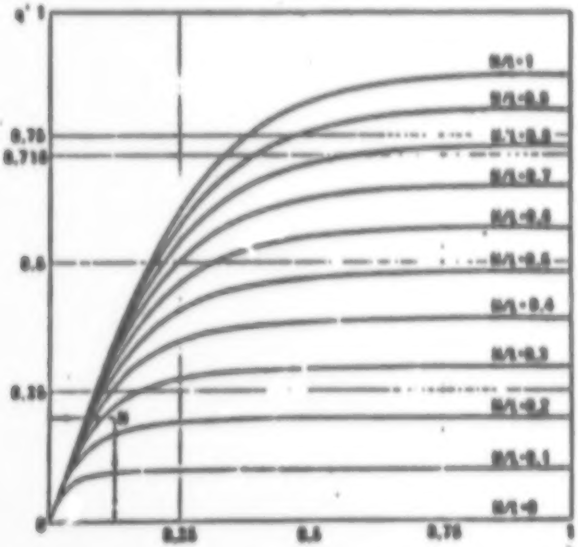

Figure 9

Abaque donnant le débit adimensionnel q' à partir du rapport H/L et du paramètre de forme b.

Chart giving the adimensional flow rate from H/L ratio and the parameter having shape b.

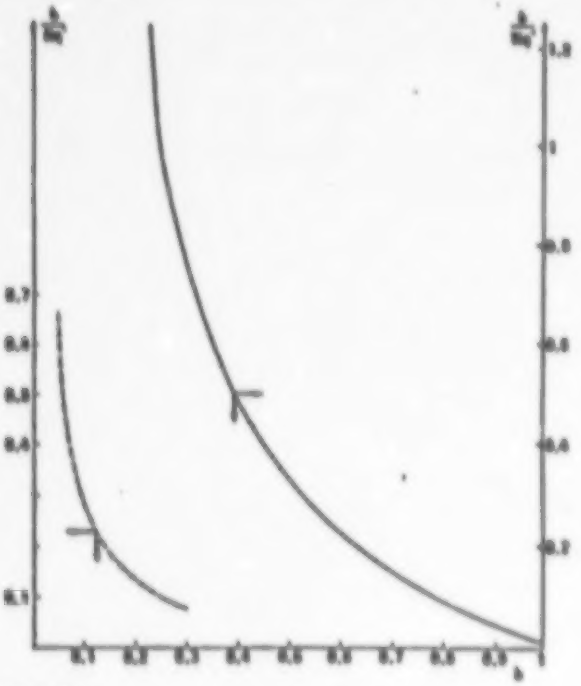

Figure 10

Abaque de correspondance du facteur $\frac{h}{Hq'}$ avec le paramètre de forme b.

Correspondence chart for the factor $\frac{h}{Hq'}$ *with the parameter having shape* b.

BIBLIOGRAPHY

1 Muskat M. - The flow of homogeneous fluids through porous media. McGraw Hill Book Company, 1937.

2 Efros D.A. - Traité d'hydraulique. Editions de Moscou.

3 Kidder R.E. - "Flow of immiscible fluids in porous media: exact solution of a free boundary problem". Journal of Applied Physics, vol. no. 27, no. 8, August 1956.

4 Cailleau Y., Chaumet P., Jeanson B., Van Quy N. - "Etude numérique et expérimentale de l'"edge coning". Rev. Inst. Franç. du Pétrole, n° Hors série, 1963. [special issue]

5 Houpeurt A. - Eléments de mécanique des fluides dans les milieux poreux. Editions Technip, 1975.

6 Giger F. - "Utilisation des fonctions analytiques pour représenter des écoulements fluides plans incompressibles". IFP report 29631, Nov. 1981.

7 Laurentiev M., Chabat B. - Méthodes de la théorie des fonctions d'une variable complexe. Editions de Moscou. French translation: Editions Mir, 1977.

8 Giger F. - "Etude analytique de l'effet d'arête d'eau créée par un drain horizontal sur une surface de séparation eau-huile". IFP report, to be published.

Final manuscript received in December 1982

767 EH
Alberta OIL SANDS
INFORMATION CENTRE

Alberta
TRANSLATION SERVICES
403/427-9693
Telex 037-2085
6950 - 113 St.
3rd Floor
Edmonton, Alberta, Canada
T6H 5V7

FRENCH-ENGLISH

(72)

ORIGINAL TRANSLATION

ALBERTA PUBLIC WORKS SUPPLY & SERVICES
CERTIFIED
Translation Service
TRUE TRANSLATION

TRANSLATED BY: MERIDEE MASCHERIN

1767 EH

Alberta OIL SANDS
INFORMATION CENTRE

L'INTERET DU FORAGE HORIZONTAL POUR L'EXPLOITATION DE GISEMENTS D'HYDROCARBURES

- (Advantages of Horizontal Drilling for Production from Hydrocarbon Fields)

F. GIGER and J. COMBE

Institut Français du Pétrole
1 et 4 avenue de Boi-Préau, BP311,
92506 Rueil-Malmaison Cedex, France

L. H. REISS

Elf-Aquitaine (Production)
Tour Générale, La Défense 9, Cedex 92,
92029 Paris La Défense, France

REVUE DE L'INSTITUT FRANÇAIS DU PETROLE
VOL. 38, N^{o} 3, MAI-JUIN 1983

à maîtriser les complétions sélectives en puits horizontal. Pour des raisons en partie semblables, les puits horizontaux possèdent des atouts pour la récupération thermique. Le positionnement précis d'une rampe d'injection à une profondeur définie dans le gisement devrait permettre d'y faire pénétrer facilement de la vapeur de façon à ce que la zone qu'elle envahit se développe régulièrement, tout en diminuant les pertes thermiques dans les épontes.

Enfin, il faut ajouter que les puits horizontaux se sont révélés, grâce aux surprenantes performances des diagraphies et du carottage, de très riches outils de connaissance de l'évolution latérale des faciès et de la répartition des fluides dans le gisement.

For fields with little vertical thickness, the productive length of a horizontal well is considerably greater than that of a vertical well. The productivity of a horizontal well increases with its length, although more slowly than this length because a logarithmic pressure-distance law comes into play. Analytical derivations as well as simulations on numerical models show that the increase in productivity may regularly attain a factor of 3 to 5. In fields having parallel vertical fractures, a horizontal well drilled perpendicularly to these fractures should cut across a great many of them and thus provide a much greater increase in productivity. In the case of fields with very heterogeneous permeability, such as karstic reservoirs, a horizontal well has a very good chance of encountering highly productive zones (case of Rospo Mare in Italy where a productivity increase of 10 and more was found in comparison with neighboring vertical wells). A study of overall productivity on the scale of the field confirms that, if vertical wells are to be replaced by horizontal wells, their number may be divided by a factor of about 4 to obtain the same production under equivalent conditions.

To prevent water (or gas) influxes during multiphase flow, a horizontal well has two advantages. It can be drilled near the top of the reservoir so as to obtain as much clearance as possible. Likewise, even with greater total production, production per unit length is less, thus locally causing more moderate stress on the oil/water or oil/gas interface. The shape of this interface is thus smoother, and calculations show that vertical sweep is more efficient, and hence recovery is greater.

Generally speaking, in multiphase flow, horizontal wells reveal all the more superiority as the mobility ratio is unfavorable, e.g. heavy oil driven by water. The phenomenon to be prevented is indeed the breakthrough of fronts, which occurs all the sooner as flow is more unstable. The steadiness of drainage among horizontal wells provides more homogeneous progression to fronts, which is especially advantageous at the beginning of production. Nonetheless, since reservoirs are more or less heterogeneous, full benefit can be drawn from such favorable effects only if selective completions can be implemented in horizontal wells.

For partly similar reasons, horizontal wells are advantageous for thermal recovery. The exact positioning of a perforated injection casing at a specific depth in a reservoir should enable steam to be fed in easily so that the zone it invades expands steadily, while decreasing heat losses into the surrounding formations.

Lastly, it should be added that horizontal wells, thanks to surprisingly good logging and coring performances, have proven to be extremely valuable instruments for determining the lateral evolution of facies and of fluid distribution in the reservoir.

Para los yacimientos de poco espesor, la longitud productiva de un pozo horizontal es mucho mas importante que la de uno vertical. La productividad de un pozo horizontal aumenta con la longitud de este, aunque mas lentamente, ya que interviene una ley presión-distancia logarítmica. Los calculos analíticos y las simulaciones con modelos numéricos indican que el aumento de productividad puede alcanzar, corrientemente, un factor de 3 a 5. En los yacimientos con fracturas verticales paralelas, un pozo horizontal dispueto perpendicularmente a ellas es susceptible de atravesarlas en gran número pudiendose así obtener aumentos de productividad mucho mas importantes. En el caso de yacimientos muy heterogêneos en la permeabilidad, como los kársticos, el pozo horizontal tiene grandes probabilidades de encontrar zonas muy productivas (caso de Rospo Mare, aumento de productividad de 10 y mas frente a la de los pozos verticales vecinos). Un estudio efectuado sobre la productividad global a la escala del yacimiento confirma que para obtener una igual producción en condiciones equivalentes, la substitución de pozos verticales por los horizontales puede permitir de dividir su número por un factor del orden de 4.

En la lucha contra las llegadas de agua (o de gas) en derrame polifásico, el pozo horizontal presenta dos ventajas. Es posible situarlo en lo alto del yacimiento de manera que se obtenga una guarda, lo mayor posible, contra el agua ; además, aún con una producción total superior, la producción lineal (por unidad de longitud), es menor, causando localmente una solicitación mas moderada de la superficie de separación crudo/agua o crudo/gas. Así pues, la forma de esta ultima es mas elastica y los calculos indican que el barrido vertical es mas eficaz y por consiguiente la recuperación mas importante.

De manera general, en derrame polifásico, los pozos horizontales presentan una superiodidad tanto mas evidente que el factor de mobilidad es desfavorable, aceite pesado desplazado por el agua por ejemplo. En efecto, el fenómeno nocivo es la rotura de los frentes, que es tanto mas precoz que el derrame es inestable. La regularidad del drenaje entre pozos horizontales contribuye a una progresión mas homogénea de los frentes, lo que es particularmente ventajosos en los comienzos de la producción. Sin embargo, como que en los yacimientos existen siempre heterogeneidades, no se podrá beneficiar completamente de estos efectos favorables que si se consigue dominar las terminaciones selectivas en pozo horizontal.

331** NOMENCLATURE

In general, the symbols used are those of the American Institute of Mining, Metallurgical and Petroleum Engineers (AIME); others have been adapted.

a: distance between centers of two neighboring horizontal wells
D: $\frac{\text{distance between two fractures or faults}}{2}$
D': $\frac{\text{length of reservoir compartment under consideration}}{2}$
E_d: displacement efficiency
E_v: ratio of volume swept by water to initial volume of oil
g: gravity
h: oil pay thickness
h_f: height of fracture
h_p: length of perforated interval of a producing well
h_{pD}: dimensionless length of perforated interval
PI_V: productivity index of a vertical well
PI_{VF}: productivity index of a fractured vertical well
PI_H: productivity index of a horizontal well
PI_{HF}: productivity index of a fractured horizontal well
k: average permeability
k': geometric mean of vertical and horizontal permeabilities
k_h: horizontal permeability
k_{rw}: relative permeability to water
k_{ro}: relative permeability to oil
k_v: vertical permeability
k_x: horizontal permeability along X axis
k_y: horizontal permeability along Y axis
ℓ: productive length of a horizontal well
L: distance from horizontal well to lateral boundary of reservoir
In: Napierian logarithm
M: mobility ratio
n: number of branches in a star-shaped drainage pattern, or number of fractured vertical wells

---

☞ *Translator's Note: See AIME Transactions, Vol. 207, 1956, pp 363-376.

Translator's Note: Numbers in margin are page numbers from original text.

N_{pD}: dimensionless cumulative production

Q: hydrous production rate

Q_c: critical flow rate from a horizontal well

Q_h: water-free production rate

$q_{c\infty}$: critical flow rate per unit length from an infinite horizontal well

r_w: well radius

r_w': radius of a well equivalent to a deviated or fractured well

r_D: dimensionless well radius

r_e: outer radius of zone drained by well, or drainage radius

r_{eD}: dimensionless drainage radius

R_e: Reynolds number

S_{wi}: initial water saturation

S_{or}: residual oil saturation

T: production time

X_f: $\frac{\text{lateral extent of fracture}}{2}$

α: inclination of a deviated well

β: multiplying factor

δ: vertical distance between middle of pay and center of fracture

θ: dip of thin reservoir bed

ΔP: difference in density between two fluids

μ: viscosity

μ_w: water viscosity

μ_o: oil viscosity

ϕ: reservoir porosity

N.B. Volumes and flows have been calculated at bottom-hole conditions

1. INTRODUCTION

The discovery of the Rospo Mare field in the Italian Adriatic prompted the Elf-Aquitaine group to turn to the concept of horizontal drilling. The problem: to develop a large European field of extremely viscous oil bounded below by an aquifer liable to quickly flood out the envisaged vertical wells through fissures. The solution: to drill horizontal wells near the reservoir roof, the lateral extent of these wells allowing them to cut across numerous fissures and thus achieve considerable total production, 332 with an average production per unit length necessitating only moderate local stress on the aquifer.

This concept had already inspired various attempts within the petroleum industry for almost half a century: star-shaped wells were drilled from mine shafts in the '40s in the United States [1], and branched wells were drilled in the '50s in the Soviet Union to increase productivity of old fields [2 and 3].

More recently, the usefulness of horizontal wells has been demonstrated in the United States and Canada [4,5,6, and 7], where such wells are being employed to overcome gas coning problems, to reach far-off objectives, and more especially (the Cold Lake project in Canada) to install slotted liners for steam injection at the bottom of reservoirs containing extremely thick oil.

The wish to put the Rospo Mare field into production in particular, and to improve well productivity and reservoir sweeping in general, resulted in the creation of a technical and scientific research project which is being headed by a scientific research organization, the Institut Français du Pétrole, and an oilfield operator, the Société Nationale Elf-Aquitaine. With the support of the European Economic Community (EEC) and a budget of fifty million francs apportioned over a five-year period, this effort has already resulted in the drilling of three horizontal wells--two in France(the Lacq Supérieur field), and one offshore (the Rospo Mare field in the Italian Adriatic), the first such well in the world [7a].

Reservoir studies and research into possible technological difficulties were carried out when the project began, with a view to deciding under which circumstances horizontal drilling would be advisable. Although the technique of horizontal drilling is not necessarily one to be used universally, there are three situations in particular which warrant its implementation. The first involves production from reservoirs where the factors likely to limit a field's productivity are thin pays, low permeability, and high oil viscosity, or some combination of all three (heavy oil or tight-gas reservoirs, for example). The second involves improving multiphase production mechanisms: water or gas coning, sweeping, and thermal recovery. And thirdly, horizontal drilling is a potential rival to hydraulic fracturing, especially in chalk, where the stone is so soft that propping agents cannot be used to keep the fracture open.

In reservoirs that are thin, low in permeability or have few fissures, the length of the well makes it possible to improve both the product $\underline{\ell k}$ (similar to the product $\underline{hk}$ in the case of vertical wells) and the probability of cutting across what are most often vertical fissures. Reservoirs making the best candidates for horizontal wells are those with a matrix lattice that is not very permeable and in which fissures or folds are not very common. If one is also looking to improve sweep efficiency by the use of a vector fluid (water, gas, steam, carbon dioxide), reservoirs making the best candidates for horizontal drilling are those which are relatively thin, contain thick oil, or have a gas coning problem. Horizontal wells are equally promising for improving recovery of edge oil or oil trapped in corners.

Let us also briefly mention here a subject that is of interest to the reservoir engineer because of the new data which can be obtained, and that is the logs conducted in horizontal wells.(1)

In the following pages we will consider the comparative productivity of different configurations of horizontal and vertical wells in homogeneous beds of various thickness. The effect of anisotropy in permeability and of vertical fractures made along a horizontal well will be analyzed. Next, a synthetic approach on the scale of an entire field will introduce the concept of well density and allow for a comparative analysis of field development using vertical and horizontal wells.

Multiphase production mechanisms involving the deformation of interfaces will then be studied for both vertical and horizontal wells, in order that the advantages of the latter may be evaluated with respect to several criteria.

2. PRODUCTIVITY OF HORIZONTAL WELLS

While pay thickness in the case of a thin reservoir a priori limits the productive length of a vertical well, this is not so for a horizontal well. However, as we shall see, productivity increases much more slowly than productive length (logarithmic law). The possibility of increasing productivity by drilling horizontal wells has been studied for some time now, and results of calculations and experiments are readily available in the literature [9 to 14]. A certain number of results expressed in analytic form make it possible to calculate the productivity of single horizontal wells or those arranged in star-shaped patterns.

2.1. Isotropic homogeneous strata

Firstly, to simplify matters, we will suppose that flow is horizontal; this amounts to supposing that the thickness of the stratum is equal to the diameter of the well (Fig. 2a). It also amounts to disregarding the loss of pressure due to the convergence of stream lines in the radial circular flow near the well as seen perpendicular to the well. The well may then be compared with a vertical fracture cutting through the entire thickness of the reservoir.

The productivity index(2) of a horizontal well that is short in relation to the drainage radius may, according to the hypotheses made, be expressed as follows(3) [15]:

$$PI_H = \frac{2\pi k}{\mu} \, \frac{h}{\mathrm{In}\left(\dfrac{1 + \sqrt{1 + (\ell/2r_e)^2}}{\ell/2r_e}\right)} \tag{1}$$

When $\ell/2r_e$ is small, this ratio can be disregarded in the term $\sqrt{1 + (\ell/2r_e)^2}$, and the expression for the productivity index then becomes:

$$PI_H = \frac{2\pi k}{\mu} \, \frac{h}{\mathrm{In}\left(\dfrac{4r_e}{\ell}\right)} \tag{2}$$

As an initial approximation, the radius of a vertical well which is equivalent to a horizontal well, that might be compared with a vertical fracture extending to the surrounding formations, is equal to one quarter the length of that horizontal well. This clearly demonstrates that the productivity index increases according to a law that depends on the logarithm of the productive length.

We obtain the same results that Prats et al [16] and Duns et al [17] obtained in a procedure in which the study of productivity increases is based on the concept of an equivalent radius (r'_w) extended to slanted wells and also to vertical fractures of limited height.

335 In the latter case, as long as the relative height of the fracture h_f in relation to the thickness of the pay h remains less than its lateral extent $2X_f$, i.e. $h - h_f \leqslant 2X_f$, we have:

$$r'_w = \frac{X_f}{2} \left[\sin\left(\pi \frac{h_f}{2h}\right) \cos\left(\pi \frac{\delta}{h}\right) \right]^{h/2X_f} \qquad (3)$$

where δ is the vertical distance between the middle of the pay and the center of the fracture.

This relation also holds true for slanted wells (Fig. 3), on the condition that:

$$\begin{aligned} 2X_f &= \frac{h}{\cos\alpha} \\ h_f &= 4r_w \qquad (4) \\ \delta &= 0.35\ h \end{aligned}$$

and, in addition $\alpha \geqslant 20^{\circ}$.

In order to account more exactly for the convergence of stream lines in the radial circular flow near a horizontal well as seen normal to the latter (Fig. 2b), an additional loss of pressure must be taken into consideration. The productivity index of a horizontal well that is short in relation to the drainage radius is then expressed as follows:

$$PI_H = 2\pi \frac{k}{\mu} \frac{1}{\frac{1}{h} \ln\left(\frac{1 + \sqrt{1 + (\ell/2r_e)^2}}{\ell/2r_e}\right) + \frac{1}{\ell} \ln\left(\frac{h}{2\pi r_w}\right)} \qquad (5)$$

In his article "Réduction du nombre de puits par l'utilisation de forages horizontaux [18][*], F. Giger confirms the validity of this expression, and proposes charts for finding the radius of a vertical well equivalent to a horizontal well for various thicknesses of isotropic homogeneous strata. We will use this method in an example given later.

2.2 Anisotropic homogeneous strata

The mechanisms of sedimentary deposition that have helped form the reservoir matrix and the tectonic forces that have sometimes fractured it are two of the principal factors contributing to the differences in values of permeability as measured along several different axes in a given sample of reservoir rock.

In describing reservoirs it is common practice to take into consideration the anisotropy in vertical permeability (k_v/k_h), and the anisotropy in horizontal permeability (k_x/k_y), along the main axes where the latter takes on extreme values. We know that for an incompressible steady-state flow the Laplace equation for potential holds. The nature of this relation makes it possible to compare the flow in a milieu having only one permeability, $\underline{k}$, with the flow in a milieu where permeabilities along the main axes are $\underline{k_i}$ ($i = x$, y or v). To do so, we have only to dilate the coordinates along each axis according to the ratio $(k/k_i)^{1/2}$ (adapted from Muskat [19]).

---

[*] Translator's Note: "Reducing the Number of Wells by Using Horizontal Drilling"

A k_v/k_h ratio of less than 1 is unfavorable for a horizontal well, as such a ratio has the same effect as reducing the length of the well.(4) 336 If both the magnitude and the direction of anisotropy in horizontal permeability can be determined, the horizontal well should be positioned so that the axis of the well coincides with the direction of lowest permeability; if such anisotropy is caused by fissuring along the vertical planes, then this would amount to placing the horizontal well perpendicular to the fissures, so that it cuts across as many of them as possible.

2.3 Multifractured horizontal wells

In the course of studies and laboratory work undertaken by Shell to improve productivity of wells drilled in tight chalk reservoirs, Duns *et al* [17] calculated that a cased horizontal well of length ℓ given five small vertical fractures (the width of each fracture being 0.075ℓ) has an equivalent radius practically identical to that of a vertical fracture of width ℓ.(5) This means that the stimulation of a horizontal well might be effected by distributing along it only five small fractures which cut through the entire thickness of the reservoir. With the help of Franlab Consultant, we developed a model which made it possible to carry out numerous simulations and clarify this result.

Figure 4 depicts the most general case of a multifractured horizontal well producing from a parallelipipedic pay. The diagram has been simplified in accordance with a certain number of hypotheses concerning the geometry of the system and the position of the horizontal well and fractures:

--the horizontal well ($r_w = 0.10$ m) is presumed to have been drilled at the center of gravity of the vertical section, the dimensions of which are fixed at:

$h = 50$ m
$2L = 400$ m

--the fractures are equidistant from each other (distance between fractures: 2D), and are repeated to infinity. In addition, the fractures are rectangular in shape and intersect both the roof and wall [sic] of the reservoir.

As the conductivity of the fractures is presumed infinite, the hydraulic potential will be the same in both fracture and well (in which, moreover, pressure losses are disregarded). All other boundaries of the simulated environment are closed (normal flux nil). We will now examine the results obtained from simulations carried out on this model.

2.3.1 Advantage of horizontal wells over fractured vertical wells

The two configurations compared in this subsection are schematized in Figure 5. Results in the form of a set of curves are also presented in this figure:

$$\frac{PI_H}{PI_{VF}} = f\left(\frac{X_f}{L}, \frac{D}{L}\right)$$

Figure 5 reveals the following:

1) When $\frac{D}{L} \leq 0.25$, a fractured vertical well is always more advantageous than a horizontal well.

2) When $\frac{D}{L} \geq 0.50$, the basic parameter of comparison becomes the lateral extent of the fracture, $\frac{X_f}{L}$. Thus, PI_H and PI_{VF} are equal for $\frac{X_f}{L} = 0.39$ when
337 $\frac{D}{L} = 1$ (point A in Figure 5); for $\frac{X_f}{L} = 0.23$ when $\frac{D}{L} = 0.75$; and for $\frac{X_f}{L} = 0.1$
when $\frac{D}{L} = 0.5$.

2.3.2 Improving horizontal wells by fracturing

Given the observations in the preceding subsection, the fracturing of horizontal wells is likely to gain considerably in importance.

The two configurations studied are schematized in Figure 6. The results in the form of a set of curves are also presented in this figure:

$$\frac{PI_{HF}}{PI_{H}} = f\left(\frac{X_f}{L}, \frac{D}{L}\right)$$

To better illustrate the degree of horizontal well fracturing, the curves have been parameterized as a function not only of $\frac{D}{L}$, but also of the number of fractures per 400-m length of well.

Figure 6 shows that, in order to triple the productivity of a horizontal well in the configuration studied:

--there must be at least 2 fractures per 400-m length of horizontal well;

--the lateral extent of the fractures, represented by $\frac{X_f}{L}$, must be greater than 0.4 in the case of two fractures, 0.250 in the case of four fractures, and 0.175 in the case of eight fractures.

2.3.3. Advantage of fractured horizontal wells over single fractured vertical wells

This comparison was carried out using the example of a reservoir 400 x 400 x 50 m, and is illustrated by the ratio of the productivity index of a vertically fractured horizontal well (1,2,4,8, and 16 equidistant fractures) to that of a fractured vertical well under the same conditions:

$$\frac{PI_{HF}}{PI_{VF}} = f\left(\frac{X_f}{L}, \text{number of well fractures}\right)$$

Figure 7a depicts the variations in $\frac{PI_{HF}}{PI_{VF}}$ that occur as a function of these two parameters. The set of curves shows that, as long as the number of fractures is less than or equal to 4, the increase in productivity always remains greater than the number of well fractures. However, if the number of wells continues to be increased a saturation effect seems to occur, and the increase in the productivity index is then related more to the size of the fractures than to their number.

339 Figure 7a concerns the basic cases defined by:

$L = 200$ m

$D' = 200$ m (number of fractures variable)

$h = 170$ m

$k_x = k_y = k$.

The influence of thickness and anisotropy, on the other hand, is shown in Figure 7b. Comparing the series of simulations with the basic case for which permeability is isotropic, we can see:

--the unfavorable effect of decreased vertical permeability on the productivity of a fractured horizontal well (cf. subsection 2.2.);

--the increased productivity of a fractured horizontal well brought about by an increase in vertical permeability (which may correspond to natural vertical fracturing) and a reduction in the height of the pay being drained.

2.3.4. Conclusions of the study on models of fractured wells

This sensitivity study on the behavior of multifractured horizontal wells made it possible to determine the circumstances under which such wells might be attractive. It is interesting to note that the ratio between the productivity index of a multifractured horizontal well and that of a fractured vertical well, since it amounts to [only] a few units, is similar to the ratio obtained when the wells are not fractured.

2.4. Developing a field using horizontal wells

Let us now consider an actual onshore oilfield, where the only problem consists in obtaining sufficient productivity to make the operation profitable. The analytical tool commonly used is the productivity index. In the expression for the productivity index of each well, certain parameters imposed by nature come into play: permeability of the reservoir rock, geometry of the reservoir, viscosity of the fluids present in the rock, and nature of the flow. Other parameters are acted on by the individuals responsible for developing the field: the geometry of the producing structure, summarized as the equivalent vertical well radius (vertical, slanted, or horizontal wells, possibly cemented, consolidated, stimulated or fractured); and the position of each well in relation to neighboring wells or reservoir limits (boundaries, discontinuities, barriers), summarized as the drainage radius.

If one wishes to improve the economic prospects of a project by modifying the geometry of the structures--by replacing vertical wells with slanted, fractured, or horizontal wells, for example--it is also advisable to reexamine the spacing between wells. The productivity index is then no longer the proper analytical criterion. Giger suggests introducing the concept of an areal productivity index, which is the product of the productivity index and the density of wells or number of wells per unit of surface area [18]. This concept makes it possible to establish comparisons between different development systems for the same field, and to demonstrate the reduction in number of wells that can be obtained by increasing the productive capacity of each well. To make the most economical choice among all variations, one needs only to know the comparative costs at a given moment for a given site.

The suggested procedure becomes even more necessary when one considers that using horizontal wells changes the scale of the size of equivalent vertical well radii customarily used in reservoir engineering from tens of centimeters to tens of meters. The influence of interference phenomena becomes considerable. To illustrate this, Figure 8 shows the productivity index of a star-shaped drainage pattern calculated according to Borisov's formula [13]:

$$PI = \frac{n\pi k}{\mu} \frac{1}{\frac{1}{h} \ln \left(\frac{1 + \sqrt{1 + (\ell/r_e)^n}}{(\ell/r_e)n/2} \right) + \frac{1}{\ell} \ln \frac{h}{2\pi r_w}} \qquad (6)$$

It can be seen from Figure 8 that the productivity index of a star-shaped drainage pattern with 4 or more branches is only slightly greater than that of a similar pattern with three branches of the same length.

341 2.5. Study of actual cases: horizontal well productivity indices

The main objective in drilling the first two horizontal wells of the Lacq Supérieur project was to perfect drilling techniques [7a]; reservoir criteria were therefore not a major consideration in drilling this type of well. Nevertheless, the wells do provide us with the opportunity to test the validity of our methods for calculating the productivity index on a concrete, 1:1-scale example.

Let us use the example of the Lacq 90 well, for which we possess production data collected over a period of more than two years.

Numerical values:

$k \sim 10$ mD

$h \sim 100$ m

$\mu \sim 0.5$ cP, the field is flooded and the oil cut produced by the wells is not greater than 10%

$r_w \sim 0.10$ m

$L \sim 300$ m

$r_e \sim 1000$ m, taking into account the extent of the zone of the Lacq Supérieur field where the well has been drilled.

Applying the chart method [18] or Merkulov's formula gives an equivalent vertical well radius $r'_w = 15$ m, from which, by applying relation (7),

$$PI_V = \frac{2\pi kh}{\mu} \frac{1}{\mathrm{In}\left(\frac{r_e}{r'_w}\right)} \qquad (7)$$

and, introducing the practical coefficient 0.0233 for a result in m^3/day/bbl, we obtain:

$$PI = \frac{0.0233 \times 2 \times 3.14 \times 10 \times 100}{0.5} \frac{1}{\mathrm{In}\left(\frac{1000}{300}\right)}$$

$$PI = 5.8 \ m^3/\text{day/bbl}$$

This value is comparable to that actually obtained from the Lacq 90 well, which is 6.5 m^3/day/bbl. The productivity index for the Lacq 90 well is approximately 4 times greater than the average of the neighboring vertical wells.

Let us also note that the results from the Rospo Mare field horizontal well, which passes through more than 600 m of a karstic--and therefore very heterogeneous--reservoir, are even more impressive. According to measurements 342 taken recently, at the commencement of production trials, the index of this well is more than ten times greater than those of neighboring wells.

Following up on the production of the entire group of horizontal wells drilled concurrently with or subsequent to this project will allow us to compare theoretical calculations to field results for a greater number of cases. However, even those results acquired to date give us confidence in the validity of our theoretical productivity calculations.

3. STUDY OF PRODUCTION IN CASES INVOLVING DEFORMATION OF BOUNDARIES BETWEEN ZONES INVADED BY DIFFERENT FLUIDS

3.1. Analytical derivations of critical flow rate

3.1.1. Vertical wells

In reservoirs where a horizontal gas/oil or water/oil boundary initially exists, a deformation (coning) of this boundary occurs when the reservoir is being drained by a well near the boundary, and such coning may lead to a breakthrough of gas or water, resulting in two-phase production (Fig. 9). The coning problem has been studied for some time, but has not yet been resolved in any exact way through analytical means. The literature contains only approximate formulas, constructed from typical groups of physical variables such as appear in a simplified model intended to evaluate the dynamic depression created by a horizontal radial circular flow [20]. The higher the initial water clearance, the more limited the open area around the well and the closer one gets to it, the more approximate the results. The latter are often presented in the following form:

$$Q_c = \beta \frac{k_h \Delta p h (h-h_p)}{\mu} \qquad (8)$$

(where, in practical units $\beta = 0.00124$ or 0.00152, according to the authors).

This formula brings to the fore an important parameter: the difference $h-h_p$ between the level of the bottom of the perforated interval and that of the initial water level (clearance). The critical flow rate also depends on the geometry of the reservoir: in particular, it decreases as the drainage radius increases, as is shown by Chierici's correlation [21]. When the drainage radius is more than 5 to 10 times the height of the oil column, the critical flow rate becomes practically independent.

By way of a reminder let us also cite other formulas where the taking into account of radial circular flow involves a potential, and the expression of this potential shows the drainage radius within a logarithmic function [12].

As concerns the practical application of these formulas, considerable differences are often observed between theoretical calculations and field measurements. The nature of the physical problem implies that the actual field results depend to a large extent on the heterogeneities of the reservoir rock immediately surrounding and under the well.

Nevertheless, the formulas do have a practical field use once they have been adjusted by a multiplying constant appropriate to a particular group of producing wells, and allow for a relatively satisfactory approach to variational tendencies during modification of the significant parameters under consideration.

As regards the study of dimensionless parameters, Muskat's analytical studies [22] reveal three such parameters that are characteristic of these configurations:

--the dimensionless drainage radius

$$r_{eD} = \frac{r_e}{h}\sqrt{\frac{k_v}{k_h}} \qquad (9)$$

343 where r_e = drainage radius; h = initial height of oil column; k_v and k_h = vertical and horizontal permeability, respectively;

--the dimensionless length of the perforated interval

$$h_{pD} = \frac{h_p}{h} \qquad (10)$$

where h_p = length of perforated interval;

--the dimensionless well radius

$$r_D = \frac{r_w}{h}\sqrt{\frac{k_v}{k_h}} \qquad (11)$$

where r_w = well radius.

In a steady-state system, these dimensionless parameters are sufficient to characterize the system.

3.1.2. Horizontal wells

The idea of increasing water clearance while maintaining sufficient productivity indices has led to the study of the behavior of horizontal wells drilled in the roof of the producing stratum, and in particular their critical flow rate.

The study of the oil/water contact and the flow of oil toward a horizontal well lends itself to the analytical method: the problem consists of a two-dimensional flow in a plane perpendicular to the axis of a well that is presumed infinite.

In his article [23], R.E. Kidder deals with boundary deformation in the case of waterfingering in a flat, thin, inclined stratum. We can attempt to use Kidder's work to study boundary movement in the case of a horizontal well by imagining that his flat, thin stratum pivots and becomes vertical, to give $\theta = \pi/2$ (Fig.10). It should be noted, however, that the absence of any upper boundary to the oil zone limits the validity of the study when one is considering horizontal wells drilled near the oil/water boundary. Nevertheless, this approach has the advantage of demonstrating how the hodograph method makes it possible to arrive at an exact parameterized expression of the oil/water boundary and to determine the critical flow rate.

D.A. Efros, for his part [24], studies the effect of water cresting created by a horizontal well located in the horizontal roof of a reservoir bed underlain by bottom water. By using the hodograph method he is able to obtain an approximate solution through the composition of several conformal transformations, and, although a certain number of approximations are involved, these are relatively unimportant. Efros succeeds in parameterizing the oil/water boundary equation and giving the value of the critical flow rate. His approach, improved and completed, is presented by Giger [25].

These analytical derivations provide an expression of the critical flow rate per unit length that is simplified when the ratio of the extent of the oil zone to its height h exceeds 5(6):

$$q_{c\infty} = \frac{k \Delta \rho g}{\mu} \frac{h^2}{\ell} \tag{12}$$

If we compare this expression to the one obtained for a vertical well, we see that the term $h\ (h-h_p)$, which characterizes the influence of the geometry of a vertical well on its critical flow rate, is replaced here by the term $\frac{h^2}{\ell}$. Let us remark that, in the case of a horizontal well located against the upper adjacent bed, there is no equivalent for the h_p term, and thus no reason for this factor to intervene.

The term $1/\ell$ would be obtained by making Dupuit's approximation [26]. Assuming the vertical permeability to be infinite, we then obtain, like Kozeny (quoted by Muskat [22]), that the free surface of a moving fluid is a ruled parabolic surface, here $\frac{h^2}{\ell}$ = constant.

344 We should comment at this point on the shape of the boundary that exists between

water and oil at a sufficiently great distance from the well. In the case of vertical wells, the impact of this distance is governed by a logarithmic function. For a given flow rate and at a sufficient distance, the values assumed by the function change only slightly, and generally the water table is considered horizontal. However, the case of infinite horizontal wells (those crossing the entire width of the reservoir) is completely different: the impact of the distance is governed by the factor $\frac{1}{\ell}$ in $\frac{h^2}{\ell}$. In this schematization, there are no longer any grounds for considering that a water table exists far from the well.

These analytical estimations of the critical flow rate may be used in the case where an infinite horizontal well crosses an entire laterally fed reservoir compartment. Up to this point we have used simulation models in the other cases.

It should be kept in mind, however, that these formulas are used to determine the influence of different parameters.

3.2. Determining critical flow rate and corresponding swept volume with numerical models

In the following paragraphs we will detail the results of our calculations on numerical models concerning the "critical" behavior of both infinite and limited horizontal wells, and also on "post-breakthrough" behavior.

3.2.1. Critical flow rate per unit length from horizontal wells

For both horizontal and vertical wells, the Rzmono model makes it possible to very rapidly calculate the critical flow rate and the volume swept by the aquifer where there is lateral feed in the two phases. The model is vertical, circular, or flat (RZ or XZ), and presupposes that there is no flow in the zone invaded by water (Muskat's hypothesis). The position of the stable cone is determined by considering the equilibrium between viscous friction and forces of gravity at the oil/water contact.

The fact that this model can be quickly and economically used allowed us to carry out a large number of simulations and vary the drainage radius, height of the oil column, and anisotropy ratio within a fairly large range of values.

More than one hundred and sixty simulations were carried out, with variations made in distance to the feed boundary (100 to 500 m), length of perforated interval (1 to 20% the height of the oil column), anisotropy ratio $\frac{k_v}{k_h}$ (from 1 to 1/100), and height of the oil column (10 to 100 m), for both infinite horizontal wells and vertical wells.

The main results obtained show that, in the range of values studied, neither h_{pD} nor r_D has any significant effect. This is due to the fact that, as long as the distance between the perforated interval and the roof of the pay or between the horizontal well and the roof of the pay is not greater than 10-20% the height of the oil column, the well may be considered as a point source at the roof. For small values of r_D--that is, small spacings between wells--the critical flow rate increases greatly. For common values of r_D (5 or more), the critical flow rate of a horizontal well is 2 to 3 times that of a vertical well.

3.2.2. Water-swept volume for infinite wells

The volume of the aquifer is also given by the model, and the curves are presented in Figure 11. The greater the distance between wells, the more significant the increase obtained by a horizontal well. For common values of r_D, the volume of the aquifer under the horizontal well, and consequently the recovery, are 4 to 6 times greater than for a vertical well (see Figure 12). Using the calculation hypotheses for this model, this volume represents the volumetric sweep efficiency at the critical flow rate.

The volumetric efficiency results obtained with the critical flow model may, as an initial approximation, be considered valid at breakthrough in a supercritical system, since we know that the volume of the aquifer at breakthrough is almost the same as that calculated at a moderately critical rate.

345

3.2.3 Critical flow rate and volumetric sweep efficiency for limited horizontal wells

For economic reasons, broken lines of horizontal wells will have to be considered. To that end a study of the critical flow rate was completed for cases in which an infinite horizontal well is replaced by a broken line of horizontal wells varying in length.

The geometric parameters that must be taken into consideration then become more numerous. Our study was limited to the case of a line of horizontal wells running parallel to a feed boundary; this may represent the configuration of a direct line-drive pattern (Figure 13). The geometry of the problem is then characterized by 3 parameters that may be reduced to two dimensionless groups: ℓ/a and L/a; L being the distance between the line of horizontal wells and the feed boundary, a the distance between the centers of two neighboring wells, and ℓ the length of a horizontal well.

346 The model used is a three-dimensional version of the critical flow model (Muskat 3D), which makes it possible to depict limited horizontal wells.

The results show (Figure 14) that the critical flow rate increases as the length of the well increases, and that the smaller the ℓ/a ratio, the greater this increase. Small breaks in a line of wells (ℓ/a in the order of 0.8 to 0.9) lower the critical flow rate only slightly, especially as the L/a ratio increases.

Let us define the volumetric sweep efficiency E_v as the ratio of the volume swept by water to the initial volume of oil. The volumetric sweep efficiency increases rapidly with ℓ/a when the latter is small. When ℓ/a is greater than 1/2, interference phenomena between extremities of horizontal wells do not allow for any great increases, at least for the values chosen.(7)

3.2.4 Simulation study of the supercritical system

In order to explore the area of flow rates greater than critical rates, simulations were carried out on the TRITRI three-phase three-dimensional model, with a view to determining rates of hydrous and water-free production before major flooding, with various fluid mobility ratios M (Figure 15).

In the absence of capillary pressure, we know that the characteristic dimen-
347 sionless parameters are [19 and 22]:

$$r_{eD} = \frac{r_e}{h}\sqrt{\frac{k_v}{k_h}} \tag{9}$$

$$h_{pD} = \frac{h_p}{h} \tag{10}$$

$$r_D = \frac{r_w}{h}\sqrt{\frac{k_v}{k_h}} \tag{11}$$

$$M = \frac{k_{ro}}{\mu_o}\,\frac{\mu_w}{k_{rw}} \tag{13}$$

$$N_{pD} = \frac{QT}{r_e^2\ h\ \phi\ (1 - S_{or} - S_{wi})} \tag{14}$$

$$R_e = \frac{\mu_h Q_h}{\Delta p \; g \; k_h \; r_e \; h} \qquad (15)$$

The first three parameters are those defined in subsection 3.1.1.; the remaining three are the mobility ratio, the dimensionless cumulative production, and the Reynolds number (ratio between forces of gravity and inertia).

In the simulation, the horizontal or vertical wells were assumed to form part of a repetitive array, in which the XY grid block was square and the boundaries were in zero flux. The simulated reservoir consisted of horizontal flat strata.

For the vertical well the grid was symmetric for X and Y, and for the horizontal well a two-dimensional YZ grid was used.

3.2.5. Increased recovery with horizontal wells

The volumetric sweep efficiency $\underline{E_v}$ was obtained by integrating over the volume where the water saturation is greater than the initial water satura-
348 tion S_{wi}. The interference ratio at breakthrough is defined as the percentage of the initial oil column invaded by water at the drainage boundary when breakthrough occurs.

For extremely unfavorable mobility ratios, the recovery ratio at breakthrough for horizontal wells is clearly greater than that for vertical wells. This advantage is maintained subsequently: for example, an increase of 6 for $M = 100$.

For less unfavorable mobility ratios(8) the increased recovery from horizontal wells remains greater at breakthrough, but tends to diminish during production involving a high percent of water. For example, for M = 10, the increase at breakthrough reaches 3.4 and then falls to 1.3 for 80% water.

As regards well spacing, the increase at breakthrough for horizontal wells in relation to vertical wells is greater as the ratio of interference between them diminishes. For example, for M = 10, the increase at breakthrough, which was 3.4 with no interference, drops to 1.6 with considerable interference.

As for the case where mobility ratios are clearly favorable, the increase in recovery, if still significant at breakthrough, becomes very slight thereafter. For M = 0.5, it drops from 2.7 to 1.02 between breakthrough and 80% water.

3.3 Superficial sweep efficiency

Where there is initially no boundary between the reservoir fluids near the wells, several types of water injection systems are possible, in particular the direct line-drive pattern. In the case where the pay is thin enough that the flow may be considered horizontal, the surface contacted by the driving fluid is almost proportional to recovery, until breakthrough.

The parameters for calculating the sweep efficiency at breakthrough are, for this type of pattern, the ratio d/a (the distance between lines of producing and injection wells in relation to the distance between the same kind of wells) and the ratio L/a for horizontal wells (the length of the well in relation to the distance between centers of two wells of the same type - see Figure 15).

Cases involving different mobility ratios were studied. With a mobility ratio equal to 1, simulations were carried out on a flow-tube model. With unfavorable mobility ratios ($M = 10$ and $M = 100$), they were carried out on a two-dimensional two-phase XY model.

Exact analytical solutions are known in the case of vertical wells for a mobility ratio (M) equal to 1. Results of experiments carried out on electrolytic models correspond to the case of horizontal wells on which the effect of limited-extent vertical fractures, shown in the XY plane as dotted lines, was studied. This pattern is equivalent to the effect of a series of horizontal wells on superficial sweep.

Simulations were carried out with $\underline{d/a}$ ratios from 1 to 2 and $\underline{L/a}$ ratios from 0 to 0.5. The ratio $\underline{L/a} = 0$ represents the standard vertical well. Results are grouped in Figure 15. We note that the flow-tube model gives results for vertical wells that come very close to Muskat's analytical solutions. For limited horizontal wells, we note that when the mobility ratio is equal to 1, results differ from those given in the literature. Indeed, we see that the increase in superficial sweep efficiency remains very low as long as $\underline{L/a}$ is less than 0.1. The smaller the $\underline{d/a}$ ratio, the greater the increase brought about by horizontal wells. This contradicts Crawford's results, which were obtained by interpolation from an insufficient number of points [10].

4. USING HORIZONTAL WELLS TO IMPLEMENT THERMAL STIMULATION METHODS

Canadian oilfield operators have been drilling steam-injection horizontal wells, in particular in the Cold Lake field [6 and 7]. The expected advantage from this type of procedure is improvement in stimulation efficiency, for the following reasons :

--Despite the viscosity of the oil in place, the productivity index of a horizontal well is greater than that of vertical wells. Using horizontal wells makes it possible to inject a greater flow of steam per well and thus to reduce the relative rate of heat loss from the steam conduction column.

--Positioning injection wells parallel to surrounding beds makes it possible to limit the proportion of thermal leaks from the producing formation towards these surrounding beds. The steam injected by a horizontal well will a priori reach a greater reservoir volume than that injected by a vertical well open its entire height, before leaks out of the formation become preponderant.

Calculations and trials on laboratory models conducted by Esso Resources Canada [5] demonstrate the influence of gravity: the umbrella of steam tends to form near the top. Accordingly, it would seem advisable to position the steam-injection horizontal well near the bottom of the zone to be stimulated. This is what Texaco has done within the framework of a pilot project that is still being operated.

5. CONCLUSION

The reservoir studies conducted within the framework of this horizontal drilling project, with the aid of theoretical work, models, and interpretation of industry results, enable us to make the statements which follow.

Compared with vertical wells, horizontal wells can increase flow or injection rates several times over. The technique should be used when, for one reason or another, hydraulic fracturing conducted from vertical wells proves ineffective. The thinner the reservoir and the higher the vertical permeability, the greater the increase that may be expected. This increase may even be tenfold in fissured reservoirs or those that are very heterogeneous; this was the case for the horizontal well drilled in the karstic reservoir of the Rospo Mare field.

If a boundary between several fluids exists in a reservoir near the well zone, production with horizontal wells should make it possible to improve the flow rate and recovery of oil severalfold, due to the increase in volumes drained. However, to benefit fully from this effect, it is necessary to perform selective completions that are adapted to the spatial heterogeneities of the matrix characteristics and reservoir fluids [27].

For draining oil that is not easily accessible, horizontal wells have two advantages: they make it possible to increase the reservoir surfaces that can be swept, and also to reach lateral regions that would not be adquately drained by vertical wells.

The repeated success of logging and coring operations has brought about great progress in our understanding of the lateral evolution of facies and fluid distribution in reservoirs.

As for enhanced recovery, horizontal wells are liable to guarantee better injection of the vector fluid--steam, for example.

Current lines of research and experimentation involve the development of selective completion and experiments with multiphase flows carried out, where possible, on physical models dekametric in scale.

The authors wish to express their thanks to all their colleagues who participated in this team effort, and in particular to C. Jain (Institut Français du Pétrole) and O. Ricard (Elf-Aquitaine), for their creative talent.

They also wish to thank the management of Elf-Aquitaine and the Institut Français du Pétrole for permission to publish these results.

BIBLIOGRAPHY

[1] Ranney, L. "Drilling wells horizontally." The Oil Weekly, Jan. 20, 1941.

[2] Grigorjan, A.M. "Les puits à ramifications horizontales." Neft. Khoz, 1976, n° 11, 19-22. Translation from Russian into French: doc. IFP ref. 29564, Oct. 1981.

[3] Grigorjan, A.M. Forage des couches productives par puits horizontaux et à complétion multiple. Moscow; "Nedra" 1969, 190 p. Translation from Russian into French: doc. IFP ref. 27746, Feb. 1980.

[4] Striegler, J. "Arco finishes fourth horizontal drainhole." Oil and Gas Journal, May 24, 1982, pp. 55-61.

[5] Butler, R.M.; Stephens, D.J. "The Gravity Drainage of Steam-Heated Heavy Oil to Parallel Horizontal Wells." Preprint n° 80-31-31, presented at the 31st annual CIM meeting, Calgary, Canada, 25-28 May, 1980.

350 [6] Loxam, D.C. "Texaco Canada Completes Unique Horizontal Drilling Program." Petroleum Engineer International, Sept. 1982, pp. 40-52.

[7] "Horizontal wells take steam to Athabasca tar." Enhanced Recovery Week, March 1, 1982, p.3.

[7a] Jourdan, A. "Le forage de puits horizontaux." Revue de l'AFTP Pétrole et techniques, n° 294, déc. 1982, p. 37.

[8] Wittrisch, Ch.; Jourdan, A. "SIMPHOR--Système d'instrumentation et de mesure en puits horizontaux." Actes du 4e Colloque annuel de diagraphies SAID, 21-23 oct. 1981.

[9] Perrine, R.L. "Well Productivity Increase from Drain Holes as Measured by Model Studies." Trans. AIME, V. 204, pp. 30-34, 1955.

[10] Landrum, B.L.; Crawford, P.B. "Effect of Drainhole Drilling on Production Capacity." JPT, Feb. 1955, pp 45-47.

[11] Roemershauser, A.E.; Hawkins, M.F. "The Effect of Slant Hole, Drainhole, and Lateral Hole Drilling on Well Productivity." JPT, Feb. 1955, pp. 11-14.

[12] Meyer, H.I.; Garder, A.O. "Mechanics of Two Immiscible Fluids in Porous Media." Journal of Applied Physics, V. 25, No. 11, Nov. 1954.

[13] Borisov, Ju. P. "Exploitation des gisements de pétrole par des puits horizontaux et à déviations multiples." Moscow: "Nedra", 1964. Translation from Russian into French: doc. IFP, ref. 28363

[14] Merkulov, V.P. "Le débit des puits déviés et horizontaux." *Neft.Khoz.*, 1958, nº 6, pp. 51-56.

[15] Houpeurt, A. *Eléments de mécanique des fluides dans les milieux poreux.* Paris: Ed. Technip, 1975.

[16] Prats, M.; Hazebroek, P.; Strickler, W.R. "Effect of vertical fractures on reservoir behavior--Compressible fluid case." *SPEJ*, June, 1962, pp. 87-94.

[17] Duns, H.; Van der Vlis, A.C.; Fernandez, Luque R. "Increasing Well Productivity in Tight Chalk Reservoirs." *10th World Petroleum Congress*, Bucharest, 1979.

[18] Giger, F. "Réduction du nombre de puits par l'utilisation de forages horizontaux." *Rev. Inst. Franç. du Pétrole*, V. 38, nº 3, mai-juin, 1983.

[19] Muskat, M. "The Performance of Bottom Water-drive Reservoirs." *Trans. AIME*, V. 165 and 170, 1946 and 1947, p. 81.

[20] Cottin, R.H. "Optimisation de la complétion et de l'exploitation d'un puits soumis au coning biphasique." *Rev. Inst. Franç. du Pétrole*, XXVI, nº 3, mars 1971, pp. 171-197.

[21] Chierici, G.L.; Ciucci, G.M.; Pizzi, G. "A Systematic Study of Gas and Water Coning By Potentiometric Models." *JPT*, Aug. 1964, pp. 923-929.

[22] Muskat, M. *The Flow of Homogeneous Fluids Through Porous Media.* Ann Arbor (Michigan): J.W. Edwards Inc., 1946.

[23] Kidder, R.E. "Flow of Immiscible Fluids in Porous Media: Exact Solution of a Free Boundary Problem." *Journal of Applied Physics*, Aug. 1956, V.27.

[23a] Cailleau, Y.; Chaumet, P.; Jeanson, B.; Van Quy, N. "Etude numérique et expérimentale de L'"edge coning." *Rev. Inst. Franç. du Pétrole*, 1963, nº hors série, p. 344. [special issue]

[24] Efros, D.A. *Etude des écoulements multiphasiques dans les milieux poreux.* Leningrad: Gostoptexizdat, 1963.

[25] Giger, F. "Evaluation théorique de l'effet d'arête d'eau sur la production par puits horizontaux." *Rev. Inst. Franç. du Pétrole*, V. 38, nº 3, mai-juin, 1983.

[26] Dupuit, J. *Etudes théoriques et pratiques sur le mouvement des eaux.* 2e éd. Paris: Dunod, 1893 (1re éd. 1863).

[27] Giger, F. "L'équipement de forages horizontaux." *Revue de l'AFTP. Pétrole et techniques*, nº 294, déc. 1982, p. 40.

Final manuscript received in February, 1983.

NOTES

(1) In horizontal drilling as in vertical drilling, the more specific information that can be obtained, the better the knowledge of the reservoir. It is for this reason that special techniques for positioning and moving measurement sondes were developed for horizontal wells. One method consists in pumping reduced-diameter sondes down the drill string so that they emerge to the right of the discovery (Schlumberger technique); the other--an original technique developed by members of our research team, the Système d'Instrumentation et de Mesure en Puits Horizontaux* (SIMPHOR, registered trade mark)--makes it possible to conduct logs by using standard-diameter sondes attached to the end of the drill string. This technique revolves around a method of electrical connection that is reliable in a muddy environment. [8]

Today, almost all logs available can be recorded in horizontal wells (at Rospo Mare CBL,GR, and CCL logs are being used in the casing; ISF, BHC, VDL, GR, BGT, and DLL logs in the open hole; and a density-neutron combination log is being used for measurement through the pipes). With logs conducted at Lacq 91 the exact portrayal of a highly fractured zone was obtained, and selective production equipment was then put into position. The quality of these logs is excellent, as can be seen in Figure 1, where a fissured zone is clearly recognizable (a matter of capital importance in reservoir engineering). It is true that the zone detected was a total loss zone in which fissures had enormous openings and consequently were able to absorb two tonnes of sand.

Together with core samples, these logs provide extremely interesting new reservoir data; in fact, they make it possible to constitute horizontal sections for the first time, and to specify lateral variations in facies and hydrocarbon distribution.

(2) The ratio of the flow produced per well and the bottom-hole pressure in that well to the average pressure prevailing in the reservoir zone drained by the well when production ends.

(3) If one wishes to use the productivity formulas with practical units (m^3/day/bbl; cP, mD, m), the multiplying coefficient 0.0233 must be introduced into the right-hand term.

(4) By way of illustration, let us take the following example:

Horizontal well:

$\ell = 500$ m $r_e = 1000$ m $k_h = 400$ mD
$h = 40$ m $k_v = 25$ mD $r_w = 0.12$ m

We will choose $k' = \sqrt{k_v k_h}$ which gives $k' = \sqrt{k_v k_h} = 100$ mD

---

*Translator's Note: Approximate English equivalent: Instrumentation and Measurement System for use in Horizontal Wells.

The relation involving the vertical element will have as factor:

$$\left(\frac{k'}{k_v}\right)^{1/2} = \left(\frac{100}{25}\right)^{1/2} = 2$$

The relation involving the horizontal element will have as factor:

$$\left(\frac{k'}{k_h}\right)^{1/2} = \left(\frac{100}{400}\right)^{1/2} = 1/2$$

The case under discussion thus amounts to:

$\ell' = 250$ m $r'_e = 500$ m $r'_w = 0.12$ m.

$h = 80$ m $k' = 100$ mD

As regards the radius, we can consider here that it hardly changes at all, i.e. $r'_w = r_w$. In fact, by the relation defined above, the circular section of the well, as seen normal to the latter, becomes an ellipse with a major vertical axis of 0.24 m and a minor horizontal axis of 0.06 m. A line of reasoning may be established similar to that leading to relation (3) in subsection 2.1, for a well equivalent to a fracture with a radius a quarter of the extent of that fracture. The ellipse with a major axis of 0.24 m is equivalent to a circle of radius 0.12 m.

In addition, let us note that if we had had to consider a vertical well or radius, $r_w = 0.12$ m, it would have been transformed by the relation into a well of half the radius, $r'_w = 0.06$ m, producing from double the height.

(5) These are theoretical calculations. The practical stimulation of horizontal wells is still at the research stage. We have not attempted it in the framework of our project; nor, to our knowledge, has Shell tested this concept on actual wells.

(6) If one wishes to use this formula with practical units, the multiplying coefficient 0.837×10^{-3} must be introduced into the right-hand term.

(7) These are as follows: $a = 400$ m; $\ell = 400$ to 800 m; $h = 10$ m.

(8) These values merely indicate tendencies; having been obtained from a limited number of specific cases, they should not be used indiscriminately.

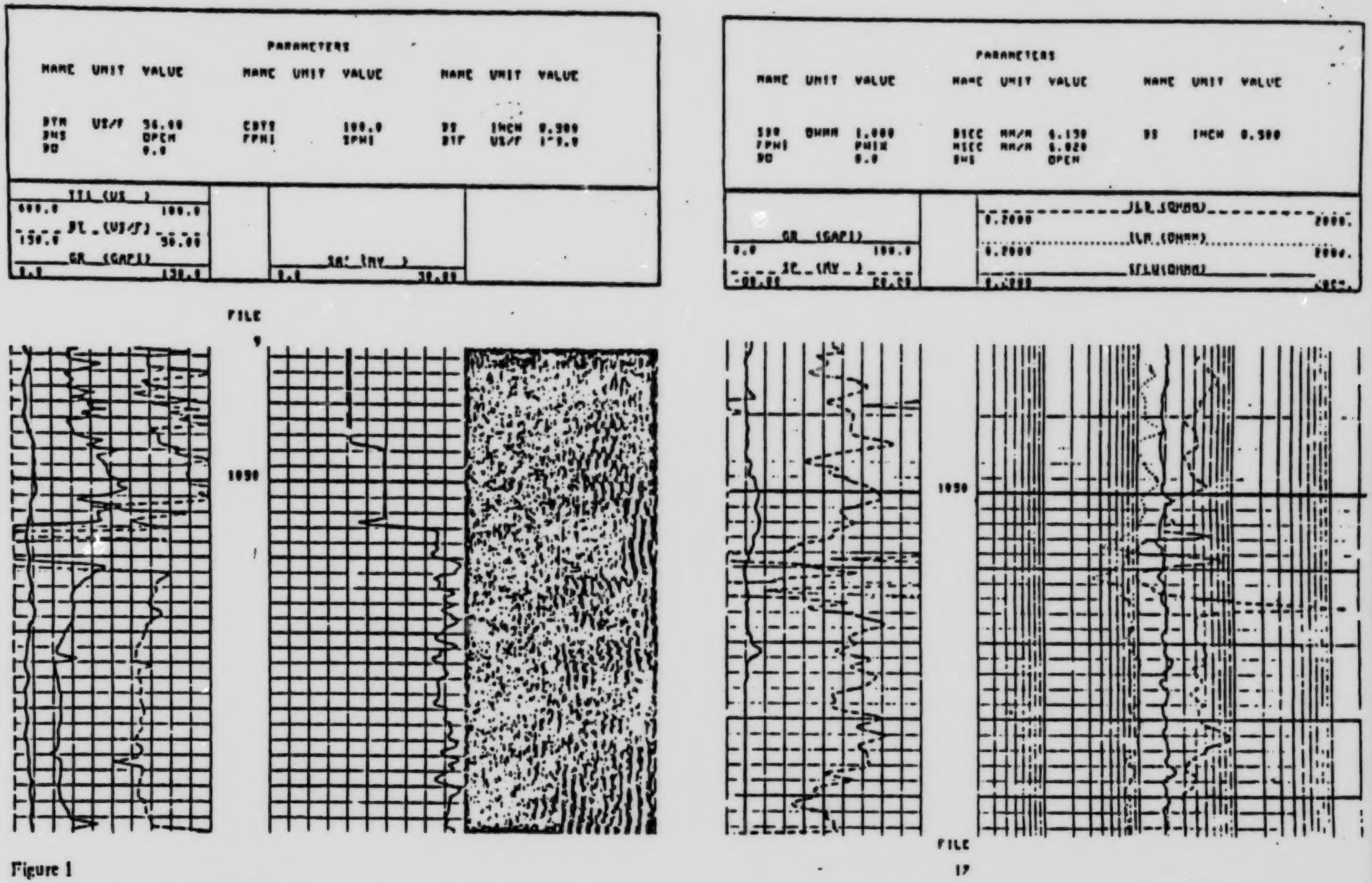

Figure 1

Diagraphies du puits horizontal Lacq 91.

Logs of the Lacq 91 horizontal well.

The fractured zone located between 1051 and 1056 m is clearly apparent on these high-quality logs. The dark area on the VDL indicates a considerable attenuation of the signal. On the transit-time record, sudden jumps indicate characteristic pulses. Induction measurements also reveal significant variations. In order to interpret the logs it was necessary to lower the signal intensity curve 3.5 m and raise the gamma ray curve 1.6 m so as to bring them to a common datum.

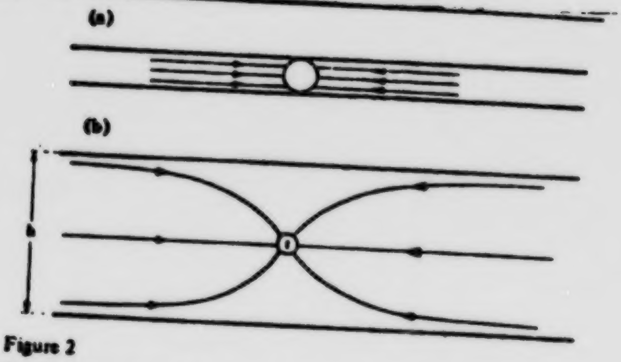

Figure 2

Coupes perpendiculaires à l'axe du drain montrant la concentration des lignes de courant à son voisinage.

Cross-section perpendicular to the axis of the horizontal well, showing the concentration of stream lines in its vicinity.

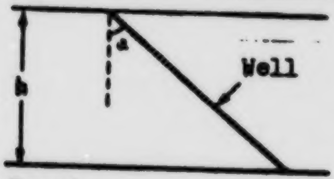

Figure 3

Puits producteur incliné.

Slanted production well.

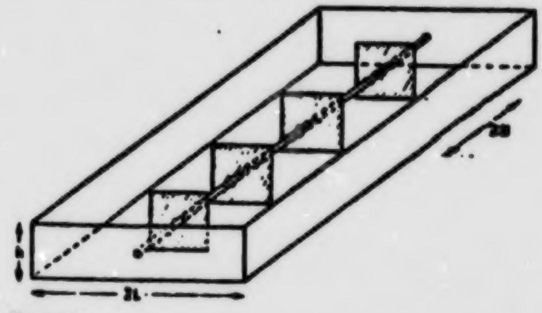

Figure 4

Forage horizontal multi-fracturé drainant une couche parallélépipédique.

Multifractured horizontal well producing from a parallelipipedic payzone.

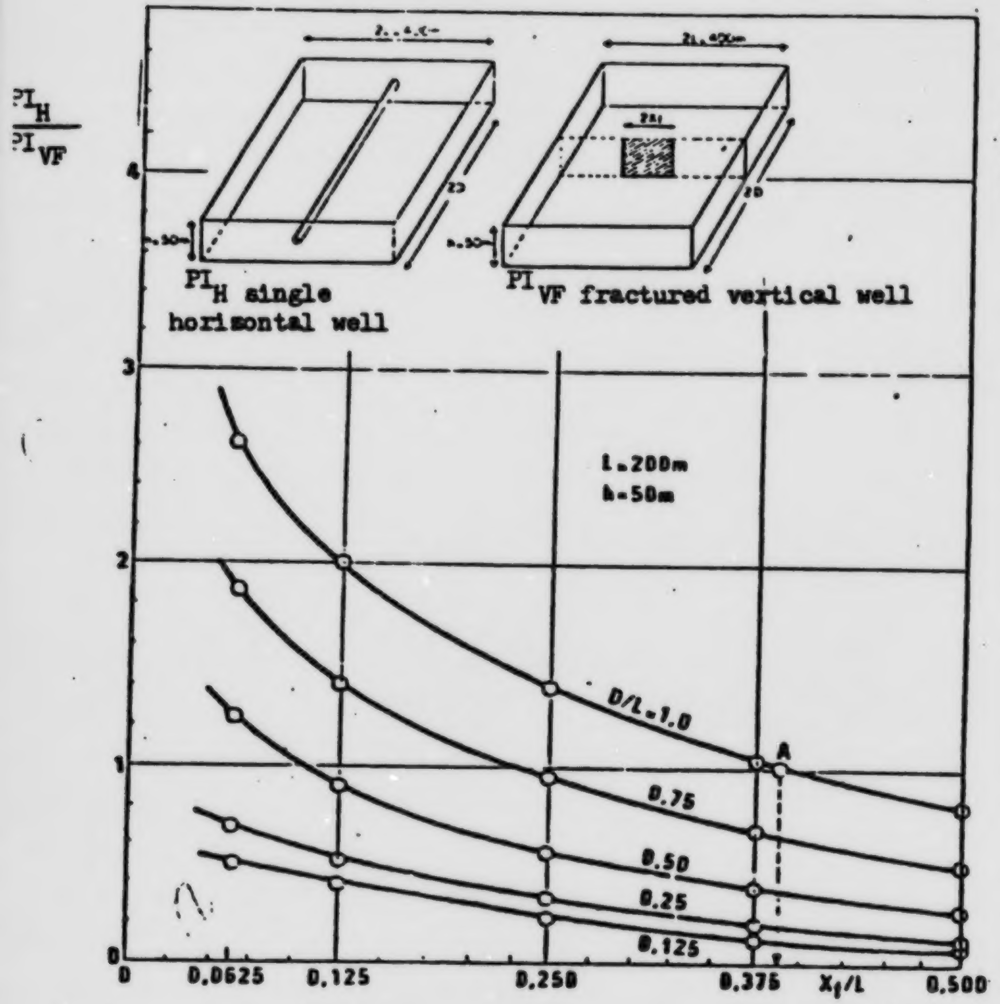

Figure 5

Intérêt du puits horizontal par rapport à un puits vertical fracturé.

Advantage of a horizontal well compared with a fractured vertical well

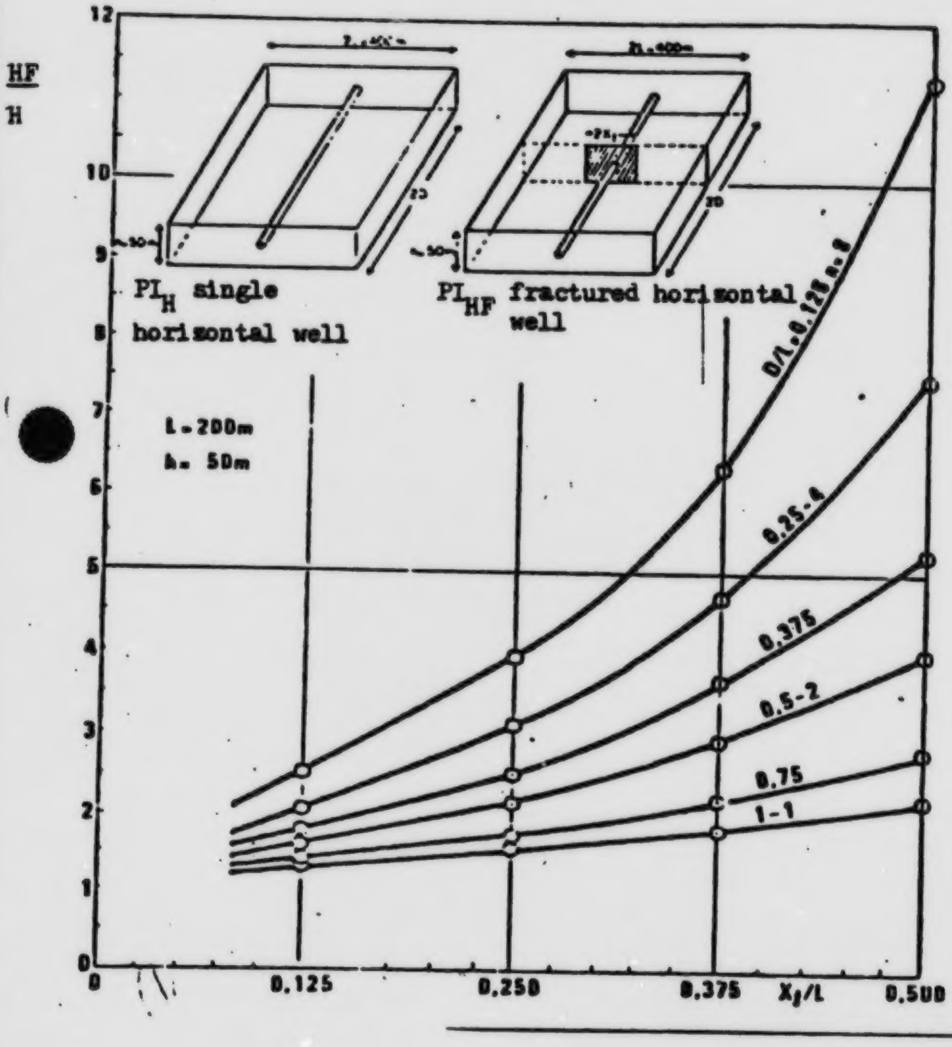

Figure 6

Valorisation du puits horizontal par des fractures.

Improving a horizontal well by fracturing.

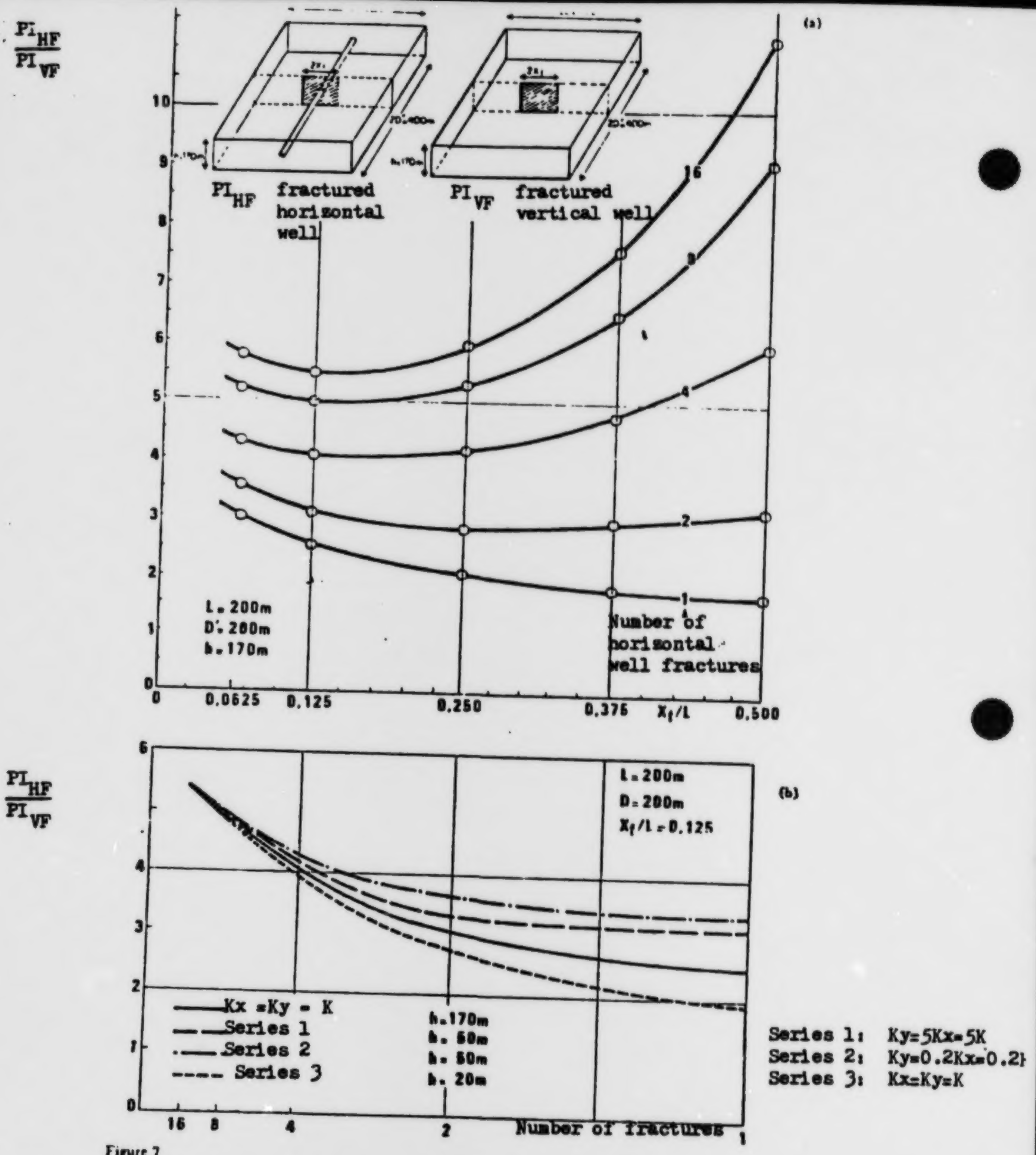

Figure 7

Intérêt du puits horizontal fracturé par rapport à un puits vertical fracturé.
(a) Effet de l'espacement entre fractures. (b) Effet de l'anisotropie et de l'épaisseur du réservoir.

*Advantage of a fractured horizontal well compared to a fractured vertical well.
(a) Effect of the distance between fractures. (b) Effect of the anisotropy and the reservoir thickness.*

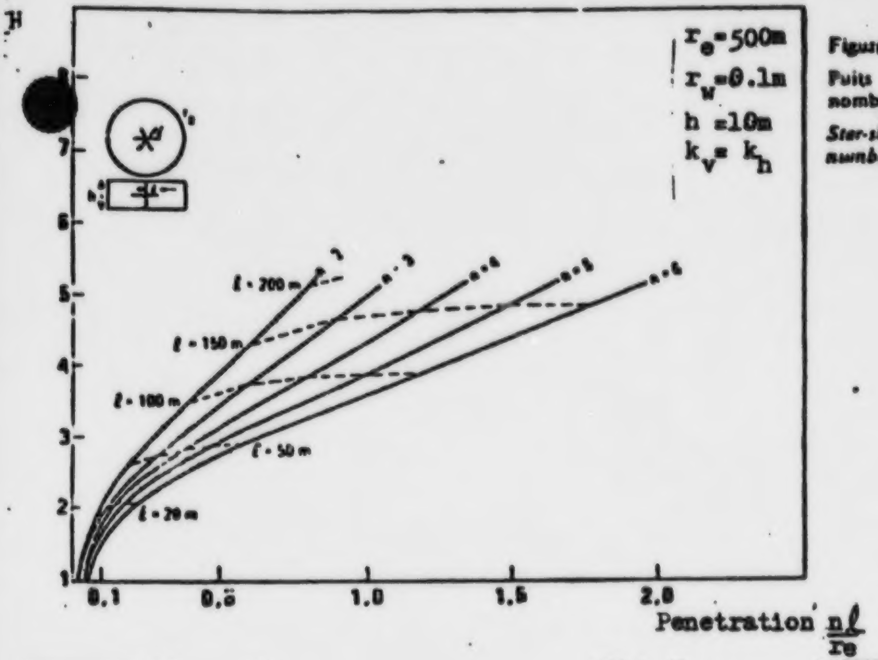

Figure 8

Puits horizontaux en étoile. Influence du nombre de branches.

Star-shaped drainage pattern. Influence of the number of branches.

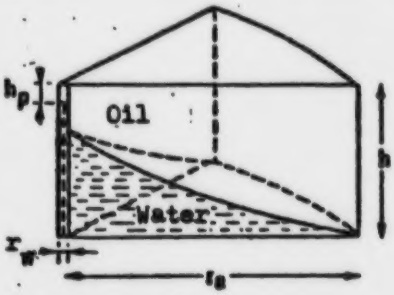
h_p
Oil
Water
h
r_w
r_e

Figure 9

Effet de cône à l'eau.

Waterconing.

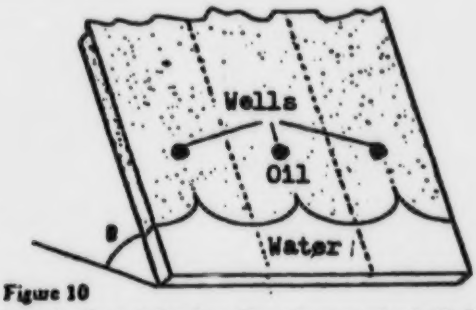
Wells
Oil
Water
θ

Figure 10

Montée d'eau de bordure d'un gisement plan incliné de faible épaisseur.

Waterfingering in a thin tilted layer.

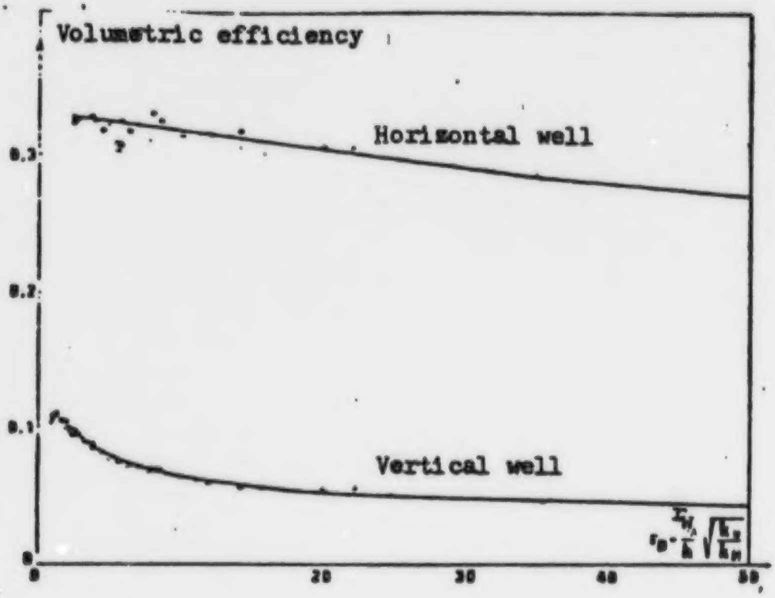

Figure 11

Efficacité volumétrique de balayage au débit critique.

Volumetric sweep efficiency at critical flow rate.

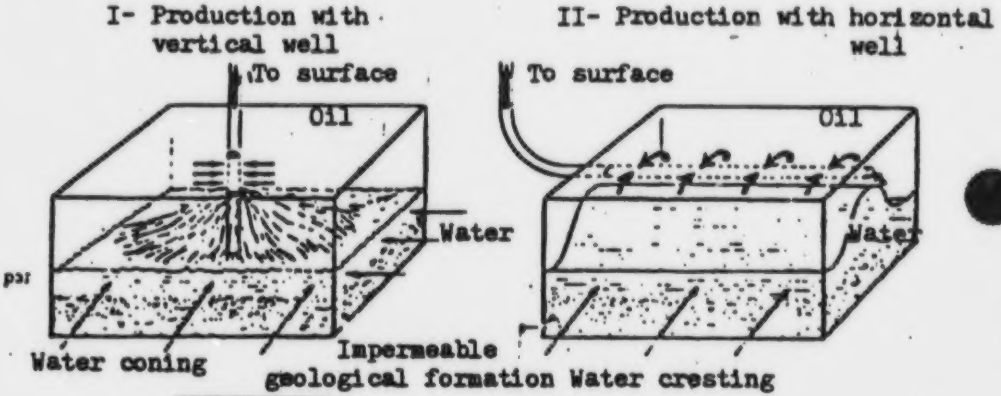
I- Production with vertical well
To surface
Oil
Water
Water coning
Impermeable geological formation
II- Production with horizontal well
To surface
Oil
Water
Water cresting

Figure 12

Déplacement de l'huile par l'eau.

Oil drive by water.

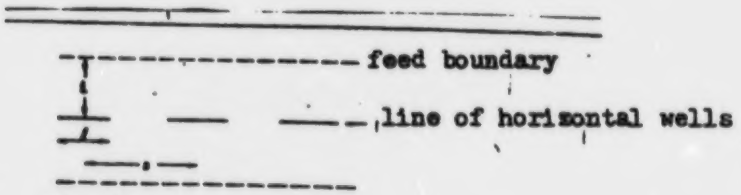
feed boundary
line of horizontal wells

Figure 13

Dispositif de puits horizontaux en ligne directe.

Horizontal wells in direct line-drive pattern.

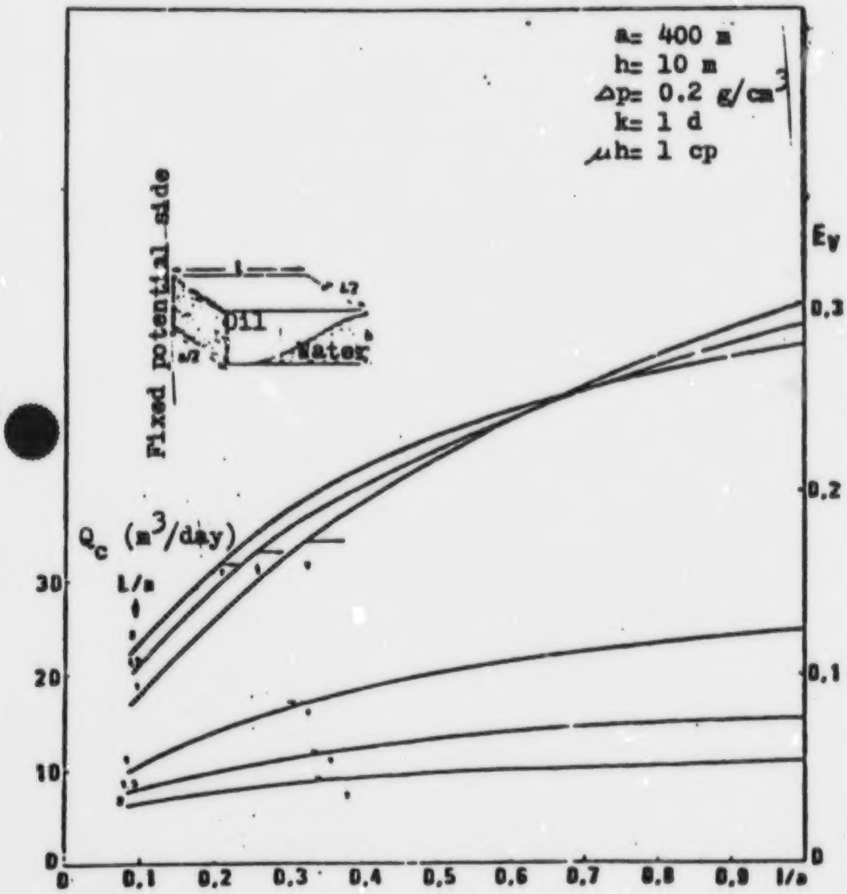

Figure 14

Débit critique et efficacité de balayage volumétrique pour un puits horizontal de longueur finie.

Critical flow rate and volumetric efficiency for a horizontal limited well.

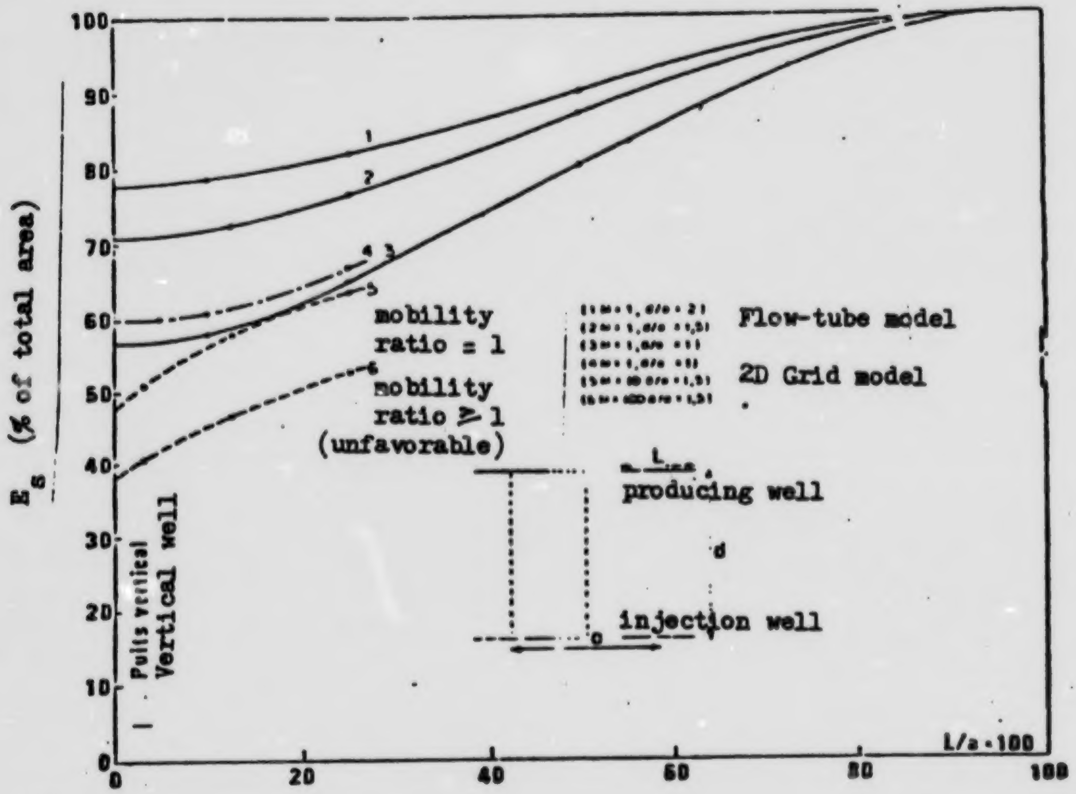

Figure 15

Balayage superficiel par puits horizontaux de longueur finie à régime supercritique.

Superficial sweep efficiency with horizontal wells of varying length (at breakthrough) in a line-drive pattern.

1769 E

Alberta OIL SANDS
INFORMATION CENTRE

Alberta

TRANSLATION SERVICES

PUBLIC WORKS, SUPPLY & SERVICES

403/427-9693
Telex 037-2055
6950 - 113 St.
3rd. Floor
Edmonton, Alberta, Canada
T6H 5V7 ~~T5J 0K5~~

73

FRENCH-ENGLISH

ORIGINAL TRANSLATION

ALBERTA PUBLIC WORKS SUPPLY & SERVICES
CERTIFIED
Jan. 16/84
J. Milne
Translation Service
TRUE TRANSLATION

TRANSLATED BY: MARY BOURNE

2 NOTATIONS

A : oil-field area
A_i : area drained by well "i"
a, b : sides of the parallelepiped rectangle (portion of formation)
B : constant
SWD : saving in well density
h : reservoir thickness
PI : productivity index
API : areal productivity index
k : permeability
Log : Napierian logarithm
ℓ : producing length of well
n : number of wells in production system D
p : well penetration into the oil-bearing stratum
q_1 : linear flow rate of the producing well
r : well radius
r' : apparent radius of the well equivalent to one horizontal well
r_e : drainage radius
RR : ratio of replacement of system D' by system D
Δp : withdrawal pressure of the producing well
μ : viscosity

In order to assist the reader in following the line of reasoning in the sequence of equations, each equation is preceded, as necessary, by one or more numbers in brackets indicating the number of the equation(s) used to establish it.

REDUCING THE NUMBER OF WELLS BY USING HORIZONTAL DRILLING [1]

351 [2]

F. Giger
Institut Français du Pétrole
1 et 4 avenue de Bois-Préau, BP 311
92506 Rueil-Malmaison Cedex, France

One of the advantages of horizontal drilling is the increase in productivity of each well. The aim of this article is to propose bases for making an analysis, such as areal productivity, so as to help the decision-maker responsible for the development of a field when confronted with an economic choice between a conventional system using vertical wells and an alternative system including other types of wells, and in particular horizontal wells. Simple and approximate solutions are proposed for evaluating the number of vertical wells that can be replaced by horizontal wells. [1]

REVUE DE L'INSTITUT FRANCAIS DU PETROLE [3]
VOL. 38, NO. 3, MAY-JUNE 1983

Translator's notes:

[1] Provided in English in the original text.
[2] Numbers shown in the margin indicate the page numbers of the original text.
[3] Approximate English equivalent: Journal of the French Petroleum Institute.

...2

I INTRODUCTION

One of the advantages of horizontal drilling is the increased productivity of each well. If comparative studies are to be carried out on each reservoir where horizontal drilling is planned, it is useful to compare, in general terms and with reference to a single well, production systems using vertical wells with different diameters, inclined wells and horizontal wells. The comparison should be made on the basis of the additional cost and the benefit involved, with the benefit expressed solely in terms of productivity.

The calculations given in the literature on this subject are limited, almost entirely, to evaluations of the productivity index. What we need in our rapidly changing economic, political and fiscal context, which is such that previously used calculation theories are frequently called into question, is an evaluation method which is relatively independent of economic data connected with the costing of a producing field and often unreliable techniques, such as discounting in particular.

The purpose of this article is to suggest analytical procedures which may help the decision-maker responsible for the development of a field decide which system - a conventional system using vertical wells (taken as a point of reference) or an alternative system using wells of a different diameter or horizontal wells - is more economical in situations where production is the same when the wells are subjected to an equal drop in bottom hole pressure (Fig. 1). We will then refer to a system of vertical wells equivalent to one horizontal well.

Consequently, this article proposes two simple methods for calculating the number of vertical wells that can be replaced by one horizontal well. One method makes use of charts, while the other uses a short BASIC language program for HP 9845 office computers.

The justification of these methods is given.

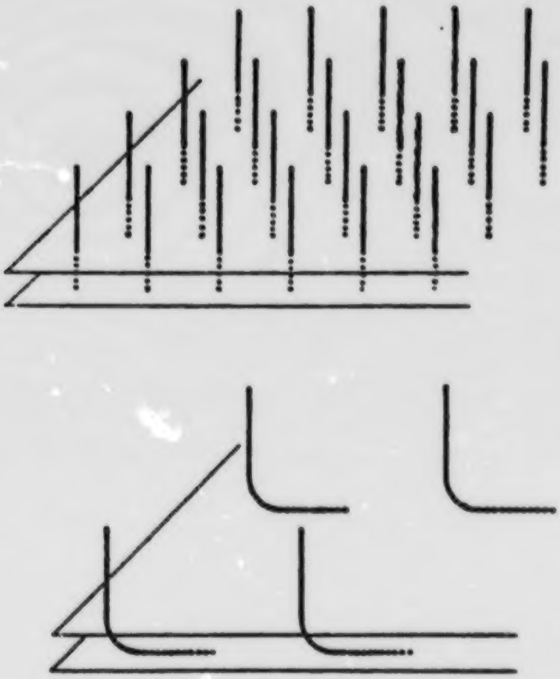

Figure 1

Equivalent production systems. [1]

53 II. SOLUTION USING CHARTS OR SHORT CALCULATION PROGRAMS

The charts shown in the attached figures provide a simple solution to the following problems:

II-A Number of vertical wells equivalent to one horizontal well with the same diameter and with given length

The calculation methods described below in II-B and II-C, used consecutively, provide an answer to this question. Let us go on to consider the following example:

- semipermanent flow
- horizontal well 500m long
- reservoir thickness, h=50m (It is assumed that vertical wells produce over their entire length.)
- radius of wells, r=0.1m
- drainage radius of vertical wells, r_e=650m

Translator's note:

[1] Provided in English in the original text.

...5

On the chart in Figure 2b, taking $r_e = 650m$, the intersection with the curve $h = 50m$ gives $r' = 76m$.

On the chart in Figure 3a, taking $r'/r = 76/0.1 = 760$, the intersection with the curve $r_e/r = 650/0.1 = 6,500$ shows that one horizontal well is equivalent to 3.[illegible]5 vertical wells.

A program in BASIC language for an [illegible] 9845 office computer, which also provides an answer to this problem, has been written by the author (1). Given the length of wells, their spacing, reservoir thickness and diameter of drilled wells, it calculates the spacing of the equivalent vertical wells and the number of vertical wells which one horizontal well replaces.

II-3 Apparent radius of a vertical well which is equivalent to a horizontal well

Figures 2a, 2b and 2c show three charts for wells with a 10cm radius and lengths of 100m, 500m and 1,000m respectively.

Using the chart showing the corresponding well length and radius, and starting from the drainage radius, r_e, as the abscissa, the apparent radius, r', is obtained as the ordinate on the curve representing the thickness of the oil-bearing stratum.

Let us consider the following example:

$$\text{Given data:}\quad \begin{cases} \text{well length } 100m \\ \text{well radius } 0.1m\ (\varnothing\ 0.2m) \\ h = 20m \\ r_e = 110m\ \ (2) \end{cases}$$

Result (Fig. 2a): $r' = 11.5m$

This is the apparent radius of a vertical well which is equivalent to one horizontal well. A program in BASIC language enables us to calculate the numerical values necessary in order to draw charts of the type shown.

---

(1) The program will be sent to readers upon request.

(2) It is to be recalled that the drainage radius is equal to 0.56 times the spacing between two neighbouring wells in a five-spot pattern.

...6

II-C Evaluation of the saving in well density by multiplying the radius "r" of a well by a given "r'/r" factor

For a given reservoir, two development systems are considered which have the same production per unit area under equal withdrawal pressure. Both are of the five-spot type but differ with respect to the radius of wells and the spacing between the wells. The radius of the reference wells is represented by "r" and that of the wells belonging to the other system by "r'". The well density is defined as the average number of wells per unit area.

Figures 3a and 3b are to be used for semipermanent and permanent flows respectively.

On each figure, it is necessary to choose from among the five curves the one which best corresponds to the ratio of the drainage radius to the radius of the reference wells (r_e/r). On Figure 3b the curves have been drawn for the Napierian logarithms of r_e/r of 5,6,7,8 and 9.

If we take r'/r as the abscissa, the saving in well density is obtained as the ordinate on the appropriate curve.

Let us take the following example:

Given data: $\begin{cases} r_e/r = 1{,}100 \\ r'/r = 115 \\ \text{permanent flow} \end{cases}$

Result (Fig. 3b): SWD = 0.61

356 A saving in well density of the order of 60% is obtained, which means that in a regular layout pattern, 10 wells with radius "r" can be replaced by 4 wells with an apparent radius "r'", or that each of the latter replaces 2.5 wells with radius "r".

III. THEORETICAL JUSTIFICATION

As a first step, calculations are provided for permanent flows, obtained in a steady state with lateral feed and average pressure from uniform drainage areas in the formation (3). Secondly, the pseudo-permanent flow is studied. Only the formulae which differ from those first obtained are rewritten.

---

(3) These theoretical results may be extended to the sweeping study for oil recovery assisted by water flooding, using the five-spot pattern if the mixed mobility ratio $\frac{k_e}{\mu_e}\,\frac{\mu_h}{k_h}$ is close to 1.

...7

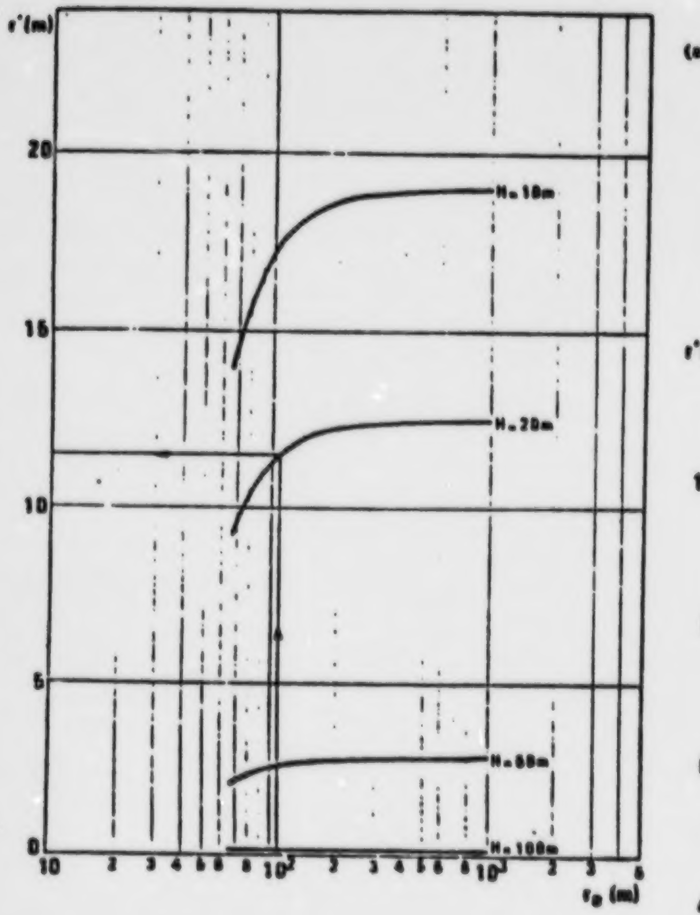

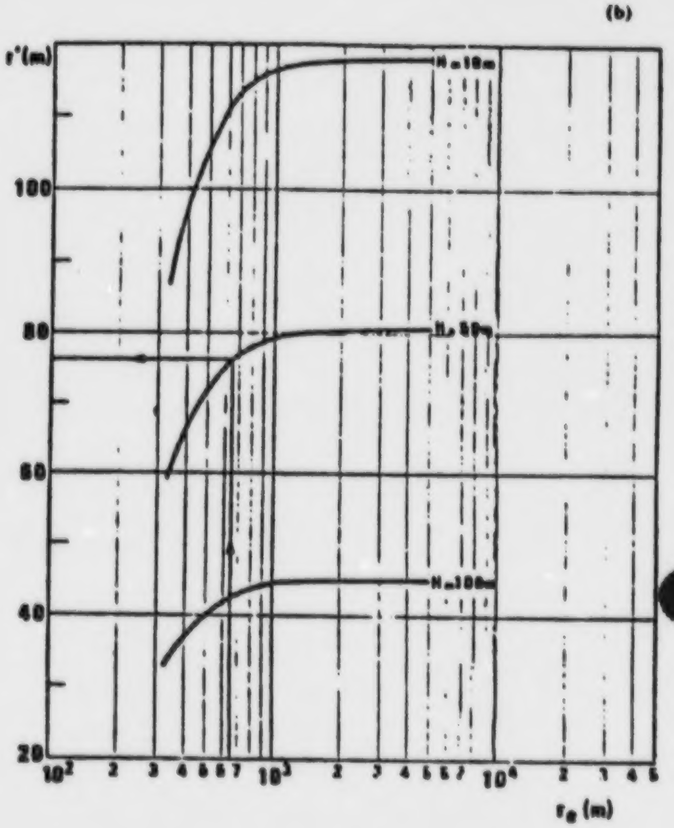

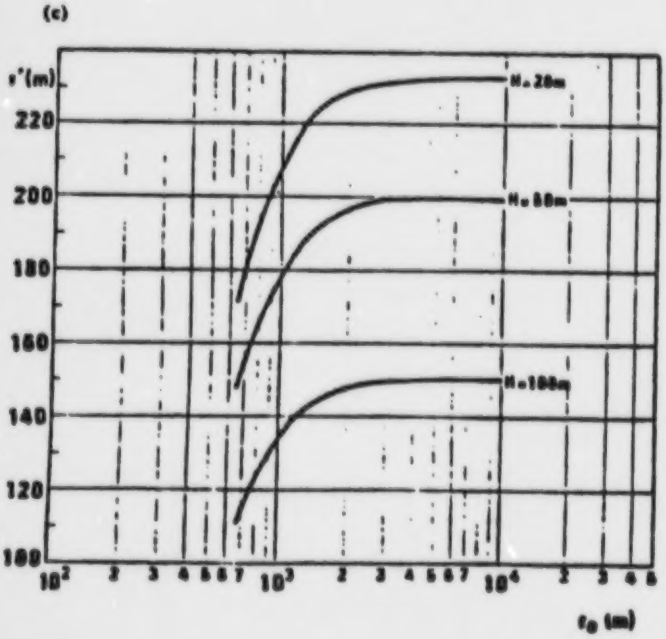

Figure 2

Radius of an equivalent vertical well

(a) Horizontal well 100m long, 0.20m in diameter
(b) Horizontal well 500m long, 0.20m in diameter
(c) Horizontal well 1000m long, 0.20m in diameter [1]

34

Translator's note:

[1] Provided in English in the original text.

...3

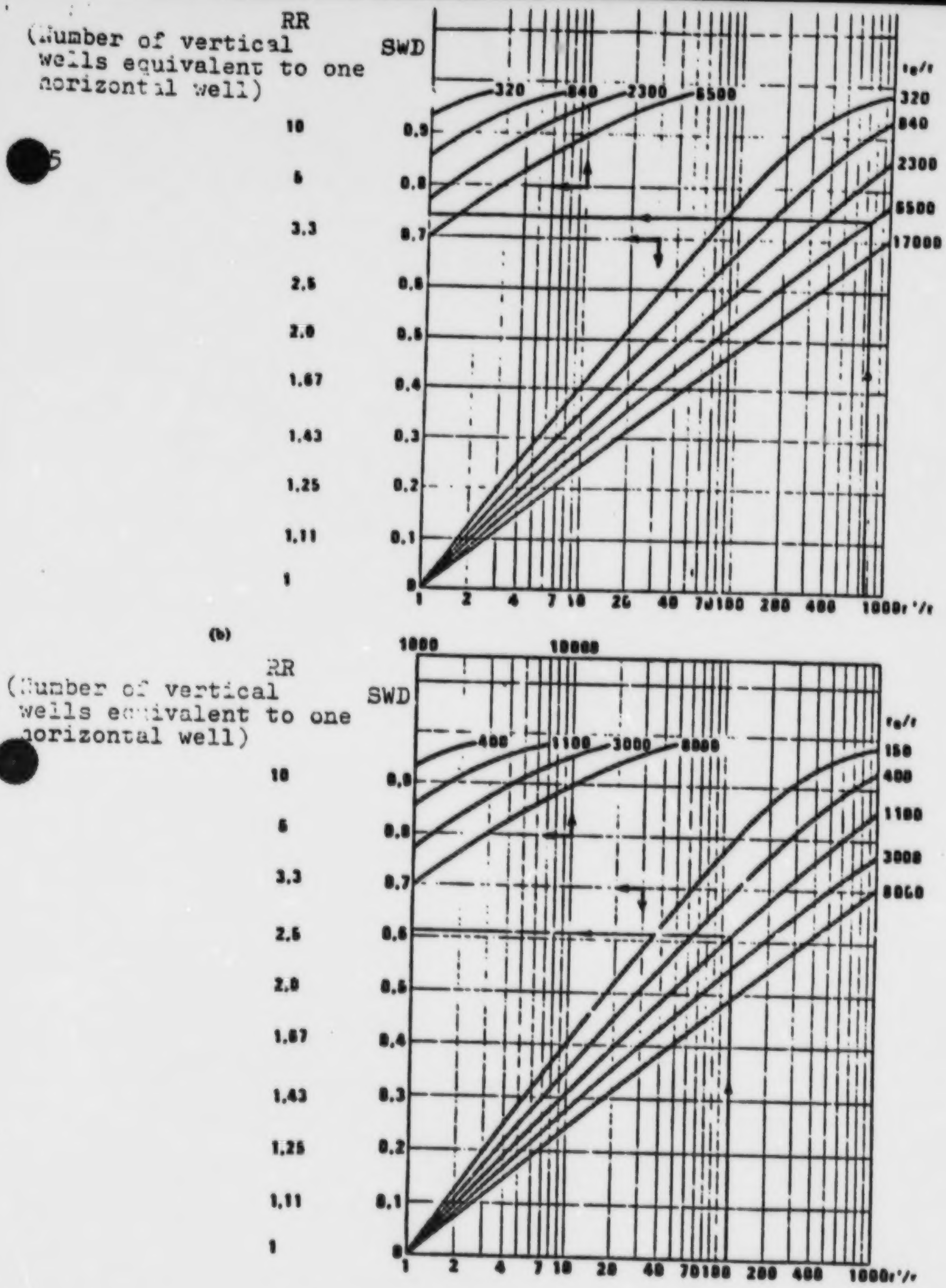

Figure 5

Vertical wells equivalent to a horizontal well
a) Semipermanent flow; b) Permanent flow [1]

Translator's note:

[1] Provided in English in the original text.

III-A Equivalent areal productivity

It is to be recalled that for a vertical well, the productivity index, defined as the ratio of the produced flow rate to the pressure drop during withdrawal, is approximately expressed by the following equation:

$$\mathrm{PI} = 2\pi \frac{k}{\mu} \frac{h}{\mathrm{Log}\left(\frac{r_e}{r}\right)} \qquad (1)$$

Let us define API_i, the areal productivity index of a well "i" draining an area A_i, as follows:

$$\mathrm{API}_i = \frac{\mathrm{PI}_i}{A_i} \qquad (2)$$

We will now apply this concept, defined for a single well, to an entire reservoir.

In a field drained by a system of wells which have the same productivity index (PI) and are regularly spaced so that the areas drained by each are equal, the areal productivity indexes are equal. The same value as that of a single well can be used to define the areal productivity index of the system of wells in the field.

In a more general manner, we will define the areal productivity index (API) of a system of wells "D" draining a field with area "A" as follows:

$$\mathrm{API}_D = \frac{\sum_{i \in D} (\mathrm{PI}_i)}{A} \qquad (3)$$

Just as two wells with the same productivity index have the same rate of production under equal withdrawal pressure, two systems of drainage wells which are draining the same field and have the same areal productivity index have the same overall rate of production under the same withdrawal pressure, assumed as equal at the bottom of all the wells.

Thus, two systems of drainage wells, D and D', containing "n" and "n'" wells respectively, will be considered equivalent with respect to productivity if they drain the same field and have the same areal productivity index.

In addition, if we assume that the wells within each system have the same productivity index and that each drains an equal area, we obtain for any two wells "i" and "j", one from each of the two systems:

$$API_i = API_j \quad i \in D, j \in D' \tag{4}$$

The wells have the same areal productivity index. They are not, however, equivalent with respect to productivity since they do not necessarily drain the same area and do not have the same productivity index. According to these hypotheses, if the drainage radius "$r_{e,i}$" of a well "i" is defined from the area drained by the well "A_i", as follows:

$$r_{e,i} = \sqrt{\frac{A_i}{\pi}} \tag{5}$$

then for the two wells "i" and "j" defined above as having the same areal productivity index, we have:

(4)(5)
$$\frac{PI_i}{(r_{e,i})^2} = \frac{PI_j}{(r_{e,j})^2} \tag{6}$$

357 III-B Saving in well density where areal productivity indexes are equal

Let us consider two systems of drainage wells, D and D', capable of draining the same field and equivalent with respect to productivity. It is assumed that the wells within each system have the same productivity index (PI_p) and drain the same area (A_p). It is also assumed that the field is large enough that any boundary effects may be disregarded.

The saving in well density (SWD) of system D', which contains n' wells, in relation to system D which contains less productive n wells, is defined as follows:

$$SWD = \frac{n - n'}{n} \tag{7}$$

...11

SWD expresses the percentage of wells which are saved in system D', in relation to system D, through an increase in the areal productivity index.

If A represents the area of the field:

$$n = \frac{A}{A_p} \qquad (8)$$

$$(5)(8) \qquad n = \frac{A}{\pi r_e^2} \qquad (9)$$

$$(7)(9) \qquad \mathrm{SWD} = 1 - \left(\frac{r_e}{r'_e}\right)^2 \qquad (10)$$

The same principle may also be used in defining the ratio of replacement (RR) of system D' by system D as the number of wells in D which one well in D' replaces. This is expressed as follows:

$$RR = \left(\frac{r'_e}{r_e}\right)^2 \qquad (10')$$

III-C Saving in well density by replacing vertical wells with radius "r" by vertical wells with radius "r'"

The same areal productivity index is obtained as follows:

$$(1)(6) \qquad \frac{2\pi kh}{\mu} \frac{1}{\mathrm{Log}\frac{r_e}{r}} \frac{1}{r_e^2} = \frac{2\pi kh}{\mu} \frac{1}{\mathrm{Log}\frac{r'_e}{r'}} \frac{1}{r'^2_e} \qquad (11)$$

$$(11) \qquad \left(\frac{r}{r_e}\right)^{-r_e^2} = \left(\frac{r'}{r'_e}\right)^{-r'^2_e} \qquad (11')$$

$$(11')(10') \qquad \frac{r'}{r} = \sqrt{RR}\left(\frac{r}{r_e}\right)^{\frac{1}{RR}-1} \qquad (12)$$

ou :

$$(10)(10')(12) \qquad r' = \frac{r}{\sqrt{1-\mathrm{SWD}}}\left(\frac{r}{r_e}\right)^{\mathrm{SWD}} \qquad (12')$$

The chart in Figure 3b shows the last equation. The curves of the SWD function (r'/r) are drawn for Log values (r_e/r), typical of those found in industrial applications. The charts may also be used to evaluate the advantage of stimulation or fracturing processes for vertical wells when the apparent radius of the well is known.

A practical example of what has just been established was given above in II-C.

III-D Productivity index of a short horizontal well

For a very thin stratum, the thickness of which is about the same as the well diameter (Fig. 4a), the pressure
358 drops only result from the flow on the horizontal plane (Fig. 5).

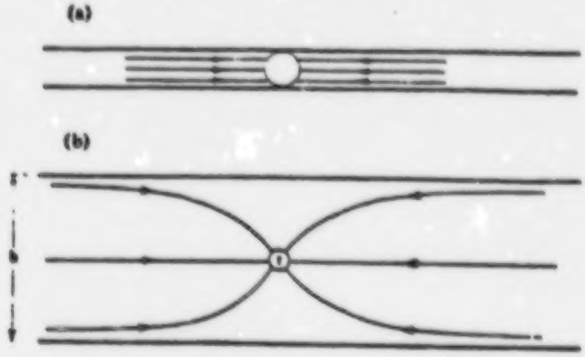

Figure 4a and 4b

Cross-section perpendicular to the axis of the horizontal well, showing the concentration of stream lines in its vicinity. [1]

The productivity index for such a well is expressed as follows (Ref. 1, p. 103; Ref. 2, p. 27):

$$\mathrm{PI} = \frac{2\pi k}{\mu} \frac{h}{\mathrm{Log}\, \dfrac{1 + \sqrt{1 + \left(\dfrac{L}{2r_e}\right)^2}}{\dfrac{L}{2r_e}}} \qquad (13)$$

This expression is only valid when the well length is short in relation to the drainage radius (r_e).

Translator's note:

[1] Provided in English in the original text.

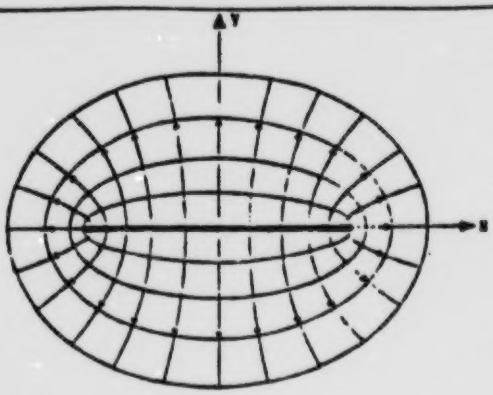

Figure 5

Pattern of stream lines moving toward a horizontal well. [1]

When the stratum is thick in relation to the well diameter, an additional pressure drop must be taken into account; this drop results from the concentration of stream lines moving toward the well in the vertical plane perpendicular to the well axis. When the well is long in relation to the thickness of the stratum and laterally fed, the pressure drop is expressed as a function of the linear flow rate (q_1) or produced flow rate per unit length (Ref. 3, p. 18)(Fig. 4b).

$$\Delta p = \frac{\mu}{k}\frac{q_1}{2\pi} \text{ Log}\left(\frac{h}{2\pi r}\right) \qquad (14)$$

The reader will have realized, on noting the logarithmic function, that the circular radial convergence of the stream lines has been taken into account.

We will consider that the pressure drop in the flow toward the well is the sum of two terms: one, which accounts for the partial penetration of the drainage area, is that established for a horizontal well in (13)(Fig. 5); the other, which accounts for the axial convergence of the stream lines, is that used to represent the circular radial flow perpendicular to the well axis.

The productivity index is then expressed as follows:

$$\overset{(13)(14)}{PI} = 2\pi\frac{k}{\mu}\,\frac{1}{\dfrac{1}{h}\text{ Log }\dfrac{1+\sqrt{1+\left(\dfrac{\mathcal{L}}{2r_e}\right)^2}}{\dfrac{\mathcal{L}}{2r_e}} + \dfrac{1}{\mathcal{L}}\text{ Log}\left(\dfrac{h}{2\pi r}\right)} \qquad (15)$$

...14

Translator's note:

[1] Provided in English in the original text.

By combining the preceding result with the evaluation, already used above, of the pressure drop resulting from the concentration of stream lines toward the well and perpendicular to its axis, we obtain the productivity index of a long well, as follows:

(14)(16)

$$PI = 2\pi\frac{k}{\mu}\frac{1}{\frac{1}{h}\,\mathrm{Argch}\left[\frac{\mathrm{ch}\ \frac{\pi}{2}\frac{a}{b}}{\sin\ \frac{\pi}{2}\frac{\mathcal{L}}{b}}\right] + \frac{1}{\mathcal{L}}\,\mathrm{Log}\left(\frac{h}{2\pi r}\right)} \quad (17)$$

It is verified that the formula again gives a known expression (Ref. 2, p. 21) when the well length ($\mathcal{L}$) is the same as side "b" of the parallelepiped, as follows:

$$(17) \qquad PI = 2\pi\frac{k}{\mu}\frac{b}{\frac{\pi}{2}\frac{a}{h} + \mathrm{Log}\left(\frac{h}{2\pi r}\right)}$$

$$\text{where } \frac{\mathcal{L}}{b} = 1 \quad (18)$$

When the well length is short in relation to side "b" of the parallelepiped, which is parallel to the well, formula 17 provides an asymptotic expression very similar to that shown in formula 15. The difference between them reflects the different conditions of supply.

III-F Equivalent radius (r') of a vertical well which would have the same productivity index as a horizontal well

The equivalent radius (r') of a vertical well which would have the same productivity index as a horizontal well that is short in relation to the drainage radius is obtained by equating the expressions of their respective indexes, (1) and (15), as follows:

(1)(15)

$$2\pi\frac{k}{\mu}\frac{h}{\mathrm{Log}\frac{r_e}{r'}} =$$

$$2\pi\frac{k}{\mu}\frac{h}{\mathrm{Log}\dfrac{1+\sqrt{1+\left(\frac{\mathcal{L}}{2r_e}\right)^2}}{\frac{\mathcal{L}}{2r_e}} + \frac{h}{\mathcal{L}}\mathrm{Log}\left(\frac{h}{2\pi r}\right)} \quad (19)$$

III-E Productivity index of a well which is laterally fed through the reservoir boundaries parallel to the well

The preceding equation was obtained for wells which are short in relation to the drainage radius; that is, small ℓ/r_e. In the case of long wells, the edge of the area drained becomes oval-shaped and the concept of drainage radius is no longer particularly adequate. A better method of accounting for flows in this case is to place the horizontal well in the centre of a parallelepiped rectangle, taken as a portion of the formation. The size and laterally-fed sides are to be defined by taking the distribution of the neighbouring wells into account.

We will now consider the production pattern shown in Figure 6, where the parallelepiped of the formation is fed
359 through the two vertical sides parallel to the well. As we did for a short well in III-D above, we will assume that the total drop in flow pressure is the sum of the pressure drops calculated on the horizontal plane and those resulting from the concentration of stream lines toward the well and perpendicular to its axis.

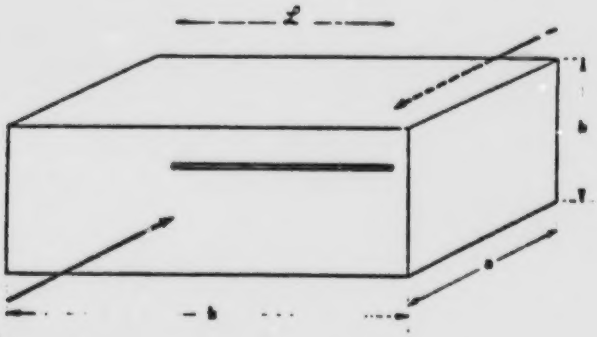

Figure 6

Long horizontal well fed laterally from two sides. [1]

Pressure drops calculated on the horizontal plane are those which would be found when drainage occurs through a vertical fracture crossing the formation from top to bottom and equal in length to the horizontal well. Such pressure drops are due to the reduced parallel flow or parallel flow with reduction in section (Ref. 1, p. 104); that is:

$$\Delta P = \frac{\mu}{k}\frac{q_1}{2\pi h}\,\mathrm{Argch}\,\frac{\mathrm{ch}\left(\frac{\pi}{2}\frac{a}{b}\right)}{\sin\left(\frac{\pi}{2}\frac{\ell}{b}\right)} \qquad (16)$$

Translator's note:

[1] Provided in English in the original text.

That is:

$$(19) \qquad r' = \frac{\mathcal{L}}{2} \frac{\left(\frac{2\pi r}{h}\right)^{h/\mathcal{L}}}{1 + \sqrt{1 + \left(\frac{\mathcal{L}}{2r_e}\right)^2}} \qquad (20)$$

This expression is not largely depedent on the drainage radius (r_e), inasmuch as the horizontal well is shorter than the drainage radius. It is verified that, for very thin layers, this expression again gives results already obtained elsewhere for two-dimensional flows and recalled above in (13).

Figures 2a, 2b and 2c show the results obtained for wells having a diameter of 0.20m and lengths of 100m, 500m and 1000m respectively. An example of the use of charts has been given above in II-A.

III-G Formulae obtained under pseudo-permanent flow

The permanent flow pattern is of limited use in representing the production mechanisms of reservoirs. Frequently the pseudo-permanent flow pattern is used (Ref. 5, p. 45), particularly when the production mechanism is similar to the expansion of an undersaturated oil.

For a vertical well, the consideration of the pseudo-steady stage involves the introduction of a fictitious skin-effect factor (Ref. 2, p. 148). This process may also be applied to the study of horizontal wells. The entire procedure described above can be followed again point by point; the formulae obtained are very similar. The reader will find them below, accompanied by an asterisk when they differ from those previously obtained. No comments are provided since the line of reasoning is based on that described above.

$$\mathrm{PI} = 2\pi \frac{k}{\mu} \frac{h}{\mathrm{Log}\left(\frac{r_e}{r}\right) - \frac{3}{4}} \qquad (1^*)$$

$$(1^*)(6) \qquad \frac{2\pi k h}{\mu} \frac{1}{\mathrm{Log}\left(\frac{r_e}{r}\right) - \frac{3}{4}} \frac{1}{r_e^2} =$$

$$\frac{2\pi k h}{\mu} \frac{1}{\mathrm{Log}\left(\frac{r_e'}{r'}\right) - \frac{3}{4}} \frac{1}{r_e'^2} \qquad (11^*)$$

$$(11^*) \qquad \left(\frac{2{,}117\, r}{r_e}\right)^2 = \left(\frac{2{,}117\, r'}{r_e'}\right)^2 \qquad (11'^*)$$

$$(10')(11^*) \quad \frac{r'}{r} = \sqrt{RR}\left(\frac{2.117\,r}{r_e}\right)^{\frac{1}{RR}-1} \qquad (12^*)$$

$$(10)(10')(12^*) \quad r' = \frac{r}{\sqrt{1-\mathrm{SWD}}}\left(\frac{2.117\,r}{r_e}\right)^{\mathrm{SWD}} \qquad (12'^*)$$

The chart in Figure 3a shows the last equation. The curves of the SWD function (r'/r) are drawn for Log values (r_e/r), typical of those found in industrial applications.

IV. CONCLUSION

This study enables us to compare vertical wells and horizontal wells from the standpoint of productivity. It should be noted that the hypotheses concerning regularity and vertical anisotropy in reservoir permeability generally favour horizontal wells. For vertically fractured reservoirs, however, more favourable results can be expected.

Still, the approach described in this study has some merit, in that it is relatively independent of the uncertainties of economic theory and introduces certain elements for analysis, such as areal productivity, which may be of assistance in studying this subject.

Simple solutions are proposed for evaluating the number of vertical wells which can be replaced by one horizontal well.

The author wishes to thank Messrs. L.H. Reiss of the Société Nationale Elf Aquitaine and J. Combe of the Institut Français du Pétrole for their advice during the writing of this article.

BIBLIOGRAPHY

1 Houpeurt A. - Eléments de mécanique des fluides dans les milieux poreux. Editions Technip, 1975.

2 Giger F. - "Utilisation des fonctions analytiques pour représenter des écoulements fluides plans incompressibles". IFP Report, Ref. 29631, Nov. 1981.

...18

3 Borisov P. Ju. - *Exploitation des gisements de pétrole par puits horizontaux et à déviations multiples.* Moscow "Nedra" 1964. Translation from Russian into French: IFP document, Ref. 20363.

4 Muskat M. - "The performance of bottom water-drive reservoirs". *Transaction AIME*, vol. 165, p. 98, 1946.

5 Chaumet P. - *Ecoulement monophasique des fluides dans les milieux poreux.* *Cours de production*, vol. III, Editions Technip, 1965.

Final manuscript received in December 1982.

010593

Alberta OIL SANDS INFORMATION CENTRE

74

UNDERGROUND-ACCESS OIL RECOVERY--A CONCEPTUAL-THEORETICAL ANALYSIS

Mervyn A. de Four
Petrotec Systems, Inc.

ABSTRACT

A conceptual and theoretical review is presented of the radial and linear *Gravity Drainage Mechanism* as it applies to oil recovery by subsurface-access (e.g., oil mining) methods. Gravity drainage as discussed herein refers to those systems in which fluid displacement is effected purely by a potential energy gradient between inflow and outflow ends and is independent of formation dip. However, it is also demonstrated that the effect of superimposed pressure drives on outflow performance is additive for potential energy terms. This gravity drainage oil recovery mechanism is known to yield high (±80% OOIP) oil recovery efficiencies but low per-well producing rates.

Possible methods of enhancing the gravity-flow rate capabilities of projects are proposed and examined theoretically. The consequences of a number of practicable but unusual upside-down well configurations and completion practices on recovery rates are quantified. Proposed configurations include various combinations of horizontal and vertical wells multi-fractured vertically and/or horizontally within common drainage areas. Probable production performance patterns for the best candidates are compared with the commonly practiced rate-enhancement approach of high-density drilling of vertical off-take wells. The relevance of several of the proposed methods to *surface* as well as *subsurface* application of the process is indicated. It is also suggested that variations of these methods can be used to enhance the recovery efficiencies of secondary and tertiary floods. Such an approach forms part of a new proprietary technology currently under development.

INTRODUCTION

Whenever the average outflow height of a fluid from a porous medium is less than its average inflow height to the system, gravity will act as a driving force to displace it outwardly. Fluid flow will continue until the system attains a minimum potential energy configuration. Such a process wherein gravity alone acts as the displacement mechanism has been termed *PURE GRAVITY DRAINAGE* (PGD) or *Gravity-Drip-Drainage*. The magnitude of the displacement force is readily identified [1] as the gradient of the fluid's average potential energy between the inflow and outflow ends. Even though some energy is lost in overcoming the resistance of the porous medium to fluid flow, the process has been shown [1, 2] to result in extremely high recovery efficiencies. Extensive laboratory experiments and limited field tests suggest that the recovery of 80% of O.O.I.P. may be possible with this process.

High recovery efficiencies are believed possible because of an unusual characteristic of certain gravity-flow systems: the development of a uniform pressure, *free-surface* during the outflow process. Such a *free-surface* is generated by the collective break-away of liquid from the upper portions of the medium as it falls to the lower level of the outflow face. This break-away process leaves behind only those oil globules trapped in dead-end or inaccessible pore spaces/channels resulting in a high fluid recovery efficiency.

Gravity-flow systems were originally studied in relation to the problems of Ground-Water Hydrology. The first comprehensive, albeit inexact, mathematical theory of the process was presented in 1863 by Dupuit-Forchheimer [3]. Although this theory proposed a solution *form* now recognized as *correct*, for system performance under specific conditions, its physical basis was incorrect in regard to the nature of the free surface. Thus extrapolations led to physically impossible conclusions. Wyckoff, Botset and Muskat [4] in 1932 studied the problem as applied both to *radial gravity drainage* or gravity drainage by radial flow into a vertical wellbore, and to linear gravity drainage. The extensive laboratory experiments and theoretical analyses conducted and published by these authors still form the basis of our current knowledge about the physics of the gravity drainage mechanism. The process is not to be confused with the down-dip *free-fall* gravity drainage observed in sloping porous media. PGD, which is the subject of this paper, is sustainable even in horizontal media of low to moderate thicknesses. The vertical free-fall rate capacity of the particular system does, however, define the upper limit to the flow rates attainable by PGD.

Gravity drainage occurs continuously, but to differing extents, in most common subsurface environments. Often, other high rate displacement

20th Intersociety Energy Conversion Engineering Conf, Miami Beach 18-23 August 1985

FIGURE 1
Schematic of an Underground-Access Oil Recovery Project

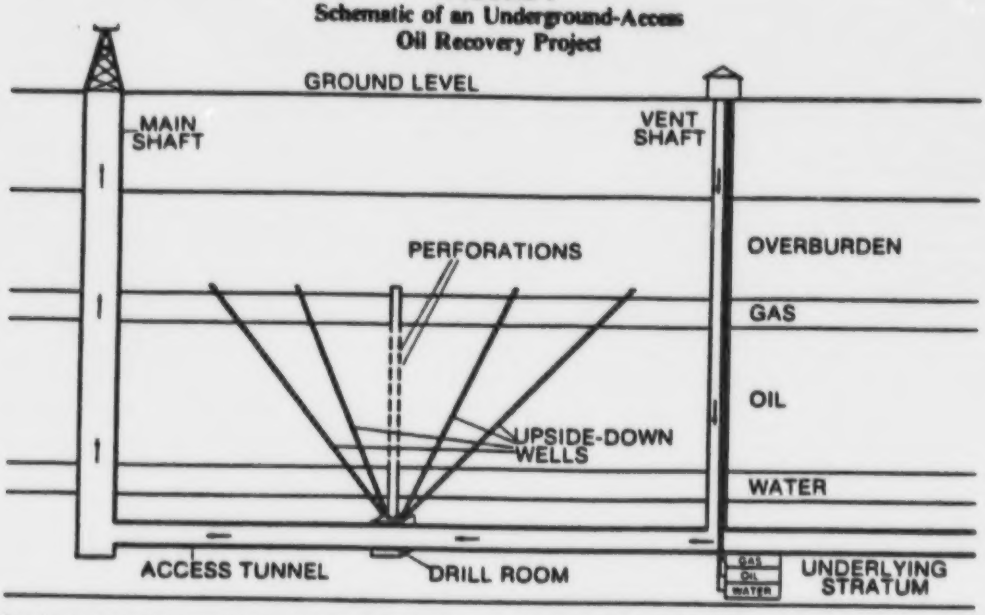

mechanisms operating concurrently, such as SGD, WD, or GCD, will obscure its contribution during primary oil recovery. In low or under-pressured reservoirs as well as in reservoirs nearing the end of their primary production cycle, gravity drainage is a distinguishable and dominant recovery mechanism. During the last decade, interest has been revived in the mechanism because of its potentially high recovery efficiency and the less than spectacular performance of current chemical EOR technologies. In fact, methods are currently being sought for rate and hence economic enhancement of its performance. One such enhancement process is that of *Underground-Access Oil Recovery* by Gravity Drainage (UOR). Pioneering studies by Energy Development Associates, Inc. [5], Golder Associates [6], Tetra Systems, Inc. [7], and others, revitalized and reinterpreted the underground-access methodology in the light of modern technology.

UOR as currently proposed and/or practiced (illustrated in Figure 1) involves:

(1) Two or more shafts (with dimensions: 8 - 15 feet in diameter) drilled vertically from ground-level to a level (seldom more than 50-100 feet) below a target oil reservoir. *At least* two shafts are generally required (except where ADIT entry is possible) for adequate subsurface ventilation;

(2) From the base of the shafts, an appropriate pattern of access tunnels (dimensions: 6'-10' x 10'-12') are created beneath the reservoir. The spacing between tunnels and their spacial pattern are determined by the desired well spacing and the maximum reach of the selected drilling equipment. Studies have shown that the tunnels are most cost efficient if placed no more than 4,000 feet below surface. This is so largely because to that depth geothermal temperatures are generally acceptable and no environmental conditioning is required. Theoretically, however, tunnels at any depth are feasible if the target resource is sufficiently productive to support the resulting cost;

(3) Wells drilled vertically upwards and at various angles to the vertical from the *access tunnels* and/or from special chambers created off them are called *drill-rooms*. The upside-down wells are usually drilled and completed at very close spacings; 75-150 feet is common. Such high offtake-well densities are economically feasible because of the short and highly effective lengths of wells. As an example, for a tunnel 100 feet below a target zone, slightly more than 100 feet of the total length of each well will be non-productive;

(4) Oil production, subsequent to well completion (by traditional methods) due to displacement by gravity flow is drip-drained into a subsurface collection system. The produced fluids are subsequently pumped to surface treatment, separation and storage facilities.

The underlying philosophy of the stated approach to UOR is therefor one of enhancing gravity drainage rates by*low-capital-cost, high density, slim-hole well drilling* while retaining the high recovery efficiencies of the process. Nonetheless, total project capital requirements are high, a large percentage of which is utilized for shaft sinking and tunnel boring. Target reservoir selection is therefore critical with regard to parameters of depth, thickness, fluid properties, and structural properties of the underlying tunneling stratum.

Horizontal wells are increasingly being utilized for the solution of specialized reservoir production problems. Such functions as decreasing the likelihood of water and gas coning by suitable placement of offtake wells [8], heavy oil and tar production via steam injection at the base of the formation [9], production from naturally fractured reservoirs by intersecting vertical fractures [10] are now being studied. Horizontal wells have also been used as alternatives to vertical and inclined wells during mine-accessed oil recovery. In this latter use, chambers are created within an oil zone, at the base of a shaft, and slimhole wells are drilled horizontally in a spoke-line radial pattern from the center of the chamber. Good production performance from horizontal wells, however, requires good vertical permeabilities and the absence of any vertical flow barriers. Furthermore, the presence of an uncased chamber within the body of the reservoir can make the subsequent application of pressure drives somewhat difficult.

Field experiments on formation fracturing from inclined wells have been successfully performed. [11]. Theoretical analyses [10] have indicated that the creation of a few multiple vertical fractures from a horizontal well can yield production performance closely equivalent to a continuous vertical fracture. Field experience [11] also suggests that it is possible to perform such techniques and that the theoretical performance potential can be achieved. Both theoretical and field studies have also verified [11, 12] that the performance of a single horizontal well can effectively replace several vertical wells.

No studies which investigate the application and adaption of such findings to the configurations of mine-accessed oil recovery in general or to recovery by the gravity drainage mechanism in particular, have appeared in the published literature. Thus, certain potentially significant advantages of horizontal wells if used singly or in combination with vertical wells have been overlooked. Additionally, the consequences on production performance of a variety of practicable surface and subsurface access configurations have not been studied. This paper will examine, conceptually and theoretically, the probable performance characteristics of some of the more promising configurations. A performance comparison with the more traditional approach is presented. Emphasis will be placed on production by the gravity-drainage mechanism and to configurations which can be installed either by underground, surface, or combination access.

THEORETICAL DISCUSSION

1. General Theory of the Gravity Drainage Mechanism

All gravity flow systems can be mathematically described and modeled as three-dimensional flow-potential problems. The velocity potential distribution, $\Phi(r)$, which describes the resulting flow system must therefore satisfy the classical LAPLACE Equation.

$$\nabla^2\Phi = 0 \qquad - - -(1)$$

For systems of interest to this study, Φ, the velocity potential vector, is best defined as follows:

$$\Phi = K(P \pm \rho g z) \qquad - - -(2)$$

Furthermore, the gravity flow systems of interest herein are characterized by the presence of a uniform pressure fluid surface which connects inflow and outflow boundaries. This surface provides the upper boundary to the flow system, and defines a *free-surface*. The following boundary conditions to the solution must therefore be satisfied:

(1) $\partial\Phi/\partial z$ = Vertical flow velocity = 0 (zero flow over the basal boundary).

(2) $\partial\Phi/\partial\hat{n}$ = 0 at the *free surface* with a normal vector n and a uniform pressure, P_o (unique shape and location of the *free surface*). - - -(3)

Appropriate selection of additional boundary conditions permits the modeling of gravity flow systems of particular geometries and flow configurations. Solution of the equation (1) requires simultaneous determination of both the magnitude of and the shape of the free surface at any point in space and time. The resulting mathematical expression involves an extremely complex integral equation for which no explicit solution (although one is theoretically guaranteed) has yet been presented.

An approximate analytical treatment of the problem was proposed by Wyckoff, Botset and Muskat in 1931 [4]. The suggested solution methodology utilized boundary condition (1) as above, a condition of constant velocity potential over the external and internal boundaries of the system, and a constant pressure above the fluid level in the porous medium. The presence of a free-surface of unknown shape was ignored, the upper boundary to the fluid system being assumed parallel to the basal boundary and to be at a height equal to that of the fluid at the external flow boundary.

Subsequent laboratory experiements conducted by Wyckoff et al [4] and independently by Caldwell [13] led to the derivation of flow relationship for the process. Experiments were performed using both radial and linear gravity flow systems and the results obtained verified the correctness of those analytical assumptions, within the limits of experimental error. Both linear and radial flow systems are of interest to this discussion. Analytical solutions for both flow configurations under the stated approximation assumptions will be examined.

The experimental work and subsequent theoretical analyses of Wyckoff, et al [4], among others, established the fact that the *superposition principle* applies for supplemental pressure drives imposed on gravity-flow systems. Thus, where a bulk pressure above the average, ΔP, exists or is applied to the system, the corresponding *equivalent* total fluid head controls recovery rates. Thus, by definition, the total fluid head available to a generalized gravity flow system is:

$$h_{total} = h_c + \Delta P/(0.433\gamma_o) \qquad - - -(4)$$

Furthermore, other analytical work [1] established that the production rate capacity of a well of any geometric configuration producing under any known form of pressure drive can be described as an equivalent simple or combined gravity flow system. This can be effected by the replacement of the normal pressure differential drive term with an equivalent gravity drive term of the form $[\mu\Delta\Phi/K]$

Application of these most significant findings to both linear and radial flow configurations will also be discussed.

2. Radial Gravity Flow

(a) Pure Radial Flow

The flow configuration for a typical radial pure-gravity flow system is as illustrated in Figure 2. Pure radial gravity flow will occur when a well vertically penetrates either completely or partially a subsurface fluid saturated porous medium having no external drive.

FIGURE 2
Flow Configuration and Experimental Streamlines for Radial Gravity Drainage into a Vertical Well

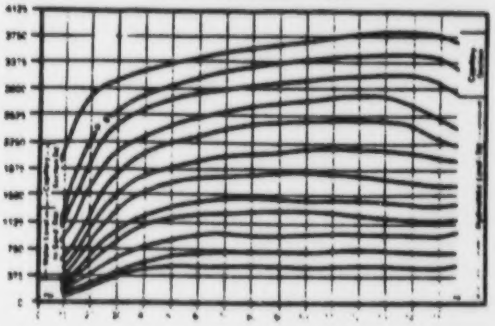

Relevant boundary conditions [4] for solution of the potential Equations (1) and (2) for a radial gravity configuration are as follows (refer to Figure (2)):

$$(1)\ @\ y = 0 \text{ and } y = h_e : \partial\Phi/\partial y = 0$$

$$(2)\ @\ r = r_e \text{ and } 0 \leq y \leq h_e : \Phi = (\kappa\gamma g/\mu)h_e$$

$$\text{and } (3)\ @\ r = r_w \quad \begin{cases} \Phi = (\kappa_o\gamma_o g/\mu_o)h_w \text{ for } 0 \leq y \leq h_w \\ \Phi = (\kappa_o\gamma_o g/\mu_o)y \text{ for } h_w \leq y \leq h_e \end{cases} \qquad \text{- - -(5)}$$

The resulting velocity potential's spacial distribution takes the form of Equation 6 [4]:

$$\Phi(r) = (\kappa_o\gamma_o g/\mu_o)\left[h_e + \frac{(h_e^2 - h_w^2)\,ln(r/r_e)}{2h_e\,ln(r_e/r_w)} - 2h_e\cdot\pi^2\sum_1^\infty \frac{\{(-1)^n - cos(n\pi h_w/h_e)\}U(\alpha_n r)cos(n\pi y/h_e)}{n^2U(\alpha_n r_w)}\right]$$

$$\text{Where: } U(\alpha_n r) = I_o(n\pi r/h_e)K_o(n\pi r_e/h_e) - I_o(n\pi r_e/h_e)K_o(n\pi r/h_e)$$

and: I_o and K_o are Bessel functions of the third kind and zero order. - - -(6)

and the corresponding flow rate relationship will be as given by Equation (7):

$$q_o = 2\pi r\int_o^{h_e}(\partial\Phi/\partial r)dy = \frac{\pi\kappa_o\gamma_o g(h_e^2 - h_w^2)}{\mu_o\,log(r_e/r_w)}$$

$$= \frac{15.35\times10^{-4}\kappa_o\gamma_o(h_e^2 - h_w^2)}{\mu_o\beta_o\,ln(r_e/r_w)} \qquad \text{- - -(7)}$$

A more general mathematical expression of the radial gravity flow rate relationship, Equation (7), based on an analogy with two dimensional radial pressure flow takes the form:

$$q_o = \frac{2\pi h_e(\Phi_e - \Phi_w)}{log(r_e/r_w)}$$

Where: $\Phi_e = (\kappa_o\gamma_o g/\mu_o)h_e$ and:
$\Phi_w = (\kappa_o\gamma_o g/\mu_o)[(h_e^2 + h_w^2/2h_e]$

- - -(8)

This form of the equation facilitates [4] consideration of composite gravity-flow systems.

(b) Composite Radial Flow

Under conditions of a superimposed pressure head on a radial gravity flow system, h_{total}, as defined in Equation (4), is the *apparent* fluid head available for gravity flow. Thus, while Φ_e is unchanged from the previous relationship, h_e still being the upper physical boundary, Φ_w is now of magnitude:

$$\Phi_w = (\kappa_o\gamma_o g/\mu_o)[(h_{total}^2 + h_w^2)/2h_{total}]$$

The resulting composite radial gravity flow relationship takes the form:

$$q_o = \frac{15.35\times10^{-4}\kappa_o\gamma_o(2h_{total}h_e - h_{total}^2 - h_w^2)}{\mu_o\beta_o ln(r_e/r_w)} \qquad \text{- - -(9)}$$

(c) Radial Flow To Vertical Fractures

The effect of a symmetrical vertical fracture of length $2L_f$ and of infinite capacity, created around a vertical wellbore, on general radial flow capacity, can be modeled by that of an otherwise identical system with an effective wellbore radius of one quarter the fracture length [14]. Thus, by physical similarity arguments identical to those presented earlier, the production performance of vertically fractured radial gravity-flow systems will be represented by Equation (10):

$$q_{of} = \frac{15.35\times10^{-4}\kappa_o\gamma_o(h_e^2 - h_w^2)}{\mu_o\beta_o ln(2r_e/L_f)} \quad \text{(Bbls/day)} \qquad \text{- - -(10)}$$

Figure (3) illustrates such a vertical fracture configuration. Multiple vertical fractures, while concievable, yield little additional productivity gains [15]. Such analyses have indicated that longer vertical fractures and higher fracture conductivities have far more significant effects than multiple but short fractures.

Subsequent discussions (see FIELD APPLICABLE CONFIGURATIONS) will present one vertical fracturing configuration wherein the findings of [15], which considered vertical wells only, may no longer be relevant.

FIGURE 3
Gravity Flow to a Vertical Well with a Single Infinite Conductivity Fracture

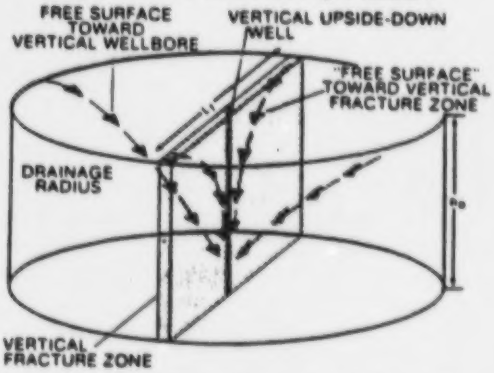
FREE SURFACE TOWARD VERTICAL WELLBORE
VERTICAL UPSIDE-DOWN WELL
"FREE SURFACE" TOWARD VERTICAL FRACTURE ZONE
DRAINAGE RADIUS
VERTICAL FRACTURE ZONE

(d) Horizontally Fractured Radial Gravity Flow

Fractures are generally created in a direction perpendicular to the least principal forces. Thus, for depths less than 1,500 feet, the formation will preferentially fracture on a horizontal plane. At greater depths, vertical fractures are more possible. Recent findings suggest [21] that steam induced fractures can be made to violate that general rule. A superposed thermal stress field can apparently alter the tectonic stress field such that the horizontal direction is preferred.

Radial gravity flow in the presence of horizontal fractures can offer yet another viable approach to rate acceleration. In view of the uncertainty about its general applicability, however, no further analysis has been presented herein.

3. Linear Gravity Flow

Pure linear gravity-flow will be observed as occurring (i) into a horizontal well or trench which has a diameter approximately equal to the thickness of the porous medium (as illustrated in Figure (4)) or (ii) into a vertical fracture zone oriented perpendicular to the flow direction. Appropriate boundary conditions for solution of the LAPLACE Equation of this configuration are as specified in Equation (11) (refer to Figure (4)):

$$(1)\ @\ y = 0 \text{ and } y = h_e : \partial\Phi/\partial y = 0$$

$$(2)\ @\ x = 0 \text{ and } 0 \le y \le h_e : \Phi = (\kappa_o \gamma_o g/\mu)h_e$$

$$\text{and } (3)\ @\ x = L : \quad \begin{array}{l} \Phi = (\kappa_o \gamma_o g/\mu_o)h_w \text{ for } 0 \le y \le h_w \\ \Phi = (\kappa_o \gamma_o g/\mu_o)y \text{ for } h_w \le y \le h_e \end{array} \qquad \text{- - -(11)}$$

FIGURE 4
Flow Configuration and Experimental Streamlines for Linear Gravity Drainage into a Horizontal Well

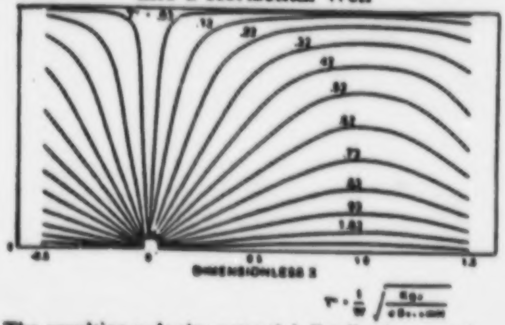

The resulting velocity potential distribution may be expressed in terms of a Fourier series of the form given by Equation (12):

$$\Phi(x) = (\kappa_o \gamma_o g/\mu_o)\Bigg[h_e - x\,\frac{h_e^2 - h_w^2}{2h_e L} + 2h_e/\pi^2 \sum_{1}^{\infty} \frac{\{(-1)^n - \cos(n\pi h_w/h_e)\}}{n^2 \sinh(n\pi L/h_e)} \cos(n\pi y/h_e)\sinh(n\pi x/h_e)\Bigg] \qquad \text{- - -(12)}$$

The corresponding flow rates will then be calculable from Equation (13):

$$q_o = 2\pi r \int_0^{h_e} (\partial\Phi/\partial r)dy = \frac{\kappa_o \gamma_o g(h_e^2 - h_w^2)}{2\mu_o L} = \frac{1.061\times10^{-4}\kappa_o \gamma_o (h_e^2 - h_w^2)}{\mu_o \beta_o L} \quad \text{(Bbls/day/ft of hole)} \qquad \text{- - -(13)}$$

4. Combination Gravity Flow Systems

A combination of radial and linear flow patterns are observed in situations where (i) a horizontal well is of diameter very much less than the thickness of the oil column being drained (i.e., d_w much less than h_e) or (ii) where the height of a vertical fracture is very much less than the formation thickness (i.e., h_f much less than h_e). Again, using earlier similarity arguments, the corresponding gravity-flow rate relationships can be derived by superposition of the two relevant velocity potentials.

The following discussion will examine production performance under each of the stated flow configurations.

(i) Horizontal Wells

(a) Single Wells

Wells penetrating the target formation horizontally exhibit differing performance patterns dependent on (i) the ratio of well length, L, to the drainage radius, r_e, (ii) the ratio of wellbore diameter, d_w, to oil column thickness, h_e, and (iii) the vertical location of the well-path within the oil column. In order to take full advantage of gravity drainage potential it is assumed that wells are always placed at the base of the continuous oil column. Figure (5) is an illustration of a possible horizontal well arrangement.

FIGURE 5
Vertically Multi-Fractured Horizontal Well Configuration

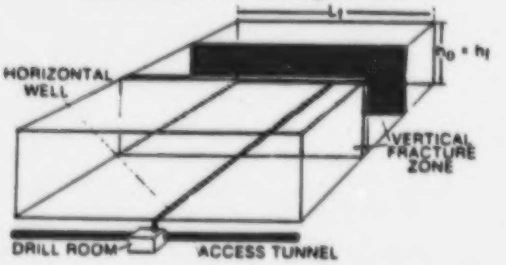

In the discussion which follows, to facilitate comparison with vertical radial flow systems and the inclusion of radial flow components linear terms are expressed in logarithmic *equivalent-wellbore-radius* form. This is in keeping with the approach used by previous authors on the subject [8, 12].

$L << r_e$ and $d_w \approx h_o$

Where the length of a horizontal well is short in relation to its drainage radius but is of a diameter such that it intersects the total oil column, the flow is purely linear. Such a flow configuration is analogous to that of a completely penetrating vertical fracture or *trench* of width d_w through the formation. If the analogous *fracture* is of perfect conductivity and the formation perfectly homogeneous, performance is identical to that of a vertical well with an equivalent fracture. Gravity flow rate performance may therefore be expressed, by suitable transformations, in the form of Equations (13), (10) or (14) below. Equation (14) modified from [18] includes conditions of semi-steady state of flow.

$$q_o = \frac{15.35\times10^{-4}\kappa_o\gamma_o h_o^2}{\mu_o\beta_o\{ln[1+\sqrt{1+(L/2r_e)^2}]/(L/2r_e) - 3/4\}} \quad \text{(Bbls/day)}$$

$\approx$ Equation (13) where $L = 2L_f$ and if $L\ (2r_e) << 1$

- - -(14)

$h_o < L << r_e$ and $d_w << h_o$

Where the horizontal well's diameter is small in relation to the thickness of the formation a radial component to the flow arises out of the convergence of flow streamlines perpendicularly downwards to the wellbore. Clearly the convergence is more acute when that well lies along the basal plane of the system and occurs over a 180 degree angle of the well surface. The total pressure drop causing flow is therefore the sum of linear and radial components yielding a semi-steady-state flow rate capability adapted from [18] of:

$$q_o = \frac{15.35\times10^{-4}\kappa_o\gamma_o h_o^2}{\mu_o\beta_o\{ln[1+\sqrt{1+(L/2r_e)^2}]/(L/2r_e) + (h_o/L)ln[h_o/(\pi r_w)] - 3/4\}}$$

(Bbls/day)

$L \approx r_e$ and $d_w << h_o$ - - -(15)

Where the length of the horizontal well approaches that of its drainage radius, the edge of the drainage area becomes oval [16] in shape. Thus, a more realistic physical representation of the system would be that of a rectangular parallelepiped of equivalent area of dimensions (w x b x h), experiencing two-sided lateral fluid flow [18, 19]. This lateral flow will be subject to a reduction in cross-sectional area as it approaches the well. A radial flow component will also arise as fluid converges towards the wellbore. The resulting semi-steady state, gravity flow relationship adapted from [18] takes the form:

$$q_o = \frac{15.35\times10^{-4}\kappa_o\gamma_o h_o^2}{\mu_o\beta_o\{cosh^{-1}[cosh(1.57w/b)/sin(1.57L/b)]+(h_o/L)ln[h_o/(\pi r)]\}}$$

(Bbls/day)

- - -(16)

(b) Multiple Wells

Horizontal or inclined wells, drilled in a spoke-like pattern from a central surface or subsurface location, are being studied and utilized for mine-accessed oil recovery. The gravity-flow performance characteristics of such multiple well patterns can be modeled from any of the previous pure or combination flow relationships (Equations (9) through (16)) by appropriate consideration of pressure interference effects. A suitable adaptation of Equation (15) for production from 'n' such wells, based on the work of Giger et al [8] and Borisov [16] would be:

$$q_o = \frac{7.675\times10^{-4}\kappa_o\gamma_o h_o^2}{\mu_o\beta_o\{ln[1+\sqrt{1+(L/2r_e)^n}]/(L/2r_e)^{n/2}+(h_o/L)ln[h_o/(\pi r_w)]-3/4\}}$$

(Bbls/day)

- - -(17)

FIGURE 6
A Field Applicable Configuration:
Multi-Fractured Vertical Well and Four Horizontal Wells

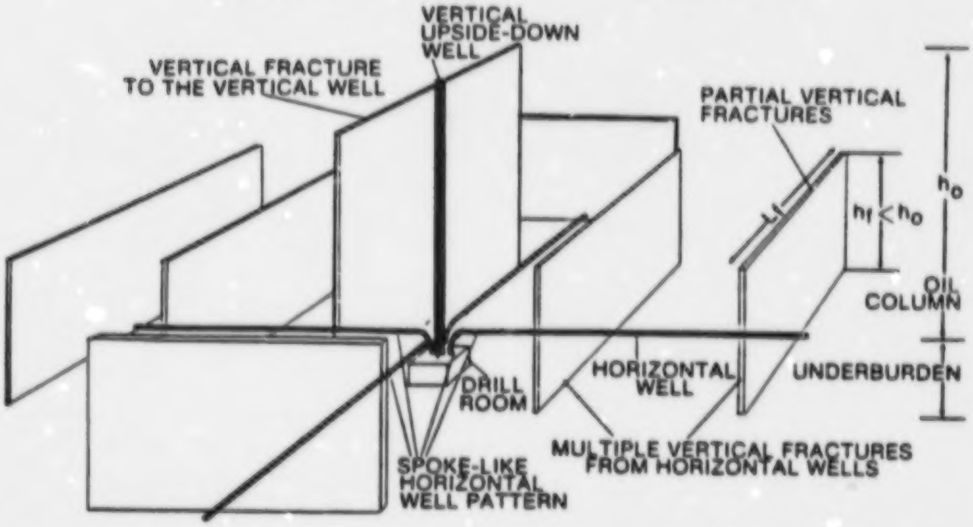
VERTICAL UPSIDE-DOWN WELL
VERTICAL FRACTURE TO THE VERTICAL WELL
PARTIAL VERTICAL FRACTURES
h_o
$h_f < h_o$
L_f
OIL COLUMN
UNDERBURDEN
HORIZONTAL WELL
DRILL ROOM
MULTIPLE VERTICAL FRACTURES FROM HORIZONTAL WELLS
SPOKE-LIKE HORIZONTAL WELL PATTERN

(ii) Short Vertical Fractures

A vertical fracture of limited vertical extent $(h - h_f < 2L_f)$ created from a vertical wellbore and with centroid 'δ' from the center of the formation, is a generalization of a common field reality. Analysis based on an equivalent-effective-wellbore-radius approach [12, 14] yields the following gravity-flow rate relationship:

$$q_o = \frac{15.35 \times 10^{-4} \kappa_o \gamma_o h_o^2}{\mu_o B_o ln\left[2r_e / \left\{L_f\left[sin(1.57h_f/h) cos(3.14d/h)\right]^{h/(2L_f)}\right\}\right]}$$

(Bbls/day) - - -(18)

FIELD APPLICABLE CONFIGURATIONS

The preceding analysis has indicated the broad range of technical possibilities for accelerating recovery rates via underground-access oil recovery in general and gravity drainage methods in particular. While many of the stated approaches are also applicable by surface-access, underground-access can increase the number of candidate reservoirs and, below certain depths, can also improve project economics. Several published and private economic studies have suggested that the profitability of projects which require high front-end investments is strongly dependent upon an early high recovery rate response. In analogous on-going or proposed projects, this objective is attained by low risk, high density drilling. Although some of the proposed methods are untried from a subsurface environment, the consequence of their successful application is a decrease in the required well density and/or a considerable increase in recovery rates. Furthermore, certain proprietary underground-access oil recovery technologies currently under development by Petrotec Systems, Inc. show the promise of accelerating flood response, improving the sweep efficiencies of secondary and tertiary floods and of increasing the probability of residual oil mobilization. These effects, if achieved either singly or collectively, will increase ultimate oil recoveries.

Two of the possible development patterns/well configurations which appear to offer the largest productivity gains with minimum drilling effort are illustrated in Figure (6) and are detailed below.

(1) This configuration consists of a single vertical well with diameter very much less than the oil column height surrounded by four equally spaced, independent, horizontal side-wells drilled in a spoke-like pattern. Vertical fractures are induced from each horizontal well (along its total length) to the vertical well extending to the top of the oil column. The final theoretical flow configuration consists of two vertical infinite conductivity fractures each of length $2L_f$ and height h_o. The fracture half-length, L_f, is assumed very much less than its drainage radius, r_e.

(2) The second configuration consists of four equally spaced, independent horizontal wells only, each of length, L, and with diameter, d_w, very much less than the oil column thickness, h_o. It is further assumed that horizontal well length will define the

system's drainage radius, r_e. This assumption is believed reasonable for the close well spacings common to underground-access methods. Each well is multi-fractured vertically where n_f (the number of fractures) is more than 5. The fractures are also of limited vertical extent, h_f.

Estimates of the order of magnitude of the ratio of production rate attainable with an enhanced system (such as configuration [1]) to that of a single, fully penetrating, vertical well can be obtained from Figures (7) and (8) (adapted from [18]).

FIGURE 7

Quantitative Comparison of the Production Performance of a Multi-Fractured Horizontal Well with a Fractured Vertical Well: Effect of the Number of Fractures and Fracture Width

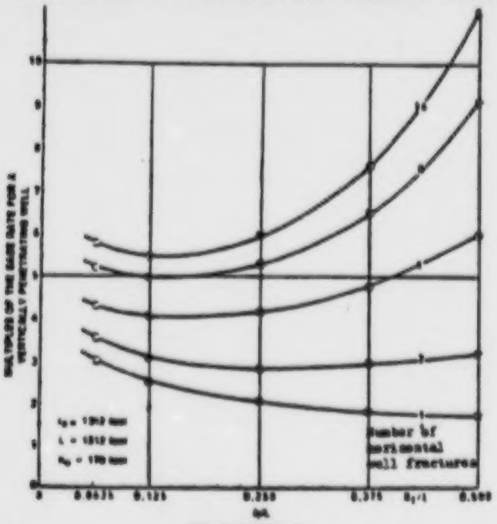

FIGURE 8

Influence of the Number of Branches and Total Well Penetration on Production Performance of Spoke-Like Well Configurations

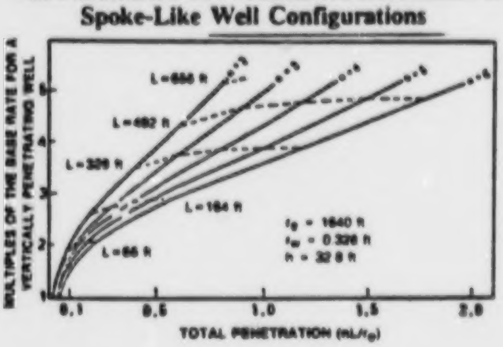

CONCLUSIONS

(1) A theoretical analysis of gravity-flow rates with several differing well configurations and with differing well completion practices suggests that considerable enhancement of production rates can be readily achieved.

(2) Some rate enhancement methodologies which appear most advantageous and practicable are:

(a) The installation, from the subsurface, of horizontal or highly inclined wells, long in comparison to the thickness of the oil column. A sufficient number of multiple vertical or horizontal fractures equally spaced along such wells will perform as a continuous fracture. The creation of such multiple fractures has been successfully field tested.

(b) The installation of satellite well groups consisting of a single vertical well with four horizontal wells surrounding it in spoke-like fashion. A vertical fracture can then be created along the total length of each horizontal well and to the vertical well.

(c) The well configuration described in (b) above can also be used for other applications. Multiple vertical or horizontal fractures of limited extent can be generated along each horizontal well *and* an extensive fracture created from the main well.

(3) These and other techniques can be applied with equal effectiveness either from the surface or subsurface. Beyond some specific depth, however, subsurface application becomes more cost effective.

(4) The theoretical analysis has also indicated, via the superposition principle, that these same methods will be advantageous during fluid pressure drive processes. Thus, adaptations of the same methodology can be utilized to improve the recovery rates and efficiencies of secondary and tertiary floods.

NOMENCLATURE

b - Breadth of Parallelepiped (ft.)
d - Depth of Parallelepiped (ft.)
g - Acceleration Due To Gravity (cm./sec^2)
h - Vertical Thickness (ft.)
K - Permeability (md.)
L - Length of Horizontal Well (ft.)
Lf - Length of Vertical Fracture (ft.)
ln - Naperian Log
log - Decimal Log
n - Direction Vector
n - Number of (quantity)
P - Pressure (psig)
r - Radius (ft.)
w - Width of Parallelepiped (ft.)
x - Horizontal Dimension (ft.)
z - Vertical Dimension (ft.)
SGD - Solution Gas Drive
WD - Water Drive
GCD - Gas-Cap Drive

SUBSCRIPTS

e - Value at Flow Boundary
f - Fracture
o - Oil
w - Water

GREEK SYMBOLS

Φ - Velocity Potential
Φ_e - Velocity Potential at Drainage Boundary
Φ_w - Velocity Potential at Wellbore
$\Delta\Phi$ - Velocity Potential Difference
γ - Specific Gravity of Oil
μ - Viscosity of Oil (cm.)
ΔP - Pressure Difference (psig.)
β - Fluid Compressibility (bbls./bbls./psi.)
δ - Distance Between Centroid of Fracture and Center of the Formation

REFERENCES

1. M. Muskat, "Flow of Homogeneous Fluids Through Porous Media", 1937.

2. Morris Muskat, "Physical Principles of Oil Production", 1981 Edition.

3. Forchheimer, Ph., "Hydraulik", 3rd Edition, 1930.

4. R.D. Wyckoff, H.G. Botset, and M. Muskat, "Flow of Liquids Through Porous Media Under The Action of Gravity", PHYSICS, 90(3), 1932.

5. Energy Development Consultants, Inc., "Mining For Petroleum: Feasibility Study" prepared for United States Department of the Interior, Bureau of Mines, Contract No. J0275002, July 1978.

6. Golder Associates, Inc., "Mining For Petroleum: Feasibility Study", prepared for United States Department of the Interior, Bureau of Mines, 1978.

7. Tetra Systems, Inc., Golden, CO 80401, Private Communications.

8. Giger, F., Combe, J., and Reiss, L.H.: "L'interet du forage horizontal pour l'exploitation des gisements d'hydrocarbures", Revue de l'Institut Francais du Petrole, Vol. 38, No. 3 (May-June 1938).

9. Butler, R.M. and Stephens, D.J., "The Gravity Drainage of Steam-Heated Heavy Oil to Parallel Horizontal Wells", Journal of Canadian Petroleum Technology, April-June, 1981, Montreal.

10. Duns, H., Van der Vlis, A.C., and Fernandez, L.R., "Increasing Well Productivity in Tight Chalk Reservoirs", 10th World Petroleum Congress, Bucharest, 1979.

11. Strubhar, M.K., Fitch, J.L., and Glenn, E.E., Jr., "Multiple, Vertical Fractures From an Inclined Wellbore - A Field Experiment", Journal of Petroleum Technology, May, 1975, 641-647.

12. Giger, F., "Reduction du nombre de puits par l'utilisation de forages horizontaux", Revue de l'Institut Francais du Petrole, Vol. 38, No. 3 (May-June, 1983).

13. Caldwell, D.H. and Babbitt, H.E., University of Illinois Engineering Experimental Station Bulletin, Service 374, January 7, 1948.

14. Prats, M., "Effect of Vertical Fractures on Reservoir Behavior--Incompressible Fluid Case", Society of Petroleum Engineers, June, 1961, 105-118.

15. McGuire, W.J. and Sikora, V.J., "The Effect of Vertical Fractures on Well Productivity", Journal of Petroleum Technology, October, 1960, 72-74.

16. Borisov, Ju. P., "Exploitation des Gisements de petrole par des puits horizontaux et a deviations multiples", Nedra, Moscow (1964), Translation from Russian to French : Institut Francais du Petrole, Rueil 28363.

17. Huygen, H.H.A. and Black, J.B., "Steam Through Horizontal Wells and Fractures — Scaled Model Tests", 2nd European Symposium on Enhanced Oil Recovery, Paris, 8-10 Nov. 1981 pg. 507.

3rd EUROPEAN MEETING ON IMPROVED OIL RECOVERY
3ème COLLOQUE EUROPEEN SUR L'AMELIORATION DE LA RECUPERATION DU PETROLE
3° CONVEGNO EUROPEO SUL MIGLIORAMENTO DELLE TECNICHE DI RECUPERO DEL PETROLIO
Roma, 16-18 Aprile 1985

010232

PROCEEDINGS
ACTES
ATTI
1

⑺⑸

FLUID FLOW IN POROUS MEDIA
ECOULEMENT DES FLUIDES DANS LES MILIEUX POREUX

WATERFLOODING AND IMMISCIBLE GAS INJECTION
INJECTION D'EAU ET DE GAZ NON MISCIBLE

THERMAL PROCESSES
PROCEDES THERMIQUES

Organization/Organisation/Organizzazione: Agip S.p.A.
Co-sponsors: Elf Italiana - Montedison - Shell Italia - Snia BPD
Società Petrolifera Italiana - Texaco - Banco di Roma

ECOULEMENT DES FLUIDES AUTOUR D'UN PUITS HORIZONTAL - ESSAIS DE PUITS

Fluid Flow in a Horizontal Well Test

F. DAVIAU*, G. MOURONVAL*, P. CURUTCHET, F. GIGER****
*Societé Nationale Elf Aquitaine (Production)
Pau, France
**Institut Français du Pétrole
Rueil-Malmaison, France

ABSTRACT

Several reservoirs provide favorable targets for profitable horizontal wells. The horizontal wells drilled and produced give very encouraging results.

This paper aims at fullfilling the need for designing and interpreting well test in horizontal wells.

The analytical solutions for the following problems are developped :

- infinite or limited reservoirs with impermeable or constant pressure boundaries.
- horizontal well with wellbore storage and skin.
- horizontal well with uniform flux or infinite conductivity

A two-fold phenomenon, specific to horizontal wells, is pointed out on the pressure charts: the early time pressure evolution is due to a circular radial flow in a vertical plane perpendicular to the well and the late time pressure behaviour corresponds to an horizontal pseudo-radial flow.

For pratical uses we describe a well test design and interpretation method which consists in :

- a semi-log analysis that provides the value of a pseudo-skin which we have defined
- a log-log analysis (with type curves drawn by a desktop computer)

Time criteria are also provided, to determine in particular the beginning of the pseudo-radial flow period.

RESUME

Un certain nombre de réservoirs constituent des cibles favorables, sur le plan économique, au forage de puits horizontaux. Les puits horizontaux réalisés et mis en production à ce jour donnent des résultats très encourageants. Il faut donc pouvoir établir le programme ("design") et interpréter un essai dans ces puits, notamment dans les cas suivants traités analytiquement :

- réservoir infini ou limité par une frontière imperméable ou maintenue à pression constante.
- puits horizontal de capacité (wellbore storage) et d'effet pariétal (skin) non nuls.
- puits avec une répartition uniforme des débits par unité de longueur ("flux uniforme") ou des pressions ("conductivité infinie").

Un phénomène nouveau, propre aux puits horizontaux, est mis en évidence sur les courbes de pression : à un écoulement radial circulaire, dans un plan vertical perpendiculaire à l'axe du puits, succède un écoulement pseudo-radial horizontal.

Pour les applications pratiques, nous décrivons une démarche commode pour préparer et interpréter un essai. Elle comporte :

- une analyse semi-log, qui fournit un pseudo-skin que nous définissons,
- une analyse log-log (avec des courbes types aisément tracées par un mini-ordinateur).

Des critères de temps sont également proposés, notamment pour déterminer le début de l'écoulement pseudo-radial.

1. INTRODUCTION

Les premiers puits horizontaux mis en production ont apporté des résultats très positifs [1 4]. Ces résultats justifient l'étude de l'écoulement des fluides autour d'un puits horizontal, dans un but pratique : la préparation (design) et l'interprétation des essais. Il devient en effet nécessaire d'être capable, pour toute configuration réelle "réservoir - puits horizontal" :

- de décider de l'opportunité d'un essai (l'essai permettra-t-il d'accéder aux informations recherchées ?)
- d'optimiser, le cas échéant, la durée de l'essai (l'essai doit être suffisamment long pour pouvoir être interprété ensuite)
- d'interpréter cet essai avec des méthodes faciles d'emploi.

Ce sont les objectifs de ce papier. En premier lieu, la solution analytique la plus simple et la plus importante est développée à savoir le comportement transitoire d'un puits, sans capacité C, ni skin S, avec un flux uniforme ; le débit par unité de longueur est alors le même en tous points du puits. Le problème est ensuite compliqué progressivement, pour aboutir à une démarche pratique applicable dans la plupart des cas réels. Notons, en particulier, que les paragraphes 2, 3 et 4 renvoient systématiquement aux solutions pour flux uniforme, détaillées en annexes. La transposition de ces solutions aux puits de conductivité infinie est décrite au paragraphe 5.

2. PUITS HORIZONTAL DANS UN RESERVOIR HOMOGENE INFINI

2-A. PRELIMINAIRE

Dans toute la suite, le puits horizontal, de longueur $2l$, reste parallèle aux épontes imperméables d'un réservoir d'épaisseur h, de conductivité k/μ et de capacité ϕc_t. Par ailleurs, toutes les hypothèses habituelles, longuement décrites dans la littérature sur les essais de puits [3,6] sont utilisées pour l'établissement de l'équation de diffusivité. La gravité est négligée, l'écoulement est monophasique et le réservoir isotrope.

2-B. PUITS DE CAPACITE ET DE SKIN NULS - RESERVOIR INFINI

Soit un puits horizontal, de rayon r_w, sans skin, situé à une distance z_w de l'éponte inférieure d'un réservoir infini (Fig. 1). Admettons qu'à l'instant initial ce puits soit mis en production avec un flux uniforme et que son débit fond soit constant et égal à qB (capacité du puits nulle).

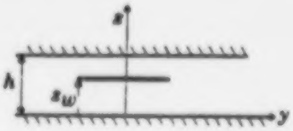

Figure 1 : Puits horizontal dans un réservoir infini.

L'évolution de la chute de pression Δp (égale à $p_i - p_{wf}$), en fonction du temps Δt au point M du puits défini par une valeur de y fixée, s'écrit rapidement par la voie analytique si on utilise les fonctions de Green [2,3]. Cette solution peut s'exprimer à l'aide des groupements de paramètres sans dimension suivants (annexe 1) :

$$p_D = \frac{2\pi kh}{qB\mu}\Delta p \qquad t_D = \frac{k\,\Delta t}{\phi\mu c_t l^2}$$

$$z_{D3} = \frac{z_w}{h}\ ;\ l_{D3} = \frac{l}{h}\ ;\ y_D = \frac{y}{l}\ ;\ r_{wD} = \frac{r_w}{l}$$

Rappelons qu'en unités métriques pratiques, p_D et t_D deviennent :

$$p_D = 5{,}356\ 10^{-4}\,\frac{kh\,\Delta p}{qB\mu}\ ;\ t_D = 3{,}557\ 10^{-6}\,\frac{k\,\Delta t}{\phi\mu c_t l^2}$$

En unités pratiques américaines, les coefficients dans p_D et t_D doivent être remplacés respectivement par : 1/141,2 et 2,64 10^{-4} La solution p_D en un point y_D du puits est de la forme (annexe 1) :

$$p_D = p_D\,(t_D,\ y_D,\ z_{D3},\ l_{D3},\ r_{wD})$$

Par raison de symétries, nous pouvons ne considérer que les cas : $z_{D3} > 0{,}5$ et $y_D > 0$

2-B-1. Différents types d'écoulement autour d'un puits horizontal

La solution précédente permet de tracer les courbes p_D (t_D) pour différentes valeurs des paramètres y_D, z_{D3}, l_{D3} et r_{wD} (paragraphes 2-B-2, 2-B-3, 2-B-4). Toutes ces courbes, portées sur des graphiques semi-log, ont un caractère commun : elles montrent toutes deux parties linéaires séparées par une transition.

Ecartons momentanément le cas très particulier où $y_D = 1$. La première des droites, observée pour les petits temps, correspond à l'écoulement radial circulaire dans un plan vertical perpendiculaire à l'axe du puits. Cet écoulement disparaît dès que les épontes du réservoir ou les extrémités ("pointes") du puits ont une influence sensible. Cet écoulement radial vertical se traduit pas une droite semi- log de pente $0.5\ \ln 10/(2l_{D3}) = 1.15/(2l_{D3})$ qui correspond à un écoulement radial circulaire dans un réservoir d'épaisseur $2l$ (on obtiendrait une pente de 1,15 si on remplaçait h par 2ℓ dans la définition de p_D). L'équation de l'écoulement radial vertical, valable pour t_D petit, est en effet (annexe 1) :

$$p_D = \frac{1}{2l_{D_3}}\left[-\frac{1}{2}\ \mathrm{Ei}\left(-\frac{x_{WD}^2}{4t_D}\right)\right]$$

$$= \frac{1}{4l_{D_3}}\cdot\left(\ln\frac{t_D}{x_{WD}^2}+0{,}809\right)\text{pour } \frac{x_{WD}^2}{4t_D} < 10^{-2} \quad (1)$$

Dans les cas particuliers où $y_D = 1$ (point M à l'extrémité du puits), l'écoulement n'est jamais radial circulaire. La solution analytique approchée pour les petites valeurs du temps s'écrit (annexe 1) :

$$p_D = \frac{1}{4l_{D_3}}\left[-\frac{1}{2}\ \mathrm{Ei}\left(-\frac{x_{WD}^2}{4t_D}\right)\right]$$

$$= \frac{1}{8l_{D_3}}\ \left(\ln\frac{t_D}{x_{WD}^2}+0{,}809\right)\text{ pour } \frac{x_{WD}^2}{4t_D} < 10^{-2} \quad (2)$$

Par conséquent, quand $y_D = 1$, la pente de la première droite semi-log est la moitié de celle observée pour les autres valeurs de y_D (équation (1)), toutes choses étant égales par ailleurs. Pour donner une idée de l'époque correspondant à la fin de l'écoulement radial vertical, deux critères approximatifs sont proposés dans l'annexe 1. L'écoulement radial vertical disparaît dès que l'une des deux conditions ci-dessous est remplie :

- l'éponte la plus proche influence la pression dans le puits, ce qui se produit quand le rayon d'investigation de l'écoulement radial circulaire vertical atteint cette éponte ; l'écoulement radial vertical est terminé pour $t_D=0.32((1-l_{D_3})/l_{D_3})^2$, formule pratique obtenue en adaptant la définition classique du rayon d'investigation.

- l'effet de pointes devient sensible dans le puits, ce qui suppose : $t_D = (1-y_D)^2/6\ (y_D \neq 1)$.

Ces critères fournissent seulement des ordres de grandeurs, néanmoins commodes car adaptés à ce qui est véritablement observable sur les courbes de pression (annexe 1). Bien entendu, le critère issu du rayon d'investigation n'est valable qu'à condition que l'effet de pointes n'ait pas déjà déformé les lignes de courant.

Quand t_D augmente, la courbe réelle s'écarte de cette première droite. Pour faciliter la compréhension, intéressons nous aux courbes qui correspondent à $\ell > h$ c'est-à-dire par exemple aux courbes des figures 2 et 3. Toutes ces courbes révèlent que, pendant la période de transition qui suit l'écoulement radial vertical, la pression p_D peut avoir deux comportements distincts :

- ou bien l'influence de l'éponte la plus proche apparaît d'abord et la courbe réelle passe au-dessus de la première droite (la pente augmente),

- ou bien l'effet de "pointes" est sensible le premier et la courbe réelle tombe sous la première droite (la pente diminue).

Une deuxième droite semi-log est ensuite rejointe. Cette droite correspond à l'écoulement pseudo-radial horizontal. Les surfaces équipotentielles ont des formes compliquées autour du puits à cause des effets de "pointes" et d'épontes. Plus elles sont distantes du puits, plus ces surfaces sont assimilables à des cylindres de révolution. Pour un temps suffisamment long, l'écoulement devient pratiquement incompressible entre le puits horizontal et la première surface équipotentielle assimilable à un cylindre de révolution. A partir de cet instant l'évolution de la pression au puits résulte uniquement du régime d'écoulement transitoire dans la région du réservoir située au-delà de cette équipotentielle cylindrique ; l'écoulement y est radial circulaire dans un plan horizontal. Ce type d'écoulement, appelé pseudo-radial, se traduit par une droite semi-log de pente 1,15 dont l'équation est en effet (annexe 1) :

$$p_D\ (t_D) = 0{,}5\ (\ln t_D + \alpha) \qquad (3)$$

où α fait intervenir la notion de skin géométrique qui sera discutée au paragraphe 2-F-2-b.

On remarque que l'époque à laquelle commence l'écoulement pseudo-radial varie assez peu d'une courbe à l'autre et qu'une fourchette apparaît déjà sur les figures 2, 3 et 4 : $0{,}8 < t_D < 3$. Nous montrerons plus loin qu'un critère beaucoup plus précis peut être adopté pour tous les cas pratiques.

2-B-2. Influence de la position du point de mesure (y_D) dans le drain

On remarque sur la figure 2 (Tableau I), que lorsque y_D augmente :

- l'effet de pointes démarre plus tôt et la chute de pression est alors plus faible

- l'époque à laquelle l'éponte la plus proche a un effet sensible, ne varie pas.

- le début de l'écoulement pseudo-radial est légèrement retardé (de $t_D = 0{,}8$ à $t_D = 3$)

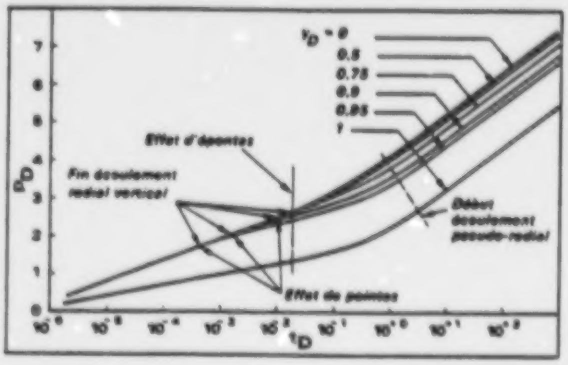

Figure 2 : Puits horizontal dans réservoir infini. Influence de y_D

Paramètres sans dimension			Exemple de valeurs correspondantes			
e_{D_3}	l_{D_3}	x_{WD}	$2l$	h	z_W	r_W
0,75	1	0,001	200m (656ft)	100m (328ft)	75m (246ft)	0,1m (0,33ft)

TABLEAU I - (Figure 2)

Dans la pratique, l'hypothèse d'une conductivité infinie dans le puits est certainement la mieux adaptée à un puits horizontal réel. Nous verrons plus loin (paragraphe 5) que la solution "flux uniforme" avec $y_D = 0,7$ permet généralement de simuler correctement un puits de conductivité infinie. Pour cette raison, et parce que l'influence de y_D est maintenant connue, nous adopterons, dans les paragraphes qui suivent, comme valeur unique de ce paramètre : $y_D = 0,7$

2-B-3. Influence de l'excentrement (e_{D_3}) du puits dans le réservoir

Les courbes de la figure 3 (Tableau II) confirment bien que l'excentrement réduit la durée de l'écoulement radial vertical : quand e_{D_3} augmente, l'influence de l'éponte la plus proche arrive plus tôt. Les valeurs de e_{D_3} choisies pour le tracé des courbes correspondent à un puits horizontal de 500 m de long distant de 0,5 m (1,6ft), 10 m (32,9ft), 25 m (82ft) et 50 m (164ft) de l'éponte la plus proche.

Le début de l'écoulement pseudo-radial ne dépend pas sensiblement de e_{D_3} et se situe toujours à des valeurs de t_D de l'ordre de 1,9 dans notre exemple.

La courbe $e_{D_3} = 0,995$ est confondue avec les autres pour t_D inférieur à $2\ 10^{-6}$ car, jusqu'à cette époque, l'éponte pourtant très proche, située à 0,5 m (1,64ft), n'agit pas encore de façon sensible sur la pression dans le puits. Ensuite, la courbe $e_{D_3} = 0,995$ devient sur le graphique semi-log, une droite de pente $1,15/l_{D_3}$ au lieu de la valeur $1,15/(2l_{D_3})$ caractéristique de l'écoulement radial vertical. Ce doublement de la pente s'explique simplement par analogie avec le cas d'un puits vertical situé près d'une barrière linéaire de perméabilité. L'application de la méthode des images permet d'écrire dans ce cas :

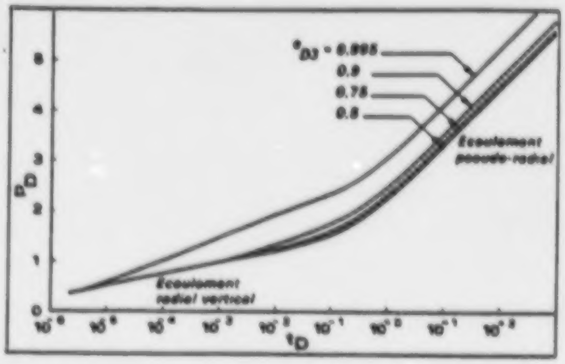

Figure 3 : Puits horizontal dans réservoir infini. Influence de e_{D_3} $y_D = 0,7$

Paramètres sans dimension			Exemple de valeurs correspondances		
y_D	l_{D_3}	x_{WD}	$2l$	h	r_W
0,7	2,5	0,0004	500m (1640ft)	100m (328ft)	0,1m (0,33ft)

TABLEAU II - (Figure 3)

$$p_D = -\frac{1}{4l_{D_3}}\left\{ Ei\left(-\frac{x_{WD}^2}{4t_D}\right) + Ei\left[-\frac{(1-e_{D_3})^2}{l_{D_3}^2\ t_D}\right]\right\}$$

ce qui, dans notre exemple, peut être approché très tôt par :

$$p_D = \frac{1}{2l_{D_3}}\left[\ln\frac{t_D}{x_{WD}^2} + 0,809 + \ln\frac{l_{D_3}\ x_{WD}}{2\ (1-e_{D_3})}\right] \quad (4)$$

Cette équation est celle d'une droite semi-log de pente $1,15/l_{D_3}$.

2-B-4. Influence de l_{D_3}

L'exemple du tableau III correspond à un puits de 500 m de long centré dans une couche d'épaisseur h de 20m (65,6ft), 50m (164ft), 100m (328ft), 200m (656ft) et 500m (1640ft)

La figure 4 montre que la pente de la première droite semi-log est égale à $1,15/(2l_{D_3})$. La pente de la deuxième droite semi-log reste inchangée et égale à 1,15. Il est intéressant de noter que l_{D_3} a un rôle, néanmoins faible, sur le début de l'écoulement pseudo-radial.

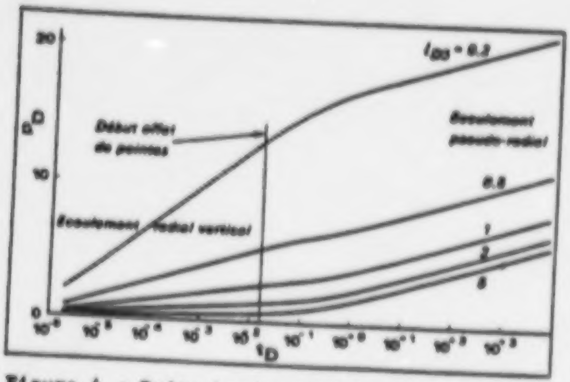

Figure 4 : Puits horizontal dans réservoir infini. Influence de l_{D_3}. $y_D = 0{,}7$.

Paramètres sans dimension			Exemple de valeurs correspondantes	
y_D	e_{D_3}	r_{wD}	$2l$	r_w
0,7	0,5	0,001	200m (656ft)	0,1m (0,33ft)

TABLEAU III - (Figure 4)

2-C. PUITS DE CAPACITE NULLE ET DE SKIN NON NUL-RESERVOIR INFINI

Par analogie avec les puits verticaux, nous définissons le skin S d'un puits horizontal en considérant que la perte de charge dans ce skin est constante, pour un débit fond constant (capacité de puits nulle).

$$\Delta p_{Skin} = \frac{qB\mu}{2\pi k.2l} S \qquad (5)$$

Dans ces conditions, pour une capacité de puits nulle, la pression sans dimension p_D d'un puits horizontal de skin non nul se déduit de la pression sans dimension p_D (S = 0) d'un puits horizontal sans skin par :

$$p_D = p_D\,(S=0) + \frac{1}{2l_{D_3}} S \qquad (6)$$

Un autre moyen de simuler un tel skin, qui se comporte comme s'il était infinitésimal, est la méthode de rayon équivalent [3,6]. Elle consiste à remplacer le puits réel, de rayon r_w et de skin S, par un puits fictif équivalent, de rayon $r'_w = r_w e^{-S}$ et de skin nul. C'est la méthode que nous utiliserons désormais car c'est la seule qui sera applicable dans tous les cas, notamment avec un puits de capacité non nulle et de skin négatif.

2-D. PUITS DE CAPACITE NON NULLE ET DE SKIN NUL-RESERVOIR INFINI

En général, les variations de débit sont imposées en tête du puits et non au fond. Il la capacité du puits qui impose une variation progressive de son débit de fond. Dans notre modèle analytique, la capacité du puits est introduite par le simulateur de H.Cinco-Ley, et al[5]. Pour adapter ce simulateur à la solution de l'annexe 1, il suffit de définir, pour un puits horizontal, une capacité de puits sans dimension C_{De} par :

$$C_{De} = C/(2\pi l^2 h\phi c_t)$$

(Le coefficient $1/(2\pi)$ doit être remplacé par 0,159 en unités métriques pratiques et par 0,89 en unités pratiques américaines).

Il apparaît, sur le graphique semi-log de la figure 6 (S = 0) ainsi obtenue, que l'effet de capacité du puits perturbe surtout l'écoulement radial vertical. La capacité du puits intervient donc surtout quand le puits horizontal se comporte comme un puits vertical dans une couche d'épaisseur 2l c'est-à-dire comme un puits vertical de capacité :

$$C_D = C/(2\pi r_w^2 .2l\phi c_t)$$

Pour faciliter la comparaison avec les courbes connues pour les puits verticaux, nous rappelons systématiquement, sur les figures 5, 6 et 7, les valeurs de C_D associées à celles des C_{D_e} utilisées dans le modèle.

2-E. PUITS DE CAPACITE ET DE SKIN NON NULS-RESERVOIR INFINI

Cette solution générale est obtenue à partir de la solution analytique de l'annexe 1, de la méthode du rayon équivalent et du simulateur de capacité de puits.

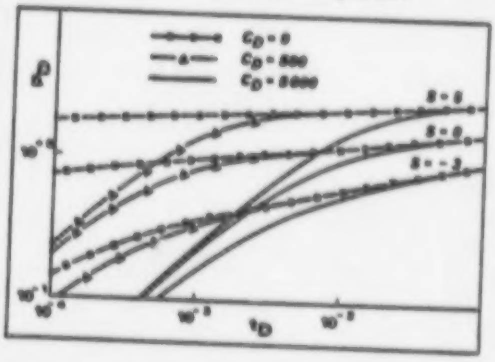

Figure 5 : Puits horizontal dans réservoir infini. Petites valeurs du temps.
$y_D = 0{,}7$ $e_{D_3} = 0{,}75$ $r_{wD} = 0{,}0004$ $l_{D_3} = 2{,}5$.

Cette solution a été comparée, pendant la période d'écoulement radial vertical, à la solution pour puits vertical, de capacité et de skin non nuls, représentée, par exemple, par la planche de courbes types

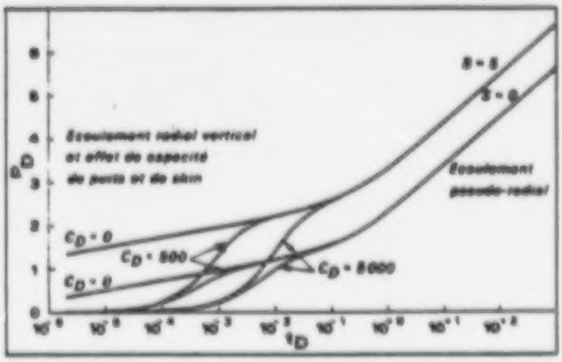

Figure 6 : Puits horizontal dans réservoir infini. Influence de C_D
$y_D = 0,7$ $e_{D_3} = 0,75$ $r_{wD} = 0,0004$ $l_{D_3} = 2,5$.

entre ces deux solutions, exactement le même écart qu'entre la solution "puits linéaire" (notre solution) et la solution "puits cylindrique" (solution d'Agarwal, et al.). En effet, notre solution, représentée sur la figure 5 pour les faibles valeurs du temps, coïncide parfaitement avec la solution d'Agarwal, et al. pour les skins positifs, nuls ou faiblement négatifs. En revanche, un skin très négatif (S = -3) introduit un rayon équivalent très grand dans ces deux solutions qui divergent alors pour les petites valeurs du temps ($t_D < 1,2\ 10^{-3}$). Cette divergence, maximale pour une capacité de puits C_D nulle, s'atténue quand C_D augmente (cas réels) : elle est négligeable, pour toutes les valeurs réalistes du temps, quand C_D est égale à 5000.

2-E-1. Existence de la première droite semi-log

Les courbes correspondant à S = 0 et S = +5 sur le graphique log-log de la figure 5, ont également été tracées sur un papier semi-log (Fig. 6). La courbe S = -3 n'a pas été reportée car elle est trop aplatie et peu lisible.

Sur la figure 6, la première droite semi- log disparaît toujours totalement à cause de l'effet de capacité du puits. L'analyse semi-log de cette première droite ne serait possible que pour des skin très négatifs et des capacités de puits faibles (effet de capacité de puits de courte durée) et si les critères du paragraphe 2-B-1 le permettaient.

Dans la plupart des cas réels, on risque fort de ne pas voir la première droite semi-log.

2-E-2. Existence de la deuxième droite semi-log

La figure 6 indique que le début de l'écoulement pseudo-radial n'est jamais retardé par l'effet de capacité du puits. Pour les configurations extrêmes représentées par les courbes de la figure 7, l'époque du début de l'écoulement pseudo-radial a été évaluée en acceptant une erreur de 10% sur la pente de la droite semi-log observée.

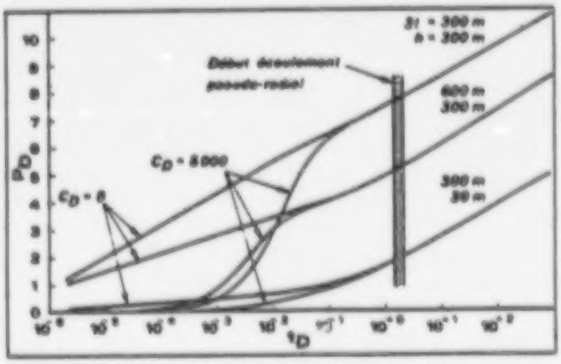

Figure 7 : Puits horizontal dans réservoir infini. Début de l'écoulement pseudo-radial
$y_D = 0,7$, $e_{D_3} = 0,75$, $C_D = 5000$.

Sur la figure 7, plusieurs valeurs sont affectées à l_{D_3}, à savoir 5, 1 et 0,5 car c'est le seul paramètre qui agit sur le début de l'écoulement pseudo-radial.

Nous pouvons alors conclure que pour toutes les configurations réalistes, l'écoulement pseudo-radial apparaît pour des valeurs de t_D comprises entre 1,5 et 2. Prenons par exemple :

$2l = 400$m (1312ft)
$\phi c_t = 10^{-7}$kPa^{-1} (0,7 10^{-6} psi^{-1})
$k/\mu = 10$md/(mPa.s) (10md/cp)

On doit alors observer le début de l'écoulement pseudo-radial à partir d'un temps t compris entre 7,1 et 9,5 jours. Pour qu'une analyse semi-log soit possible, il faudra donc attendre des temps au moins 3 fois plus grands. Pour les faibles valeurs de la conductivité et les puits longs, on atteint rapidement des durées d'essais extrêmement élevées. Ce critère sera donc fondamental pour évaluer la durée minimale nécessaire d'un essai pour qu'il soit ensuite interprétable.

2-F. INTERPRETATION D'UN ESSAI DANS UN PUITS HORIZONTAL

2-F-1. Généralités

Soit un puits horizontal mis en production avec un débit en tête constant depuis son ouverture et situé dans un réservoir qui se comporte comme s'il était infini. Les pressions enregistrées au fond du puits pendant cette période de débit peuvent être interprétées par des méthodes analogues aux méthodes classiques : analyse log-log et analyse semi-log.

Nous avons mis en évidence deux sortes d'écoulements qui conduisent à des "droites semi-log". Le problème essentiel est de savoir positionner ces droites, quand elles existent. Dans ce but, nous avons établi des critères très simples (paragraphe 2 - B-1 et 2-E-2 et tableau V). Cependant, la durée pendant laquelle l'effet de capacité de puits est sensible, reste difficile à estimer et la meilleure méthode consiste à :

- générer des courbes types à l'aide de la solution de l'annexe 1.
- jouer sur les paramètres inconnus pour trouver une courbe type qui soit bien calée sur les points expérimentaux.

Une telle simulation analytique permettra de déceler les éventuelles droites semi-log et conduira également à une première estimation des paramètres et à une meilleure compréhension des phénomènes. Dans tous les cas, l'analyse semi-log constituera à la fois la base de l'interprétation et la méthode la plus simple à employer.

2-F-2. Analyse semi-log

2-F-2-a. Ecoulement radial vertical

Supposons que l'effet de capacité de puits ne dure pas assez longtemps pour masquer la première droite semi-log. L'équation de cette droite peut s'écrire, en combinant (1) et (5) ou (6) :

$$P_i - P_{wf}(t) = \frac{qB\mu}{4\pi k.2l} . \left(\ln \frac{k_t}{\phi\mu c_t r_w^2} + 0,809 + 2S\right) \qquad (7)$$

L'analyse semi-log classique est donc applicable à cette droite à condition de remplacer dans les formules l'épaisseur h de la couche par la longueur de 2l du puits. En particulier, la pente m de la droite semi-log permet de calculer k.2l, d'où l'on déduit la perméabilité moyenne observée lors de l'écoulement radial circulaire dans un plan vertical, normal au puits. Les formules s'écrivent :

$$k = - \frac{C_1\, qB\mu}{m.2l}$$

$$S = 1,15 \left(\frac{P_{1hre} - P_i}{m} - \log \frac{k}{\phi\mu c_t r_w^2} + C_2\right)$$

avec, en unités métriques pratiques :
$C_1 = 2,149\ 10^3$ $C_2 = 5,10$
et en unités pratiques américaines :
$C_1 = 162,6$ $C_2 = 3,23$

2-F-2-b. Ecoulement pseudo-radial

Si l'essai a duré suffisamment longtemps et si les frontières n'ont pas influencé le puits trop tôt, l'écoulement pseudo-radial peut être observé. L'équation de la droite semi-log correspondante s'écrit, en combinant (5) et (A -4) :

$$P_i - P_{wf}(t) = \frac{qB\mu}{4\pi kh} \left(\ln \frac{kt}{\phi\mu c_t r_w^2} + 0,809 + 2S'\right) \qquad (8)$$

$$\text{où : } S' = (h/(2l))\, S + S_g \qquad (9)$$

S_g étant le pseudo skin ou skin géométrique qui caractérise la diminution des pertes de charges enregistrée si on remplace un puits vertical par un puits horizontal. Le skin géométrique est négatif et, pour les cas pratiques, peut être évalué par la formule (A-5) (annexe 1) :

$$S_g = \ln \frac{2\, x_{wD}}{(2\pi x_{wD}\, l_{D_3})^{1/(2l_{D_3})}}$$

Dans l'exemple représenté par les figures 5 et 6, la valeur calculée pour S_g serait de -6,1. La formule (A-5) devient moins précise pour les très fortes excentrements comme cela est signalé dans l'annexe 1. Les formules classiques sont directement applicables. Elles donnent :

- la valeur de kh, où k est la perméabilité moyenne lointaine qui gouverne l'écoulement radial circulaire horizontal.
- la valeur du skin global S', qui conduit ensuite à S par l'intermédiaire de l'équation (9), le skin géométrique S_g ayant été calculé au préalable à l'aide de (A-5).

3 - PUITS HORIZONTAL DANS UN RESERVOIR HOMOGENE LIMITE PAR DES FRONTIERES IMPERMEABLES

Nous nous attachons à décrire les phénomènes liés aux frontières c'est-à-dire les phénomènes qui marquent la fin du régime transitoire. Pour simplifier la présentation, nous négligeons la capacité et le skin du puits dont les effets, déjà étudiés, n'apporteraient rien de plus à la démarche que nous allons suivre.

La position du puits horizontal, dans le réservoir supposé limité par une frontière rectangulaire imperméable est schématisée sur la figure 8.

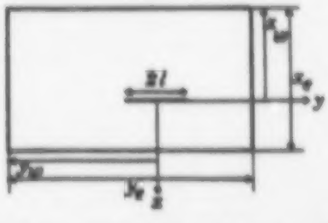

Figure 8 : Puits horizontal dans réservoir limité.

La géométrie de ce système est déterminée par les 4 paramètres supplémentaires suivants :
$l_{D_1} = \ell / x_e \quad l_{D_2} = \ell / y_e \quad e_{D_1} = x_W / x_e \quad e_{D_2} = y_W / y_e$

La solution analytique pour un flux uniforme dans le puits, donnée dans l'annexe 2, est de la forme :
$p_D = p_D\,(t_D,\, y_D,\, l_{D_1},\, l_{D_2}, l_{D_3},\, e_{D_1},\, e_{D_2},\, e_{D_3},\, x_{WD})$.

Par raison de symétrie, nous pouvons nous limiter, moyennant certaines précautions (annexe 2) aux valeurs d'excentrement adimensionnel e_D supérieures à 0,5.

La solution pour un puits de conductivité infinie est toujours assimilable à la solution "flux uniforme" avec $y_D = \pm\, 0{,}7$ dans le cas : $e_{D_2} = 0{,}5$ (cf annexe 2).

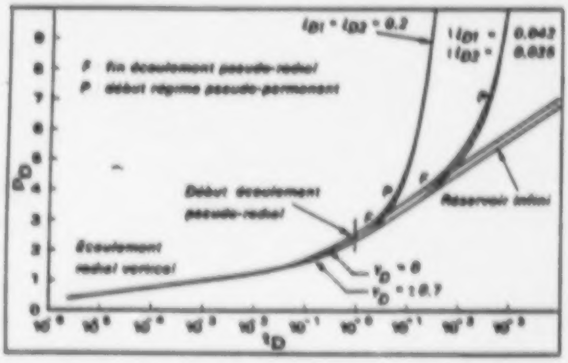

Figure 9 : Puits horizontal dans réservoir limité par des frontières imperméables.

Figure 9	Paramètre sans dimension				
	y_D	e_{D_3}	l_{D_3}	C_D	S
Paramètres communs	0 ± 0,7	0,75	2,5	0	0
	e_{D_1}	e_{D_2}	l_{D_1}	l_{D_2}	x_{WD}
Géométrie N° 1	0,5	0,5	0,2	0,2	0,0004
Géométrie N° 2	0,75	0,5	0,042	0,025	-0,0004
Géométrie N° 3	RESERVOIR INFINI				0,0004

	Exemple de valeurs correspondantes			
	2ℓ	h	x_W	r_W
Paramètres communs	500m (1640ft)	100m (328ft)	75m (246ft)	0,1m (0,33ft)
	x_e	y_e	x_w	y_w
Géométrie N° 1	1250m (4101ft)	1250m (4101ft)	625m (2051ft)	625m (2051ft)
Géométrie N° 2	6000m (19685ft)	10000m (32808ft)	4500m (14764ft)	5000m (16404ft)
Géométrie N° 3	RESERVOIR INFINI			

TABLEAU IV - (Figure 9)

La solution de l'annexe 2 a été contrôlée en prenant : $y_e = 2\ell$, $h = x_e$ et $e_{D_1} = e_{D_2} = e_{D_3} = 0{,}5$. Notre solution coïncide alors parfaitement avec celle obtenue pour un puits vertical centré dans un réservoir d'épaisseur 2ℓ, limité par une frontière imperméable carrée (côté de longueur $x_e = h$)^6. Pour les petites valeurs du temps, le puits se comporte comme si le réservoir était infini car les effets des frontières ne sont pas encore ressentis (courbes confondues sur la figure 9).

Après un temps suffisamment long, on observe, sur un graphique cartésien, une droite dont la pente est ,

$$\frac{dp_D}{dt_D} = 2\pi\, l_{D_1}\, l_{D_2}, \text{ soit } \frac{dp}{dt} = -\frac{qB}{x_e y_e h \phi c_t}$$

pente caractéristique du régime pseudo-permanent. Les courbes correspondant à $y_D = \pm\, 0{,}7$ sont toujours confondues puisque $e_{D_2} = 0{,}5$.

Un phénomène important apparaît sur ces courbes de la figure 9. La droite semi-log, caractéristique de l'écoulement pseudo-radial, est absente dans le cas de la géométrie n° 1 de cette figure car le régime transitoire se termine très tôt sous l'effet des frontières. Comme, par ailleurs, l'écoulement radial vertical est le plus souvent masqué par la capacité du puits, un essai effectué dans le cas de la géométrie n° 1 risque fort d'être ininterprétable, aucune analyse semi-log ne pouvant être effectuée.

Avant de décider un test dans un puits horizontal, il est donc indispensable d'estimer au préalable l'époque de la fin de l'écoulement pseudo-radial. Pour cela, la meilleure méthode consiste à générer une courbe type prévisionnelle, à l'aide de la solution analytique de l'annexe 2, comme pour la figure 9.

Nous avons également cherché un critère qui permet de prévoir, approximativement mais rapidement, la fin de l'écoulement pseudo-radial. Dans ce but, nous avons tracé de nombreuses courbes à l'aide de la solution (A-6) avec diverses valeurs de l_{D_1}, l_{D_2}, e_{D_1}, e_{D_2} et y_D.

A l'époque Δt de la fin de l'écoulement pseudo-radial, nous avons associé le temps t_{D_0} rapporté, non plus à ℓ^2, mais au carré de la distance du centre du puits horizontal à la frontière la plus proche. Suivant les cas, la frontière la plus proche peut être parallèle ou perpendiculaire au puits. Nous avons donc :

$$t_{D_0} = \left(\frac{l_{D_1}}{1-e_{D_1}}\right)^2 t_D \text{ ou } t_{D_0} = \left(\frac{l_{D_2}}{1-e_{D_2}}\right)^2 t_D$$

pour $e_{D_1} \geqslant 0{,}5$ $e_{D_2} \geqslant 0{,}5$

Nous avons trouvé, pour toutes les configurations traitées, que t_{D0} variait de 0,3 à 0,5. Comme il ne s'agit que d'un critère approximatif, nous adoptons t_{D0} = 0,4. Dans les géométries n°^{s} 1 et 2 du tableau IV, ce critère conduit à prévoir la fin de l'écoulement pseudo-radial aux valeurs respectives suivantes : $t_{D1} = 2,5$ et $t_{D2} = 14,3$, qui sont cohérentes avec la figure 9. Prenons encore, par exemple :
$2l = 400m$ (1312ft)
$\phi c_t = 10^{-7} kPa^{-1}$ (0,7 10^{-6} psi^{-1}).
k/μ=10md/(mPa.s) (10md/cp).

Les valeurs t_{D1} et t_{D2} correspondent alors aux temps réels de 12 et 68 jours.

4. PUITS HORIZONTAL DANS UN RESERVOIR HOMOGENE LIMITE PAR UNE FRONTIERE MAINTENUE A PRESSION CONSTANTE

Les hypothèses et les configurations traitées ici sont les mêmes que dans le paragraphe précédent (fig. 8). La frontière rectangulaire est cette fois maintenue à pression constante.

La solution analytique, détaillée dans l'annexe 3, a permis de tracer les courbes de la figure 10, les valeurs des paramètres étant toujours celles du tableau IV.

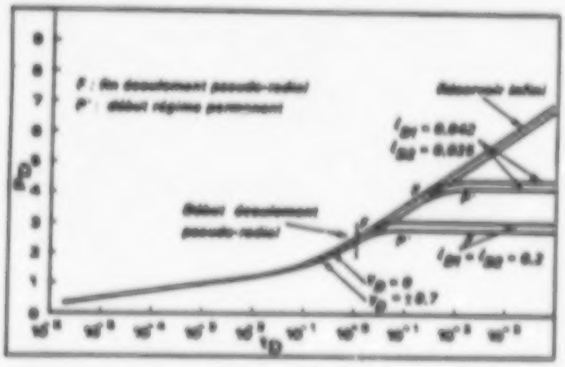

Figure 10 : Puits horizontal dans réservoir avec frontières maintenues à pression constante.

L'établissement de l'écoulement permanent, à partir duquel la pression p_D garde une valeur constante, apparaît clairement sur ces courbes.

Les conclusions et les critères, établis au paragraphe 3 et concernant la fin de l'écoulement pseudo-radial, restent inchangés. Ils sont donc encore directement applicables quand les frontières sont maintenues à pression constante. Nous sommes donc en mesure de proposer des critères de temps valables pour toutes les configurations (Tableau V où e_{D1}>0,5 e_{D2}>0,5 e_{D3}>0,5)

	Ecoulement radial vertical	
	Début	Fin
t_D	Fin effet de capacité de puits	$\min\left[\frac{(1-y_D)^2}{6};0,32\left(\frac{1-e_{D1}}{l_{D1}}\right)^2\right]$
	Ecoulement pseudo-radial	
	Début	Fin
t_D	1,5 à 2	$\min\left[0,4\left(\frac{1-e_{D1}}{l_{D1}}\right)^2;0,4\left(\frac{1-e_{D2}}{l_{D2}}\right)^2\right]$

TABLEAU V

5. SOLUTION APPROCHEE POUR UN PUITS HORIZONTAL DE CONDUCTIVITE INFINIE

Un puits horizontal réel se comporte certainement comme un puits de conductivité infinie. Par analogie avec les résultats connus pour une fracture hydraulique verticale, on pouvait espérer que la solution pour un puits de conductivité infinie soit assimilable à la solution "flux uniforme" obtenue pour une valeur fixe de y_D (appelée "point équivalent") à déterminer.

Le modèle utilisé pour effectuer cette recherche [7] du point équivalent y_D, simule le drain horizontal par une succession de sources ponctuelles. Il est alors possible de fixer le débit de chaque source ponctuelle et, par conséquent, de simuler aussi bien un puits de conductivité infinie qu'un puits avec flux uniforme.

Les résultats de ce modèle concordent parfaitement, avec les nôtres. Tous les cas traités par G. Ruez [7], montrent que, pour les longueurs vraisemblables des puits horizontaux, la valeur de y_D cherchée reste comprise entre 0,67 et 0,72. Par ailleurs, les courbes (flux uniforme) correspondant à ces deux valeurs de y_D sont extrêmement voisines. La solution "flux uniforme" avec $y_D = 0,7$ est donc généralement une approximation tout à fait acceptable pour simuler le comportement d'un puits de conductivité infinie. Rappelons seulement que ce résultat est valable pendant tout le régime transitoire (c'est-à-dire jusqu'à la fin de l'écoulement pseudo-radial) et n'est théoriquement extrapolable aux réservoirs limités que si $e_{D2} = 0,5$ (annexe 2).

6. CONCLUSIONS

Nous avons étudié le comportement d'un puits horizontal avec flux uniforme ou conductivité infinie, de capacité et de skin non nuls, mis en production, dans un réservoir infini ou limité (frontière imperméable ou à pression imposée).

Des solutions analytiques facilement exploitables par un mini-ordinateur ont été développées. Le simulateur analytique ainsi obtenu est un outil extrêmement utile pour le "design" et l'interprétation d'un essai dans un puits horizontal.

Nous avons mis en évidence la succession de deux types d'écoulement caractéristiques des puits horizontaux : un écoulement radial vertical puis un écoulement pseudo-radial horizontal.

Ces deux types d'écoulement donnent lieu, dans les cas favorables, à des droites semi-log, auxquelles on peut adapter l'analyse semi-log classique (en introduisant un skin géométrique).

Enfin, des critères de temps commodes (tableau V) ont été établis, pour prévoir le début et la fin de chacun de ces types d'écoulement, susceptibles de donner lieu à une analyse semi-log.

En pratique, l'écoulement radial vertical initial sera très souvent masqué par l'effet de capacité de puits. Il faudra donc impérativement s'assurer, avant de décider un essai dans un puits horizontal, que l'écoulement pseudo-radial pourra être observé c'est-à-dire que les frontières du réservoir ne perturberont pas trop tôt la pression dans le puits ou que la durée de l'essai ne sera pas prohibitive.

Si ces conditions ne sont pas respectées, l'essai risque fort d'être ininterprétable. Ce contrôle pourra être effectué grâce aux critères du tableau V ou mieux, à l'aide des solutions analytiques décrites dans les annexes.

Remerciements

Les auteurs sont reconnaissants à la Société Elf Aquitaine et à l'Institut Français du Pétrole d'avoir autorisé cette publication. Ils remercient tous ceux qui ont participé à cet effort et plus particulièrement G.Rues SNEA(P), P.Ménégatti SNEA(P) et L.H.Reiss SNEA(P).

Unités pratiques

	Pour convertir en		Multiplier par
	Unités pratiques américaines	Unités métriques pratiques	
Longueur	ft	m	$3,048\ 10^{-1}$
Perméabilité	md	md	1,0
Pression	psi	kPa	6,895
Température	°R	K	$5,555\ 10^{-1}$
Temps	hr	h	1,0
Viscosité	cp	mPa.s	1,0
Volume	bbl	m^3	$1,59\ 10^{-1}$
Volume	cu ft	m^3	$2,832\ 10^{-2}$

TABLEAU VI

Fonctions :

e^x fonction exponentielle

$\ln(x)$ logarithme népérien

$$\mathrm{erf}(x) = \frac{2}{\sqrt{\pi}} \int_0^x e^{-u^2}\, du$$

$$-\,\mathrm{Ei}(-x) = \int_x^{\infty} \frac{e^{-u}}{u}\, du$$

Bibliographie

1. L.H. REISS, A.P.L. JOURDAN, F.M. GIGER and P.A. ARMESSEN : "Offshore and Onshore European Horizontal Wells" OTC 4791 (1984).
2. A.C. GRINGARTEN, H.J. RAMEY Jr : "The use of source and Green's functions in solving unsteady-flow problems in reservoirs" Trans, AIME, vol 255 (1973)
3. F.DAVIAU : "Interprétation des essais de puits : les méthodes nouvelles" Cours Ecole Nationale Supérieure du Pétrole et des Moteurs. Réf. 31 770. Décembre 1983 (A paraître aux éditions Technip).
4. F.GIGER : "Réduction du nombre de puits pour l'utilisation des forages horizontaux" Rev. Inst. Franç. du Pétrole, vol. 38, n° 3, mai-juin 1983.
5. H.CINCO-LEY, F.SAMANIEGO "Effect of wellbore storage and damage on the transient pressure behavior of vertically fractured wells "SPE6752 (1977).
6. R.C. EARLOUGHER Jr : "Advances in well test analysis", Monograph Series, SPE of AIME Dallas (1977).
7. G.RUEZ : Communication personnelle.

ANNEXE 1

PUITS HORIZONTAL AVEC FLUX UNIFORME DANS UN RESERVOIR HOMOGENE INFINI

A - SOLUTION ANALYTIQUE

Nous conservons les notations et les hypothèses du paragraphe 2 et de la figure 1. La solution analytique du problème s'établit aisément à l'aide des fonctions de Green [3] et en particulier, des fonctions répertoriées par A.C. Gringarten, et al[2].

La pression dans le puits, écrite avec nos groupements de paramètres, sans dimension est donnée par l'équation (A-1) du tableau VII

Cette expression est invariante quand on change y_D en $-y_D$ ou e_{D3} en $1-e_{D3}$.

Pour simplifier la suite, notons respectivement $f_1\ (\tau_D)$, $f_2\ (\tau_D)$ et $f_3\ (\tau_D)$ les trois termes qui interviennent sous le signe "intégrale" de (A-1).

B. SOLUTIONS APPROCHEES - CRITERES DE TEMPS

B.1. Petites valeurs du temps

Les comportements asymptotiques des fonctions f_1, f_2 et f_3 quand τ_D tend vers zéro sont connus. δ étant la distance entre le point de mesure M (y_D) et l'extrémité du drain la plus proche, nous avons, pour τ_D petit[2] :

- $f_2(\tau_D)=2$ pour $y_D \neq 1 (kt/(\phi\mu c_t \delta^2) < 1/20)$
- $f_2(\tau_D)=1$ pour $y_D = 1\ (kt/(\phi\mu c_t \ell^2) < 1/20)$
- $f_3\ (\tau_D) = 1/(2 l_{D3} \sqrt{\pi \tau_D})$

La solution approchée de (A1) pour τ_D petit s'écrit alors, quand y_D est différent de 1 (écoulement radial vertical) :

$$p_D\ (t_D) = \frac{1}{4 l_{D3}} \int_0^{t_D} \frac{e^{-\pi y_D^2/4\tau_D}}{\tau_D}\, d\tau_D$$

$$= \frac{1}{2 l_{D3}} \cdot \left[- \frac{1}{2}\, \mathrm{Ei}\ (- \frac{\pi y_D^2}{4 t_D}) \right] \qquad \text{(A-2)}$$

Si $y_D = 1$, le coefficient $1/(2 l_{D3})$ devient $1/(4 l_{D3})$.

L'approximation de la fonction $f_2\ (\tau_D)$ n'est plus valable quand l'effet de pointes est ressenti. Mais le critère donné ci-dessus, en fonction de δ, concerne directement la fonction $f_2\ (\tau_D)$ et se révèle beaucoup trop sévère si on l'applique brutalement à la fonction p_D. L'analyse de toutes les courbes générées par (A-1) nous a montré qu'un critère beaucoup mieux adapté à la fonction p_D est obtenue en remplaçant 1/20 par 1/6. Nous retiendrons donc que l'effet de pointe est ressenti dès que $t_D > (1-y_D)^2/6$ en unités cohérentes.

L'approximation de $f_3\ (\tau_D)$ devient illicite dès que l'éponte la plus proche influence la pression dans le drain. Tant que l'écoulement est radial vertical, le problème est identique à celui d'un puits vertical situé à une distance "d" d'une faille étanche. Dans ce cas classique, la formule du rayon d'investigation ($kt/(\phi\mu c_t d^2)=0,25$) donne systématiquement des valeurs trop faibles pour le temps. C'est pourquoi nous lui préférons : $kt/(\phi\mu c_t d^2)=0,32$. Un puits horizontal ne sera donc influencé par l'éponte la plus proche que pour :

$$t_D > 0,32 \left(\frac{1 - e_{D3}}{l_{D3}}\right)^2 \quad (e_{D3} > 0,5)$$

B.2. Grandes valeurs du temps

Quand τ_D devient très grand, nous avons cette fois :

$$f_1\ (\tau_D) = \frac{1}{\sqrt{\tau_D}}\ ,\ f_2\ (\tau_D) = \frac{2}{\sqrt{\pi\tau_D}}\ ,\ f_3\ (\tau_D) = 1$$

La solution (A1) conduit alors à l'équation de l'écoulement pseudo-radial :

$$p_D\ (t_D) = 0,5\ (\ln t_D + \alpha) \qquad \text{(A-3)}$$

C. SKIN GEOMETRIQUE

Dans (A-3), le terme α englobe plusieurs phénomènes qu'il est essentiel de bien distinguer (paragraphe 2P-2-b). Supposons ici que le skin réel S du puits soit nul. Par définition de l'écoulement pseudo-radial (paragraphe 2-B-1), la perte de charge, dans la région où les lignes de courant sont déformées par la présence du drain, est constante et se traduit par un pseudo-skin (ou skin géométrique S_g) négatif. S_g dépend de la configuration réservoir-puits horizontal. La loi de l'écoulement pseudo-radial s'écrit, pour S nul :

$$P_i - P_{wf}\ (t) = \frac{qB\mu}{4\pi kh}\ (\ln \frac{kt}{\phi\mu c_t r_w^2} + 0,809 + 2\ S_g) \qquad \text{(A-4)}$$

Pendant l'écoulement pseudo-radial, le comportement d'un puits horizontal de skin géométrique S_g est donc identique au comportement d'un puits vertical de rayon $r'_w = r_w\, e^{-S_g}$. Or, nous connaissons par ailleurs[4] la relation entre r'_w et r_w dans le cas d'un drain horizontal de conductivité infinie, centré dans le réservoir. Cette relation s'écrit :

$$r'_w = \frac{\ell\ (2\pi r_w/h)^{h/2\ell}}{1 + \sqrt{1-(\ell/r_e)^2}}$$

où r_e est le rayon de drainage du puits. Ici, l'écoulement pseudo-radial étant atteint, nous pouvons supposer que $\ell/r_e \ll 1$ et la relation précédente peut alors être simplifiée.

Nous en déduisons le skin géométrique pour un drain centré :

$$S_g = \ln \frac{r_w}{r'_w} = \ln \frac{2\ r_{wD}}{(2\pi r_{wD} l_{D3})^{1/(2 l_{D3})}} \qquad \text{(A-5)}$$

Cette formule est valable pour le cas qui nous intéresse c'est-à-dire pour un puits de conductivité infinie. Elle a été établie avec un puits centré mais l'erreur commise pour des excentrements raisonnables

...

est faible. Reprenons l'exemple des figures 5 et 6 où l'excentrement est $e_{D_3} = 0,75$. Nous avons évalué le skin géométrique à partir de la formule (A-5) qui suppose $l_{D_3} = 0,5$ et nous avons recalculé les pressions pendant l'écoulement pseudo-radial à l'aide de la loi logarithmique (A-4). La comparaison entre ces valeurs calculées et les valeurs relevées sur la figure 6 montrent que la formule (A-5) introduit une erreur sur les pressions, de l'ordre de 3% seulement. En pratique, la formule (A-5) permet d'estimer S_g avec une précision largement suffisante sauf peut être dans le cas de puits très excentrés (excentrements très supérieurs à 0,75) où la valeur obtenue pour S_g devra être regardée comme un ordre de grandeur.

ANNEXE 2

PUITS HORIZONTAL AVEC FLUX UNIFORME DANS UN RESERVOIR HOMOGENE LIMITE (FRONTIERE IMPERMEABLE)

A. SOLUTION ANALYTIQUE

Une démarche analogue à celle de l'annexe 1 conduit à la solution au puits, écrite avec les groupements de paramètres supplémentaires du paragraphe 3 (Fig. 1 et 8) : équation (A-6) Tableau VII.

B. REMARQUE

Par raison de symétrie, nous pouvons restreindre notre champ d'étude aux cas :

$e_{D_1} > 0,5$; $e_{D_2} > 0,5$; $e_{D_3} > 0,5$

Les résultats sont en effet identiques, quand on change e_{D_1} en $1-e_{D_1}$, à condition de remplacer x_{WD} par $-x_{WD}$, ou e_{D_2} en $1-e_{D_2}$, à condition de remplacer y_D par $-y_D$.

Notons, en particulier, que lorsque e_{D_2} est peu différent de 0,5, la pression est la même en y_D et en $-y_D$. On peut admettre alors que la solution "flux uniforme" avec $y_D = \pm 0,7$, simule toujours correctement un drain de conductivité infinie.

Mais cette conclusion ne peut pas être généralisée aux cas $e_{D_2} \neq 0,5$ pour lesquels nous pouvons seulement remarquer que, lorsque y_D varie, les courbes obtenues ne sont jamais très éloignées l'une de l'autre.

ANNEXE 3

PUITS HORIZONTAL AVEC FLUX UNIFORME DANS UN RESERVOIR HOMOGENE DONT LA FRONTIERE EST MAINTENUE A PRESSION CONSTANTE

La méthode utilisée pour résoudre ce problème est tout à fait similaire à celle de l'annexe 2 et conduit à l'équation (A-7) du tableau VII.

Les remarques faites dans l'annexe 2 restent valables ici.

ANNEXE 1

$$p_D(t_D) = \frac{\sqrt{\pi}}{4}\int_0^{t_D}\frac{e^{-x_{wD}^2/4\tau_D}}{\sqrt{\tau_D}}\left(\mathrm{erf}\,\frac{1+y_D}{2\sqrt{\tau_D}} + \mathrm{erf}\,\frac{1-y_D}{2\sqrt{\tau_D}}\right).\left[1+2\sum_{n=1}^{\infty} e^{-n^2\pi^2 l_{D_3}^2\tau_D}.\cos^2(n\pi e_{D_3})\right]d\tau_D \qquad \text{(A-1)}$$

ANNEXE 2

$$p_D(t_D)=2\pi l_{D_1} l_{D_2}\int_0^{t_D}\left\{1+2\sum_{n=1}^{\infty} e^{-n^2\pi^2 l_{D_1}^2\tau_D}.\cos(n\pi e_{D_1}).\cos[n\pi(e_{D_1}+x_{wD}l_{D_1})]\right\}.\left\{1+\frac{2}{\pi l_{D_2}}\sum_{n=1}^{\infty}\frac{1}{n}e^{-n^2\pi^2 l_{D_2}^2\tau_D}\right.$$

$$\left..\sin(n\pi l_{D_2}).\cos(n\pi e_{D_2}).\cos[n\pi(e_{D_2}+y_D l_{D_2})]\right\}.\left\{1+2\sum_{n=1}^{\infty} e^{-n^2\pi^2 l_{D_3}^2\tau_D}.\cos^2(n\pi e_{D_3})\right\}d\tau_D \qquad \text{(A-6)}$$

ANNEXE 3

$$p_D(t_D) = 8 l_{D_1}\int_0^{t_D}\left\{\sum_{n=1}^{\infty} e^{-n^2\pi^2 l_{D_1}^2\tau_D}.\sin(n\pi e_{D_1})\,.\sin[n\pi(e_{D_1}+x_{wD}l_{D_1})]\right\}.\left\{\sum_{n=1}^{\infty}\frac{1}{n}e^{-n^2\pi^2 l_{D_2}^2\tau_D}\,.\sin(n\pi l_{D_2}).\right.$$

$$\left..\sin(n\pi e_{D_2})\sin[n\pi(e_{D_2}+y_D l_{D_2})]\right\}.\left\{1+2\sum_{n=1}^{\infty} e^{-n^2\pi^2 l_{D_3}^2\tau_D}.\cos^2(n\pi e_{D_3})\right\}d\tau_D \qquad \text{(A-7)}$$

TABLEAU VII

9010607

Alberta OIL SANDS
INFORMATION CENTRE

SPE
Society of Petroleum Engineers

SPE 14250

(76)

Pressure Drawdown and Buildup Analysis of Horizontal Wells in Anisotropic Media

by P.A. Goode and R.K.M. Thambynayagam, *Sohio Petroleum Co.*

SPE Members

Copyright 1985, Society of Petroleum Engineers

This paper was prepared for presentation at the 60th Annual Technical Conference and Exhibition of the Society of Petroleum Engineers held in Las Vegas, NV September 22-25, 1985.

This paper was selected for presentation by an SPE Program Committee following review of information contained in an abstract submitted by the author(s). Contents of the paper, as presented, have not been reviewed by the Society of Petroleum Engineers and are subject to correction by the author(s). The material, as presented, does not necessarily reflect any position of the Society of Petroleum Engineers, its officers, or members. Papers presented at SPE meetings are subject to publication review by Editorial Committees of the Society of Petroleum Engineers. Permission to copy is restricted to an abstract of not more than 300 words. Illustrations may not be copied. The abstract should contain conspicuous acknowledgment of where and by whom the paper is presented. Write Publications Manager, SPE, P.O. Box 833836, Richardson, TX 75083-3836. Telex, 730989 SPEDAL.

ABSTRACT

An analytical solution is presented for the pressure response during drawdown and buildup of a horizontal well. This method results from solving the 3D diffusion equation using successive integral transforms. Simplified solutions for short, intermediate and long time, which exhibit straight line sections when pressure is graphed against time, are presented. The validity of the method is demonstrated by comparison with results generated numerically by a reservoir simulator and with an analogous analytical solution. Methods for analyzing pressure drawdown and buildup data are presented with worked examples. The method allows reservoir characteristics, including permeability, skin and distance to boundaries, to be determined. The early time effects, where the well behaves as if it were in an infinite reservoir, are also discussed. Expressions to determine times to critical events, which are important for well test design, are presented.

INTRODUCTION

The idea of using horizontal wells to increase the area of reservoir contacted dates back to the early 1940's.[1-13] But until recently, very few horizontal wells have been drilled in the non-communist world. There has been little incentive to spend additional money on a new technique when most reservoirs can be economically produced by conventional techniques such as stimulation by fracturing. For a long time, hydraulic fracturing has been a potential rival to horizontal drilling. Although compared with vertical wells, horizontal wells could increase injection or production rates several times over. However, the technique was considered only when stimulation by hydraulic fracturing from vertical wells was not feasible, or not practicable.

Recently, the usefulness of horizontal wells has been demonstrated in North America[14-28] and Western Europe.[29-44] With the present day technology, horizontal drainhole distances that are much longer than the fracture lengths achieved by hydraulic fracturing are possible at moderate costs. ARCO[14-15] in 1979, rejuvenated their high GOR wells by horizontal drainholes. Serious gas coning problems were thus overcome. The danger of extending into the gas cap had precluded hydraulic fracturing. In 1978, Esso Resources[18], Canada drilled a horizontal well at the Cold Lake Leming Pilot to field-test thermally aided gravity drainage processes. Texaco[16-17] Canada, in 1980, completed a drilling program to tap an unconsolidated bituminous sand at shallow depths in its Athabasca Lease.

In Western Europe, between 1979 and 1983, Societe Nationale Elf-Aquitaine, in association with the Institut Francais du Petrole, drilled four horizontal wells in oil-bearing reservoirs. Three of these wells are located in the Lac Superieur and Castera Lou fields[29-33] in France. The fourth one is offshore in the Karstic reservoir of the Rospo Mare field[34] in the Italian part of the Adriatic sea. The reservoirs consist of thin, soft, vertically-fractured, tight formations with fluid interface problems and have been found to be ideal candidates for horizontal wells. When the Rospo Mare Pilot was initiated, it was reported[33] that productivity was twenty times greater in the horizontal well compared to that of the neighboring vertical and deviated wells. The horizontal well intersected several voids and was positioned to obtain the greatest possible height above the water oil contact. Lower, near-wellbore drawdown prevented water from coning.

Several researchers[5-9,45-48] have studied horizontal well productivity. Efros[47] and, later, Giger[48] considered the relative economics of the horizontal wells on overall productivity by studying the geometry and spacing of the horizontal wells. Giger[49] investigated the merits of the horizontal wells in preventing water and gas influxes during multiphase flow. His calculations show that horizontal wells

References and illustrations at end of paper.

provide greater sweep efficiencies. Giger[31] also studied the use of horizontal wells to improve oil recovery in formations with fluid interface problems.

Recently, Butler et al[50-54], Joshi and Threlkeld[55], Griffin and Trofimenkoff[56] and Rial[57] have conducted laboratory studies on thermally-aided gravity drainage of viscous oil in horizontal wells. Huygen and Black[58] investigated the problem of cyclic steam stimulation through horizontal wells and have had encouraging results. Despite the unfavorable mobility ratios associated with heavy oils, horizontal wells provide a more homogeneous steam front and a much greater injectivity index than does a vertical well.

Although horizontal drilling activities have been the focus of much attention during recent years, there appears to have been no study in the area of pressure transient analysis of horizontal wells. The accomplishments so far must be augmented by attempts to understand pressure data from well testing. Cinco et al[59] presented analytic solutions of unsteady-state pressure distribution created by a directionally drilled well in an anisotropic medium. Gringarten et al[60], Raghavan et al[61] and Rodriguez et al[62] have obtained analytic solutions to the problem of transient flow of fluids towards fully and partially penetrating vertical fractures. These solutions correspond closely to that of horizontal wells. The mathematical method applied to solve these problems was based on the use of Green's and Source Functions whose usefulness in solving such problems has been demonstrated by Gringarten and Ramey[63]. The derivation of these solutions and the form of the results are, however, complicated and the extension of the methods to analysis of pressure transient data from horizontal wells is not immediately apparent.

The purpose of this paper is to present a straightforward analytic solution for the pressure drawdown and buildup associated with testing a horizontal well in an undersaturated oil zone. This method is the result of an elegant mathematical procedure using successive integral transforms (Laplace and Fourier). The paper highlights one of the problems with Laplace transforms, which is, that they are sometimes difficult to analytically invert. On the other hand, if they can be analytically inverted, as will be seen in this paper, the resulting solution is often more elegant and easily followed. The reason for this is that the solution of the diffusivity equation, by integral transforms, is usually in terms of functions (eg: Exponential integral, Error functions or Bessel functions) which are familiar to the petroleum industry and are generally free of badly behaved integrals that require numerical evaluation. One of the drawbacks of the application of Fourier transforms is that the resulting solution is usually in the form of an infinite series which can be slow in converging. The problem studied in this paper is a classic example of how the physical nature of the problem can be used to simplify such solutions containing infinite series without any loss of accuracy.

In order to demonstrate the validity of the derivation, the analytic solutions are compared with the results of extensive numerical studies undertaken as part of this work and an existing analogous analytical solution. Sample calculations are presented to illustrate the determination of reservoir characteristics, including permeabilities and skin factor.

The present, "state of the art", well testing theory does not provide for well test interpretation of horizontal wells. The theory presented in this paper fills this void.

THEORY

Mathematical Solution

The physical model considered in this analysis consists of an infinite conductivity horizontal well located at the center of a semi-infinite homogeneous and anisotropic medium of uniform thickness and width. The formation fluid properties are independent of pressure. A slightly compressible fluid of constant compressibility is produced through the horizontal well. Gravity effects are neglected. The model is illustrated in Figure 1.

The partial differential equation governing the isothermal fluid flow in this medium is given by,

$$\left(\frac{\phi\mu c}{k_y}\right)\frac{\partial p}{\partial t} = \left(\frac{\partial^2 p}{\partial y^2}\right) + \frac{k_z}{k_y}\left(\frac{\partial^2 p}{\partial z^2}\right) + \frac{k_x}{k_y}\left(\frac{\partial^2 p}{\partial x^2}\right) \qquad \ldots(1)$$

The initial and boundary conditions are:

1). The reservoir pressure is initially constant.

2). The reservoir is assumed to be semi-infinite. The pressure at infinity is not affected by the pressure disturbance at the wellbore.

3). In order to develop the solution as a first approximation, the horizontal well is replaced with a thin strip source of width (b-a) and length (l-d). This provides a mathematically tractable boundary condition at the wellbore. This assumption will be later removed and the horizontal well reinstated with its original configuration. During the drawdown period uniform flux along the length of the wellbore is assumed. However, as will be seen later, this restriction is accounted for in the final solution. No fluid will be entering the wellbore during the buildup period.

4). No fluid flow across the over or under burden.

5). No fluid flow across the lateral extremities of the reservoir.

The foregoing may be written mathematically as follows:

(i) $p = p_i$ at $t = 0$ for all x, y and z

(ii) $p = p_i$ as $y \longrightarrow \infty$ for all x, z and t

$$\text{(iii)} \quad \lim_{y \to 0} \int_a^b \int_d^l \left(\frac{\partial p}{\partial y}\right) dx\,dz = \begin{cases} \left.\begin{cases} 0 & 0 \le x \le d \\ \left.\begin{cases} 0 & 0 \le z \le a \\ -\frac{q\mu}{2k_y} & a < z \le b \\ 0 & b < z \le H_z \end{cases}\right\} & d < x \le l \\ 0 & l < x \le H \end{cases}\right\} & 0 \le t < t_p \\ 0 & t > t_p \end{cases}$$

(iv) $\frac{\partial p}{\partial z} = 0$ at $z = 0$ and $z = H_z$

(v) $\frac{\partial p}{\partial x} = 0$ at $x = 0$ and $x = H_x$

The general solution of the problem is obtained by successive application of Laplace and finite Fourier integral cosine transforms. The complete derivation is resented in Appendix A. The general solution is given Equation (A9). By setting y = 0 in Equation (A9) nd converting to field units, an expression is obtained for pressure response at the wellbore during isothermal drawdown and buildup and is given by Equation (A10).

In most practical cases $v_x \ll v_z$ (i.e. $H_x \gg H_z$), that is the width of the reservoir is much greater than the thickness of the formation. In the case where the reservoir is infinite in the x direction, $v_x \rightarrow 0$. By using this physical characteristics of the reservoir and introducing the Van Everdingen[64] mechanical skin factor into Equation (A10), the pressure response at the wellbore during drawdown and buildup is given by:

Pressure Drawdown

$$p_i - p_{wf} = \frac{282.4\, q\mu B_o}{H_x H_z k_y}\left[\sqrt{\pi\tau} + \frac{H_x}{v_x}\sum_{n=1}^{\infty}\frac{1}{n}\,\mathrm{erf}(v_x n\sqrt{\tau})\, X_n \mathrm{Cos}(nX) + \frac{H_x H_z}{(s-d)v_z}\sum_{m=1}^{\infty}\frac{1}{m}\,\mathrm{erf}(v_z m\sqrt{\tau})\, Z_m \mathrm{Cos}(mZ) + \frac{H_z H_x\sqrt{k_y/k_z}}{2\,(s-d)}\, S_m\right]_{0<\tau<\tau_o} \quad \ldots(2)$$

Pressure Buildup

$$p_i - p_{ws} = \frac{282.4\, q\mu B_o}{H_x H_z k_y}\left[\sqrt{\pi}(\sqrt{\tau} - \sqrt{\Delta\tau}) + \frac{H_x}{v_x}\sum_{n=1}^{\infty}\frac{1}{n}\left\{\mathrm{erf}(v_x n\sqrt{\tau}) - \mathrm{erf}(v_x n\sqrt{\Delta\tau})\right\} X_n \mathrm{Cos}(nX) + \frac{H_x H_z}{(s-d)v_z}\sum_{m=1}^{\infty}\frac{1}{m}\left\{\mathrm{erf}(v_z m\sqrt{\tau}) - \mathrm{erf}(v_z m\sqrt{\Delta\tau})\right\} Z_m \mathrm{Cos}(mZ)\right]_{\tau>\tau_o} \quad \ldots(3)$$

where

$$X_n = \left[\mathrm{Sin}\left\{\frac{n\pi s}{H_x}\right\} - \mathrm{Sin}\left\{\frac{n\pi d}{H_x}\right\}\right] / (n(s-d)) \quad \ldots(4)$$

$$Z_m = \left[\mathrm{Sin}\left\{\frac{m\pi}{H_z}(H_s + 2r_w')\right\} - \mathrm{Sin}\left\{\frac{m\pi}{H_z}(H_s - 2r_w')\right\}\right] / (m\,(4r_w')) \quad \ldots(5)$$

$$r_w' = r_w\left(\frac{k_z}{k_y}\right)^{1/4} \quad \ldots(6)$$

$$X = \frac{\pi}{H_x}(0.131\, s + 0.869\, d) \quad \ldots(7)$$

$$Z = \frac{\pi}{H_z}(H_s + 1.47 r_w') \quad \ldots(8)$$

$$v_x = \left(\frac{\pi}{H_x}\right)\sqrt{\frac{k_x}{k_y}} \quad \ldots(9)$$

$$v_z = \left(\frac{\pi}{H_z}\right)\sqrt{\frac{k_z}{k_y}} \quad \ldots(10)$$

$$\tau = \frac{.000264\, k_y t}{\phi\mu c_t} \quad \ldots(11)$$

$$\Delta\tau = \tau - \tau_o \quad \ldots(12)$$

and S_m is the mechanical skin factor.

n the derivation of Equations (2) and (3) for pressure drawdown and buildup, the thin strip source approximation has been removed using an effective wellbore radius equal to one quarter the strip width, as suggested by Prats[65] and multiplying by the fourth root of the permeability ratio of the y and z dimensions to account for anisotropy. This substitution may be written mathematically as:

$$(b-a) = 4\, r_w\left(\frac{k_z}{k_y}\right)^{1/4} \quad \ldots(13)$$

Furthermore, the flux density over the well may be assumed uniform and the pressure taken at an "effective average", which is at a dimensionless distance of .869 from either of the extremities of the well, provided the well is placed in the center of the formation. If the well is placed at either of the boundaries, the "effective average" pressure is at .738 of the distance from the end of the well that is adjacent to the boundary. For a well placed between these two extremes the "effective average" will be at .869 until the transient hits the nearer boundary, at which time it will start to move toward .738. For this intermediate case the steady state position for the "effective average" will be at some point between .869 and .738 depending upon the location of the well relative to the boundaries. Gringarten[60] suggested a distance of .866, however .869 better satisfies his Equation (10). Muskat[66] found a similar result for partially penetrating wells. Figure 2 presents a graph of the flux distribution along the strip source as calculated by Gringarten. The same distribution applies for an infinite conductivity horizontal well.

Pressure Drawdown

The general expression for the pressure drawdown Equation (2) can be approximated and simplified by considering the following time intervals separately. An analytical derivation of the following may be found in Appendix B.

(i) Early Times.

The flow is radial around the well. This is equivalent to a fully penetrating, vertical well in an infinite reservoir. For this time period, Equation (2) reduces to:

$$p_i - p_{wf} = \frac{162.6\, q\mu B_o}{\sqrt{k_z k_y}\,(s-d)}\left[\mathrm{Log}\left(\frac{\sqrt{k_y k_z}\,t}{\phi\mu c r_w^2}\right) - 3.227 + 0.868\, S_m\right] \quad \ldots(14)$$

(ii) Intermediate Times.

As the well is generally long compared to the formation thickness, a period of linear flow may develop once the pressure transient hits the upper and lower boundary. This period results from the spread of the flow beyond the ends ofthe well being negligible.

$$p_i - p_{wf} = \frac{8.128\, qB_o}{(s-d)\, H_z}\sqrt{\frac{\mu t}{k_y\phi c_t}} + \frac{141.2\, q\mu B_o}{(s-d)\sqrt{k_y k_z}}(S_z + S_m) \quad \ldots(15)$$

Where the pseudo skin S_z can be visualized as the skin due to partial penetration in the vertical direction.

$$S_z = \frac{0.07958\, H_z}{r_w}\left[\psi(\eta_1) + \psi(\eta_2) - \psi(\eta_3) - \psi(\eta_4)\right] \quad \ldots(16)$$

$\psi(\eta)$ is known as the Spence function, which was first identified by Clausen[61] in 1832. Later, Ashour and Sabri[63] numerically evaluated Clausen's integral and presented it in tabular form. A graphical representation of this function in given in Figure 3.

$$\psi(\eta) = \sum_{m=1}^{\infty}\frac{\mathrm{Sin}(m\eta)}{m^2} = -\int_0^{\eta}\mathrm{Log}\left[2\,\mathrm{Sin}\left\{\frac{u}{2}\right\}\right] du \quad \ldots(17)$$

$$\eta_1 = 0.52 \frac{\pi}{H_z} r'_w \qquad \text{...(18)}$$

$$\eta_2 = \frac{\pi}{H_z} (2H_s + 3.48 r'_w) \qquad \text{...(19)}$$

$$\eta_3 = -3.48 \frac{\pi}{H_z} r'_w \qquad \text{...(20)}$$

and

$$\eta_4 = \frac{\pi}{H_z}\left(2H_s - 0.52 r'_w\right) \qquad \text{...(21)}$$

(iii) Late Intermediate Time.

During this time period a second radial flow pattern will develop, this time, in the x-y plane. For this case, Equation (2) reduces to:

$$p_i - p_{wf} = \frac{162.6\, q\mu B_o}{H_z\sqrt{k_x k_y}}\left[\mathrm{Log}\left(\frac{k_x t}{\phi\mu c(L-d)^2}\right) - 2.023\right] + \frac{141.2\, q\mu B_o}{(L-d)\sqrt{k_y k_z}}(S_z + S_m) \qquad \text{...(22)}$$

(iv) Late Time.

The pressure transient has now reached the outer boundaries in the x direction thus yielding the second linear and final flow period. Equation (2) can be simplified to:

$$p_i - p_{wf} = \frac{8.128\, qB_o}{H_z H_x}\sqrt{\frac{\mu t}{k_y \phi c_t}} + \frac{141.2\, q\mu B_o}{(L-d)\sqrt{k_y k_z}}(S_z + S_x + S_m) \qquad \text{...(23)}$$

ere the pseudo skin S_x is due to partial penetration n the x direction.

$$S_x = \frac{0.3183\, H_x}{\sqrt{k_z/k_x}\, H_z}\left[\psi(\ell_1) + \psi(\ell_2) - \psi(\ell_3) - \psi(\ell_4)\right] \qquad \text{...(24)}$$

where

$$\ell_1 = 0.13 \frac{\pi}{H_x}(L-d) \qquad \text{...(25)}$$

$$\ell_2 = \frac{\pi}{H_x}(1.87 L + 0.13 d) \qquad \text{...(26)}$$

$$\ell_3 = -0.87 \frac{\pi}{H_x}(L-d) \qquad \text{...(27)}$$

and

$$\ell_4 = \frac{\pi}{H_x}(0.87 L + 1.13 d) \qquad \text{...(28)}$$

A plot of bottom-hole pressure versus the logarithm of time would exhibit two linear sections corresponding to the two radial flow periods that occur during early and late intermediate times given by equations (14) and (22). The first linear section, corresponding to early time, has a slope defined by the length of the horizontal well and by the effective isotropic permeability in the y-z plane. The mechanical skin S_m defines the intercept. The second linear section corresponding to the "Late intermediate" time radial flow has a slope defined by the thickness of the formation and the effective isotropic permeability in the x-y plane. For this flow period to develop, the length of the horizontal well should be sufficiently ort compared to the width of the reservoir. Since e pseudo skin can be expressed analytically, the mechanical skin can be obtained from the intercept.

The two linear flow periods given by equations (15) and (23) can be analyzed by a pressure versus the square root of time plot. The first linear flow period corresponds to intermediate time. For the complete development of this flow period, the length of the well should be sufficiently long compared to the thickness of the formation. The slope of the linear section resulting from the pressure versus square root of time plot is defined by the square root of the mobility in the y direction, the thickness of the formation and the length of the well. This is expected since during this period the pressure transient has reached the over and under burden and the linear flow pattern is constrained to the length of the well. The mechanical skin can be calculated from the intercept.

The second linear flow period corresponds to late time, where the pressure transient has reached all four boundaries. Naturally, this flow period will only exist for a reservoir with a finite width. As expected, the slope of the linear section is defined by the entire area ($H_x H_z$) of the formation open to flow and the square root of the mobility normal to this area. Once again, since analytical expressions exist for the pseudo skins, the mechanical skin can be calculated from the intercept.

The different time periods that may occur during a horizontal well test will be illustrated later in the paper by worked examples.

Approximate Times for Flow Periods

The early time radial flow period approximated by Equation (4) ends at:

$$t_{erf1} = \frac{190.0 (H_z)^{2.095} (r_w)^{-0.095}\, \phi\mu c_t}{k_z} \qquad \text{...(29)}$$

The "Intermediate time" linear flow period approximated by Equation (15) ends at

$$t_{elf1} = \frac{20.8\, \phi\mu c_t (L-d)^2}{k_x} \qquad \text{...(30)}$$

If the time calculated by Equation (29) is greater than that of Equation (30) it means the length of the well is not sufficiently long compared to the thickness of the formation, for this flow period to develop.

The second radial flow period corresponding to the "Late intermediate time" approximated by Equation (22) begins at:

$$t_{brf2} = \frac{1230.0 (L-d)^2 \phi\mu c_t}{k_x} \qquad \text{...(31)}$$

and for a reservoir of finite width, ends at:

$$t_{erf2} = 297.0 \frac{(L+d)^{2.095} (L-d)^{-0.095}\, \phi\mu c_t}{k_x} \qquad \text{...(32)}$$

If the time calculated by Equation (31) is larger than that of Equation (32), it means that the extremities of the well are close to the reservoir boundaries and that there is insufficient room in the reservoir for the second radial flow to develop. As the width of the reservoir $H_x \longrightarrow \infty$, time calculated by Equation (32) will also tend to infinity, that is the final linear flow period will only develop for a reservoir of finite width. The time approximation Equations (29) to (32) were developed empirically. It should be noted that by observing a plot of pressure versus the square root of time, for the late time linear section, Equation (32) may be used to estimate d. If the well is not in the center, d will be the distance to the nearest boundary.

Pressure Buildup

o buildup scenarios have been considered. The first, d probably most common is the case where the reservoir is infinite (i.e. $H_x \longrightarrow \infty$). The second is that of a reservoir of finite width. In this case, the pressure transient has reached the final linear flow period prior to shut-in.

As in the pressure drawdown case, the general expression fur pressure buildup Equation (3) can be simplified by considering the different time periods separately.

(i) Early Times.

This flow period corresponds to the first radial flow period.

Case 1. Infinite Reservoir. ($H_x \longrightarrow \infty$)

Equation (3) reduces to:

$$p_i - p_{ws} = \frac{162.6\, q\mu B_o}{\sqrt{k_z k_y}\,(L-d)}\left[\mathrm{Log}\left[\frac{t_o + \Delta t}{\Delta t}\right] + \gamma_1\right] \qquad \ldots(33)$$

where

$$\gamma_1 = \frac{(L-d)}{H_z}\sqrt{\frac{k_z}{k_x}}\left[\mathrm{Log}\left[\frac{k_x t}{\phi\mu c_t (L-d)^2}\right] - 2.023\right] - \mathrm{Log}(t)$$

$$- \mathrm{Log}\left[\frac{\sqrt{k_z k_y}}{\phi\mu c_t r_w^2}\right] + 3.227 + .868\, S_z \qquad \ldots(34)$$

se 2. Reservoir of Finite Width, H_x

Equation (3) reduces to:

$$p_i - p_{ws} = \frac{162.6\, q\mu B_o}{\sqrt{k_y k_z}\,(L-d)}\left[\mathrm{Log}\left[\frac{t_o + \Delta t}{\Delta t}\right] + \gamma_2\right] \qquad \ldots(35)$$

where

$$\gamma_2 = \frac{0.05\,(L-d)}{H_z H_x}\sqrt{\frac{k_z t}{\phi\mu c_t}} - \mathrm{Log}\left[\frac{\sqrt{k_y k_z}\,t}{\phi\mu c_t r_w^2}\right] + 3.227 + .868\,(S_z + S_x) \qquad \ldots(36)$$

Since $t_o \gg \Delta t$, $\log(t_o + \Delta t) = \log(t) \simeq$ constant and γ_1 and γ_2 may be considered constant. A plot of ΔP versus log $\{(t_o + \Delta t)/\Delta t\}$ yields straight lines for both Equations (33) and (35). The slope of the straight line is defined by the length of the well and the effective isotropic permeability in the y-z plane.

(ii) Intermediate times.

This time period corresponds to the first linear flow period

Case 1. Infinite Reservoir ($H_x \longrightarrow \infty$)

Equation (3) reduces to:

$$p_i - p_{ws} = \frac{8.128\, qB_o}{H_z (L-d)}\sqrt{\frac{\mu \Delta t}{k_y \phi c_t}} + \gamma_3 \qquad \ldots(37)$$

where

$$\gamma_3 = \frac{162.6\, q\mu B_o}{H_z \sqrt{k_x k_y}}\left[\mathrm{Log}\left(\frac{k_x t}{\phi\mu c_t (L-d)^2}\right) - 2.023\right] \qquad \ldots(38)$$

Case 2. Reservoir of Finite Width, H_x

$$p_i - p_{ws} = \frac{8.128\, qB_o}{H_z (L-d)}\sqrt{\frac{\mu}{k_y \phi c_t}}\left[\sqrt{\Delta t} - \frac{(L-d)\sqrt{t}}{H_x}\right] + \frac{141.2\, q\mu B_o}{(L-d)\sqrt{k_y k_z}}\, S_x \qquad \ldots(39)$$

A plot of Δp versus $\sqrt{\Delta t}$ of both Equations (37) and (39) will form a straight line. The straight line slope is defined by the area equal to the product of the length of the well and the thickness of the formation and the square root of the mobility normal to this area.

(iii) Late Intermediate Time.

This time period will correspond to the second radial flow period.

Case 1. Infinite Reservoir ($H_x \longrightarrow \infty$)

This will be the final flow period for this case and Equation (3) reduces to

$$p_i - p_{ws} = \frac{162.6\, q\mu B_o}{H_z \sqrt{k_x k_y}}\left[\mathrm{Log}\left(\frac{t_o + \Delta t}{\Delta t}\right)\right] \qquad \ldots(40)$$

The Horner plot of Equation (40) extrapolates to the original reservoir pressure. Note that the pressure is independent of the well dimensions. The slope of the straight line is defined by the thickness of the formation and by the effective isotropic permeability in the x-y plane.

Case 2. Reservoir of Finite Width, H_x

Equation (3) simplifies to:

$$p_i - p_{ws} = \frac{162.6\, q\mu B_o}{H_z \sqrt{k_x k_y}}\left[\mathrm{Log}\left[\frac{t_o + \Delta t}{\Delta t}\right] + \gamma_4\right] \qquad \ldots(41)$$

where

$$\gamma_4 = \frac{0.05}{H_x}\sqrt{\frac{k_x t}{\phi\mu c_t}} - \mathrm{Log}\left[\frac{k_x t}{\phi\mu c_t (L-d)^2}\right] + 2.023 + .868\, S_x \qquad \ldots(42)$$

Generally, the initial part of the Horner plot generated by Equation (41) will be a straight line. However, as the shut-in time gets longer, and when the inequality $t_o \gg \Delta t$ does not hold, the Horner plot will not be a straight line. The slope of the initial straight line is defined by the thickness of the formation and the effective isotropic permeability in the x-y plane.

(iv) Late Time.

This will be a second linear flow period and will not exist for the infinite reservoir case.

Case 2. Reservoir of Finite Width, H_x

$$p_i - p_{ws} = \frac{8.128\, qB_o}{H_z H_x}\sqrt{\frac{\mu}{k_y \phi c_t}}\,(\sqrt{t} - \sqrt{\Delta t}) \qquad \ldots(43)$$

A plot of pressure versus $(\sqrt{t} - \sqrt{\Delta t})$ will produce a straight line, which will extrapolate to p_i, the initial pressure at $(\sqrt{t} - \sqrt{\Delta t}) = 0$. The slope of the straight line is defined by the entire area open to flow and the square root of the mobility normal to this area.

Skin Effect

By considering the different time periods separately, 'he conventional mechanical skin factor can be ;eveloped.

Skin Factors For Drawdown

(i) Early Time.

The first radial flow period:

$$s_m = 1.151\left[\frac{p_i - p_{wf(1hr)}}{m_{1r}} - \mathrm{Log}\left(\frac{\sqrt{k_y k_z}}{\phi\mu c_t r_w^2}\right) + 3.227\right] \quad \ldots(44)$$

Where m_{1r} is the slope of the linear section corresponding to the first radial flow period and $p_{wf(1hr)}$ is the pressure at t = 1 hour, the linear section of the semilog plot being extrapolated to this time, if necessary. It should be noted that the damaged area near the wellbore may extend a finite distance into the formation and thus may influence the shape of the early sections of the drawdown.

(ii) Intermediate Time.

The first linear flow period.

$$s_m = \frac{0.058}{H_z}\sqrt{\frac{k_z}{\phi\mu c_t}}\left[\frac{p_i - p_{wf(0hr)}}{m_{1\ell}}\right] - S_z \quad \ldots(45)$$

Where $m_{1\ell}$ is the slope of the linear section 'orresponding to the first linear period and $p_{wf(0hr)}$ s the pressure at zero hours, obtained by extrapolating the plot back to this time.

(iii) Late Intermediate Time

The second radial flow period.

$$s_m = \frac{1.151(\ell-d)}{H_z}\sqrt{\frac{k_z}{k_x}}\left[\frac{p_i - p_{wf(1hr)}}{m_{2r}} - \mathrm{Log}\left(\frac{k_x}{\phi\mu c_t(\ell-d)^2}\right) + 2.023\right] - S_z \quad \ldots(46)$$

Where m_{2r} is the slope of the linear section corresponding to the second radial flow period and $p_{wf(1hr)}$ is the pressure resulting from the extrapolation of the linear section back to t = 1 hour.

(iv) Late Time.

The second linear flow period.

$$s_m = \frac{0.058(\ell-d)}{H_x H_z}\sqrt{\frac{k_z}{\phi\mu c_t}}\left[\frac{p_i - p_{wf(0hr)}}{m_{2\ell}}\right] - (S_z + S_x) \quad \ldots(47)$$

Where $m_{2\ell}$ is the slope of the linear section corresponding to the second linear flow period.

Skin Factors for Buildup

The skin factor can be determined by subtracting the theoretical equations for the linear buildups 'rresponding to various time periods from the pressure ,rawdown equation. Different formulations for determining skin are required for the case of the infinite reservoir ($H_x \longrightarrow \infty$) and the semi-infinite case. The resulting expressions for skin factor are:

1. Infinite Reservoir

(i) Early Time.

$$s_m = 1.151\left[\frac{p_{ws(1hr)} - p_{wf}}{m_{1r}} - \mathrm{Log}\left(\frac{\sqrt{k_y k_z}}{\phi\mu c_t r_w^2}\right) + 3.227\right] \quad \ldots(48)$$

Where p_{wf} is the final bottom hole flowing pressure at the time of shut-in.

(ii) Intermediate Time.

$$s_m = \frac{0.058}{H_z}\sqrt{\frac{k_z}{\phi\mu c_t}}\left[\frac{p_{ws(0hr)} - p_{wf}}{m_{1\ell}}\right] - S_z \quad \ldots(49)$$

(iii) Late Intermediate Time.

$$s_m = \frac{1.151(\ell-d)}{H_z}\sqrt{\frac{k_z}{k_x}}\left[\frac{p_{ws(1hr)} - p_{wf}}{m_{2r}} - \mathrm{Log}\left(\frac{k_x}{\phi\mu c_t(\ell-d)^2}\right) + 2.023\right] - S_z \quad \ldots(50)$$

2. Reservoir of Finite Width (The pressure transient has reached the boundaries in the x direction during drawdown)

For "Early time", "Intermediate time" and "Late intermediate time", the mechanical skin factors are given by Equations (48), (49) and (50), respectively.

iv) Late Time

$$s_m = \frac{0.058(\ell-d)}{H_z H_x}\sqrt{\frac{k_z}{\phi\mu c_t}}\left[\frac{p_{ws(0hr)} - p_{wf}}{m_{2\ell}}\right] - (S_z + S_x) \quad \ldots(51)$$

Verification and Discussion of Results

Pressure drawdown and buildup for a horizontal well completed in a reservoir of finite width, but of infinite length, will exhibit four distinct flow regimes, as illustrated in Figures 4 through 7. The first flow period will be radial around the well. The well will exhibit the pressure response of a fully penetrating vertical well, of height (ℓ-d), completed in an infinite reservoir.

If the well is sufficiently long in relation to the formation thickness a second flow period will develop when the pressure pulse reaches the over and underburden boundaries. This flow period will result in linear flow and is analogous to that of a vertical fracture. If the well is not long compared to the formation thickness, then this period of flow will not develop and there will be a lengthy transition period between the first and third flow periods.

The third flow period will be a period of radial flow around the well, in the plane of the formation. This period would be analogous to radial flow around a vertical well. If the width of the reservoir, H_x is not large compared to the length of the well, this flow period may not develop and a long transition period will be present. The time functions, Equations (29-32) may be used to determine which of the flow periods will be present.

Finally, the pressure pulse will reach the boundaries at x = 0 and x = H_x. This period of flow will be linear and analogous to that of a vertical fracture, with an additional pressure drop due to partial penetration in both the x and z directions. If the reservoir is infinite, this period of flow will not develop.

The analytical model was verified by performing numerical simulation using a conventional, fully implicit, black oil reservoir simulator. The data used in the comparison are given in Table 1. The well was represented by ten horizontal sections, as shown in Figure 8. Figure 9 shows a comparison of the results of the analytical solution for pressure drawdown analysis with that of the numerical simulator. The results are in good agreement. The slight discrepancy during the early times is due to the numerical error associated with the gridding. The verification justifies the assumption of constant flux and shows that this assumption can be removed by taking the pressure, at an effective average, at a dimensionless distance of 0.869 from either of the extremities of the well when it is placed in the center of the formation.

In addition to verifying the solution with numerical simulation, a verification against an established analytical procedure was also performed. If H_x is finite and H_z is infinite, the horizontal well can be considered to be a partially penetrating wellbore. As gravity is ignored, no error will develop due to the rotation of the coordinate system. Of course, as H_x is not much greater than H_z, the assumptions applied to reduce Equation (A10) to Equations (2) and (3) are not valid and the full form of the solution must be used.

A semilog plot of pressure drawdown versus log time is plotted as Figure 10. The data used is tabulated on the figure. These results are seen compared to the analytic solution developed by Hantush[6] and later by Kazemi and Seth[7]. Good agreement is found between the two solutions. The slight discrepancy for early time (10^{-4} hours) is a result of the horizontal well being described as a strip, with a width equal to $4r_w$. The strip initially exhibits linear flow whereas the Hantush solution is cast in radial coordinates and initially exhibits radial flow.

The solutions become identical at 0.0003 hours (1 sec). This illustrates the validity of considering the horizontal well as a strip and replacing the width by four times the wellbore radius.

The solutions presented in this paper are also applicable to problems involving partially penetrating fractures. Analytic solutions have been developed for partially penetrating fractures[8-10,11-13] and the solution could be verified against any of these. This work, however, was not performed and a discussion of partially penetrating fractures is considered beyond the scope of this paper.

Examples of Application

Synthetically generated pressure versus time data is used to illustrate the methods for analyzing pressure build-up test in horizontal wellbores.

Example 1

This example considers a horizontal well completed in the center of an isotropic, semi-infinite (slab) reservoir. The flow period was sufficiently long to obtain the final linear flow period. Table 1 gives the reservoir and fluid characteristics.

Figure 9 shows a semi-log graph of Δp versus t for the entire drawdown period. It should be noted that two straight line sections are present, the second one ends with a curvature upward, illustrating the effect of the boundary.

The time to the end of the first radial flow period is obtained from Equation (29):

$$t_{erf1} = \frac{190.0 \times (220)^{2.095} \times (.354)^{-0.095} \times .1 \times 1.5 \times 3E\text{-}5}{100}$$
$$= .76 \text{ hours}$$

The semilog slope for this section $m_{1r} = 14.63$ psi/cycle and $\Delta p_{wf(1hr)} = 73.4$ psi as shown in Figure 11. From Equation (14), k is calculated.

$$k = \frac{162.6 \times 3000 \times 1.5 \times 1}{14.63 \times 500} = 100.0 \text{ md}$$

and the skin factor from Equation (44):

$$S_m = 1.151 \left[\frac{73.4}{14.63} - \text{Log}\left(\frac{100}{1.5 \times .1 \times 3E\text{-}5 \times (.354)^2}\right) + 3.227\right] = 0$$

If the first linear flow period is present, it will end at a time obtained from Equation (30).

$$t_{elf1} = \frac{20.8 \times .1 \times 1.5 \times 3E\text{-}5 \times 500^2}{100} = .234 \text{ hours}$$

Since $t_{erf1} > t_{elf1}$ the first linear flow period is not present in this example. This is a result of the well not being sufficiently long with respect to the formation thickness.

The late intermediate time radial flow period will begin at t_{brf2}, which is obtained from Equation (31):

$$t_{brf2} = \frac{1230 \times 500^2 \times .1 \times 1.5 \times 3E\text{-}5}{100} = 13.84 \text{ hours}$$

and will end at t_{erf2}, obtained from Equation (32):

$$t_{erf2} = \frac{297 \times 2100^{2.095} \times 500^{-0.095} \times .1 \times 1.5 \times 3E\text{-}5}{100}$$
$$= 67.5 \text{ hours}$$

Figure 12 shows a semi-log graph of the pressure drawdown versus time for late intermediate time radial flow. The semilog straight line has a slope $m_{2r} = 33.2$ psi/cycle and $\Delta p_{wf(1hr)} = 56.1$ psi.

The permeability is obtained from the slope of Equation (22) as:

$$k = \frac{162.6 \times 3000 \times 1.5 \times 1}{33.2 \times 220} = 100.0 \text{ md}$$

and the skin factor from Equation (46):

$$S_m = \frac{1.151 \times 500 \times 10}{220 \times 10}\left[\frac{56.1}{33.2} - \text{Log}\left(\frac{100}{.1 \times 1.5 \times 3E\text{-}5 \times 500^2}\right) + 2.023\right] - S_z$$
$$= 4.6 - S_z$$

and from Equation (16):

$$S_z = \frac{.07958 \times 220}{.354}\left[\psi(.00263) + \psi(3.159) - \psi(-.0176) - \psi(3.139)\right]$$
$$= 4.6$$

therefore,

$$S_m = 0$$

Figure 13 shows a graph of the pressure drawdown (Δp) versus $\sqrt{t}$ for the late time data. A straight line is formed at $\sqrt{t} = 8$ hour$^{1/2}$ which has slope of $m_{2L} = 3.73$ psi/hour$^{1/2}$ and $\Delta p_{wf(0hr)} = 87.3$psi. Equation (23) can now be used to calculate the permeability.

$$k = \left(\frac{8.128 \times 3000 \times 1 \times 1.225}{220 \times 2100 \times 3.73 \times 1.732E{-3}}\right)^2 = 100 \text{ md}$$

and the skin factor follows from Equation (47):

$$S_m = \frac{.050 \times 500 \times 10}{220 \times 2100 \times .002121}\left(\frac{87.2}{3.73}\right) - 4.6 - S_z = 2.28 - S_z$$

Where, from Equation (24):

$$S_z = \frac{.3183 \times 2100}{1 \times 220}\left[\psi(.897) + \psi(3.79) - \psi(-.63) - \psi(3.04)\right] = 2.28$$

therefore

$$S_m = 0$$

For an isotropic reservoir, it is not necessary to evaluate the reservoir characteristics from each of the flow periods, however, having two or more of the flow periods present does provide for a consistency check of the results.

Example 2

This example differs from the previous example, in that, the reservoir is anisotropic and infinite ($H_x \rightarrow \infty$). The reservoir and fluid characteristics are provided in Table 2.

Figure 14 shows a semilog graph of Δp versus t for the entire drawdown period. The drawdown period was sufficiently long to achieve radial flow in the plane of the formation, giving rise to a straight line section for the late time data. Equation (31) can be used to check that radial flow was established.

$$t_{erf2} = \frac{1230 \times 1000^2 \times .1 \times 1.5 \times 3E{-5}}{50} = 110.7 \text{ hours}$$

The data for this example is interpreted using the build-up period. As the reservoir is infinite, the late time radial flow period will be the final flow period. Therefore, the build-up will result from the shut-in period being superimposed upon radial flow in the plane of the formation.

The time to the end of the early time radial flow period is obtained from Equation (29):

$$t_{erf1} = \frac{190.0 \times (60)^{2.095} \times (.25)^{-0.095} \times .1 \times 1.5 \times 3E{-5}}{25}$$
$$= .2 \text{ hours}$$

From Figure 15, which is a graph of Horner time versus pressure, a slope m_{1r} =21.9 psi/cycle and $p_{ws(1hr)}$ = 3681.6 psia are obtained. The effective permeability in the y-z plane is obtained using Equation (33):

$$\sqrt{k_y k_z} = \frac{162.6 \times 3000 \times 1.5 \times 1.5}{21.9 \times 1000} = 50 \text{ md}$$

and the skin obtained from Equation (48):

$$S_m = 1.151\left[\frac{3681.6 - 3482.8}{21.9} - \text{Log}\left[\frac{50}{.1 \times 1.5 \times 3E{-5} \times .354^2}\right] + 3.227\right]$$
$$= 5$$

The first linear flow period will be present if $t_{erf1} < t_{elf1}$. From Equation (30):

$$t_{elf1} = 1.87 \text{ hours}$$

Figure 16, which is a graph of pressure versus $\sqrt{t}$ reveals a linear section of slope m_{1L} = 43.1 psi/hour$^{1/2}$ and $p_{ws(0hr)}$= 3647.4 psia. The permeability, k_y may be obtained from Equation (37):

$$k_y = \left(\frac{8.128 \times 3000 \times 1.225 \times 1.5}{43.1 \times 1000 \times 1.73E{-3}}\right)^2 = 100 \text{ md}$$

therefore,

$$k_z = \left(\frac{50}{10}\right)^2 = 25 \text{ md}$$

The skin can be obtained for this flow period using Equation (49):

$$S_m = \frac{.050 \times 5}{60 \times (.1 \times 1.5 \times 3E{-5})^{1/2}}\left(\frac{3647.4 - 3482.8}{43.1}\right) - 3.6 = 5$$

As this example is for an infinite reservoir, the radial flow in the plane of the formation will be the final flow period. The straight line section on Figure 9 has a slope m_{2r} = 258 psi/cycle and $p_{ws(1hr)}$ = 3395.5 psia. The final radial period develops after t_{brf1} hours, which was calculated above to be 110.7 hours.

The evaluation of the slope for this section of the Horner plot will yield $\sqrt{k_x k_y}$, which will enable k_x to be evaluated. Using Equation (40):

$$\sqrt{k_x k_y} = \frac{162.6 \times 3000 \times 1.5 \times 1.5}{60 \times 258.7} = 70.71$$

therefore $k_x = \left(\frac{70.71}{10}\right)^2 = 50$ md

The skin may be obtained from Equation (50):

$$S_m = \frac{1.151 \times 1000 \times 5}{60 \times 7.07}\left[\frac{3395.5 - 3482.8}{258.7} - \text{Log}\left[\frac{50}{.1 \times 1.5 \times 3E{-5} \times 100}\right] + 2.023\right]$$
$$- 3.64 = 5$$

By examination of Equation (40) it is seen that as Horner time approaches unity the pressure will approach the original reservoir pressure. The straight line section indicating radial flow in the plane of the formation will extrapolate to p_i. In this example the straight line section extrapolates to p_i= 4000 psia.

Conclusions

1. Analytic solutions are presented for the pressure response during drawdown and subsequent pressure buildup of a horizontal well.
2. The use of the equations, as illustrated by field examples, allows the directional permeabilities, average reservoir pressure and the mechanical skin factor to be calculated.
3. The uniform flux density over the horizontal well can be corrected by taking the pressure at an "effective average". If the well is at the center of the formation, this is at a dimensionless distance of .869 from either of the extremities. If the well is placed at either of the boundaries this will be at a dimensionless distance of 0.738 from the end of the well that is adjacent to the boundary.
4. The predictions of the analytic solutions are in good agreement with that of the numerical simulator and established analogous analytical results.
5. Replacing the strip source by an effective well radius of one-fourth the strip thickness, as

suggested by Prats, gives a good approximation to the horizontal well.

NOMENCLATURE:

A_{nm} = Arbitrary constant

a = Vertical distance from the top reservoir boundary to the top edge of the horizontal strip source, ft(m)

B_{nm} = Arbitrary constant.

B_o = Oil formation volume factor, RB/STB

b = Vertical distance from the top reservoir boundary to the bottom of the horizontal strip source, ft(m)

c_t = Total compressibility, psi^{-1} (pa^{-1})

d = Lateral distance from the left reservoir boundary to the near end of the well, ft(m)

H = Reservoir thickness, ft(m)

k = Permeability, md

ℓ = Lateral distance from the left reservoir boundary to the far end of the well, ft(m)

m = Fourier transform variable.

n = Fourier transform variable.

p = Pressure, psia(pa)

p_i = Initial pressure, psia(pa)

= Dimensionless pressure = $\dfrac{p_i - p}{\left(\frac{q\mu}{2k_y}\right)}$

$\bar{P}$ = Finite Fourier cosine transform of P in the x coordinate

= $\int_0^\pi P \,\mathrm{Cos}(nx)dx$

$\bar{\bar{P}}$ = Finite Fourier cosine transform of $\bar{P}$ in the z coordinate

= $\int_0^\pi \bar{P} \,\mathrm{Cos}(mz)dz$

$\bar{\bar{\bar{P}}}$ = Laplace transform of $\bar{\bar{P}}$

= $\int_0^\infty \bar{\bar{P}} e^{-st}dt$

q = Volumetric flow rate, STB/D(m^3/D)

r_w = Wellbore radius, ft(m)

r'_w = $r_w \left(\frac{k_z}{k_y}\right)^{1/4}$, ft(m)

s = Laplace transform variable

S_m = Mechanical skin factor

S_x = Skin due to partial penetration in the x direction

S_z = Skin due to partial penetration in the z direction

t = time, hour(s)

x = Lateral coordinate, ft(m)

X = Dimensionless lateral coordinate, $\pi x/H_x$

y = Longitudinal coordinate, ft(m)

z = Vertical coordinate, ft(m)

Z = Dimensionless vertical coordinate, $\pi z/H_z$

Greek Letters

β = $\left(\frac{\phi\mu c}{k_y}\right)$

ϕ = Porosity, fraction

$\psi(\xi)$ = Spence function

μ = Viscosity, cp(pa.s)

ν_x = $\left(\frac{\pi}{H_x}\right)\sqrt{\frac{k_x}{k_y}}$

ν_z = $\left(\frac{\pi}{H_z}\right)\sqrt{\frac{k_z}{k_y}}$

τ = $0.000264t/\beta$, ft^2 $(^2)$

τ_o = $0.000264t_o/\beta$, ft^2 (m^2)

$\Delta\tau$ = $\tau - \tau_o$, ft^2 (m^2)

ξ,η = Arguments to Spence function

Δ = Difference

Subscripts

brf2 = beginning of radial flow two.
elf1 = end of linear flow one.
erf1 = end of radial flow one.
erf2 = end of radial flow two.
i = initial
f = flux per unit length.
m = mechanical.
s = standoff.
wf = drawdown.
ws = buildup.
x = coordinate indicator.
y = coordinate indicator.
z = coordinate indicator.
0hr = extrapolated to zero hours.
1hr = extrapolated to one hour.
1ℓ = first linear flow period.
2ℓ = second linear flow period.
1r = first radial flow period.
2r = second radial flow period.

Acknowledgement

The authors thank the management of SOHIO Petroleum Company for permission to publish this paper. They also gratefully acknowledge the assistance of Laura Fujikawa and Angie Lingad during the preparation of the paper.

REFERENCES

1). Ranney, L.: Drilling Wells Horizontally, The Oil Weekly, January 20, 1941.

2). Stormont, D. H.: Increasing Drainage of Oil into the Well by Drainhole Drilling, The Oil and Gas Journal, pp. 105-108, 145, August 17, 1983.

3). Higgins, R. V.: Factors that Influence Gravity Drainage. The Petroleum Engineer, pp. B-83 to B-92, May, 1953.

Eastman, H. J.: Lateral Drainhole Drilling. The Petroleum Engineer, pp. B-57 to B-73, November, 1954.

5). Perrine, R. L.: Well Productivity Increase from Drainholes as Measured by Model Studies, Petroleum Transactions, AIME, Vol. 204, 1955.

6). Roemershauser, A. E. and Hawkins, Jr., M. F.: The Effect of Slant Hole, Drainhole and Lateral Hole Drilling on Well Productivity, JPT, February, 1955.

7). Landrum, B. L. and Crawford, P. B.: Effect of Drainhole Drilling on Production Capacity, JPT, February, 1955.

8). Merkulov, V. P.: Le debit des puits devies et horizontaux, Neft. Khoz., 1958, n^{o}6, pp. 51-56.

9). Borisov, Ju. P.: Exploitation des gisements de petrole par des puits horizontaux et a deviations multiples. Moscow: "Nedra", 1964. Translation from Russian into French: doc. IFP, ref. 28363.

10). Colamasi,C. and delle Canne, A.: Drainhole Drilling in Sicily, World Oil, March 1963.

11). Holbert, D. R.: Method of Drilling a Curved Bore, U. S. Patent No. 3, 398, 804 August 27, 1968.

2). Grigorjan, M. M.: Les puits a ramification horizontales, Neft Khoz.n^{o}11, 19-22. Translation from Russian into French: doc. IFP ref. 29564, October, 1981.

13). Grigorjan, A. M.: Forage des couches productives par puits horizontaux et a completion multiple. Moscow: "Nedra" 1969, 190 p. Translation from Russian into French: doc. IFP ref. February 1980.

14). Striegler, J.: ARCO Finishes Fourth Horizontal Drainhole, Technology, OGJ, May 24, 1982.

15). Cawvey, J. L.: ARCO', Empire Abo Unit Horizontal Drainhole Program Advances, Well Servicing, July/August, 1981.

16). Loxam, D. C.: Texas Canada Completes Unique Horizontal Drilling Program, Petroleum Engineering International, September, 1982.

17). Horizontal Wells Take Steam To Athabasca Tar, Enhanced Recovery Week, March 1, 1982, p.3.

18). Bezgirr, G. E. and Morkiw, I. A.: Esso Resources Horizontal Hole Project at Cold Lake, Petroleum Society of CIM, No. 79-30-10, May, 1979.

19). Moore, W. D.: ARCO Drills Horizontal Drainhole for Better Reservoir Placement, OGJ, September 15, 1980.

20). Killough, J. E. and Foster, Jr., A. P.: Reservoir Simulation of the Empire Abo Field: The Use of Pseudos in a Multilayered System, SPEJ, October 1979.

21). Pitts, J. P.: ARCO's Lea County Drainhole Proves a Success, Drill Bit., August, 1980.

22). Technical Advances Broaden Use of Highly Deviated and Horizontal Drilling Methods, JPT, February, 1981.

23). Stramp, R. L.: The Use of Horizontal Drainholes in the Empire Abo Unit, SPE Paper No. 9221, presented at the Society of Petroleum Engineers 55th Annual Technical Conference, September 21-24, 1980, Dallas, Texas.

24). Wash R.: ARCO's Fourth Successful Drainhole Drilled in Cased Hole, Drill Bit, September, 1981.

25). Holbert, D. R.: New Interest in Drainhole Drilling Revives Technology, Word Oil, March, 1981.

26). Holbert, D. R.: Variables in Kickoff Remain First Consideration during Drainhole Drilling OGJ, February 9, 1981.

27). Holbert, D. R.: Special Practices Allow High Angle Drilling, OGJ, February 16, 1981.

28). Pugh, G. E.: Drilling of Three Horizontal Hole Pattern Fort McMurray, Alberta, Preprint, paper n^{o}82-83-68 presented at the 33rd annual technical meeting of the Petroleum Society of CIM, Calgary, Canada (June 6-9, 1982).

29). Astier, B., Jourdan, A., and Baron G.: Elf Well Turns 90° - and stays there, Petroleum Engineering International, January, 1981.

30). Jourdan, A., and Baron, G.: Elf drills 1,000+ Ft Horizontally, Petroleum Engineering International (September, 1981).

31). Giger, F.: L'equipment de forages horizontaux, Petrole et Techniques, Revue de l'Association Francaise des Techniciens du Petrole, no 294 (December 1982) 40-42.

32). Giger, F., Combe, J., Reiss L. H.: L'interet du forage horizontal pour l'exploitation des gisements d'hydrocarbures, Revue de l'Institut Francais du Petrole, (Advantages of Horizontal drilling for production from hydrocarbon fields) Vol. 38, n^{o}3 (May-June 1983).

33). Giger, F. M., Jourdan, A. P.: The Four Horizontal Wells Producing Oil in Western Europe, Presented at the Fifth Annual "Advances in Petroleum Recovery and Upgrading Technology Conference", June 14 & 15, 1984 Alberta,Canada.

34). Jourdan, A.: Le forage de puits horizontaux, Revue de l'AFTP Petrole et techniques, n^{o}294, December 1982, p. 37-39.

35). Wittrisch, C., Jourdan, A.: Horizontal Well Logging by Simphor, Transaction of the VIIIth European Formation Evaluation Symposium, London (March 14-15, 1983).

6). Bleakley, W. B.: IFP and Elf Aquitaine Solve Horizontal Well Logging problem, Petroleum Engineering International (November 15, 1983).

37). Jourdan, A. P. and Baron, G.: Horizontal Well Proves Productivity Advantages, Petroleum Engineer International, October, 1984.

38). Reiss, L., Jourdan, A. P., Giger,F. M. and Armessen, P. A.: Off Onshore European Horizontal Wells, paper n^{o}4791, Offshore Technology Conference, Houston, 1984.

39). Elf Tries Horizontal Drilling to Tap Heavy Oil, Oil and Gas Journal, pp. 48 (August 1, 1983).

40). Elf to Attempt Deep Horizontal Well, Oil and Gas Journal, pp. 48-49 (December 26, 1983).

41). Giannesini, J. F.: Horizontal Wells, PetroAsia, January - February, 1984.

42). Sandru, L., Carpeniseaunu, D. and Ionoscu, L.: Improvement of Oil Recovery by Mining Methods, World Petroleum Congress, Bucharest, 1979 - S.P. 9.

43). Bleakley, W. F.: IPF and Elf-Aquitaine Solve Horizontal Well Logging Problem, Petroleum Engineering International, November 15, 1983.

44). Giger, F. M. and Reiss, L. H.: Reservoir Engineering Aspects of Horizontal Drilling, SPE 13024, Presented at the 59th Annual Technical Conference and Exhibition held in Houston, Texas, September 16-19, 1984.

45). Duns, H., Van der Vlis, A. C., Fernandez, Luque R.: Increasing Well Productivity in Tight Chalk Reservoirs, 10th World Petroleum Congress,Bucharest, 1979.

46). Houpeurt, A.: Elements de mecanique des fluides dans les milieux poreux. Paris: Ed. Technip, 1975.

47). Efros, D. A.: Etude des ecoulements multiphasiques dans les milieux poreux. Leningrad: Gostoptexizdat, 1963.

48). Giger, F.: Reduction du nombre de puits par l'utilisation de forages horizontaux, Revue de l'Institut francais du Petrole, Vol. 38, no 3 (May-June 1983).

49). Giger, F.: Theoretical Evaluation of Effect of Water Cresting on Production by Horizontal Wells, Revue De L'Institut Francais Du Petrole, Vol. 38, No. 3 (May-June 1983).

50). Butler, R. M.: The Potential of Horizontal Wells, presented at the fifth annual "Advances in Petroleum Recovery and Upgrading Technology" Conference, June 14 & 15, 1984 Calgary, Alberta, Canada.

51). Butler, R. M. and Stephens, D. J.: The Gravity Drainage of Steam - Heated Heavy Oil to Parallel Horizontal Wells, Journal of Canadian Petroleum Technology, Vol. 20 (2), pp. 90-96, April-June 1981.

52). Butler, R. M., McNab, G. S. and Lo, H. Y.: Theoretical Studies on the Gravity Drainage of Heavy Oil During In-Situ Steam Heating, The Canadian Journal of Chemical Engineering, Vol. 59,pp. 455-460 (August, 1981).

53). Butler, R. M.: Stephens, D. J., Weiss, M.: The Vertical Growth of Steam Chambers in the In-Situ Thermal Recovery of Heavy Oils, Proc. 30th Can. Chem. Eng. Conf., Edmonton, Alberta, Volume 4, pp. 1152-1167, 1980.

54). Butler, R. M.: New Interpretation of the Meaning of the Exponent "m" in the Gravity Drainage Theory from Continuously Steamed Wells, Proc. 2nd World Cong. Chem. Eng. 1981.

55). Joshi, S. D. and Threlkeld, C. B.: Laboratory Studies of Thermally Aided Gravity Drainage Using Horizontal Wells, presented at the fifth annual "Advances in Petroleum Recovery and Upgrading Technology" Conference, June 14 & 15, 1984, Calgary, Alberta, Canada.

56). Griffin, P. J. and Trofimenkoff, P. N.: Laboratory Studies of the Steam - Assisted Gravity Drainage Process, presented at the fifth annual "Advances in Petroleum Recovery and Upgrading Technology" Conference, June 14 & 15, 1984, Calgary, Alberta, Canada.

57). Rial, R. M.: 3D Thermal Simulation Using a Horizontal Wellbore for Steamflooding, SPE 13076, Presented at the 59th Annual Technical Conference and Exhibition held in Houston, Texas, September 16-19, 1984.

58). Huygen, H. H. A. and Black, J. B.: Steaming Through Horizontal Wells and Fractures - Scaled Model Tests, Proceedings of 2nd European Symposium on Enhanced Oil Recovery, Paris, pp. 507-517 (November 8-10, 1982).

59). Cinco, H., Miller, F. G. and Ramey, Jr. H. J.: Unsteady-State Pressure Distribution Created By a Directionally Drilled Well, JPT, November, 1978.

60). Gringarten, A. C., Ramey, H. J. and Raghavan,R.: Unsteady-State Pressure Distribution Created by a Well with a Single Infinite - Conductivity Vertical Fracture, SPEJ, August, 1974.

61). Raghavan,R., Uraiet, A. and Thomas G. W.: Vertical Fracture Height: Effect on Transient Flow Behavior, SPE 6016, Presented at the 51st Annual Fall Technical Conference and Exhibition, SPE of AIME, New Orleans, October 3-6, 1976.

62). Rodriguez, F., Horne, R. N. and Cinco, H.: Partially Penetrating Fractures: Pressure Transient Analysis of an Inifinite Conductivity Fracture, SPE 12743. Paper presented at the California Regional Meeting, Long Beach, CA, April 11-13, 1984.

63). Gringarten, A.C. and Ramey, Jr., H. J.: The Use of Source and Green's Functions in Solving Unsteady Flow Problems in Reservoir, SPEJ, 285-296; Trans., AIME Vol. 255, October 1973.

64). Van Everdingen, A. F.: The Skin Effect and its Impediment to Fluid Flow into a Wellbore, Trans AIME, 198: 171-176, 1953.

65). Prats, M.: Effect of Vertical Fractures on Reservoir Behavior - Incompressible Fluid Case, SPEJ, June, 1961.

66). Muskat, M.: The Flow of Homogeneous Fluids through Porous Media, McGraw-Hill Book Company, 1937.

67). Clausen, T.: Uber die Zerlegung reeller gebrochener Funktionen, J. f. d. reine u. angew. Math. (Crelle), V. 8, 1832, p. 298-300.

68). Ashour, A. and Sabri, A.: Tabulation of the Spence Function Mathematical Tables and other Aids to Computation, National Academy of Sciences, Vol. X, No. 54, April 1956

69). Hantush, M.: Advances in Hydroscience, Ven Te Chow, Ed., Academic Press, New York and London, 1964.

70). Kazemi, H. and Seth, M. S.: Effect of Anistropy and Stratification on Transient Analysis of Wells with Restricted Flow Entry, JPT, May 1969.

71). Earlougher, R. C.: Advances in Well Test Analysis. Monograph Volume 5, Society of Petroleum Engineers of AIME, Dallas, 1977.

72). Tinsley, J. M., Williams, J. R., Tiner, R. L., and Malone, W. T.: Increase Vertical Fracture Height - Its Effect on Steady - State Production, J. Pet. Tech., May, 1969.

73). Mao, M. L.: Performance of Vertically-Fractured Wells with a Finite Conductivity Fracture, Ph. D. Dissertation, Stanford University, California (May 1977).

74). Abramowitz, M. and Stegun, I. A.: Handbook of Mathematical Functions with Formulas, Graphs and Mathematical Tables, Dover Publications, Inc. New York, N. Y. (1972).

75). Tranter, C. J.: Integral Transforms in Mathematical Physics, 3rd Edition John Wiley & Sons, Inc., New York, 1966.

Appendix A

Derivation of Pressure Drawdown and Buildup Equations

To facilitate solution of the problem, the following variables are introduced.

$$P = \frac{p_i - p}{\left(\frac{[illegible]}{[illegible]}\right)_y}$$

$$\rho = \left[\frac{\phi\mu c_t}{k_y}\right]$$

$$\tau = \frac{t}{\rho} = \left[\frac{k_y t}{\phi\mu c_t}\right] \qquad \text{...(A1)}$$

$$\nu_z = \left(\frac{1}{h_z}\right)\sqrt{\frac{k_z}{k_y}} \quad , \quad \nu_x = \left(\frac{1}{h_x}\right)\sqrt{\frac{k_x}{k_y}}$$

and

$$Z = \frac{\pi z}{h_z} \quad , \quad X = \frac{\pi x}{h_x}$$

Substitution of these new variables into the partial differential equation and initial and boundary conditions yields.

$$\frac{\partial P}{\partial \tau} = \left[\frac{\partial^2 P}{\partial y^2}\right] + \nu_z^2\left[\frac{\partial^2 P}{\partial Z^2}\right] + \nu_x^2\left[\frac{\partial^2 P}{\partial X^2}\right] \qquad \text{...(A2)}$$

The initial and boundary conditions are:

(i) $P = 0$ at $\tau = 0$ for all X, y and Z

(ii) $P = 0$ as $y \longrightarrow \infty$ for all X and Z

(iii)
$$\left[\frac{h_z h_x}{\pi^2}\right]\lim_{y\to 0}\int_{\frac{\pi z_1}{h_z}}^{\frac{\pi z_2}{h_z}}\int_{\frac{\pi x_1}{h_x}}^{\frac{\pi x_2}{h_x}}\left(\frac{\partial P}{\partial y}\right)dX\,dZ = \begin{cases} \begin{bmatrix} \begin{cases} 0 & 0 \le Z < \frac{\pi z_1}{h_z} \\ 1 & \frac{\pi z_1}{h_z} < Z < \frac{\pi z_2}{h_z} \\ 0 & \frac{\pi z_2}{h_z} < Z \le \pi \end{cases} & \begin{matrix} 0 < X \le \frac{\pi x_1}{h_x} \\ \frac{\pi x_1}{h_x} < X < \frac{\pi x_2}{h_x} \\ \frac{\pi x_2}{h_x} < X \le \pi \end{matrix} \end{bmatrix} & 0 < \tau \le \tau_o \\ 0 & \tau > \tau_o \end{cases}$$

(iv) $\frac{\partial P}{\partial Z} = 0$ at $Z = 0$ and π for all τ, X and y

(v) $\frac{\partial P}{\partial X} = 0$ at $X = 0$ and π for all τ, Z and y

Application of the finite Fourier cosine transform to the X coordinate of the differential equation and boundary condition yields.

$$\frac{\partial \bar P}{\partial \tau} = \left[\frac{\partial^2 \bar P}{\partial y^2}\right] - (\nu_x n)^2\,\bar P + \nu_z^2\left[\frac{\partial^2 \bar P}{\partial Z^2}\right] \qquad \text{...(A3)}$$

where $\bar P = \int_0^\pi P\,\text{Cos}(nX)dX$

Initial and boundary conditions are

(i) $\bar P = 0$ at $\tau = 0$

(ii) $\bar P = 0$ as $y \longrightarrow \infty$

(iii)
$$\frac{h_z}{\pi}\,(\ldots)\lim_{y\to 0}\int_{\frac{\pi z_1}{h_z}}^{\frac{\pi z_2}{h_z}}\left[\frac{\partial \bar P}{\partial y}\right]dZ = \begin{cases} \begin{cases} 0 & 0 \le Z \le \frac{\pi z_1}{h_z} \\ \frac{1}{n}\left[\sin\frac{n\pi x_2}{h_x} - \sin\frac{n\pi x_1}{h_x}\right] & \frac{\pi z_1}{h_z} < Z \le \frac{\pi z_2}{h_z} \\ 0 & \frac{\pi z_2}{h_z} < Z \le \pi \end{cases} & ; \ 0 \le \tau \le \tau_o \\ 0 & ; \ \tau > \tau_o \end{cases}$$

(iv) $\frac{\partial \bar P}{\partial Z} = 0$ at $Z = 0$ and π for all τ, X and y

Where n is the Fourier transform variable. The boundary condition (v) has been accounted for in the transformation of the $(\partial^2 P/\partial X^2)$ term in the partial differential Equation (A2).

Application of the finite Fourier cosine transform to the Z coordinate of differential Equation (A3) and boundary conditions yields:

$$\frac{\partial \bar{\bar P}}{\partial \tau} = \left[\frac{\partial^2 \bar{\bar P}}{\partial y^2}\right] - \left\{(\nu_x n)^2 + (\nu_z m)^2\right\}\bar{\bar P} \qquad \text{...(A4)}$$

where $\bar{\bar P} = \int_0^\pi \bar P\,\text{Cos}(mZ)dZ$

Initial and boundary conditions are

(i) $\tilde{P} = 0$ at $t = 0$

(ii) $\tilde{P} = 0$ at $y \to \infty$

(iii) $$\lim_{y\to 0}\left[(L-d)(b-a)\frac{\partial \tilde{P}}{\partial y}\right] = \begin{cases} \frac{1}{nm}\left[\sin\frac{n\pi L}{x_e} - \sin\frac{n\pi d}{x_e}\right]\left[\sin\frac{m\pi b}{z_e} - \sin\frac{m\pi a}{z_e}\right] & ; 0 \le t \le t_0 \\ 0 & ; t > t_0 \end{cases}$$

Where m is the Fourier transform variable. The boundary condition (iv) has been accounted for in the transformation of the $(\partial^2 P/\partial Z^2)$ term in the partial differential Equation (A3). Now the application of a Laplace transform to the differential Equation (A4) and boundary conditions (ii) and (iii) yields.

$$\frac{d^2\bar{\tilde{P}}}{dy^2} - \left(s + (\gamma_x n)^2 + (\gamma_z m)^2\right)\bar{\tilde{P}} = 0 \qquad \ldots(A5)$$

where $\bar{\tilde{P}} = \int_0^\infty \tilde{P} e^{-st}\,dt$

with

(ii) $\bar{\tilde{P}} = 0$ at $y \to \infty$

(iii) $$\lim_{y\to 0}\left[(L-d)(b-a)\frac{d\bar{\tilde{P}}}{dy}\right] =$$

$$\left[\sin\frac{n\pi L}{x_e} - \sin\frac{n\pi d}{x_e}\right]\left[\sin\frac{m\pi b}{z_e} - \sin\frac{m\pi a}{z_e}\right]\left[\frac{1 - e^{-st_0}}{mns}\right]$$

Where s is the Laplace transform variable (not to be confused with the skin factor). The initial condition (i) has been accounted for in the transformation of the time derivative in the partial differential Equation (A4).

The general solution of the ordinary differential Equation (A5) is:

$$\bar{\tilde{P}} = A_{nm}e^{-\sqrt{(s + (\gamma_x n)^2 + (\gamma_z m)^2)}\,y} + B_{nm}e^{\sqrt{(s + (\gamma_x n)^2 + (\gamma_z m)^2)}\,y} \qquad \ldots(A6)$$

From boundary condition (ii)

$B_{nm} = 0$

From boundary condition (iii)

$$A_{nm} = \frac{\left(e^{-st_0} - 1\right)}{nm(L-d)(b-a)s\sqrt{s + (\gamma_x n)^2 + (\gamma_z m)^2}} \times \left[\sin\frac{n\pi L}{x_e} - \sin\frac{n\pi d}{x_e}\right]\left[\sin\frac{m\pi b}{z_e} - \sin\frac{m\pi a}{z_e}\right]$$

Substituting for A and B in Equation (A6)

$$\bar{\tilde{P}} = \frac{\left(1 - e^{-st_0}\right)e^{-\sqrt{(s + (\gamma_x n)^2 + (\gamma_z m)^2)}\,y}}{nm(L-d)(b-a)s\sqrt{s + (\gamma_x n)^2 + (\gamma_z m)^2}} \times \left[\sin\frac{n\pi L}{x_e} - \sin\frac{n\pi d}{x_e}\right]\left[\sin\frac{m\pi b}{z_e} - \sin\frac{m\pi a}{z_e}\right] \qquad \ldots(A7)$$

Whose inverse Laplace transform[74,75] is:

$$\tilde{P} = \begin{cases} G_{nm}(t,y)\,R_nR_m & ; 0 \le t \le t_0 \\ \left(G_{nm}(t,y) - G_{nm}(t-t_0,y)\right)R_nR_m & ; t > t_0 \end{cases} \qquad \ldots(A8)$$

where

$$G_{nm}(t,y) = \frac{1}{\sqrt{\pi}}\int_0^t \frac{e^{-\left[((\gamma_x n)^2 + (\gamma_z m)^2)\,u + \frac{y^2}{4u}\right]}}{\sqrt{u}}\,du$$

; Both m and n are not equal to zero at the same time.

$$= \frac{2}{\sqrt{\pi}}\int_0^{\sqrt{t}} e^{-\left[((\gamma_x n)^2 + (\gamma_z m)^2)\,u^2 + \frac{y^2}{4u^2}\right]}\,du$$

$$= \frac{1}{2\sqrt{(\gamma_x n)^2 + (\gamma_z m)^2}}\left[e^{-\sqrt{((\gamma_x n)^2 + (\gamma_z m)^2)}\,y} \times \left\{1 + \operatorname{erf}\left(\sqrt{((\gamma_x n)^2 + (\gamma_z m)^2)t} - \frac{y}{2\sqrt{t}}\right)\right\} - e^{\sqrt{((\gamma_x n)^2 + (\gamma_z m)^2)}\,y}\operatorname{erfc}\left(\sqrt{((\gamma_x n)^2 + (\gamma_z m)^2)t} + \frac{y}{2\sqrt{t}}\right)\right]$$

$$G_{00}(t,y) = \frac{2}{\sqrt{\pi}}\int_0^{\sqrt{t}} e^{-\frac{y^2}{4u^2}}\,du \qquad ; n = m = 0$$

$$= 2\sqrt{\frac{t}{\pi}}\,e^{-\frac{y^2}{4t}} - y\operatorname{erfc}\left(\frac{y}{2\sqrt{t}}\right) = 2\sqrt{t}\operatorname{ierfc}\left(\frac{y}{2\sqrt{t}}\right)$$

and

$$R_n = \left[\sin\left(\frac{n\pi L}{x_e}\right) - \sin\left(\frac{n\pi d}{x_e}\right)\right] / \left(n(L-d)\right)$$

$$R_m = \left[\sin\left(\frac{m\pi b}{z_e}\right) - \sin\left(\frac{m\pi a}{z_e}\right)\right] / \left(m(b-a)\right)$$

The successive inverse Fourier cosine transforms[73] of Equation (A8) yields.

$$P = \begin{cases} \frac{G_{00}(t,y)}{x_e z_e} + \frac{2}{\pi z_e}\sum_{n=1}^{\infty} G_{n0}(t,y)\,R_n\cos(nX) + \frac{2}{\pi x_e}\sum_{m=1}^{\infty} G_{0m}(t,y)\,R_m\cos(mZ) + \frac{4}{\pi^2}\sum_{n=1}^{\infty}\sum_{m=1}^{\infty} G_{nm}(t,y)\,R_nR_m\cos(nX)\cos(mZ) & ; 0 \le t \le t_0 \\ \left(G_{00}(t,y) - G_{00}(t-t_0,y)\right)\frac{1}{x_e z_e} + \frac{2}{\pi z_e}\sum_{n=1}^{\infty}\left(G_{n0}(t,y) - G_{n0}(t-t_0,y)\right)R_n\cos(nX) + \frac{2}{\pi x_e}\sum_{m=1}^{\infty}\left(G_{0m}(t,y) - G_{0m}(t-t_0,y)\right)R_m\cos(mZ) + \frac{4}{\pi^2}\sum_{n=1}^{\infty}\sum_{m=1}^{\infty}\left(G_{nm}(t,y) - G_{nm}(t-t_0,y)\right)R_nR_m\cos(nX)\cos(mZ) & ; t > t_0 \end{cases} \qquad \ldots(A9)$$

When y = 0 (i.e. at the wellbore)

$$G_{nm}(t,0) = \frac{\operatorname{erf}\left[\sqrt{((\gamma_x n)^2 + (\gamma_z m)^2)t}\right]}{\sqrt{((\gamma_x n)^2 + (\gamma_z m)^2)}}$$

and $G_{00}(t,0) = 2\sqrt{\frac{t}{\pi}}$

Setting y = 0 in Equation (A9) and converting to field units the following expression is obtained for the pressure response at the wellbore during isothermal drawdown and buildup, respectively.

$$p_i - p = \begin{cases} \dfrac{282.4\, q\mu B_o}{H_x H_z k_y}\left[\sqrt{\pi\tau} + \dfrac{H_x}{\nu_x}\displaystyle\sum_{n=1}^{\infty}\dfrac{\operatorname{erf}(\nu_x n\sqrt{\tau})}{n} F_n \cos(nX)\right. \\ + \dfrac{H_z}{\nu_z}\displaystyle\sum_{m=1}^{\infty}\dfrac{\operatorname{erf}(\nu_z m\sqrt{\tau})}{m} F_m \cos(mZ) \\ \left. + \dfrac{H_x H_z}{\pi}\displaystyle\sum_{n=1}^{\infty}\sum_{m=1}^{\infty}\dfrac{\operatorname{erf}\left[\sqrt{((\nu_x n)^2 + (\nu_z m)^2)\tau}\right]}{\sqrt{(\nu_x n)^2 + (\nu_z m)^2}} F_n F_m \cos(nX)\cos(mZ)\right] & ;\ 0<\tau<\tau_o \\ \dfrac{282.4\, q\mu B_o}{H_x H_z k_y}\left[\sqrt{\pi}\left(\sqrt{\tau} - \sqrt{\tau-\tau_o}\right)\right. \\ + \dfrac{H_x}{\nu_x}\displaystyle\sum_{n=1}^{\infty}\dfrac{1}{n}\left(\operatorname{erf}(\nu_x n\sqrt{\tau}) - \operatorname{erf}(\nu_x n\sqrt{\tau-\tau_o})\right) F_n\cos(nX) \\ + \dfrac{H_z}{\nu_z}\displaystyle\sum_{m=1}^{\infty}\dfrac{1}{m}\left(\operatorname{erf}(\nu_z m\sqrt{\tau}) - \operatorname{erf}(\nu_z m\sqrt{\tau-\tau_o})\right) F_m\cos(mZ) \\ + \dfrac{2 H_x H_z}{\pi}\displaystyle\sum_{n=1}^{\infty}\sum_{m=1}^{\infty}\left[\dfrac{\operatorname{erf}\left(\sqrt{((\nu_x n)^2 + (\nu_z m)^2)\tau}\right)}{\sqrt{(\nu_x n)^2 + (\nu_z m)^2}}\right. \\ \left. - \dfrac{\operatorname{erf}\left(\sqrt{((\nu_x n)^2 + (\nu_z m)^2)(\tau-\tau_o)}\right)}{\sqrt{(\nu_x n)^2 + (\nu_z m)^2}}\right] \\ \left. \cdot F_n F_m \cos(nX)\cos(mZ)\right] & ;\ \tau>\tau_o \end{cases} \quad \text{...(A10)}$$

Appendix B

Detailed derivation of pressure drawdown and buildup equations for the different time periods.

From Appendix A:

$$p_i - p_{wf} = \frac{282.4\, q\mu B_o}{H_z H_x k_y}\left[\sqrt{\pi\tau} + \frac{H_x}{\nu_x}\sum_{n=1}^{\infty}\frac{1}{n}\operatorname{erf}(\nu_x n\sqrt{\tau}) F_n\cos(nX)\right.$$

$$+ \frac{H_z}{\nu_z}\sum_{m=1}^{\infty}\frac{1}{m}\operatorname{erf}(\nu_z m)\sqrt{\tau}\, F_m\cos(mZ) \quad \text{...(B1)}$$

$$\left. + \frac{2 H_x H_z}{\pi}\sum_{n=1}^{\infty}\sum_{m=1}^{\infty}\frac{\operatorname{erf}\left(\sqrt{((\nu_x n)^2 + (\nu_z m)^2)\tau}\right)}{\sqrt{(\nu_x n)^2 + (\nu_z m)^2}} F_m F_n\cos(nX)\cos(mZ)\right]$$

in general $H_x \gg H_z \Rightarrow \nu_x \ll \nu_z$, therefore

$$\sum_{n=1}^{\infty}\sum_{m=1}^{\infty}\frac{\operatorname{erf}\left(\sqrt{((\nu_x n)^2 + (\nu_z m)^2)\tau}\right)}{\sqrt{(\nu_x n)^2 + (\nu_z m)^2}} F_m F_n\cos(nX)\operatorname{Cox}(mZ)$$

$$\approx \sum_{n=1}^{\infty} F_n\cos(nX)\sum_{m=1}^{\infty}\frac{\operatorname{erf}(\nu_z m\sqrt{\tau})}{\nu_z m} F_m F_n\cos(mZ) \quad \text{...(B2)}$$

for $H_x > 10H_z$ this approximation is within 0.01% if the strip source is sufficiently long with respect to its width.

$$\sum_{n=1}^{\infty} F_n\cos(nX) = \sum_{n=1}^{\infty}\left[\sin\left[\frac{n\pi\ell}{H_x}\right] - \sin\left[\frac{nd\pi}{H_x}\right]\right]\frac{\cos(nX)}{n(\ell-d)} \quad \text{...(B3)}$$

where $X = \frac{\pi x}{H_x}$

$$= \frac{1}{2(\ell-d)}\sum_{n=1}^{\infty}\frac{1}{n}\left[\sin\left[\frac{n\pi(\ell-x)}{H_x}\right] + \sin\left[\frac{n\pi(\ell+x)}{H_x}\right] - \sin\left[\frac{n\pi(d-x)}{H_x}\right]\right.$$

$$\left. - \sin\left[\frac{n\pi(d+x)}{H_x}\right]\right] \quad \text{...(B4)}$$

ince $\sum_{n=1}^{\infty}\frac{\sin(nX)}{n} = \frac{1}{2}(\pi - x)$, $0<x<\pi$ ...(B5)

$$= \frac{\pi}{2}\left[\frac{1}{(\ell-d)} - \frac{1}{H_x}\right]$$

Equation (B2) becomes:

$$= \frac{\pi}{2}\left[\frac{1}{(\ell-d)} - \frac{1}{H_x}\right]\frac{1}{\nu_z}\sum_{m=1}^{\infty}\frac{\operatorname{erf}(\nu_z m\sqrt{\tau})}{m} F_m\cos(mZ) \quad \text{...(B6)}$$

(B1) may now be rewritten:

$$p_i - p_{wf} = \frac{282.4\, q\mu B_o}{H_z H_x k_y}\left[\sqrt{\pi\tau} + \frac{H_x}{\nu_x}\sum_{n=1}^{\infty}\frac{\operatorname{erf}(\nu_x n\sqrt{\tau})}{n} F_n\cos(nX)\right. \quad \text{...(B7)}$$

$$\left. + \frac{H_x H_z}{(\ell-d)\nu_z}\sum_{m=1}^{\infty}\frac{\operatorname{erf}(\nu_z m\sqrt{\tau})}{m} F_m\cos(mZ)\right]$$

At this point substitutions for x and z suggested by Gringarten and Muskat, and for r_w suggested by Prats may be made. The following substitutions apply.

$$X = \frac{\pi}{H_x}(.131\,\ell + .869\,d) \quad , \quad Z = \frac{\pi}{H_z}(.131\,b + .869\,a)$$

and

$$r_w' = r_w\left[\frac{k_z}{k_y}\right]^{1/4} = \frac{(b-a)}{4}$$

The substitutions for X and Z account for the difference between uniform flux and constant wellbore pressure. The permeability ratio multiplying the wellbore radius, is to account for the effects of anisotropy.

Following these substitution

$$F_m = \frac{\left[\sin\left[\frac{m\pi(H_s + 2r_w')}{H_z}\right] - \sin\left[\frac{m\pi(H_s - 2r_w')}{H_z}\right]\right]}{4m\pi r_w'} \quad \text{...(B8)}$$

For small x: $\operatorname{erf}(x) \approx \frac{2}{\sqrt{\pi}}x$ (<.1, <1% error) ...(B9)

Therefore for early time,

$$\frac{1}{\nu_x}\sum_{n=1}^{\infty}\frac{\operatorname{erf}(\nu_x n\sqrt{\tau})}{n} F_n\cos(nX) = \frac{\pi}{2}\left[\frac{1}{(\ell-d)} - \frac{1}{H_x}\right]\frac{2}{\sqrt{\pi}} \quad \text{...(B10)}$$

The term containing r_w' would behave in a similar fashion, however, the width of the equivalent fracture is so small that this approximation would only be valid for unrealistically small times, but would be of interest if considering a partially penetrating fracture of significant width.

also for early time,

$$\sum_{m=1}^{\infty}\frac{\operatorname{erf}(\nu_z n\sqrt{\tau})}{m} F_m\cos(mZ)$$

$$= \frac{1.8089}{H_z}\left[\log\left[\frac{\tau k_z}{r_w^2 k_y}\right] + .352\right] - \frac{\nu_z\sqrt{\pi\tau}}{H_z} \quad \text{...(B11)}$$

This relationship was determined numerically.

Substituting (B10) and (B11) into (B7) gives:

$$p_i - p_{wf} = \frac{162.6\, q\mu B_o}{\sqrt{k_z k_y}(\ell-d)}\left[\log\left[\frac{\sqrt{k_y k_z}\,t}{\phi\mu c_t r_w^2}\right] - 3.227\right] \quad \text{...(B12)}$$

Early Intermediate Time.

for x > 1.8, $\operatorname{erf}(x) \approx 1$

Therefore F_m will become constant and equal to:

$$\frac{1}{\;r_w'}\left[\psi(\eta_1)+\psi(\eta_2)-\psi(\eta_3)-\psi(\eta_4)\right]=\Omega_z \qquad \text{...(B13)}$$

where $\psi(\eta)=\sum_{n=1}^{\infty}\frac{\operatorname{Sin}(n\eta)}{n^2}$ and is known as the Spence Function.

$$\eta_1=\frac{.52\pi r_w'}{H_z}\ ,\quad \eta_2=\frac{\pi}{H_z}(2z+3.48r_w')$$

$$\eta_3=\frac{-3.48\pi r_w'}{H_z}\ ,\quad \eta_4=\frac{\pi}{H_z}(2z-.52r_w')$$

Ω_1 represents a "pseudo skin" per unit length resulting from flow travelling in the z direction toward the well.

Substituting Ω_1 and Equation (B10) into (B7)

$$p_i-p_{ws}=\frac{8.128\ qB_o}{H_z(\ell-d)}\sqrt{\frac{\mu t}{k_y\phi c_t}}+\frac{282.4\ q\mu B_o\pi}{(\ell-d)\sqrt{k_zk_y}H_z}\Omega_z \qquad \text{...(B14)}$$

Redetermining the "pseudo skin" per unit length term in terms of the familiar van Everdingen skin factor.

$$S_z=.6366\ H_z\Omega_z \qquad \text{...(B15)}$$

Substituting (B15) into (B14) yields.

$$p_i-p_{ws}=\frac{8.128\ qB_o}{H_z(\ell-d)}\sqrt{\frac{\mu t}{k_y\phi c_t}}+\frac{141.2\ q\mu B_o}{(\ell-d)\sqrt{k_yk_z}}S_z \qquad \text{...(B16)}$$

Late Intermediate Time.

During this period the term containing X_n will assume the approximation described by (B11) as follows.

$$\sum_{n=1}^{\infty}\frac{\operatorname{erf}(\nu_x n\sqrt{T})}{n}X_n\operatorname{Cos}(nX)$$

$$=\frac{1.8089}{H_x}\left[\operatorname{Log}\left(\frac{\tau k_x}{(\ell-d)^2k_y}\right)+1.556\right]-\frac{\nu_x}{H_x}\sqrt{\pi\tau} \qquad \text{...(B17)}$$

Substituting (B17), (B13), and (B15) into (B7) yields:

$$p_i-p_{ws}=\frac{162.6\ q\mu B_o}{H_z\sqrt{k_xk_y}}\left[\operatorname{Log}\left(\frac{k_xt}{\phi\mu c_t(\ell-d)^2}\right)-2.023\right]+\frac{141.2\ q\mu B_o}{(\ell-d)\sqrt{k_yk_z}}S_z \qquad \text{...(B18)}$$

Late Time

For late time the term containing X_n will become constant and have a form similar to (B13).

$$\Omega_x=\frac{1}{2(\ell-d)}\left[\psi(\zeta_1)+\psi(\zeta_2)-\psi(\zeta_3)-\psi(\zeta_4)\right] \qquad \text{...(B19)}$$

where

$$\zeta_1=\frac{.13\pi(\ell-d)}{H_x}\ ,\quad \zeta_2=\frac{\pi(1.87\ \ell+.13\ d)}{H_x}$$

$$\zeta_3=-.87\ \pi\ (\ell-d)\ ,\quad \zeta_4=\frac{\pi(.87\ \ell+1.13\ d)}{H_x}$$

Ω_x represents a "pseudo skin" per unit length resulting from flow travelling in the x direction toward the well.

Defining the "pseudo skin" to be consistent with S_z.

$$S_x=\frac{.6366\ H_x(\ell-d)}{H_z\sqrt{k_x/k_z}}\Omega_x \qquad \text{...(B20)}$$

Substituting (B18), (B19), and (B20) into (B7).

$$p_i-p_{ws}=\frac{8.128\ qB_o}{H_zH_x}\sqrt{\frac{\mu t}{k_y\phi c_t}}+\frac{141.2\ q\mu B_o}{(\ell-d)\sqrt{k_yk_z}}\left\{S_z+S_x\right\} \qquad \text{...(B21)}$$

The buildup section of Equation (A10) can be analytically reduced to similar simplified sections. The authors leave this to the readers.

TABLE 1

Reservoir and Fluid Properties for Example 1

k_x = 100 md
k_y = 100 md
k_z = 100 md
ϕ = .1
c_t = 3.0×10^{-5} psi^{-1}
H_z = 220 ft
H_y = 2100 ft
r_w = .354 ft
Length = 500 ft
y = 1050 ft
z = 110 ft
q = 3000 STB/D
μ = 1.5 cp
B_o = 1.5 RB/STB
s_m = 0

TABLE 2

Reservoir and Fluid Properties for Example 2

k_x = 50 md
k_y = 100 md
k_z = 25 md
ϕ = .1
c_t = 3.0×10^{-5} psi^{-1}
H_z = 110 ft
H_y = ∞ ft
r_w = .354 ft
Length = 1500 ft
z = 110 ft
q = 3000 STB/D
μ = 1.5 cp
B_o = 1.5 RB/STB
S_m = 5

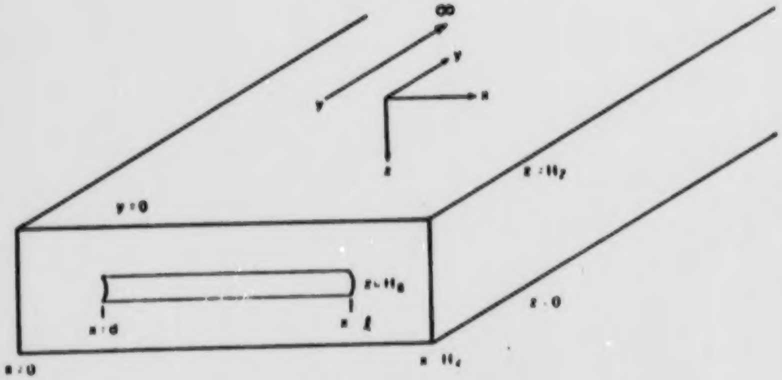
∞
y
y
x
z
z = H_T
y = 0
z = H_0
z = 0
x = d
x = ℓ
x = 0
x = H_x

FIGURE 1. HORIZONTAL WELL MODEL

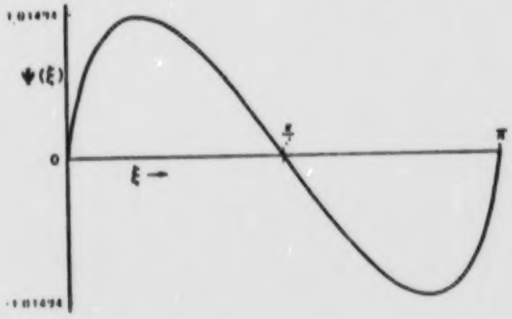

FIGURE 2. SPENCE FUNCTION

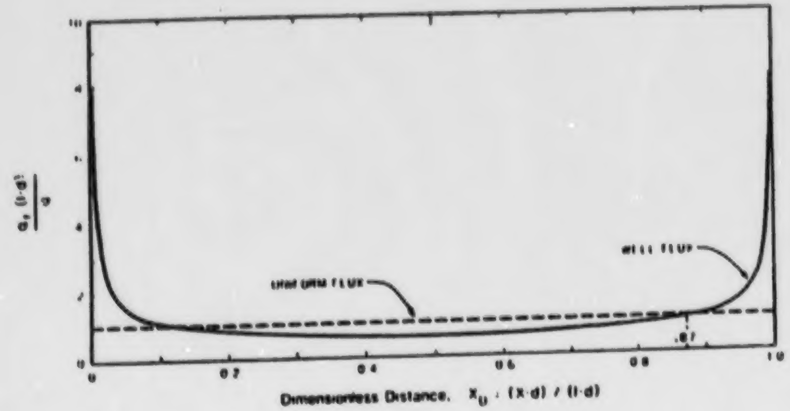

FIGURE 3. FLUX DISTRIBUTION ALONG THE STRIP SOURCE

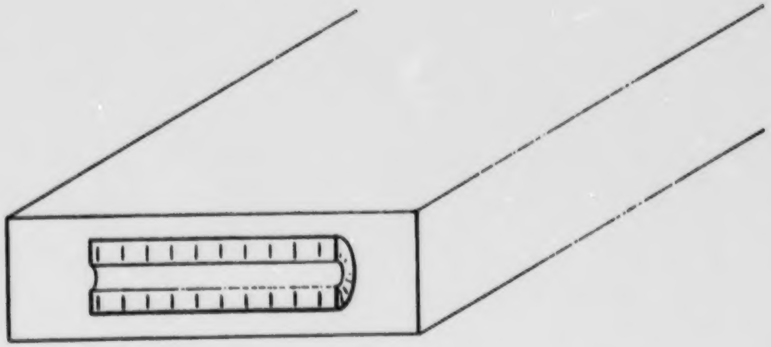

FIGURE 4. EARLY TIME RADIAL FLOW

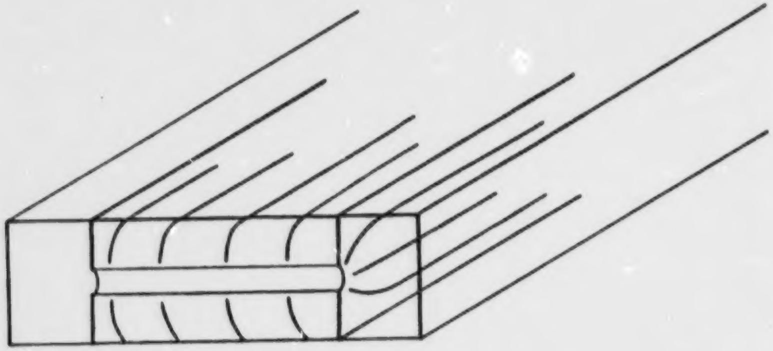

FIGURE 5. INTERMEDIATE TIME LINEAR FLOW

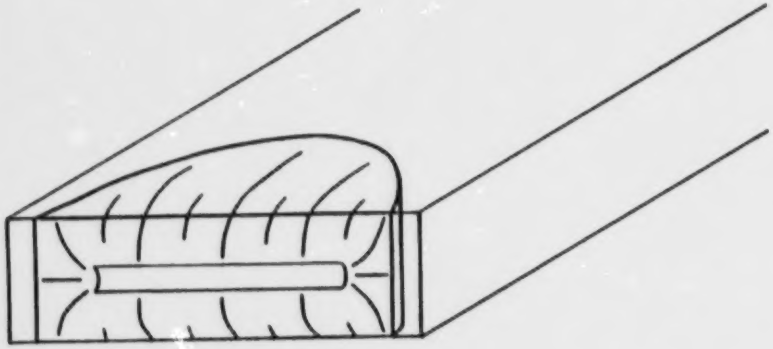

FIGURE 6. LATE INTERMEDIATE TIME RADIAL FLOW

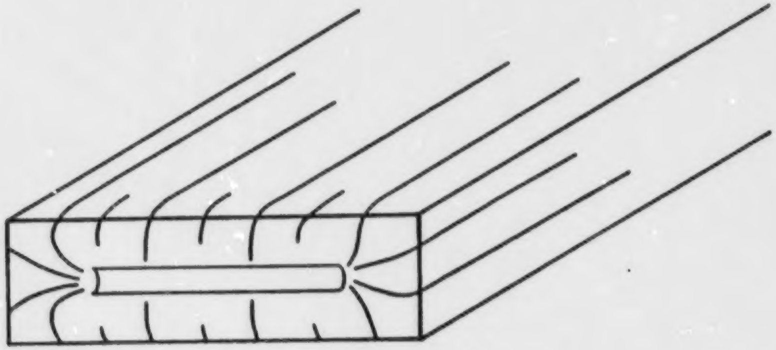

FIGURE 7. LATE TIME LINEAR FLOW

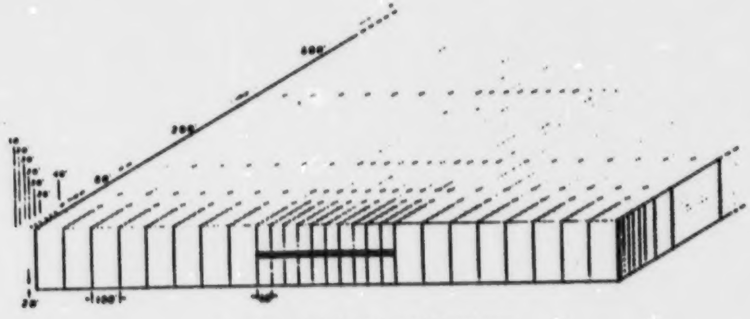

FIGURE 8 HORIZONTAL WELLBORE GRID

COMPARISON OF SIMULATED PRESSURE DRAWDOWN AGAINST ANALYTIC SOLUTION
EXAMPLE 1

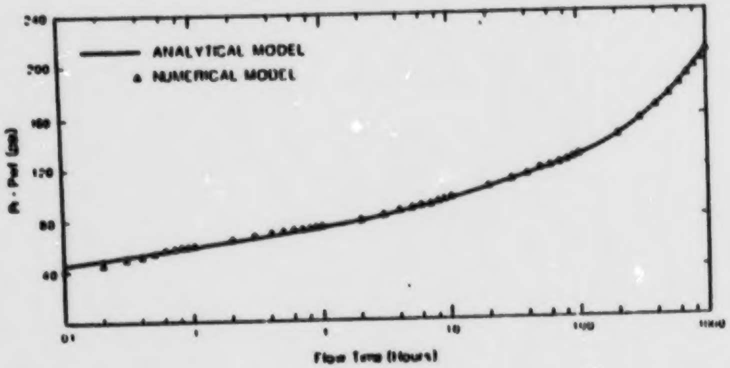

FIGURE 9. COMPARISON OF SIMULATED PRESSURE DRAWDOWN AGAINST ANALYTIC SOLUTION EXAMPLE 1

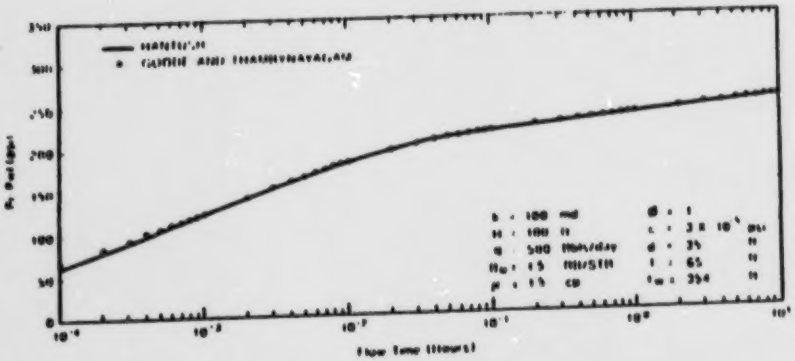

FIGURE 10. A COMPARISON OF HANTUSH PARTIALLY PENETRATING SOLUTION AGAINST GOODE AND THAMBYNAYAGAM ANALYTIC SOLUTION.

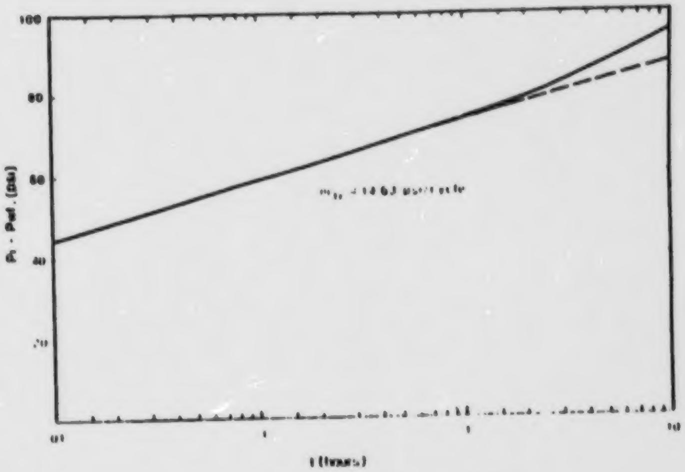

FIGURE 11. EXAMPLE 1. EARLY TIME RADIAL FLOW PERIOD

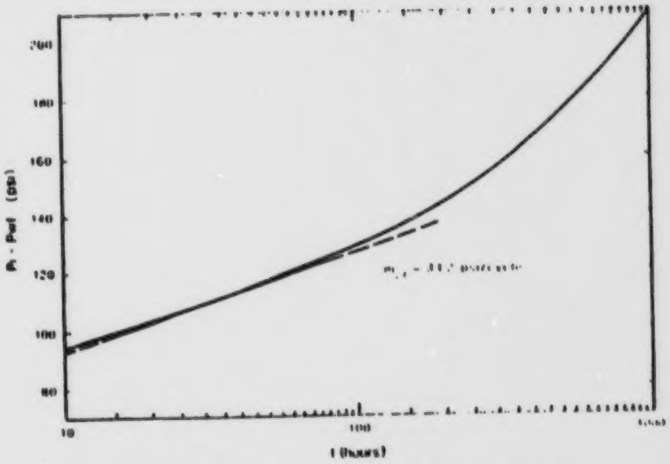

FIGURE 12. EXAMPLE 1. LATE INTERMEDIATE TIME RADIAL FLOW PERIOD

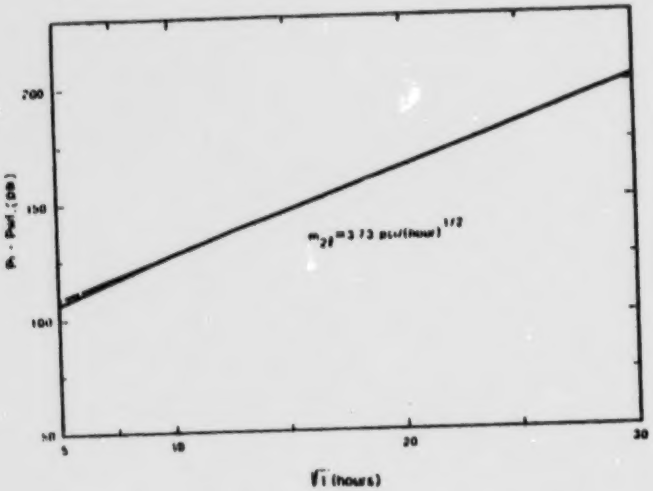

FIGURE 13. EXAMPLE 1. LATE TIME LINEAR FLOW

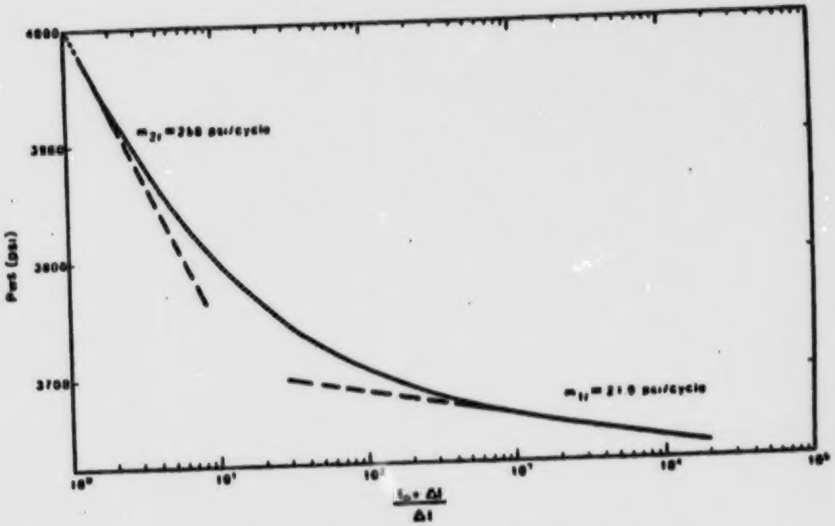

FIGURE 15. EXAMPLE 2. HORNER TIME VERSUS PRESSURE

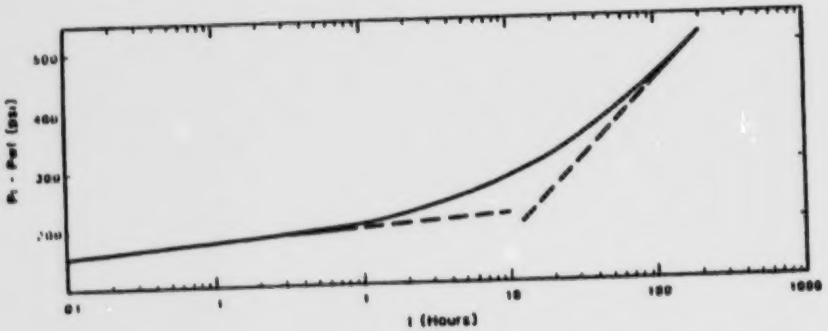

FIGURE 14. EXAMPLE 2. COMPLETE DRAWDOWN PERIOD

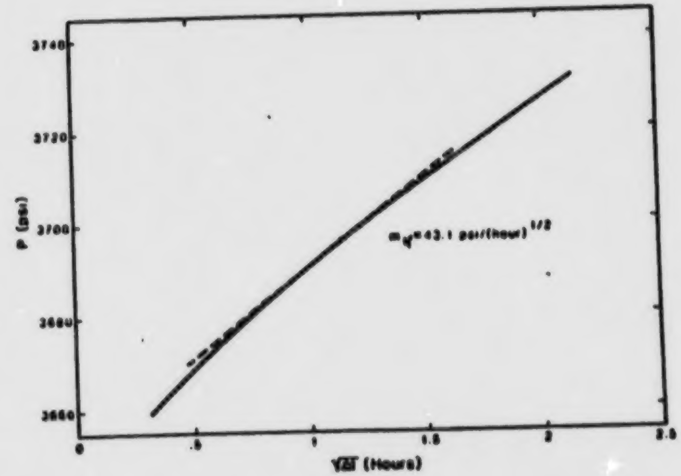

FIGURE 16. EXAMPLE 2. INTERMEDIATE TIME LINEAR FLOW PERIOD

6566 H

Alberta
OIL SANDS TECHNOLOGY &
RESEARCH AUTHORITY
Library and Information Services

SPE
Society of Petroleum Engineers of AIME

PE 15116

(77)

Pressure Transient Analysis for Wells With Horizontal Drainholes

by M.D. Clonts, *ARCO Alaska Inc.*, and H.J. Ramey Jr., *Stanford U.*

SPE Members

This paper was prepared for presentation at the 56th California Regional Meeting of the Society of Petroleum Engineers held in Oakland, CA, April 2–4, 1986.

This paper was selected for presentation by an SPE Program Committee following review of information contained in an abstract submitted by the author(s). Contents of the paper, as presented, have not been reviewed by the Society of Petroleum Engineers and are subject to correction by the author(s). The material, as presented, does not necessarily reflect any position of the Society of Petroleum Engineers, its officers, or members. Papers presented at SPE meetings are subject to publication review by Editorial Committees of the Society of Petroleum Engineers. Permission to copy is restricted to an abstract of not more than 300 words. Illustrations may not be copied. The abstract should contain conspicuous acknowledgment of where and by whom the paper is presented. Write Publications Manager, SPE, P.O. Box 833836, Richardson, TX 75083-3836. Telex, 730989. SPEDAL

ABSTRACT

Drainholes have been drilled in several areas of the world and there is a need to understand these drainage systems for accurate well test analysis. This study presents an analytical solution for the transient pressure response of a uniform flux horizontal drainhole in an anisotropic reservoir of finite thickness. The solution also applies for a reservoir with multiple drainholes in a vertical array. The solution shows that there are two possible types of transient pressure behavior depending on the length of the drainhole relative to the height of the reservoir. If the drainhole is short, initial radial flow perpendicular to the drainhole axis is followed by a transition to a pseudo-radial flow period. If the drainhole length is long relative to the reservoir height, the initial radial flow period ends rapidly and transient pressure behavior becomes identical to that of a uniform flux vertical fracture.

The pressure transient response for multiple drainholes is identical to the single drainhole solution if dimensionless variables are defined relative to the number of drainholes. Consequently, the pressure response of a uniform flux vertical fracture can also be approximated by a vertical array of drainholes. The pressure response for infinite conductivity drainholes is also suggested by analogy to the infinite conductivity vertical fracture solution.

Log-log type curves are presented for various drainhole radii and can be used in the conventional manner to determine reservoir characteristics including directional permeability or drainhole half length. Short and long time approximations are presented along with appropriate time limits. Finally, conditions for greater productivity than with vertical wells or hydraulic fractures are presented.

INTRODUCTION

Drainholes are horizontal bores drilled from a vertical wellbore to increase production. The purpose of this study is to present a means for understanding these systems using pressure transient analysis. Recently, many applications of horizontal drainholes have been attempted or suggested.[1-34] This increased popularity is due mainly to attractive economics and better drilling technology.[1] Applications for drainholes includes: productivity index increases, injectivity index increases, greater sweep efficiencies by line flooding from one drainhole to another, water and gas coning reduction[5-8], penetration of narrowly missed target zones, intersection of naturally occurring vertical fractures and reduced wellbore damage.[1]

The available drainhole literature can be categorized by areas of operational feasibility, productivity increases, and EOR applications. The operational feasibility literature documents the development of flexible drill collars with better directional drilling.[1-4] These technological advances have reduced the amount of risk involved in drilling horizontal drainholes. Areas of the world where horizontal bores have been drilled with positive results include California,[25] Texas,[5-8] France,[4,9] Italy[26] and the USSR.[10-12]

The first studies on drainhole productivity using potentiometric models were presented in the mid-1950's by Perrine,[27] Roemershauser and Hawkins,[28] and Landrum and Crawford.[29] These three studies concluded that (1) drainhole length is of primary importance to productivity, (2) additional drainhole footage is more effective on a single well than are additional drainholes, and (3) increases in productivity are proportional to the combined length of all drainholes in the system until a point is reached were additional benefit per added foot begins to diminish. The conclusions of these reports are explained by the drainhole pseudo skin factor presented in this study.

Publications have been presented in the early 1980's that give analytical expressions and field results for determining expected productivity increases.[9,30-32] The studies showed that horizontal bores were most advantageous for:

- tight reservoirs, specially if vertical fractures are suspected
- thin beds
- thin oil columns or a small density difference between water and oil
- soft formations such as chalk that are likely to collapse

The third area of drainhole literature is EOR applications of drainholes. The primary work in this area is from Canadian production of heavy crudes.[14-17] Suggested or applied uses include continuous steam injection, cyclic injection production techniques, production of tight chalk formations and gravity drainage of steam-heated oil through parallel drainholes.[14-24]

Although no published studies on the pressure transient analysis of horizontal drainholes currently exist, several studies in the pressure transient analysis literature are applicable to this study. First is the partially-penetrating uniform flux fracture solution presented analytically by Raghavan et al.[33] The general vertical fracture solution presented analytically for infinite conductivity and uniform flux fractures by Gringarten et al.[34] will be used to find similarities with the horizontal drainhole pressure transient response. A third study of interest is the pressure transient response for a slanted wellbore presented by Cinco.[35] Limiting cases of these three studies approximate the drainhole case and can be used for checking the drainhole solution.

PROBLEM DESCRIPTION

A solution to the pressure transient response of horizontal drainholes was derived using instantaneous source functions together

---

References and illustrations at end of paper.

with the Newman product method. The combined application of these two methods for petroleum engineering problems was presented by Gringarten and Ramey[36].

A physical description of the problem is illustrated in Fig. 1. A drainhole is represented as a constant-rate line source of length $2x_f$ in a reservoir of height h with impermeable upper and lower boundaries. The reservoir is infinite in the x and y directions, with directional permeabilities of k_x, k_y and k_z. The drainhole is located at height z_w above the bottom of the reservoir. The center of the drainhole is defined by x_w and y_w the distances from the origin in the x and y directions respectively.

The equation governing flow is the diffusivity equation as derived from the continuity equation, an equation of state, and Darcy's Law[37,38]:

$$\eta_x\frac{\partial^2 p(M,t)}{\partial x^2}+\eta_y\frac{\partial^2 p(M,t)}{\partial y^2}+\eta_z\frac{\partial^2 p(M,t)}{\partial z^2}-\frac{\partial p(M,t)}{\partial t}=0 \qquad (1)$$

where:

$$\eta_j=\frac{k_j}{\phi\mu c}\ ,\ j=x,y,z\ or\ r \qquad (2)$$

The instantaneous source function for the drainhole configuration shown in Fig. 1 can be obtained using the Newman product method[39]. If a source-reservoir system can be represented as the intersection of three one-dimensional source-reservoir systems, then the instantaneous uniform flux source function is defined by the product of the three one-dimensional instantaneous source functions.

Many instantaneous source functions useful in pressure transient analysis have been presented previously by Gringarten and Ramey[36]. These instantaneous source functions were used to generate the instantaneous source function for the drainhole-reservoir configuration. The system shown in Fig. 1 can be thought of as the intersection of three one-dimensional systems as shown in Fig. 2.

The following dimensionless variables were used.

$$x_D=(1+\frac{x-x_w}{x_f})\sqrt{\frac{k_y}{k_x}}-1 \qquad (3)$$

$$y_D=\frac{y-y_w}{x_f} \qquad (4)$$

$$z_D=\frac{z-z_w}{x_f}\sqrt{\frac{k_y}{k_z}} \qquad (5)$$

$$z_{wD}=\frac{z_w}{h} \qquad (6)$$

$$L_D=\frac{x_f}{h}\sqrt{\frac{k_z}{k_y}} \qquad (7)$$

$$t_D=\frac{k_y t}{\mu\phi c x_f^2} \qquad (8)$$

Appendix A presents a derivation of the analytical solution given by Eq. (9).

$$p_D(x_D,y_D,z_D,z_{wD},L_D,t_D)=\frac{\sqrt{\pi}}{4}\int_0^{t_D}[1+2\sum_{n=1}^{\infty}\exp\left[-n^2\pi^2L_D^2t'_D\right]\cos n\pi z_{wD}$$

$$\cdot\cos n\pi(z_DL_D+z_{wD})][erf\frac{(1+x_D)}{2\sqrt{t'_D}}+erf\frac{(1-x_D)}{2\sqrt{t'_D}}][\frac{\exp\left[-\frac{y_D^2}{4t'_D}\right]}{\sqrt{t'_D}}]dt'_D \qquad (9)$$

The analytical solution can not be expressed by known functions except for some limiting cases. To obtain solutions for a desired location or system configuration, it was necessary to evaluate the solution using Simpson's Rule. A computer program was obtained from Roland N. Horne which was used previously by Horne and Temeng[40]. The program uses Simpson's Rule to evaluate definite integrals given an instantaneous function. The program was modified to solve the definite integral of the drainhole instantaneous source function. Tabulated results of dimensionless pressure vs time are given in Tables 1-4 for various dimensionless drainhole lengths and radii. These figures correspond to the pressure response at the center of a drainhole with dimensionless drainhole radius $r_{D_w}=Y_D$. Type curves for the tabulated results are shown in Figs. 3-6.

Verification of Solution

Three cases found in the literature were considered for verification of the solution. These are[33-35]:

1. Partially Penetrating Uniform Fracture[33]

   let $\frac{h_f}{x_f}\rightarrow 0$

2. General Uniform Flux Fracture Solution[34]

   let $L_D\rightarrow >10$

3. Slanted Wellbore[35]

   let $\theta_w\rightarrow 90°$

The partially-penetrating, uniform-flux fracture solution should approach the drainhole solution when the completion interval, h_f, relative to the fracture half length, x_f, approaches 0. Unfortunately, the values of $\frac{h_f}{x_f}$ presented by Raghavan were not small enough for the drainhole solution to approximate the partially-penetrating, uniform-flux fracture results.

The uniform flux, fully-penetrating vertical fracture solution was solved analytically by Gringarten and Ramey. Results discussed later show that the solution to a multiple vertical array of drainholes does approach the uniform flux vertical fracture solution as the number of drainholes in the reservoir increases.

Verification was obtained from the slanted wellbore solution although solutions were only presented for deviations from vertical up to 75°. Cinco defined the variable θ_w as the well deviation from vertical and plotted p_{wD} vs. t_D for various $h_D=\frac{h}{r_w}$. To match the drainhole solution, the slanted wellbore was approximated as a horizontal drainhole with the same horizontal projection as a w slanted at 75°. Fig. 7 shows the results of the match. The solutions are within 1 % at all times. The results verify the drainho solution and suggest that small variations from the horizontal do not significantly affect the pressure transient response.

SHORT-TIME APPROXIMATION

A short-time approximation may be derived by approximating an instantaneous source function for each of the three component systems as shown in Appendix B. The resulting equation is:

$$p_D = -\frac{1}{4L_D} Ei\left[-\frac{x_D^2+y_D^2}{4t_D}\right] \tag{10}$$

This form of the short-time approximation is identical to the expression for radial flow when $x_D^2+y_D^2$ is replaced by r_D^2,[44], indicating that early flow toward a drainhole is radial. The end of this radial flow period is given by Eq. (11).

$$t_{e_D} \le min \begin{cases} \dfrac{(1-X_D)^2}{20} \\ \dfrac{\left[Z_D + \dfrac{2}{L_D}(Z_{w_D}-1)\right]^2}{20} \\ \dfrac{\left[Z_D + 2\dfrac{Z_{w_D}}{L_D}\right]^2}{20} \end{cases} \tag{11}$$

Combining the conditions for the natural logarithmic approximation with Eq. (11) defines the conditions that must be present for a graph of the short-time dimensionless pressure drop against the log of dimensionless time to be a straight line within 1%:

$$100(x_D^2+y_D^2) < \min \begin{cases} \dfrac{(1-x_D)^2}{20} \\ \dfrac{[z_D+2\dfrac{z_{wD}}{L_D}]^2}{20} \\ \dfrac{[z_D+\dfrac{2}{L_D}(z_{wD}-1)]^2}{20} \end{cases} \tag{12}$$

If Eq.(12) is satisfied, a semilog straight line will begin at a t_D defined by the left side of Eq. (12), and end at a t_D defined by the right side. The short-time approximation has a slope of $0.5756L_D^{-1}$ when graphed on semilog graph paper. Thus, either the drainhole half length or $\sqrt{\frac{k_z}{k_y}}$ can be determined if skin and storage effects become negligible before the end of the short time flow period. The short-time approximation is not a function of x_D, showing that this approximation is also the short-time solution for the infinite-conductivity drainhole.

If L_D is large, the initial radial flow ends quickly, and the short-time approximation in Eq. (10) is not accurate even at reasonably small times. Figure 3 shows that for such cases the early time log-log graph of P_D vs t_D is a straight line of slope $\frac{1}{2}$. Such behavior indicates that early flow is linear for large L_D.

LONG-TIME APPROXIMATION

The long-time behavior of the pressure transient response due [illegible] a uniform-flux drainhole was determined by referring to the instantaneous source functions for each of the three component systems in Fig. 2 used to generate the problem.

Derivation in Appendix C yields:

$$p_D(x_D,y_D,z_D,z_{wD},L_D,t_D) = \frac{\sqrt{\pi}}{4}\int_0^{t_{pD}}[1+2\sum_{n=1}^{\infty}\exp\left[-n^2\pi^2L_D^2t'_D\right]\cos n\pi z_{wD}$$

$$\cos n\pi(z_DL_D+z_{wD}))][erf\frac{(1+x_D)}{2\sqrt{t'_D}}+erf\frac{(1-x_D)}{2\sqrt{t'_D}}][\frac{\exp\left[-\dfrac{y_D^2}{4t'_D}\right]}{\sqrt{t'_D}}]dt'_D$$

$$+\int_{t_{pD}}^{t_D}\frac{1}{2t_D}\,dt_D \tag{13}$$

Equation 13 applies when t_D is greater than that for the beginning of the pseudo-radial flow period, t_{pD}, as defined from Appendix C by:

$$t_{pD} = \max \begin{cases} \dfrac{5}{\pi^2L_D^2} \\ 25y_D^2 \\ \dfrac{25}{3}(\dfrac{1}{2}+x_D)^2 \\ \dfrac{25}{3}(\dfrac{1}{2}-x_D)^2 \end{cases} \tag{14}$$

Letting p_{pD} equal the first term on the right, in Eq.(13), then the long-term approximation can be simplified to:

$$p_D = p_{pD} + \frac{1}{2}\ln\frac{t_D}{t_{pD}} \tag{15}$$

That late-time pressure drop is a constant plus $\frac{1}{2}\ln t_D$ indicates that flow is pseudo-radial after t_{pD} is reached. This is expected since all wellbore configurations in an infinite slab reservoir system should eventually reach a pseudo-radial flow period indicated by a 1.1515 semilog slope. Equation (14) can be used with type curve matching to determine if the appropriate semilog straight line was reached during a well test or to estimate well test duration requirements.

WELL TEST APPLICATIONS

The analysis of well test data for horizontal drainholes can be conducted with the type curves in Figs. 3-7 using conventional type curve matching procedures presented in the literature[46]. Type curves for a particular drainhole radius can be generated using Eq. (9) and Simpson's Rule. The definitions of dimensionless drainhole variables suggest that the permeabilities in all three directions could be evaluated through the match point technique if all the other variables in the respective dimensionless group are known. The L_D match point yields the ratio of k_z to k_y and the p_D match point yields k_y. The x_D match point combined with other directional permeability data yields $\frac{k_y}{k_x}$. The $\phi\mu c$ constant may be determined by the time match, similarly to conventional type curve matching. Note that k_z can not be determined from well test data if L_D>10 because flow in the vertical direction no longer influences pressure drop. This observation is reflected by the convergence of the pressure response lines to a single envelope of curves for L_D>10.

In addition to the semilog techniques previously mentioned, well test data can also be used to determine the skin factor for the well.[46] The conditions for the start of the long-time flow approximations define the beginning of the appropriate semilog straight line. The magnitude of drainhole damage can be determined by subtracting the drain hole pseudo skin factor, to be presented from the total skin factor. The result yields a mechanical skin factor which is positive for a damaged drainhole, and negative for a stimulated drainhole.

EXTENSION TO MULTIPLE DRAINHOLES

Since multiple drainholes have also been drilled in some reservoirs[1,25], the pressure transient solution for a multiple drainhole system was investigated. A physical representation of the multiple drainhole system is given in Fig. 8. The system is identical to the single drainhole system except that several drainholes are present in a vertical array. In Fig. 8 the number of drainholes is three, although the solution is general for any number of drainholes.

The general solution for a single drainhole was obtained by multipling together the instantaneous source functions for each of the three component systems:

$$S(x_D,y_D,z_D,t_D) = S(x_D,t_D) \cdot S(y_D,t_D) \cdot S(z_D,t_D) \tag{16}$$

The instantaneous source function in the z-direction was obtained by the method of images as described by Matthews et al[48]. The configuration of the drainhole system in Fig. 1 is represented mathematically as an infinite array of drainholes stacked vertically a distance h apart as shown on the left side of Fig. 9. The solid lines between the drainholes are generated by the infinite array of drainholes, and represent no-flow boundaries in the reservoir. A no-flow boundary exists between each drainhole, and the choice of which two to represent the upper and lower reservoir boundaries defines the number of drainholes in the reservoir.

The solution for the multiple-drainhole case can be considered as m identical solutions to the single drainhole case stacked vertically where m is the number of drainholes. The multiple drainhole solution requires redefinition of only the dimensionless variables with respect to the number of drainholes in the reservoir. If L_D and z_{wD} are defined by Eqs.(17) and (18), then the dimensionless pressure for any point in the reservoir is given by Eq.(19).

$$L_D = \frac{m x_f}{h}\sqrt{\frac{k_z}{k_y}} \tag{17}$$

$$z_{wD} = \frac{z_w m}{h} \tag{18}$$

$$p_D(x_D,y_D,z_D,z_{wD},L_D,t_D) = \frac{\sqrt{\pi}}{4}\int_0^{t_D}\left[1+2\sum_{n=1}^{\infty}\exp\left(-n^2\pi^2L_D^2t'_D\right)\cos n\pi z_{wD}\right.$$

$$\left.\cos n\pi(z_DL_D+z_{wD})\right]\left[erf\frac{(1+x_D)}{2\sqrt{t'_D}}+erf\frac{(1-x_D)}{2\sqrt{t'_D}}\right]\left[\frac{\exp\left[-\frac{y_D^2}{4t'_D}\right]}{\sqrt{t'_D}}\right]dt'_D \tag{19}$$

Equation (19) is the same equation as that for the single-drainhole solution, Eq.(9). Note that the definitions for dimensionless variables are also equivalent to the single-drainhole case when m=1.

Because the pressure response equation is the same as for a single drainhole, the results previously presented are also valid for the multiple-drainhole solution.

SIMILARITY TO VERTICAL FRACTURES

As the number of drainholes in a vertical array in a reservoir increases, the pressure transient solution to the drainhole problem should approach the solution for a uniform-flux vertical fracture case. It was noted previously that early flow into the drainhole is linear toward the drainhole if the dimensionless length of the drainhole is greater than 5 to 10. This behavior at short time is similar to a vertical fracture where flow is also linear in the y-direction. Intuitively, one would expect that later flow periods also represent the vertical fracture case.

The uniform flux vertical fracture solution is included with the type curve in Fig. 3. The two solutions are identical for for L_D>10. The similarity has also been proven mathematically[54].

$$p_D(x_D,y_D,z_D,z_{wD},L_D,t_D) = \frac{\sqrt{\pi}}{4}\int_0^{t_D}\left[erf\frac{(1+x_D)}{2\sqrt{t'_D}}+erf\frac{(1-x_D)}{2\sqrt{t'_D}}\right]\cdot\left[\frac{\exp\left[-\frac{y_D^2}{4t'_D}\right]}{\sqrt{t'_D}}\right]dt'_D \tag{20}$$

when:

$$L_D > 10, \tag{21}$$

or;

$$\frac{m\,x_f}{h}\sqrt{\frac{k_z}{k_y}} > 10 \tag{22}$$

Eq.(20) is identical to the general expression for the uniform-flux vertical fracture as presented by Gringarten and Ramey[34]. Eq. (22) shows that the uniform-flux vertical fracture pressure transient response can also be reproduced by increasing the number of drainholes.

Since the drainhole solution is identical to Gringarten and Ramey's solution for the vertical fracture, several special solutions can be directly inferred from that study. The expression for dimensionless pressure along the plane of a vertical fracture (y_D=0) is also the dimensionless pressure drop along the drainhole and is given by Eq.(23):

$$p_D(x_D,z_D,z_{wD},L_D,t_D) = \frac{\sqrt{\pi}}{4}\int_0^{t_D}\frac{1}{\sqrt{t'_D}}\left[erf\frac{(1+x_D)}{2\sqrt{t'_D}}+erf\frac{(1-x_D)}{2\sqrt{t'_D}}\right]dt'_D \tag{23}$$

From the vertical fracture solution, the dimensionless pressure drop at y_D=0 and z_D=0 for a drainhole is given as:

$$p_D(x_D,t_D) = \frac{1}{2}(\pi t_D)^{\frac{1}{2}}\left[erf\frac{(1+x_D)}{2\sqrt{t_D}}+erf\frac{(1-x_D)}{2\sqrt{t_D}}\right]$$

$$\frac{(1-x_D)}{4}\,Ei\left[\frac{(1-x_D)^2}{4t_D}\right]-\frac{(1+x_D)}{4}\,Ei\left[\frac{(1+x_D)^2}{4t_D}\right] \tag{24}$$

The short-time approximation for large L_D can be defined directly from the vertical fracture solution as:

$$p_D(x_D,y_D,t_D) = \sqrt{\pi t_D}\exp\left(-\frac{y_D^2}{4t_D}\right) - |y_D|erfc\left(\frac{|y_D|}{2\sqrt{t_D}}\right) \tag{25}$$

and along the drainhole (y_D=0) :

$$p_D(x_D,t_D) = \sqrt{\pi t_D} \tag{26}$$

EXTENSION TO INFINITE-CONDUCTIVITY DRAINHOLES

The similarity between the drainhole and the vertical fracture cases suggests that other properties of the vertical fracture solution may be applicable to the drainhole solution. The pressure transient response to an infinite-conductivity drainhole should be considered since most drainholes are drilled and cased. Thus resistance to flow in the drainholes is negligible.

The infinite-conductivity solution for the fully-penetrating vertical fracture has been solved by several methods in the literature[34,49,50]. It has been shown that the pressure drop along an infinite-conductivity vertical fracture can be obtained from the uniform-flux solution by calculating P_D for y_D=0 and x_D=0.732. The result is[34]:

$$P_{wD}(t_D) = \frac{1}{2}\sqrt{\pi t_D}\left[erf(\frac{0.134}{\sqrt{t_D}})+erf(\frac{0.866}{\sqrt{t_D}})\right]$$

$$-\,0.067Ei(-\frac{0.018}{t_D}) - 0.433Ei(-\frac{0.759}{t_D}) \qquad (27)$$

This equation was correct for all points along an infinite-conductivity vertical fracture for late and early times, and was assumed correct for all time. Of course the fracture result followed the previous result (x_D=0.75) obtained by Muskat[51] for a well with partial penetration at steady state.

Equation (27) was derived by Gringarten and Ramey directly from the uniform-flux vertical fracture solution, Eq.(20). Consequently, Eq.(27) should also hold for infinite-conductivity drainhole with L_D>10.0.

Fig. 5 shows a graph of the infinite-conductivity fracture solution is equivalent to the drainhole solution evaluated at x_D=0.732 when L_D>10. By analogy, it is probable that the uniform-flux drainhole solution evaluated at x_D=0.732 also represents the dimensionless pressure along an infinite conductivity drainhole for L_D less than 10. Of course an infinite-conductivity drainhole could be represented a number of constant-flux segments and the flux along the drainhole determined as a function of time to prove this speculation. This step was beyond the objectives of this study.

DRAINHOLE PSEUDO SKIN FACTOR

A pseudo skin factor for drainholes was developed to compare drainhole productivity with that of vertical wells, and hydraulic fractures. Because the long-time flow for a drainhole has been shown to be pseudo-radial, it would be expected that a drainhole pseudo skin function should become constant at late time. The constant value reached by the pseudo skin function at late time has been defined[52] as the pseudo skin factor, *s*, and is a function of space and system geometry, but not time. The pseudo skin factor for a uniform-flux drainhole system can be derived by analyzing the appropriate long-time approximations.

During late time the line source solution can be expressed as[44]:

$$p_D=\frac{1}{2}\left[\ln\frac{t_D}{x_D^2+y_D^2}+0.80907\right] \qquad (28)$$

The long term approximation for the dimensionless pressure in Eq.(15) can be used with Eq.(28) to obtain the drainhole pseudo skin factor:

$$s=p_{wD}-\frac{1}{2}\ln t_{wD}+\ln\frac{r_w}{x_f}-0.4045 \qquad (29)$$

Where p_{wD} and t_{wD} are given by Eqs.(13) and (14).

Fig. 10 shows the pseudo skin factor at the wellbore graphed vs. L_D for various dimensionless drainhole radii, $\frac{r_{dh}}{x_f}$. The condition for negative pseudo skin factors is suggested by the following observation from Fig. 10:

$$\left[s+\ln\frac{x_f}{r_w}\right]_{at\,L_D=1/2}=\ln\frac{x_f}{r_{dh}} \qquad (30)$$

Eq.(30) implies that if r_w=r_{dh} then the pseudo skin factor for a drainhole is 0 when L_D=$\frac{1}{2}$. In general, the pseudo skin factor is negative if:

$$\frac{m\,x_f}{h}\sqrt{\frac{k_z}{k_y}}>\frac{1}{2} \qquad (31)$$

In isotropic reservoirs, the pseudo skin factor is negative when the drainhole halflength is longer than the reservoir height. A large k_z should also help achieve the condition of Eq. 31. Such could be the case for reservoirs with natural fractures. Eq.(31) also suggests that reservoirs with thin beds could benefit from observations. Field results from France as reported by Giger et al.[9] support these observations.

The three potentiometric studies[27-29] of drainholes expressed results in terms of productivity increases. One of the principle observations from the studies was that increases in productivity are proportional to the combined length of all drainholes in the system until a point is reached were additional benefit per added foot begins to diminish[28]. The negative unit slope in Fig. (10) confirms that productivity increases are directly proportional to the combined length of the drainholes. It also shows that the benefit to productivity does gradually decrease for each added foot beyond a certain amount. The potentiometric studies also observed that increases in drainhole length were more important than drainhole radius increases[29]. Fig. 10 illustrates this observation and shows that productivity is not a function of drainhole radius for L_D>10. A third observation from the potentiometric studies was that additional drainhole length was better than increasing the number of drainholes[27]. Figure 10 shows that for L_D>10, the only means for decreasing the pseudo skin factor is to increase the drainhole half length, L_D.

Figure 10 shows that for L_D>10:

$$s=1+\ln(\frac{r_w}{x_f}) \qquad (32)$$

This expression for the pseudo skin factor is equivalent to the pseudo skin factor for a uniform-flux vertical fracture[34]. The apparent conclusion from Eq.(32) is that productivity increases from a drainhole may be as great as a uniform-flux vertical fracture of the same length for L_D>10. The uniform-flux fracture case is very close to the infinite-fracture permeability case. Most hydraulic fractures have a finite conductivity that limits the effective fracture length[53]. A drilled and cased drainhole should behave with infinite internal (wellbore) conductivity, although a skin effect may be present. Thus a drainhole may have a lower pseudo skin factor than a finite conductivity hydraulic fracture. Another observation is that if k_y>k_x, then fracture orientation is most likely in only the high permeability direction, while drainholes could be directionally drilled in the direction of low permeability for higher productivity. The orientation of a hydraulic fracture most likely occurs perpendicular to the principal axis of stress. If the reservoir contains naturally occurring fractures, hydraulic fracturing would be expected to form parallel to natural fractures and not enhance flow potential. Finally, it may be possible to obtain greater drainhole half lengths[9] than with vertical fractures. Since one of the three previous observations will usually be pertinent, drainhole productivity may sometimes be greater than the productivity of hydraulic fractures in the same formation. Drainholes offer an alternative to hydraulic fracturing that has important and unique advantages in certain situations.

CONCLUSIONS

There are two possible types of transient pressure behavior depending on effective dimensionless drainhole half-length. If L_D < 10, flow is characterized by an initial radial flow perpendicular to the drainhole axis followed by a transition to a pseudo-radial flow period. If $L_D>10$, the initial radial flow period ends instantaneously for all practical purposes. Flow is then characterized by early time linear flow followed by a transition to late time pseudo-radial flow.

Log-log type curves are presented for various drainhole radii. Through type curve matches of p_D-t_D-L_D and x_D , permeability in three directions and $\phi\mu c$ can possibly be determined. The conditions for the start of the long time flow approximations define the beginning of the appropriate semilog straight line. Analysis of the semilog straight line will yield a skin factor which can be used with the drainhole pseudo skin factor to determine whether a drainhole is damaged or stimulated.

For cases where $L_D>10$, the uniform flux drainhole solution matches the uniform flux vertical fracture solution. From the definition of L_D, the similarity between drainholes and vertical fractures is directly proportional to the ratios $\frac{x_f}{h}$ and $\sqrt{\frac{k_x}{k_y}}$.

The study demonstrated that the pressure transient response for multiple drainholes is identical to the single drainhole solution if dimensionless variables are defined relative to the number of drainholes. Consequently, a drainhole system will also approximate a vertical fracture if several drainholes are present.

Evaluation of the uniform flux drainhole solution for $x_D = 0.732$ showed that the drainhole pressure transient response for $L_D>10$ was equivalent to the infinite conductivity vertical fracture. The early time solution for the infinite conductivity drainhole is given by the early time solution for the uniform flux case. The type curves presented can be used to determine reservoir characteristics and mechanical conditions similarly to the uniform flux drainhole case.

The drainhole pseudo skin factor defines situations were drainholes will be more productive than vertical wells. Drainholes are preferable to a vertical well if $\frac{x_f}{h}>\frac{1}{2}$. The performance of drainholes compared to vertical wells is further enhanced if $k_x>k_y$, or if the reservoir contains more than one drainhole.

The drainhole pseudo skin factor for $L_D>10$ is identical to the pseudo skin factor for a uniform flux vertical fracture. In practice however, drainholes may have higher productivities than hydraulic fractures because (1) drainholes may be drilled to greater lengths than hydraulic fractures, (2) they can provide maximum productivity in reservoirs where $k_x \neq k_y$ through directional drainhole orientation, and (3) cased drainholes will have infinite wellbore conductivity acting, while a fracture of the same length will have some finite conductivity.

These statements are not intended to say that drainholes are always, or even sometimes, superior to a hydraulic fracture on the same well. Under certain conditions, the performance of a drainhole may exceed that of a hydraulic fracture on the same well. However, economics of the results has not been considered in this study. Horizontal directional drilling is difficult and costly. But the potential for improved well performance and improved well control make drain hole completions a very attractive target for the oil industry.

Obvious omissions in this study include consideration of a skin effect on the surface of the drainhole and wellbore (as well as drainhole) storage. Because of the similarity between drainhole and fracture solutions, it did not appear worthwhile to add the complexity of these issues. Neither have an important effect on the performance of high-conductivity fractures, and thus would have a small effect on the performance of a drainhole.

This study was actually inspired by field well test data that indicated a high-conductivity fracture was present in wells completed in an unconsolidated sand in Canada producing a heavy oil. One theory was that sand production of a complete sand-size distribution led to formation of "worm holes". We believed that a linear "worm hole" might appear very much like a high-conductivity vertical fracture, and set out on this study to answer an academic question. The answer is an unqualified conclusion that long "worm holes" (drainholes) can appear very much like vertical fractures as far as pressure transient data is concerned. This was not a major guess in the light of Cinco's work[35].

A surprising and perhaps more important finding, is that drainholes may exceed the performance of vertical fractures for some formations. For such formations, it is already known that there is a maximum effective fracture length for a specific frac[illegible] permeability-fracture width product. The added advantage [illegible] directional drilling the drainhole adds a new degree of freedom to such a well completion. This could have a major impact on anisotropic or fractured formations, and in EOR operations.

The question of comparative economics between fracturing and drainhole completions remains. However the obvious interest in drainholes in the recent literature signals that horizontal directional drilling and completions are here to stay. A major new tool is about to be added to drilling and production. The state of this art of engineering's time has come.

NOMENCLATURE

c = Total reservoir compressibility
h = Reservoir height
h_D = Dimensionless reservoir height based on r_w
h_f = Fracture height
k_i = Permeability in the i direction
L_D = Dimensionless drainhole half length
M = Pressure point
m = Number of drainholes in reservoir
P = Source point
p = Pressure
p_D = Dimensionless pressure using k_y
p_i = Initial reservoir pressure
p_{wD} = Dimensionless Wellbore Pressure
q = Flow rate per unit length of source
q_w = Total flow rate
r = radius
S = Instantaneous source function
s = Pseudo skin factor
t = Time
t_D = Dimensionless time using x_f and k_y
t_{Dw} = Dimensionless time using r_w
x,y,z = Space coordinates
x_w,y_w,z_w = Drainhole center space coordinates
x_f = Drainhole or Fracture half length
z_e = Vertical distance between drainhole no-flow boundaries

GREEK SYMBOLS

Δp = Pressure change from initial
δ = Horizontal distance from the pressure point to the nearest drainhole tip
η_i = Diffusivity constant in the i direction
θ_w = Angle of well inclination from vertical
μ = Viscosity
ϕ = Porosity
σ = Pseudo skin function
τ = Integration variable

SUBSCRIPTS

c = Critical
D = Dimensionless
dh = Drainhole
f = Fracture
l = Beginning of late time flow period
s = End of short time flow period
w = Well

ACKNOWLEDGMENTS

The authors would like to express appreciation to Professor Ro[illegible]nd Horne for providing portions of the computer program used in this study. Financial support was received from Stanford University Petroleum Research Institute, Department of Energy Contract No. DE-ACO3-81SF-11564; Society of Petroleum Engineers, Los Angeles Basin Section; Stanford Geothermal Program, Department of Energy Contract No. DE-AS03-80SF11459; and the Department of Petroleum Engineering, Stanford University. Computer time was provided by the Department of Petroleum Engineering, Stanford University.

REFERENCES

1. Hyland, C.R.: "Drain Hole Drilling - An Idea Whose Time is Now," paper SPE 12792 presented at the SPE 1984 California Regional Meeting, Long Beach, March 25-26, 1984.

2. Holbert, D.R.: "Variables in Kickoff Remain First Consideration During Drainhole Drilling," *Oil and Gas Journal* (Feb. 9, 1981) 121-131.

3. Holbert, D.R.: "Special Practices Allow High-Angle Drilling," *Oil and Gas Journal* (Feb. 16, 1981) 91-99.

4. Dorel, M.: "Horizontal Drilling Methods Proven in Three Test Wells," *World Oil* (May 1983).

5. Stamp, R.L.: "The Use of Horizontal Drainhole in the Empire Abo Unit," paper SPE 9221 presented at the SPE 55th annual Technical Conference, Dallas, Sept. 21-24, 1980.

Wash, R.: "ARCO's Fourth Successful Drainhole Drilled in Cased Hole," *Drill Bit* (Sept. 1981).

7. Monroe, W. D.: "ARCO Drills Horizontal Drainhole for Better Reservoir Placement," *Oil and Gas Journal* (Sept. 15, 1980).

8. Striegler, J.: "ARCO Finishes Fourth Horizontal Drainhole," *Oil and Gas Journal* (May 24, 1982).

9. Giger, F.M., Reiss. L.H. and Jourdan, A.P.: "The Reservoir Engineering Aspects of Horizontal Drilling," paper SPE 13024 presented at the SPE 59th Annual Technical Conference and Exhibit, Houston, Sept. 16-19, 1984.

10. Baturin, A.I., Khalyavkin, V.I. and Musatkin, A.A.: "Experimental Drilling of Horizontal Well 196 at the Novouzybashevskiy Field of Bashkiriya," *Bashk. Gos. Nauchno-Issled. Proektn. Inst. Neft. Prom-sti.* (1979) 34-40.

11. Kovalenko, K.I.: "Promising Production Plans for Exploratory Oil and Gas Drilling Using Horizontal Wells," *Tr. Vses. Neft. Nauhno-Issled. Geologorazved. Inst.* (1981) 92-99.

12. Bragin, V.A., Garushev, A.R., Kldalov, I.V. and Orel, V.E.: "Operation of some Kuban Oil Fields in Late Stages," *Neftegazov. Geol. Geofiz.* (1970) 7-10.

13. Astier, B., Jourdan, A. and Baron, G.: "Elf Well Turns 90° and Stays There," *Petroleum Engineer* (Jan. 1981) 40-44.

14. Quinn, P.C. and Meyer, R.F.: "Mine-assisted in situ Project: An Update," *Long-term Energy Resources*, UNITAR International Conference on Long-term Energy Resources, (1981) 1, 505-509.

15. Towson, D.E. and Meyer, R.F.: "Current in situ Oil Sands Pilot Projects in Alberta, Canada," *Long-term Energy Resources*, UNITAR International Conference on Long-term Energy Rresources, (1981) 1, 499-503.

16. Butler, R.M. and Stephens, D.J.: "Gravity Drainage of Steam-Heated Heavy Oil to Parallel Horizontal Wells," *J. Can. Pet. Tech.* (1982) 90-96.

17. Smith, G.W., Butler, R.M., Meyer, R.F. and Steele, C.T.: "Studies on the use of Tunnels and Horizontal Wells for Recovery of Heavy Crudes," *Future of Heavy Crude and Tar Sands* (1981) 455-459.

18. Allen, J.C.: "Method and Apparatus for Recovering High Viscosity Oils," U.S. Patent No. 4,434,849 (1981).

19. Levinson, L.M., Garris, O.V., Khakimov, M.M., Kotskulich, Ya.S. and Vdovin, K.I.: "Development of Wells at Fields of Highly Viscous and Nonflowing Oils of the Tatar ASSR," *Tekhnol. Buren. Neft. Gazov. Skvazhin* (1982) 98-102.

20. Luque, R.F., Duns, H. and van der Vlis, A.C.: "Research on Approved Hydrocarbon Recovery from Chalk Deposits," *New Technologies for Exploration and Exploitation of Oil and Gas Resources*, (1979) 2,1162-1170.

21. Willman, B.T.: "Method of Treating Reservoirs Containing Very Viscous Crude Oil or Bitumen," Assignees: Exxon Production Research Co., U.S. Patent No. 4,390,067 (1983).

22. Ware, C.H.: *Evaluation of Alternatives For Production of Heavy Oil Using Mining, Drilling, and Steam Stimulation*, Commercialization Insights, Tampa, 1982.

23. Butler, R.M.: "Method for Oil Recovery Using a Horizontal Well With Indirect Heating," Assignees: Exxon Production Research Co., U.S. Patent No. 4,085,803 (1978).

24. Willman, B.T.: "Thermal Recovery of Viscous Hydrocarbons Using Arrays of Radially Spaced Horizontal Wells," Assignees: Exxon Production Research Co., U.S. Patent No. 4,296,969 (1981).

25. Stormont, D.H.: "Increasing Drainage of Oil into Well by Drain-hole Drilling," *Oil and Gas Journal* (Aug. 17, 1953) 105-108,145.

26. Colamasi, C. and delle Canne, A.: "Drainhole Drilling Successful in Sicily," *World Oil* (March 1963) 88.

27. Perrine, R.L.: "Well Productivity Increase from Drain Holes as Measured by Model Studies," *Trans.*, AIME (1955) 204,30-34.

28. Roemershauser, A.E. and Hawkins, M.F.: "The Effect of Slant Hole, Drainhole, and Lateral Hole Drilling on Well Productivity," *J. Pet. Tech. (Feb. 1955) 11-14.*

29. Landrum, B.L. and Crawford, P.B.: "Effect of Drainhole Drilling on Production Capacity," *Trans.*, AIME (1955) 204,271-273.

30. Borisov, Ju. P.: *Exploitation des Gisements de petrole par des puits horizontaux et a deviations multiples*, Nedra, Moscow (1964); Translation from Russian to French - Institut Francais du Petrole, Rueil 28363.

31. Merkulov, V.P.: "Le debit des puits devies et horizontaux," *Neft. Khoz* (1958) 6, 51-56.

32. Giger, F.: "Reduction du Nombre de Puits par l'Utilisation de Forages Horizontaux," *Revue de l'Institut Francais du Petrole*, 38, No. 3 (May-June 1983).

33. Raghavan, R., Uraiet, A. and Thomas, G.W.: "Vertical Fracture Height: Effect on Transient Flow Behavior," paper SPE 6016, presented at the SPE 51st Annual Technical Conference and Exhibition, New Orleans, Oct. 3-6, 1976.

34. Gringarten, A.C., Ramey, H.J., Jr. and Raghavan, R.: "Unsteady State Pressure Distributions Created by a Well with a Single Infinite Conductivity Vertical Fracture," *Soc. Pet. Eng. J.* (Aug. 1974) 347-360.

35. Cinco-Ley, H.: "Unsteady-State Pressure Distributions Created by a Slanted Well or a Well with a Slanted Fracture," PhD dissertation, Stanford U., Stanford, CA (May 1974).

36. Gringarten, A.C. and Ramey, H.J., Jr.: "The Use of Source and Green's Functions in Solving Unsteady-Flow Problems in Reservoirs," *Soc. Pet. Eng. J.* (Oct. 1973) 295-296; *Trans.*, AIME, 255.

37. Matthews, C.S. and Russell, D.G.: *Pressure Buildup and Flow Tests in Wells*, Monograph Series, SPE, Dallas (1967) 1.

38. Hubbert, M.K.: "Darcy's law and the Field Equations of the Flow of Underground Fluids," *Trans.*, AIME (1956) 207, 222-239.

39. Newman, A.B.: "Heating and Colling Rectangular and Cylindrical Solids," *Ind. and Eng. Chem.* (1936) 28, 545.

40. Horne, R.N. and Temeng, K.O.: "The Recognition and Location of Pinch-Out Boundaries by Pressure Transient Analysis," paper SPE 9905 presented at the SPE 1981 California Regional Meeting, Bakersfield, March 25-26, 1981.

41. Gringarten, A.C. and Ramey, H.J., Jr.: "Unsteady-State Pressure Distributions Created by a Well with a Single Horizontal Fracture, Partial Penetration, or Restricted Entry," *Soc. Pet. Eng. J.* (Aug. 1974) 413-426; *Trans.*, AIME, 257.

42. Hantush, M.S.: "Nonsteady Flow to a Well Partially Penetrating an Infinite Leaky Aquifer," *Proceedings*, Iraq Scientific Society (1957).

43. Gringarten, A.C.: "The Use of Source and Green's Functions in the Solution of Unsteady Flow Problems in Reservoirs," Pub. ITTE 71-9, Dept. of Civil Engineering, U. of California at Berkeley (Dec. 1971).

44. Earlougher, R.C., Jr.: *Advances in Well Test Analysis*, Monograph Series, SPE, Dallas (1977) 5.

45. *Handbook of Mathematical Functions*, M. Abramowitz and I.A. Stegun (eds.), Dover Publications, Inc., New York City (1964).

46. Ramey, H.J., Jr.: "Practical Use of Modern Well Test Analysis," paper SPE 5878 presented at the SPE 1976 California Regional Meeting, Long Beach, April 8-9, 1976.

47. White, C.D.: "Propagation of Cavities in Unconsolidated Sand," M.S. Report, Stanford U. (Dec. 1982).

48. Matthews, C.S., Brons, F. and Hazebroek, P.: "A Method for Determination of Average Pressure in a Bounded Reservoir," *Trans.*, AIME (1954) 201, 182-191.

49. Russell, D.G. and Truit, N.E.: "Transient Pressure Behavior in Vertically Fractured Reservoirs," *J. Pet. Tech.* (Oct. 1964) 1159-1170; *Trans., AIME, 231.*

50. van Everdingen, A. F. and Meyer, L.J.: "Analysis of Buildup Curves Obtained After Well Treatment," *J. Pet. Tech.* (April 1971) 513-524; *Trans.*, AIME, 251.

51. Muskat, M.: *The Flow of Homogeneous Fluids Through Porous Media*, J. W. Edwards, Inc., Ann Arbor, Mich. (1946) 273.

52. Brons, F. and Marting, V.E.: "The Effect of Restricted Fluid Entry on Well Productivity," *J. Pet. Tech.* (Feb. 1961) 172-174; *Trans.*, AIME, 222.

53. Cinco-Ley, H., Samaniego-V., F. and Dominguez-A., N.: "Transient Pressure Behavior for a Well With a Finite-Conductivity Vertical Fracture," paper SPE 6014 presented at the SPE 51st Annual Technical Conference and Exhibition, New Orleans, Oct. 3-6, 1976.

54. Clonts, M.D.: "Pressure Transient Analysis of Well with Horizontal Drainholes", M.S. Report, Stanford University, June 1985.

APPENDIX A

Solution Derivation

A general expression for pressure drop is:

$$\Delta p(M,t)=\frac{1}{\phi c}\int_0^t q(\tau)S(M,t-\tau)d\tau \tag{A-1}$$

In Eq. (A-1) *S* is the instantaneous uniform flux source function for the particular source-reservoir system. Referring to Fig. 2, the first source is a slab source infinite in the *y* and *z* directions and of thickness $2x_f$. The instantaneous source function for an infinite slab source is given in Ref. 36 as:

$$S(x,t)=\frac{1}{2}\left[erf\frac{\frac{x_f}{2}+(x-x_w)}{2\sqrt{\eta_x t}}+erf\frac{\frac{x_f}{2}-(x-x_w)}{2\sqrt{\eta_x t}}\right] \tag{A-2}$$

The second instantaneous source is that for an infinite plane source in the x-z plane. The instantaneous source function for an infinite plane source is given by Ref. 36 as:

$$S(y,t)=\frac{\exp\left[\frac{(y-y_w)^2}{4\eta_y t}\right]}{2\sqrt{\pi\eta_y t}} \tag{A-3}$$

The third instantaneous source function is that for an infinite plane source in a slab reservoir. This is also presented by Gringarten and Ramey[36] as:

$$S(z,t)=\frac{1}{h}\left[1+2\sum_{n=1}^{\infty}\exp\left[\frac{n^2\pi^2\eta_z t}{h^2}\right]\cos n\pi\frac{z_w}{h}\cos n\pi\frac{z}{h}\right] \tag{A-4}$$

Fig. 2 shows that the intersection of Eqs. (A-2), (A-3), and (A-4) is the necessary configuration describing the drainhole system. By the principle of the Newman product method, the instantaneous source function for the drainhole system is given as the product of e three individual source functions. The instantaneous source ction for the drainhole system is:

$$S(x,y,z,t)=\frac{1}{h}\left[1+2\sum_{n=1}^{\infty}\exp\left(-\frac{n^2\pi^2\eta_z t}{h^2}\right)\cos n\pi\frac{z_w}{h}\cos n\pi\frac{z}{h}\right]$$

$$\frac{1}{2}\left[erf\frac{\frac{x_f}{2}+(x-x_w)}{2\sqrt{\eta_x t}}+erf\frac{\frac{x_f}{2}-(x-x_w)}{2\sqrt{\eta_x t}}\right]\frac{\exp\left[-\frac{(y-y_w)^2}{4\eta_y\tau}\right]}{2\sqrt{\pi\eta_y t}} \qquad \text{(A-5)}$$

Substituting Eq.(A-5) into Eq.(A-1) yields the pressure drop at any point M due to the drainhole:

$$\Delta p(x,y,z,t)=\frac{1}{\phi c}\int_0^t q(\tau)\frac{1}{h}\left[1+2\sum_{n=1}^{\infty}\exp\left(-\frac{n^2\pi^2\eta_z\tau}{h^2}\right)\cos n\pi\frac{z_w}{h}\cos n\pi\frac{z}{h}\right]$$

$$\frac{1}{2}\left[erf\frac{\frac{x_f}{2}+(x-x_w)}{2\sqrt{\eta_x\tau}}+erf\frac{\frac{x_f}{2}-(x-x_w)}{2\sqrt{\eta_x\tau}}\right]\frac{\exp\left[-\frac{(y-y_w)^2}{4\eta_y\tau}\right]}{2\sqrt{\pi\eta_y\tau}}\,d\tau \qquad \text{(A-6)}$$

where

$$q_w=2x_f q \qquad \text{(A-7)}$$

e total flowrate, q_w, is assumed constant, and the flowrate per unit length, $q(\tau)$, can be removed from the integral.

The relation between Δp and p_D is given by Eq. (A-8).

$$p_D=\frac{2\pi k_r h\Delta p}{q_w\mu} \qquad \text{(A-8)}$$

Combining Eqs. (A-1), (A-8) and the dimensionless variable definitions yields the dimensionless pressure drop at any point in the drainhole system given by Eq. (9).

APPENDIX B

Short-Time Approximation Derivation

For small values of t_D the expression:

$$erf\left[\frac{x}{2\sqrt{t_D}}\right]\rightarrow\pm 1 \qquad \text{(B-1)}$$

approaches unity for positive values of x, and approaches negative one for negative values of x. Thus, the instantaneous source function given by Eq. (A-2) is unity at early time. The proper time limit for this approximation is presented by Gringarten and Ramey[36] as:

$$t\le\frac{\delta^2}{20\eta_x} \qquad \text{for } |x|<x_f \qquad \text{(B-2)}$$

where δ is defined as the minimum distance to the nearest source boundary. For the drainhole problem, the minimum distance is the distance from x to x_f.

$$\delta=|x-x_f| \qquad \text{(B-3)}$$

From Eq.(B-2) the short time approximation for the dimensionless instantaneous source function is given by Eqs.(B-4),(B-5), and (B-6) for points between the tips of the drainhole, on the tips, and beyond the drainhole, respectively.

$$S(x,t)=1 \qquad \text{(B-4)}$$

$$S(x,t)=\frac{1}{2} \qquad \text{(B-5)}$$

$$S(x,t)=0 \qquad \text{(B-6)}$$

At early times, there is no flow in the reservoir beyond the edges of the drainhole from Eq.(B-6). The appropriate time limit maybe obtained by combining Eqs.(B-2) and (B-3). This maximum time is the end of the short-time flow period, t_{eD}, and is given in Eqs.(B-7) and (B-8).

$$t_{eD}\le\frac{(1-x_D)^2}{20} \qquad x_D\neq 1 \qquad \text{(B-7)}$$

$$t_{eD}\le\frac{1}{20} \qquad x_D=1 \qquad \text{(B-8)}$$

The instantaneous source function for an infinite plane in a slab reservoir, Eq.(A-4), can be approximated at short time by Eq.(B-9).[36,43]

$$S(z,t)=\frac{1}{2\sqrt{\pi\eta_z t}}\exp\left[-\frac{(z-z_w)^2}{4\eta_z t}\right] \qquad \text{(B-9)}$$

when:

$$\max\left\{\begin{array}{c}\frac{\eta_z t}{(z+z_w)^2}\\ \frac{\eta_z t}{(z+z_w-2h)^2}\end{array}\right.\le\frac{1}{20} \qquad \text{(B-10)}$$

Substituting the definitions for dimensionless variables from Eqs.(3) through (8) into Eq.(B.9) yields the following dimensionless short-time approximation of Eq.(A-4):

$$S(Z_D,t_D)=\sqrt{\frac{k_y}{k_x}}\cdot\frac{1}{2x_f\sqrt{\pi t_D}}\exp\left[-\frac{z_D^2}{4t_D}\right] \qquad \text{(B-11)}$$

when:

$$t_{2D}\le\min\left\{\begin{array}{c}\frac{[z_D+\frac{2}{L_D}(z_{wD}-1)]^2}{20}\\ \frac{[z_D+2\frac{z_{wD}}{L_D}]^2}{20}\end{array}\right. \qquad \text{(B-12)}$$

The short-time approximation for the drainhole system is the product of the three short-time instantaneous source approximations, Eqs.(B-11), (B-4) and (A-4). The result is Eq.(B-13):

$$S(x_D,y_D,z_D,t_D)=\sqrt{\frac{k_y}{k_x}}\frac{1}{2x_f\sqrt{\pi t_D}}\exp\left[-\frac{x_D^2}{4t_D}\right]\cdot 1$$

$$\cdot\frac{1}{2x_f\sqrt{\pi t_D}}\exp\left[-\frac{y_D^2}{4t_D}\right] \qquad \text{(B-13)}$$

Substituting Eq.(B-13) into Eq.(9) yields:

$$p_D(y_D,z_D,t_D)=\frac{h}{4x_f}\sqrt{\frac{k_y}{k_x}}\int_0^{t_D}\frac{\exp\left[-\frac{x_D^2+y_D^2}{4t'_D}\right]}{t'_D}dt'_D \qquad \text{(B-14)}$$

Eq.(B-14) can be expressed in terms of the exponential integral as shown by Eq.(10).

APPENDIX C

Long-Time Approximation Derivation:

The instantaneous source function for an infinite plane source in an infinite slab reservoir, Eq.(A-4), can be approximated[36] within 1 % by $\frac{1}{h}$ in Eq.(C-1):

$$S(z,t)=\frac{1}{h}\left[1+2\sum_{n=1}^{\infty}\exp\left[-\frac{n^2\pi^2\eta_z t}{h^2}\right]\cos n\pi\frac{z_w}{h}\cos n\pi\frac{z}{h}\right]\to\frac{1}{h} \qquad \text{(C-1)}$$

when:

$$t\geq\frac{5h^2}{\pi^2\eta_z}\ , \qquad \text{(C-2)}$$

or:

$$t_D\geq\frac{5}{\pi^2L_D^2} \qquad \text{(C-2a)}$$

The instantaneous source function for an infinite plane source, Eq.(A-3), can be approximated by expanding the exponential term[45] as in Eq.(C-3):

$$S(y,t)=\frac{\exp-\frac{(y-y_w)^2}{4\eta_y t}}{2\sqrt{\pi\eta_y t}}=\frac{1}{2x_f\sqrt{\pi t_D}}\left[1-\frac{y_D^2}{4t_D}+\frac{y_D^2}{32t_D^2}+O(\frac{1}{t_D^3})\right] \qquad \text{(C-3)}$$

The left hand side of Eq.(3.3) can be approximated by the first term in the expansion when:

$$\frac{1}{2x_f\sqrt{\pi t_D}}\geq\frac{100y_D^2}{4t_D\cdot 2x_f\sqrt{\pi t_D}} \qquad \text{(C-4)}$$

or:

$$t_D\geq 25y_D^2 \qquad \text{(C-5)}$$

The third instantaneous source function, Eq.(A-2), can be approximated by expansion of the error function[45].

$$erf\left[\frac{\frac{1}{2}+x_D}{2\sqrt{t_D}}\right]=\frac{2}{\sqrt{\pi}}\sum_{n=0}^{\infty}\frac{(-1)^n\left[\frac{\frac{1}{2}+x_D}{2\sqrt{t_D}}\right]^{2n+1}}{n!(2n+1)}$$

$$=\frac{\frac{1}{2}+x_D}{\sqrt{\pi t_D}}-\frac{(\frac{1}{2}+x_D)^3}{12\sqrt{\pi t_D^3}}+O\left[\frac{1}{t_D^{5/2}}\right] \qquad \text{(C-6)}$$

The first term is an accurate expression of the error function within 1% when:

$$\frac{\frac{1}{2}+x_D}{\sqrt{\pi t_D}}\geq\frac{100(\frac{1}{2}+x_D)^3}{12\sqrt{\pi t_D^3}} \qquad \text{(C-7)}$$

or:

$$t_D\geq\frac{25}{3}(\frac{1}{2}+x_D)^2 \qquad \text{(C-8)}$$

Similarly, the second error function is approximated within one percent by:

$$erf\left[\frac{\frac{1}{2}-x_D}{2\sqrt{t_D}}\right]=\frac{\frac{1}{2}-x_D}{\sqrt{\pi t_D}} \qquad \text{(C-9)}$$

when:

$$t_D\geq\frac{25}{3}(\frac{1}{2}-x_D)^2 \qquad \text{(C-10)}$$

The instantaneous source function for a drainhole may be determined by substituting Eqs.(C-1), (C-3), (C-6), and (C-9) into the general expression for the drainhole instantaneous source function, Eq.(A-5):

$$S(X_D,Y_D,Z_D,Z_{w_D},L_D,t_D)=\frac{1}{h}\cdot\frac{1}{2x_f\sqrt{\pi t_D}}\cdot\frac{1}{2}\left[\frac{\frac{1}{2}+x_D}{\sqrt{\pi t_D}}+\frac{\frac{1}{2}-x_D}{\sqrt{\pi t_D}}\right] \qquad \text{(C-11)}$$

The dimensionless pressure long-time approximation is then found by combining Eq.(C-11) with Eq.(9) to obtain Eq. (13).

APPENDIX D

Multiple Drainhole Solution Derivation

The dimensionless pressure drop can be defined in terms of the total height of the reservoir, h, and the total flowrate from all the drainholes, q_{t}.

$$p_D=\frac{2\pi k_y h\Delta p}{q_t\mu} \qquad \text{(D-1)}$$

where

$$h=z_e\,m \qquad \text{(D-2)}$$

$$q_w = 2\, x_f\, m\, q \qquad \text{(D-3)}$$

stituting Eqs.(D.2) and (D.3) into Eq.(D.1) shows that the m's ancel and the dimensionless pressure, as defined, is equal to the definition for dimensionless pressure in Eq.(A-8).

The pressure transient response is given by replacing h with z_e in Eq.(9):

$$\Delta p(x,y,z,t) = \frac{1}{\phi c}\int_0^t q(\tau)\frac{1}{z_e}\left[1+2\sum_{n=1}^{\infty}\exp\left(-\frac{n^2\pi^2\eta_z\tau}{z_e^2}\right)\cos n\pi\frac{z_w}{z_e}\cos n\pi\frac{z}{z_e}\right]$$

$$\frac{1}{2}\left[erf\frac{\frac{x_f}{2}+(x-x_w)}{2\sqrt{\eta_x\tau}} + erf\frac{\frac{x_f}{2}-(x-x_w)}{2\sqrt{\eta_x\tau}}\right]\frac{\exp\left[-\frac{(y-y_w)^2}{4\eta_y\tau}\right]}{2\sqrt{\pi\eta_y\tau}}\,d\tau \qquad \text{(D-4)}$$

Substituting Eqs.(D.1-3) into Eq.(D.4) yields:

$$p_D = \frac{2\pi k_y h m}{m q \mu\phi c x_f h}\int_0^t\left[1+2\sum_{n=1}^{\infty}\exp\left(-\frac{n^2\pi^2\eta_z\tau m^2}{h^2}\right)\cos n\pi\frac{z_w m}{h}\cos n\pi\frac{z m}{h}\right]$$

$$\left[erf\frac{\frac{x_f}{2}+(x-x_w)}{2\sqrt{\eta_x\tau}} + erf\frac{\frac{x_f}{2}-(x-x_w)}{2\sqrt{\eta_x\tau}}\right]\frac{\exp\left[-\frac{(y-y_w)^2}{4\eta_y\tau}\right]}{2\sqrt{\pi\eta_y\tau}}\,d\tau \qquad \text{(D-5)}$$

Eq.(D.5) suggests that the dimensionless variables x_D, y_D, z_D, and t_D should still be as previously defined. Thus:

$$p_D = \frac{\sqrt{\pi}}{4}\int_0^{t_D}\left[1+2\sum_{n=1}^{\infty}\exp\left(-\frac{n^2\pi^2\eta_z t'_D x_f^2 m^2}{\eta_y h^2}\right)\cos n\pi\frac{z_w m}{h}\cos n\pi\frac{z m}{h}\right]$$

$$\cdot\left[erf\frac{1+x_D}{2\sqrt{t'_D}} + erf\frac{1-x_D}{2\sqrt{t'_D}}\right]\cdot\left[\frac{\exp\left(-\frac{y_D^2}{4t'_D}\right)}{\sqrt{t'_D}}\right]dt'_D \qquad \text{(D-6)}$$

If L_D and Z_{w_D} are defined by Eqs. (17) and (18) then Eq. (19) follows.

TABLE 1 - Dimensionless Pressure for a Uniform Flux Drainhole in an Infinite Slab Reservoir for x_D=0 and r_{Dw}=0.0005

XD = 0.0 YD = 0.5e-03 ZD = 0.0 ZWH = 0.5000

LD TD	1.250d-01	2.500d-01	5.000d-01	1.000d+00	2.500d+00	1.000d+01	5.000d+01
1.00e-04	1.3529e+01	6.8026e+00	3.4014e+00	1.7007e+00	6.8027e-01	1.7007e-01	3.6243e-02
1.00e-03	1.8135e+01	9.1054e+00	4.5528e+00	2.2764e+00	9.1056e-01	2.2888e-01	7.4564e-02
1.00e-02	2.2741e+01	1.1409e+01	5.7045e+00	2.8522e+00	1.1416e+00	3.5034e-01	1.9577e-01
1.00e-01	2.7334e+01	1.3705e+01	6.8527e+00	3.4386e+00	1.5285e+00	7.3188e-01	5.7731e-01
1.00e+00	3.0913e+01	1.5499e+01	7.8863e+00	4.3271e+00	2.4146e+00	1.6180e+00	1.4634e+00
1.00e+01	3.2472e+01	1.6639e+01	9.0019e+00	5.4427e+00	3.5302e+00	2.7336e+00	2.5790e+00
1.00e+02	3.3620e+01	1.7787e+01	1.0150e+01	6.5907e+00	4.6782e+00	3.8816e+00	3.7270e+00
1.00e+03	3.4772e+01	1.8938e+01	1.1301e+01	7.7420e+00	5.8295e+00	5.0329e+00	4.8783e+00
1.00e+04	3.5923e+01	2.0090e+01	1.2453e+01	8.8937e+00	6.9812e+00	6.1845e+00	6.0300e+00
1.00e+05	3.7075e+01	2.1242e+01	1.3605e+01	1.0045e+01	8.1329e+00	7.3363e+00	7.1817e+00
1.00e+06	3.8227e+01	2.2393e+01	1.4756e+01	1.1197e+01	9.2846e+00	8.4880e+00	8.3334e+00
1.00e+07	3.9378e+01	2.3545e+01	1.5908e+01	1.2349e+01	1.0436e+01	9.6397e+00	9.4851e+00

TABLE 2 - Dimensionless Pressure for a Uniform Flux Drainhole in an Infinite Slab Reservoir for x_D=0 and r_{Dw}=0.005

XD = 0.0 YD = 0.5e-02 ZD = 0.0 ZWH = 0.5000

LD TD	1.250d-01	2.500d-01	5.000d-01	1.000d+00	2.500d+00	1.000d+01	5.000d+01
1.00e-04	4.5126e+00	2.2571e+00	1.1285e+00	5.6426e-01	2.2571e-01	5.6426e-02	1.3298e-02
1.00e-03	9.0086e+00	4.5051e+00	2.2525e+00	1.1263e+00	4.5051e-01	1.1386e-01	5.0880e-02
1.00e-02	1.3604e+01	6.8029e+00	3.4014e+00	1.7007e+00	6.8104e-01	2.3508e-01	1.7185e-01
1.00e-01	1.8196e+01	9.0987e+00	4.5494e+00	2.2870e+00	1.0678e+00	6.1654e-01	5.5331e-01
1.00e+00	2.1774e+01	1.0892e+01	5.5830e+00	3.1754e+00	1.9539e+00	1.5026e+00	1.4394e+00
1.00e+01	2.3334e+01	1.2032e+01	6.6986e+00	4.2911e+00	3.0695e+00	2.6182e+00	2.5550e+00
1.00e+02	2.4482e+01	1.3180e+01	7.8465e+00	5.4390e+00	4.2175e+00	3.7662e+00	3.7030e+00
1.00e+03	2.5633e+01	1.4332e+01	8.9979e+00	6.5904e+00	5.3688e+00	4.9175e+00	4.8543e+00
1.00e+04	2.6785e+01	1.5483e+01	1.0150e+01	7.7420e+00	6.5205e+00	6.0692e+00	6.0060e+00
1.00e+05	2.7936e+01	1.6635e+01	1.1301e+01	8.8937e+00	7.6722e+00	7.2209e+00	7.1577e+00
1.00e+06	2.9088e+01	1.7787e+01	1.2453e+01	1.0045e+01	8.8239e+00	8.3726e+00	8.3094e+00
1.00e+07	3.0240e+01	1.8938e+01	1.3605e+01	1.1197e+01	9.9756e+00	9.5243e+00	9.4611e+00

TABLE 3 - Dimensionless Pressure for a Uniform Flux Drainhole in an Infinite Slab Reservoir
for x_D=0.732 and r_{Dw}=0.0005

XD = 0.732 YD = 0.5e-03 ZD = 0.0 ZWH = 0.5000

LD TD	1.250d-01	2.500d-01	5.000d-01	1.000d+00	2.500d+00	1.000d+01	5.000d+01
1.00e-04	1.3529e+01	6.8026e+00	3.4014e+00	1.7007e+00	6.8027e-01	1.7007e-01	3.6243e-02
1.00e-03	1.8135e+01	9.1054e+00	4.5528e+00	2.2764e+00	9.1056e-01	2.2888e-01	7.4564e-02
1.00e-02	2.2721e+01	1.1399e+01	5.6994e+00	2.8497e+00	1.1406e+00	3.4956e-01	1.9498e-01
1.00e-01	2.6657e+01	1.3366e+01	6.6833e+00	3.3510e+00	1.4638e+00	6.6767e-01	5.1310e-01
1.00e+00	2.9461e+01	1.4773e+01	7.5022e+00	4.0614e+00	2.1724e+00	1.3763e+00	1.2218e+00
1.00e+01	3.0938e+01	1.5860e+01	8.5667e+00	5.1260e+00	3.2370e+00	2.4409e+00	2.2863e+00
1.00e+02	3.2080e+01	1.7002e+01	9.7087e+00	6.2680e+00	4.3790e+00	3.5829e+00	3.4283e+00
1.00e+03	3.3231e+01	1.8152e+01	1.0859e+01	7.4187e+00	5.5297e+00	4.7336e+00	4.5791e+00
1.00e+04	3.4383e+01	1.9304e+01	1.2011e+01	8.5704e+00	6.6813e+00	5.8852e+00	5.7307e+00
1.00e+05	3.5534e+01	2.0456e+01	1.3163e+01	9.7220e+00	7.8330e+00	7.0369e+00	6.8824e+00
1.00e+06	3.6686e+01	2.1607e+01	1.4314e+01	1.0874e+01	8.9847e+00	8.1886e+00	8.0341e+00
1.00e+07	3.7838e+01	2.2759e+01	1.5466e+01	1.2025e+01	1.0136e+01	9.3403e+00	9.1858e+00

TABLE 4 - Dimensionless Pressure for a Uniform Flux Drainhole in an Infinite Slab Reservoir
for x_D=0.732 and r_{Dw}=0.005

XD = 0.732 YD = 0.5e-02 ZD = 0.0 ZWH = 0.5000

LD TD	1.250d-01	2.500d-01	5.000d-01	1.000d+00	2.500d+00	1.000d+01	5.000d+01
1.00e-04	4.5126e+00	2.2571e+00	1.1285e+00	5.6426e-01	2.2571e-01	5.6426e-02	1.3298e-02
1.00e-03	9.0086e+00	4.5051e+00	2.2525e+00	1.1263e+00	4.5051e-01	1.1386e-01	5.0880e-02
1.00e-02	1.3584e+01	6.7927e+00	3.3964e+00	1.6982e+00	6.8001e-01	2.3430e-01	1.7106e-01
1.00e-01	1.7518e+01	8.7600e+00	4.3800e+00	2.1994e+00	1.0031e+00	5.5234e-01	4.8911e-01
1.00e+00	2.0323e+01	1.0166e+01	5.1989e+00	2.9098e+00	1.7117e+00	1.2610e+00	1.1978e+00
1.00e+01	2.1800e+01	1.1253e+01	6.2634e+00	3.9743e+00	2.7763e+00	2.3255e+00	2.2623e+00
1.00e+02	2.2942e+01	1.2395e+01	7.4054e+00	5.1164e+00	3.9183e+00	3.4676e+00	3.4043e+00
1.00e+03	2.4093e+01	1.3546e+01	8.5562e+00	6.2671e+00	5.0690e+00	4.6183e+00	4.5550e+00
1.00e+04	2.5245e+01	1.4697e+01	9.7078e+00	7.4187e+00	6.2206e+00	5.7699e+00	5.7067e+00
1.00e+05	2.6396e+01	1.5849e+01	1.0859e+01	8.5704e+00	7.3723e+00	6.9216e+00	6.8583e+00
1.00e+06	2.7548e+01	1.7001e+01	1.2011e+01	9.7221e+00	8.5240e+00	8.0733e+00	8.0101e+00
1.00e+07	2.8700e+01	1.8153e+01	1.3163e+01	1.0874e+01	9.6757e+00	9.2250e+00	9.1618e+00

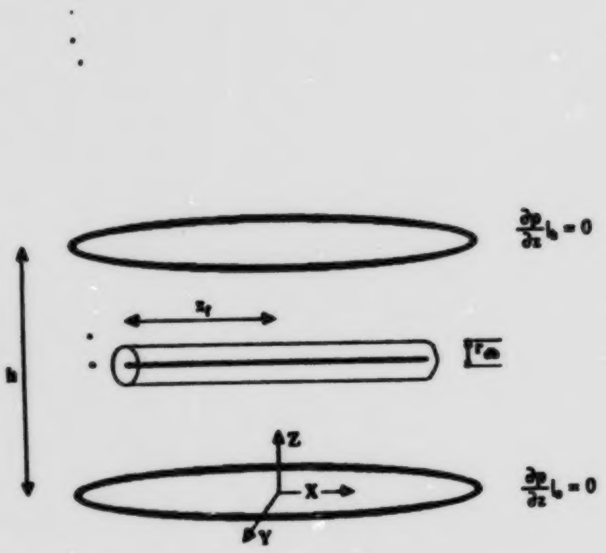
h
z_f
r_w
$\frac{\partial p}{\partial z}|_h = 0$
$\frac{\partial p}{\partial z}|_0 = 0$
Z
X
Y

Fig. 1—Physical representation of single drainhole system.

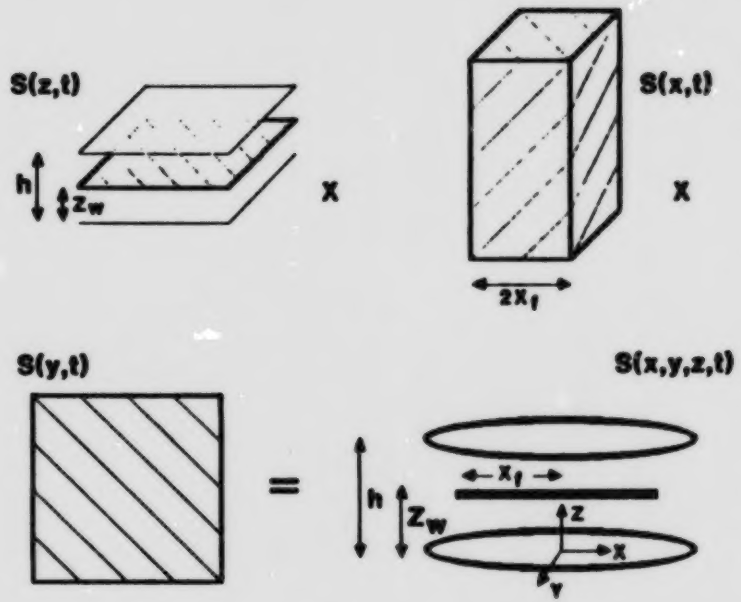
S(z,t)
h
Z_w
X
S(x,t)
X
$2X_f$
S(y,t)
=
S(x,y,z,t)
h
Z_w
X_f
Z
X
Y

Fig. 2—Newman product representation of single drainhole system.

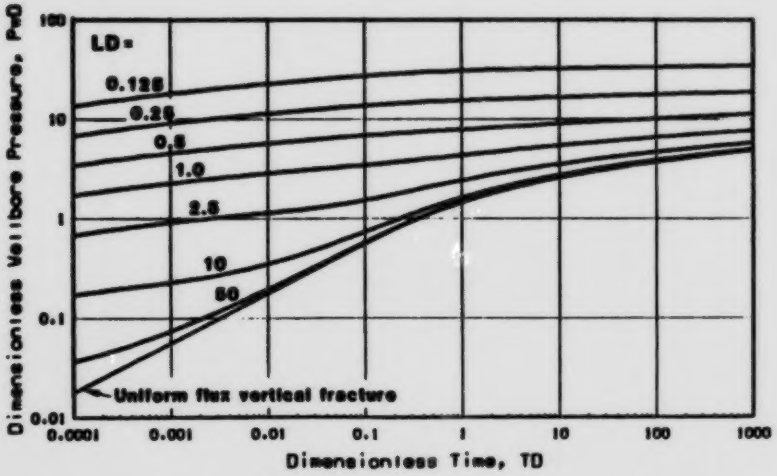

Fig. 3—p_{wD} vs. t_D for a uniform flux dr[illegible] in an infinite slab reservoir for $z_D = 0$ and $r_{wD} = 0.0005$.

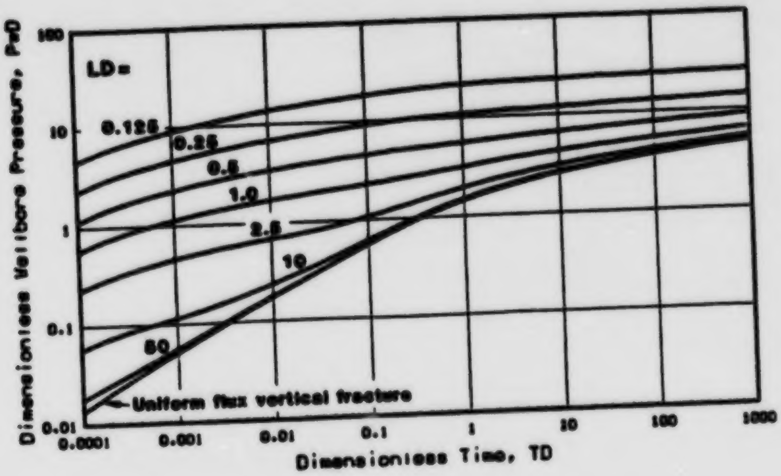

Fig. 4—p_{wD} vs. t_D for a uniform flux drainhole in an infinite slab reservoir for $z_D = 0$ and $r_{wD} = 0.005$.

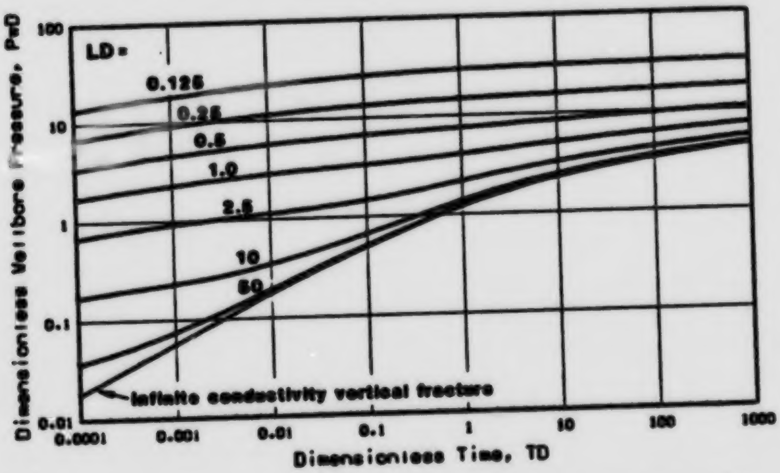

Fig. 5—p_{wD} vs. t_D for a uniform flux drainhole in an infinite slab reservoir for $z_D = 0.732$ and $r_{wD} = 0.0005$.

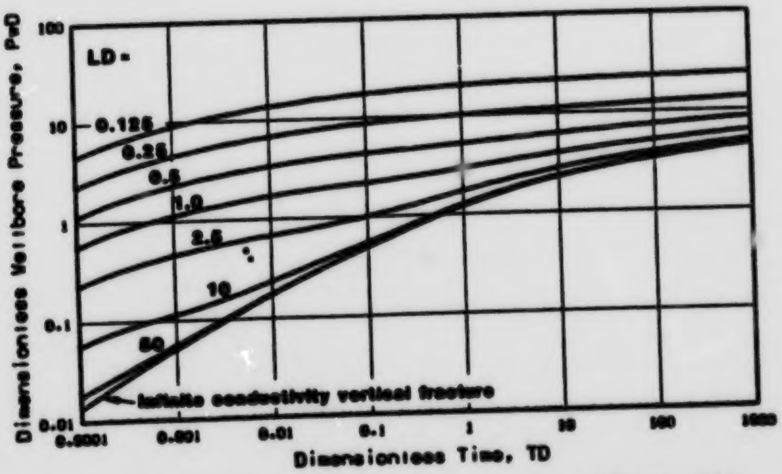

Fig. 6—p_{wD} vs. t_D for a uniform flux drainhole in an infinite slab reservoir for $z_D = 0.732$ and $r_{wD} = 0.005$.

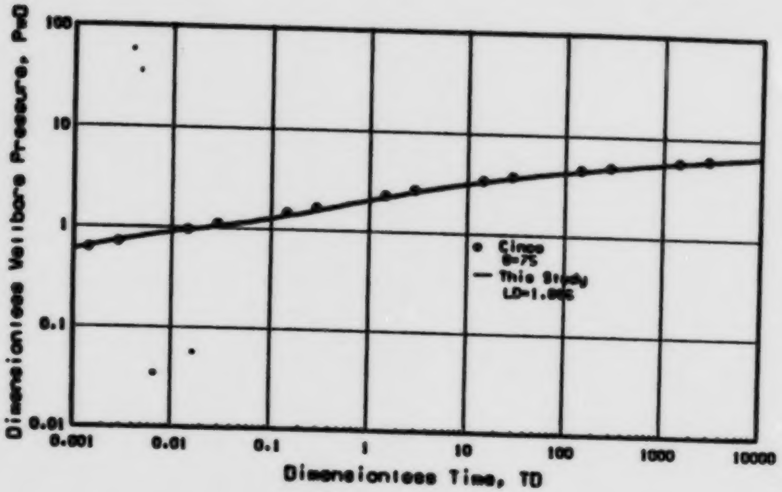

Fig. 7—Comparison of drainhole solution and Cinco solution for a 75° slanted wellbore.

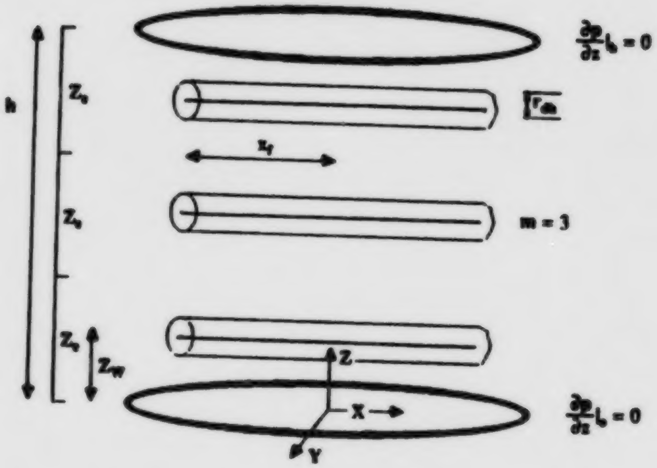
h
Z_e
Z_e
Z_e
Z_w
x_f
r_w
m = 3
Z
X
Y
$\frac{\partial p}{\partial z}\big|_h = 0$
$\frac{\partial p}{\partial z}\big|_0 = 0$

Fig. 8—Physical representation of multiple drainhole system.

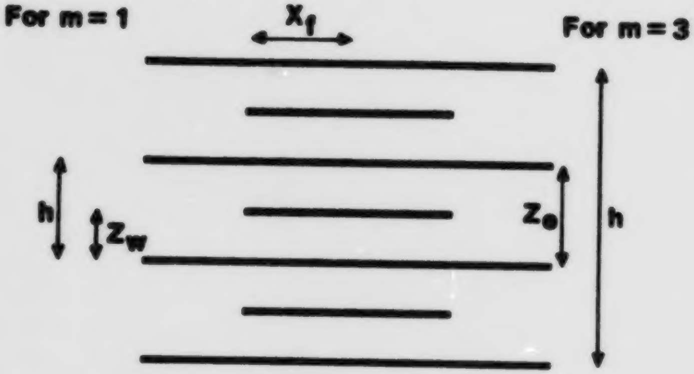
For m = 1
For m = 3
X_f
h
Z_w
Z_e
h

Fig. 9—Newman product representation of multiple drainhole system.

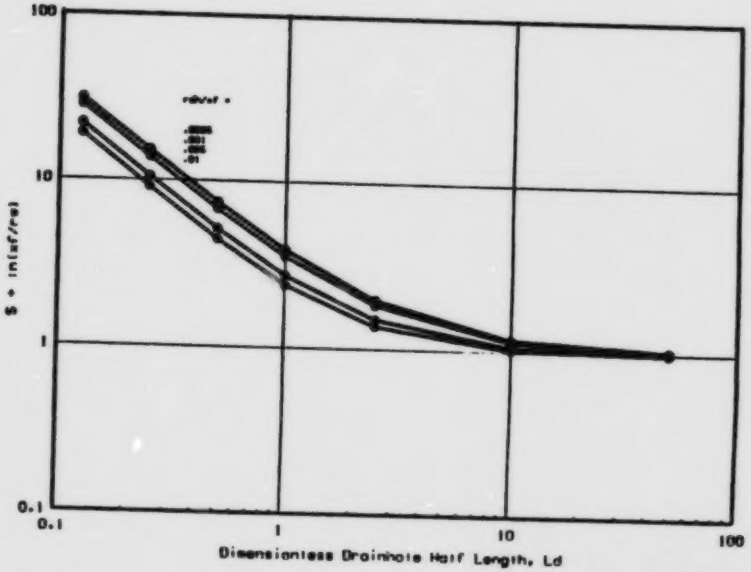

Fig. 10—Uniform flux drainhole pseudo skin factor vs. dimensionless drainhole half length for v [illegible] a-

SPE
Society of Petroleum Engineers

SPE 15430

78

Some Practical Formulas To Predict Horizontal Well Behavior

by B.J. Karcher,* *Elf Aquitaine*, and F.M. Giger** and J. Combe, *Inst. Français du Pétrole*

*SPE Member
**SPE Member now with Horwell SA

Copyright 1986, Society of Petroleum Engineers

This paper was prepared for presentation at the 61st Annual Technical Conference and Exhibition of the Society of Petroleum Engineers held in New Orleans, LA October 5–8, 1986.

This paper was selected for presentation by an SPE Program Committee following review of information contained in an abstract submitted by the author(s). Contents of the paper, as presented, have not been reviewed by the Society of Petroleum Engineers and are subject to correction by the author(s). The material, as presented, does not necessarily reflect any position of the Society of Petroleum Engineers, its officers, or members. Papers presented at SPE meetings are subject to publication review by Editorial Committees of the Society of Petroleum Engineers. Permission to copy is restricted to an abstract of not more than 300 words. Illustrations may not be copied. The abstract should contain conspicuous acknowledgment of where and by whom the paper is presented. Write Publications Manager, SPE, P.O. Box 833836, Richardson, TX 75083-3836. Telex, 730989 SPEDAL.

ABSTRACT

Horizontal and drainhole drilling have been used successfully to increase productivity of wells in the past years. Many formulae can be used to compute the productivity of horizontal or slanted wells compared to vertical ones. One objective of this work is to recall the proper way to use these formulae and to recall the assumptions made that may limit their use. The increase of productivity due to longer perforated interval increases as the logarithm of length and can reach values of two or three times the vertical well.

Also presented is a sample calculation of the influence of natural or artificial fractures on well productivity : a horizontal well may take advantage from an existing fracture network, much better than a vertical well would have. This is because the most permeable fractures are the open ones which have their planes parallel to the largest stress, and the largest stress is generally vertical because of rock weight. The productivity of a drainhole in a fractured medium can raise to 10 times the productivity of the drainhole alone.

Another improvement expected from horizontal wells is a larger flexibility regarding coning problems : it is possible to produce with an interface while keeping a good productivity and a high critical rate. The analytical means for critical rate computation are reviewed with their assumptions. Model computations give the examples of supercritical production in the bottom water drive case. The advantage of horizontal well is important at water breakthrough but does not increase much after and even decreases for favorable mobility ratios. Short drainholes may perform as well as horizontal wells if their distance allows a large interference of cones.

The third way of using horizontal wells is to increase areal sweep efficiency in regular pattern floods. The pattern showing the poorest efficiency is the direct line drive. Using horizontal wells drilled along the lines of producers can bring the areal sweep efficiency close to perfection. In that particular use, horizontal wells act like artificial fractures, with the advantage that their orientation can be controlled.

References and illustrations at end of paper.

INTRODUCTION

Drilling horizontal wells (1-4) and drainholes (5-6) to increase productivity has been proved successful in several field tests. The comparison of the productivity of horizontal wells with vertical wells, slanted wells or fractured wells, has first been studied using potentiometric models (7-9) and is now possible using analytical formulae in the pseudo steady state approximation (10-15) and more recently in the transient pressure response (16-17). Uncautious use of some of these methods may lead to errors if the limiting assumptions are forgotten : some of them need to be recalled and a comparison with the experiments and numerical models is used to check the validity of such formulae.

The homogeneous case is first considered, then the anisotropic case and finally a case with sparse fractures.

The coning problem occurs for fields produced with wells located above the water oil contact or below the gas oil contact (19-20). In such cases, when the well is produced at a high rate, the phase with higher mobility breaks through the oil and the well production becomes diphasic.

In cases with high mobility contrast between oil and gas or water, the oil production after the breakthrough may become negligible (22). In some cases, there exists a critical rate below which the production remains water free (19, 20, 23-27) : these are the cases where a steady state boundary condition can be found. Actual field conditions are not truly steady state, but the time lapse until breakthrough due to excessive rate is much smaller than the one due to the boundary condition. Critical rates predictions for vertical wells are compared using a numerical model to solve the cone equilibrium problem. Supercritical production in a bottom water drive reservoir needs also to be investigated. Configurations studied numerically include the infinite horizontal well, limited horizontal well and groups of horizontal or slanted drainholes.

The areal sweep efficiency increase due to horizontal drilling is not really new. The topic has been quite extensively studied in the case of natural or induced fractures (28), and the results can be directly applied to horizontal wells if the layer is not too thick so that the flow could be considered as plane. The efficiency in the case of the direct line drive is calculated using a streamtube numerical model and checked against known analytical solutions (29) for a unit mobility ratio.

PRODUCTIVITY

The reference case will be the productivity of a single vertical well in a circular drainage area. The productivity index calculated in the pseudo steady state approximation is given by :

$$PI_v = \frac{2\ \pi\ k_h\ H}{\mu\ B\ \ \ln \frac{Re}{R_w}} \quad \ldots\ldots\ldots\ldots\ldots\ldots\ldots (1)$$

The productivity of a fractured vertical well can be estimated assuming that :

- the fracture height equals the reservoir height,
- the fracture is plane, centered on the well,
- the drainage radius is large with regard to fracture length,
- the fracture is supposed to have an infinite conductivity.

The equipotential surfaces are then ellipses and far enough, can be approximated by circles (10), hence the formula valid if fracture length is small compared to drainage radius.

$$PI_{vf} = \frac{2\ \pi\ k_h\ H}{\mu\ B\ \ln \left(\frac{2\ Re}{L} + \sqrt{\left(\frac{2\ Re}{L} \right)^2 - 1} \right)} \quad \ldots .\ (2)$$

or

$$PI_{vf} = \frac{2\ \pi\ k_h\ H}{\mu\ B\ \ \ \text{arc cosh} \left(\frac{2\ Re}{L} \right)} \quad \ldots\ldots\ldots\ldots (3)$$

If the ratio L/2Re is very small, the 1 under the square root of equation 2 may be neglected and the formula can be simplified into :

$$PI_{vf} = \frac{2\ \pi\ k_h\ H}{\mu\ B\ \ \ln \left(\frac{4\ Re}{L} \right)} \quad \ldots\ldots\ldots\ldots\ldots\ldots (4)$$

The productivity index of a single horizontal well in a circular drainage area can be calculated in the same way as the fracture if the layer is thin enough so that the flow can be considered as plane even around the drain bore. This gives the formula presented by Merkulov (12) for a drainhole of length L :

$$PI_f = \frac{2\ \pi\ k_h\ H}{\mu\ B\ \ \ln \left(\frac{2\ Re}{L} + \sqrt{\left(\frac{2\ Re}{L} \right)^2 + 1} \right)} \quad \ldots .. (5)$$

Note the difference of sign between equations (2) and (5) which is due to the approximation of the equipotential circle by an ellipse by equating the large diameter or the small diameter to the circle diameter.This should introduce a small difference only as far as the approximation is justified, i.e. as long as the drain length is small compared to the external radius.

A more precise way to compute horizontal well productivity is to assume a plane flow everywhere as in the step before, and to assume a radial flow in the vertical plane perpendicular to the drain for distances to the drain lower than the half thickness of the layer, this leads to an expression more suitable when the layer is not thin (10) as shown on figure 1a.

$$PI_f = \frac{2 \pi k_H\ H}{\mu\ B} \cdot \frac{1}{\ln \left(\frac{2\ Re}{L} + \sqrt{\left(\frac{2\ Re}{L} \right)^2 - 1} \right) + \frac{H}{L} \ln \frac{H}{2 \pi R_w}} \quad \ldots .. (6)$$

This method may be extended to more complicated drainhole geometry, including slanted wells (12) drilled as shown on figure 1b :

$$P_h = \frac{2\ \pi\ k_h\ H\ \ n}{\mu\ B} \cdot \frac{1}{\frac{\pi b}{L} + \frac{H}{L} \ln \frac{H}{2 \pi R_w} - \frac{H}{L} \left(\ln \frac{a+c}{2\ c} + 1 \right) + \ln \frac{2 Re^n \left[1 - \left(d/Re \right)^{2n} \right]}{n\ (a+b)\ d^{n-1}}} \quad \ldots\ldots\ldots\ldots (7)$$

where :

n is the number of drainholes

$a = L/2 + H$

$b = \sqrt{2H\ (L + 2H)}$

$c = L/2$

d is the horizontal distance of drainhole center to the center of the drainage area.

e is the vertical distance of drainhole axis to the middle of the layer (figure 1c)

and

$$l = 0.426 \frac{L}{2H} - 9.7 \left(\frac{e}{H}\right)^{\prime} + 1.28 \frac{e}{H} + 4.45$$

for a horizontal drainhole, and

$$l = 0.4 \frac{L}{2H} + 4$$

for a slanted well crossing the entire layer.

By taking d, the distance between drainhole center and axis, equal to L/2, this equation gives results similar to equation 7 for a single centered horizontal well with length 2L.

The transient pressure analysis has also given solutions to this problem for cases where the drainage radius is large enough so that the pseudo radial flow occurs and then give the productivity increase as a pseudo skin factor (16-17) for these late times.

Other solutions allow to compute productivity in cases where the drainage area is not large compared to the drain length. The easiest solutions are for the case of the infinice drainhole in the pseudo steady state approximation :

. for the unit length of a drainhole in a parallelipedic area with the outer vertical boundary parallel to the drain at distance D, kept at a constant potential (14), as in figure 1d :

$$PI_h = \frac{2 \pi k_h}{\mu B \left(\frac{\pi}{4} \frac{D}{H} + \ln \frac{H}{2 \pi R_w} \right)} \qquad \ldots\ldots\ldots\ldots\ldots(8)$$

. for the unit length of a drainhole with a closed boundary on one side and an infinite reservoir on the other side (figure 2), the solution obtained for a vertical well applies, just by exchanging the width and height of the system (15)

$$PI_h = \frac{4 \pi k_h}{\mu B} \; \frac{1}{\frac{4\pi}{H} D + 2 \ln \frac{H}{2\pi Rw} + \ln \frac{2}{1 - \cos \frac{\pi}{H} (H - 2e - Rw)}} \qquad ..(9)$$

. for all closed domains especially parallelepipedic ones, the shape factor method can be applied (18) by exchanging width and height as in the former example.

In these types of geometry, fractured vertical wells productivity can be calculated using the same formula by simply removing the term characterizing the flow restriction around the well bore.

Application of all the methods and formulae described leads to productivity increases of the order of two to three for usual drain length.

For instance, with an external radius of 200 m, a reservoir height of 50 m, a well radius of 0.1 m, a drain of length 2 L = 20 m (n = 2), the equation 7 gives a ratio of 0.5564 over vertical well, while formula 6 gives 0.5195 and formula 5 gives a result of 2.06. This reduction of productivity is due to the fact that the perforated length of drainholes is 20 m, smaller than the vertical hole (50 m). In this example, the layer is very thick and formula 5 is much too optimistic. If we choose now H = 10 m, the same ratios are :

equation 7 : 1.46

equation 6 : 1.50

equation 5 : 2.06

This proves that the horizontal well will not yield a better productivy than a vertical well unless the perforated length is higher. Table 1 and figure 3 give more examples, showing the order of magnitude of the increase in productivity that can be hoped. It can be seen in figure that equations 6 and 7 yield very similar results and that horizontal and slanted well with same perforated length have the same productivity.

PRODUCTIVITY IN ANISOTROPIC MEDIUM

Very often the geological history of the reservoir rock makes the vertical permeability in the vertical direction smaller than horizontal permeability because of shale beds. In other cases, the presence of numerous fractures leads to a greater vertical permeability.

The ratio of productivity of horizontal or slanted wells to that of a vertical length can be calculated using the equations described before according to their hypothesis. For instance equations 1 to 5 assume the flow is plane and hence will not take into account the vertical permeability. The usual transformation dictated by dimensional analysis (10) consists in multiplying all distances by the square root of the ratio of the average permeability to the permeability in that direction. The average permeability is calculated using geometric average.

Equation 7 can be extended to the anisotropic case for a single drainhole or a slanted well of length L by letting d = o, n = 1 in equation 7 and applying the scaling method :

$$PI_h = \frac{2 \pi k_h}{\mu B} \; \frac{1}{\frac{\pi b}{L'} + \frac{H'}{L'} \ln \frac{H'}{2\pi R_w} - \frac{H'}{L'} \left(\ln \frac{a'+c'}{2 c'} + l' \right) + \ln \frac{2 Re}{a' + b'}} \qquad \ldots\ldots\ldots\ldots\ldots(10)$$

Where a', b', c', l' are calculated as in equation 7, using :

$H' = H \sqrt{k_h/k_v}$ instead of H,

$L' = L$ for a horizontal drainhole,

$l' = \sqrt{L^2 + H'^2} - H'$ for a slanted well.

Vertical permeability greater than horizontal can only favor the horizontal wells, but this dependence of anisotropy is unfavorable to horizontal well if vertical permeability is lower than horizontal permeability, and this effect may be very important as shown on table 2.

The slanted wells suffer less at high permeabilities, but need large deviation angles to achieve the same length as the drainhole.

The warning should nevertheless be kept in mind when questioning about the opportunity to drill a horizontal well rather than deviated ones.

PRODUCTIVITY WITH FRACTURES

The productivity improvement that may be expected from vertical fractures has been studied using a numerical finite difference model solving the pseudo steady state flow equations for wells and fractures located in a closed area.

The disposition chosen is presented in figure 4. The infinite horizontal well is located in the middle of the square drainage area. Fractures are supposed to be vertical planes crossing the whole reservoir height, with a length smaller than the drainage area width L. The drainage area width is 8 times the height H.

The productivity of a fracture with the same length as the horizontal well and full vertical penetration will always be larger than the productivity of the well because of the linear flow instead of radial flow around well bore. A horizontal well that crosses vertical fractures perpendicular to its axis benefits dramatically from this effect. Results for an infinite drainhole illustrate this in this case. Figure 5 shows the improvement of productivity that can be expected from the fractures. The increase shown is the ratio of productivity of horizontal well crossing fractures to the productivity of the same horizontal well in homogeneous medium. It is plotted against dimensionless fracture width. The different curves are for the number of fractures crossed. A single vertical well in the same drainage area would cross at the most one fracture. With one fracture crossed, productivity increase does not exceed 1.5 for the maximum fracture length studied of 0.5D. In this case, the drainhole still participates in flow. When the well crosses 8 fractures (if the drainage area width is 400 m, that makes a fracture every 50 m) the increase reaches 12. At that point, most of the production comes from the fractures. This study points out the real interest in terms of productivity, of horizontal wells, and how they should be used : when the field geology is well known the well can be oriented perpendicular to the main fractures and then achieve really high productivity index increases.

DRAINHOLES AND CONING

Coning of water or gas is the phenomenom that occurs when a well is produced in the oil zone with an interface initially present on the vertical of the well.

The more mobile phase, gas or water, tends to channel towards the perforations.
What will happen depends on the boundary conditions which can be :

- constant interface elevation at a finite distance,
- free surface boundary condition (velocity directed toward the source at a given distance)
- constant potential in the water or gas zone.

Actual field conditions will never be so precisely defined but will be approximately represented at a given point in time by one of these : the first type of boundary condition can characterize an isolated well with a small rate compared to field volume with a strong lateral aquifer that maintains pressure. The second type is for a well with a large rate compared to the oil in place such that vertical velocity of water oil contact is noticeable. The third type will suit to a well located above the water oil contact surrounded by other production wells.

Previous experimental studies (19-22) seem to show that the critical rate might depend only weakly on the boundary conditions of the first and third type. However it does depend on some parameters describing the system that can be written in dimensionless form (22) :

. the dimensionless drainage radius

$$R_{eD} = \frac{Re}{H}\sqrt{\frac{k_v}{k_h}}$$

. the dimensionless well penetration

$$H_{pD} = \frac{Hp}{H}$$

. the dimensionless well radius

$$R_{wD} = \frac{R_w}{H}\sqrt{\frac{k_v}{k_h}}$$

. the mobility ratio

$$M = \frac{k_{rw}}{\mu w} / \frac{k_{ro}}{\mu o}$$

. the Reynolds number (ratio of viscous to gravity forces) :

$$N = \frac{\mu \quad Q}{g \; H \; k_h \; R_e}$$

Analytical solutions to the critical rate problem for horizontal wells were found for several types of boundary conditions, in the case of an infinite horizontal well :

. first type of boundary condition (27) : the solution neglects the flow restriction due to immobile water in the cone, which should give an optimistic evaluation of critical rate.

. second type of boundary condition (23-25) with a horizontal well drilled at the top of the reservoir, the critical rate is nearly independant of drainage radius and the oil height H is difficult to choose (26) ; this is due to the assumption of free surface at a large distance, hence these solutions must not be used for small values of dimensionless drainage radius :

after Efros (24) :

$$q_c = \frac{k_h \;\Delta\rho g \;H^2}{\mu B \left(D + \sqrt{D^2 + \frac{H^2}{3}} \right)} \qquad \text{..................(10)}$$

after Giger (25) :

$$q_c = \frac{k_h}{\mu B} \Delta\rho g \,\frac{H^2}{D} \left(1 - \frac{1}{6} \left(\frac{H}{D} \right)^4 \right) \qquad \text{...........(11)}$$

These two formulae yield very similar results.

. third type of boundary condition : there cannot be, stricto sensu, a true critical rate, but each time, assuming the height of the oil zone, and a distribution of potentials, it is possible to estimate the critical value for the infinite horizontal well (26) during a bottom water drive :

$$q_c = \frac{3}{2} \;\frac{k_h \Delta\rho g_D}{\mu B} \left[\sqrt{1 + \frac{16}{3} \;\frac{H^4}{D^2}} \; - 1 \right] \text{......(12)}$$

Results of these analytical computations were compared with a numerical model, which solves the problem of cone equilibrium with constant height of cone at finite distance (first type of boundary condition). The model solves the potential of incompressible flow in the oil zone by iterating on cone position. Water is not mobile in the cone and oil potential is kept constant at the outer vertical boundary in the radial case and on one or several of the four vertical boundaries in the general three dimensional case. Results of this comparison between a vertical well and an infinite drain are presented in figure 6 for critical rates and figure 7 for oil recovery. Results are plotted as functions of dimensionless drainage radius as defined above. The critical rate is presented in dimensionless form. The actual value is to be calculated as indicated using density contrast in Kg/L, k_h in mD, viscosity in mPa.s and length in meters to give the rate in m^3/D.

Note in the figures that at low values of the dimensionless radius R_{eD} the results are strange : this is because as the height becomes greater than the drainage radius the boundary condition becomes more and more non physical and solutions silly (the cone must stay fixed at the boundary and with a horizontal tangent at that point due to the constant potential).

The parameters were varied to check the validity of the dimensionless parameters. This proves the numerical model and the dimensional analysis to be consistent.

Results for the vertical well and the infinite drain are related to the same drained volume. They show that the critical rate of the horizontal well is two to three times higher than the vertical well. In terms of sweep efficiency, the advantage of the horizontal well is yet more impressive : more than three times. This is easy to understand by simple geometric considerations : the vertical well raises a cone and the horizontal well raises a ridge with nearly the same lateral section as the cone but extended under the whole length of drain. The volume of a cone of height H (H - Hp more precisely) and base R is :

$$V_v = \frac{1}{3} \quad R^2 \;(H - Hp)$$

which represents only a small portion of the cylinder of radius R and height H. The volume of the ridge with the same cone width at its base and length L is :

$$V_H = V_v + L\,R\,(H - Hp)$$

assuming that the ridge is composed of two half cones surrounding a prism.

Whith the values H = 100 m, Hp = 10 m, R = 150 m, L = 400 m, this gives a ratio of these volumes of 3.5 which reflects very well the results obtained.

Results also show that, in the range studied, dimensionless penetrations of the vertical well from 1 to 20 %, dimensionless well radius from 0.001 to 0.01, have no noticeable influence.

To complete this study of critical rate, the same model was used to investigate cases with more complicated geometry.

. Effect of limited drain length : the geometry is the same as for the infinite drainhole case, a square drainage area with constant potential on boundaries parallel to the drain as on figure 1d. The model grid is completed to be fully three dimensional (it was only two dimensional for the infinite drain case), and the drain is perforated only on a portion of its length. Simulations were performed using a dimensionless drainage radius of 40 with D = 400 m and H = 10 m. Oil viscosity is 1 mPa.s and the density contrast is 0.2 Kg/L. With these values, the results of figure 8 show that the increase in critical rate is substantial from the small drainhole length but does not vary much for large drain length.

On the contrary the recovery efficiency is sensitive to drain length at all times. This can easily be understood from the geometrical considerations exposed on the cones and ridges.

. Comparison between horizontal and vertical drainholes : A geometry including a square cross (4 horizontal drainholes) with a length of 10 m was compared to a single well and 4 vertical drainholes with the same distance of 10 m to the center (that would result of a kickoff point for drainholes located above the reservoir top). The drainage square area length was varied from 100 to 500 m, the other parameters remaining as in the former case. The results of the critical rate and recovery efficiency showed a suprisingly good agreement : looking at these results, there is nearly no difference. This can be explained by the small size of the cross that makes the cone very flat in the square between the 4 wells. The critical rate of this well with its 4 drainholes of 10 meters each is nearly equivalent to a single 40 meters horizontal well in the same drainage area but its recovery is smaller (5.3 % against 9 %).

AFTER BREAKTHROUGH BEHAVIOR

Production after breakthrough is important in coning cases. Even if the rate can be kept below the critical rate during a long time, diphasic production will decrease towards a zero value along with the remaining oil height. It is worth knowing how much of the advantage of horizontal wells is kept when cumulative production reaches its economic limit. The case of production at supercritical rates is also worth considering. The case of bottom water drive was choosen to represent the situation of a well located in a drainage area closed by the surrounding wells of the field. This part of the study was performed using a three phase three dimensional numerical simulator. Parameters investigated include the drainage radius, rate and mobility ratio. In the absence of capillary pressure, the dimensional analysis of the problem allows to present the results using the previously defined dimensionless parameters (22) R_{eD}, H_{pD}, R_{wD}, M, N, and the dimensionless cumulative oil production :

$$N_{pD} = Q\,T / (R_e^2\ H\,\varphi\,(1 - Sor - Swi))$$

The vertical well case simulated the quarter of the square drainage area, using symmetric grid increments in the X and Y directions . The infinite horizontal well is simulated in two dimensions only, representing the unit length of an infinite well, with the same grid blocks in X direction as for the vertical well and the length of the single grid increment in the Y direction adjusted to keep the drainage area square.

. influence of mobility ratio : results show different behavior for favorable and unfavorable mobility ratios (table 3) : In all cases at water breakthough the vertical well is behind the horizontal well in terms of recovery, by factors of 1.5 (M = 0.5) to 3 or even 8 for very high mobility ratio.

This advantage is not kept in the favorable mobility case : final recoveries are quite the same, all of these being very good (the displacement is very stable because of mobility and gravity). When mobility ratio is unfavorable, the advantage is not kept as a ratio but the oil production during diphasic production period is almost the same for the two wells. Hence a ten points advantage at breakthrough will remain at the end. Notice that after water breakthrough, even with a mobility ratio of 400, oil production continues (from 1 % to some 12 %) although it takes a long time because of the high water oil ratio. This is a consequence of the strong bottom water influx that allows production by maintaining pressure.

. Influence of rate : rates were adjusted for each simulation at a constant ratio compared to the critical rate predicted by the steady state model described here before. Some runs were performed with different rates to check its influence. In the favorable mobility case, two runs at 2 and 10 times the critical rate did not exhibit any major sensitivity. In the unfavorable mobility case, the runs for the horizontal well show a degredation of recovery (from 11.6 % down to 6.3 %) as rate is increased from 22 to 42 times the critical rate. This proves there was still at this rate a favorable influence of gravity to improve sweep efficiency.

. Influence of drainage radius : in this configuration of bottom water drive, the water oil contacts goes up on boundaries as oil is produced. It is expected that the smaller the dimensionless radius, the higher the sweep efficiency, because of interference between wells causing a more vertical displacement. In the favorable mobility runs, increasing the radius causes the breakthrough recovery to decrease but final recoveries are once again less sensitive. In the unfavorable mobility runs, the behavior is the same although emphasized.

AREAL SWEEP EFFICIENCY

Another potential improvement brought by use of horizontal wells may be to increase horizontal sweep efficiency. Many reservoirs are produced by waterflooding using regular patterns as five spots or line drive. The oil recovery is nearly proportional to the area swept if the producting layer is thin and the pattern away from water-oil or gas-oil contacts. The areal sweep efficiency of such patterns is not maximum in most cases, especially those with rectangular drainage areas. Hence the idea to improve areal sweep efficiency by using horizontal injector or producer wells. The well orientation can then be chosen according to flow pattern so as to maximize the area swept. The influence of fractures is quite similar and has already been studied for the five spot pattern (28).

The main advantage of horizontal wells in such configuration is that the well orientation can chosen, which is very difficult using hydraulic fracturation.

We give an example for the direct line drive pattern that seemed to us to be favorable to horizontal wells. The recovery depends on the shape of the pattern through the ratio D/a of distance D between the line of injectors and the line of producers to the distance a between two adjacent wells of same type. The pattern including horizontal wells drilled in the axis of producers and injectors lines has a sweep efficiency depending also on the ratio L/a of length of drain L to the distance a between wells. Two cases were studied : the first one with a unit mobility ratio and the second with water more mobile than oil.

The case with unit mobility ratio allows us to use a streamtube model as the streamlines of flow do not change during flooding (figure 9). Under this assumption and using equal rate flow tubes, the recovery at water breakthrough may be calculated from the pore volume of the shortest tube without having to compute the displacement. The results presented on figure shows a very good agreement with the analytical solutions obtained for vertical wells. It also shows that a small horizontal well length does not improve the sweep efficiency. Of course for a total penetration (L/a = 1) the sweep efficiency reaches 100 %. For penetrations between 0 and 1, the maximum recovery increase is obtained for penetrations around 50 %.

Another case with unfavorable mobility ratio was computed using a standard finite difference two dimensional two phase water oil numerical model. Results show a reasonable agreement with the streamtube model for the unit mobility ratio (figure 10). Two other model runs with mobility ratios of 10 and 100 show that the increase in sweep efficiency can be noticeable even for small drain penetrations of 10 or 20 %.

CONCLUSIONS

- Productivity index formulae estimate an increase in productivity of 2 to 5 over the equivalent vertical well in an homogenous medium.
- Slanted holes may have a higher productivity than a horizontal one for an equal perforated length if the vertical permeability is very low.
- Crossing a natural vertical fractures network may increase the productivity gain over the vertical well to highs of 10 or more. This appears to be the best target for productivity.
- Critical rates in coning problems may be multiplied by a factor of two and recoveries by more than three at near critical rates.
- Supercritical production brings the same gains at breakthrough but these do not augment after, except in cases of unfavorable mobility ratios.
- Areal sweep efficiency of the direct line drive may approach unity through the use of horizontal wells and a high increase in oil recovery over the vertical wells is reached with drains only half the continuous line.

NOMENCLATURE

B = volume factor

D = distance between two lines of horizontal wells

d = distance between drain center and drainage area center

e = drainhole excentricity (distance between middle of layer and drain axis)

g = acceleration of gravity

H = thickness of the reservoir

k = permeability of the porous media

L = length of the horizontal well

M = mobility ratio

N = Reynolds number

PI = productivity index

q = rate of a horizontal well per unit length

Q = production rate

R = radius

S_{or} = residual oil saturation

S_{wi} = connate water saturation

T = time

Greek symbols

Δ = difference operator

φ = porosity

μ = viscosity

ρ = specific gravity

Subscripts and Superscripts

c = critical

D = dimensionless

e = external (drainage)

f = fracture

h = horizontal

o = oil

p = perforated

v = vertical

w = well

AKNOWLEDGEMENTS

The authors thank the Institut Français du Pétrole and the Société Nationale Elf aquitaine for permission to publish this paper.

REFERENCES

1. Dore, M.: "Horizontal Drilling Methods Proven in Three Test Wells," World Oil (May 1983).
2. Yager, D., "Esso Drills World's Longest Horizontal Well" The Roughneck, January 1985.
3. Jourdan, A.P., Reiss, L.H., Joly, E., "Horizontal Wells : the Worlwide State-of-the-art, as of 1986". Presented at the SPE International Meeting on Petroleum Engineering, Beijing, China, 17-20 March, 1986. SPE 14067.
4. Reiss, L.H., Jourdan, A.P., Giger, F.M. and Armessen, P.A. : "Off onshore European horizontal wells," paper OTC 4791. Presented at the 1984 Offshore Technology Conference, Houston.
5. Striegler, J.: "ARCO Finishes Fourth Horizontal Drainhole," Oil and Gas Journal (May 24, 1982).
6. Hyland, C.R.: "Drain Hole Drilling - An Idea Whose Time is Now," paper SPE 12792 presented at the SPE 1984 California Regional Meeting, Long Beach, March 25-26, 1984.
7. Perrine, R.L.: "Well Productivity Increase from Drain Holes as Measured by Model Studies," Trans., AIME (1955) 204, 30-34.
8. Roemershauser, A.E. and Hawkins, M.F.: "The effect of Slant Hole, Drainhole, and Lateral Hole Drilling on Well Productivity," J. Pet. Tech. (Feb. 1955) 11-14.
9. Landrum, B.L. and Crawford, P.B.: "Effect of Drainhole Drilling on Production Capacity," Trans., AIME (1955) 204, 271-273.
10. Muskat, M.: The Flow of Homogeneous Fluids Through Porous Media, J.W. Edwards, Inc., Ann Arbor, Mich. (1946) 273.
11. Borisov, Ju. P.: "Exploitation des gisements de pétrole par des puits horizontaux et à déviations multiples," Nedra, Moscow (1964), Translation from Russian to French : Institut français du Pétrole, Rueil 28363.
12. Merkulov, V.P.: "Le débit des puits déviés et horizontaux," Neft. Khoz (1958) 6, 51-56 (in Russian).
13. Giger, F.: "Réduction du nombre de puits par l'utilisation de forages horizontaux", Revue de l'Institut Français du Pétrole, vol 38, N° 3 (May-June 1983) (in French).
14. Giger, F.: "Horizontal wells productions techniques in heterogeneous reservoirs", paper SPE 13710 presented at the 1985 SPE Middle East Meeting, Bahrain, March 11-14, 1985.
15. Pyckhacev, G.B., "Underground Hydraulics", Moscow, 1961, 260-264 (in Russian).
16. Daviau, F., Bourdarot, G., Mouronval, G., Curutchet, P.: "Pressure Analysis for Horizontal Wells". SPE 14251 presented at SPE Annual Technical Conference and Exhibition, Las Vegas, Nevada, September 22-25, 1985. .
17. Clonts, M.D, Ramey, H.J. Jr: "Pressure transient analysis for wells with horizontal drainholes", paper SPE 15116 presented at the 1986 SPE California Regional Meeting, Oakland, April 2-4, 1986.
18. Earlougher, R.C. Jr: "Advances in well test analysis", SPE Monograph Series, Dallas, 1977, 5.
19. Muskat, M.: "The performance of Bottom water drive Reservoirs", Trans. AIME, 1947, 70, 81-111.
20. Chiericci, G.L., Giucci, G.M., Pizzi, G.: "A systematic study of gas and water coning by potentiometric models", J.P.T., Aug. 1964, 923929.
21. Sobocinsky, D.P., Cornelius, A.J.: "a correlation for predicting water coning time", J.P.T., May 1965, 594.
22. Hutchinson, T.S., Kemp, C.E.: "An extended analysis of bottom water drive reser[illegible] performance", Trans. AIME, 207, 1956, 256-[illegible]
23. Kidder, R.E.: "Flow of immiscible fluids in porous media : exact solution of a freee boundary problem," Journal of Applied Physics, Ang. (1956), 27.
24. Efros, D.A.: "Study of multiphase flows in porous media, Gastoptexizdat, Leningrad, 1963 (in Russian).
25. Giger, F.: "Evaluation théorique de l'effet d'arête d'eau sur la production par puits horizontaux," Revue de l'Institut Français du Pétrole, Vol. 38, N° 3, (May-June 1983) (in French).
26. Giger, F.: "Analytical 2-D models of water cresting before breakthrough for horizontal wells" paper SPE n° 15378, to be presented at 61st SPE annual Meeting, New Orleans, Oct. 5-8, 1986.
27. Chaperon, I.: "Theoretical study of water oil gas coning towards vertical and horizontal wells - subcritical and critical rates" paper SPE n°15377 to be presented at 61st SPE annual Meeting, New Orleans, Oct. 5-8, 1986.
28. Crawford, P.B., Collins, R.E.: "Estimated Effect of Vertical Fractures on Secondary Recovery" Trans. AIME, V. 201, 1954, 19[illegible].
29. Muskat, M., Wyckoff, R.D.: "A Theoretical Analysis of Water-Flooding Networks" trans. AIME, V. 107, 1934, 62-76.

Table 1

Influence of Drain length and number of Drainholes on Productivity Increase over Vertical Well

(Re = 400 m, H = 10 m, Rw = 0.1 m)

Dimensionless Drain length L / Re	Productivity Increase PIh / PIv			
	n = 1	n = 2	n = 3	n = 4
0.05	1.384	1.845	2.027	2.117
0.10	1.825	2.422	2.636	2.731
0.20	2.410	3.277	3.576	3.697
0.30	2.884	4.044	4.448	4.605
0.40	3.332	4.815	5.351	5.555
0.50	3.787	5.635	6.334	6.599

Table 2

Influence of Permeability Anisotropy on Productivity Increase of Horizontal and Slanted Wells

(Re = 200 m, L = 100 m, Rw = 0.1 m)

Anisotropy Ratio Kv / Kh	Horizontal well PIh / PIv		Slanted Well PIs / PIv	
	H = 10 m	H = 50 m	H = 10 m	H = 50 m
100.	3.973	3.864	3.962	3.589
10.	3.784	3.424	3.774	3.181
1.	3.104	1.691	3.104	1.691
0.1	1.024	0.227	1.360	1.040
0.01	0.113	0.022	1.030	1.024
0.001	0.011	0.002	1.024	1.024

Table 3

Comparison of Breakthrough and Ultimate Recoveries of Vertical and Infinite Horizontal Well in Bottom Water Drive with Supercritical Rate

General Parameters	Well Type	Q/Qc	Oil Recovery at Water Breakthrough	Oil Recovery at 80 % Water Cut
M = 0.5 K = 200 mD D = 100 m	V H H	1.6 2.2 9.0	37.5 55.2 52.7	84.1 85.3 84.0
M = 0.5 K = 200 mD D = 200 m	V H	10.2 9.8	14.1 36.6	77.1 78.8
M = 10 K = 1000 mD D = 200 m	V H	10.2 9.8	10.2 31.5	29.7 39.5
M = 10 K = 1000 mD D = 400 m	V H	13.5 10.7	0.7 5.2	11.0 31.0
M = 200 Kh= 1000 mD Kv= 100 mD D = 400 m	V H V H	21.0 21.0 42.0 42.0	0.13 1.07 0.13 0.87	1.5 11.8 1.2 6.3

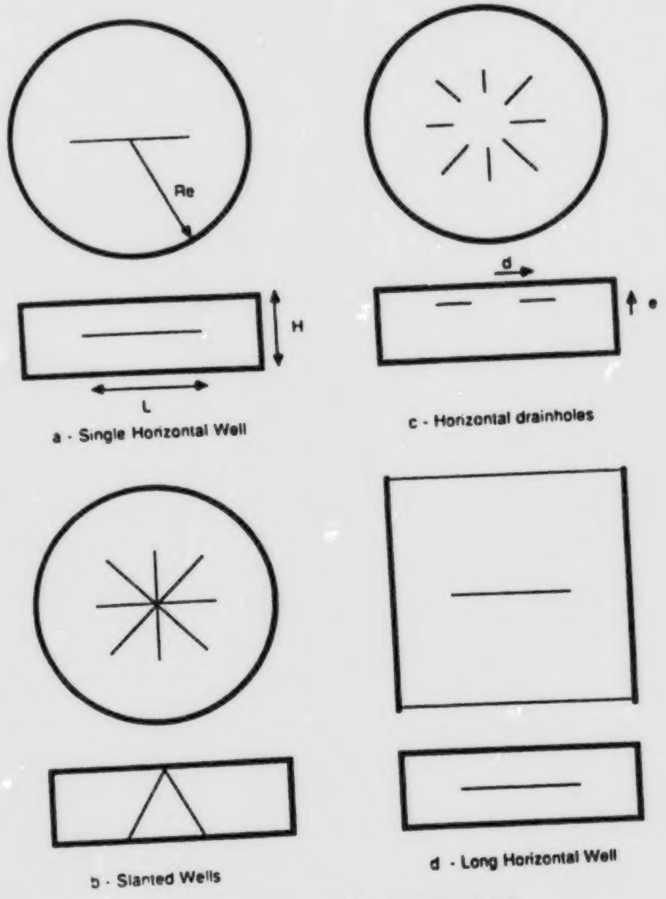

a - Single Horizontal Well

c - Horizontal drainholes

b - Slanted Wells

d - Long Horizontal Well

Fig. 1—Dispositions of single wells or group of wells.

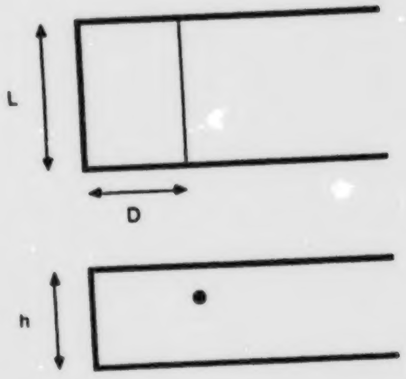

Horizontal well in a semi infinite medium

Fig. 2—Infinite horizontal well located in a semi-infinite drainage area.

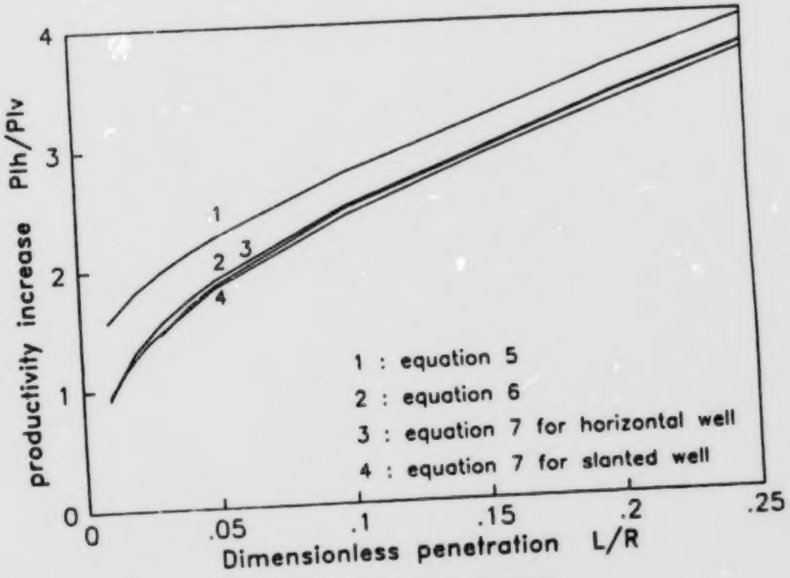

Fig. 3—Comparison of results of Eqs. 5 through 7.

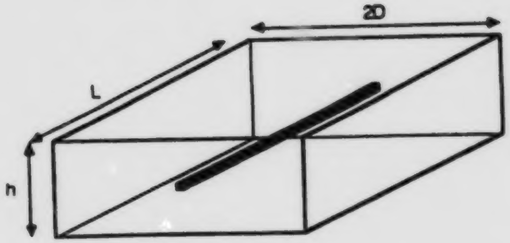

infinite drainhole unfractured

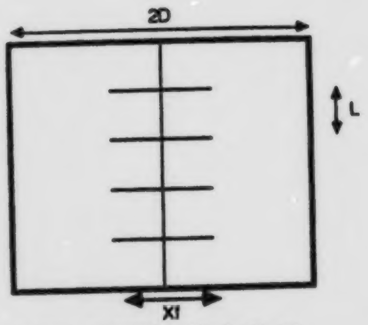

Infinite drainhole with fractures

Fig. 4—Infinite drainhole in a square drainage area, crossing fractures.

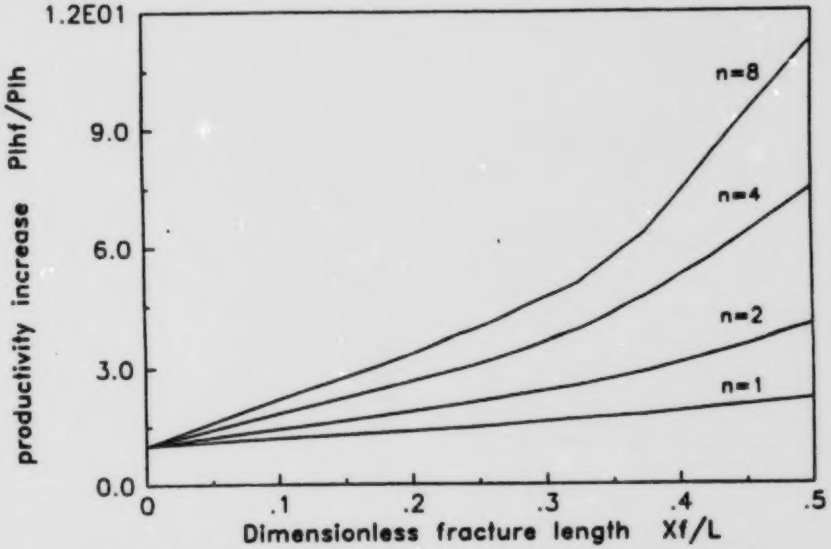

Fig. 5—Productivity increase of fractured horizontal wells vs. fractures width and number of fractures.

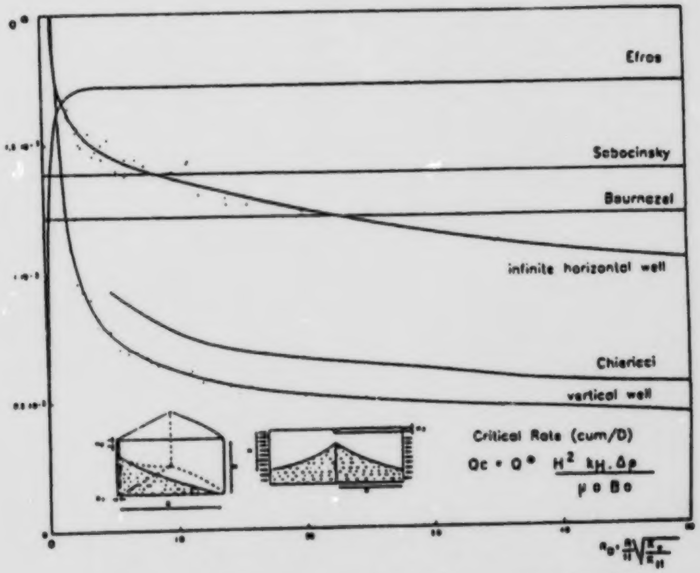

Fig. 6—Comparison of critical rate predictions for vertical and infinite horizontal well.

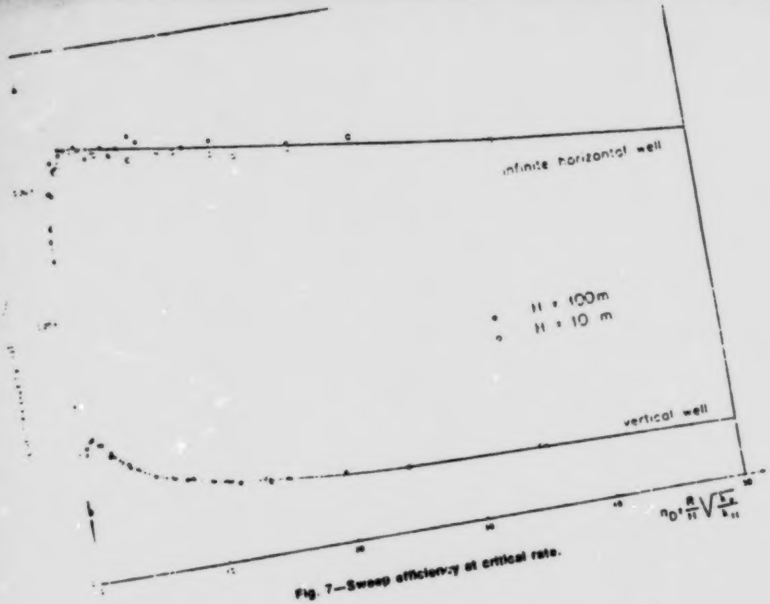

Fig. 7—Sweep efficiency at critical rate.

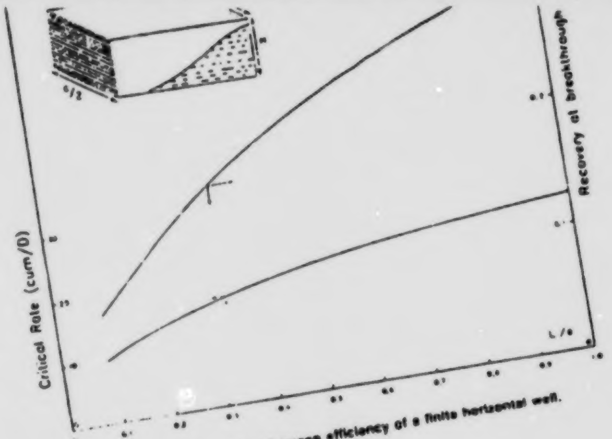

Fig. 8—Critical rate and sweep efficiency of a finite horizontal well.

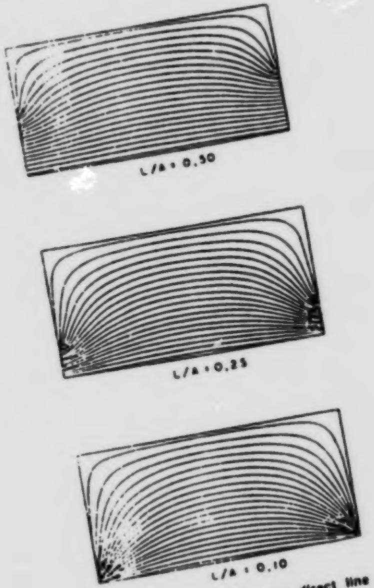

Fig. 9—Streamlines in the direct line drive with unit mobility ratio for various drainhole length.

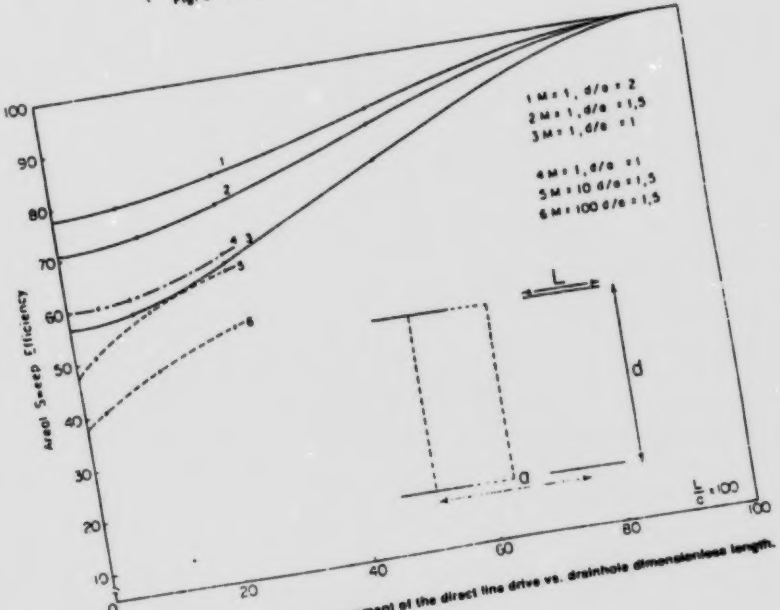

Fig. 10—Areal sweep efficiency improvement of the direct line drive vs. drainhole dimensionless length.

010161

(79)

SPE

Society of Petroleum Engineers of AIME

Alberta OIL SANDS
INFORMATION CENTRE

SPE 13710

Horizontal Wells Production Techniques in Heterogeneous Reservoirs

by F.M. Giger, *Inst. Français du Pétrole*

SPE Member

Copyright 1985, Society of Petroleum Engineers

This paper was presented at the SPE 1985 Middle East Oil Technical Conference and Exhibition held in Bahrain, March 11–14, 1985. The material is subject to correction by the author. Permission to copy is restricted to an abstract of not more than 300 words. Write SPE, Box 833836, Richardson, Texas 75083-3836. Telex: 730989 SPE DAL.

ABSTRACT

Two advantages of oil production with horizontal wells are the increase in productivity of each well and a new approach to solving reservoir-engineering problems resulting from heterogeneities. The aim of this paper is to propose elements of analysis focusing on flowline patterns and pressure distribution in an oil field. These elements should be of help to decision-makers when faced with an economic choice between spudding vertical or horizontal wells and eventually fracturing them.

INTRODUCTION

Drilling and production from several horizontal wells by Elf Aquitaine and the Institut Français du Pétrole[1,2] has shown the need to do some thinking about the heterogeneities of permeability encountered in a reservoir. Since a horizontal well is open over 300 m (1000 ft) in the same horizontal layer, two consequences must be drawn. First, hydraulically speaking, when seen in a horizontal plane the well is closely bound to a wide area of the reservoir. Second, in stratified reservoirs only one or, at most, a few strata are intersected by the producing length of the well. Hence impervious shale interbedding may be very detrimental to its productivity.

Experience has shown how heterogeneous carbonate fissured reservoirs are, even along a horizontal profile that remains in the same layer. Besides the extremely valuable new geological information obtained on how facies evolve, this experience induces us to take into consideration the occurrence of lateral heterogeneities when evaluating horizontal wells and comparing them with vertical wells.

The effects of heterogeneities on flow mechanisms and the influence of feed mechanisms on productivity will illustrate how different the behaviors of horizontal and vertical wells are as well as when fractures look more like one another.

EFFECTS OF HETEROGENEITY ON FLOW MECHANISMS

Anisotropy

The sedimentation process and the fracturing that may follow it, usually create local inhomogeneities in the porous matrix of a reservoir. If the mean dimensions of the heterogeneous domains are small enough in comparison to the dimensions of the entire domain of fluid flow, then their random distribution on a large scale will often result in an averaging-out effect. Reservoir engineers represent this effect, which is called anisotropy[3], by three permeabilities, k_x, k_y and k_z. An application of this method to the estimating of the productivity index of horizontal wells has been developed by F. Giger et al.[1]

Multilayer and Multiphase Reservoirs

Let us consider an oil reservoir with an active bottom water drive. Let us suppose that a layer with very poor vertical permeability compared to the oil-zone matrix lies just above the water-oil transition zone. The poor permeability in this layer might be due to shaly interbedding, for instance. The bottoms of the oil-producing wells in such a reservoir will be situated higher than the level of the shaly interbedding to prevent water coning. Soon after the beginning of oil production, drainage through the shaly interbedding will cause a limited oil flow to vertically enter into the part of the reservoir above the interbedding. In a first approximation it might be assumed that the surface flow vertically entering into the upper part of the reservoir is uniform because of the weak permeability barrier. Let us call this feed mechanism bottom drive.

References and illustrations at end of

If the thickness of the upper part of the reservoir is favorable to the implementation of horizontal wells under the criteria defined for homogeneous reservoirs[1], it is worthwhile to investigate such implementation in greater detail. The study of the effects of feed mechanisms on productivity hereunder focuses on a comparison between bottom drive mechanisms and conventional lateral feed.

Nevertheless, the fact should be borne in mind that any eventualy poor connection between adjacent beds with good permeability might act as a major drawback to efficient production with horizontal wells. This is the case, for instance, if impervious interbedding is found in fissured limestones[4]. Indeed, a horizontal well in stratified horizons intersects only a limited number of horizontal strata, and its advantages over vertical wells disappears if the flowlines cannot vertically cross the horizontal interbedding boundaries in its immediate vicinity. On the other hand, the productivity of vertical wells remains unchanged even if the adjacent horizontal beds are isolated[5].

Other reservoir configurations may lead to the same assumption of uniform vertical feed. For instance, an oil ring in which the stack of layers imbibed by oil is more or less protected from the gas-cap and the water-zone by strata with lower vertical permeability will be subjected, during oil production, to vertical feed mechanisms from above and below. If the low-permeability strata are 30 m (100 ft) to 100 m (300 ft) apart, the possibility of producing the reservoir by horizontal wells should be assessed. The analytical equations to be used will then be the same as the ones for a bottom drive mechanism.

Even multiphase homogeneous-permeability reservoirs, provided the water-oil and gas-oil interfaces remain almost flat during production, provide potential applications of concepts similar to the bottom drive mechanism.

Lateral Permeability Variations

Referring to a geological investigation limited to the use of vertical wells, Muskat[9] in 1949 noted the impossibility of determining random lateral variations in permeability. Now, thanks to horizontal drilling and coring[2], their lateral occurrence and distribution can be observed. Intersecting the rock matrix horizontally in the reservoir provides extremely valuable information to be analyzed over hundreds of feet on as small a scale as necessary.

The strong influence of the quality of the vertical connection between adjacent beds having different permeabilities has already been described above. On the other hand, since the linear flow q or the flow gathered per unit of perforated length is smaller, the pressure drawdown along the horizontal axis perpendicular to the horizontal well under steady state condition is almost linear (Fig. 1) because of almost parallel flow toward the well[6,7]. This aspect is explained hereunder in greater detail. Because loss of head in the close vicinity of a horizontal well is much less than that around a vertical well, the impact of horizontal permeability on productivity is very small in the first case as compared to the second one. Another favorable aspect of horizontal well is that its perforated length is greater than the scale of heterogeneity. According to Zeito[8] who studied the stratigraphy of the Grand Junction basin in Colorado, the Price basin in Utah and the Cairo basin in Illinois, three types of sandstone deposits with interbedded shale intercalations may be distinguished, i.e. maritime, channel and deltaic. Data given for the last two of them show that the thickness of channel deposits varies between 12 m (36 ft) and 40 m (120 ft), while their length is between 23 m (70 ft) and 60 m (180 ft). In the deltaic deposits the thickness of the high-permeability domains is about 40 m (120 ft), and their length reaches 100 m (300 ft) to 320 m (960 ft). These heterogeneity dimensions are small in comparison to the lateral extension of 500 m (1500 ft) of a horizontal well.

The horizontal well drilled in the Rospo Mare karsts is an industrial example of the high economic value of horizontal wells in very heterogeneous reservoirs[3]. The horizontal well gives very high productivity because it encounters the fractures and vugs in the karstic system, whereas vertical and slanted wells produce at only a limited rate through the compact carbonate rock in which permeability is very low. The great economic superiority of horizontal wells there is the reason why Elf Aquitaine and AGIP decided to develop the Rospo Mare field with horizontal wells alone[1].

POTENTIAL INTEREST OF FRACTURING HORIZONTAL WELLS

Because horizontal wells are good ways to take advantage of heterogeneities, when there is no natural heterogeneity in a specific reservoir, an effort might be made to create such heterogeneities. Hydraulic fracturing is a way of synthetically creating heterogeneity in a reservoir. Therefore, as soon as reliable methods of cementing horizontal wells are industrially available, the idea of hydraulically fracturing such wells will arise[9].

Figure 2 gives a theoretical case to illustrate the productivity ratio of fractured horizontal wells to fractured vertical wells. The wells drain box-shaped layers. With the conductivity of the fracture assumed to be infinite, the hydraulic potential will be the same in the crack and in the well when head losses are neglected. All the other boundaries of the simulated area are assumed to be impervious (null normal flux). In the reservoir block shown, it can be seen that a greater extension of the fractures is more profitable for the horizontal as compared to the vertical well only if the horizontal well crosses more than four fractures.

The network shows that, as long as the number of cracks remains fewer than four, the gain in productivity is invariably greater than the number of cracks in the drain. On the other hand, if the number of cracks continues to be increased, a saturation effect appears to occur, and the gain in the productivity index is then much more closely linked to the size of the cracks.

Such results also apply to naturally fractured reservoirs and confirm previous developments dealing with horizontal permeability anisotropy. A horizontal well is an effective tool for hitting fractures and for producing from them.

INFLUENCE OF FEED MECHANISMS ON PRODUCTIVITY

Experience gained by reservoir engineers from studying oil-field production by vertical wells shows that the feed mechanism usually has little effect on productivity. A comparative analysis of flowlines and of the loss of head around vertical (Fig. 3) and horizontal wells and around fractures (Fig. 4) indicates when a different conclusion must be drawn.

Vertical Wells

The productivity index for a vertical well, as defined by the ratio of the produced flow rate to pressure drop during withdrawal, is expressed approximately by the following equation[3]:

$$PI_V = \frac{2\pi k}{\mu} \quad \frac{h}{\ln\left(\frac{r_{ev}}{r_{wv}}\right)} \qquad (1)$$

The equations given in this paper are for use with SI units unless otherwise specified. A multiplication factor of 0.0145 must be used in the equations for the productivity index when the following units are used: ft, bbl, day, psi, md and cp, as well as 2 π and logarithms with a base of ten. Including 2 π and logarithms with a base of ten, a multiplication factor of 0.0233 must be used with the following units: m, m^3, day, bar, md and cp.

Equation (1) is determined for lateral feed with radius r_{ev}. The pressure drop that is created is given by Equation (2):

$$P_e - P_w = \frac{\mu}{2\pi k h} \quad \ln\left(\frac{r_{ev}}{r_{wv}}\right) Q \qquad (2)$$

Let us now consider a bottom drive feed with uniform areal feed flow. This means that, everywhere in the reservoir, the vertically entering flow is proportional to the surface area, f ds. The pressure drop between the lateral boundary of the reservoir at radius r'_{ev} and the well is (see Appendix A):

$$P'_e - P'_w = \frac{\mu}{2\pi k h} \quad \left[\ln\left(\frac{r_{ev}}{r_{wv}}\right) - \frac{1}{2}\right] Q' \qquad (3)$$

The productivity index of the well is:

$$PI'_V = \frac{2\pi k}{\mu} \quad \frac{h}{\ln\left(\frac{r_{ev}}{r_{wv}}\right) - \frac{1}{2}} \qquad (4)$$

Therefore, bottom drive feed has a limited effect on the productivity equations, e.g. a pseudoskin value of -0.5.

Hydraulically-Fractured Vertical Wells

One way of improving the productivity of a vertical well is to fracture the rock matrix in the reservoir around it. Therefore, it is worthwhile including fractured vertical wells in a comparison between horizontal and vertical wells.

The fractures considered in this paper are rectangular in shape and intersect the top and bottom of the reservoir. The hydraulic potential is the same in the crack and in the well connected to it. The productivity index for such a fractured well is expressed as follows[3,6]:

$$PI_{VF} = \frac{2\pi k}{\mu} \quad \frac{h}{\operatorname{arccosh}\left(\frac{2\, r_e}{L}\right)} \qquad (5)$$

This equation is valid only when the ratio of fracture length, L, to drainage radius, r_e, is small. When this ratio is negligible, the productivity-index equation becomes:

$$PI_{VF} = \frac{2\pi k}{\mu} \quad \frac{h}{\ln\left(\frac{r_e}{L/4}\right)} \qquad (6)$$

As shown by Muskat, this equation proves that a limited-length fracture, L, is equivalent to a vertical well with radius r'_w:

$$r'_w = \frac{L}{4} \qquad (7)$$

The simple Equation (7) is applicable provided that the extension of the fracture is small. Otherwise, Equation (5) shows that a more complex interaction occurs between the fracture and the feed boundary. Flow is no longer radial. Its equipotentials are not circular but elliptical (see Fig. 4).

In any case, with hydraulically-fractured vertical wells the extension of the fracture remaining open is rather small compared to the outside radius. This is the only case that will be considered in studying the influence of bottom drive feed.

The same conclusion as for a vertical well is obtained, i.e. a pseudoskin value of -0.5 appears to take bottom drive feed into consideration:

$$PI'_{VF} = \frac{2\pi k}{\mu} \frac{h}{\ln\left(\frac{r_e}{L/4}\right) - \frac{1}{2}} \qquad (8)$$

Extended Fracture in a Box-Shaped Reservoir

With long fractures the edge of the area drained becomes oval-shaped, and the concept of drainage radius is no longer very suitable. A better method of accounting for such flows is to place the long fracture in the center of a parallelepiped rectangle taken is a portion of the formation (Fig. 5). The size and laterally-fed sides must be determined by taking the distribution of the neighboring wells or the boundaries of the reservoir into account.

Let us now consider the production pattern shown in Figure 5, where the parallelepiped of the formation is fed through the two vertical sides parallel to the fracture. The flowlines are parallel to the horizontal plane. The problem is two-dimensional, and pressure drop calculated on the horizontal plane results from reduced parallel flow or to parallel flow with a reduction of cross-section[10]. This means that:

$$P_L - P_F = \frac{\mu}{2\pi k h} \quad \operatorname{arccosh}\left[\frac{\cosh\left(\frac{\pi}{2} \frac{a}{b}\right)}{\sin\left(\frac{\pi}{2} \frac{L}{b}\right)}\right] Q \qquad (9)$$

If the extension of fracture L equals the length of rectangle b, Equation (9) can be simplified as follows:

$$P_L - P_F = \frac{\mu}{4k h} \frac{a}{h b} Q \qquad (10)$$

This is the result obtained directly for parallel flow. The productivity index is:

$$PI_{FL} = \frac{4k}{\mu} \frac{h b}{a} \qquad (11)$$

With bottom drive feed the pressure difference between the lateral boundaries and the fracture becomes (see Appendix B):

$$P'_L - P'_F = \frac{\mu}{8k} \frac{a}{h b} Q \qquad (12)$$

And the productivity index is:

$$PI'_{FL} = \frac{8k}{\mu} \frac{h b}{a} \qquad (13)$$

Hence bottom drive feed has considerable effect on productivity values:

$$PI'_{FL} = 2\, PI_{FL} \qquad (14)$$

When the extension, L, of the fracture is smaller than the length of rectangle b, Equation (14) does not exactly apply, although it still gives the order of magnitude that can be expected.

Flowlines and Pressure Drop in the Vicinity of a Horizontal Well

In the vicinity of a long horizontal well, the flowlines are radial in planes perpendicular to its axis (Fig. 6). To demonstrate this, let us imagine a 90° rotation of the reservoir block in such a way that the horizontal well becomes vertical. Indeed, the local shape of the flowline system is basically the same as for a vertical well that would be used to produce from a thick and narrow reservoir closed laterally by two impervious boundaries. Additional pressure drop is caused by the concentration of streamlines toward the drain seen in the vertical plane perpendicular to the axis of this plane. For a drain situated in the middle of the layer and fed laterally, this is expressed as a function of linear flow q or flow collected per unit length[8] by:

$$\Delta P = \frac{\mu}{2\pi k} \ln\left(\frac{h}{2\pi\, r_{WH}}\right) q \qquad (15)$$

It can be seen from the logarithmic function that the circular radial convergence of the streamlines has been taken into account.

Short Horizontal Wells

For fields with little vertical thickness, which are good targets for implementing horizontal wells, the productive length of such wells is considerably greater than the thickness of the layer. Hence the main part of most of the flowlines is horizontal in planes perpendicular to the horizontal well, and it bends only in its close vicinity to hit it (Fig. 6). Since the pattern of flowlines running toward a horizontal well is very similar to the one obtained around a vertical fracture with an extension equal to the length of the well, pressure drops are partly the same in both cases.

For the horizontal well the pressure drop in flow toward the well is the sum of two terms. The first term is the one established for a vertical fracture in Equation (5), and it takes the partial penetration of the drainage area into account (Fig. 4). The other term is the one established in Equation (15) to represent circular radial flow in the plane perpendicular to the axis of the horizontal well, and it takes the axial convergence of the streamlines into count:

$$P_e - P_H = \frac{\mu}{2\pi k}\left[\frac{1}{h} \operatorname{arccosh}\left(\frac{2 r_e}{L}\right) + \frac{1}{L} \ln\left(\frac{h}{2\pi r_{wH}}\right)\right] Q \quad (16)$$

The productivity index is then expressed by:

$$PI_H = 2\pi \frac{k}{\mu} \frac{1}{\frac{1}{h} \operatorname{arccosh}\left(\frac{2 r_e}{L}\right) + \frac{1}{L} \ln\left(\frac{h}{2\pi r_{wH}}\right)} \quad (17)$$

The denominator in this equation consists of two terms. The lefthand one corresponds to the pressure drop a long way away from the horizontal well and is the same as the one used for hydraulically fractured wells. The righthand term in the denominator corresponds to the streamlines converging on the horizontal cross-section of the well.

Long Horizontal Wells

The preceding equation was derived for horizontal wells which are small compared to the drainage radius, i.e. a small L/r_e ratio. For long wells the edge of the drain zone becomes oval, and the concept of drainage radius is no longer suitable. For ascertaining flows it then becomes more odent to place the horizontal well in the ter of a rectangular parallelepiped ased on the shape of the reservoir and on the size and the faces fed, which are to be defined on the basis of the distribution of the neighboring wells.

Let us now look at the production scheme given in Figure 7 where the parallelepiped reservoir is fed via two vertical faces parallel to the well. In a way similar to the approach used above for a short well, we will assume that total flowpressure loss is the sum of the pressure losses calculated in the horizontal plane as well as of the pressure losses resulting from the concentration of the streamlines toward the well as seen in the plane perpendicular to the axis of this well.

The pressure losses calculated in the horizontal plane are those that were found for drainage through a vertical fracture traversing the reservoir from top to bottom and having an extent equal to the length of the horizontal well (Equation (9)). By combining this result with the evaluation (Equation (15)) previously used for the pressure loss resulting from the concentration of streamlines toward the well as seen in a plane perpendicular to its axis, productivity of a long horizontal well obtained:

$$PI_H = 2\pi \frac{k}{\mu} \frac{1}{\frac{1}{h} \operatorname{arccosh}\left[\frac{\cosh\left(\frac{\pi}{2} \frac{a}{b}\right)}{\sin\left(\frac{\pi}{2} \frac{L}{b}\right)}\right] + \frac{1}{L} \ln\left(\frac{h}{2\pi r_{wH}}\right)} \quad (18)$$

When the well has the same length L as the parallel side b of the parallelepiped, this equation assumes a simple expression that would be easy to establish directly[6]:

$$PI_H = 2\pi \frac{k}{\mu} \frac{b}{\frac{\pi}{2} \frac{a}{h} + \ln\left(\frac{h}{2\pi r_{wH}}\right)} \quad (19)$$

For well lengths that are short compared to length b of the side of the parallelepiped parallel to the well, Equation (18) gives an asymptotic expression that is very similar to the one in Equation (17). The differences between them represent different feed conditions.

With bottom drive feed the difference in pressure between the lateral boundaries and the well having length L = b is the sum of what is obtained with a long fracture and a pressure drop in the vicinity of the horizontal well:

$$P'_e - P'_H = \frac{\mu}{k b}\left[\frac{a}{8 h} + \frac{1}{2\pi} \ln\left(\frac{h}{2\pi r_{wH}}\right)\right] Q' \quad (20)$$

CONCLUSIONS

The productivity of a horizontal well is less sensitive to unfavorable heterogeneities in the vicinity of the well than with a vertical well. The open production length and the pressure profile are such that the horizontal well takes better advantage of high-permeability zones while diminishing the impact of low-permeability horizontal variations. Only horizontal impermeable interbedding is more detrimental to a horizontal well than to a vertical one.

As soon as the length of a horizontal becomes appreciable in relation to the size of the reservoir, the productivity of this well is sensitive to the nature of the feed mechanism. Some cases of bottom water drive are even more favorable to horizontal wells than is lateral feed.

NOMENCLATURE

a = side of the parallelipippedic rectangle block of formation perpendicular to the fracture or the horizontal well

arccosh = inverse hyperbolic cosine function[11]

$$\operatorname{arccosh}(x) = \ln\left[x + (x^2 - 1)^{\frac{1}{2}}\right] \quad (x \geqslant 1)$$

b = side of the parallelipippedic rectangle block of formation parallel to the fracture or the horizontal well

cosh = hyperbolic cosine function[11]

$$\cosh(z) = \frac{1}{2}\left[\exp(z) + \exp(-z)\right]$$

ds = differential surfacic element

exp = exponential function

f = surfacic flow entering the layer vertically

h = thickness of the layer or of the reservoir

k = permeability

l = length of the horizontal well or of the fracture

ln = Napierian logarithm

p = pressure

PI = productivity index

q = linear production rate of a horizontal well (or a fracture)

Q = production rate

Q'(r) = flow rate entering radially the cylinder with axis the well and with a radius r

Q'(x) = flow rate

r = radius

sin = sine function

x = absisse

y = ordinate

Greek

Δ = difference

μ = viscosity

Subscripts and Superscripts

e = external (drainage)

F = fissure

H = horizontal

L = lateral border of the reservoir (or lateral feed)

V = vertical

W = well

X = along the x axis

Y = along the y axis

Z = along the z axis

' = with bottom drive feed or equivalent

ACKNOWLEDGEMENTS

The author wishes to thank the Institut Français du Pétrole and Société Nationale Elf Aquitaine for encouragement to publish this paper.

REFERENCES

1. Giger, F.M., Reiss, L.H. and Jourdan, A.P. : "The Reservoir Engineering Aspects of Horizontal Drilling," SPE paper 13024, 1984 SPE Annual Technical Conference, Houston, TX.

2. Reiss, L.H., Jourdan, A.P., Giger, F.M. and Armessen, P.A.: "Offshore and Onshore European Horizontal Wells," OTC paper 4791, 1984 OTC, Houston, TX.

3. Muskat, M.: The Flow of Homogeneous Fluids through Porous Media, I.H.R.D.C., Boston, 1982.

4. Reiss, L.H.: The Reservoir Engineering Aspects of Fractured Formations, Editions Technip, Paris, 1980.

5. Muskat, M.: Physical Principles of Oil Production, I.H.R.D.C., Boston, 1981.

6. Giger, F.: "Réduction du nombre de puits par l'utilisation de forages horizontaux," Revue de l'IFP, vol. 38, No. 3, (May-June 1983).

7. Giannesini, J.F.: "Horizontal Wells, a Today's Technology," Petrossis Jan-Feb. 1984.

8. Zeito, G.A.: "Interbedding of shales breaks and reservoir heterogeneities," J.P.T., October 1965.

9. Duns, H., van der Vlis, A.C., Fernandez Luque, R.: "Increasing Well Productivity in Tight Chalk Reservoirs," 10th World Petroleum Congress, Bucarest, 1979, Romania.

10. Houpeurt, A.: Eléments de mécanique des fluides dans les milieux poreux, Editions Technip, Paris, 1975.

11. Abramowitz, M. and Stegun, I.: Handbook of Mathematical Functions, Dover, New York, 1972.

APPENDIX A

VERTICAL WELL WITH BOTTOM-DRIVE FEED

The Darcy equation with axisymmetric flow becomes:

$$\frac{dP'}{dr} = \frac{\mu}{2\pi k h} \cdot \frac{Q'(r)}{r} \qquad (A.1)$$

The assumption of uniform surface flow f entering the reservoir vertically can be written:

$$\frac{dQ'}{dr} = -2\pi \; r f \qquad (A.2)$$

There is no lateral feed at the external radial boundary:

$$Q'(r_e) = 0 \qquad (A.3)$$

ations (A.2) and (A.3) give the flow e entering the cylinder whose axis is the well and with radius r:

$$Q'(r) = \pi \quad (r_e^2 - r^2)\, f \tag{A.4}$$

The production rate of the well is:

$$Q' = \pi \quad r_e^2 \quad f \tag{A.5}$$

Equations (A.1) and (A.4) give the pressure distribution:

$$P'(r) - P'_e = \frac{\mu}{2\, k\, h}\left[r_e^2 \ \ln\left(\frac{r}{r_e}\right) - \frac{r^2}{2} + \frac{r_e^2}{2}\right] f \tag{A.6}$$

The pressure drop between the lateral boundary of the reservoir a radius r'_{ev} and the well is:

$$P'_e - P'_w = \frac{\mu}{2\pi\, k\, h}\left[\ln\left(\frac{r_e}{r_{wv}}\right) - \frac{1}{2}\right] Q' \tag{A.7}$$

APPENDIX B

EXTENDED FRACTURE WITH BOTTOM-DRIVE FEED

By taking advantage of the symmetry on both sides of the plane of the fracture as in Fig. 5 the Darcy equation can be written:

$$\frac{d\, P'}{d\, x} = \frac{\mu}{k\, h\, b} \quad \frac{Q'}{2} \quad (x) \tag{B.1}$$

ere Q'(x)/2 is the flow rate through the rectangular cross-section of the box-shaped layer parallel to the fracture and at the x abscissa. The factor of 1/2 multiplied by Q'(x) allows for the symmetry of the problem. The assumption of uniform surface flow f entering the layer vertically can be written:

$$\frac{d\, Q'}{2\, d\, x} = -\, b\, f \tag{B.2}$$

There is no lateral feed at the external boundary:

$$\frac{Q'}{2}\left(\frac{a}{2}\right) = 0 \tag{B.3}$$

Equations (B.2) and (B.3) give the flow rate entering through the rectangular cross-section of the layer at the x abscissa:

$$\frac{Q'}{2}\,(x) = b\left(\frac{a}{2} - x\right) \ f \tag{B.4}$$

The producing rate of the fracture is:

$$Q' = a\, b\, f \tag{B.5}$$

Equations (B.1) and (B.4) give the pressure distribution:

$$P'_e - P'(x) = \frac{\mu}{2\, k\, h}\left(x - \frac{a}{2}\right)^2 \ f \tag{B.6}$$

The pressure drop between the lateral boundary of the reservoir and the fracture is:

$$P'_e - P'_F = \frac{\mu}{k} \ \frac{a^2}{8\, h} \quad f \tag{B.7}$$

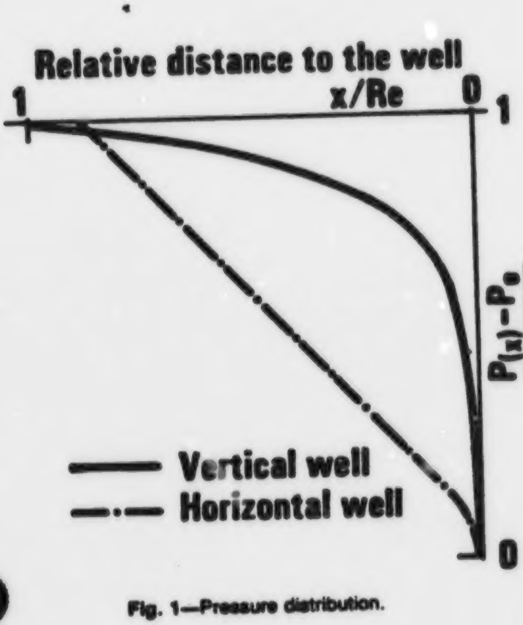

Fig. 1—Pressure distribution.

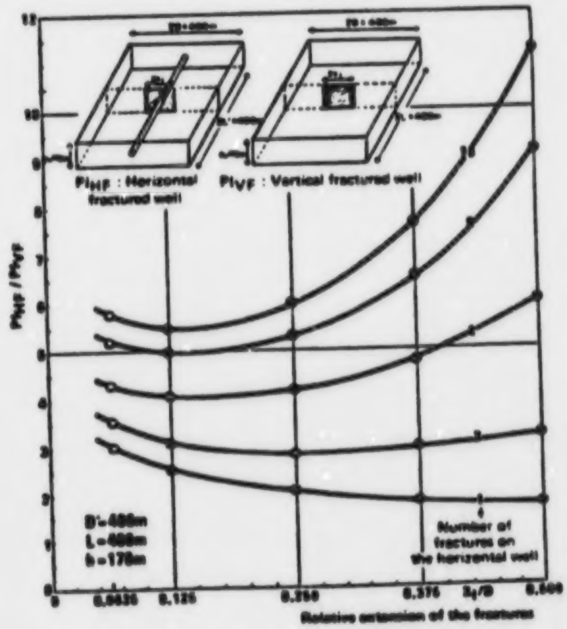

Fig. 2—Fractured horizontal and vertical wells.

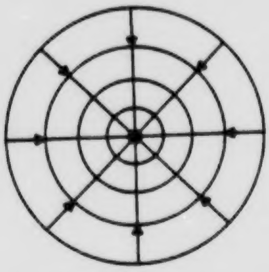

Fig. 3—Radial stream lines moving toward a vertical well.

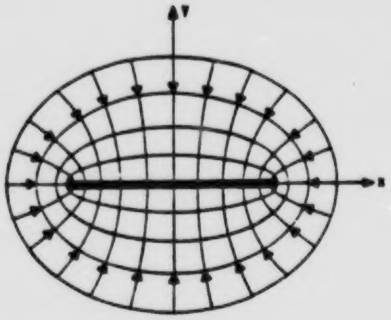

Fig. 4—Stream lines moving toward a horizontal well.

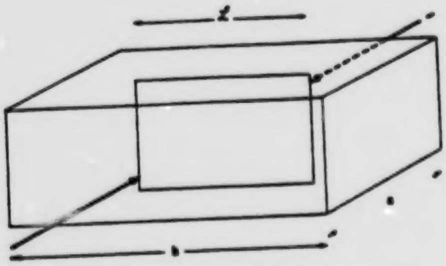

Fig. 5—Long vertical fracture fed laterally.

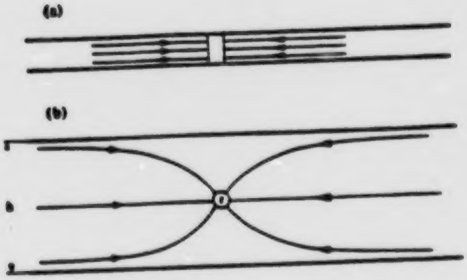

Fig. 6—Stream lines in a cross section perpendicular to the axis of a fracture and of a horizontal well.

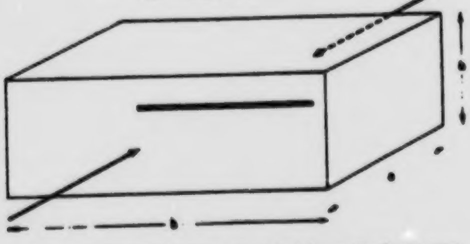

Fig. 7—Long horizontal well fed laterally from two sides.

SPE
Society of Petroleum Engineers

SPE 15378

80

Analytic 2-D Models of Water Cresting Before Breakthrough for Horizontal Wells

by F.M. Giger, *Inst. Français du Pétrole*

SPE Member now with Horwell SA

Copyright 1986, Society of Petroleum Engineers

This paper was prepared for presentation at the 61st Annual Technical Conference and Exhibition of the Society of Petroleum Engineers held in New Orleans, LA October 5-8, 1986

This paper was selected for presentation by an SPE Program Committee following review of information contained in an abstract submitted by the author(s). Contents of the paper, as presented, have not been reviewed by the Society of Petroleum Engineers and are subject to correction by the author(s). The material, as presented, does not necessarily reflect any position of the Society of Petroleum Engineers, its officers, or members. Papers presented at SPE meetings are subject to publication review by Editorial Committees of the Society of Petroleum Engineers. Permission to copy is restricted to an abstract of not more than 300 words. Illustrations may not be copied. The abstract should contain conspicuous acknowledgment of where and by whom the paper is presented. Write Publications Manager, SPE, P.O. Box 833836, Richardson, TX 75083-3836. Telex, 730989 SPEDAL

ABSTRACT

Production with horizontal wells offers a new approach to reduce water coning effect during oil production.

This paper evaluates what effect water cresting under a horizontal well will have and determines the critical flowrate by fully analytic 2-D methods developed in a vertical plane perpendicular to the axis of the horizontal well.

Three production mechanisms are successively considered : Lateral edge drive, gas cap drive and bottom waterdrive.

The theory gives the value of the critical flowrate in each case. A major achievement of this theory is the proof of a decreasing value of the critical flowrate with cumulative production of the bottom waterdrive mechanism.

Results are presented on graphs for a quick use. Case studies exemplify a simple evaluation method to help solving practical engineering problems.

INTRODUCTION

Whatever method is envisaged today for producing a deposit of oil comprising a contact surface with water or gas near to the well, there is a so called "critical" flowrate which cannot be exceeded without leading rapidly to the entry of water or gas into the well. In the case of a vertical producing well, the effect is called water coning, a frequently encountered phenomenon which introduces vital constraints upon the production rate of the field and the oil recovery.

Physical theory explains this phenomenon of deformation of the water-oil contact surface by the pressure sink created by the dynamic flow of the oil towards the drainage system. Its effect is intuitive with the higher convergence of flow stream-lines and the rapid increase of pressure gradient.

For the vertical well, where the flow is of the radial-circular type in first approximation, sharp gradients appear in the neighbourhood of the well. Its trace is limited to a single point in a horizontal plane. For the reasons stated above, the gradients induce water to rise in its immediate surroundings. Reference to the horizontal plane is justified by the fact that this latter extends parallel to the initial oil-water plane, following the greatest dimensions of the deposit.

This observation leads us to expect that a horizontal drain, open over its entire length and for which the trace on a horizontal plane is a segment of a straight line, will give a much more favourable flow both in respect to occurrences of water (in so far as the gradients are shallower) and in respect to the sweep efficiency (due to the disappearance of the individual points of the production system using vertical wells).

The aim of this paper is to present analytical solutions which describe the shape of the water crest created by a horizontal drain used for producing a deposit of oil bounded by an oil-water contact surface. As a matter of fact, the rise of water below a horizontal well does not create a cone but a crest and the expression of water cresting is proposed here to describe the phenomenon. The horizontal well is situated near the roof of the reservoir for the lateral edge drive and the bottom waterdrive cases.

References and illustrations at end of paper.

The calculations provide an evaluation of the critical flowrate.

PHYSICS OF THE WATER-OIL SURFACE

Physical Schematic Representation

The diagramatic examples studied deal with the formation of water crests when the oil contained in a reservoir stratum is brought into production by means of an infinite drain situated close to its horizontal roof. After Muskat[1], the flows are approximated by a piston type flow scheme. Phenomena of capillarity are not taken into account. Displacement efficiency is supposed to be complete.

The nature of the problem enables us to deal with it in the plane perpendicular to the axis of the drain. It is therefore a permanent and incompressible two-dimensional fluid flow in a porous medium. The velocity field therefore derives from a scalar potential, the Laplace operator of which is zero.

Expression in the form of equations

The state of equilibrium of the pressures on each side of the oil/water separation surface can be written with the assistance of the Darcy equation (1) to take into account the dynamic pressure potential created by the flow of oil and the difference between the hydrostatic pressures in the oil and in the water resulting from the difference in their densities (2).

$$\overrightarrow{\text{grad}}\ \Phi = -\frac{\mu_o}{k}\ \vec{v} \qquad (1)$$

$$\frac{d\Phi}{dy} = (\rho_o - \rho_w)\ g \qquad (2)$$

By introducing the angle α which the separation surface makes with the horizontal at one point, the local equation of this latter is expressed as follows :

$$||v|| = \frac{k}{\mu_o}\ (\rho_w - \rho_o)\ g\ \ |\sin\alpha| \qquad (3)$$

The problems can be solved by using the hodograph method as explained by Muskat[1] or Kidder[2]. Appendix A describes the resolution method.

LATERAL EDGE DRIVE

Description of the case

Let us consider the part of the reservoir shown in the cross-section of Figure 1. The horizontal well is near the top of the oil column in order to have the maximum distance from the initial water oil contact. The aquifer is almost non active and the production mechanism is a symmetric lateral drive in the oil zone. As the well is under steady production, a water crest forms below the horizontal well.

The flow conditions at the borders are Neumann conditions with no flow on the A-C line to represent the impervious top of the reservoir and the equation (3) for the free oil-water boundary. Dirichlet conditions of defined potential value are applied to the well and to the edges.

How is the shape of the water crest related with the linear flowrate ?

Shape of the water oil contact

The general solution is obtained without any approximation improving an approach proposed by D.A. Efros[3,4] (See Appendix A). It provides the shape of the oil-water separation line with the following parametric expression where θ is the parameter.

$$x = \frac{c\theta + c(\theta)\left[\frac{\pi\theta^2}{4} - \frac{1}{2\pi}\left[\ln\left(1+e^{-\pi|\theta|}\right)\right]^2 - \frac{s\left(\frac{1}{e^{\pi|\theta|}+1}\right)}{\pi} + \frac{\pi}{12}\right]}{c + \ln 2}\ h \qquad (4)$$

$$y = -\left[1 + \frac{\ln\left[\cosh\left(\frac{\pi}{2}\theta\right)\right]}{c + \ln 2}\right] h \qquad (5)$$

Where x and y are the abscissa and ordinate of a moving point describing the boundary of the water crest. h is the vertical distance between the top of the water crest and the top of the reservoir. c is a positive parameter that will be discussed hereafter. The volumetric rate of oil production from the well per unit length, q is :

$$q = \frac{\pi\ k\ \Delta\rho\ g}{\mu_o}\ \ \frac{h}{c + \ln 2} \qquad (6)$$

Regarding the system of equations (4) to (6), two data taken out of c, h, q and also a point having x_1 and y_1 as coordinates and belonging to the W.O.C. are sufficient to define a solution.

For instance, Figure 2 shows the family of adimensional curves with coordinates x* = x/h and y* = y/h representing the W.O.C. defined by the parameter c. As their top is at a point with -1 as ordinate, a homothetia of factor h with center the origin of coordinates B gives the effective shape of the W.O.C. in the reservoir. Parameter c is related with the largest angle made by the W.O.C. with the horizontal. High c values correspond to limited cresting effect.

Small c values correspond to high cresting effect. Critical flow is obtained for c = 0.

Far from the well, the shape of the water crest is a branch of parabola -the Dupuit parabola- with equation :

$$y^2\left[\frac{c+\ln 2}{h}\right]^2 - x\pi\frac{c+\ln 2}{h} - \frac{\pi^2}{12} - c^2 = 0 \qquad (7)$$

On the other side, the water crest may be described by the symmetric branch of the parabola with respect to the y axis.

Far from the well, from rough evaluations, the two last expressions may be combined and simplified :

$$q = \frac{k_H(\rho_w - \rho_o)\, g}{\mu_o} \frac{y^2}{x} \qquad (8)$$

Written with the practical units in surface conditions, m, md, g/cm^3, cp, d, this expression is :

$$q = 8.37\ E\text{-}4\ \frac{k_H(\rho_w - \rho_o)}{B_o\ \mu_o} \frac{y^2}{x} \qquad (9)$$

The multiplication factor is 0.49 E-3 with the following units : bbl/D, md, g/cm^3, ft, cp.

These results presented earlier[5]* may be obtained easily as a solution of the problem solved using the Dupuit-Forchheimer approximation[6-9]. In this approximation, the pressure drops in the flowing oil are those resulting only from the horizontal component of the velocity vector. Pressure drops caused by the vertical motion of the oil are simply omitted. This omission is valid at some distance from the well but leads to discrepancies in its vicinity where the flow lines are far from being horizontal.

Critical flowrate

Critical flowrate q_c is obtained in equations (4) to (6) when c equals 0. Then :

$$h = \frac{\ln 2}{\pi} \frac{\mu_o}{k\,\Delta\rho\, g} q_c \qquad (10)$$

$$\frac{x}{h} = \frac{c(\theta)\left[\frac{\pi\theta^2}{4} - \frac{1}{2\pi}\left[\ln\left(1+e^{-\pi|\theta|}\right)\right]^2 - \frac{\left(\frac{1}{e^{\pi|\theta|}+1}\right)}{\pi} + \frac{\pi}{12}\right]}{\ln 2} \qquad (11)$$

$$y = -h\left[1 + \frac{\ln\left[\cosh\left(\frac{\pi}{2}\theta\right)\right]}{\ln 2}\right] \qquad (12)$$

The summit of W.O.C. is then sharp (Figure 3).

Discussion of the model

The parabolic shape of the water oil contact at some distance from the well makes its practical use difficult.

As there is no horizontal asymptote to the parabola, there is no answer to the question of a reservoir engineer asking how the initial position of the water oil contact could be represented by the present model.

At this point we must make a comment about the subject of the shape of the boundary between the water and the oil at a sufficiently large distance from the well. For the vertical wells, the impact of this distance occurs within the logarithmic function. For a given flow-rate, and at a sufficient distance, the values assumed by this function evolve only slightly and it is usually considered that a horizontal water level exists. Matters are different from the infinite horizontal wells (or those completely crossing the width of a deposit) ; the impact of the distance intervenes by the factor 1/x in y^2/x. We are no longer entitled to consider that a water level far from the well exists in this representation.

Even if the flow close to the well may be depicted as a lateral flow of an incompressible fluid, at some distance from it, the production mechanism is usually a sweep by the moving water oil contact eventually combined with the expansion of the compressible oil. The geometry of the parallel flow towards the horizontal well points out how the hypothesis taken are different from the actual reservoir conditions, whereas the radial circular flow towards a vertical well corrects, to some extend, discrepancies originating in vague hypothesis.

Therefore, one should avoid to use a description of the lateral edge drive as made here for a different use than a study of the local deformation of the water-oil contact below the horizontal well. The interest of this model lies in its ability to describe the watercrest and its deformation in the vicinity of the horizontal well at any flow up to the critical flowrate. It will be used this way in a following chapter in this paper.

---

* In the former presentation, i.e. eq (5) of SPE 13024, the reader should correct L by l, lateral distance from the horizontal well.

GAS CAP DRIVE

Description of the case

The reservoir which is now considered is shown in the cross-section of Figure 4. Some water lies beneath the oil column but the aquifer is not active. The production mechanism is a gas drive. When the well will be put on stream, a water crest will rise below the well. Anyway, as soon as the height of the water crest reaches the value corresponding to the stabilized flow-rate of oil, it will remain at this value because the aquifer is not active. On the other hand, due to the gas drive mechanism, the oil production results from the downward motion of the gas-oil contact. Therefore, for a given forecasted flowrate, one may expect to produce water-free but an ultimate breakthrough of gas into the well is unavoidable. Given an expected flow-rate, the optimum location of the horizontal well is the lowest one for which no water will enter the well.

We will determine the vertical distance from the initial W.O.C. at which the horizontal well should be drilled to allow the water-free expected flow-rate and we will describe the shape of the water crest.

At this stage, we will not focus on the evolution of the shape of the gas-oil contact and therefore, we will consider the equivalent cross-section where oil influx at the top of the oil column allows a steady-state flow pattern in the oil zone. (Figure 5)

Shape of the water oil contact

The equations describing the state of equilibrium of the pressures on each side of the oil/water separation surface are the same as for the lateral edge drive, the only difference between both cases being the different conditions at the borders of the flowing oil zone. A Dirichlet condition is applied to the upper border and a Neumann condition with no flow is applied to the lateral borders.

The mathematical solution of this problem has been derived by Y.Cailleau[10] et al. Appendix B presents the results for subcritical flowrates which lead to very long mathematical expressions. (See Figure 14)

Critical flow rate

The equations for critical flowrate are obtained from those of Appendix B for $\beta = \pi$ and match with the results of R. E. Kidder[2].

At critical flow rate, the vertical distance of the well from the initial W.O.C. is :

$$B = \frac{D}{2\pi} \ln \left[1 + \frac{2 \mu_o q_c}{k \Delta\rho g D} \right] + \left[\frac{\mu_o q_c}{\pi k \Delta\rho g} \ln \left[1 + \frac{k \Delta\rho g D}{2 \mu_o q_c} \right] \right] \qquad (13)$$

The height of the water crest is then :

$$H = \frac{\mu_o q_c}{\pi k \Delta\rho g} \ln \left[1 + \frac{k \Delta\rho g D}{\mu_o q_c} \right] \qquad (14)$$

The graph in Figure 6 gives the relations between the dimensionless critical flow

$$q_c^* = \frac{\mu_o q_c}{g \Delta\rho k D} \qquad (15)$$

the dimensionless distance of the well from the initial W.O.C.

$$B^* = \frac{2B}{D} \qquad (16)$$

and the dimensionless height of the water crest

$$H^* = \frac{2H}{D} \qquad (17)$$

Example : Determination of the critical linear flow associated with a position of the horizontal well.

Let us consider an example :

B = 60m (193 ft)

B_o = 1.25

D = 400m (1320 ft)

$k = k_H$ = 100md

$\rho_w - \rho_o$ = 0.1 g/cm^3

μ_o = 50cp

We enter with an ordinate of 0.3 on the B* curve of Figure 6 and we obtain a dimensionless critical flow q^*_c of 0.25 and a dimensionless height of the water crest H* of 0.25 . The results are :

$$q_c = q_c^* \; 8.37\,E\text{-}4 \; \frac{k_H\,(\rho_w - \rho_o)\,D}{B_o\;\mu_o} \qquad (18)$$

q_c = 1.34 E-2 m^3/d/m (2.58 E-2 bbl/D/ft)

$$H = B \; \frac{H^*}{B^*} \qquad (19)$$

H = 50m (164 ft)

Expression (18) is written with the practical units in surface conditions, m, md, g/cm^3, cp, d. The multiplication factor is 0.49 E-3 with the following units : bbl/D, md, g/cm^3, ft, cp.

Discussion of the model

The lateral no flow boundaries may represent the border of the reservoir as well as the limits of drainage areas between several parallel horizontal wells.

The depicted production mechanism is a gas cap drive. When the G.O.C. arrives close to the well a gas cresting effect will appear. This effect has not been studied here but should be looked at in an actual reservoir.

This model is not aimed to represent a solution gas drive and although it may give an approximative evaluation of the critical rate in such a case, one has to be very cautious about results obtained that way.

Theoretically speaking, if there is no bottom water-drive at all, the conservation of the volume of water implies that the level of the W.O.C. will go down at the lateral boundaries at the same time as when the apex will rise below the well. The derivations have been presented here in assuming this effect negligeable. As a matter of fact B and H are established with respect of the level of the W.O.C. at the lateral boundaries. The analytical description of the W.O.C. given in Appendix B allows to make the correction stating that the mean level of the W.O.C. does not vary by reckoning the volume swept during the creation of the apex.

BOTTOM WATER DRIVE

Description of the case

Let us consider the reservoir shown in the cross section of Figure 7. Now the lateral sides are impervious and the aquifer is active.

The production mechanism is a bottom water drive. The water crest that will form below the well as soon as it will be put on stream is shown in Figure 8.

The boundary conditions are Neumann conditions with no flow at the G_oA, AC and CG'_o lines to represent the impervious top of the reservoir and the tight vertical sides. The equation (3) is taken for the description of the water oil contact. Although its slow vertical movement creates the oil sweep necessary for production, it could be considered to have at any time the near equilibrium shape that results from the oil flow lines pattern.

Shape of the water oil contact

At some distance from the well we use the Dupuit-Forchheimer approximation that has been shown above to be accurate enough (See appendix C).

There, on both sides, the shape of the water oil contact is an ellipse with a horizontal tangent close to the sides.

$$y^2 - y_{G'}^2 + \frac{\mu_o\; q}{k_H\,\Delta\rho\, gD}\left(\frac{D}{2} - |x|\right)^2 = 0 \qquad (20)$$

For practical use, this tangent is to be matched with the initial W.O.C.

Now if we consider the area of the flow domain in the vicinity of the well, one notices that the pattern of the flow lines is the same as for the lateral drive described earlier in the paper.

As the Dupuit-Forchheimer approximation does not lead to accurate results close to the well, it is then advisable to use the exact solution for the shape of the boundary obtained earlier for the lateral edge drive mechanism.

A fit of the ellipse with the Dupuit parabola permits to define the related exact description of the water oil contact close to the well and the parameter c (See Appendix C)

Critical flow rate

$$q_c = \frac{3}{2}\;\frac{k_H\,\Delta\rho\, gD}{\mu_o}\left[\left(1 + \frac{16}{3}\,\frac{y_{G'}^2}{D^2}\right)^{1/2} - 1\right] \qquad (21)$$

At some distance from the well, the shape of the W.O.C. is described by an ellipse on both sides by replacing q by q_c in equation (20).

Below the well, the shape of the W.O.C. is given by the equation (10) and the parametric expressions (11) and (12).

Water-free oil production

If the well is put on stream at a steady production rate smaller than the critical rate, the bottom water drive induces the slow upward sweep of the W.O.C. $|y_{G'}|$ decreases as time is passing . Equation (21) shows that q_c decreases with $|y_{G'}|$ and, at a time t_c, q_c gets equal to the production rate. At this time water begins to appear in the production :

$$t_c = \frac{A_{sc}}{q_c} \phi \; (1 - S_w - S_{oR}) \qquad (22)$$

where the expression of A_{sc} is given in Appendix C. The cumulative production is at that time :

$$n_c = \frac{t_c \; q_c \; L}{B_o} \qquad (23)$$

If no water production is allowed, the production rate of the well will have to be gradually reduced in such a way that it will be at any time smaller than the critical rate related to the level of the W.O.C.

Example

When writing with the practical units in surface conditions, m, md, g/cm^3, cp, d, m^3/d one has to replace g by 8.34 E-4/B_o. The multiplicating factor replacing g is 0.49 E-3/B_o with the following units : bbl/D, md, g/cm^3, ft, cp.

Taking the same values as before, and with :

$$y_{G'} = -\,60\text{m} \quad (-\,193\text{ft})$$

The critical flowrate is :

$$q_c = 4.67\text{ E-3 m}^3\text{/d/m} \quad (9.0\text{ E-3 bbl/D/ft})$$

Discussion of the model

Comparison of critical rate values obtained with the bottom water drive model with those obtained with an inadequate use of the lateral edge drive model shows that the last ones are about one half of the first ones for large D and x. This .5 factor comes from a simple comparison of the Dupuit parabolas and ellipses.

The values of critical rates obtained with the present model, as well as with the former ones, might appear rather small. After Muskat[1], critical flowrate has been characterized by the arrival of the first drop of water into the well, but production engineers will probably not notice it. This first drop of water does not mean a massive breakthrough.

More experience of production of horizontal wells in multiphasic reservoirs is needed to determine how conservative the present theory is in comparison with their actual behavior. The same need of evaluating the gap between theory and practice has been encountered with vertical wells. It was fulfilled by establishing correlations obtained in comparing theory and practice. A similar approach is proposed here for horizontal wells.

CONCLUSION

The major achievements of this theory are :

- The description of the oil water boundary by exact analytical equations for lateral edge drive, gas cap drive and bottom water drive.
- Reserves about a proper use of the lateral edge drive model with incompressible fluids.
- The best position of a horizontal well with respect to its productive rate for the gas cap drive model with a non active aquifer.
- the proof of a decreasing value of the critical flowrate with cumulative production for the bottom water drive mechanism and its expression.

Discussion on the validity of the theory and examples are provided, allowing its safe application.

All the results pertaining to the W.O.C. are applicable to gas cresting problems.

AKNOWLEDGEMENTS

The author thanks the Institut Français du Pétrole, HORWELL and the Société Nationale Elf Aquitaine for granting permission to publish this paper.

NOMENCLATURE

A = area

B = vertical distance of the well from the W.O.C. at the lateral boundaries

B_o = oil formation volume factor

c = shape parameter of the W.O.C.

D = lateral dimension of the reservoir block or spacing between horizontal wells

f = reciprocal of the velocity

g = gravity acceleration

h = distance of the summit of the water crest to the top of the reservoir

i = square root of -1

H = height of the water crest

k = permeability

L = length of the horizontal well

n = cumulative production

q = linear flowrate, or flow collected by the horizontal well per unit of length

S = saturation

t = time

u = oil flow

v = oil velocity

w = complex flow potential

x = abscissa

y = ordinate

z = complex coordinate

Greek

α = angle of the W.O.C. with the horizontal

β = twice the largest angle made by the W.O.C. with the horizontal

$\Delta\rho$ = difference of fluid densities $\rho_w - \rho_o$

ζ = complex coordinate

θ = parameter

μ = viscosity

ρ = density

τ = complex coordinate

ϕ = porosity

Φ = flow potential

Suscripts and superscripts

* designates dimensionless terms

c = critical

E' = of point E'

G' = of point G'

H = horizontal

o = oil

R = irreducible

S = swept by the W.O.C.

w = water

Fonctions

ln = Napierian logarithm

s = Dilogarithm [13] : $s(x) = \int_1^x \frac{\ln t}{1-t}\,dt$

ε = Fonction sign : $\varepsilon(x) = \frac{x}{|x|}$

REFERENCES

1. Muskat, M. : "The Flow of Homogeneous Fluids through Porous media", I.H.R.D.C., Boston, (1982). (First edition by Mc Graw-Hill 1937)

2. Kidder, R.E. : "Flow of immiscible fluids in porous media : exact solution of a free boundary problem", Journal of Applied Physics, vol. 27, 8 (August 1956).

3. Efros, D.A. : "Study of multiphase flows in porous media", Gastoptexizdat, Leningrad 1963 (in Russian).

4. Giger, F. : "Evaluation théorique de l'effet d'arête d'eau sur la production par puits horizontaux", Revue de l'Institut Français du Pétrole, Vol. 38, 3 (May-June 1983).

5. Giger, F.M., Reiss, L.H. and Jourdan, A.P. : "The Reservoir Engineering Aspects of Horizontal Drilling", SPE paper 13024, 1984 SPE Annual Technical Conference, Houston.

6. Dupuit, J. : "Etudes théoriques et Pratiques sur le Mouvement des eaux", 2nd Ed., Dunod, Paris (1863).

7. Forchheimer, Ph. : "Hydraulik Encyklopädie der Mathematischen Wissenschaften", 4.20. B.G. Teubner, Leipzig (1901-1908).

8. Hantush, M.S. : "On the validity of the Dupuit-Forchheimer well discharge formula", Journal of Geological Research, Vol. 67, 6 (June 1962).

9. De Wiest, R.J. : "History of the Dupuit-Forchheimer Assumptions on groundwater Hydraulics", Transactions of the ASAE (1965) p. 508.

10. Cailleau, Y., Chaumet, P., Jeanson, B., Van Quy, N. : "Etude Numérique et Expérimentale de l'"Edge Coning"", Revue de l'IFP, Special issue (1963).

11. Houpeurt, A. : "Eléments de mécanique des fluides dans les milieux poreux", Editions Technip, Paris (1975).

12. Laurentiev, M. and Chabat, B. : "Méthodes de la théorie des fonctions d'une variable complexe", Editions de Moscou, French translation : Editions Mir (1977).

13. Abramowitz, M. and Stegun, A. : "Handbook of mathematical fonctions", Dover publications, New York (1970).

APPENDIX A

THE HODOGRAPH METHOD OF CALCULATION

The hodograph method[1] has been applied to this problem by D.A. Efros[3]. A hodograph is a representation of a dynamic system in space of velocities; one point in the system has the components of its velocity vector for coordinates in this representation.

On the hodograph (Figure 9) the separation surface appears as a portion of a circle covered twice by the image of the moving point M.

Method of solving the problem

The aim of the calculations is to deduce the shape of the separation surface, i.e. the boundary of the fluid flow characterised by equation (3). The method consists in carrying out a series of conformal transformations* which make it possible to map the flow shown in Figure 1 which we are trying to identify with an initial flow which is completely known, particularly at its boundaries.

By introducing a complex potential w of the flow after rendering the variables dimensionless, the reciprocal f of the velocity can be expressed with the help of w in the flow area :

$$f = \frac{dz^*}{dw} \qquad (A1)$$

With the help of (3), the W.O.C. is represented by :

$$f = \frac{e^{i\alpha}}{\sin\alpha} \qquad (A2)$$

This latter expression characterises the boundary of the fluid flow considered in a simple manner as is shown by Figure 10 drawn in the plane of the variable f. The image of the point M which follows on the water-oil boundary on Figure 1, follows portions of the straight line Im(z) = +i on Figure 10, the images of the portions of a circle in Figure 9 by inversion of centre E.

The initial flow chosen is that created by an infinite horizontal well situated in the roof of a reservoir stratum bounded by two horizontal walls and only containing oil. Figure 11 represents a section of the reservoir perpendicular to the axis of the well. The stream lines parallel to the walls far from the well converge towards it at B.

In this plane, perpendicular to the axis of the well, the flow is represented by the equation (A3)

$$\frac{dw}{d\zeta} = -\frac{\pi}{2\,(c+\ln 2)} \cot\left(\frac{\pi i \zeta}{2}\right) \qquad (A3)$$

Carrying out the calculations

In view of the fact that Figures 9,10 and 11 are symmetrical with respect to the vertical axis, it is sufficient to consider only one half of each of them.

It is useful to introduce an intermediate variable τ defined in a quarter plane as shown in Figure 12.

We shall now define two conformal transformations of this quarter plane τ in Figure 12 towards the planes f and ζ respectively represented by Figures 10 and 11. For an explanation of the Schwartz-Christoffel method used, the reader may refer to reference (11), p. 108 or to reference (12), p. 159. Composing the transformations in accordance with the diagram below will supply a tranformation of the plane ζ towards the plane f :

$$\begin{tikzcd} & \tau \arrow[dl, "G"'] \arrow[dr, "F"] & \\ \zeta \arrow[rr, "F \circ G^{-1}"] & & f \end{tikzcd}$$

---

* A geometric transformation is called conformal if and only if all angles between intersecting curves remain unchanged.

$$G(\tau) = i\left(\frac{\arctan(\tau - 1)^{\frac{1}{2}}}{\pi/2} - 1\right) \qquad (A4)$$

$$(\tau) = -\frac{2i}{\pi}\arctan(\tau - 1)^{\frac{1}{2}} + c(\tau - 1)^{\frac{1}{2}} + 1 \qquad (A5)$$

Therefore :

$$FoG^{-1}(\zeta) = -\frac{2}{\pi}c\ i\tan\left(i\frac{\pi\zeta}{2}\right) - \zeta \qquad (A6)$$

The composition of F and the reciprocal of G gives the transformation of the plane τ (Figure 12) to the plane $f = dz^*/dw$ (Figure 10).

$$\frac{dz^*}{d\tau} = \frac{dz^*}{dw}\ \frac{dw}{d\tau} \qquad (A7)$$

We can establish the description of the W.O.C. in the physical space by integration and, bearing in mind the boundary conditions, we obtain :

$$z^* = \frac{c\zeta + \frac{\pi}{2}\int_0^{\zeta} it\ \mathrm{cotan}\left(\frac{\pi it}{2}\right)dt}{c + \ln 2} \qquad (A8)$$

Where z* is the space variable, complex and dimensionless, of the plane perpendicular to the axis of the well in which we studied the formation of the water crest. The conformal transformation written in (A8) solves the problem in mathematical terms because it establishes a correspondence between the physical planes of a well-known flow represented by Figure 11 and of the flow above the water crest, also known from now on (See Figure 1).

APPENDIX B

SHAPE OF THE W.O.C. FOR A GAS CAP DRIVE

The mathematical solution of this problem has been derived without any approximation by Y. Cailleau et al[10].

The method of resolution is exactly the same as for the lateral drive case. The shape of the oil water separation line has the following parametric expressions with θ as parameter :

$$x = \frac{B}{2} - \frac{B}{2\pi}\left[\theta + 2(q^*+1)\arctan\frac{\sin\theta\tan\frac{\beta}{2}}{\left[\left(\frac{q^*}{q^*+1}\right)^2 + \tan^2\frac{\beta}{2}\right]^{\frac{1}{2}} + \frac{q^*}{q^*+1} - \cos\theta\tan\frac{\beta}{2}} - 2q^*\arctan\frac{\sin\theta}{\mathrm{cotan}\frac{\beta}{4} - \cos\theta}\right] \qquad (B1)$$

$$y = \frac{\mu_o q}{2\pi\Delta\rho g k}\ln\left[\frac{1 - \sin\frac{\beta}{2}}{\left[\left(\frac{q^*}{q^*+1}\right)^2 + \tan^2\frac{\beta}{2}\right]^{\frac{1}{2}} - \tan\frac{\beta}{2}}\ \frac{\left[\left(\frac{q^*}{q^*+1}\right)^2 + \tan^2\frac{\beta}{2}\right]^{\frac{1}{2}} - \cos\theta\tan\frac{\beta}{2}}{1 - \cos\theta\sin\frac{\beta}{2}}\right] \qquad (B2)$$

Where the adimensional flow $q^* = \mu_o q/(\Delta\rho gkD)$.

The parameter θ is in the $(0,\pi)$ interval and the top of the W.O.C. is obtained for $\theta = \pi/2$. Examples of such shapes for $q^* = 0.25$ are shown in Figure 14.

β, twice the highest angle made by the W.O.C. with the horizontal is related with the adimensional vertical distance $B^* = 2B/D$ of the well from the W.O.C. at the lateral boundaries and the adimensional flow as follows :

$$B^* = \frac{2q^*}{\pi}\ln\left\{1 - \frac{\mathrm{cotan}\frac{\beta}{4} - \frac{\left[\left(\frac{q^*}{q^*+1}\right)^2 + \tan^2\frac{\beta}{2}\right]^{\frac{1}{2}} + \frac{q^*}{q^*+1}}{\tan\frac{\beta}{2}}}{\frac{\left[\left(\frac{q^*}{q^*+1}\right)^2 + \tan^2\frac{\beta}{2}\right]^{\frac{1}{2}} + \frac{q^*}{q^*+1}}{\tan\frac{\beta}{2}\ \tan\frac{\beta}{4}} - 1}\right\}$$

$$-\frac{1}{\pi}\ln\frac{\mathrm{cotan}\frac{\beta}{4} - \frac{\left[\left(\frac{q^*}{q^*+1}\right)^2 + \tan^2\frac{\beta}{2}\right]^{\frac{1}{2}} + \frac{q^*}{q^*+1}}{\tan\frac{\beta}{2}}}{\frac{\left[\left(\frac{q^*}{q^*+1}\right)^2 + \tan^2\frac{\beta}{2}\right]^{\frac{1}{2}} + \frac{q^*}{q^*+1}}{\tan\frac{\beta}{2}\ \tan\frac{\beta}{4}} - 1} \qquad (B3)$$

For each value of B*, an adimensional W.O.C. line may be drawn, knowing the value of β which is in the $(0,\pi)$ interval. The critical flow is obtained for $\beta = \pi$.

The top of the W.O.C. is horizontal except for the case of critical flow where it becomes sharp as for the lateral edge drive.

For $\beta = \pi$, one may check that the previous equations match with the derivations made by R.E. Kidder[2] for critical flow only (See Figure 14).

APPENDIX C

Development of a water crest in an oil column during production with a horizontal well.

HYPOTHESIS

- Horizontal well of infinite length : 2D problem
- Oil column with an impervious horizontal boundary at its top and an aquifer at its bottom
- Lateral tight boundaries
- Oil production with piston like sweeping by water under Muskat scheme
- Incompressible fluids

BASIC EQUATIONS

The horizontal flowrate u is supported by the vertical movement of the W.O.C. It tends towards zero at both the lateral boundaries.

$$|u| = \frac{q}{D} \left(|x| - \frac{D}{2} \right) \qquad \text{(C1)}$$

Allowing for the Dupuit-Forchheimer approximations, equations (1) and (2) yield :

$$\frac{dy}{dx} = \frac{\mu_o}{k_H \Delta\rho g} \frac{u}{y} \qquad \text{(C2)}$$

SHAPE OF THE W.O.C. WITH DUPUIT-FORCHHEIMER APPROXIMATION

Knowing the ordinate $y_{G'}$ of the W.O.C. at the lateral boundaries, the integration of equation (B2) gives the description of the W.O.C. at some distance from the well.

$$y^2 - y_{G'}^2 + \frac{\mu_o q}{k_H \Delta\rho g D} \left(\frac{D}{2} - |x| \right)^2 = 0 \qquad \text{(C3)}$$

The shape of the W.O.C. is made of two parts of ellipses.

SHAPE OF THE W.O.C. BELOW THE WELL

Below the well, the fit of one of these ellipses with a Dupuit parabola (Figure 13), described by equation (7), provides the value of the c parameter and a point E' with coordinates $0, y_{E'}$ of the Dupuit parabola.

$$c^2 = \pi^2 \left[\left[\frac{k_H \Delta\rho g}{\mu_o q} y_{G'} \right]^2 - \frac{k_H \Delta\rho g}{\mu_o q} \frac{D}{4} - \frac{1}{12} \right] \qquad \text{(C4)}$$

$$y_{E'} = - \frac{\mu_o q}{k_H \Delta\rho g} \left(\frac{c^2}{\pi^2} + \frac{1}{12} \right)^{½} \qquad \text{(C5)}$$

Therefore, using equation (6) :

$$h = \frac{\mu_o q}{k_H \Delta\rho g} \frac{c + \ln 2}{\pi} \qquad \text{(C6)}$$

The local shape of the W.O.C. below the well is now defined as c and h are known.

CRITICAL FLOWRATE

The critical flowrate is obtained for c = 0 :

$$q_c = \frac{3}{2} \frac{k_H \Delta\rho g}{\mu_o} D \left[\left[1 + \frac{16}{3} \frac{y_{G'}^2}{D^2} \right]^{½} - 1 \right] \qquad \text{(C7)}$$

The area A_{sc} swept by the W.O.C. is then :

$$A_{sc} = -D y_{G'_o} - \frac{\mu_o q_c}{k_H \Delta\rho g} \left[\frac{D}{4\sqrt{3}} + \left[\frac{k_H \Delta\rho g}{\mu_o q_c} \frac{D}{4} + \frac{1}{12} \right] \right.$$

$$\left. \left[\frac{\mu_o q_c D}{k_H \Delta\rho g} \right]^{½} \arccos \left[\frac{k_H \Delta\rho g}{\mu_o q_c} \frac{D}{48} + \frac{1}{144} \right]^{-½} \right] \qquad \text{(C8)}$$

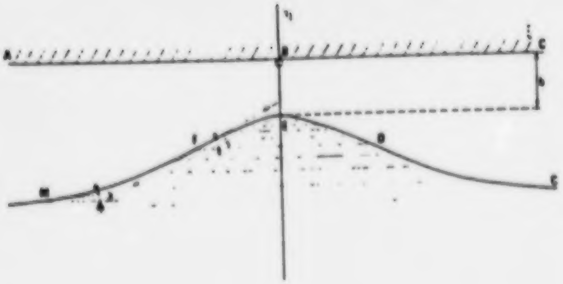

Fig. 1—Lateral edge drive.

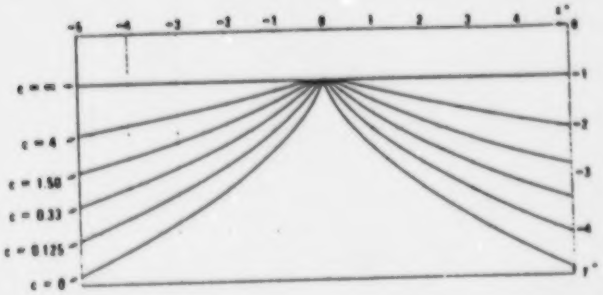

Fig. 2—Adimensional W.O.C. curves.

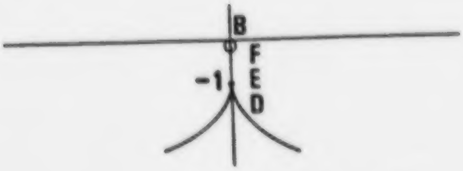

Fig. 3—Summit of W.O.C. at critical rate.

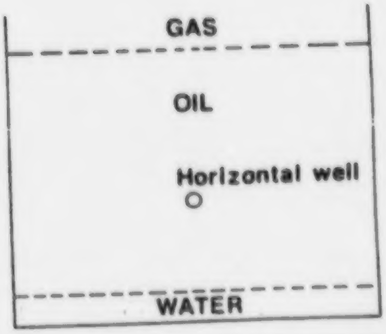
GAS
OIL
Horizontal well
WATER

Fig. 4—Gas-cap drive case before production.

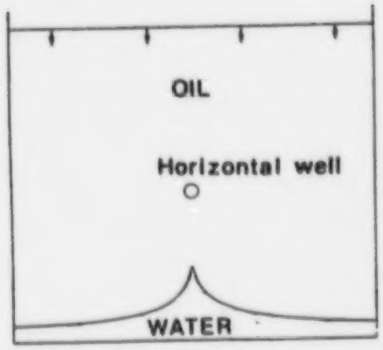
OIL
Horizontal well
WATER

Fig. 5—Gas-cap drive case during production.

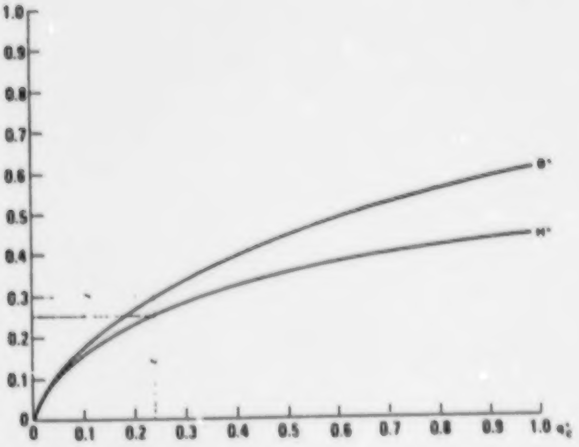

Fig. 6—Gas-cap drive graph.

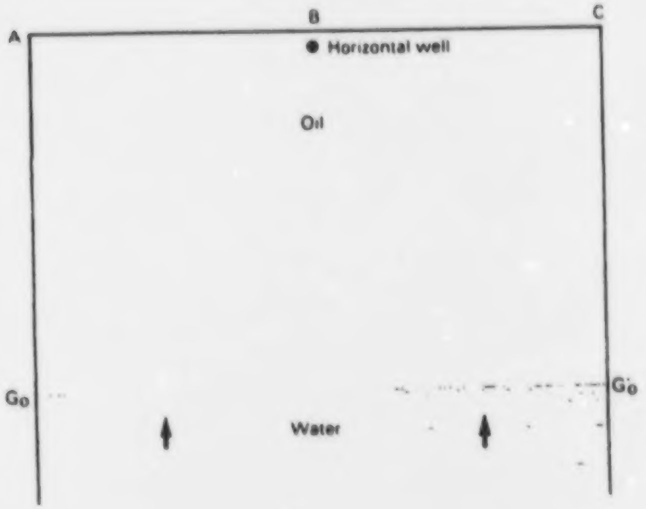
A
B
C
Horizontal well
Oil
G_o
G_o'
Water

Fig. 7—Bottomwater-drive case before production.

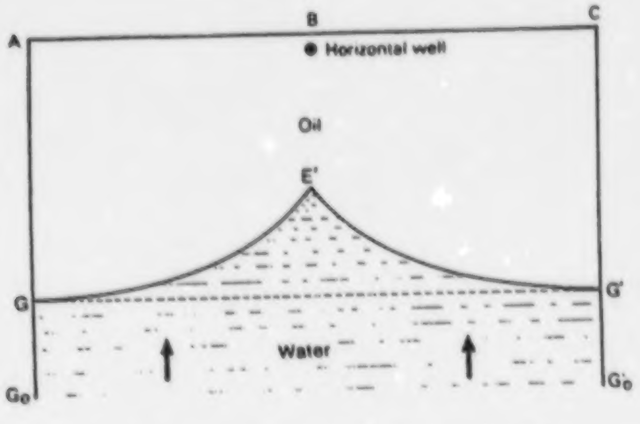
A
B
C
Horizontal well
Oil
E'
G
G'
Water
G₀
G'₀

Fig. 8—Bottomwater-drive case during production.

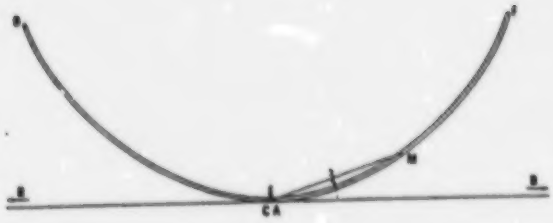

Fig. 9—Hodograph plane.

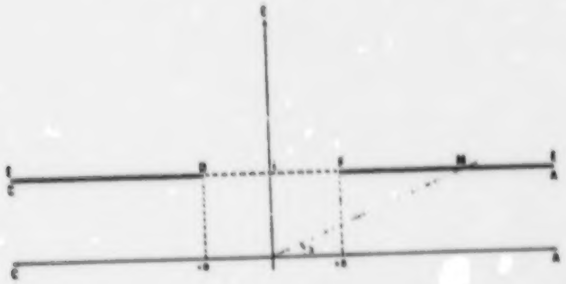

Fig. 10—Plane dz°/dw.

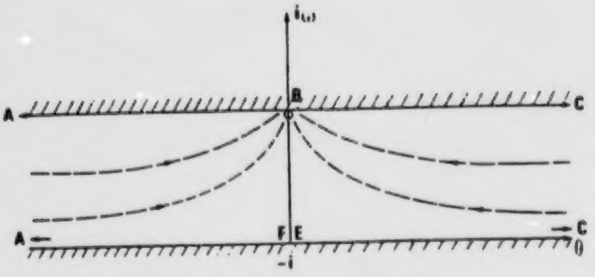

iω
A
B
C
A
F E
C
-i
0

Fig. 11—Initial flow in plane ζ.

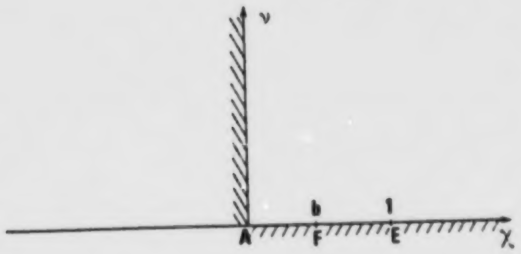

Fig. 12—Quarter plane τ.

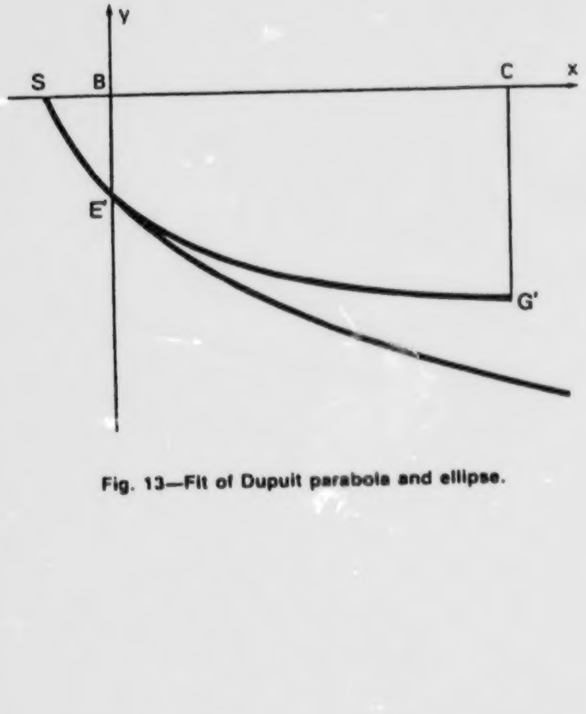

Fig. 13—Fit of Dupuit parabola and ellipse.

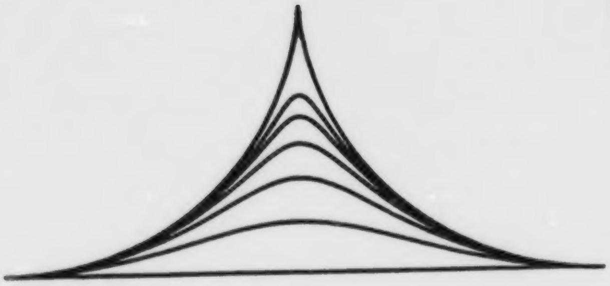

Fig. 14—W.O.C. shapes for the gas-cap drive case.

SPE
Society of Petroleum Engineers

(81)

SPE 15377

Theoretical Study of Coning Toward Horizontal and Vertical Wells in Anisotropic Formations: Subcritical and Critical Rates

by I. Chaperon, *TOTAL-CFP*
SPE Member

Copyright 1986, Society of Petroleum Engineers

This paper was prepared for presentation at the 61st Annual Technical Conference and Exhibition of the Society of Petroleum Engineers held in New Orleans, LA October 5-8, 1986

This paper was selected for presentation by an SPE Program Committee following review of information contained in an abstract submitted by the author(s). Contents of the paper, as presented, have not been reviewed by the Society of Petroleum Engineers and are subject to correction by the author(s). The material, as presented, does not necessarily reflect any position of the Society of Petroleum Engineers, its officers, or members. Papers presented at SPE meetings are subject to publication review by Editorial Committees of the Society of Petroleum Engineers. Permission to copy is restricted to an abstract of not more than 300 words. Illustrations may not be copied. The abstract should contain conspicuous acknowledgment of where and by whom the paper is presented. Write Publications Manager, SPE, P.O. Box 833836, Richardson, TX 75083-3836. Telex, 730989 SPEDAL.

ABSTRACT

Stable cones created by a horizontal well drilled with maximum clearance from the unwanted fluid are studied (Muskat[9] type approach, using pertinent viscous flow potential), yielding practical values for the critical rate per unit length of a horizontal well, and for the critical cone elevation, depending on both vertical and horizontal permeabilities, oil thickness, both fluid gravities, and oil viscosity. Critical rate weakly decreases when vertical permeability decreases.

The same type of analysis is repeated for a vertical well completed over a very short interval (modelized as a point source) also with maximum clearance from the gas cap or water table, yielding values of critical rate and cone height for the vertical well. In this case the critical rate slightly increases when vertical permeability decreases.

The outcome of a comparison between both types of wells shows that a critical cone comes closer to the horizontal well than to the vertical well. Also horizontal wells generally allow higher critical rates than vertical wells, however this advantage lessens with increased anisotropy. Very simple formulas are provided to evaluate what gain in critical rate may be obtained from a horizontal well.

INTRODUCTION

The use of horizontal wells to produce hydrocarbon reservoirs appears as a possible solution to some particular drainage problems such as isolated low productivity layers, the will of restricting coning phenomena and maintaining monophasic production. Also these may be a solution to environmental problems (highly deviated wells are enough, ending horizontal is not the key factor in this case). So far the best application of horizontal wells is the pilot development of a tight karstic formation with some high permeability fractures[1] that a horizontal well is likely to intercept (which is statistically almost impossible for a vertical wells), containing highly viscous oil in presence of a bottom water drive.

However, horizontal wells do not solve all problems, and even when one horizontal well produces twice more than a vertical one, is it worth the investment (and risk) as compared to two regular wells ? To answer this kind of question that a reservoir or production engineer is often faced with, it is necessary to study in details how oil flows towards a horizontal well as compared to a vertical well : changes in flow lines, influence of vertical and horizontal permeabilities, changes in viscous flow potential far from and close to the well. These detailed studies should provide simple formulas (and a guide to how and when to apply them) that anyone may use for evaluation purposes. Most reservoir engineering results of the french research group "FORHOR" have been gathered and presented in ref. 2, for practical use. Concerning coning, one ideal case only was published[3] but cannot be applied as such.

The scope of the present paper is to provide a simple and practical estimate of the critical rate to be expected from a horizontal well in realistic conditions (steady-state or pseudo-steady-state, anisotropic formation), and compare it to that of a vertical well to estimate a possible gain in rates. It concerns static stable cones or crests as illustrated by Fig. 1 but not diphasic production. Water cones (vertical wells) or crests (horizontal wells) follow the same equations as gas, except for the fact that they form below the wells instead of above. The descriptions hereafter concern oil flow in presence of a gas cap so as to avoid repetition of the reverse case of oil above water.

References and illustrations at end of paper

I. STABLE CRESTS CREATED BY HORIZONTAL WELLS

For simplicity the horizontal well is assumed to be located at the very bottom of the oil zone so as to minimize gas cresting. When end effects are neglected flow takes place in x - z planes, as shown on Fig. 2, so we study a cross section of the well, orthogonal to the well axis (2D analysis).

Derivations are made in the case of isotropic permeability first, results are then extended to the more general case of anisotropic formations, and the effect of anisotropy will be outlined.

. Isotropic permeability

In the reservoir, flow is essentially linear (in x direction, no vertical component of velocities), except very close to the well, where flow lines converge towards the well and flow geometry becomes radial (in x-z planes). Fig. 2. illustrates an immobile gas crest above a horizontal well.

The approach is identical to that used by Muskat[9] : Equilibrium conditions are stated first. This requires expression of viscous flow potential pertinent to the geometry of the flow created by a horizontal well. However, as in Muskat, the presence of the immobile crest which reduces the cross section (assumed constant for true linear flow) is not taken into consideration as such. Since the flow potential that we use does take radial flow convergence towards the line x = 0 and z = 0 (well) into account, the oil flow that would occur in the zone actually invaded by the immobile crest is negligible.

In the main derivation, steady-state potential is used. However the results may then be extended to a no flow boundary at X_e, using $X_A = X_e/2$ (See § IV and App. E).

Viscous oil flow potential of this 2D flow combining both radial flow close to the well and linear flow far aside (x>>h), is the same with or without a cone - see flow lines on fig. 2 - (Had we used linear flow potential only, as done by Dupuit[4], the restriction of flow cross section close to the well could not have been neglected. Dupuit's formula shows a rate per unit length proportional to H^2/X_A, and a parabolic shape of interface $h^2(x)=H^2x/X_A$. One of his assumptions is that vertical component of velocity is much less than horizontal (because drainage is by a long ditch and not by a horizontal well). This does not apply in our case).

The general form of flow potential was derived from a solution given by Houpeurt[5] for the case of an infinite row of vertical wells. When applied to 2D flow in vertical planes with no flow limits at z = 0 and h, towards a horizontal well located at z = 0 (very top or bottom of the layer, this gives (in Darcy units) :

$$\Phi(x,z) = \frac{Q\mu}{2\pi Lk}\, Log\left(ch\, \frac{\pi x}{h} - \cos \frac{\pi z}{h} \right) \tag{1}$$

Notice that the viscous potential has an analytical form which produces nearly radial flow when x/h → 0 and nearly linear flow when x/h → ∞ (or x → X_A). This expression describes flow in the whole layer, both close to and far from the well.

Considering potential difference between a point A on the interface far from the well, with coordinates (X_A, h) and S the apex of the cone with coordinates (O, Z_S) (See Fig. 2), the viscous flow potential difference must equal that of gravity potential difference so that static equilibrium be achieved.

This first equation gives a relationship between distance from the well to the apex of a crest in equilibrium, and the dimensionless corresponding rate (equation A.8 in Appendix A). It is illustrated on Fig.3.

Starting from a small cone ($Z_S/h = 1$), q_l^* increases as the cone extends further down and a maximum (q_l^* max or q_{lc}^*) is observed for a critical cone location Z_{Sc}. Cones extending lower than Z_{Sc} can be in equilibrium (with rates q_l^* less than q_{lc}^*), but these cones are unstable meaning that if a perturbation occurs they immediately accelerate towards the well.

Dynamic equilibrium requires an additional stability condition : buoyancy forces must be stronger than viscous forces so that in case of a perturbation, the cone does not accelerate towards the well but comes back to its equilibrium position. This provides a second equation (A-9).

Combining equilibrium and stability equations yields an implicit equation for Z_{Sc}, the critical cone location. Its solutions are tabulated on Table 1, together with the corresponding dimensionless critical rate. In practical units, for isotropic formations, rate per unit length in reservoir conditions is :

$$Q_{lc} = \frac{Q_c}{L} = 3.486\,10^{-5}\left(\frac{\Delta\rho\, k\, h}{\mu} \right) q_{lc}^{*} \left(\frac{X_A}{h} \right) \tag{2}$$

(Q_{lc} in $m^3/h/m$; ρ in g/cm^3 ; h in m ; k in mD ; μ in cp).

. Anisotropy

Except at the ends of the well, flow is bidimensional in x-z planes, therefore the change in variables to be used to convert an anisotropic case to isotropic form affects x and z coordinates only (this study being 2D, it does not concern end effects at all). The transformation is such that :

$$k_x \frac{\partial^2 P}{\partial x^2} + k_z \frac{\partial^2 P}{\partial z^2} = k' \left(\frac{\partial^2 P}{\partial x'^2} + \frac{\partial^2 P}{\partial z'^2} \right) \tag{3}$$

x, y, z should be principal permeability axes. This is most often the case for z, and it can be demonstrated that the well axis should be on the axis of minimum permeability (one of the principal axes) to maximize production.

Since the viscous potential has an analytical form which produces nearly radial flow when x/h → 0 and nearly linear flow when x/h → ∞ (or x → X_A), this unique change of variables will automatically work for the whole range of x (around the well, far aside from the well and any intermediate location aside from the well).

When k_h > k_v, the change invariables increases z dimensions and reduces x dimensions by a factor $(k_h/k_v)^{1/4}$ while y dimensions remain unchanged. The transformed system (x', z') behaves as isotropic, thus equation (2) does apply to x',z',k', ρ'. Coming back to actual coordinates gives the general expression for critical rate per unit length of a horizontal well in practical units.

$$\boxed{\frac{Q_c}{L} = 3.486\ 10^{-5}\Delta\rho\, h\, \frac{k_h}{\mu}\left(\frac{k_v}{k_h}\right)^{1/2} q^{*}_{lc}\left(\frac{X_A}{h}\left(\frac{k_v}{k_h}\right)^{1/2}\right)} \quad (4)$$

(Q_{lc} in $m^3/h/m$; ρ in g/cm^3 ; h in m ; k in mD ; μ in cp). Note that q_{lc}^* has to be evaluated for $\alpha=(X_A/h)(k_v/k_h)^{1/2}$. Its values are found from Table 1. q_{lc}^* is also plotted versus $\alpha=(X_A/h)(k_v/k_h)^{1/2}$ on fig.F4.

It may be noticed that the product $F = \alpha\, q_{lc}^*(\alpha)$ is fairly constant over a wide range of values of α. Thus we may also write Q_c (= L Q_{lc}), in the following way applicable only for $1 \le L/W \le 4$ - (see App. D) :

$$Q_c = 3.486\ 10^{-5}\frac{L}{X_A}(\Delta\rho\, h)\left(\frac{k_h h}{\mu}\right)F \quad (5)$$

with f = 4 for $(X_A/h)(k_v/k_h)^{1/2} < 6$. F increases slowly afterwards, reaches 5 when $(X_A/h)(k_v/k_h)^{1/2}$ reaches 20 (see Table 1).

When F = 4 we get the quick and simple estimate for critical rate of a horizontal well of length L (and W = L) :

$$Q_c = 1.4\ 10^{-4}\frac{L}{X_A}(\Delta\rho\, h)\frac{k_h h}{\mu} \quad (6)$$

(Q_{lc} in $m^3/h/m$; ρ in g/cm^3 ; h in m ; k in mD ; μ in cp). This latter form shows that when $(X_A/h)(k_v/k_h)^{1/2} < 6$ the critical rate of a horizontal well is quasi-independent of anistropy but quite sensitive to lateral boundaries (Q_c increases as $(X_A)^{-1}$). Main parameters are the same as in Dupuit's formula[4] ($Q/L - h^2/X_A$).

. Example :
Let us consider a horizontal well in an oil layer just below a gas cap (See parameters on Table 2).

When $k_h/k_v = 10$: $\alpha = (X_A/h)(k_v/k_h)^{1/2} = 13$.

from Table 1 or Fig. 4 one gets q_{lc}^* (α=13) = 0.3695 (or the value of function F : F = 4.80).

$Q_{lc} = 0.0078\ m^3/h/m$ of well.

Thus total critical rate is :

$Q_{ch} = L \times 0.0079\ m^3/h = 3.95\ m^3/h$.

Following is a table showing the effect of vertical permeability on horizontal well critical rate ($Q = L\ Q_l$; rates in reservoir conditions).

k_v/k_h	1	1/10	1/100
α	40	13	4
Z_{sc}/h	0.0434	0.1163	0.3053
q_{lc}^*	0.137	0.3695	1.040
F	5.48	4.80	4.16
Q_{lc}	0.0093	0.0079	0.0071
Q_c (m^3/h)	4.65	3.95	3.55

One observes that when vertical permeability decreases (k_h being kept constant), critical rate decreases and the critical cone stays further away from the well.

II. STABLE CONES CREATED BY VERTICAL WELLS

In this mathematical formulation, the vertical well is assumed to be completed on a very short interval at the bottom of the oil zone so as to minimize the risk of coning. The upper limit is represented by a no flow plane at z = h (initial gas oil contact) thus in the reservoir pseudo radial flow prevails except very close to the well where flow is hemispherical. Figure 5. illustrates an immobile gas cone above a vertical well. Reading it upside down shows the case of a water cone below a vertical well.

Again, derivations are made in the case of isotropic permeability for clarity first, the results are then extended to anisotropic formations providing general equations to evaluate critical rate.

a. Isotropic permeability

As in §I, one states equilibrium and stability conditions. So we first need an expression of viscous flow potential pertinent to this problem. One way of deriving it is to start from hemispherical flow towards a well (represented as a point source) located at the origin (x = y = z = 0) of a semi-infinite porous medium limited by a no flow plane (z = 0) representing the impermeable lower boundary in case of gas coning. Then since the other no flow limit at z = h (h << lateral extension of drainage area X_A) has to be accounted for because flow is restricted in a thin layer (and not hemispherical), one uses the method of image wells : an infinite row of point sources located as mirror images of the actual well interfere with it. Their location is illustrated on Fig. 6.

Thus viscous flow potential for oil flow within a limited layer of thickness h, towards a point well located at the bottom of the layer is Φ, a summation of all ψ created by the infinite series of image wells. It applies close to the well $r = r_w$ (where flow is nearly hemispherical) as well as far from the well ($r >> r_w$) (where flow is nearly radial).

This is a steady-state potential. However the following results apply to pseudo-steady-state (no flow limit at r_e) by using $r_A = 0.607\ r_e$) in equation 7 or 9. (See Discussions : § IV and App. E).

The equilibrium condition gives a relationship between rate and cone elevation (eq. B.5). This is illustrated on Fig. 7 where q^* is the dimensionless form of rate (same definition as eq. 7). Starting from a small cone (Z_S/h = 1) q^* increases as the cone extends further down and a maximum (q^* max or q^*_c) is observed for a critical cone height Z_{Sc}. Cones extending lower than Z_{Sc} can be in equilibrium (with rates q^* less than q_c^*), but these cones are unstable meaning that if a perturbation occurs they immediately accelerate towards the well.

Critical rate is the maximum possible rate. It also satisfies the stability condition. The order of magnitude for q_c^* is 1 (See App. B for calculation).

The numerical value of critical rate of a vertical well in practical units (Q_{lc} in $m^3/h/m$; ρ in g/cm^3 ; h in m ; k in mD ; μ in cp) for isotropic permeability is :

$$Q_c = 3.486\ 10^{-5}\ (kh/\mu)(\Delta\rho\, h)\, q_c^* \quad (7)$$

with $q_c^* = 1 \pm 25\,\%$, given by Table 3.

q_c^* is a weak function of radius r_A (which is usually not included in most used equations such as Bournazel[6]. This is because such formulas were derived from model experiments where r_A was fixed).

b. Anistropic permeability

Vertical permeability is usually lower than horizontal permeability (except in fractured formations). However after an adequate change in variables, the isotropic case solutions may be used in the anisotropic case. If x, y, z are the principal axes of permeability, as flow takes place in all three dimensions, the change in variables affects x, y, and z coordinates. This transform is not the same as for the horizontal well. Since the viscous flow potential has a unique analytical form which produces nearly hemispherical flow close to the well ($x, y, z \to 0$) and nearly radial flow far from the well (x, and $y \gg r_w$), the change in variables applies equaly to all regions of flow.

the tranformed (or ") system behaves as isotropic if :

$$k''\left(\frac{\partial^2 P}{\partial x''^2} + \frac{\partial^2 P}{\partial y''^2} + \frac{\partial^2 P}{\partial y''^2}\right) = k_x \frac{\partial P}{\partial x} + k_y \frac{\partial P}{\partial y} + k_z \frac{\partial P}{\partial z} \tag{8}$$

As equation (7) applies to isotropic media it may be written for the double prime system only. Coming then back to actual variables yields the equation for critical rate of a vertical well (of small penetration) in an anisotropic formation :

$$Q_c = 3.486\ 10^{-5}\left(\frac{k_h h}{\mu}\right)(\Delta\rho\, h)\, q_c^*\left(\left(\frac{r_A}{h}\right)\left(\frac{k_v}{k_h}\right)^{1/2}\right) \tag{9}$$

(Q_c in m^3/h ; k_n in mD ; h in m ; μ in cp ; ρ in g/cm^3).

$q_c^* = 1 \pm 25\,\%$ (see App. B and Table 3).

Anisotropy plays a role in the evaluation of q_c^*, which has to be calculated as a function of $\alpha = (r_A/h)(k_v/k_h)^{1/2}$. It has been found from this derivation that drainage radius does play a role in the value of critical rate, since anisotropy induces a change in variables. The tranformed dimensionless value of drainage radius (r_A/h) is $(r_A/h)(k_v/k_h)^{1/2}$.

. Example :

For the example described in Table 2 we have :

$$\left(\frac{k_v}{k_h}\right)^{1/2} = \sqrt{1}$$

$$\alpha = \left(\frac{r_A}{h}\right)\left(\frac{k_v}{k_h}\right)^{1/2} = 1.3$$

$$q_c^* = 0.8962 \quad , \quad \frac{Z_c}{h} = 0.37$$

Q_c = 1.48 m^3/h/day (res. conditions)

k_v/k_h = 1 and 1/100 would yield Q_c = 1.27 m^3/h and 2 m^3/h respectively (See Table 3). As opposed to horizontal wells, critical rate for vertical wells increases when vertical permeability drecreases. Bournazel formula[6] (for any k_v/k_h) gives Q_{cB} = 2.4 m^3/h (asymptotic approach on breakthrough time, experimental models).

III. GAIN IN CRITICAL RATES

The practical question which the reservoir engineer is usually asked is how much more will one get from a horizontal well ? Thus a simple indicator for gain in critical rates should be of practical use. Using equations (5) and (9) yields :

$$\frac{Q_{ch}}{Q_{cv}} = \frac{L}{X_A}\,\frac{F}{q_c^*} \tag{10}$$

Since $F = 4$ and $q_c^* = 1$ a quick order of magnitude for gain in critical rates is $4L/X_A$ (applies for L = W). For a more precise estimate, one should use the proper value of F (Table 1) and the proper value of q_c^* (Table 3).

It is also observed by comparing Figures 3 and 7 that critical cones or crests come closer to horizontal wells than to vertical wells.

. Example :

We consider the two vells of § I and § II (Table 2) in three cases of anisotropy, namely : $k_v = k_h$, $k_h/10$, and $k_h/100$.

Cone or crest apex location, critical rate of horizontal and 500m-long vertical wells, and their ratio are given below.

k_v/k_h	1	1/10	1/100
Z_{Sc}/h (hor) Z_{Sc}/h (vert) Q_{chor} (m^3/h) Q_{cvert} (m^3/h)	0.043 0.35 4.65 1.25	0.116 0.37 3.95 1.48	0.305 0.43 3.55 2.00
Q_{ch}/Q_{cv}	3.70	2.70	1.80

This comparison shows that horizontal well critical rate is less sensitive to anisotropy than vertical well is. The effects are in opposite ways, thus the ratio is finally rather sensitive to the degree of anisotropy.

IV. DISCUSSION :

Constant pressure versus no flow boundaries (steady-state and pseudo-steady-state).

This makes hardly any difference for a vertical well, however, the problem has to be studied in more details for horizontal wells.

. For a vertical well, one knows that the cone forms only locally, very close to the well and that at the actual drainage radius r_A the free interface is flat (at its initial location). Thus, there is no ambiguity for calculating h, it is easy to say that, at radius r_A, interface elevation is h. (initial oil thickness). Critical rates have been established (§ II) for true steady-state. They will apply just as well for pseudo-steady-state if one uses r_A in the critical rate calculation (with $r_A = 0.607\ r_e$, r_e being the distance from the well to the actual no flow boundary). With this trick, $(\Phi_A - \Phi_S)$ using steady-state viscous flow potential is equal to the actual ($\Phi_e - \Phi_g$) pseudo-steady-state viscous flow potential of the bounded system (See App. E). (However, since the only feed (so called "bottom drive") is from the fluid which is coning, one has to adjust h from time to time during the well life, using simple material balance, so that cumulative oil production be balanced by a rise of average water level, or by expansion of gas-cap hence lowering of average GOC level).

. For a horizontal well draining a realistic oil layer, the ideal solution shown by Efros[7] and Giger[3] cannot be used as such : they show that the interface is tilted with asymptotic parabolic shape (meaning that nowhere it tends to its initial shape, but instead, at some distance from the well, it drops lower than initial WOC, as low as infinity). Recent modifications attempt to extend this mathematical solution to more realistic cases[8].

The scope of the present paper is to provide a quick estimate of critical rates for practical cases. The derivations here have assumed steady-state flow from distance X_A (where interface elevation is h).

For the case of no flow at lateral boundary ($x = X_e$), which happens when drainage is achieved by several wells, or when the oil extension has some physical no flow boundaries, one could work again the derivation, replacing the steady-state potential by a pseudo-steady-state potential including a series of images wells located at $x_n = \pm 2\ n\ X_A$, $z_n = 0$. There is also a quicker way (slightly less precise though) : it is to notice that there is a value of X_A for which linear flow potential for steady-state has the same value as pseudo-steady-state linear flow potential at the actual no flow boundary X_e in the equations of viscous flow potential ($X_A = X_e/2$ see App. E).Thus we still write that at boundary $x = X_e$ and $z = h$, viscous flow potential balances that of gravity. Thus h is the actual interface elevation at the no flow boundary, and equations 2, 4 5 and 6 apply, provided one uses $X_A = X_e/2$.

(Also during the life of the well h will need to be adjusted from time to time for vertical quasi-static elevation of WOC or lowering of GOC that may be estimated from material balance).

SUMMARY

Critical rates of horizontal and vertical wells :
(Q_{lc} in $m^3/h/m$; ρ in g/cm^3 ; h in m ; k in mD ; μ in cp).

. Steady-state :

$$Q_{ch} = \beta \frac{L}{X_A} F(\alpha) \quad \textit{with } F(\alpha) \textit{ from Table 1} \tag{11)or}$$

$$Q_{ch} = 4\beta \frac{L}{X_A} \quad \textit{for} \quad 1 \le \alpha \le 13 \tag{12}$$

$$Q_{cv} = \beta q_c^*(\alpha) \quad \textit{with } q_c^*(\alpha) \textit{ from Table 3} \tag{13)or}$$

Q_c [illegible] $\beta(1 + 2.5$ [illegible] for $1 \le \alpha \le 40$ (14)

Gain [illegible] $4L/X_A$ for $1 \le \alpha \le 1$[illegible] (15)

$$\alpha = \left(\frac{X_A}{h}\right)\left(\frac{k_v}{k_h}\right)^{1/2} \ (hor) \quad or \quad \alpha = \left(\frac{r_A}{h}\right)\left(\frac{k_v}{k_h}\right)^{1/2} \ (vert) \tag{16}$$

$$\beta = 3.486\ 10^{-5} (\Delta\rho\ h) \left(\frac{k_h h}{\mu}\right) \tag{17}$$

. Pseudo-steady-state : (no flow boundary at $x = X_e$ or $r = r_e$) :
replace X_A by $X_e/2$ and r_A by 0.607 r_e in above equations .
. Remindal : these equations are derived from a 2D study, therefore they apply when W < 4L only.

CONCLUSIONS

A simple equation is provided to estimate critical rate of horizontal wells in anisotropic formations. It shows that critical rate per unit length increases as horizontal transmissivity of the layer (k_h h/μ) and initial oil thickness (h), and decreases as well-to-lateral-boundary distance. The actual value of vertical permeability has very little influence on rate ; increased k_v weakly increases critical rate and keeps the critical crest further away from the well.

An estimate of critical rate of a vertical well in an anisotropic formation - including the influence of distance between well and boundary - is also derived, which is more sensitive to anisotropy : critical rate slightly increases when vertical permeability decreases, but critical cone elevation does not change significantly.

It is observed that critical cones come usually closer to horizontal wells than to vertical wells.

The outcome of a critical rate comparison is that horizontal wells may allow higher critical rates than vertical wells, but this advantage lessens when vertical permeability decreases.

Therefore the actual gain in critical rate to expect from a horizontal well should be estimated carefully from key parameters (L and X_A ; k_v/k_h and r_A to a lesser degree).

ACKNOWLEDGEMENTS

The author wishes to thank Mr THOMERE, Head of Reservoir Engineering Departement in TOTAL CFP for his advice and his permission to publish this paper.
She also acknowledges M.M. REISS and KARCHER from ELF-ALQUITAINE, and M.M. COMBE and GIGER from IFP for forum type discussions.

REFERENCES

1. L. H. REISS, A. P. L. JOURDAN, F.M. GIGER and P. A. ARMESSEN : "Offshore and Onshore European Horizontal Wells", OTC 4791, presented at the 16th Annual OTC in Houston, Texas, May 7 - 9, 1984.

2. B. KARCHER, F. GIGER, J. COMBE : "Some Practical Formulas to Predict Horizontal Wells behaviour", SPE 15430, to be presented at the 61st SPE fall meeting in New Orleans, Louisiana, october 5 - 8, 1986.

3. F. GIGER : "Evaluation théorique de l'effet d'arrête d'eau sur la production par puits horizontaux" (Theoretical study of water cresting effect on production by horizontal wells). *Revue de l'Institut Français du Pétrole* vol. 38 n° 3, Mai - Juin 1983. (English translation available at the Alberta Oil Sands Information Center, Edmonton, Alta, CANADA, ref 1769.)

4. J. DUPUIT : *Etudes théoriques et pratiques sur le mouvement des eaux.* Dunod - Paris 1863. (Theoretical and Practical studies on underground water movement).

5. A. HOUPEURT : *Elements de mécanique des fluides dans les milieux poreux* (Elements of fluid mechanics in porous media). Editions Technip, Paris, 1975.

6. BOURNAZEL and B. JEANSON : "Fast Water Coning Evaluation Method". SPE 3628, presented at 46th SPE fall meeting - 1971.

7. D. A. EFROS : "*Study of Multiphase Flows in Porous Media*". Gastoptexizdat, Leningrad, 1963.

8. F. GIGER : "Analitic 2D Models of Water Cresting Before Breakthrough for Horizontal Wells". Paper SPE 15378, to be presented at the 61st SPE fall meeting in New Orleans, Louisiana, October 5 - 8, 1986.

9. M. MUSKAT : *The Flow of Homogenous Fluids Through Porous Media.* Reprinted by I.H.R.D.C., Boston (1982).

10. I. W. AMYX, D. BASS, and R. L. WHITING : *Petroleum Reservoir Engineering Physical Properties.* Mc GRAW HILL, N. Y., 1960.

NOMENCLATURE

ch : hyperbolic cosine (ch (x) = $(e^{x} + e^{-x})/2$)
cos : trigonometric cosine (cos(0) = cos (π) = 1)
F : dimensionless function : F = $\alpha\, q_{cl}^{*}(\alpha)$
g : gravity constant
g/cm^3 : gram per cubic centimeter (1 g/cm^3 = 62.43 lb/cuft)
h : initial oil thickness (or interface elevation at X_A or (r_A) - (see also m^3/h)
h(x) : interface elevation at abscissa x in Dupuit formula
H : interface elevation at r_A in Dupuit formula (H = h(r_A))
k : permeability to oil
L : horizontal well length
Log : base e logarithm (Log (e) = 1)
m : meters (1 m = 3.28 ft)
m^3/h : cubic meters per hour (1m^3/h = 151 BOPD)
P : pressure
Q : actual oil rate (m^3/h) in reservoir conditions
r : radial distance from vertical well
r_A : drainage radius for steady-state(where interface elevation is h) or r_A = 0.607 r_e, by definition, for pseudo-steady-state
r_e : location of actual no flow boundary for pseudo-steady-state
sh : hyperbolic sine (sh(x) = $(e^{x} - e^{-x})/2$)
W : length (in y dimension) of drainage volume for a horizontal well (should be less than 4 L)
x, X : abscissa (aside from the horizontal well
X_A : location of a constant pressure boundary or abscissa where interface level is known to be h, for steady-state flow. In the pseudo-steady-state case, by definition : $X_A = 0.5\ X_e$
X_e : location of an actual no flow boundary (where interface level is h)
y : coordinate along horizontal well axis
z, Z : coordinate along vertical axis (well is at z=0)
Z_S : well to cone apex distance
α : dimensionless proup : $\alpha = (x_A/h)(k_v/k_h)^{1/2}$ for horizontal wells, or $\alpha = (r_A/h)(k_v/k_h)^{1/2}$) for vertical wells
β : 3.486 10^{-5} ($\Delta\rho$ h) (k_h h/μ) m^3/h
Δ : difference
Ψ : hemispherical viscous flow potential
Φ : actual viscous flow potential, or gravity potential
μ : oil viscosity
π : constant = 3.1415...
ρ : density

__Subscripts__ :

B : from Bournazel formula
c : critical
h : in horizontal direction (permeability) ; or for horizontal well (rates)
l : per unit length of horizontal well
S : at cone or crest apex
v : in vertical direction (k_v) ; or for vertical well
x : in x direction (permeability)
y : in y direction (permeability)
z : in z direction (permeability)

__Superscripts__ :

* : dimensionless
' : transformed variables (2D flow changed to isotropic)
" : transformed variables (3D flow changed to isotropic)

APPENDIX A
ANALYSIS OF STABLE CONES CREATED BY HORIZONTAL WELLS

a. __Isotropic formation__

. Flow potential

A well sitting close to the bottom of a layer of thickness h (case a) is equivalent to a well of double rate in the middle of a double thickness layer (case b).

The flow potential for case (b) is in the shape of A Log (ch ax - cos by) (which is a close form for an infinite sum of image wells)^5. Constants are chosen so that diffusivity equation be satisfied (eq. A.1), that planes z = 0 and z = h be no flow boundaries (eq. A.2), and Darcy law be satisfied at the well (eq. A.3).

(Equations A.1 to A.11 are either in Darcy units, or dimensionless).

$$\frac{\partial^2\Phi}{\partial x^2} + \frac{\partial^2\Phi}{\partial z^2} = 0 \qquad (A.1)$$

$$\frac{\partial \Phi}{\partial z} = 0 \quad for \quad z = 0 \quad and \quad z = h \tag{A.2}$$

$$\frac{Q}{\pi r L} = - \frac{k}{\mu} \overrightarrow{grad}\, \Phi \quad when \quad (x,y) \rightarrow (r,w) \tag{A.3}$$

$$\Phi(x,z) = \frac{Q\mu}{2\pi L k} Log\left(ch \frac{\pi x}{h} - cos \frac{\pi z}{h}\right) \tag{A.4}$$

The potential in equation A.4 satisfies equations A.1 to A.3. Using this close form of potential, the same kind of analysis is applied to stable cones around a horizontal well as was done by Muskat[9] in the case of vertical wells.

Considering potential difference between a point A on the interface far from the well, with coordinates (X_A, h) and S the apex of the cone with coordinates (O, Z_S) as illustrated on Fig. 2, the potential difference may be expressed by equation A.5 (viscous flow potential) or A.6 (gravity potential), static equilibrium being achieved when A.5 = A.6.

$$\Phi_A - \Phi_S = \frac{Q\mu}{2\pi L k} Log\left(\frac{1 + ch \frac{\pi X_A}{h}}{1 - cos \frac{\pi Z_S}{h}}\right) \tag{A.5}$$

$$\Phi_A - \Phi_S = \Delta\rho\, g(h - Z_S) \tag{A.6}$$

therefore the rate per unit length corresponding to a static cone at height Z_S is :

$$Q_l = \frac{Q}{L} = \Delta\rho\, g\, h \frac{k}{\mu} q_l^{*} \tag{A.7}$$

where q_l^{*} the dimensionless rate per unit length satisfies equation A.8 :

$$q_l^{*} = \frac{2\pi\left(1 - \frac{Z_S}{h}\right)}{Log\left(\frac{1 + ch \frac{\pi X_A}{h}}{1 - cos \frac{\pi Z_S}{h}}\right)} \tag{A.8}$$

Its solutions are shown on Fig. 3.

In addition, we require a stable equilibrium.
The limit of stability is given by equation A.9 :

$$\Delta\rho\, g = \frac{Q\mu}{L k h} \frac{sin \frac{\pi Z_S}{h}}{1 - cos \frac{\pi Z_S}{h}} \tag{A.9}$$

Combining A.5, A.6 and A.9 yields an implicit equation for Z_{Sc}, the critical cone height :

$$\left(1 - \frac{Z_{Sc}}{h}\right) = \frac{1 - cos \frac{\pi Z_{Sc}}{h}}{sin \frac{\pi Z_{Sc}}{h}} \; Log\left(\frac{ch \frac{\pi X_A}{h} + 1}{1 - cos \frac{\pi Z_{Sc}}{h}}\right) \tag{A.10}$$

Critical rate is also the maximum rate, it corresponds to equation A.8, written for critical value of Z_S, i.e. Z_{Sc}, the solution of implicit equation A.10.

The critical rate in dimensionless form may thus be written in a simpler way :

$$q_{lc}^{*} = 2 \frac{1 - cos \frac{\pi Z_{Sc}}{h}}{sin \frac{\pi Z_{Sc}}{h}} \tag{A.11}$$

The implicit equation A.10 has been solved for various values of X_A/h. Critical cone heights and dimensionless rates are reported in table 1 and Fig. 4.

In practical units, the value of critical rate per unit length in reservoir conditions is given by equation A.12 (a or b).

$$Q_{lc} = \frac{Q_c}{L} = 3.486\, 10^{-5}\left(\frac{\Delta\rho\, k\, h}{\mu}\right) 2 \frac{1 - cos \frac{\pi Z_{Sc}}{h}}{sin \frac{\pi Z_{Sc}}{h}} \tag{A.12.a}$$

$$Q_{lc} = \frac{Q_c}{L} = 3.486\, 10^{-5}\left(\frac{\Delta\rho\, k\, h}{\mu}\right) q_{lc}^{*}\left(\frac{X_A}{h}\right) \tag{A.12.b}$$

where q_{lc}^{*} and Z_{Sc}/h are functions of X_A/h tabulated in table 1 and plotted on Fig. 4 (Q_l = $m^3/h/m$; $\Delta\rho$ = g/cm^3 ; h : m ; k : mD ; μ : cp).

b. Anisotropy

Except at the ends of the well, flow is bidimensional in x-z planes, therefore the change in variables to be used to convert an anisotropic case to isotropic form affects x and z coordinates only.

$$a = \frac{k_h}{k_v} = \frac{k_x}{k_z} \tag{A.13}$$

$$k' = (k_x k_z)^{\frac{1}{2}} = k_h\, a^{-\frac{1}{2}} \tag{A.14}$$

$$x' = x\left(\frac{k'}{k_x}\right)^{\frac{1}{2}} = x\, a^{-\frac{1}{4}} \tag{A.15}$$

$$z' = z\left(\frac{k'}{k_z}\right)^{\frac{1}{2}} = z\, a^{-\frac{1}{4}} \tag{A.16}$$

$$\mu' = \mu\, a^{-\frac{1}{4}} \tag{A.17}$$

Equations A.14 to A.16 allow transformation of the diffusivity equation into isotropic form :

$$\frac{\partial^2 \Phi}{\partial x'^2} + \frac{\partial^2 \Phi}{\partial z'^2} = 0 \tag{A.18}$$

Equation A.17 is necessary to keep gravity forces unchanged.

Rate is invariant in this change of coordinates, so is L (y dimension). Equation A.12b holds in the prime system only :

$$Q_{lc} = \frac{Q_c}{L} = (\Delta\rho g h)'\left(\frac{k'}{\mu}\right)q^*_{lc}\left(\frac{X'_A}{h'}\right) \quad (A.19)$$

$$(\Delta\rho g h)' = \Delta\rho g h \quad (A.20)$$

$$k' = k_h\, a^{-\frac{1}{2}} \quad (A.21)$$

$$\frac{X'_A}{h'} = \left(\frac{X_A}{h}\right)a^{-\frac{1}{2}} \quad (A.22)$$

Therefore the general equation for critical rate (reservoir conditions) in practical units is the following :

$$\frac{Q_c}{L} = 3.486\ 10^{-5}\,\Delta\rho\, h\,\frac{k_h}{\mu}\left(\frac{k_v}{k_h}\right)^{1/2} q^*_{lc}\left(\frac{X_A}{h}\left(\frac{k_v}{k_h}\right)^{1/2}\right) \quad (A.23)$$

(Q/L : m^3/h/m ; $\Delta\rho$: g/cm^3, h : m ; k_h : mD)

q_{lc}^* is a function of α. Numerical values are tabulated (Table 1) and plotted Fig. 4 together with the product F = $\alpha\, q_l^*(\alpha)$ with $\alpha = (X_A/h)\,(k_v/k_h)^{1/2}$.

Since F is nearly constant (F = 4 for α = 1, + 4 % at α = 4 ; + 10 % at α = 6 ; + 20 % at α = 13 ; + 37 % at α = 40), the following expression outlines the important parameters better :

$$\boxed{Q_C = 3.486\ 10^{-5}\,(\Delta\rho\, h)\left(\frac{k_h\, h}{\mu}\right)\frac{L.F}{X_A}} \quad (A.24)$$

(F = 4 see Table 1 or Fig. 4)

APPENDIX B
ANALYSIS OF STABLE CONES CREATED BY A VERTICAL WELL

The well has a low penetration ratio (hp << h) and maximum clearance (well touches the impermeable boundary). Thus it is represented as a point source.

a. Isotropic formation

The flow potential corresponding to hemispherical flow induced by a point source located at the origin of a semi-infinite porous medium, limited by a no flow plane at z = 0 is :

$$\varphi(M) = \frac{Q\mu}{2\pi k}\left(-\frac{1}{r}\right) \quad (B.1)$$

where r is the distance between the well point z = 0, x = y = 0 and any point M.

However in the case of a limited oil column of thickness h, the no - flow boundary (z = h) may be accounted for by the method of images. The image well locations are $z_n = \pm 2\,n\,h$, $x_n = 0$ (Fig. 6).

The viscous flow potential for oil flow within a limited layer of thickness h, towards a point well located at the bottom of the layer is Φ a summation of all φ's created by the infinite series of image wells. It applies close to the well ($r = r_w$, where flow is nearly hemispherical) as well as far from the well ($r >> r_w$, where flow is nearly radial). If we consider a point A, far from the well on the gas oil interface with coordinates (r_A, h), and S the apex of a gas cone in equilibrium with coordinates (o, Z_S) above a vertical well producing at rate Q (reservoir conditions), the potential difference may be expressed as follows :

$$\Phi_A - \Phi_S = \frac{Q\mu}{2\pi k}\sum_{n=-\infty}^{+\infty}\left|\frac{1}{|Z_S + 2nh|} - \frac{1}{\left(r_A^2 + (Z_S + 2nh)^2\right)^{1/2}}\right| \quad (B.2)$$

The infinite sum in equation B.2 does converge rapidly because each term is equivalent to $1/(2n)^2$. Σ has been evaluated with 20 images for practical purposes.

Potential of gravity forces :

$$\Phi_A - \Phi_S = \Delta\rho\, g\,(h - Z_S) \quad (B.3)$$

Equilibrium condition : (B.2 = B.3)

$$\Delta\rho\, g\, h\left(1 - \frac{Z_S}{h}\right) = \left(\frac{Q\mu}{2\pi k h}\right)\Sigma$$

with

$$\Sigma = \sum_{n=-\infty}^{+\infty}\frac{1}{|Z_S + 2nh|} - \frac{1}{\left|r_A^2 + (Z_S + 2nh)^2\right|^{1/2}} \quad (B.4)$$

Thus a cone in equilibrium at elevation Z_S corresponds to one rate Q (Z_S) as precised by equation B.5.

$$Q = \frac{1}{\Sigma}\,\frac{k\,h}{\mu}\,(\Delta\rho\, g\, h)\,2\pi\left(1 - \frac{Z_S}{h}\right) \quad (B.5)$$

Equations B.5 and B.6 define dimensionless rate q^*, Σ is given in equation B.4.

$$q^* = 2\pi\left(1 - \frac{Z_S}{h}\right)/\Sigma \quad (B.6)$$

In addition to static equilibrium, dynamic equilibrium should be achieved, meaning that if a perturbation of the interface occurs, buoyancy will be stronger than viscous forces.

Stability condition may be stated as follows :

$$\Delta\rho\, g \geq \frac{d}{dZ_S}(\Phi_A - \Phi_S) \quad (B.7)$$

The maximum and critical rate corresponds to an = sign in B.7. q^*, the dimensionless oil rate, is plotted versus cone height on Fig.7, corresponding to equation B.6. q^* max or q^*_c is observed for a critical cone height Z_{Sc} solved in next §..

Equations B.1 through B.7 are in Darcy units, equation B.6 is dimensionless.

Numerical values for critical rate (reservoir conditions) may be obtained as follows :

$$Q_c = 3.486\ 10^{-5}\left(\frac{k\,h}{\mu}\right)(\Delta\rho\, h)\, q_c^* \quad (B.8)$$

with the following units :

Q m^3/h , k mD , h m , μ cp , $\Delta\rho$ g/cm^3

b. Anisotropic permeability

If x, y, z are the principal axes of permeability, as flow takes place in all three dimensions, the following variables should be used :

$$a = \frac{k_h}{k_v} = \frac{k_x}{k_z} = \frac{k_y}{k_z} \qquad \text{(B.9)}$$

$$k'' = (k_x k_y k_z)^{1/3} = k_x a^{-1/3} = k_h a^{-1/3} \qquad \text{(B.10)}$$

$$x'' = x\left(\frac{k''}{k_x}\right)^{1/2} = a^{-1/6} \qquad \text{(B.11)}$$

$$y'' = y\left(\frac{k''}{k_y}\right)^{1/2} = y\, a^{-1/6} \qquad \text{(B.12)}$$

$$z'' = z\left(\frac{k''}{k_z}\right)^{1/2} = z\, a^{1/3} \qquad \text{(B.13)}$$

$$(\Delta\rho\, g)'' = (\Delta\rho\, g)\left(\frac{z}{z''}\right) = \Delta\rho\, g\, a^{-1/3} \qquad \text{(B.14)}$$

Equations B.10 to B.13 allow the diffusivity equation to be identical to the isotropic case, and equation B.14 is necessary for gravity forces to remain unchanged. (Here, one has assumed $k_x = k_y$. However one may use : $a = k_x/k_z$, $b = k_y/k_z$, and the definitions remain the same (first parts of equations B.10 to B.14)).

With these changes, Q is invariant. Equation B.8 applies in the double prime system of coordinates only :

$$Q = 3.486\ 10^{-5}\,(k''\,h'')\,(\Delta\rho\, g\, h)''\, q_c^*\left(\frac{r''_A}{h''}\right) \qquad \text{(B.15)}$$

$k''h'' = k_h\, h$ (from equations B.10 and B.13)
$(\Delta\rho\, g\, h)'' = \Delta\rho\, g\, h$ (from equations B.13 and B.14)
$r''_A/h'' = (r_A/h)\,(k_v/k_h)^{1/2}$ (from equations B.11 to B.13)

So the general equation for critical rate in reservoir conditions is the following

$$Q_c = 3.486\ 10^{-5}\left(\frac{k_h\, h}{\mu}\right)(\Delta\rho\, h)\, q_c^*\left(\left(\frac{r_A}{h}\right)\left(\frac{k_v}{k_h}\right)^{1/2}\right) \qquad \text{(B.16)}$$

(Q is in m^3/h, k_h in mD, h in m, μ in cp, ρ in g/cm^3).

q_c^* is a function of $a = (r_A/h)\,(k_v/k_h)^{1/2}$, this is the only place where anisotropy plays a role. q_c^* function (together with critical cone locations) is shown on Table 3. Other cases may be calculated from equations B.2 to B.15, using the appropriate expression of Σ.

APPENDIX C

Pressure loss in the well itself

As critical rates are very low they correspond to low pressure drops in the reservoir. Therefore it is necessary to check whether pressure loss along the well length may be neglected, so that each unit length of well behave the same (except both ends because of end effects when well length is less than drainage length).

For laminar flow, a pipe of inner diameter r behaves as a medium of permeability $k = 12.5\ 10^6\ r^6$ (k in Darcy, r in cm) (analogy between Poiseuille's[10] and Darcy's equations. Flow takes place in vertical planes, and each unit length of well collects the same influx, thus the total rate flowing in the well (or pipe) is :

$$Q(x) = \left(\frac{Q}{L}\right) x \qquad \text{(C.1)}$$

From Darcy law :

$$dp = \left(\frac{Q}{L}\right) \mu x\, dx/kA = \left(\frac{Q}{L}\right) \mu x\, dx/12.5\ 10^6\, \pi r^4 \qquad \text{(C.2)}$$

Integrating from x = L to 0

$$\Delta P = \frac{\frac{Q}{L}\,\mu\,\frac{L^2}{2}}{12.5\ 10^6\, \pi r^4} \qquad \text{(C.3)}$$

$$\Delta P = 3.6\ 10^{-5}\ atm \quad for\ \ L = 500\ m \qquad \text{(C.4)}$$

The order of magnitude of drawdown in the formation being around one atmosphere at critical rate, the pressure losses for laminar flow may be considered as negligible.

APPENDIX D

Total rate versus rate per unit length of horizontal well.

a. No flow planes at y = 0 and y = L (L = well length)
This happens when the well is really extending between two parallel sealing faults, or fully crosses a narrow channel, or when the wells are drilled in a line with barely any space between each other (on y axis).

In these cases, total rate is rate per unit length (Q_l or Q/L) derived in this paper, times actual well length L.

b. Y dimension of drainage volume (W) somewhat larger than well length ($1 \le W/L \le 4$)
In this case, far from the ends, flow is the same as case (a). However rate per unit length increases close to the ends. Radial flow towards both ends of the well occurs.

It has been observed (by 3D simulations of monophasic flow towards a horizontal well which does not reach the boundaries of the drainage volume) that the total rate range lies between LQ_l and $1.25\ L\ Q_l$ when $W < 2\, a^{1/4}\, L$ (i.e. W < 4L when $a = k_h/k_v = 10$).

This range should not be significantly changed when coning is concerned.

Thus to keep calculations simple, one uses $Q = L\ Q_l$, throughout this paper, knowing that this may be an understatement, but within the accuracy of the practical estimates that are presented in this paper.

c. Well length is much less than interwell distance (in Y direction).
In this case, flow is essentially radial and the gain in total rate (linear + radial as compared to radial only) should be studied by 3D analytical or numerical studies. Also in this case, productivity index formulas derived from a 2D analysis cannot apply.

APPENDIX E :
STEADY-STATE AND PSEUDO-STEADY-STATE

a. Vertical well :
Steady-state between radii r and r_w (radial flow)

$$\frac{\partial^2 P}{\partial x^2} + \frac{\partial^2 P}{\partial y^2} = 0 \tag{E.1}$$

$$\left| P(r) - P(r_w) \right|_{SS} = c \, ln \left(\frac{r}{r_w} \right) \tag{E.2}$$

Pseudo-steady-state : no flow accross boundary $r = r_e$. $(\partial P/\partial r) = 0$ at r_e

$$\frac{\partial^2 P}{\partial x^2} + \frac{\partial^2 P}{\partial y^2} = - c \tag{E.3}$$

$$\left| P(r_e) - P(r_w) \right|_{SS} = c \left(ln \frac{r_e}{r_w} - \frac{r_e^2 - r_w^2}{2 r_e^2} \right) \tag{E.4}$$

Pseudo-steady-state potential at r_e equals steady-state potential at r if :

$$ln \frac{r}{r_w} = ln \frac{r_e}{r_w} - \frac{1}{2} \tag{E.5}$$

This is satisfied for one value of r only, that we name r_A :

$$r_A = 0.607 \, r_e \tag{E.6}$$

b. Horizontal well
Steady-state linear flow :

$$\frac{\partial^2 P}{\partial x^2} = 0 \tag{E.7}$$

$$\left| P(x) - P(X_o) \right|_{SS} = A \, (x - X_o) \tag{E.8}$$

Pseudo-steady-state : no flow at $x = X_e$

$$\frac{\partial^2 P}{\partial x^2} = - C \tag{E.9}$$

$$\frac{\partial P}{\partial x} = C \, (X_e - x) \tag{E.10}$$

$$\left| P(x) - P(X_o) \right|_{PSS} = C \, (x - X_o) \left| X_e - \frac{x + X_o}{2} \right| \tag{E.11}$$

Same well rate in the two cases (at X_o), thus :

$$A = C \, (X_e - X_o) \tag{E.12}$$

Pseudo-steady-state potential at X_e (no flow boundary) equals steady-state potential at x if :

$$\left| P(X_e) - P(X_o) \right|_{PSS} \quad \left| P(x) - P(X_o) \right|_{SS} \tag{E.13}$$

This is achieved for one particular value of x, that we name X_A. From E.8, E.11 and E.12, one gets

$$X_A \quad \frac{X_o + X_e}{2} \tag{E.14}$$

α	Z_{Sc}/h	q_{lc}^*	$F = \alpha q_{lc}^*(\alpha)$
1	.7050	4.003	4.003
2	.5021	2.013	4.026
3	.3803	1.361	4.083
4	.3053	1.040	4.160
5	.2557	0.849	4.245
7	.1946	0.631	4.417
10	.1450	0.464	6.64
13	.1163	0.3695	4.80
20	.0804	0.254	5.08
30	.0562	0.177	5.31
40	.0434	0.137	5.48
70	.0260	0.082	5.74

TABLE 1 - Horizontal well : Critical cone heights, dimensionless critical rates, and function F for various values of $\alpha = (X_A/h)\,(k_v/k_h)^{1/2}$

Example :
Gas coning or cresting (oil well)

k_h = 70 mD
k_v = 7 mD
h = 24.4 m
$\Delta\rho$ = 0.48 g/cm^3 (gas/oil)
μ = 0.42 cp
r_w = 0.1 m
r_A = 1000 m (vert. well)
or X_A = 1000 m (hor. well)
L = 500 m (hor. well)
W = L m (hor. well)

TABLE 2 : Example parameters

α	Z_{Sc}/h	q_c^*	[illegible]
4	0.43	1.2133	2.95
13	0.37	0.8962	4.42
40	0.34	0.7676	5.32

TABLE 3 - Vertical well - Critical cone parameters for α = 4, 13, 40 (α $(r_A/h)\,(k_v/k_h)^{1/2}$)

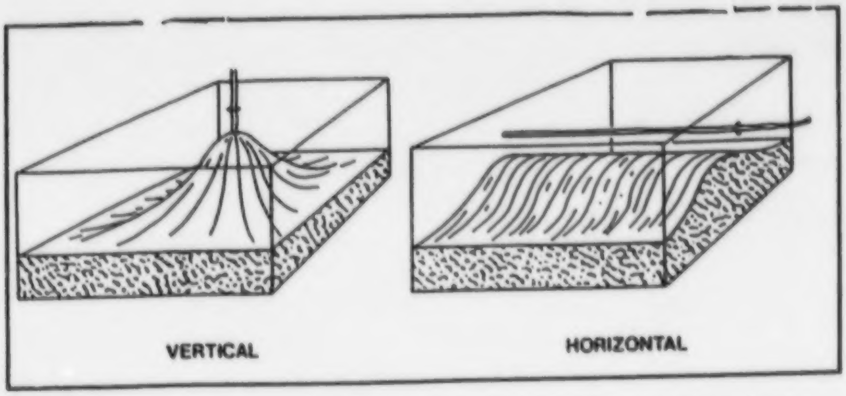
VERTICAL
HORIZONTAL

Fig. 1—Water coning toward a vertical well and cresting toward a horizontal well.

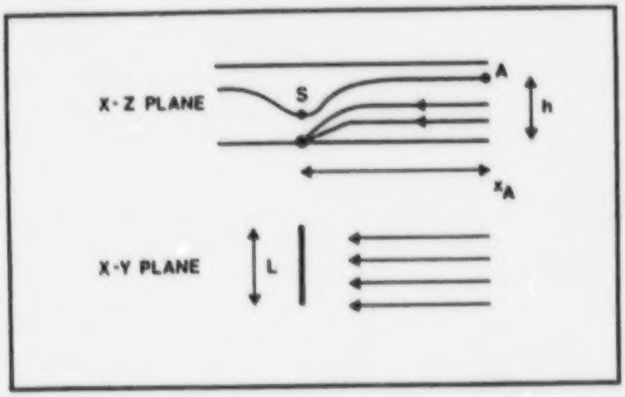
X-Z PLANE
S
A
h
x_A
X-Y PLANE
L

Fig. 2—Immobile gas crest above a horizontal well—flowlines in oil.

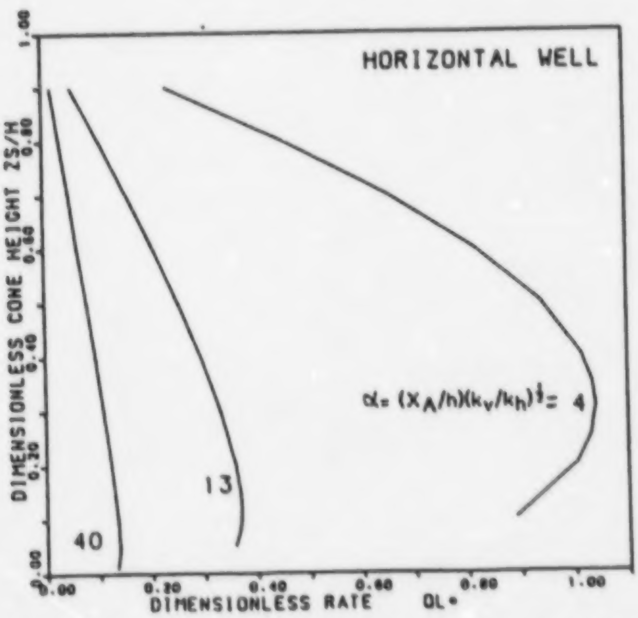

Fig. 3—Crest apex to well distance vs. rate for crests in equilibrium (horizontal well).

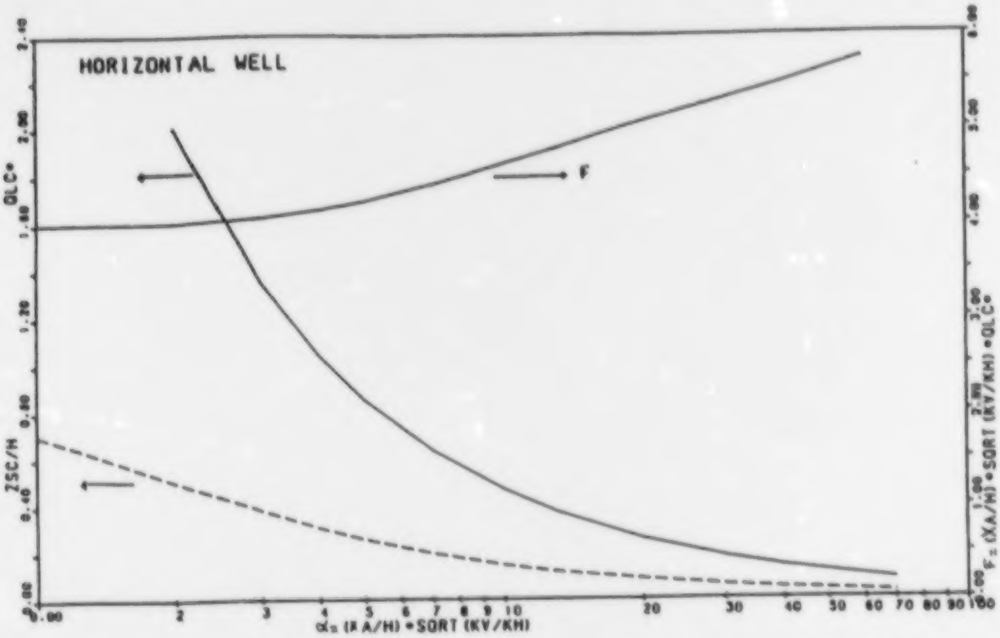

Fig. 4—Dimensionless critical rates, crest apex location and F function vs. α [with $\alpha = (x_A/h)(K_V K_h^{1/2})$].

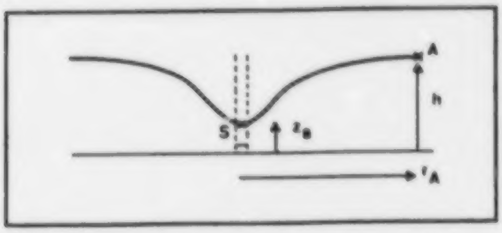

Fig. 5—Immobile gas cone above a vertical well.

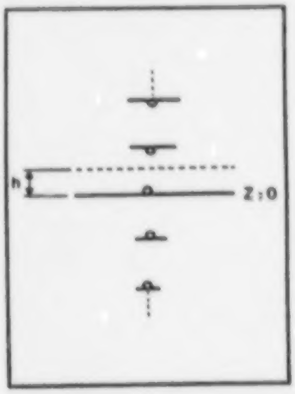

Fig. 6—Row of image wells to generate a no flow boundary at z = h ($z_n = \pm 2\ nh$).

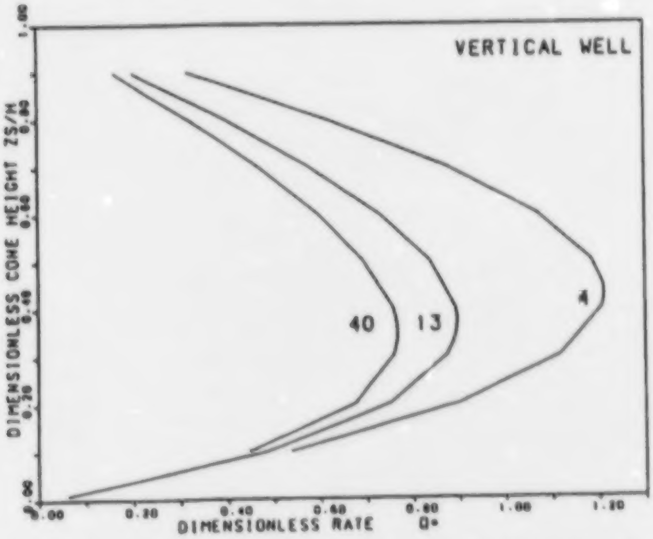

Fig. 7—Cone-apex to well distance vs. rate for cones in equilibrium (vertical wells).

0066

0074

Alberta OIL SANDS
INFORMATION CENTER

THEORETICAL STUDIES ON THE GRAVITY DRAINAGE OF HEAVY OIL DURING IN-SITU STEAM HEATING

BY

R.M. BUTLER

G.S. McNAB

H.Y. LO

Esso Resources Canada Limited

(82)

For presentation at the 29th Canadian Chemical Engineering Conference, Sarnia, Ontario, Sept. 30 - Oct. 3, 1979.

006674

ABSTRACT

One concept for the in-situ production of oil from the tar sands involves the continuous injection of steam into a growing steam-saturated volume or steam chamber. Steam flows to the boundary of the chamber, condenses and gives up its heat to the surrounding oil sands. The condensate and heated oil flow by gravity to a production well located at the bottom of a chamber and they are removed continuously. The well may consist of a horizontal slotted pipe. This paper describes the theory of operation of such a process.

39-974

IN-SITU RECOVERY OF HEAVY OILS

FACTORS:

- ○ LARGE THICK RESERVOIRS
- ○ HIGH POROSITY & PERMEABILITY
- ○ HIGH IN-SITU OIL VISCOSITY

Introduction - Vugraph #1

Today I am going to discuss a new concept for the in-situ production of heavy crudes by steam heating which we have been working on at Esso Resources in Calgary.

The idea for our work arose from a desire to develop a continuous means for removing oil from the reservoir more completely, more quickly, and with lower use of energy. All in-situ recovery processes for reservoirs such as ours at Cold Lake are influenced by the factors shown in this vugraph.

The reservoirs are large and thick. They generally have high porosity and permeability. Frequently they are more or less continuous. These factors are, of course, desirable.

The main obstacle to recovery lies in the very high in-situ oil viscosity. Although the oil is liquid at reservoir conditions its very high viscosity makes it behave almost like a solid. The idea of using steam to recover the oil is thus almost akin to a process of steam melting.

The main problem in using steam is one of achieving contact. A well drilled into the reservoir will not allow steam to be injected at an appreciable rate because the pores are already filled with essentially immobile bitumen. Steam can be injected if pressures high enough to achieve fracturing are employed. The steam then enters into narrow fractures. However, oil recovery may be moderate, since steam tends to be restricted to the region affected by the fracture.

In the development of the concepts which I am discussing today, we started with the objective of developing a means whereby steam could be introduced continuously and the condensate removed as it formed together with the oil which had been heated. The general idea is shown in the next vugraph.

39-575

GRAVITY DRAINAGE CONCEPT

- STEAM CONDENSES AT CHAMBER INTERFACE
- OIL & CONDENSATE DRAIN TO WELL AT BOTTOM
- FLOW IS CAUSED BY GRAVITY
- CHAMBER GROWS — UP & SIDEWAYS

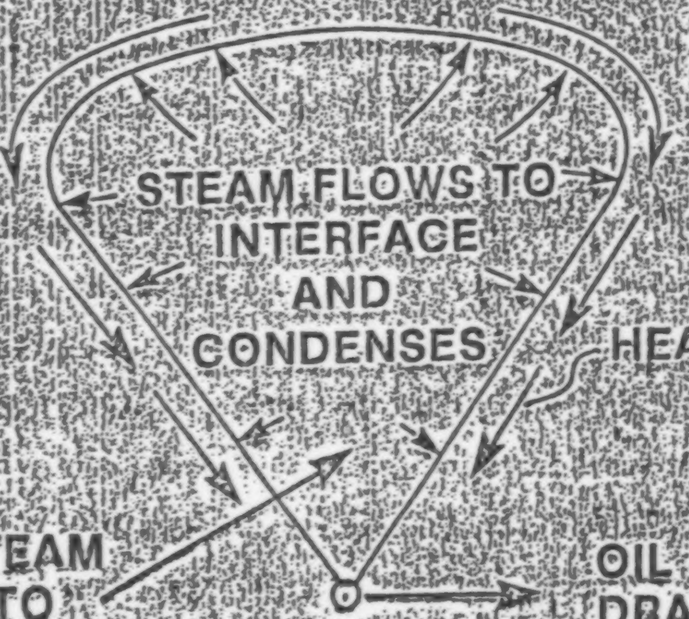

STEAM FLOWS TO
INTERFACE
AND
CONDENSES

HEATED OIL FLOWS
TO WELL

CONTINUOUS STEAM
INJECTION INTO
"STEAM CHAMBER"

OIL & CONDENSATE
DRAIN CONTINUOUSLY

Vugraph #2 - Gravity Drainage Concept

The basic idea is that if steam is introduced near the bottom of the reservoir it will tend to rise and the heavier condensate and heated oil will tend to fall to the bottom. Means must be provided for introducing the steam, initially quite near to the bottom, and for removing the liquids as they drain to a location near to where the steam is introduced. As the liquids drain, space is left in the reservoir for more steam to flow in. The mechanism is shown schematically in the diagram. The figure is of a vertical section above a horizontal well placed at the bottom. A steam chamber is formed above the well and steam is injected continuously into this chamber by means of another well placed somewhat above the production well. A steam pressure is maintained. The chamber is surrounded by colder oil sand. Steam flows through the sand within the chamber to the interface and condenses. The liberated heat is conducted into the colder oil sand. This causes the oil near the interface to become heated and permits it to drain by gravity towards the well. The condensate also drains. As the oil is removed the steam chamber becomes larger by growing upwards and sideways. The pressure within the steam chamber can remain essentially constant. Flow is caused by gravity. Oil and water condensate drain downwards and steam rises.

In some respects the process is analogous to that of water draining from a bathtub drainhole. Steam does not push the oil out of the reservoir anymore than the air pushes the water from the tub.

In our initial analysis of this concept it appeared to us that the rate of growth upwards of the steam chamber would be larger than that sideways. Eventually the upwards growth would be limited by the top of the reservoir and the sideways growth would then become critical. The next vugraph shows how steam chambers might grow for a series of parallel horizontal production wells in a reservoir.

39-576

DIAGRAM SHOWING GROWTH OF STEAM CHAMBER ABOVE ADJACENT HORIZONTAL WELLS

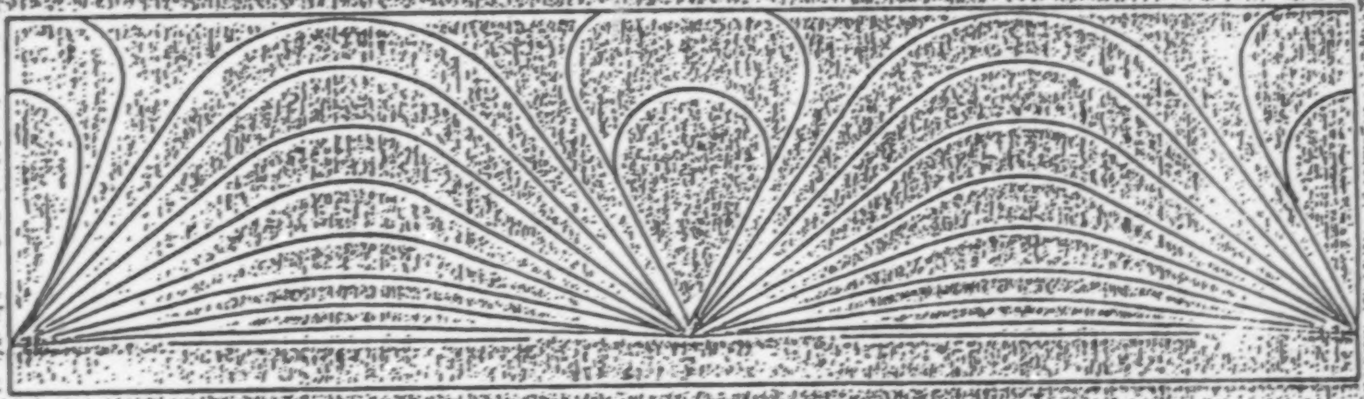

Vugraph #3 - Diagram Showing Growth of Steam Above Adjacent Horizontal Wells

Here a horizontal well shown in the centre of the diagram is flanked by similar wells on either side. The positions of the interface are shown diagramatically at successive periods of time. Initially the steam chambers grow rapidly to the top of the reservoir and then spread sideways. After a period they intermingle and form a single steam layer above the oil. Heating continues and oil drains to the horizontal wells. It will be noted that this method may allow almost complete coverage of the reservoir volume.

In our studies we concentrated initially on the rate at which such steam chambers could grow sideways and I am going to show you some of our theoretical results in this area.

GRAVITY DRAINAGE RELATIONS

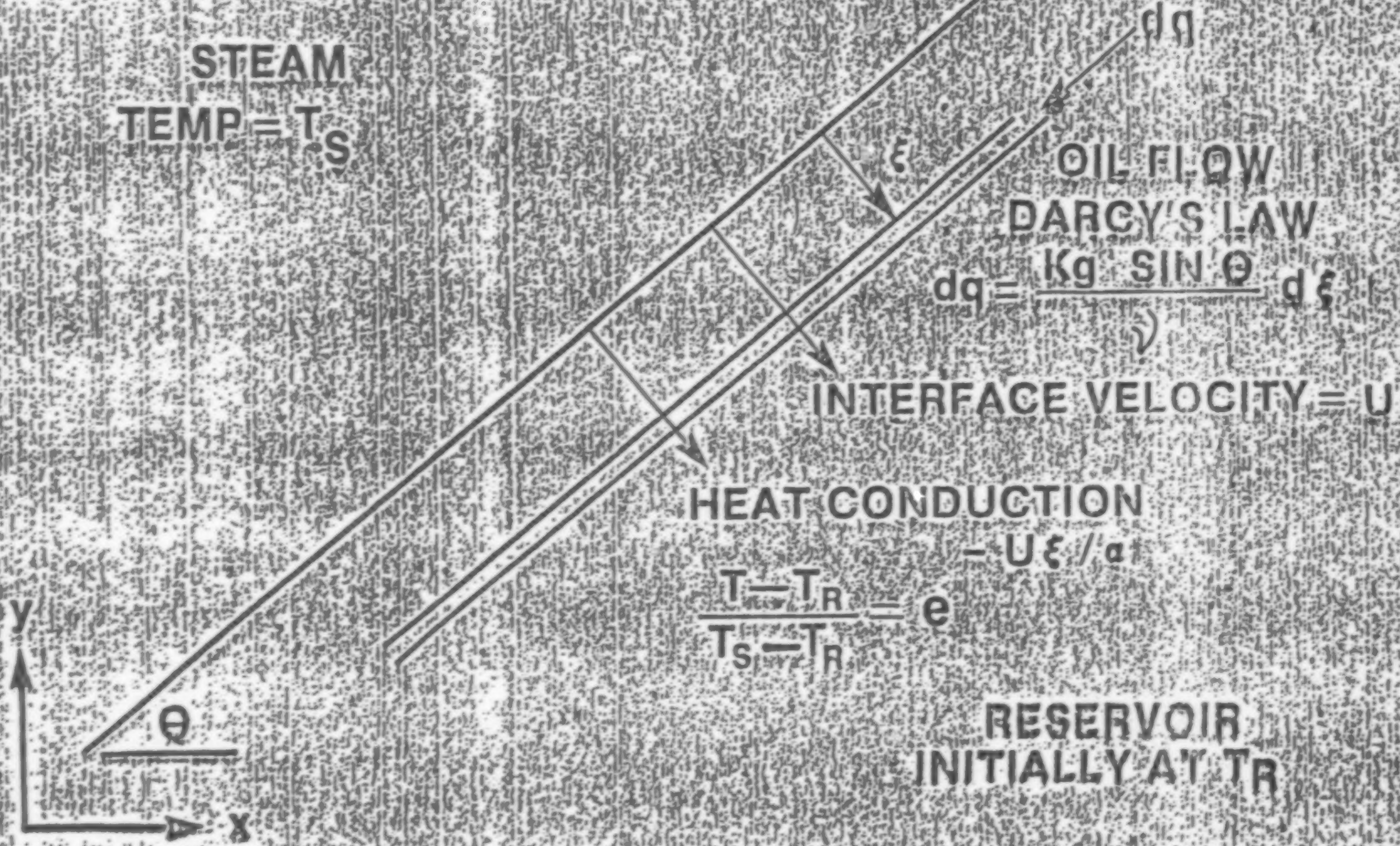

STEAM
TEMP = T_S

OIL FLOW
DARCY'S LAW

$$dq = \frac{Kg \ \mathrm{SIN}\ \Theta}{\nu} d\xi$$

INTERFACE VELOCITY = U

HEAT CONDUCTION

$$\frac{T - T_R}{T_S - T_R} = e^{-U\xi/\alpha}$$

RESERVOIR
INITIALLY AT T_R

Vugraph #4 - Gravity Drainage Relations

This diagram shows a small section of the interface between the steam and the oil. Condensate from the steam runs down the steam side of the interface and is assumed in the theory not to affect the process. In the region shown the interface is assumed to be inclined at an angle θ from horizontal. θ is a function of location along the interface.

Oil is assumed to run parallel to the interface as in the little element shown at a distance ξ from the surface. The rate of flow in the element dq is given by Darcy's law which results in the expression shown.

It is assumed that the interface is moving locally at a velocity U as shown on the green overlay.

Ahead of the interface the temperature falls, starting at the steam temperature T_s and going to the reservoir temperature T_r. If the interface is moving at a constant velocity U the heat conduction equation gives the temperature distribution shown in blue. This assumes that the only heat transfer mechanism is that of conduction normal to the interface. The two equations shown on this vugraph are listed as 1 and 2 on the next.

39–578

GRAVITY DRAINAGE THEORY

$$q = kg \text{ Sin } \Theta \int_0^\infty \frac{d\xi}{\nu} \qquad (1)$$

$$\left(\frac{T - T_R}{T_S - T_R}\right) = e^{-U\xi/\alpha} \qquad (2)$$

$$\left(\frac{\nu_S}{\nu}\right) = \left(\frac{T - T_R}{T_S - T_R}\right)^m \qquad (3)$$

$$\int_0^\infty \frac{d\xi}{\nu} = \alpha / Um \qquad s \qquad (4)$$

$$q = kg\,\alpha \text{ Sin } \Theta / Um\,\nu_S \qquad (5)$$

Vugraph #5 - Gravity Drainage Theory

Equation 1 is now the integrated form of the Darcy equation. Equation 2 is the same as on the previous vugraph. In order to evaluate the integral of equation 1, it is necessary to express the oil viscosity as a function of the distance from the interface. Equation 2 defines the temperature as a function of this distance and this is combined with equation 3 which shows the variation of viscosity with temperature. This particular equation is a suitable approximation for this purpose and when combined with equation 2 gives a particularly simple mathematical result. For heavy crudes, such as that at Cold Lake, a value of the exponent m equal to 3 can be employed. The resulting integral is evaluated in equation 4 and when this is substituted back in the Darcy equation 1, equation 5 results.

39-579

GRAVITY DRAINAGE THEORY (cont.)

$$\frac{\partial q}{\partial x} = \phi S_o \frac{\partial y}{\partial t} \qquad (6)$$

$$U = -\cos\Theta \frac{\partial y}{\partial t} \qquad (7)$$

$$\int_0^q q\,dq = \int_0^{\Delta H} \frac{\phi S_o K g a}{m \nu_s}\,dy \qquad (8)$$

$$q = \sqrt{\frac{2 \phi S_o K g a \Delta H}{m \nu_s}} \qquad (9)$$

one side

Vugraph #6 - Gravity Drainage Theory (cont.)

The quantity of oil draining downwards, q, increases as the oil flows towards the bottom of the reservoir. The rate of change of q with distance is related to the movement of the interface by a material balance equation such as 6. The rate of movement of the interface is related to the velocity U by equation 7. Equations 5, 6 and 7 can be combined and rearranged to give equation 8 which may be integrated to give the overall rate of drainage q as a function of the various parameters. Numerical results using this equation are described later in the talk.

Equation 9 estimates the drainage of oil down a hypothetical interface which is free to move continuously into a cold infinite reservoir as the steam chamber expands. In practical cases when the bottom of the chamber surface is tied to a production well, it overestimates the rate somewhat. It is nevertheless very useful for estimating the approximate rate at which drainage can occur.

39-580

GRAVITY DRAINAGE IN VISUAL MODEL

$$B_2 = \frac{m\,K g H}{\phi\, S_o\, \alpha\, \gamma_s}$$

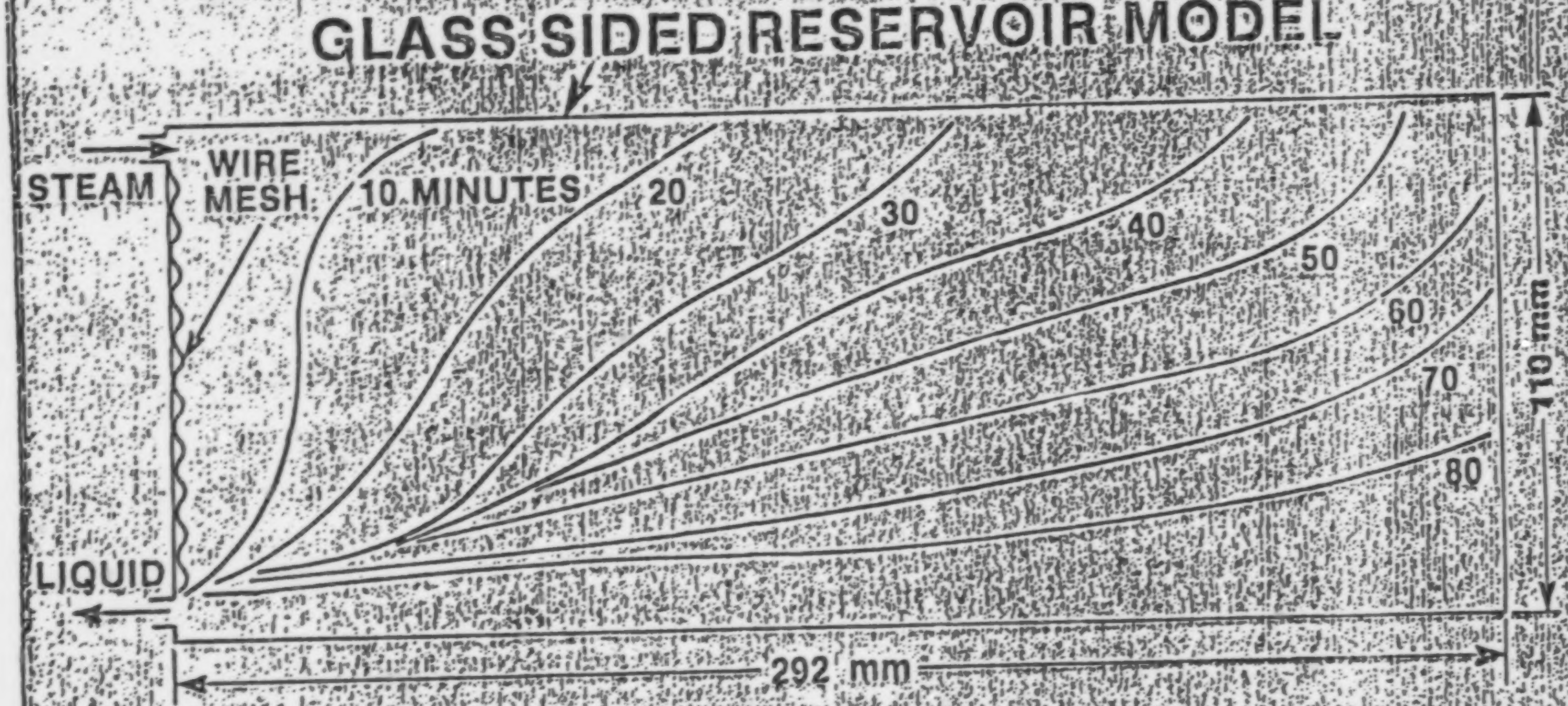
GLASS SIDED RESERVOIR MODEL
STEAM
WIRE MESH
10 MINUTES
20
30
40
50
60
70
80
LIQUID
110 mm
292 mm

Vugraph #7 - Gravity Drainage in Visual Model

Some of the experiments which we have carried out in our laboratory have involved the use of glass sided reservoir models operated at atmospheric pressure. The results of an experiment of this type are shown in vugraph #7. Here a glass sided model 29 cm long by 11 cm high and 2 1/2 cm thick was filled with glass beads and saturated with Cold Lake crude. A wire mesh was placed along the left hand vertical side of the model to represent a fracture. Steam at atmospheric pressure was introduced into the top of the model and liquids allowed to drain from the bottom as shown. The permeability of the glass beads was chosen so as to make the dimensionless number B_2 shown at the top of the vugraph the same in the model as it would be in the full scale reservoir. This makes the model dimensionally similar to the field.

The position of the interface at 10 minute intervals is shown in the figure. It will be noted that the oil was drained in a systematic manner. It is believed that the tendency of the interface lines to curve upwards near the right hand edge of the model was due to heat losses through the edges of the model. For the particular conditions chosen for this experiment, 10 minutes is about equivalent to 1.6 years in the full scale field example.

DRAINAGE FROM GLASS MODEL

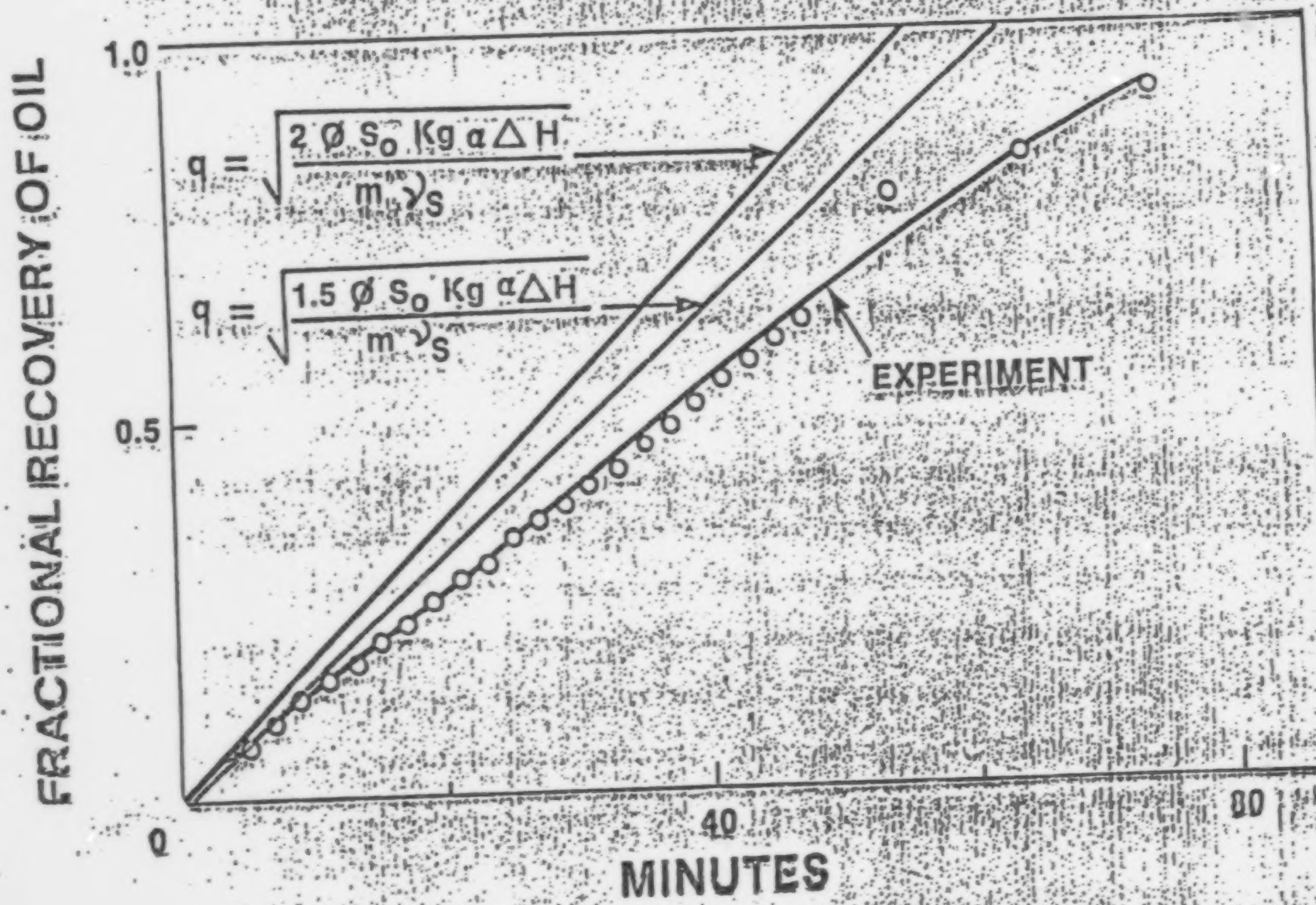

Vugraph #8 - Drainage From Glass Model

The recovery of oil from the model is plotted against time in this vugraph and the results are compared with the recovery predicted by the previously derived equation. The observed rate was of the same order as that predicted but slightly slower. The agreement is encouraging. The lower observed experimental rate is due to factors not recognized in the derivation of the equation. The effective head is smaller than assumed in the theory because of depletion and because of the need to maintain the position of the lower end of the interface at the well. A more recent equation which we have developed results in a factor 1.5 in place of the 2 of the original equation. As may be seen from the overlay, this happens to result in better agreement with the initial rate observed in this experiment.

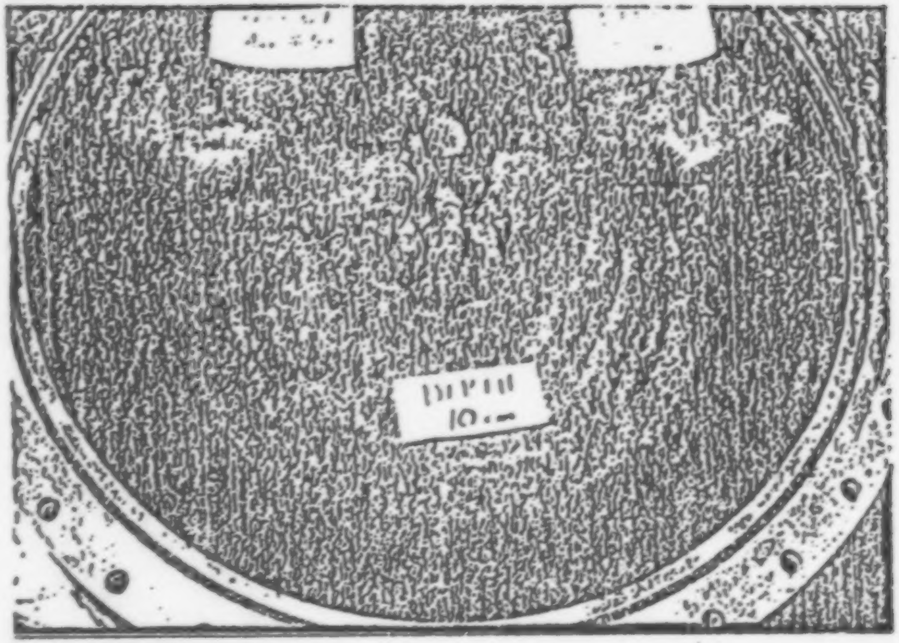

9. Photograph of Pressurized Scaled, Laboratory Physical Model

The top of the model has been removed following an experiment. The nearer half of the reservoir has been excavated to a depth of 10 cm. The circular steam chamber surrounding the vertical injection well can be seen clearly. The production well was below the injection well.

ugraph #9 - Photograph of Leached Reservoir Around a Radial Production Well
In a Pressure Model

As well as experiments with atmospheric pressure, visual models such as that shown previously, we ave carried out gravity drainage experiments using a scaled, pressurized laboratory physical reservoir odel. These experiments have used Cold Lake crude with steam pressures of the order of a few MPa. This articular photograph shows a section through one of these reservoir models after the oil had been partially roduced by gravity drainage. In this particular experiment, steam was introduced in a vertical well ositioned slightly above a vertical production well. The flow was thus radial rather than linear. The olume from which the oil has drained can be clearly seen in the photograph.

Production rates in these experiments were of the same order as predicted by gravity drainage elationships after allowance for the effects of radial rather than linear flow.

39-582

CALCULATED DRAINAGE RATE — FOR COLD LAKE CRUDE

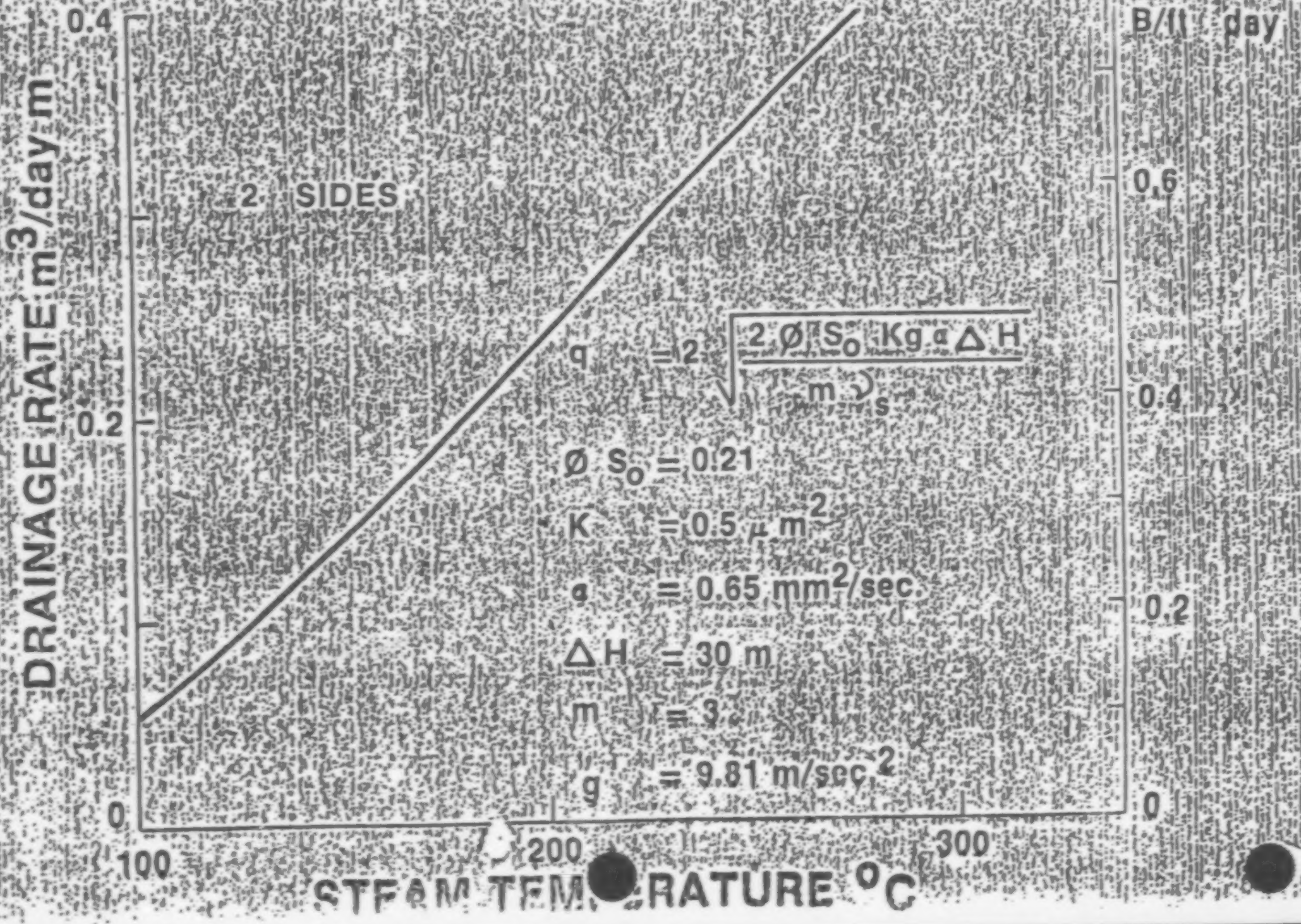

$$q = 2\sqrt{\frac{2\,\phi\,S_o\,K g\,\alpha\,\Delta H}{m\,\nu_s}}$$

$\phi\ S_o = 0.21$

$K = 0.5\ \mu m^2$

$\alpha = 0.65\ mm^2/sec$

$\Delta H = 30\ m$

$m = 3$

$g = 9.81\ m/sec^2$

ugraph #10 - Calculated Drainage Rate

This vugraph shows the rate at which Cold Lake crude is predicted to drain to a horizontal well sing the simple equation developed previously. Values of the parameters assumed are also shown. The predicted rainage rate increases with steam temperature because of the reduced value of the oil viscosity at steam emperature, v_s. Rates from about .05 to .4 m^3/day per metre of horizontal well (0.1 to 0.7 barrels/ft/day) re predicted. Thus, for example, at a steam temperature of 200° C a well 2,000 ft. long may be expected to roduce about 800 barrels of oil per day. This is calculated from the simple equation shown. Maximum rates f the order of about 80% of this are more realistic. Also, of course, as reservoir depletion occurs the vailable head, ΔH, decreases and the rate declines. When the reservoir is about three-quarters depleted, the rainage rate may only be about 50% of that calculated by the equation.

If a vertical production well rather than a horizontal one were employed then the initial effective rainage length would be only the circumference of the well, which at most would only be 2 or 3 feet. As rainage occurred this effective length would increase somewhat but the overall rate would be disappointingly mall. In order to make effective use of gravity drainage, horizontal wells are preferred because of the ncreased effective contact with the reservoir.

The calculated rates shown in the vugraph assume that the steam chamber reaches to the top of the eservoir. Initially it may be much smaller. If this is the case, then the drainage rate will increase as the mber grows upwards, i.e. as ΔH increases. This initial process can be accelerated by injecting steam itially at above fracturing pressure and creating a fracture above the production well. It is advisable in is case to locate the horizontal production well along the fracture trend direction.

39-583

CONCLUSIONS

- CONTINUOUS DRAINAGE TO A HORIZONTAL WELL AT THE BASE OF A GROWING STEAM CHAMBER IS AN ATTRACTIVE IN-SITU PRODUCTION POSSIBILITY
- HIGH RECOVERY
- CAN USE LP STEAM
- PREDICTED RATES ARE OF THE ORDER OF $0.15\ m^3/\text{day}\ m$ (0.3 B/D ft.)
- $q = 2\sqrt{\dfrac{2\,\phi\,S_o\,K g\,\alpha\,\Delta H}{m\,\nu_s}}$ (two sides)

Vugraph #11 - Conclusions

Continuous drainage to a horizontal well at the base of a growing steam chamber appears to be an attractive in-situ production possibility. It has the potential to provide higher recovery and potentially can be used with low pressure steam. The rate of drainage to such a well is calculated to be of the order of .3 barrels oil per day per foot of well. Finally an equation has been developed which allows one to estimate the effect of the major variables.

008084

Theoretical Studies on the Gravity Drainage of Heavy Oil During In-Situ Steam Heating (1)

(83) Alberta OIL SANDS INFORMATION CENTRE

R.M. BUTLER, G.S. McNAB and H.Y. LO
Esso Resources Canada Limited, Calgary, Alberta, Canada

One concept for the in-situ production of oil from the tar sands involves the continuous injection of steam into a growing steam-saturated volume or steam chamber. Steam flow to the boundary of the chamber, condenses and gives up its heat to the surrounding oil sands. The condensate and heated oil flow by gravity to a production well located at the bottom of a chamber and are removed continuously. The well may consist of a horizontal slotted pipe. This paper describes the theory of operation of such a process and an equation is derived which predicts the rate of drainage.

Un concept pour la production "in situ" d'huile à partir des sables bitumineux implique l'injection continue de valeur d'eau dans un volume croissant saturé de vapeur d'eau, ou chambre de vapeur d'eau. La vapeur s'écoule jusqu'à la limite de la chambre, se condense et cède sa chaleur aux sables bitumineux qui l'entourent. Le condensat et l'huile chauffée se rendent par gravité à un puits de production situé au bas de la chambre d'où on les prélève de manière continue. Le puits peut consister en un tube horizontal, rainuré. On décrit, dans le présent travail, la théorie du fonctionnement du procédé et l'on a établi une équation permettant de prédire la vitesse de drainage.

This paper considers a method for in-situ recovery of heavy crude using steam-assisted gravity drainage. The basic concept, a theoretical analysis, and some experimental laboratory data are included.

Heavy oils can be divided into two types: the conventional oils which can be produced by primary methods, and the tarry bitumen which is virtually immobile in the reservoir. The latter is represented by the Cold Lake, Peace River, Wabasca and Athabasca deposits in Alberta, Canada. The fluids in reservoirs such as these have very high viscosities under reservoir conditions and will not flow, even through the very porous matrix of the unconsolidated sand reservoir. Oil density is close to that of water. This bitumen can be recovered economically by strip-mining if the deposit is close to the surface but the major part of such oil is too deep and can only be recovered by in-situ methods. Such techniques involve reducing the viscosity of the oil in place.

Both non-thermal and thermal methods can reduce the bitumen's viscosity. Non-thermal methods include concepts such as solvent dilution. Thermal techniques employ steam, fire or electricity to heat the oil. A recent review of the field containing 46 references has been given by Prats[1]. There is some overlap, of course, as methods can be combined and there are many possible variations. The technique described in this paper uses steam to heat the bitumen.

The application of steam can be divided into two main categories: cyclic steam stimulation ("huff-and-puff"), and steam flooding. In the former case, high pressure steam is injected into the reservoir, some soaking time is allowed, and then the same well is allowed to flow back. The flow of water and steam carries the heated bitumen to the wellbore. It is moved to the surface either by means of its own pressure or, in the later stages, by pumping.

Steam flooding uses separate injection wells and producers. Steam is injected into the reservoir and proceeds along a natural or artificial path between wells. The flow of water and steam carries oil with it. A variation of this approach employs hot water rather than steam.

Both approaches can be economic but may have some inherent difficulties which limit displacement efficiency. First, the fluid flow is relatively rapid and can break up the oil phase into droplets, leaving a significant amount behind. Secondly, oil and other fluids flow simultaneously through the same section of the bed, thereby reducing the relative permeability of the sand. These factors tend to increase the amount of steam and water required to move a given volume of bitumen. The steam-assisted gravity drainage technique described in this paper reduces these two effects and should increase both the ultimate oil recovery and the energy efficiency.

Concept

The huff-and-puff and steam flood processes can both be considered as "drive" mechanisms, that is, the steam (or hot water) pushes the oil towards the collection well. This mechanism has problems in that the steam or water is much less viscous than the oil and hence fingering and poor sweep efficiencies can occur. Related to this, oil flow is hindered as both phases share the same section of

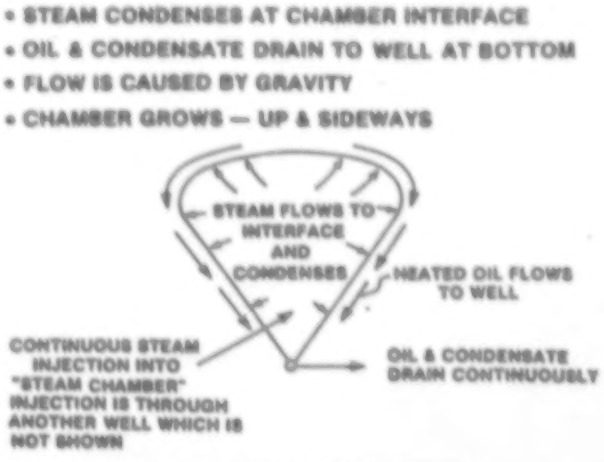
• STEAM CONDENSES AT CHAMBER INTERFACE
• OIL & CONDENSATE DRAIN TO WELL AT BOTTOM
• FLOW IS CAUSED BY GRAVITY
• CHAMBER GROWS — UP & SIDEWAYS
STEAM FLOWS TO INTERFACE AND CONDENSES
HEATED OIL FLOWS TO WELL
CONTINUOUS STEAM INJECTION INTO "STEAM CHAMBER" INJECTION IS THROUGH ANOTHER WELL WHICH IS NOT SHOWN
OIL & CONDENSATE DRAIN CONTINUOUSLY

Figure 1 – Gravity drainage concept.

---

(1) This paper was presented at the 29th Canadian Chemical Engineering Conference in Sarnia, Ontario, on October 1, 1979.

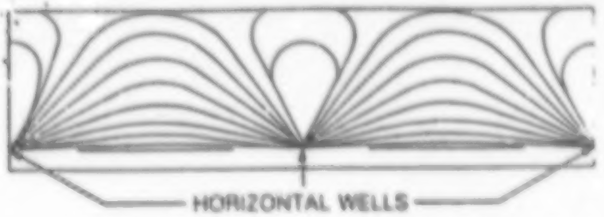

Figure 2 – Diagram showing growth of steam chamber above adjacent horizontal wells.

reservoir. In addition, since flow is rapid, the oil tends to be dispersed and capillary forces ensure that droplets will be left behind. In the recovery method described here, these factors are improved since oil and the other phases have separate flow paths and displacement is slow.

Gravity drainage concept

In the development of the concept discussed below, the objective was to develop a means whereby steam could be introduced continuously and the condensate removed as it formed together with the oil which had been heated. The concept is shown in Figure 1.

The basic idea is that if steam is introduced near the bottom of the reservoir it will tend to rise and the heavier condensate and heated oil will tend to fall to the bottom. Means are provided for introducing the steam, initially quite near to the bottom, and for removing the liquids as they drain to a location near to where the steam is introduced. As the liquids drain, space is left in the reservoir for more steam to flow in. The mechanism is shown schematically in the figure. This shows a vertical section above a horizontal well placed at the bottom. A steam chamber is formed above the well and steam is injected continuously into this chamber by means of another well placed close to and usually somewhat above the production well. A steam pressure is maintained. The chamber is surrounded by colder oil sand. Steam flows through the sand within the chamber to the interface and condenses. The liberated heat is conducted into the colder oil sand. This causes the oil near the interface to become heated and permits it to drain by gravity towards the well. The condensate also drains. As the oil is removed the steam chamber becomes larger by growing upwards and sideways. The pressure within the steam chamber remains essentially constant. Flow is caused by gravity. Oil and water condensate drain downwards and steam rises.

In some respects the process is analogous to that of water draining from a bathtub drainhole. Steam does not push the oil out of the reservoir anymore than the air pushes the water from the tub.

It has long been realized that the gravity drainage of conventional crude oil beneath a gas cap can produce unusually high oil recoveries. A recent paper by Dykstra[2] summarizes work in this area. Terwilliger et al[3] have shown that the recovery varies in an inverse manner with the drainage rate. Increasing the rate by lowering the production well pressure tends to leave additional liquid behind in the gas saturated region.

While the dynamic hold-up of oil in the gas saturated region is significant it is relatively small, for drainage in a steam chamber, since the viscosity of oil within the chamber is very low compared to the average viscosity of the oil draining below and around it. The average oil saturation in the steam chamber can be estimated using the following integrated form of Cardwell and Parsons[4] Equation (28).

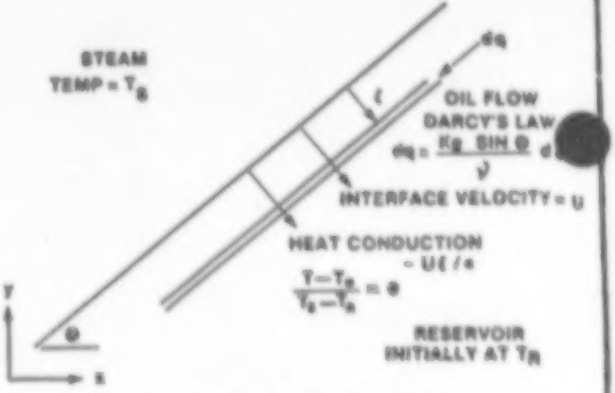

Figure 3 – Gravity drainage relations.

$$\overline{S}_o = \left(\frac{\nu_s \phi Z}{b K g t}\right)^{1/(b-1)} \left(\frac{b-1}{b}\right) \qquad (1)$$

where $\overline{S}_o$ is the average oil saturation in the steam chamber of thickness Z (i.e. $H\text{-}y = Z$) and b is the exponent in Cardwell and Parsons relative permeability equation. If b is set equal to a typical value of 3.5 and Z is set equal to the maximum possible value H then Equation (1) becomes:

$$\overline{S}_o = 0.43 \left(\frac{\nu_s \phi H}{K g t}\right)^{0.4} \qquad (2)$$

Typical field values are: $\nu_s = 0.452$ m²/d; $\phi = 0.$ $H = 30.5$ m; $Kg = 0.072$ m²/d²; $t = 1000$ d.

Then $\overline{S}_o = 0.14$. The oil saturation in the steam chamber is neglected in the following theory but as is noted later it can be allowed for by using a reduced value for the initial oil saturation.

In the initial analysis of this concept it appeared to us that the rate of growth upwards of the steam chamber would be larger than that sideways. Eventually the upwards growth would be limited by the top of the reservoir and the sideways growth would then become critical. Figure 2 shows how steam chambers are expected to grow for a series of parallel horizontal production wells in a reservoir. A horizontal well shown in the centre of the diagram is flanked by similar wells on either side. The positions of the interface are shown diagrammatically at successive periods of time. The steam chambers grow to the top of the reservoir and then spread sideways. After a period they intermingle and form a single steam layer above the oil. Heating continues and oil drains to the horizontal wells. It will be noted that this method allows almost complete coverage of the reservoir volume.

In our theoretical studies we concentrated initially on the rate at which such steam chambers could grow sideways. This theory is discussed in this paper.

Darcy's law

Figure 3 shows a small part of the drainage interface. It is a vertical section. Oil heated by steam is flowing approximately parallel to the interface down towards the well somewhere below the left of the diagram. The steam is at temperature T_s and

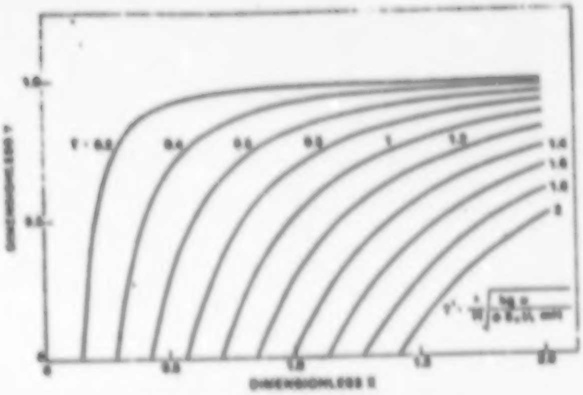

Figure 4 – Calculated interface curves.

the reservoir is initially at T_R. At the interface which, in the section shown, is inclined at an angle θ to the horizontal, steam is condensing. The interface is at temperature T_s. Heat is transferred into the cooler reservoir by conduction. As one proceeds from the interface into the reservoir, successive layers of material become cooler. At a distance ξ from the interface, the kinetic viscosity of the oil is ν and Darcy's law gives the equation shown on the figure for the rate of drainage of oil dq within the element $d\xi$. If the interface velocity is U, measured normal to the interface, and it is assumed that heat transfer is by conduction, then the temperature ahead of the interface for a steady state advance is given by Equation (3).

$$\frac{T - T_R}{T_s - T_R} = \exp(-U\xi/\alpha) \qquad (3)$$

High values of U result in a rapidly decreasing temperature and low values give a slowly falling temperature. Integration of the differential Darcy's law equation shown results in:

$$Q = Kg\operatorname{Sin}\theta \int_0^\infty \frac{d\xi}{\nu} \qquad (4)$$

For the purpose of this paper it will be assumed that the variation of viscosity with temperature can be represented by an equation of the form:

$$\frac{\nu_s}{\nu} = \left(\frac{T - T_R}{T_s - T_R}\right)^m \qquad (5)$$

This form of expression is particularly suitable since it represents the variation of viscosity with temperature well for a range near to the steam temperature and since it results in a simple final equation. For heavy crudes under typical conditions m has a value of 3 to 4. General correlations for choosing m will be discussed in a future paper.

In order to apply this equation it is necessary to specify the steam temperature T_s and the corresponding viscosity ν_s, the reservoir temperature T_R and the exponent m. This viscosity equation allows the evaluation of the integral of Equation (4) in a simple way. It may be seen that the temperature term may be readily eliminated and that the substitution of the expression for ν allows the integral to be evaluated with the result:

$$\int_0^\infty \frac{d\xi}{\nu} = \frac{\alpha}{U}\,\frac{1}{m\nu_s} \qquad (6)$$

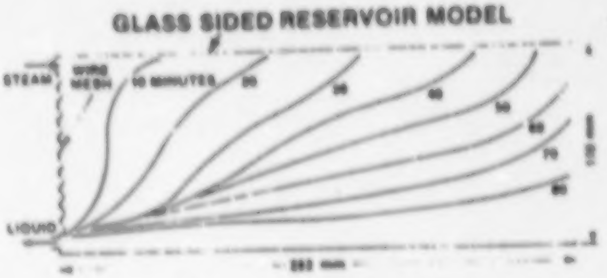

Figure 5 – Gravity drainage in visual model.

Integrated flow

Substituting Equation (6) into Equation (4) results in the following relationship:

$$Q = \frac{Kg\alpha\operatorname{Sin}\theta}{m\nu_s U} \qquad (7)$$

This equation is not the final answer since it involves the unknown variables U and $\operatorname{Sin}\theta$.

There is a trivial solution to the equation which is of some interest. It will be noted that Q can be any arbitrary constant if both U and θ are equal to 0. This results does have a physical significance although it is a very unrealistic approximation. It will be referred to again later.

Material balance

Consider again the small area shown in Figure 3. If the interface is advancing, then oil must be flowing out of the area shown faster than it is flowing in. The rate of increase of the oil flow across the section is thus related to the rate of advance of the interface. The appropriate material balance relationship is:

$$\left(\frac{\partial Q}{\partial x}\right) = \phi S_o \left(\frac{\partial y}{\partial t}\right) \qquad (8)$$

Velocity

In Equation (7), the rate of movement of the interface is involved in the term $(\partial y/\partial t)$. This is related to the velocity U by the expression:

$$U = -\operatorname{Cos}\theta \left(\frac{\partial y}{\partial t}\right) \qquad (9)$$

Note that in this expression, the term $(\partial y/\partial t)$ may be expected to be negative. Substituting U from Equation (9) in Equation (7), and recalling that $\tan\theta$ is equal to $\operatorname{Sin}\theta$ divided by $\operatorname{Cos}\theta$ and that it is also $(\partial y/\partial x)$, and substituting $(\partial y/\partial t)$ from Equation (8) in the resulting equation, gives:

$$Q = -\frac{Kg\alpha\operatorname{Sin}\theta}{m\nu_s\operatorname{Cos}\theta\left(\frac{\partial y}{\partial t}\right)} \qquad (10)$$

$$= -\frac{Kg\alpha}{m\nu_s}\,\frac{\left(\frac{\partial y}{\partial x}\right)}{\left(\frac{\partial y}{\partial t}\right)} = -\frac{Kg\alpha\phi S_o}{m\nu_s}\left(\frac{\partial y}{\partial Q}\right)$$

This may be rearranged and integrated to give:

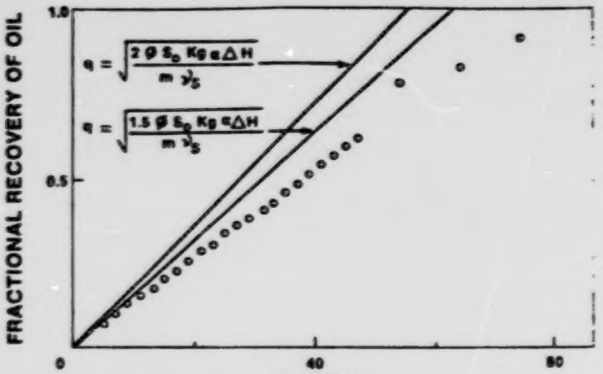

Figure 6 – Drainage from visual model.

$$\int_0^Q Q\,dQ = \int_0^{\Delta H} \frac{\phi S_o Kg\alpha}{m\nu_s}\,dy$$

Which results in the following expression for the total rate of drainage of oil at a height y:

$$Q = \sqrt{\frac{2\phi S_o Kg\alpha(H-y)}{m\nu_s}} \qquad (11)$$

Position of interface

The horizontal velocity of the interface is given by:

$$\left(\frac{\partial x}{\partial t}\right)_y = \left(\frac{\partial y}{\partial t}\right)_x \Big/ \left(\frac{\partial y}{\partial x}\right)_t \qquad (12)$$

Combining this with Equation (8) and differentiating Equation (11) to obtain $(\partial Q/\partial y)$ gives:

$$\left(\frac{\partial x}{\partial t}\right)_y = \frac{1}{\phi S_o}\left(\frac{\partial Q}{\partial y}\right) = \sqrt{\frac{Kg\alpha}{2\phi S_o m\nu_s(H-y)}} \qquad (13)$$

Hence, if it is assumed that the steam chamber is initially a vertical plane above the well, the horizontal displacement x is given as a function of time t and height y by the relationship:

$$x = t\sqrt{\frac{Kg\alpha}{2\phi S_o m\nu_s(H-y)}} \qquad (14)$$

This may also be solved for y with the result:

$$y = H - \frac{Kg\alpha}{2\phi S_o m\nu_s}\left(\frac{t}{x}\right)^2 \qquad (15)$$

Equation (14) may also be written in dimensionless form as:

$$Y = 1 - \frac{1}{2}\left(\frac{T'}{X}\right)^2 \qquad (16)$$

where the variables are:

$Y = y/H$

$X = x/H$

$$T' = \frac{t}{H}\sqrt{\frac{Kg\alpha}{\phi S_o \nu_s m H}} \qquad (17)$$

Values of Y calculated from Equation (16) have been plotted against X in Figure 4.

It will be noted that a characteristic of this set of curves is that the lower part of the interface moves away from the production well. If the well were at the origin of Figure 4, then as time increases it will be necessary for the oil to move further and further horizontally towards the well after it drains to the bottom. In the discussion of Equation (7), it was pointed out that a solution based on the assumptions made was that oil could indeed move horizontally along a stationary interface. The reason for this is that it is assumed that there is an infinite amount of material beyond the interface and that if the interface is stationary, this oil is at temperature T_r. Thus for a finite flow, only an infinitesimal gravity head is required. This is not realistic. However, the concept of two interfacial curves with the oil sliding down the more vertical one and then moving along a less inclined curve to the well is conceivable, and in practice something of this sort must occur. For this reason, the rates calculated by Equation (11) are recognized as being somewhat too high; the head is not all available to move [illegible] down the interface since some of the head is requi[illegible] to transport oil horizontally to the well. A modified equation in which the constant 2 in Equation (11) is replaced by 1.5 has been derived and this will be described in a later paper. The rate predicted by this modified equation is 87% of that given by Equation (11).

TABLE 1

CORRESPONDING MODEL AND FIELD PARAMETERS

	MODEL	FIELD
m	3.9	3.9
Kg m³/d²	1079 (15000 Darcies)	0.072 (1.0 Darcies)
H m	0.105	30.5
α m²/d	0.0557	0.0557
ν_s m²/d	12.25 (98° C)	0.452 (216° C)
ϕS_o	0.4	0.21
B_3	1619	1619
$\alpha t/mH^2$	1.3t(1)	1.5×10^{-3}t(1)
(1) t in days		

Scaled visual model

Some of the experiments which we have carried out in our laboratory have involved the use of glass sided reservoir models operated at atmospheric pressure. The results of an experiment of this type are shown in Figure 5. A glass sided model 25 cm long by 11 cm high and 2.5 cm thick was filled with glass beads and saturated with Cold Lake crude. A wire mesh was placed along the left hand vertical side of the model to represent a fracture. Steam at atmospheric pressure was introduced into the top of the model and liquids allowed to drain from the bottom as shown. The permeability of the glass beads was chosen so as to make the model dimensionally similar to the field.

If the theory described previously were complete and accurate the dimensional similarity between the model and the field could be achieved by making the dimensionless time as determined by Equation (17) the same for the model as in the field. Thus, for example, for a given value of T' Equation [illegible] predicts a specific curve of Y vs X.

Examination of Equation (17) indicates that with the above restriction alone it would be possible to compensate for a low permeability K by employing a matrix with a high thermal diffusivity α. The compensation here is based on the idea that the

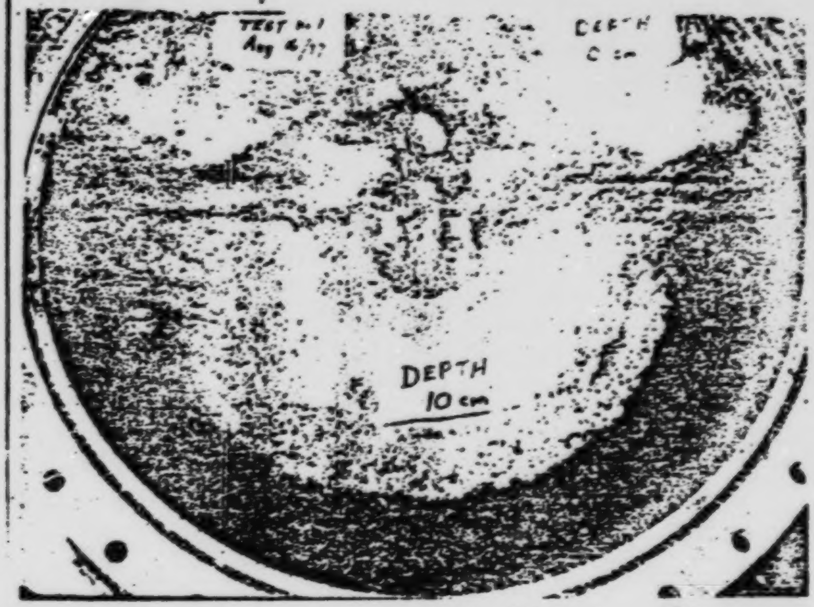

Figure 7 – Photograph of high pressure gravity drainage model. Steam was introduced through a vertical central well and drained oil was removed from a well located immediately below it. Following the completion of the experiment the model was opened and a 10 cm layer of sand was removed from the front half of the model. The interface around the steam chamber can be seen in the picture.

low K would be allowed for because with the higher thermal diffusivity the heated layer in the reservoir would be thicker. Such a compensation is only realistic if there is, indeed, a sufficient depth for heat flow to occur, i.e. the assumption that the reservoir extends to infinity which is implicit in Equation (4) may be unrealistic.

An analysis of this problem has shown that a condition for dimensional similarity which overcomes this problem is that not only should T' as given by Equation (17) be the same for the model and the field but also that the dimensionless number B_2 as given by the following equation should be made the same:

$$B_2 = \frac{mKgH}{\phi S_o \alpha \nu_s} \qquad (18)$$

If T' and B_2 are the same for the model and the field, then other combinations of T' and B_2 are also equal in the model and the field, e.g.

$$(T')(B_2) = Kgt/\phi S_o \nu_s H \qquad (19)$$

$$\text{and } T'/B_2 = (\alpha t/mH^2) \qquad (20)$$

For dimensional similarity it is necessary that B_2 as defined by Equation (18) be the same and the corresponding times can be compared, with identical results, using any one of the dimensionless time numbers(1) given by Equations (17), (19) or (20).

For the model experiment shown here the corresponding model and field conditions are given in Table 1. Ten minutes for the model is equivalent to: $1.3/(1.5 \times 10^{-5}) \times 10$ min or, 1.6 years in the field.

The position of the interface at 10 min intervals is shown in Figure 5. It will be noted that the oil was drained in a systematic manner. It is believed that the tendency of the interface lines to curve upwards near the right hand edge of the model was due to heat losses through the edges of the model. As was shown above, 10 min is about equivalent to 1.6 years in a full scale field example, for the particular conditions chosen for this experiment.

The recovery of oil from the model is plotted against time in Figure 6 and the results are compared with the recovery predicted by Equation (11). The observed rate was of the same order as that predicted but slightly slower. The agreement is encouraging. The lower observed experimental rate is due to factors not recognized in the derivation of the equation. The effective head is smaller than assumed in the theory because of depletion and because of the need to maintain the position of the lower end of the interface at the well. The modified equation with a factor 1.5 in place of the 2 results in better agreement with the initial rate observed in this experiment.

Sealed pressurized physical models

As well as experiments with atmospheric pressure, visual models such as that shown previously, gravity drainage experiments have been carried out using a scaled, pressurized reservoir model. These experiments have used Cold Lake crude with steam pressures of the order of 3 MPa. Figure 7 is a photograph of a horizontal section through one of these reservoir models after the oil had been partially produced by gravity drainage. The spectacular difference between the cleaned steam zone and the undrained sand can be clearly seen in the photograph. In this particular experiment, steam was introduced in a vertical well which was slightly above a vertical production well. Figure 8 shows the well arrangement of the model and the position of the steam front for a typical experiment. The flow was radial rather than linear.

Production rates in these experiments were of the same order as predicted by theoretical gravity drainage relationships which made allowance for the effects of radial rather than linear flow.

Calculated drainage rates

Figure 9 shows the calculated rate at which Cold Lake crude is predicted to drain to a horizontal well using Equation (11). Values of the parameters assumed are also shown. The predicted drainage rate increases with steam temperature because of

---

(1) The dimensionless time defined by Equation (19) is quite similar to the "drainage modulus x time" referred to in a recent paper on gravity drainage by H. Dykstra Ref. (8).

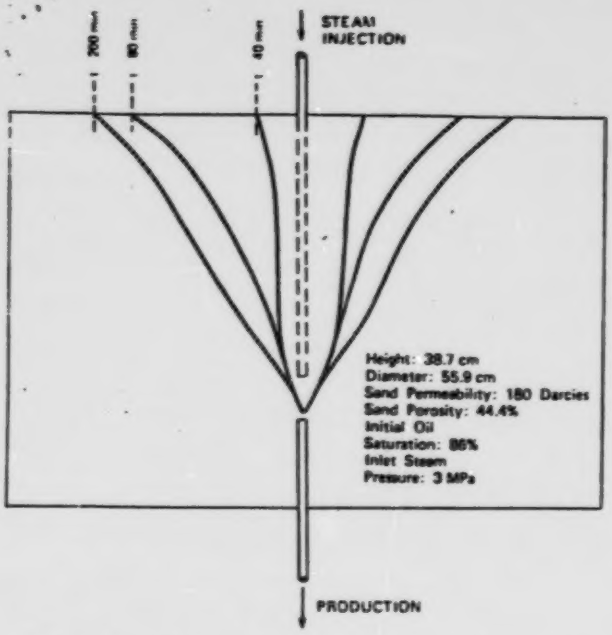

Figure 8 – Position of steam front in pressurized model.

the reduced value of the oil viscosity at steam temperature, ν_s. Rates from about 0.05 to 0.4 m^3/d per metre of horizontal well (0.1 to 0.7 barrels/ft/day) are predicted. Thus, for example, at a steam temperature of 200°C a well 600 m long may be expected to produce about 120 m^3 of oil per day. This is calculated from the simple equation shown. Maximum rates of the order of about 80% of this are more realistic. Also, of course, as reservoir depletion occurs the available head, ΔH, decreases and the rate declines. When the reservoir is about three-quarters depleted, the drainage rate may only be about 50% of that calculated by the equation.

If a vertical production well rather than a horizontal one were employed then the initial effective drainage length would be only the circumference of the well, which would only be 60 to 90 cm. As drainage occurred this effective length would increase somewhat but the overall rate would probably be disappointingly small. In order to make effective use of gravity drainage, horizontal wells are preferred because of the increased effective contact with the reservoir.

The calculated rates shown in the figure assume that the steam chamber reaches to the top of the reservoir. Initially it may be much smaller. A future paper will describe a theory which predicts the rate of rise of such chambers. This will describe how the drainage rate increases as the chamber grows upwards, i.e. as ΔH increases. The initial process can be accelerated by injecting steam initially at above fracturing pressure and creating a fracture above the production well. It is advisable in this case to locate the horizontal production well along the fracture trend direction.

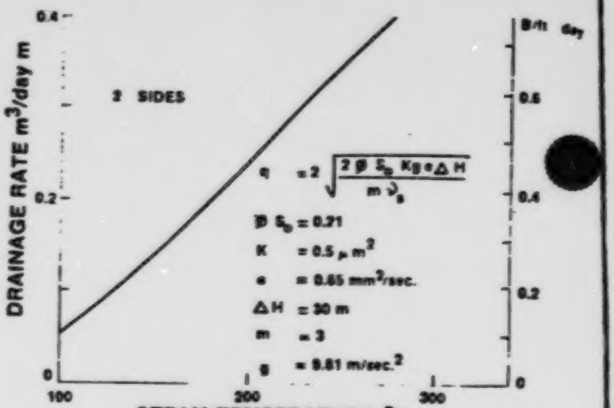

Figure 9 – Calculated drainage rate for Cold Lake crude in reservoir.

Conclusions

Continuous drainage to a horizontal well at the base of a growing steam chamber appears to be an attractive possibility for the in-situ production of heavy crudes. It has the potential to provide higher recovery and potentially can be used with low pressure steam. The rate of drainage of heavy oil to such a well calculated to be of the order of 0.16 m^3/d per metre (0.3 barrels per day per foot) of well. An equation has been developed which allows the estimation of the effect of the major variables upon the drainage rate.

Nomenclature

b = the exponent in the equation $K_r = S^b$ as used by Cardwell and Parsons
B_2 = dimensionless number defined by Equation (18)
g = the acceleration due to gravity, m/d^2
H = the distance from the bottom of the reservoir to the top in meters
m = a dimensionless constant which is dependent upon conditions used and upon the nature of the heavy oil
K = the effective permeability to oil flow. It will normall about 40% of the total permeability, m^2
Q = the oil drainage rate in volume per unit length of well per unit time, m^3/(m · d) for each side of the chamber. Q must be multiplied by 2 to obtain the total flow
$\overline{S}_o$ = the initial oil saturation, or, more correctly, the difference between the initial oil saturation and the residual saturation
T = temperature at a distance ξ from interface, °C
T' = dimensionless time defined by equation (17)
T_R = initial reservoir temperature, °C
T_s = steam temperature, °C
x = the horizontal coordinate
X = x/H
y = the distance from the bottom of the reservoir to the bottom of the steam chamber in metres
Y = y/H
Z = depth of steam chamber (H–y), m
α = the thermal diffusivity of the reservoir material, m^2/d
θ = angle of inclination of interface as defined in Figure 3
ν_s = the viscosity of the oil at steam temperature, e.g. m^2/d
ξ = the perpendicular distance from interface, m
ϕ = the porosity

References

(1) Prats, M.: "A Current Appraisal of Thermal Recovery', J. Pet Technol. 1129-1136 (Aug. 1978).

(2) Dykstra, H.: "The Prediction of Oil Recovery by Gravity Drainage", J. Pet. Technol. 818-830 (May 1978).

(3) Terwilliger, P.L., Wilsey, L.E., Hall, H.N., Bridges, P.M., and Moise, R.A.: "An Experimental and Theoretical Investigation of Gravity Drainage Performance", Trans. AIME 192, 285-296 (1951).

(4) Cardwell, W.T. and Parsons, R.L.: "Gravity Dra Theory", Trans. AIME 146, 28-53 (1942).

Manuscript received April 24, 1980; accepted for publication January 5, 1981.

SPE

Society of Petroleum Engineers of AIME

SPE 13076

84

3D Thermal Simulation Using a Horizontal Wellbore for Steamflooding

by R.M. Rial, *Mobil Oil Corp.*

SPE Member

Copyright 1984 Society of Petroleum Engineers of AIME

This paper was presented at the 59th Annual Technical Conference and Exhibition held in Houston, Texas, September 16–19, 1984. The material is subject to correction by the author. Permission to copy is restricted to an abstract of not more than 300 words. Write SPE, 6200 North Central Expressway, Drawer 64706, Dallas, Texas 75206 USA. Telex 730989 SPEDAL.

ABSTRACT

Steamflooding has been used for years in enhanced oil recovery. However, the use of a horizontal wellbore for injection is a relatively new application that could improve process efficiency. This paper explores the effect of a horizontal wellbore for steamflooding using a three-dimension thermal simulator. Using a Primos 1, and lately a Cray-1, a comparison was made between a conventional vertical wellbore and a horizontal wellbore model.

The data used were representative of the Kern River Field, Kern County, California. The results of the two models showed a 13% increase in oil recovery for a horizontal wellbore. The temperature and oil phase saturation distribution revealed an improved sweep efficiency with a horizontal wellbore. For a five year period the horizontal model had production of 214.14 MSTB (64% OOIP) compared to 163.61 MSTB (51% OOIP) for the vertical model. After 15 years the horizontal model produced 237.55 MSTB (71% OOIP) and the vertical model produced 194.01 MSTB (58% OOIP). The heat transmissibility was higher throughout the grid system using the horizontal model.

A horizontal wellbore proved to enhance oil recovery for steamflooding using the data and simulation developed. There are also possible applications to other enhance oil recovery processes.

INTRODUCTION

In 1980, over 60% of the active enhanced oil recovery projects in the United States were continuous steamfloods. Heavy-oil fields, in California particularly, produced an estimated 400,000 BBLS of oil by using steam floods. Steamflooding has been the most widely used of all EOR processes. This may be attributed to the high recovery efficiency and relatively low cost of displacing oil with steam. This paper examines the application and discusses the effect of a horizontal wellbore for steamflooding.

The conventional procedure for a steamflood project utilizes a vertical wellbore. Depending on the pattern and well spacing, the injected steam displaces the oil through a reservoir and produces it through a vertical production well. The purpose of this paper is to examine whether or not a horizontal wellbore will enhance oil recovery from a steamflood. The effects on sweep efficiency, heat distribution, heat transmissibility, and cumulative production will be included in determining the success of this idea.

A thermal simulator was developed to analyze the effect on steam flooding by using a horizontal wellbore for injection. Simulation was chosen because it is a relatively inexpensive way to determine the feasibility and effectiveness of such a proposed idea. It is also a reliable way to predict performance in a reservoir environment.

The approach taken included simulating a steam drive project from a horizontal wellbore at the bottom of a heavy-oil reservoir. A three dimensional numerical model was developed that would account for three-phase flow, steam distillation, and temperature dependent relative permeability. This model describes flow by Darcy flow and includes gravity, viscous, and capillary forces.

The input data used for the steam drive model was the result of collective research from published data. It was representative of the Kern River Field, Kern County, California. The results of the horizontal wellbore model were compared to the results of the vertical wellbore model. Both simulation runs used the same input data, therefore the results are comparable under the given conditions and parameters.

References and illustrations at end of paper.

THEORY

Model Description

The grid for the steam drive model used a 4-layered, 7x7 Cartesian system. The model was a 2.5 acre 1/4 five spot using 9 point difference, Figure 1. To simulate a horizontal wellbore, the model defined steam injection in six grid blocks along the edge of the bottom layer. Each injection point simulates injection as if a horizontal well was drilled in the same location. This is a possible estimation of how steam injection will behave for a horizontal wellbore. The vertical producing well was located in the center of the opposite edge of the grid system, Figure 2.

The three-dimension, three-phase numerical simulator was patterned after a model described by Coats et al.[1] The model consists of the necessary equations that consider transport of mass and energy, mass and energy balances, heat losses to overburden and underburden layers, and constraints on sums of liquid and gas phase mole fractures. The simulator equations are basically volumetric material balances for each phase in each grid block. Flow in the adjacent blocks are represented by Darcy's Law. The mass and energy balance equations were programed in finite difference form.

The simulator program assumes a lower oil viscosity at the higher temperature and pressure tends to result in increased oil recovery. Initially the reservoir rock is assured to be homogeneous, isotropic, incompressible, in thermal equilibrium with adjacent layers, and uniformly saturated with gas, water and oil.

The model consists of five equations expressing:

(1) conservation of energy,

(2) conservation of mass for water, steam and oil,

(3) steam-water equilibrium.

- water

$$-qc+V/\Delta t\,\delta(\phi b_w S_w)=\Delta(T_w(\Delta P_w-\gamma_w\Delta Z))-q_w$$

- steam

$$qc+V/\Delta t\,\delta(\phi b_g S_g)=\Delta(T_g(\Delta P_g-\gamma_g\Delta Z))-qg$$

- oil

$$V/\Delta t\,\delta(\phi b_o S_o)=\Delta(T_o(\Delta P_o-\gamma_o\Delta Z))-q_o$$

- energy

$$V/\Delta t\ (\phi(b_w S_w U_w+b_o S_o U_o+b_g S_g U_g)+$$

$$(1-\phi)(\rho C_p)_R T)=\Delta(T_h\Delta P)+\Delta(T_c\Delta T)-q_l-q_h$$

- equilibrium $T=Ts(p)$

Flow transmissibilities between two blocks requires average interblock values of Kr, FVF, μ, and H. In practice, Kr and H data are weighted 100% upstream. Tables of Kr and Pc vs saturation are read into the simulator for 2P, W-O and G-O systems. Three phase Kr is calculated using Stone's method. Linear interpolation is used between adjacent entries within the tables.

Viscosities are entered into the simulator as a tabular function of temperature. Interpolation between adjacent entries is performed assuming linearity of log μ vs log T.

ϕ, oil and water FVF are expressed as a function of P and T.

$$b_w=b_{wi}(1+C_w(P-P_i)-C_{tw}(T-T_i))$$

$$b_o=b_{oi}(1+C_o(P-P_i)-C_{to}(T-T_i))$$

$$\phi=\phi_i(1+C_r(P-P_i))$$

Internal energies of water and oil are represented as:

$$U_w=U_{wi}+C_{pw}(T-T_i)$$

$$U_o=C_{po}(T-T_i)$$

The condensation term (mass transfer) is eliminated by combining the water and steam equations. Mass and energy balance equations are solved simultaneously. Water transmissibilities are handled implicitly. The equilibrium equation can be expanded if steam is present as:

$$T_{n+1}=T_s(P_{n+1})=T_{sn}+T_{sp}\,\delta P$$

$$\text{where } T_{sp}=\frac{Tsn+1-Tsn}{Pn+1-Pn}$$

If no steam is present at t_{n+1} then:

$$\delta S_g=-S_{gn}$$

Final simulation equations are expressed in terms of δSg, δSw, δT, and δP. This accounts for coefficients $C_{i,j}$ and residuals R_i.

The implicit production rates are calculated:

$$q_{m,u+1}=q_{m,n}\,\delta P+q_{m,sw}\,\delta S_w+q_{m,sg}\,\delta S_g$$

Productivity index for a single layer:

$$PI=\frac{\pi\ 2Kh}{\ln re/rw-1/2+s}\times\frac{.0063}{5.615}$$

rc=equivalent radius of the grid block

The production rate of phase m:

$$q_m=PI\ \frac{Krm\ bm}{\mu\ m}(P-P_{well})$$

The total liquid production rate (RB/D):

$$q^*=PI\ (K_{rw}/\mu_w+K_{ro}/\mu_o)(P-P_{well})$$

Saturation and temperature coefficient are recorded for each grid block at each time step. S and T are during the next time step are averaged for flow in x,y, and z directions.

Experimental data has shown that temperature dependence on relative permeability has improved calculated results. Relative permeability curves were read at the original reservoir temperature and converted to forms of Krw, Krow, Krog. Krg versus S_w and were allowed to change with temperature. The relative permeability to oil, Kro, was obtained using Stone's method.[2]

Discussion of Data

The input data used for both the vertical and horizontal models were essentially the same. The data set was developed from an abundance of published field data representing Kern River Field. Table 2 contains component PVT properties for the three phase system. The gas and oil viscosities are presented as a function of temperature in Table 3. Temperature dependent relative permeabilities were estimated and presented in Table 4.

The depth of the reservoir is assumed to be 600 feet, and a dip angle of 15° was used. The grid block thickness, permeability, specific gravity, formation, oil and water compressibilities, specific, reservoir thermal conductivity, thermal expansion, and fluid saturation are tabulated in Table 5.

Application of Equipment and Process

Two computers were used to effectively obtain the results. Simulation runs were performed on Primos-1. Due to the storage and CPU time involved a Cray-1 was used at a later date. The Primos-1 was used to interpolate and sort through the available data and results. The first set of runs were performed using a horizontal wellbore for injection along one edge and a vertical production wellbore in the opposite corner of the grid system. The conventional steamflood had a injector and a producer in the opposite corners. After analyzing the resutls it was concluded that the two models were difficult to compare. This was remedied by moving the producing well in the horizontal model to the center edge of the grid system, figure 1. Then, for the vertical model, both the injector and producer are placed at the center edges of the grid system, figure 2. This produced better results for comparison.

DISCUSSION OF RESULTS

The effectiveness or non-effectiveness of a horizontal wellbore was gauged by comparing the two models under the same conditions and properties. Three categories were examined: (1) cumulative production (2) heat transmissibility (3) areal sweep. The temperature and saturation distribution at each time step were included in the results. The heat transmissibility of both models was also analyzed to determine how much heat has reached the reservoir.

Temperature and Saturation Distribution

The temperature and saturation changes caused by steam injection can be seen by comparing figures 3, 4, 5 and 6. It is obvious that the use of a horizontal model not only had a greater effect on the steam bank development than the vertical model, but a more effective sweep. Over a five year period the even temperature distribution, shown in figures 3b and 4b, signifies greatly increased oil displacement. The saturation distribution demonstrated to have the same effect in figure 6b for the horizontal model. The oil phase saturation is much lower across the grid system for the horizontal model, whereas the vertical model demonstrated higher oil phase saturations along the edges. The temperature and saturation distributions indicate a distinct advantage of the horizontal model. The steam front showed an even, consistent reach across the grid system. The oil phase saturation for both models at the end of ten years is shown in figure 7. These numbers represent a diagonal cross-section from injector to producer. As saturations progress toward the producing well, the horizontal model revealed lower oil saturations left by displacement. After ten years the vertical model had 58% oil phase saturation in the bottom layer after having 71% at one year. During the same time period, the horizontal model demonstrated an oil phase saturation of 68% for one year and 23% for ten years.

Sweep Efficiency

Rate of injection, steam quality, and kinematic viscosities of the steam and crude at steam tempreature are the chief determinants of steam drive efficiency. These factors are assumed to account for the most representative conditions possible. The dual sweep efficiency of the two models showed a distinct difference in method. The horizontal model had an areal sweep efficiency of 84% for the ten year period. The vertical model showed an areal sweep efficiency of 73%. The important aspect of these efficiencies are not the size, but the improvement due to the horizontal model. These efficiencies are averaged from grid block to adjacent grid block. This could create some error over the extent of the entire model. However, by examining the distribution of the temperature and oil phase saturation, it is understandable that the horizontal model would have a much higher sweep efficiency.

Movement of Heat

The degree of success from a steamflood is determined by the amount of heat transmitted to the outer reaches of the reservoir. The heat transmitted through the grid blocks was calculated and shown in figure 9. For both models the flow patterns demonstrated changes as the steam front moved from the injector to producer. The vertical model demonstrated a radial flow toward the producing well. However, this model leaves areas toward the sides of the grid system untouched, figure 3 and 5. The horizontal model demonstrates an even progression from the injector. At a greater distance the flow resembles a radial movement as in the temperature profile. The comparison reveals that the horizontal model covered more of the grid system and reached further out with more heat. This indicates that more heat reached the oil, therefore lowering the oil viscosity and producing more oil.

PRODUCTION

The production of the two methods studied provides the best insight into their effectiveness. For years steam injection has provided an effective

effective way to enhance heavy oil recovery. Examination of production results for each model demonstrates a clear pattern. Figure 8 shows the cumulative production over 15 years. The horizontal wellbore demonstrated a higher, steeper production curve within the first five years. Steam was effectively displacing oil during this period. Between five and ten years, however, this curve began to level off and was projected to approximately 71% recovery of OOIP. After only five years the production is 214.13 MSTB, 69% of OOIP. From the same five year period, the vertical model showed only 163.01 MSTB, or 51% of the OOIP. The 15 year projection shows the horizontal model producing 237.55 MSTB. The vertical model produced 194.01 MSTB. Table 6 shows the yearly breakdown of cumulative production.

Table 6 and figure 8 demonstrate the potential that the simulation model will produce for both the horizontal and vertical wellbores. Comparison of the production curves reveals a 13% increase in production by a horizontal wellbore over the conventionally used vertical wellbore for steamflooding. In terms of the simulation model, this equates to an increase of 50.82 MSTB for five years and 55.20 MSTB for ten years. This is impressive in that the operator can receive most of the production in the first five years.

RECOMMENDATIONS

(1) Correlations are needed between reservoir and wellbore properties to modify Darcy's Law for a horizontal wellbore. This should include both reservoir simulation and laboratory experiments to develop an analytical and numerical equation.

(2) Since there exists an advantage for steamflooding using a horizontal wellbore, further investigation is needed into other areas:

- other EOR processes, waterflood, polymer, etc.
- Tar-sand reservoirs
- primary oil and gas production
- horizontal wellbore for both injector and producer
- economics of such projects

CONCLUSIONS

(1) Under the reservoir conditions and parameters assigned, the simulator produced reasonable results. A horizontal wellbore model demonstrated to have a more consistent areal sweep than the conventional vertical wellbore model.

(2) Temperature and oil phase saturation distributions that a horizontal wellbore was more efficient than the vertical wellbore for steamflooding.

(3) When a horizontal wellbore was simulated for steam injection, it produced 71% of the OOIP for 15 years. The vertical wellbore model produced 58% OOIP for the same time period.

(4) The horizontal wellbore model swept more heat through the grid system and produced more BTU's than the conventional vertical wellbore model.

(5) Further investigation into other EOR processes needs to be researched.

ACKNOWLEDGEMENT

A great deal of credit is due S. Robert Aydelatte for his encouragement, direction and critical review while putting this project together.

NOMENCLATURE

C	Compressibility, vol/vol-psi
C_p	Specific het, Btu/lb-F°
C_r	Rock formation compressibility
C_t	Thermal expansion coefficient, vol/vol/-F°
H	Enthalpy, BTU/mol
K_{rw}	Relative permeability to water
K_{row}	Relative permeability to oil in water-oil two phase system
K_{rg}	Relative permeability to gas
K_{rog}	Relative permeability to oil in gas-oil two phase system
K_{rwro}	Relative permeability to water at residual oil S_{orw}
K_{rocw}	Relative permeability to oil at ineducible water saturation S_{wir}
K_{rg}	Relative permeability to gas at residual oil S_{org}
P	Oil pressure, psia
P_i	Initial reservoirs pressure
PI	Productivity index
q_h	Enthalpy production rate, Btu/day
q_h	Heat loss rate, Btu/day
S	Fluid saturation fraction
t	Time, days
T	Temperature, °F
T_i	Initial reservoir temperature
U	Internal energy, Btu/mol
V	Grid block volume, reservoir bbls.
x,y,z	Cartesian coordinates, ft

x_i	Mole fraction component i in oil phase
y_i	Mole fraction component i in gas phase
Z	Depth, vertically downward, ft.
z	Gas phase compressibility factor

Greek

δ	Time difference operator
ρ	Molar density, mole/Rb
μ	Viscosity, cp
ϕ	Porosity, fraction
ϕ_i	Porosity at P_i
T	Transmissibility
T_c	Heat conduction transmissibility

Subscripts

g	Gas
i	Hydrocarbon component number
n	Time level
o	Oil
s	Steam
w	Water
OB	Overburden

Difference Operators

$$\cdots\cdots\ \Delta(T_w \Delta p_w) = \Delta_x(Tw\Delta_x p_w) + \Delta y$$

$$(T_w \Delta_y p_w) + \Delta_z(T_w \Delta_z p_z)$$

$$\cdots\cdots\ \Delta_x(Tw\Delta_x Pw) = T_{wi+1/2,j,k}$$

$$(P_{witi,o,k} - P_{wi,j,k})$$

$$-T_{wi-1/2,vjk}(P_{wi,j,k} - P_{wi-1,j,k})$$

REFERENCES

1. Coats, K. H.: George, W. D.; Chu, Chieh; and Marcum, B.E.: "Three Dimension Simulation of Steamflooding," Soc. Pet. Eng. J. (December 1974).
2. Stone, H. L. "Estimation of Three-Phase Relative Permeability and Residual Oil Data," J. Can. Pet. Tech. (October-December 1973).

BIBLIOGRAPHY

Aydelotte, S. Robert; Pope, Gary A.: "A Simplified Predictive Model for Steamdrive Performance," J. Pet. Tech. (May 1983).

Coats, K. H.: Meldan, R. F.; Shipley, R. G.: "Cyclic Gas/Steam Stimulation of Heavy-Oil Wells," J. Pet. Tech. (October 1981).

Coats, K. H.: "In-Situ Combustion Model," Soc. Pet. Eng. J. (December 1974).

Coats, K. H.; George, W. D.; Chu, Chieh; and Marcum, B. E.: "Three Dimensional Simulation of Steamflooding," Soc. Pet. Eng. J. (December 1974).

Coats, K. H.: "Simulation of Steamflooding with Distillation and Solution Gas," Soc. Pet. Eng. (October 1976).

Coats, K. H.: "A Highly Implicit Steamflood Model," Soc. Pet. Eng. J. (October 1978).

Crookson, R. B.; Culham, W. E.; and Chen, W. H.: "Numerical Simulation Model for Thermal Recovery Processes," Soc. Pet. Eng. J. (February 1979).

Dietrich, J. K.: "Relative Permeability During Cyclic Steam Stimulation of Heavy Oil Reservoirs," SPE Paper No. 7968

Farouq, Ali, SM. M.: "A Comprehensive Wellbore Steam/Water Flow Model for Steam Injection and Geothermal Applications," Soc. Pet. Eng. J. (October 1981).

Farouq, Ali, S. M.: "Marx and Langenheim's Model of Steam Injection," Producer's Monthly (November 1966).

Lewin and Associates, Inc.: "Economics of Enhanced Oil Recovery," Final Report, DOE/BETC/2628-2 (May 1981).

Loxam, D. C.: "Texaco Canada Completes Unique Horizontal Drilling Program," Petroleum Engineer International, (September, 1982).

Marx, J. W. and Langenheim, R. H.: "Reservoir Heating by Hot Fluid Injection," Trans, AIME (1959) Vol. 198, 79-92.

Moughamian, J. M.; Woo, P. T.; Dekessian, B. O.; Fitzgerald, J. G.: "Simulation and Design of Steam Drive in a Vertical Reservoir," J. Pet. Tech. (July 1982).

Price, H. S. and Coats, K. H.: "Direct Methods in Reservoir Simulation," Soc. Pet. Eng. J. (June 1974).

Stone, H. L.: "Estimation of Three-Phase Relative Permeability and Residual Oil Data," J. Can. Pet. Tech. (October-December 1973).

Yortsos, Y. C. and Gavalar, G. R.: "Analytical Modeling of Oil Recovery by Steam Injection." Soc. Pet. Eng. J. (April 1981).

Table 1

Relative Permeability at 100^{0}F

Water-oil Functions			Gas-oil Functions		
Sw	Krw	Krow	Sg	Krg	Krog
.15	0.000	1.000	.33	0.000	1.000
.24	0.003	0.673	.41	0.009	0.781
.34	0.021	0.413	.48	0.043	0.590
.43	0.057	0.219	.55	0.099	0.427
.53	0.117	0.087	.63	0.182	0.291
.72	0.205	0.016	.70	0.291	0.182
.81	0.323	0.000	.77	0.427	0.099
.91	0.664	0.000	.85	0.590	0.043
1.00	0.891	0.000	.93	0.781	0.009
			1.00	1.000	0.000

Table 2

Component PVT Properties

	Water	Oil	Gas
Mole wt.	18.0	400.0	23.2
Critical Pressure (PSIA)	3206.2	0.0	663.9
Critical Temperature (^{0}R)	1165.4	0.0	419.7
Compressibility (1/PSI)	0.0	0.32×10^{-5}	0.227×10^{-3}
Thermal Expansion Coefficient (1/^{0}F)	0.0	0.32×10^{-3}	0.495×10^{-2}
Heat of vaporization (BTU/LB)	0.0	0.0	180.0
Stock-Tank Density (lb/cu ft)	62.4	60.58	0.0

Table 3

Gas and Oil Viscosity

Temp.	Gas Viscosity, cp Phase			Oil Viscosity, cp Phase		
	Water	Oil	Gas	Water	Oil	Gas
110	0.0	1.70	0.0111	0.0	407	0.0
130	0.0	1.33	0.0114	0.0	149	0.0
150	0.0	1.06	0.0117	0.0	66.1	0.0
170	0.0	0.86	0.0210	0.0	33.8	0.0
190	0.0	0.71	0.0124	0.0	19.3	0.0
210	0.0	0.59	0.0127	0.0	12.0	0.0
230	0.0	0.50	0.0130	0.0	8.0	0.0
250	0.0	0.43	0.0133	0.0	5.6	0.0
270	0.0	0.36	0.0137	0.0	4.1	0.0
290	0.0	0.31	0.0140	0.0	3.1	0.0
310	0.0	0.27	0.0143	0.0	2.4	0.0
330	0.0	0.23	0.0146	0.0	1.9	0.0
350	0.0	0.21	0.0149	0.0	1.6	0.0
370	0.0	0.18	0.0153	0.0	1.3	0.0
390	0.0	0.16	0.0156	0.0	1.1	0.0
410	0.0	0.14	0.0159	0.0	0.9	0.0
430	0.0	0.13	0.0162	0.0	0.8	0.0
450	0.0	0.12	0.0165	0.0	0.7	0.0
470	0.0	0.10	0.0168	0.0	0.6	0.0
490	0.0	0.08	0.0170	0.0	0.5	0.0

Table 4

Relative Permeability - Dependence

Temp	Swc	Swir	Sorw	Sorg	Krwro	Krocw
100	0.15	0.15	0.33	0.18	0.30	1.00
200	0.20	0.20	0.22	0.13	0.44	1.00
300	0.23	0.25	0.15	0.09	0.62	1.00
400	0.30	0.30	0.10	0.06	0.62	1.00
500	0.35	0.35	0.08	0.04	0.62	1.00

Table 5

Input Data Used

Depth, ft.	600
Compressibility (1/PSI)	7.35×10^{-4}
Porosity, fraction	0.34
Initial Temperature (^{o}F)	95.0
Initial Pressure (PSIA)	82.6
Rock Specific Heat (BTU/cu ft ^{o}F)	35.0
Reservoir Dip, degree	15.0
Connate Water Saturation	0.15
Residual Water Saturation	0.15
Residual Oil Saturation (w-o flow)	0.30
Residual Oil Saturation (g-o flow)	0.18
Critical Gas Saturation	0.00
Residual Gas Saturation	0.00
Oil Saturation in Initial Gas Cap	0.18
Flow Rate (bbl/D)	300.0
Steam Quality	0.75

Table 6

Yearly Production

Year	Horizontal Model		Vertical Model	
	Oil Production (MMSTB)	% OOIP	Oil Production (MMSTB)	% OOIP
1	20.44	6.0	12.06	3.6
2	75.09	22.4	47.59	14.2
3	154.50	46.1	93.84	28.0
4	195.05	58.2	146.79	43.8
5	214.13	64.0	163.61	51.0
6	221.19	66.0	177.29	52.9
7	227.23	67.8	182.98	54.6
8	229.57	68.5	184.99	55.2
9	231.58	69.1	187.68	56.0
10	233.93	69.8	189.02	56.4
15	237.55	70.8	194.01	57.9

Table 7

Grid Block Parameters

	Layers			
	1 (top)	2	3	4 (bottom)
Thickness, ft.	12	9	20	30
Permeability, md.	5.500	5,500	2,000	1,400
Porosity, fraction	.34	.34	.34	.34
Depth, ft.	606	616	631	656
Initial Gas Phase Pressure, psia	55.5	60.0	66.5	78.0
Initial Water Phase Saturation	.28	.28	.30	.32
Initial Oil Phase Saturation	.72	.72	.70	.68
Pore Volume, bbls	409.7	307.3	785.2	1,024

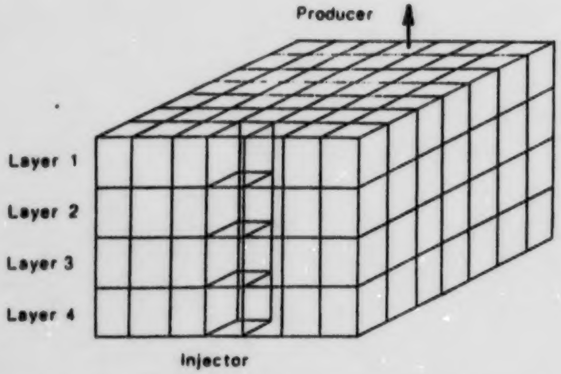

Fig. 1—Conventional vertical wellbore 7 X 7 X 4, 2.5-acre, one-fourth five-spot with 9 point difference.

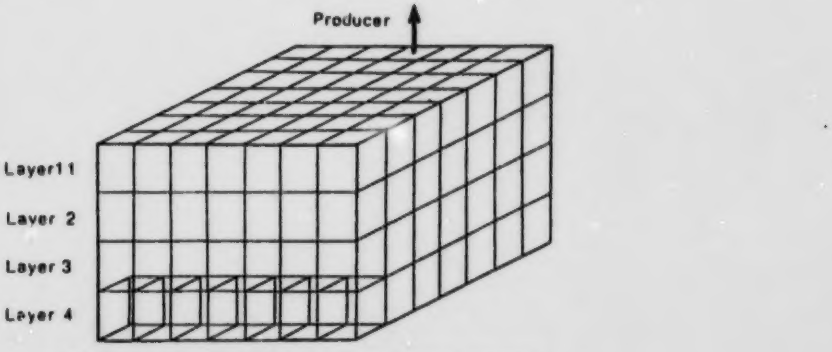

Fig. 2—Horizontal wellbore model injection into bottom six grid blocks.

Figure 3 - Temperature Distribution for Vertical Model

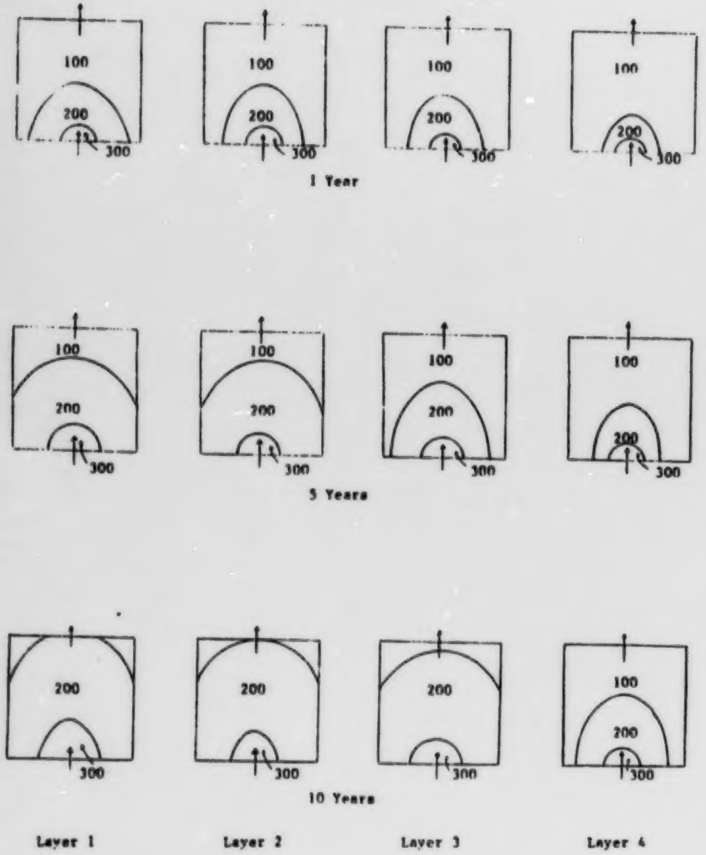
100
200
300
1 Year
5 Years
10 Years
Layer 1
Layer 2
Layer 3
Layer 4

Figure 4 - Temperature Distribution for Horizontal Model

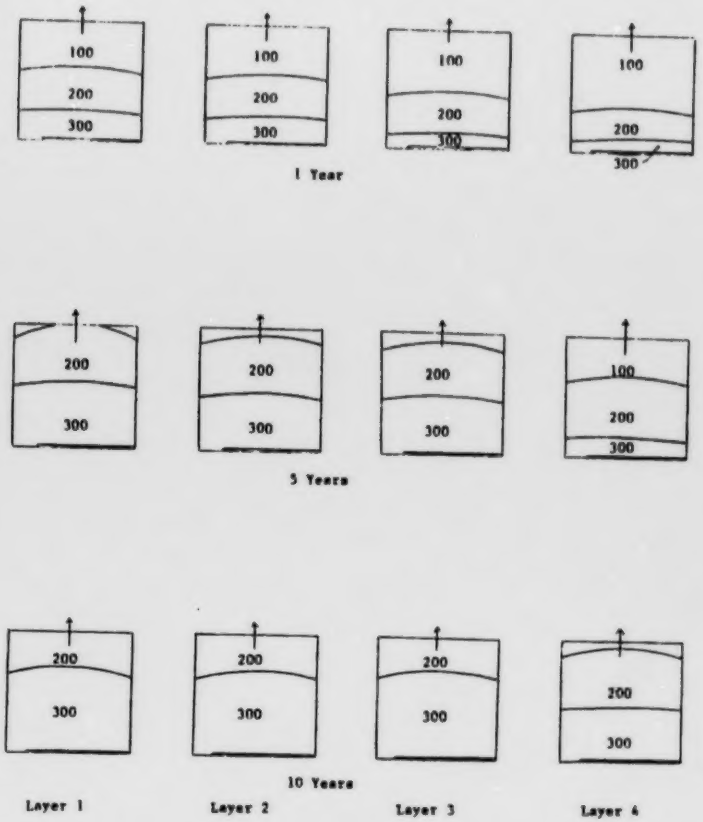
100
200
300
1 Year
5 Years
10 Years
Layer 1
Layer 2
Layer 3
Layer 4

Figure 5 - Oil Phase Saturation Distribution
for Vertical Model

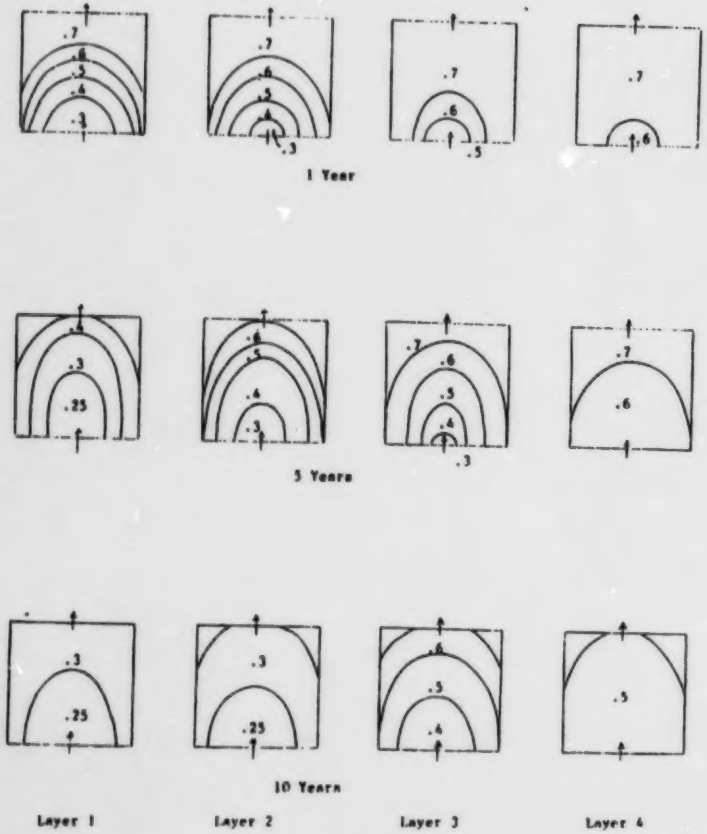

Figure 6 - Oil Phase Saturation Distribution
for Horizontal Model

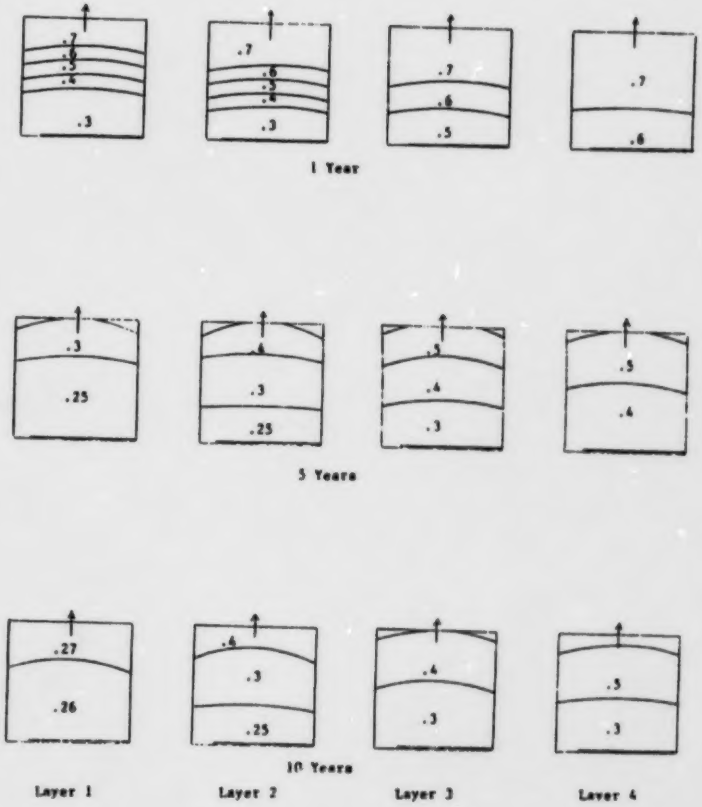

Layer	Grid Blocks 1	2	3	4	5	6	7
1	.38	.39	.41	.43	.46	.48	.50
2	.27	.28	.29	.30	.34	.38	.41
3	.24	.25	.25	.27	.29	.30	.32
4	.23	.23	.24	.25	.27	.27	.28

Layer	Grid Blocks 1	2	3	4	5	6	7
1	.39	.40	.41	.43	.45	.47	.48
2	.27	.28	.29	.30	.33	.35	.37
3	.24	.25	.26	.27	.29	.31	.32
4	.24	.24	.25	.27	.28	.28	.29

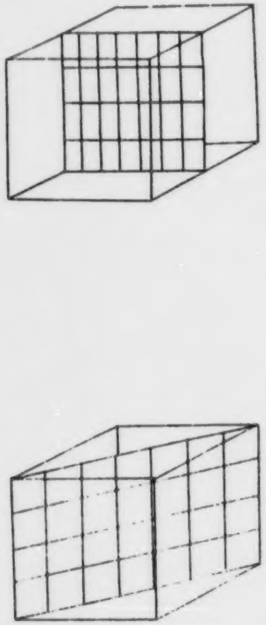

FIGURE 7

Oil Phase Saturation Distrubtion for
Ten years

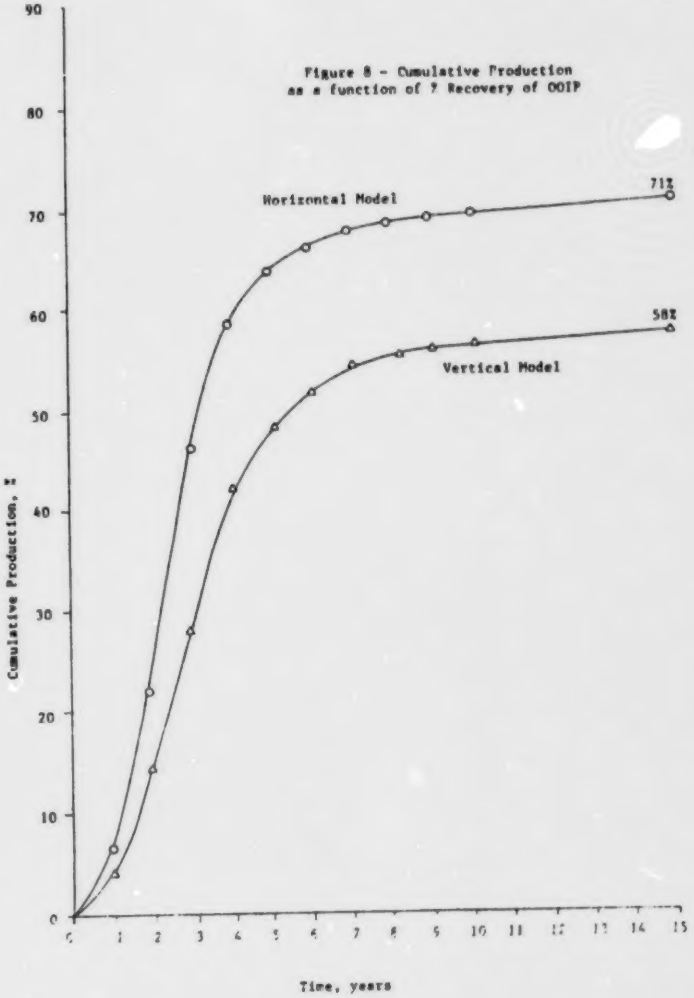

Figure 8 - Cumulative Production
as a function of ? Recovery of OOIP

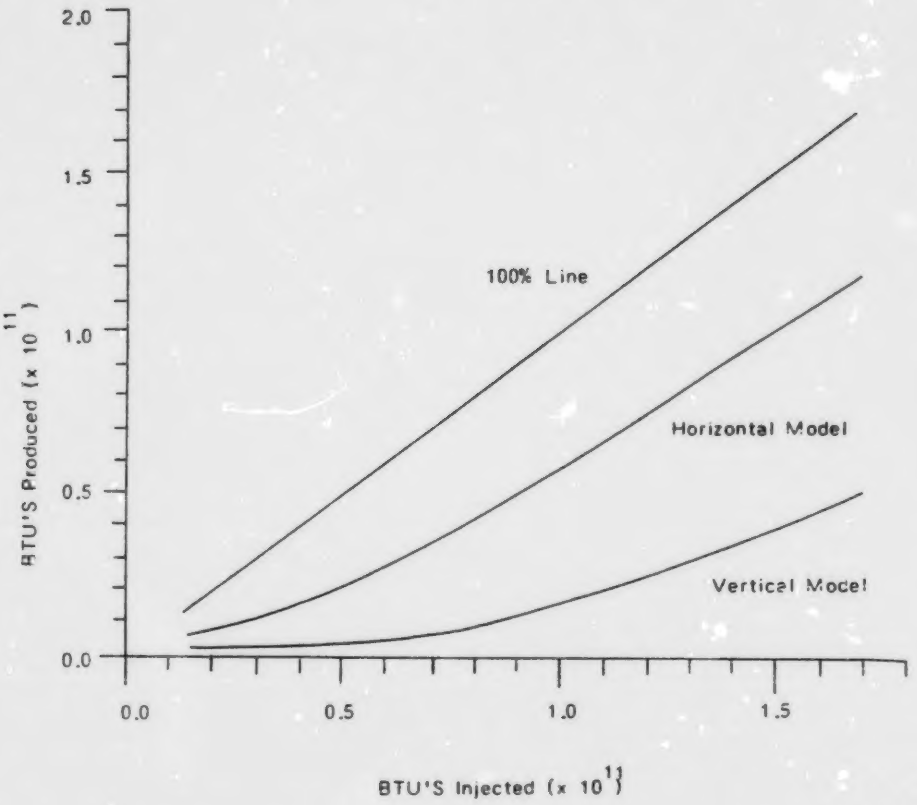

Figure 5 - Comparison of BTU'S Injected against BTU'S Produced

010292

OIL SANDS
INF CENTRE

PETROLEUM SOCIETY OF CIM

PAPER NO. 85-36-28

THIS IS A PREPRINT — SUBJECT TO CORRECTION

85

PREDICTING STEAM RECOVERY OF ATHABASCA OIL THROUGH HORIZONTAL WELLS

by
S. Jain
A. Khosla
Petro-Canada Resources

PUBLICATION RIGHTS RESERVED
THIS PAPER IS TO BE PRESENTED AT THE 36TH ANNUAL TECHNICAL MEETING OF THE PETROLEUM SOCIETY OF CIM HELD JOINTLY WITH THE CANADIAN SOCIETY OF PETROLEUM GEOLOGISTS IN EDMONTON JUNE 2-5, 1985. DISCUSSION OF THIS PAPER IS INVITED. SUCH DISCUSSION MAY BE PRESENTED AT THE TECHNICAL MEETING AND WILL BE CONSIDERED FOR PUBLICATION IN CIM JOURNALS IF FILED IN WRITING WITH THE TECHNICAL PROGRAM CHAIRMAN PRIOR TO THE CONCLUSION OF THE MEETING.

ABSTRACT

This paper describes the development of operating strategies and production performance predictions for horizontal wells drilled from a tunnel as well as surface deviated horizontal wells in combination with vertical wells. Scientific Software Intercomp's Steam and Therm Model were used for the studies. The reservoir considered in this investigation had characteristics similar to the Athabasca McMurray formation. Steamdrive was used as the primary recovery process.

Three configurations were studied. The first configuration involved two 150 m long horizontal wells spaced 60 m apart. Computer model studies led to the development of an effective operating strategy with an oil production capability of about 22 m³/d and an SOR of 5.5. Predicted oil recovery was 58% of the original oil-in-place in a seven year operation. The second configuration studied involved a horizontal well (300 m long) and a vertical well in communication with it. With steam continuously injected into the horizontal well, the vertical well produced at a rate of approximately 12.5 m³/d of oil at an SOR of 8.6 for about 6 years. The third configuration had a horizontal well with two vertical wells in combination with it to create a heated plane over the horizontal well. In this case, Butler's concept of a steam chamber and gravity drainage was modelled. The horizontal well was 400 m long with two vertical wells located over it, equidistant from its two ends. The modelling study showed that continuous steam injection into the vertical wells resulted in horizontal well oil production capability (after initial stimulation) of about 50 m³/d with an SOR of 8. The well life was calculated to be 7.5 years.

INTRODUCTION

In 1978 Petro-Canada, as operator for a five party group including Esso Resources Canada Ltd., Husky Oil Ltd., Canada Cities Service (now Canadian Occidental Ltd.) and Gulf Canada Ltd. initiated the MAISP Project at an outcrop near Fort McMurray. Three horizontal wells were drilled and completed in the oil sands. The purpose of this surface demonstration was to investigate the feasibility of horizontal well drilling and completion to increase confidence in proceeding to an underground test and to obtain data for the design of an underground test. This test project demonstrated that long horizontal wells could be successfully drilled, completed and operated. Though the production was a secondary objective of the project, the production results were also encouraging. During production, two modes of steam operation were tested, hot finger stimulation and steamdrive. After about a month of operation in the hot finger mode, interwell communication was achieved between two wells spaced 8 m apart. The pilot was abandoned after one and one half years of operation(1). Because of the success of the pilot, computer simulation and design studies were carried out in-house to further explore the potential of horizontal well processes for recovering oil from the Athabasca oil sands deposits.

This paper deals with a study of tnree configurations of horizontal and/or vertical wells. The first configuration consisted of two parallel horizontal wells 150 m long and about 60 m apart reflecting a repeated pattern of 0.9 ha. While studying the process, completion and operation of the wells was assumed to be from a tunnel in a system of shafts and tunnels. A steamdrive process was evaluated. The second configuration consisted of a surface deviated horizontal well 300 m long in communication with a vertical well. Steam was continuously injected through the horizontal well and the vertical well acted as the producer. The third process, based on Butler's Steam Chamber Concept(2) consisted of a system of one surface deviated horizontal and two vertical wells. The length of the horizontal well was assumed to be 400 m and the vertical wells were located above the horizontal well equidistant from its ends. Steam was injected above fracture pressure in the the vertical wells to create a vertical heating plane parallel to the horizontal well and the fluids were produced from the horizontal well.

Parallel Horizontal Wells

In this case, the potential of the steamdrive recovery process was evaluated. In order to be realistic, the typical McMurray formation description and rock properties shown in Table 1 were developed from actual cores and logs of one of the core-holes drilled by Petro-Canada in the Northern Athabasca leases. The configuration, considered in this evaluation, is shown in Figure 1A. The horizontal length was limited to 150 m in anticipation of problems in recompleting hot wells in order to improve the sweep efficiency. The other-data, such as viscosity are shown in Table 2. Temperature dependent relative permeability data developed from other history match studies were used.

Model Formulation

Scientific Software Intercomp's three-component steam model (1982 version) was slightly modified to accept actual wellbore geometry in the well grid block. A well-cell concept was developed by Petro-Canada in order to simulate the fluid and thermal flow in and around the well in a realistic manner. One disadvantage of this method was higher CPU cost. To offset that an optimized grid system of 210 blocks was used to simulate the steam stimulation/drive process. With the symmetry in a repeated pattern configuration, half wells were simulated. Also note that the two horizontal wells are located in a reservoir zone of 55% water saturation to assist in achieving well to well communication in a reasonable time. Open hole completion with slotted liners was assumed. Tubing in both the wells extended 3.75 m into the horizontal portion from the wellheads (see Figure 1B).

Operating Strategy

Many cases were run to reach a nearly optimal strategy. Without going into the details, various well placements, grid sizes, steam stimulation injection rates and slugs, time for reversing well functions etc. were studied. The results from the following nearly optimal strategy are discussed:

(i) Initial Well Stimulation

Inject 70% quality steam at 3 600 kPa (below fracture pressure) at a temperature of 250°C in well #1 at a maximum rate of 240 m^3/d (CWE) while flowing well #2. At 100 days, switch steam injection to well #2 at the same conditions while flowing well #1. Produce wells against a BHFP of 1 000 kPa.

(ii) Initiating Steamdrive

From 100 days to 730 days, continuously injected steam into well #2 while producing fluids from well #1.

(iii) Recompleting the Injector

From 730 days to 900 days discontinue steam injection in well #2 while continuing production from well #1. This depressurization process facilitates recompletion of the injector. At 900 days recomplete the injector so that the tubing, initially located 3.75 m from the wellhead is now at 90 m from the wellhead (middle of model block J=3). Use packers around the tubing at 30 m from the wellhead so that injection occurs from 120 m zone along the injector beyond 30 m (see Figure 1C).

Operate with steam injection in well #2 from 900 to 1200 days with production from well # 1.

(iv) Recompleting the Producer

At 1200 days, recomplete the producer also in the manner defined earlier (see Figure 1C). Continue the injection and production process to 2400 days.

Results

The simulation model was actually run up to 2200 days at which time oil was being produced at a rate of 22.5 m^3/d. The oil rate was extrapolated until it reached a limit of 5 m^3/d (see Figure 2) giving a well life of about 2 400 days (6½ years). During the life of the wells, 53 000 m^3 of bitumen was produced at a calendar day oil rate of 22 m^3/d recovering approximately 58% of the OOIP. At the end of the operation, an SOR and a WOR of 5.5 and 5.4 were achieved (see Figure 3).

To decide on the appropriate time for recompleting the wells, a curve for cumulative OSR vs cumulative steam injected/total pore volume was plotted (see Figure 4). A dip in the curve indicated that steam was not sweeping any additional reservoir resulting in a drop in oil production. After about two years of injection/production, a decline in OSR was observed which corresponded to 0.75 pore volume of cumulative steam injected. Steam injection was stopped at this point and the injection well was recompleted. Before recompleting the injector, the reservoir was depressurized to facilitate recompletion. Sensitivity runs showed that before the recompletion of the injector, pressure cycling in stages by pressurizing the reservoir, blowdown and production, pressure maintenance, production cycling and injection cycling did not improve the oil production.

After recompleting the injector, injection and production were carried out up to 1200 days. At this point cumulative OSR again declined (see Figure 4) and the producer was recompleted. Injection and production operations were carried out to 2 400 days until the OSR flattened out (see Figure 4).

Initially when the tubing in each of the wells was located 3.75 metres from the wellhead, heat front breakthrough (fluid breakthrough) was achieved at about 230 days up to 30 m along the well from the wellhead (in model blocks J=1 and J=2, see Figure 5). This was indicated by a sudden increase in the injection rates (see Figure 2) followed by a gradual decrease in the steam rate as steam swept additional reservoir along the well (also due to the grid block size effect). Because of recompletion of the wells, close to 1 600 days, fluid broke through beyond 30 m from the wellhead increasing the oil production rate (see Figure 2). At 2 200 days, the steam injection rate began to drop and so did the oil production rate indicating most of the mobile oil was swept from the reservoir. At 2 200 days, the average temperature in the entire reservoir was about 220°C (see Figure 6).

Because of the numerical grid block sizes and the form in which the results are presented by the model, it could not be accurately determined whether the fluid communication was formed along the entire length of the wells or not.

B. Combination of a Horizontal and a Vertical Well

In this case performance of a single 300 m long surface deviated horizontal well in communication with a vertical well was analyzed (Figure 7). To minimize sand production problems steam was injected through the horizontal well and fluids were produced through the vertical well assumed to have a deep sump. Once again, a typical McMurray reservoir description was used (Table 3). Note that in this case there is no high injectivity zone. Viscosity data used are given in Table 4 and the relative permeability data were obtained from the history match of a single well operation in the same formation.

Model Formulation

The steam process performance for an isolated pattern, was simulated using Scientific Software Intercomp's steam 3-D, 3-component model (1982 version). The horizontal and the vertical wells were defined using the well cell concept. For a sufficient but cost effective technical evaluation, only half of the system was simulated. The reservoir was sliced into half by vertically cutting the model block J=1 (see Figure 7). For the study, in order to have a better areal description, five vertical slices were used in the "Y" direction (perpendicular to the horizontal well in the horizontal plane) and ten formation layers were used in the "Z" (vertical) direction to take into account the vertical hetrogenities.

Well Descriptions

The horizontal well was located in model layer Z=7, in the 72% oil saturated zone. In the model, the vertical well was assumed to be in communication with the horizontal well. The horizontal well was assumed to have an open hole completion with slotted liner. The vertical well had about 5.2 metres of perforations. Because of flow conditions prevailing in the vertical well, a BHP of 4 250 kPa was used.

Operating Strategy

Once again the results are discussed with respect to a nearly optimal injection/production strategy developed through extensive simulation. The horizontal well was first stimulated by injecting 65% quality steam (bottomhole), at a pressure of 7 600 kPa and temperature of 290°C at a rate of 200 m³/d (CWE).

The horizontal well was stimulated for about six months. At the end of six months, the vertical producer was allowed to flow against a BHP of 4 250 kPa, and the steam injection rate was cut down to 100 m³/d to minimize sand dislocation. Initially, from 190 to 830 days the fluids were produced at a maximum rate of 90 m³/d so that the material balance in the formation is such that the temperature and pressure within the formation increase to heat up the additional reservoir volume. The production rates were increased to 100 m³/d and 110 m³/d at 830 and 1 090 days. From 1 090 days to 2 210 days, total fluid production rate was maintained at 110 m³/d. At 2 210 days, the steam injection was stopped and the total fluid production rate was increased to 200 m³/d (blowdown). The pressures, temperatures, oil saturations and gas saturations along the horizontal well, 16 m away (i.e. in the centre of grid block J=3) are given in Figures 8 and 9 for comparison purposes.

Results

At the end of about 6 years of operation, about 28 000 m³ of oil was produced with a calendar day oil rate of about 12.5 m³/day and SOR of 8.7 (Figures 10 & 11). For a commercial project, assuming a spacing of 60 m between two horizontal wells, this translates into a recovery of 25% of the OOIP.

C. Surface Deviated Horizontal Well With a Parallel Heated Plane

This case is of extreme interest as initial work by Butler (Reference 2) shows that higher productivity and recovery is achievable from horizontal wells by taking advantage of gravity drainage. The steam chamber process consists of continuously injecting steam into a growing steam chamber formed above and along a horizontal production well. In this process, the steam injection rate is controlled so as to maintain a contstant steam pressure within the chamber. Steam flows to the edge of the chamber and condenses. This heats the oil which drains from around the walls of the chamber to the production well below.

Performance of a 400 m long surface deviated horizontal well drilled on-trend and two vertical wells located over the horizontal well were considered. Vertical wells were spaced 200 m from each other equidistant from the ends of the horizontal well and offset by 3 m (see Figure 12). Steam was continuously injected through the vertical wells above formation fracture pressure to create a heated plane and reservoir fluids were continuously produced from the horizontal well. For this study, the reservoir description of McMurray channel sand was used and is given in Table 5. Viscosity and the relative permeability data were derived from other studies. Viscosity data are given in Table 6.

The two vertical wells were initially stimulated while keeping the horizontal producer shut in to create a heated front parallel to and over the horizontal producer. This was followed by continuous injection into the vertical wells while letting the horizontal well flow. This process is a slight deviation of Butler's concept because instead of creating a steam chamber, a heated zone is created over the horizontal well and the oil flows because of gravitational forces and the pressure differential between the formation and the horizontal producer.

Model Formulation

The performance of an isolated system was evaluated using Scientific Software Intercomp's 3-component, 3-phase Therm model (2.1.3, 1983 version). To define the wells in the model, the built-in option using the implicit pressure calculations for the wells was used. A half system of the wells was simulated by a total of 560 grid blocks with ten slices along the completed interval of the horizontal well (x-direction). The horizontal well was located in the sixth layer in the "Z" direction as shown in Figure 12.

Reservoir Description and the Well Data

The reservoir description used for this study is given in Table 5. The horizontal well was located in a 73% oil saturated zone. The vertical wells were not in direct communication with the horizontal well and are located 3 m away from the horizontal well considering the deviation due to drilling. The horizontal well was assumed to have an open hole completion with a slotted liner.

Optimized Strategy

The function of the vertical injectors was basically to create a heated plane along the length of the horizontal producer. In order to achieve this, one cycle of injection and production was performed on both the vertical wells before initiating the continuous injection and production mode.

The vertical wells were huffed and puffed sequentially in order to attain well to well communication on-trend. Steam with 70% bottomhole quality was injected at a rate of 225 m³/d (CWE) at a BHP of 5 500 kPa and BHT of 200°C in the vertical well #1 for 50 days. Thereafter, the well was produced at a total fluid production rate of 50 m³/d for 150 days and during this time, steam was injected in vertical well #2 at the same conditions as in well #1. This well was also produced for about 150 days at a total fluid production rate of 50 m³/d.

After the completion of one cycle, steam was injected in both the vertical wells simultaneously at a rate of 225 m³/d/well at a BHP of 5 500 kPa. High injection rates were maintained so as to obtain a bottomhole steam quality of 70% and a temperature of 280°C. The horizontal producer was allowed to produce against a BHP of 4 200 kPa created by the fluid column in the tubing. Injection and production profiles are given in Figure 13.

Results

After operating the wells for about 7.8 years, about 142 000 m³ of oil was produced at a calendar day rate of 50 m³/d, which amounts to a recovery of about 59% of OOIP for a confined pattern having a well spacing of 75 m. This cumulative oil was produced at an SOR of 8.3 and a WOR of 8.2 for the reservoir studied (Figure 14).

This study was carried out for an unconfined pattern. At about 350 days, heat losses to the overburden and the underburden increased sharply as the temperature front reached the top of the formation. In the model, because of the grid block sizes and the injection pressures used, a 100% steam chamber was not observed. Following 350 days, the rate of heat losses increased steadily as the heated front grew in size. Since the fluids were produced at a constant rate, the heat production rate was almost constant. However, the rate at which net heat was injected into the formation declined steadily, affecting the growth of the heated volume and resulted in a decline in oil production. Oil production rate peaked at about 1 800 days (Figure 13).

Results obtained from the simulation study were compared with the results obtained using the equations developed by Dr. R.M. Butler (Figures 13 & 14). It was found that the oil production rates in both the cases have the same trend, except that in the simulation case, oil rates lag behind the rates obtained from Butler's equations. Assuming that it will take about one cycle of injection and production in the vertical wells to create a heated plane over the horizontal well, oil production rates and SOR's obtained using Butler's calculations have been plotted from 250 days onwards for the purposes of comparison. The model developed by Butler, predicts an SOR of almost half that predicted by the simulation model. This could be explained by three factors:

(i) The theory developed by Dr. R.M. Butler assumes the existence of heated plane over the horizontal well from day 1.

(ii) Butler's theory doesn't take into account the reservoir hetrogenities while the simulation model does.

(iii) Grid block sizes in the simulation model affect the predicted rates, however, the cumulative oil production over the well life is not affected.

In the simulation study, injection and production rates from the well were kept at a level so as to maintain a pressure of 4 300 kPa within the reservoir. It was done so that the fluids could flow through the producer without pumping. Cumulative SOR was high when the wells were operated in the cyclic mode (see Figure 14) and dropped when the wells were brought into continuous injection/production mode.

CONCLUSIONS

A. Parallel Horizontal Wells

1) The results indicate that for a steamdrive process, completing both the horizontal wells in a formation zone having relatively higher water saturation (in the order of 40-55%), can provide sufficient injectivity (below formation fracture pressure) to create the hot communication between wells required to initiate the steamdrive process. To achieve early hot communication between the wells, a single steam injection cycle of about 100 days can give satisfactory results.

2) Selective recompletion of the injector and the producer will be necessary to maximize sweep efficiency from 150 m long horizontal wells.

3) A near optimal strategy of the type described herein can lead to about 58% recovery from a 0.9 ha pattern with an average rate of 22.5 m³/calendar day. A Steam-oil ratio and water-oil ratio of the order of 5.5 and 5.4 can be achieved.

B. Combination of a Horizontal and a Vertical Well

1) For the reservoir considered herein, a continuous injection and production process for a 300 m long horizontal well, gives the best results after one injection cycle of approximately 6 months.

2) Sensitivity studies indicated that increasing the injection rate not greater than 100 m³/d (CWE) and increasing the total fluid production rate improve the oil production rate.

3) In the continuous steaming process, a higher oil production rate can be achieved at the expense of higher SOR and WOR. Using such a system, it is possible to recover about 25% of the original-oil-in-place in a 1.8 ha pattern at a calendar day oil rate of about 12.5 m³/d and SOR of 8.7 over a period of 6 years.

C. Surface Deviated Horizontal Well With a Heated Parallel Plane

1) High bitumen production can be achieved by creating a heated plane using a system of a 400 m long horizontal well and two vertical wells. The results of the study indicate that from a 3 ha pattern about 59% of OOIP can be produced from such a system over a period of about 7.8 years

with an average rate of 50 m^3/d and an SOR of 8.3.

REFERENCES

1. TOWSON, D.E., "Mine Assisted In Situ Project" presented at UNITAR/AAPG Conference, Santa Maria, California October 29 to November 2, 1984.

2. BUTLER, R.M., STEPHENS, D.J. and WEISS, M., "The Vertical Growth of Steam Chambers in the In-Situ Thermal Recovery of Heavy Oils", presented at Canadian Chemical Engineering Conference, Montreal, Quebec, 1981.

TABLE 1

RESERVOIR DESCRIPTION

LAYER #	THICKNESS m	So	Sw	Sg	Kh md	Kv md	ø
1	3.0	0.43	0.55	0.02	1 000	400	0.29
2	2.5	0.73	0.25	0.02	1 500	600	0.33
3	1.5	0.83	0.15	0.02	1 500	600	0.33
4	1.0	0.68	0.30	0.02	1 000	400	0.34
5	3.0	0.81	0.17	0.02	1 500	600	0.35
6	4.0	0.83	0.15	0.02	1 500	600	0.35
7	3.0	0.68	0.30	0.02	1 500	600	0.33
8	0.75	0.43	0.55	0.02	500	200	0.25
9	2.25	0.78	0.20	0.02	1 500	600	0.35
10	1.00	0.0	1.0	0.0	2 000	800	0.25

Reservoir Rock Heat Capacity = 2 937.5 KJ/m^3-°C
Reservoir Thermal Conductivity = 150.0 KJ/d-m-°C
Overburden Heat Capacity = 2 682.6 KJ/m^3-°C
Overburden Thermal Conductivity = 187.5 KJ/d-m-°C
Underburden Heat Capacity = 2 012.4 KJ/m^3-°C
Underburden Thermal Conductivity = 146.0 KJ/d-m-°C

TABLE 2

TEMPERATURE, °C	OIL VISCOSITY, MPa.s
10.0	2 730 000
65.6	2 030
121.1	75.2
176.7	13.3
232.2	4.69
287.8	2.32
343.3	1.38
398.9	0.916
454.4	0.659
510.0	0.502

TABLE 3

RESERVOIR DESCRIPTION

LAYER #	THICKNESS m	So	Sw	Kh md	Kv md	ø
1	4.0	0.65	0.35	1 800	720	0.34
2	5.5	0.62	0.38	1 800	720	0.34
3	5.0	0.67	0.33	1 800	720	0.34
4	3.0	0.57	0.43	1 800	720	0.34
5	3.0	0.73	0.27	1 650	660	0.32
6	2.2	0.72	0.28	1 800	720	0.32
7	0.8	0.72	0.28	1 800	720	0.32
8	4.4	0.66	0.34	2 000	800	0.35

Reservoir Rock Heat Capacity = 2 937.5 KJ/m^3-°C
Reservoir Thermal Conductivity = 150.0 KJ/d-m-°C
Overburden Heat Capacity = 2 682.6 KJ/m^3-°C
Overburden Thermal Conductivity = 187.5 KJ/d-m-°C
Underburden Heat Capacity = 2 012.4 KJ/m^3-°C
Underburden Thermal Conductivity = 146.0 KJ/d-m-°C

TABLE 4

TEMPERATURE, °C	OIL VISCOSITY, MPa's
25.0	434,000
80.6	1,030
136.1	56.2
191.7	12.3
247.2	5.16
302.8	3.03
358.3	2.15
413.9	1.71
469.4	1.46
525.0	1.31

TABLE 5

RESERVOIR DESCRIPTION

LAYER #	THICKNESS m	So	Sw	Sg	Kh md	Kv md	ɸ
1	3.3	0.64	0.36	0.0	600	60	0.32
2	8.2	0.77	0.21	0.02	1 800	720	0.34
3	8.0	0.78	0.19	0.03	1 800	720	0.34
4	3.0	0.76	0.24	0.0	1 800	720	0.31
5	5.0	0.75	0.24	0.01	1 800	720	0.34
6	4.0	0.73	0.26	0.01	1 800	720	0.36
7	2.0	0.57	0.43	0.0	800	80	0.32

Reservoir Rock Heat Capacity = 2 347.5 KJ/m³-°C
Reservoir Thermal Conductivity = 150.0 KJ/d-m-°C
Overburden Heat Capacity = 2 400.0 KJ/m³-°C
Overburden Thermal Conductivity = 155.0 KJ/d-m-°C
Underburden Heat Capacity = 2 500.0 KJ/m³-°C
Underburden Thermal Conductivity = 160.0 KJ/d-m-°C

TABLE 6

TEMPERATURE, °C	OIL VISCOSITY (cp)
25.0	435,000
69.9	2,280
114.8	135
159.7	25.5
182.1	14.2
204.6	8.73
227.0	5.82
271.9	3.05
294.4	2.33
339.3	1.48
384.1	1.01
429.0	0.73

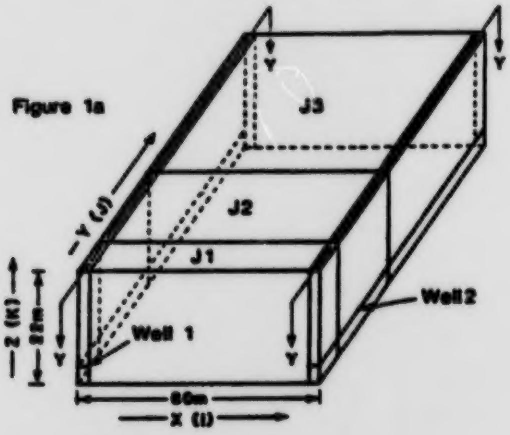

Figure 1a

Y
Y
J3
— Y (J) —
J2
J1
— Z (K) —
Well 1
Y
Y
Well2
60m
— X (I) —

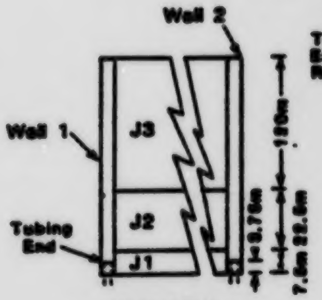
Well 2
Well 1
J3
J2
J1
Tubing End
180m
3.75m
7.5m 22.5m

TOP VIEW
Tubing Ends 3.75m
From Wellheads
(Before Recompletion)

Figure 1b

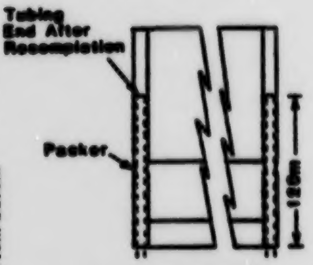
Tubing End After Recompletion
Packer
120m

TOP VIEW
Tubing Ends 120m
From Wellheads
(After Recompletion)

Figure 1c

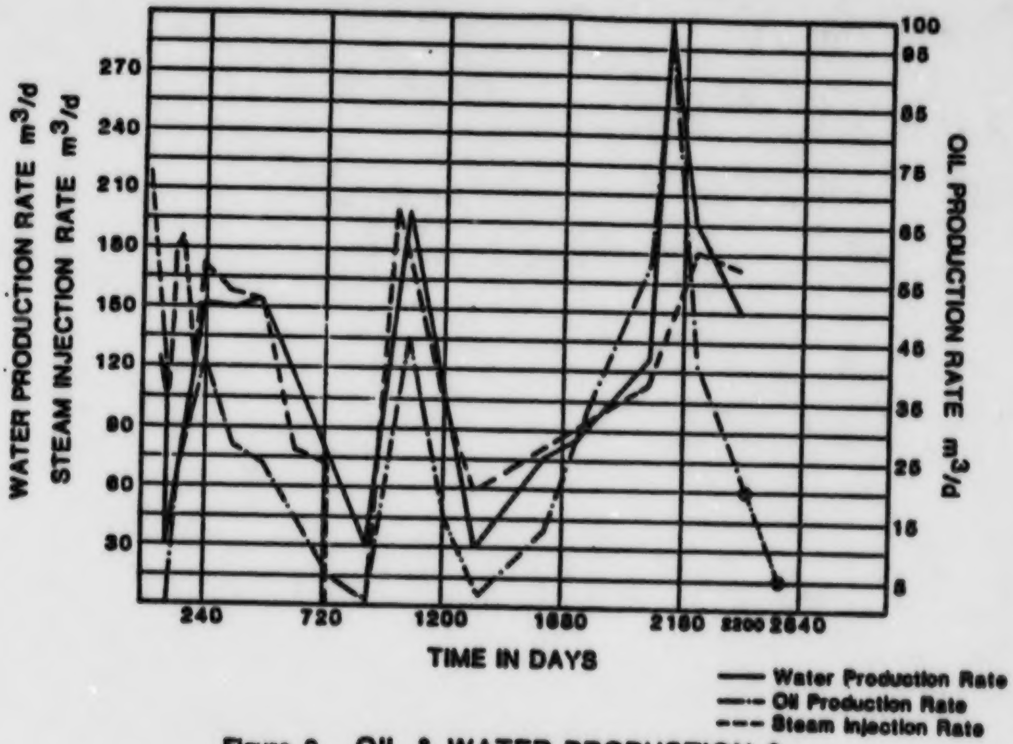

Figure 2 OIL & WATER PRODUCTION & STEAM INJECTION RATES VS TIME IN DAYS

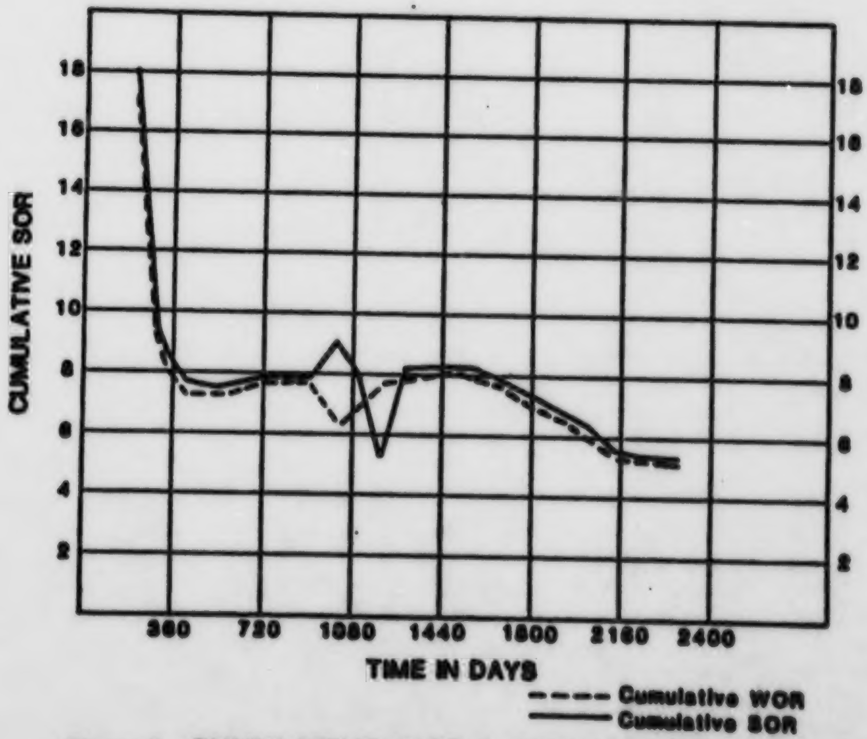

Figure 3 CUMULATIVE WOR & SOR VS TIME IN DAYS

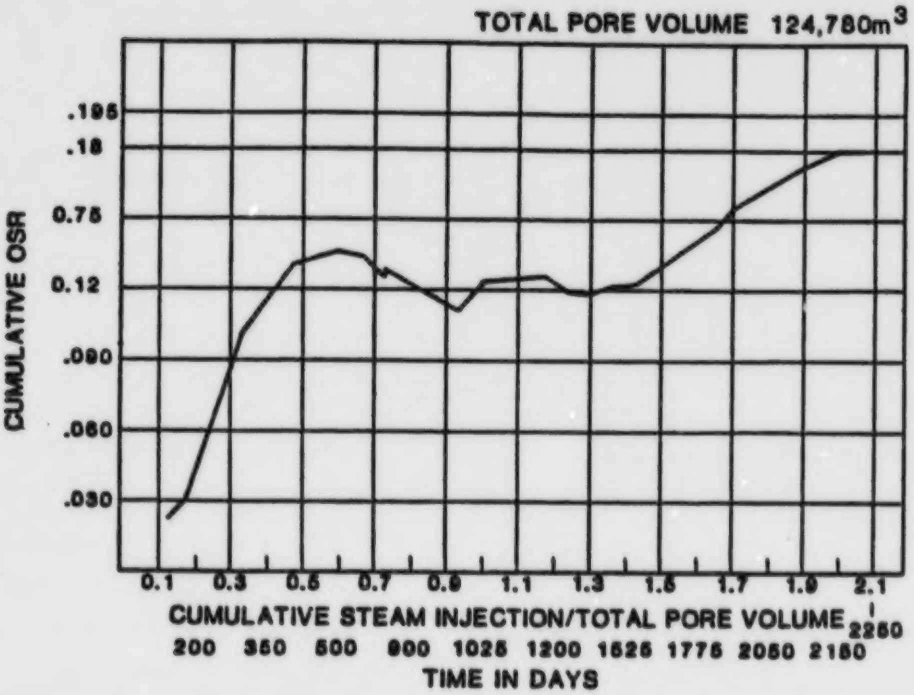

Figure 4

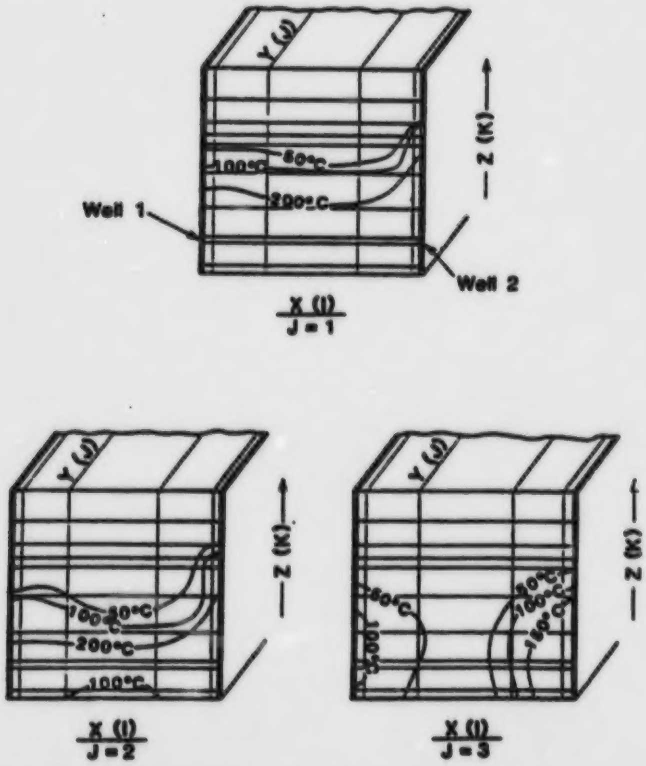
Y (J)
Z (K)
100°C
50°C
200°C
Well 1
Well 2
X (I)
J = 1
Y (J)
Z (K)
100°C
50°C
200°C
100°C
X (I)
J = 2
Y (J)
Z (K)
50°C
100°C
50°C
100°C
150°C
X (I)
J = 3

Figure 5 POSITION OF HEAT FRONT IN BLOCKS
J = 1,2 & 3 AT 242 DAYS

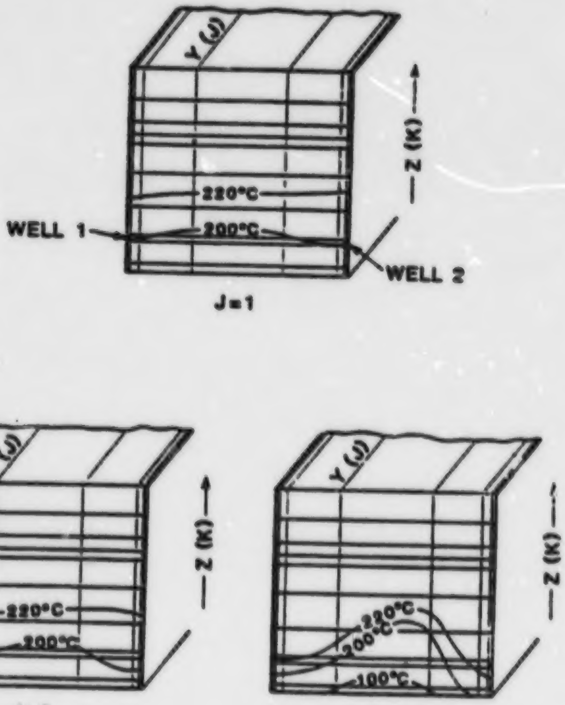
Y (J)
Z (K)
220°C
200°C
WELL 1
WELL 2
J=1
100°C

J=2 J=3

Figure 6 TEMPERATURES IN BLOCKS J=1,2&3 AFTER 2200 DAYS

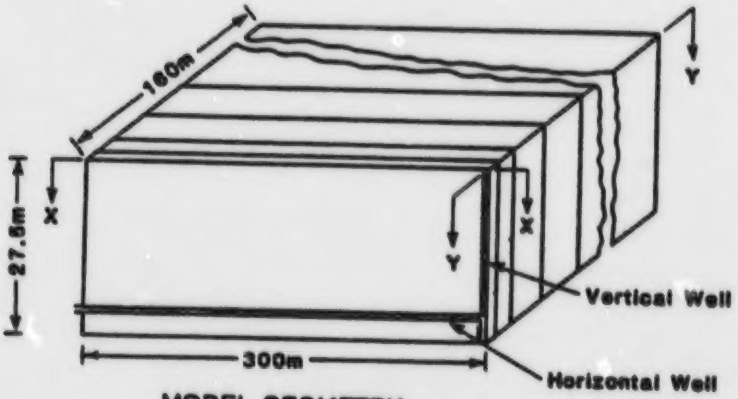
160m
27.5m
X
Y
X
Y
Vertical Well
Horizontal Well
300m

MODEL GEOMETRY

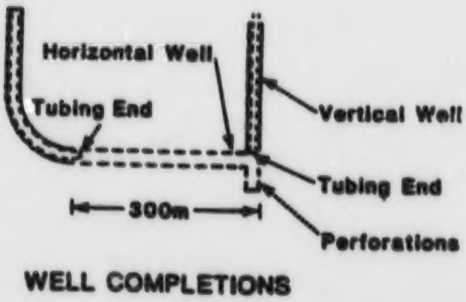
Horizontal Well
Tubing End
Vertical Well
Tubing End
300m
Perforations

WELL COMPLETIONS

Figure 7

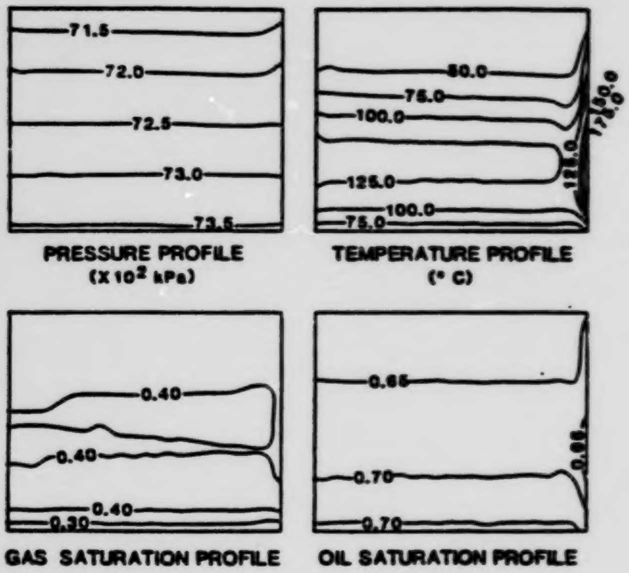

Figure 8 PRESSURE, TEMPERATURE & SATURATIONS PROFILES IN BLOCK J = 3 AFTER 190 DAYS

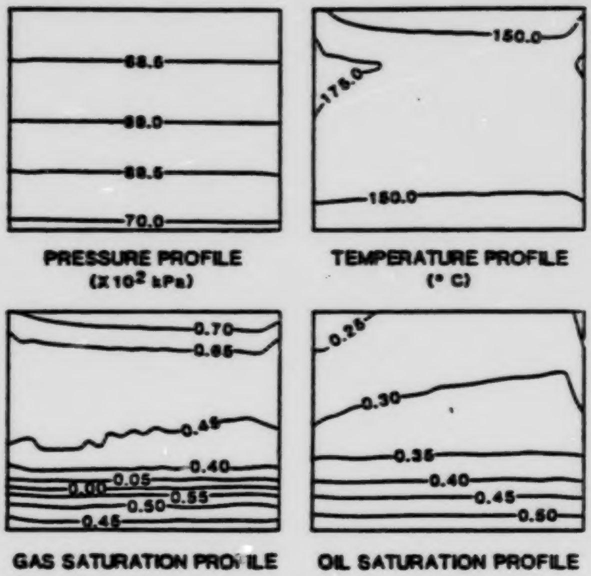

Figure 9 PRESSURE, TEMPERATURE & SATURATIONS PROFILE IN BLOCK J = 3 AFTER 2240 DAYS

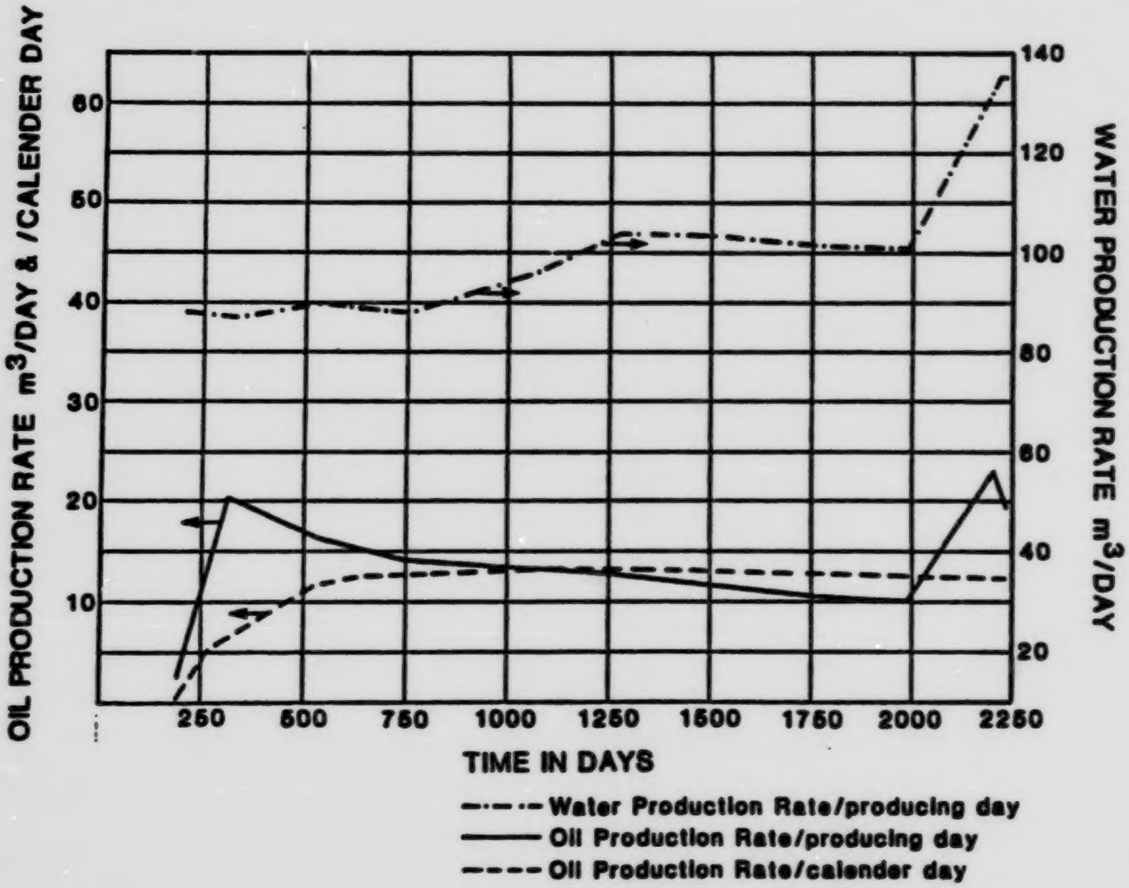

Figure 10

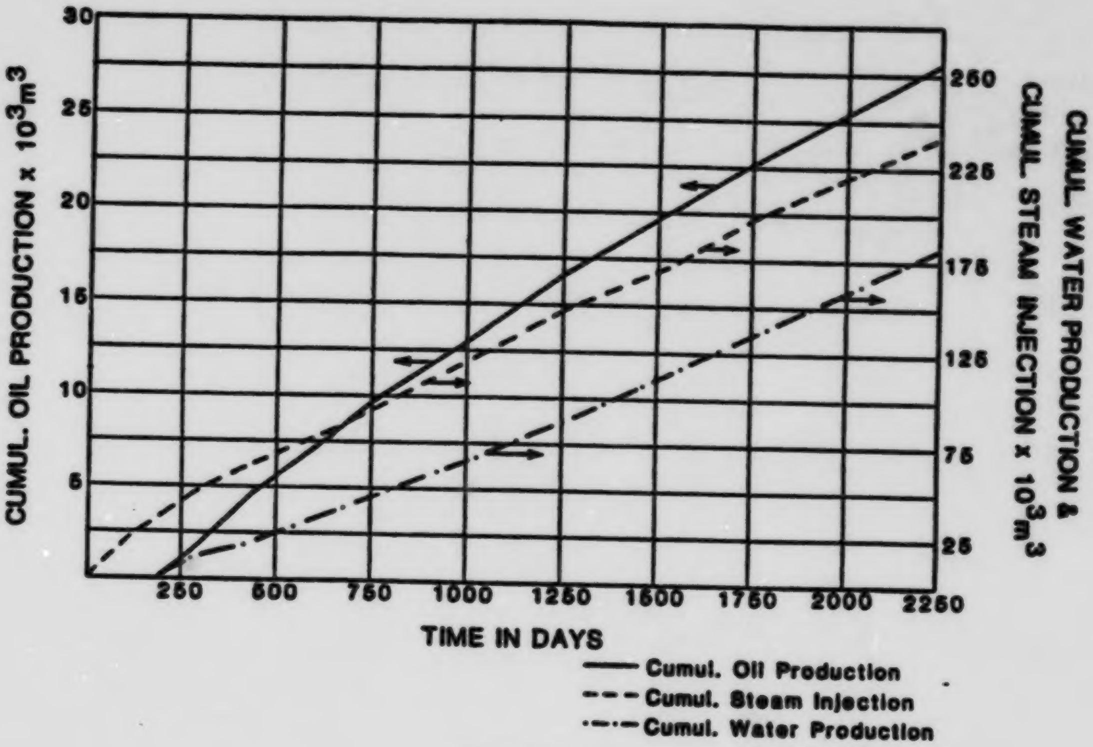

Figure 11

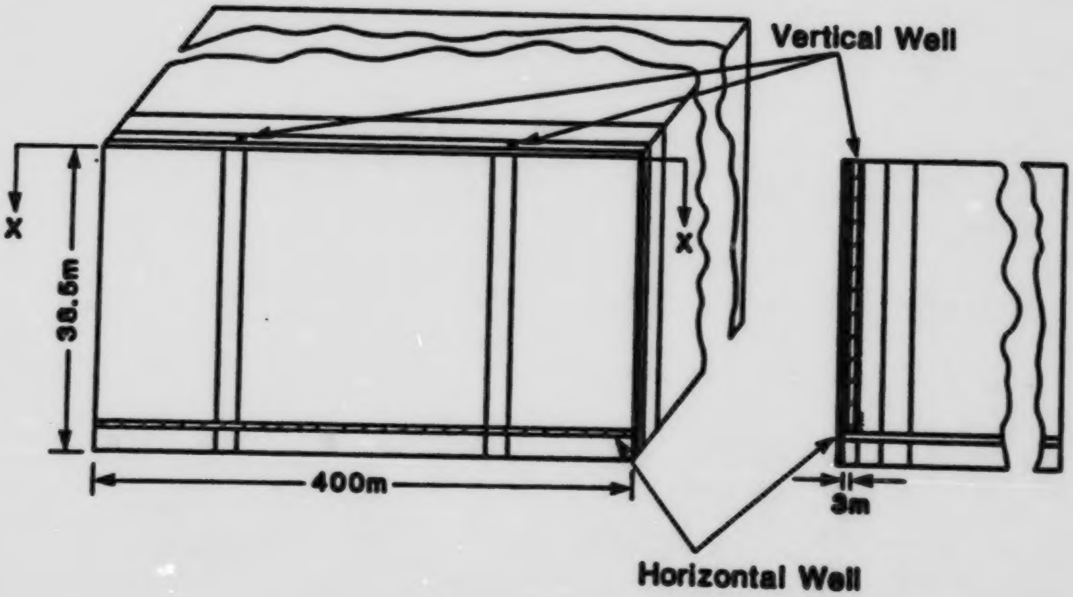
Vertical Well
X
X
36.5m
400m
3m
Horizontal Well

Figure 12

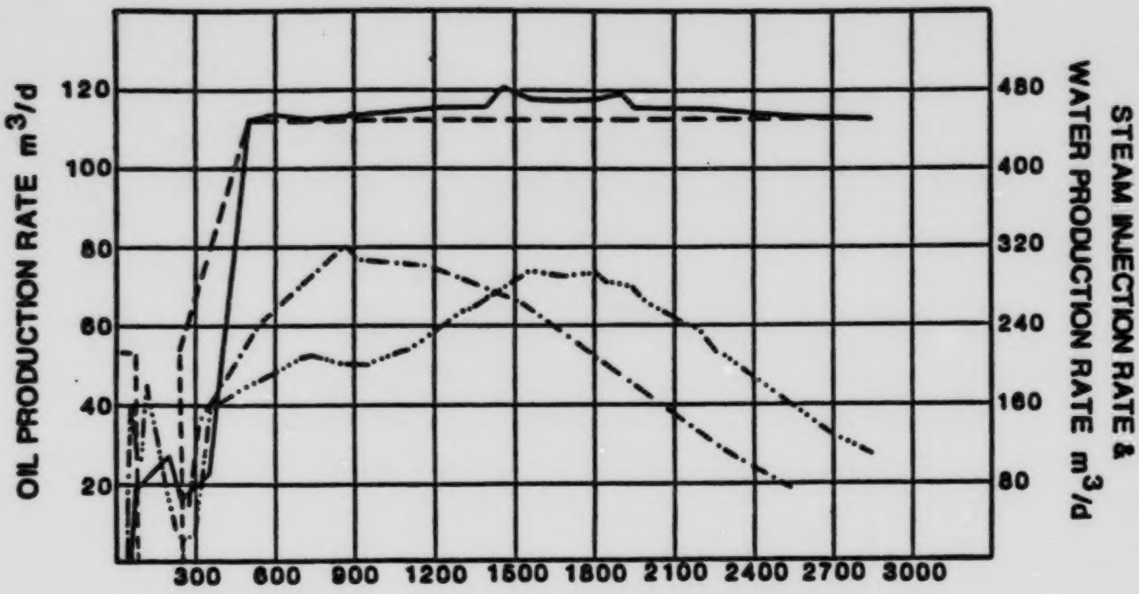

Figure 13

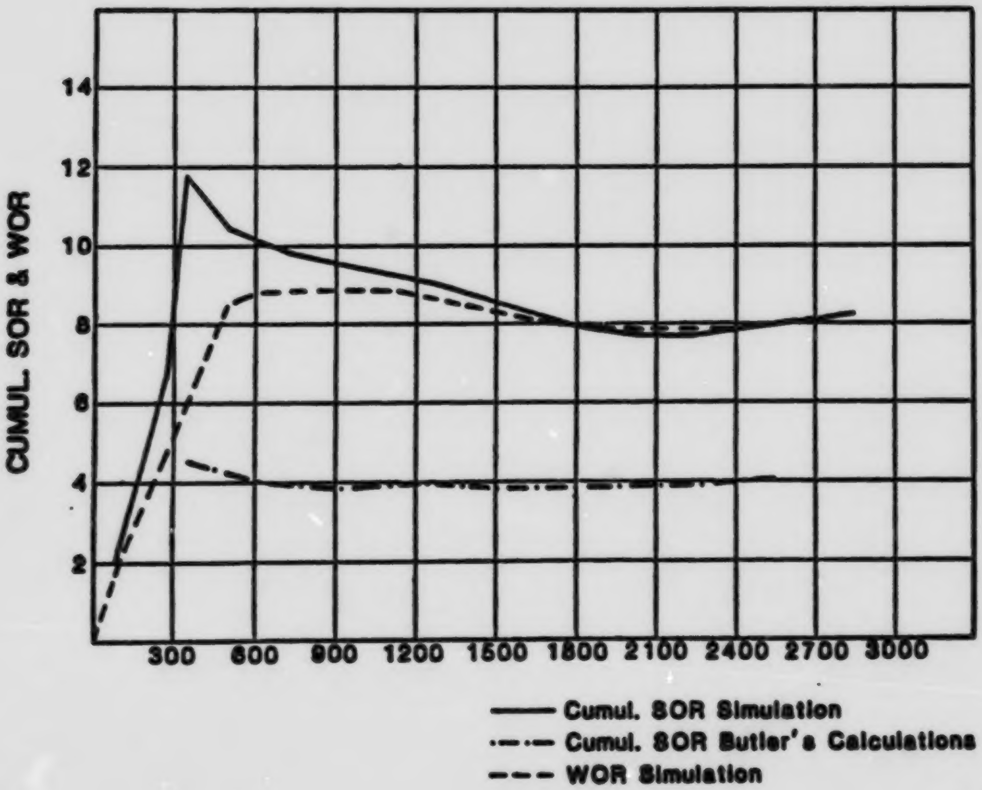

Figure 14

010295

Advances in Petroleum Recovery & Upgrading Technology

1985

Edmonton Convention Centre
June 6 - 7, 1985

ALBERTA OIL SANDS
TECHNOLOGY AND
RESEARCH AUTHORITY
500 Highfield Place
10010 - 106 Street
Edmonton, Alberta, Canada
T5J 3L8
403/427-7623
Telex 037-3519

AOSTRA

86

SESSION 1

PAPER 3

POTENTIAL OF HORIZONTAL WELL PROCESSES

A. Khosla
Petro Canada Inc.

G. Cordell
AOSTRA

Calgary, Alberta

POTENTIAL OF HORIZONTAL WELL PROCESSES

A. Khosla
Petro Canada Inc.

G. Cordell
AOSTRA

ABSTRACT

This paper describes the technical and economic effectiveness of horizontal wells in recovering bitumen from the Athabasca McMurray formation encountered at a depth greater than 350 m. Two recovery processes were evaluated: (a) the steam Stimulation/Drive Process; and (b) the Steam Assisted Gravity Drainage Process. The performance is compared with that of vertical wells using the cyclic steam recovery process. A representative reservoir description and characteristics for the McMurray formation were used. This evaluation study showed that horizontal wells perform more favourably than vertical wells provided that the recovery process can be applied in the field as perceived in this study. Those aspects of horizontal well technology that need to be further evaluated through field piloting are also discussed.

INTRODUCTION

During the period of 1978 to 1981, a consortium of five companies, Petro-Canada Inc., Husky Oil Ltd., Canada-Cities Service Ltd. (now Canadian Occidental Petroleum Ltd.), Esso Resources Canada Ltd., and Gulf Canada Resources Ltd. demonstrated that long horizontal holes could be successfully drilled, completed, and operated in the oil sands (1). Petro-Canada was the Operator of this project called MAISP (Mine Assisted In Situ Project). The field comprising of three horizontal wells (two 330 m and one 543 m long) was carried out at an outcrop near Fort McMurray. The project successfully ended in March, 1981. Utilizing the stimulation/pressure cycling process, 850 m³ of oil was produced at an SOR of 16. In view of the low steam temperature (170°C) and long preheating time for one of the three wells, the production peformance was considered encouraging. During the same period, Esso began field testing of horizontal wells for application to their Cold Lake acreage. Butler (2) conceptualized the steam assisted gravity drainage process. Although information on Esso's project is not publically available, it is believed that the first test well showed that steam assisted gravity drainage process was a feasible recovery process. Since then many companies have put their effort on the use of horizontal wells: Conoco's horizontal well project in Oklahoma, Texaco in Athabasca and Esso Resources in Cold Lake (3, 4, 5). AOSTRA, in 1984, presented the industry with the idea of constructing an Underground Test Facility (UTF) at a cost of about 50 million dollars, where some of the potential steam based horizontal well processes can be field tested. It is an excellent opportunity for the oil industry to test their ideas in a "field laboratory". With the advances in drilling technology (6) and also increased understanding of the McMurray resource, the oil industry is having a serious look at the horizontal wells and their edge over the vertical wells.

This paper, presents the technical and economic effectiveness of horizontal wells in recovering bitumen from the Athabasca McMurray formation at a depth greater than 350 m where vertical fractures are imminent. In an attempt to answer the question of "why horizontal wells" the relative performance of vertical wells is compared with that of horizontal wells in terms of recovery, oil production rates and supply price.

HORIZONTAL WELL PROCESSES

Results from two recovery processes are presented herein:

(i) Steam Stimulation/Flood Process
(ii) Steam Assisted Gravity Drainage Process

The Steamflood Process is considered to be applicable to the McMurray Formation, provided that well to well communication can be achieved. Its potential increases in thick reservoirs as gravity drainage increases oil production rates at nominal steam expense and overall recovery is greatly improved. Evidently, reservoirs having some mobility at the bottom of the zone of interest are more suitable for this process.

For reservoirs which have almost no injectivity, it is difficult to create horizontal fractures at a virgin stress state of the formation at depths greater than 300 m. Horizontal steam drive is not considered feasible because of the mobility variance between injected steam and the highly viscous bitumen. A steam drive in this instance would tend to short circuit by fingering steam between horizontal wells. On the other hand, injectivity can be increased by initially fracturing vertically with vertical wells and recovering fluids from a horizontal producer beneath the injector wells. Butler (2) has shown that such a process, although slow, is very promising in terms of high recovery as well as high oil rates.

This paper investigates the applicability of horizontal wells in two separate reservoir environments. One reservoir has good initial fluid mobility at the base (for Steam Flood Processes) and a second reservoir has minimal initial fluid mobility (for the Steam Assisted Gravity Drainage Process).

VERTICAL WELL PROCESSES

The steam stimulation and steam flood processes are equally applicable to vertical wells. Gravity drainage is an integral part of these processes. In this paper, only the steam stimulation process with vertical fractures has been evaluated because of its application for oil sands commercialization. Furthermore, vertical well, vertical fracture performance is evaluated in two different reservoirs described above, as a means of comparison of horizontal well processes investigated to vertical well performance.

BASIS OF PERFORMANCE PREDICTION

A typical McMurray reservoir description has been formulated from a core hole evaluation program carried out by Petro-Canada (see Figure 1). The high water saturation at the base of this reservoir makes it amenable to steam drive because of the initial good fluid mobility through the base of the reservoir. Recognizing that often no bottom water exists in the Athabasca sands a second reservoir characterization was formulated and served as the reservoir environment which had minimal initial injectivity at below formation fracture pressure (see Figure 2). The only difference between the reservoir characterizations is that the bottom six meters of pay in the first case has good water mobility and in the second reservoir environment the water mobility is negligible.

Bitumen viscosity and relative permeability data used in the reservoir studies are given in Figures 3 through 5. The relative permeability curves used in this study were obtained from a prior study carried out by AOSTRA for a reservoir slightly different to the Petro-Canada reservoir. A comparison of the simulation results obtained from one of the cases of this study to actual field performance for a isolated vertical fractured well is given in Table 1. Performance predicted from the simulator for this study is comparable to the performance obtained from an actual field environment and operating strategy, thereby giving credence to the results reported herein.

For a reservoir with a net pay of 15 m, a well spacing of 2.4 ha was considered appropriate. Table 2 summarizes the well spacing and bitumen reserves in place for each particular well configuration investigated. A total of 77 000 m^3 of bitumen is in place for each repeatable well pattern investigated with the basal water reservoir. To ensure a meaningful comparison of performance for each well configuration the well spacing was maintained at 2.4 ha for all but one of the studies.

VERTICAL WELL CONFIGURATIONS AND OPERATING STRATEGIES INVESTIGATED

In total, seven separate numerical simulation studies were completed to compare horizontal well performance to the vertical well performance. The Computer Modelling Group's ISCOM 3.0 model was used for the numerical simulation studies. Two vertical well studies were carried out using an 11 x 5 x 3 cartesian grid for the simulations. The only difference between the two vertical well studies was that the water mobility at the base of the reservoir was different. In the attached figures one case is called vertical well with high water at the bottom and the second is identified by vertical well with high bitumen at the bottom. These represent good water mobility and minimal initial fluid mobility cases, respectively.

The creal vertical well pattern for a commercial operation is depicted in Figure 6. The interwell distance is twice as long in the vertical fracture direction relative to the direction perpendicular to the fracture, because most of the injected fluid and energy remains in the vicinity of the vertical fracture. The 2:1 rectangular well spacing enhances recovery of the bitumen reserves in place.

One quarter of one vertical well was simulated due to symmetry of the well configuration and the fluid distribution. Figure 7 depicts the volume of symmetry simulated for the two vertical well cases.

The operating strategy employed for the two vertical well cases involved injection of 71% quality steam at the sand face at a rate of 250 m^3/d for 28 days. A total of 7 000 m^3 of steam were injected during each injection phase, at and above the formation fracture pressure of 9 000 kPa. During the production phase the vertical fracture closed and the well was produced until the bitumen rate decreased below 1 m^3/d. The production period ranged between 70 and 100 days.

The performance of the vertical wells was terminated after 3 years of operation because the intantaneous oil-steam ratios became less than 0.10 m^3/m^3 which indicated that further steam injection cycles would be uneconomic.

HORIZONTAL WELL CONFIGURATIONS AND OPERATING STRATEGIES INVESTIGATED

A total of 5 separate numerical simulation runs were completed to assess performance from horizontal wells. Four of the runs incorporated the high mobile water saturation interval at the base of the reservoir (see Figure 1) while the fifth study had minimal initial fluid injectivity at the base as depicted in Figure 2. The five horizontal well runs were:

1) Horizontal well steam drive on 2.4 ha/well spacing with bottom water using an 11 x 6 x 5 cartesian grid for the simulations (Figure 8).

2) Horizontal well steam drive on 2.4 ha/well spacing with bottom water and a doubling of the areal horizontal permeability in the bottom water interval over 100 m of the 500 m horizontal well length (Figure 9).

   The areal horizontal permeability variation was intended to represent the channel sands nature of the Athabasca deposit in terms of areally variant reservoir characteristics. This second study was designed to assess the risk of premature steam breakthough at the producing well along 20% of the total well length, in terms of cumulative bitumen recovery. Once steam breakthrough occurred, the horizontal wells were placed on steam stimulation cycles at below fracture pressure.

3) Horizontal well steam drive on 4.8 ha/well spacing with identical reservoir characterization as Case 2 above. Once steam breakthrough occurred along 20% of the production horizontal well, both the injection and production wells were placed on cyclic steam stimulation at below fracture pressure. The study was designed to assess the improvement on recovery with double the well spacing, recognizing that areal variations in horizontal permeability may exist.

4) Steam assisted gravity drainage utilizing vertical wells as the injectors and 500 m long horizontal wells as the producers. The vertical wells were perforated over 3 m of length and 3 m from the top of the formation. The wells were initially vertically fractured to achieve communication to the horizontal production well. Steam was injected at 9 000 kPa into the injectors and the average production pressure along the horizontal well was 8 950 kPa. The high bottom water interval existed for Case 4. Figure 10 depicts the horizontal-vertical well configuration.

5) Steam assisted gravity drainage utilizing vertical wells as the injectors and 500 m long horizontal wells as the producers. The only difference to Case 4 above was that a high bitumen saturation interval replaced the high water saturation zone at the base of the reservoir.

The areal horizontal well and vertical well patterns for a commercial operation are depicted in Figures 11 and 12 for the steam drive and gravity assisted steam drainage cases. The well spacing was maintained at 2.4 ha (except for Case 3) to provide a direct comparison to the vertical well performance.

Performance Comparison

Table 3 summarizes the performance of the horizontal and vertical well configurations studied. Comparing first the performance for cyclic steamed vertical wells, by increasing the average overall reservoir oil saturation from 67% (high water at base) to 80% (high bitumen at base) increases the bitumen productivity by 30%, from 7 500 m^3 to 9 800 m^3 after 3 years of operation. Similarly the oil steam ratio improves by 60% for the high bitumen saturated reservoir case because injected steam is more efficiently used to heat bitumen as opposed to water as that which exists in the high basal water saturation case. Therefore, reservoirs that have high bitumen saturations may be expected to outperform reservoirs with basal water for cyclic steam vertical fracture operations. A 20% increase in average oil saturation resulted in a 30% increase in oil production.

Comparing the vertical cyclic steam well completed in the high basal water reservoir to the horizontal well steam drive strategies indicated that performance from horizontal wells would be superior to performance from vertical wells in terms of: 1) the cumulative bitumen produced; 2) oil steam ratios and 3) calendar day oil rate. Even with a high permeable path that creates a steam finger between the injector and producer horizontal wells the performance can be expected to be better than the vertical well because of the initial good drive between the wells before

steam breakthrough. Once steam breakthrough occurs at the producer horizontal well, performance from cyclically steaming the horizontal wells can be expected to be at par with the vertical wells. Steam channelling between horizontal wells will affect performance substantially but not to the extent that performance will be poorer than the vertical wells, assuming that a high permeable channel exists over 20% of the length of the horizontal well.

If areal horizontal permeability variations exist, doubling the horizontal steam drive well spacing from 2.4 ha to 4.8 ha could minimize the risk of unacceptable performance. The steam breakthrough time to the producer is increased from 240 days to 700 days thereby enabling improved sweep vertically above the high permeable areal channel and hence improved productivity over that of the 2.4 ha well spacing.

For horizontal well steam drives in basal water the performance would be comparable to vertical cyclic steam wells in terms of oil steam ratio. However, a higher recovery of the reserves in place could be expected from the horizontal well which may offset the higher cost of drilling the horizontal wells (see Table 4).

The results from the numerical simulation studies have determined that the preferred exploitation scheme for the two reservoir environments investigated would be to drill horizontal production wells with vertical injection wells directly above the drainage horizontal well. For a 500 m long horizontal producer, with two vertical injectors above, bitumen production can be expected to be 7 times greater than from a single vertical cyclic steam well on the same well spacing. In addition, an improvement of between 10 to 20% could be expected in the oil steam ratio for the high bitumen reservoir case and high basal water cases respectively. The steam assisted gravity drainage process is the most robust of the processes investigated in terms of being able to recover oil at high rates from two distinctly different reservoirs.

There are two major explanations for the improvement in performance with vertical injectors and horizontal producers over that of straight vertical cyclic steam wells. The first is that the reservoir operating temperature is maintained close to the steam injection temperature always for the horizontal well case because steam is continuously injected above the horizontal producer and hence correspondingly the bitumen viscosity is maintained low. On the other hand, for the cyclic steam vertical wells by drawing the pressure of the reservoir down to close to 200 kPa during production the corresponding saturated steam temperature is much lower which in turn results in a high bitumen viscosity. Bitumen does not flow as readily to vertical production wells because of its lower temperature and higher viscosity in comparison to maintaining a high steam chamber temperature through continuous injection of steam, for the steam assisted gravity drainage recovery strategy.

The second reason for the better performance is that steam is never produced from the horizontal production well whereas during the early phase of production from the vertical well, for each cycle of operation, steam is produced which decreases the oil steam ratio because of the inefficiency associated with producing the steam. The vertical injector-horizontal producer concept, because of gravity segregation, maintains a liquid level of water steam condensate and bitumen above the horizontal well with the steam chamber above it and hence the injected steam is very efficiently utilized.

Table 4 depicts the energy efficiency of each process. The horizontal-vertical well gravity drainage process produces 20% less energy than the cyclic steam vertical wells and hence uses the 20% additional energy, in part, to heat more bitumen. Table 4 illustrates that heat losses from all processes are comparable, within the 20 to 30% range of the total energy injected at the sand face for each case study.

In summary, technically the vertical steam injector with horizontal producer steam assisted gravity drainage provides the highest recovery of the reserves-in-place surpassing that of vertical cyclic steam stimulation by 7.0 times (see Table 4). The higher recovery of the reserves in place is accounted for by the fact that for each 2.4 ha spacing the horizontal well has 500 m of wellbore in contact with the reservoir compared to the vertical well on the same spacing which has 15 m of well in contact with the reservoir. Tied to the higher recovery of reserves in place for the horizontal well steam gravity drainage process is an improved oil steam ratio and calendar day oil rate. The results from this study have demonstrated that for two different reservoir environments the vertical steam injector-horizontal producer well configuration is technically superior to solely cyclic steam stimulation wells.

ECONOMICS

A supply price analysis was carried out for a system of horizontal well versus vertical well development strategies. The analysis was based on a 10 000 BOPD plant for a 20 year supply period. Production forecasts were developed on the basis of wells coming on production to be drilled and equipped in the previous year. The analysis indicated a supply price of $25.90/bbl for a system of horizontal wells as opposed to $28.70/bbl for vertical wells when discounted at 10% (see Table 5 for development costs comparison). The analysis further pointed out that higher recoveries and rates (approximately four times the cyclic steam process) associated with a horizontal well system do offer a definite advantage over the vertical wells development strategy when developing a finite acreage. With a limited resource base, the horizontal well development strategy would achieve much higher commercial rates provided that the additional capital is available.

AREAS FOR PILOTING

The analysis presented herein clearly demonstrates the advantages of horizontal wells over vertical wells. Therefore, it becomes necessary to check that the assumptions made in the analysis of horizontal well processes are realistic and practically achievable. Some of the aspects of horizontal wells where some field testing is needed are discussed below:

Shafts, Tunnels and Horizontal Well Drilling

AOSTRA realized the need to first test the technical as well as economical feasibility of drilling shafts and tunnels in the oil sands and Devonian Limestone. A rig for drilling the horizontal wells from tunnels is being designed by AOSTRA. The field work has already begun at the site Township 93 - Range 12. Success in this area would be a major step towards the utilization of horizontal wells for the shallower oil sand deposits. For deeper deposits with possible incompetent underburden (Devonian), it becomes important that the technology of drilling horizontal wells from the surface should also be developed. Comparative economics will indicate the option that should be used in field development. Petro-Canada has the capability whereas it is believed that Esso is already testing the horizontal well drilling technology in the Cold Lake area. Texaco Drilling Company (6) from Houston has demonstrated the feasibility of drilling approximately 200 m long horizontal holes from vertical wells.

Application to McMurray, Channel Sands

McMurray deposits in the Athabsaca area are in the form of channel sands. It is believed that the general depositional trend of these sands is NE-SW. In Petro-Canada's experience, a sufficiently accurate knowledge of the extent, minerology and richness of the resource is essential. The channel trends must be determined, if horizontal wells with steam assisted gravity drainage process are to be used in producing this type of resource. Lack of knowledge in this area can lead to problems if long horizontal wells cut through either poorer sands or the banks of the channel sands. Risk involved in this venture is quite high. AOSTRA has carried out a high density vertical core hole program at the UTF resource site. This is an opportunity where the risk of drilling long horizontal wells through the rich sand can be assessed at a low cost.

Risks Associated With Pattern Operation of Horiztonal Wells

In the case of steam assisted gravity drainage and/or steamdrive process, it is important that the risk associated with sequential flooding from one project area to the next should be assessed. In other words, what are the chances of success to flood the next pattern once the first one is depleted which now is a potential thief zone. Would a buffer zone be required? What is the geometrical size of this buffer zone? This problem may be somewhat alleviated by drilling horizontal wells along the length and patterns across the width of the McMurray channel. Once again, at the UTF site, it is possible to study the overall extent affected by the injected steam and then develop means for controlling the loss of steam to the preflooded zones. This combined with the knowledge of the resource shape, appropriate pattern configurations and operating strategies can be studied using computer modelling techniques.

There are many other areas where information is lacking: such as well completions and their competency, effect of reservoir heterogeneities on the process performance, optimization of horizontal well lengths, workovers etc. Therefore, it is important to further analyze the work presented in this paper in an iterative manner as advances are made.

CONCLUSIONS

1. The numerical simulation studies indicate that technically horizontal well processes can perform significantly better than vertical steam stimulated wells, in each of the two reservoir environments investigated, both in terms of the calendar day oil rate and ultimate oil recovery of the reserves in place.

2. Steamdrive horizontal wells must be carefully operated to minimize the risk of early steam breakthrough, along only a small portion of the horizontal well, which reduces oil recovery due to steam short circuiting.

3. The higher recoveries and rates (at least four times the cycle steam process) associated with horizontal well system offer a definite advantage over field development with the vertical wells.

4. With a limited resource base, the horizontal well development strategy would achieve much higher commercial rates provided that the additional capital is available.

ACKNOWLEDGEMENT

The authors wish to express their appreciation to Petro-Canada and Alberta Oil Sands Technology and Research Authority for permission to publish this paper.

REFERENCES

1. Towson, D.E., "The Mine Assisted In Situ Project", Presented at UNITAR/AAPG Conference, Santa Monica, California, October 29 to November 2, 1984.

2. Butler, R.M., Stephens, D.J. abd Weiss, M., "The Vertical Growth of Steam Chamber in the In-Situ Thermal Recovery of Heavy Oils", Proc. 2nd World Cong. Chem. Eng., 2, Montreal, October, 1981.

3. "Conoco Producing from Second Wyo. Oil Mine", Enhanced Recovery Week, Jan. 24, 1983, P.3.

4. Loxam, D.C., "Texaco Canada Completes Unique Horizontal Drilling Program", Petroleum Engineer International, September, 1982.

5. Bezaise, G.E. and Markiw, I.A., "Esso Resources Horizontal Hole Project at Cold Lake", 30th Annual meeting of Petroleum Society of CIM, Banff, May 8 - 11, 1979.

6. Texas Eastern Drilling Systems Inc. - Improved Lateral Completion Technology (LCT), 1984.

TABLE 1

COMPARISON OF NUMERICAL SIMULATOR RESULTS TO ACTUAL FIELD RESULTS FOR A WELL DEPTH GREATER THAN 350 m AND UNDER CYCLIC STEAM STIMULATION

	NUMERICAL SIMULATOR RESULTS FROM THIS STUDY	ACTUAL FIELD HISTORY RESULTS (RESERVOIR & OIL CHARACTERISTICS SLIGHTLY DIFFERENT)
Number of Steam Stimulation cycles	5	5
Total Operating Days	500	554
Steam Injected (m^3)	35,000	22,836
Oil Produced (m^3)	4,368	3,229
Oil-Steam Ratio (m^3/m^3)	0.125	0.141
Calendar Day Oil Rate (m^3/day)	8.74	5.83

TABLE 2

RESERVOIR VOLUMES PER REPEATABLE PATTERN

PROCESS	REPEATABLE PATTERN SPACING ha	OIL-IN-PLACE m^3	WATER-IN-PLACE m^3
Cyclic Steam High Oil Sat.	2.42	91,480	22,866
Cyclic Steam Low Oil Sat.	2.42	77,584	36,762
Horizontal Well Homogeneous Reservoir	2.25	72,148	34,185
Horizontal Well High Perm Path	2.36	75,755	35,894
Horizontal Well High Perm Path	4.72	151,510	71,789
Horizontal Well Gravity Assist-Low Oil Sat.	2.40	76,924	36,463
Horizontal Well Gravity Assist-High Oil Sat.	2.40	90,344	23,065

TABLE 3

COMPARISON BETWEEN HORIZONTAL AND VERTICAL WELL PERFORMANCE PER REPEATABLE PATTERN

PROCESS	OPERATING LIFE (Years)	CUMULATIVE STEAM INJECTED (m^3)	CUMULATIVE BITUMEN PRODUCED (m^3)	CUMULATIVE WATER PRODUCED (m^3)	CUMULATIVE OIL-STEAM RATIO (m^3/m^3)	CUMULATIVE DAY OIL RATE (m^3/d)
VERTICAL						
Cyclic Steam High Water Sat.	3	70,000	7,500	78,000	0.11	6.8
Cylic Steam High Bitumen Sat.	3	56,000	9,800	56,800	0.18	9.0
HORIZONTAL						
Steam Drive No Variations	3	267,000	61,400	308,000	0.23	56.1
Steam Drive Permeable Path	3	119,000	12,000	158,000	0.10	11.0
Steam Drive Double Spacing	3	275,000	38,500	380,000	0.14	35.2
Gravity Drainage High Water Sat.	4	346,000	56,800	343,700	0.16	38.9
Gravity Drainage High Bitumen Sat.	4	342,000	69,600	327,000	0.20	47.7

TABLE 4

PROCESS COMPARISON FOR THE RECOVERY OF RESERVES IN PLACE

PROCESS	% OF BITUMEN IN PLACE RECOVERED	% OF ENERGY INJECTED LOST TO OVER & UNDER BURDEN	% OF ENERGY INJECTED THAT WAS PRODUCED
VERTICAL			
Cyclic Steam High Water at Bottom	9.7%	22%	63%
Cyclic Steam	10.7%	22%	58%
HORIZONTAL			
Steam Drive no Areal Variations	85.0%	29%	42%
Steam Drive Permeable Path at Bottom	15.8%	27%	46%
Steam Drive Double Spacing - Perm. Path	25.4%	28%	43%
Gravity Drainage-High Water at Bottom	73.8%	29%	41%
Gravity Drainage-High Bitumen at Bottom	77.0%	28%	42%

TABLE 5

Development Costs Comparison ($1985)

Horizontal Well System VS Vertical Well (Cyclic Steam)

Plant Size: 10 000 BOPD Plant Life: 20 Years

	Vertical Wells	Horizontal Wells
New Satellite Cost $MM	2.35	2.97
Used Satellite Cost $MM	1.38	1.75
Well Drilling Cost $MM	0.25	1.00
New Well Completion $MM	0.07	0.50
Used Well Completion $MM	0.04	0.40
Fixed Operating Cost $/bbl *	7.00	8.40
No. of Wells Drilled $MM	1170	165
Total Tangible Costs $MM	279	215
Total Intangible Costs $MM	292	165
Operating Costs (Gross) ** $MM	1280	1294
Undiscounted Supply Price $/bbl	25.7	23.2
Supply Price $/bbl Discounted @ 10%	28.7	25.9

*Operations/workovers = 21%
Maintenance = 20%
Central Plant = 28%
Admin./Technical = 31%

** 4% built-in inflation in gas price assumed

** Transportation/Tariff assumes oil deliveries to Edmonton.
Cost developed by authors from publicly available data.

RESERVOIR CHARACTERIZATION - BOTTOM WATER CASE

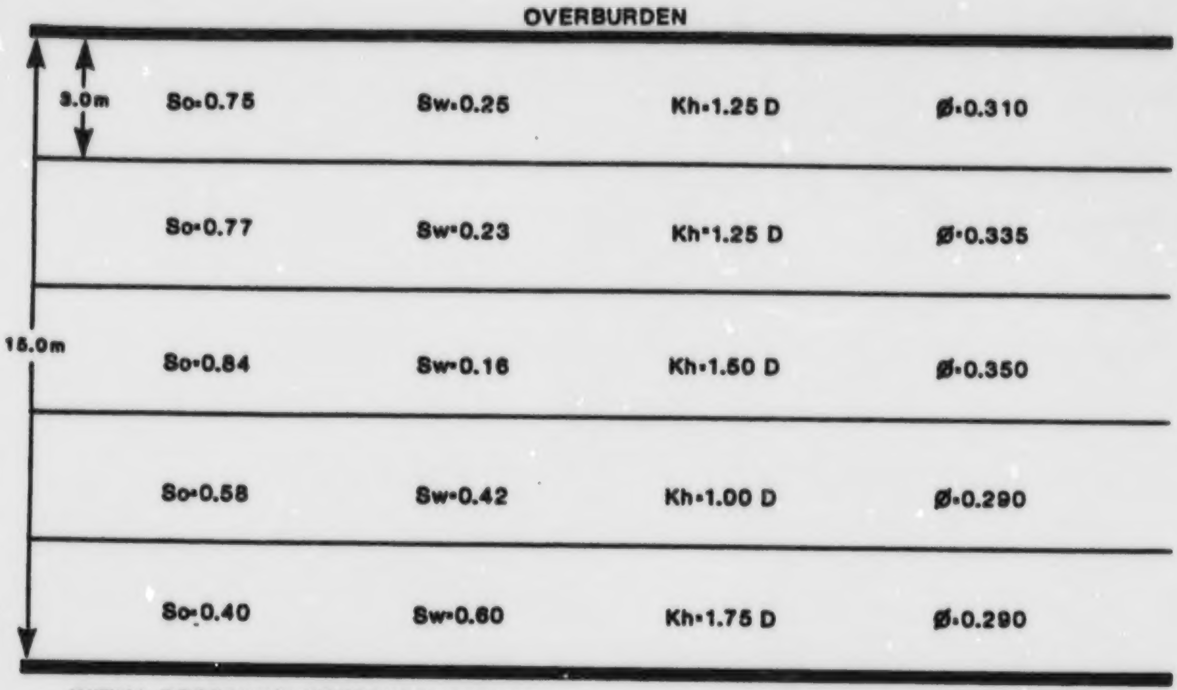

So=0.75	Sw=0.25	Kh=1.25 D	Ø=0.310
So=0.77	Sw=0.23	Kh=1.25 D	Ø=0.335
So=0.84	Sw=0.16	Kh=1.50 D	Ø=0.350
So=0.58	Sw=0.42	Kh=1.00 D	Ø=0.290
So=0.40	Sw=0.60	Kh=1.75 D	Ø=0.290

INITIAL RESERVOIR PRESSURE = 2200 kPa   RESERVOIR TEMPERATURE = 10°C

Figure 1

RESERVOIR CHARACTERIZATION - HIGH BITUMEN CASE

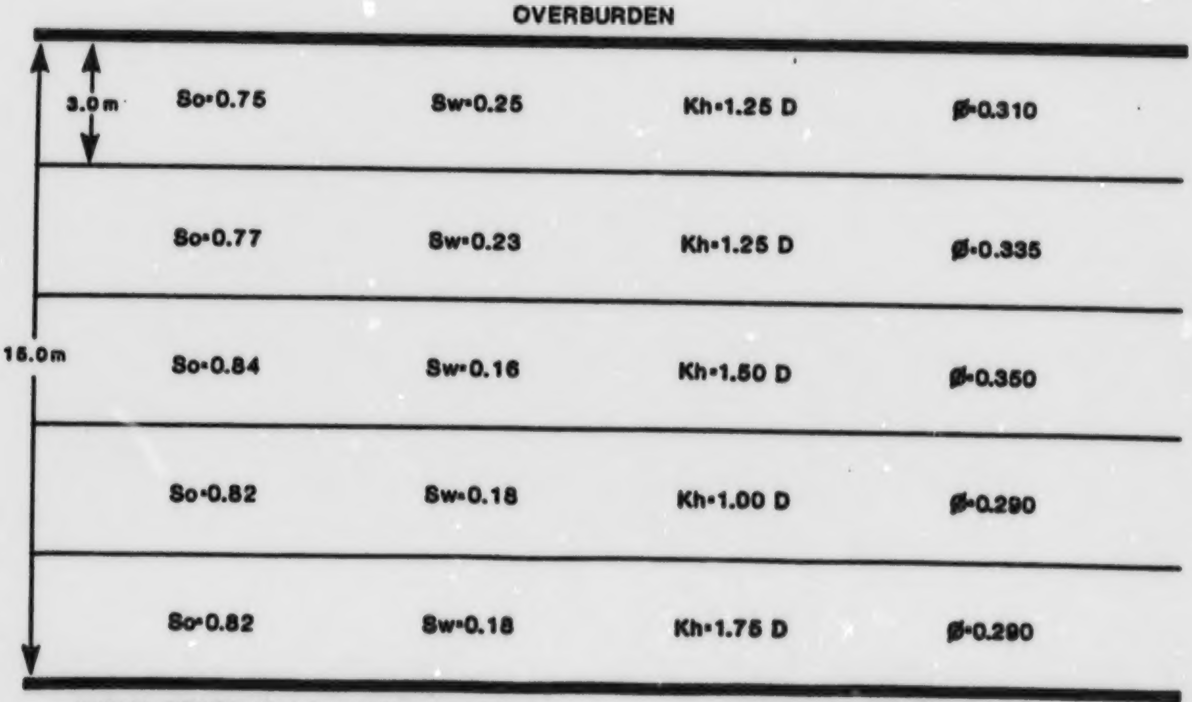

So=0.75	Sw=0.25	Kh=1.25 D	Ø=0.310
So=0.77	Sw=0.23	Kh=1.25 D	Ø=0.335
So=0.84	Sw=0.16	Kh=1.50 D	Ø=0.350
So=0.82	Sw=0.18	Kh=1.00 D	Ø=0.290
So=0.82	Sw=0.18	Kh=1.75 D	Ø=0.290

INITIAL RESERVOIR PRESSURE = 2200 kPa   RESERVOIR TEMPERATURE = 10° C

VISCOSITY- TEMPERATURE CHART
OIL VISCOSITY VS TEMPERATURE

(OIL DENSITY 1030 kgm/m^3 (5.9° API))

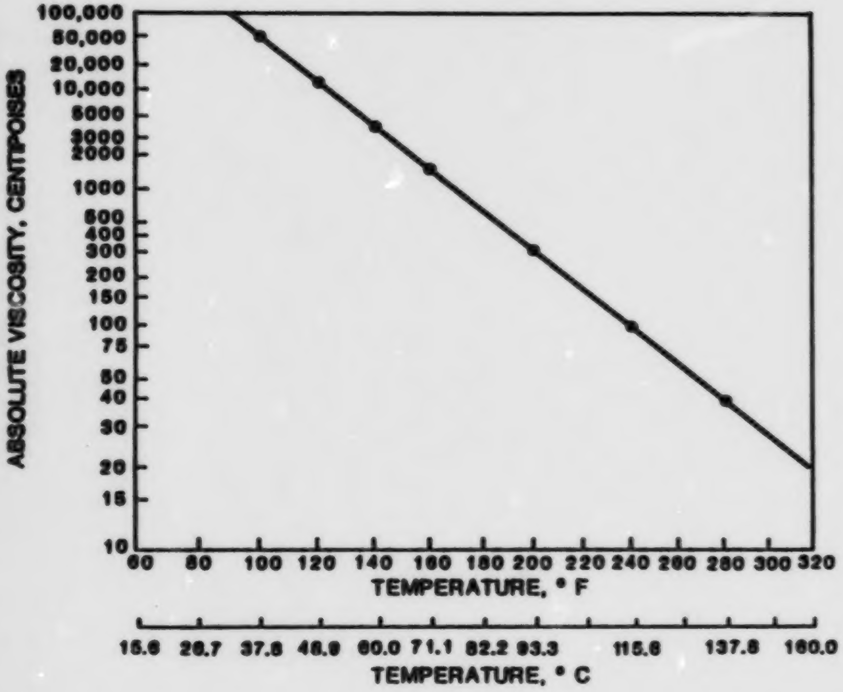

Figure 3

WATER AND GAS RELATIVE PERMEABILITY CURVES

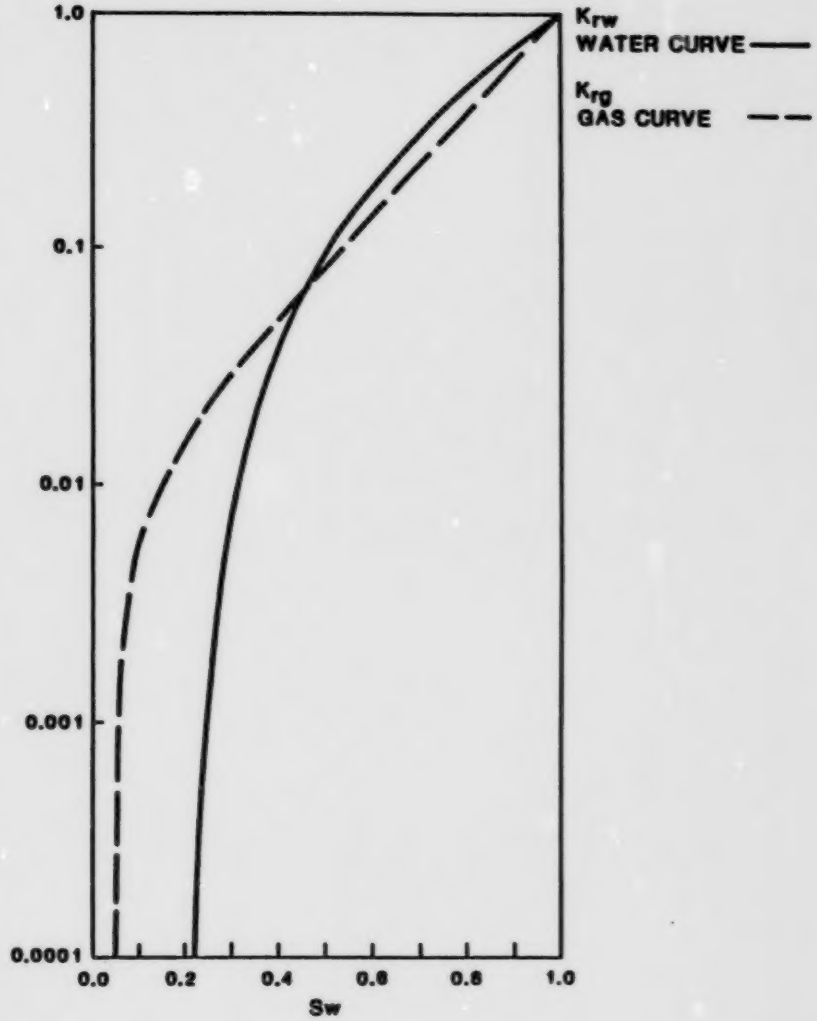

Figure 4

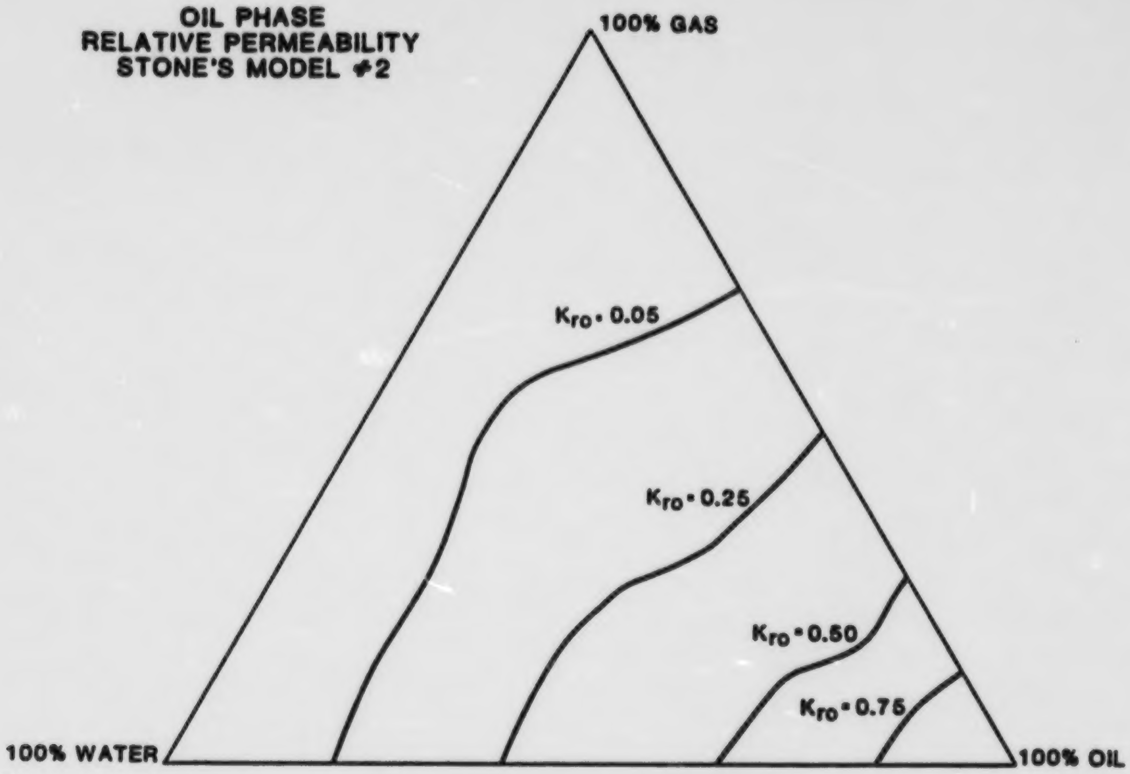

Figure 5

COMMERCIAL OPERATION - VERTICAL WELL PATTERN SPACING

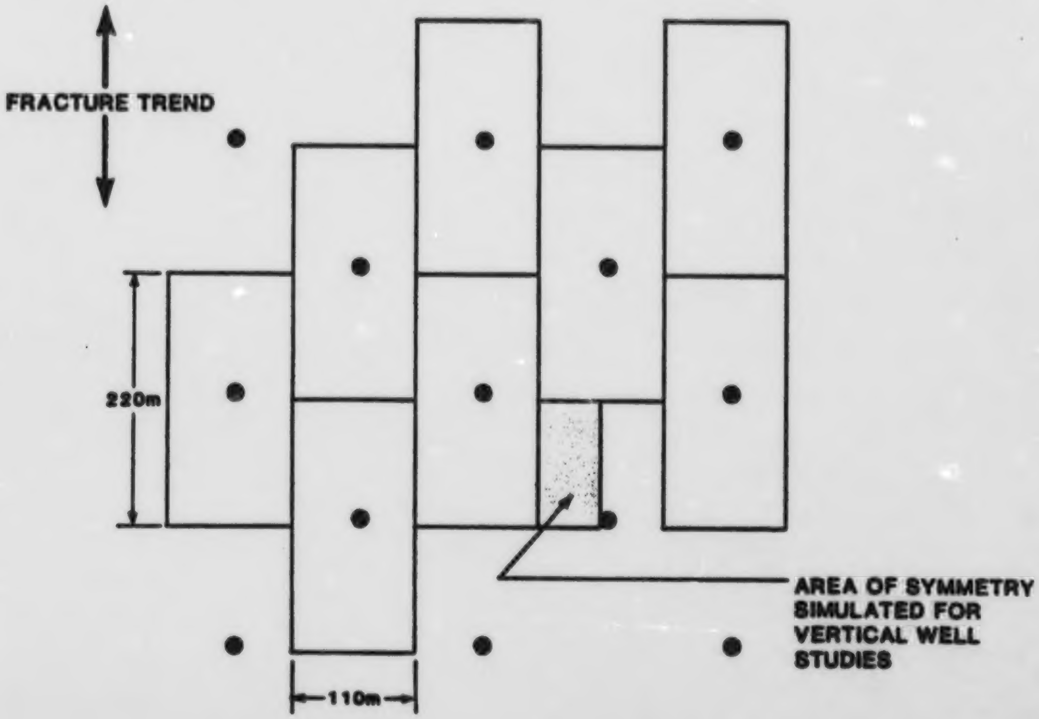
FRACTURE TREND
220m
110m
AREA OF SYMMETRY
SIMULATED FOR
VERTICAL WELL
STUDIES

Figure 6

CYCLIC STEAM RESERVOIR DEPICTION AND OPERATING STRATEGY
(1/4 OF AN ISOLATED VERTICAL WELL SIMULATED - NOT TO SCALE)

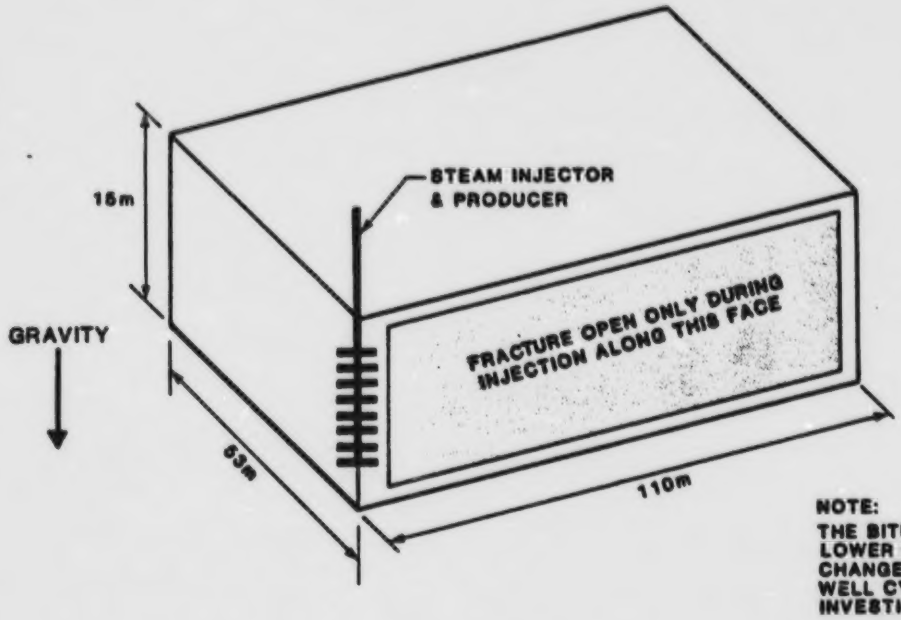
15m
STEAM INJECTOR
& PRODUCER
GRAVITY
FRACTURE OPEN ONLY DURING
INJECTION ALONG THIS FACE
53m
110m

OPERATING STRATEGY

INJECT 7000 m^3 OF 71% QUALITY STEAM AT SAND FACE OVER 28 DAYS

PRODUCE FOR BETWEEN 70 AND 100 DAYS UNTIL OIL RATE REACHES 1.0 m^3/d

NOTE:
THE BITUMEN SATURATION IN THE LOWER 6m OF RESERVOIR WAS CHANGED BETWEEN THE 2 VERTICAL WELL CYCLIC STEAM CASES INVESTIGATED

Figure 7

HORIZONTAL WELL INTERWELL STEAM DRIVE FOR BOTTOM WATER RESERVOIR
(1/2 OF HORIZONTAL WELLS SIMULATED - NOT TO SCALE)

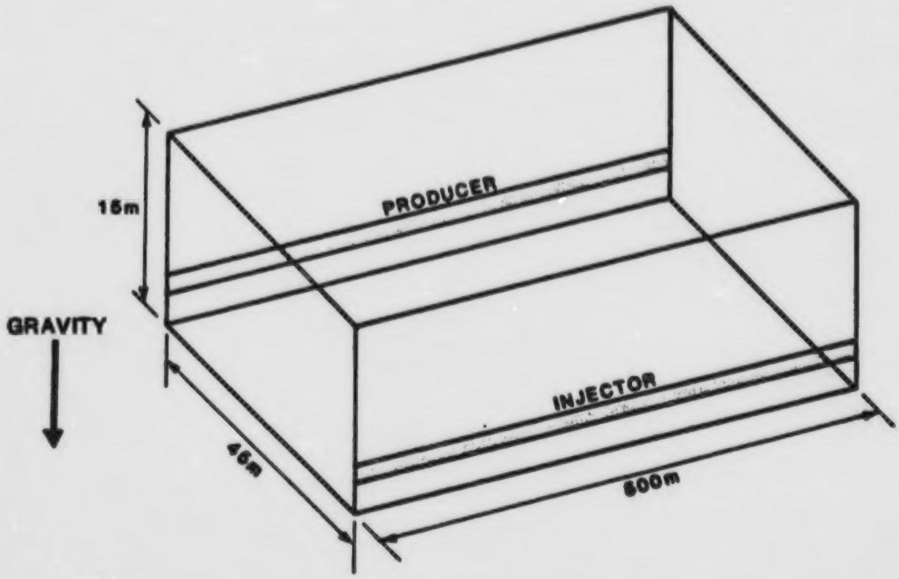
15m
PRODUCER
GRAVITY
INJECTOR
46m
600m

OPERATING STRATEGY

INJECT INTO INJECTER AT 275 m^3/d OF 71% QUALITY STEAM

PRODUCE FROM PRODUCER AT 350 m^3/d

Figure 8

HIGH PERMEABILITY CHANNEL BETWEEN INJECTOR AND PRODUCER
(1/2 OF HORIZONTAL WELLS SIMULATED - NOT TO SCALE)

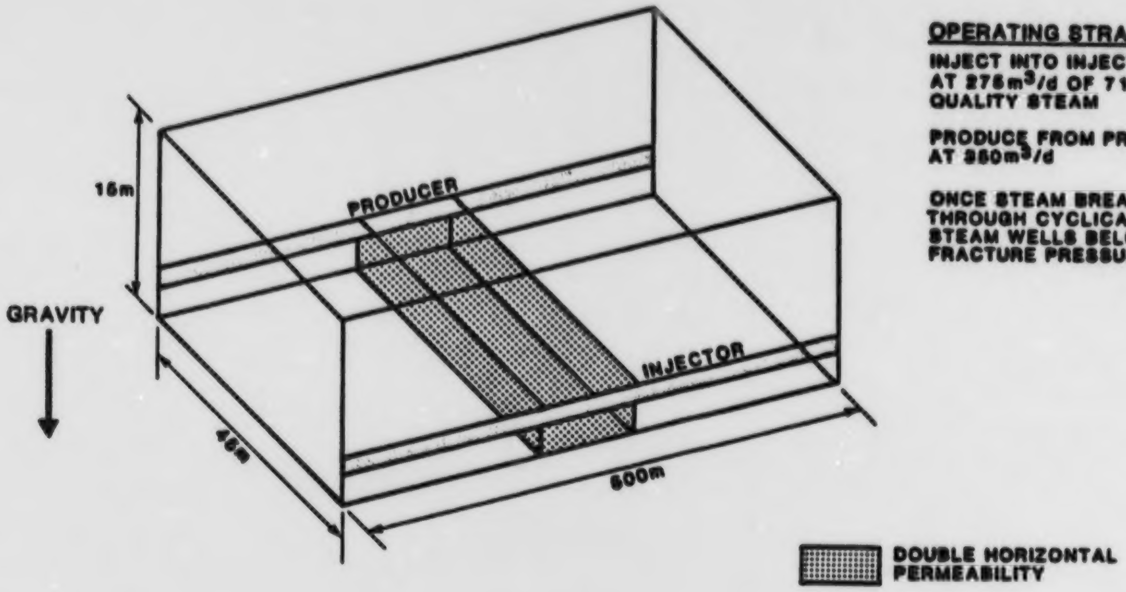
15m
PRODUCER
GRAVITY
INJECTOR
45m
500m
▦ DOUBLE HORIZONTAL PERMEABILITY

OPERATING STRATEGY

INJECT INTO INJECTOR
AT 275m^3/d OF 71%
QUALITY STEAM

PRODUCE FROM PRODUCER
AT 350m^3/d

ONCE STEAM BREAKS
THROUGH CYCLICALLY
STEAM WELLS BELOW
FRACTURE PRESSURE

Figure 9

GRAVITY ASSISTED STEAM DRAINAGE INTO HORIZONTAL WELLS
(1/2 OF REPEATABLE PATTERN SIMULATED - NOT TO SCALE)

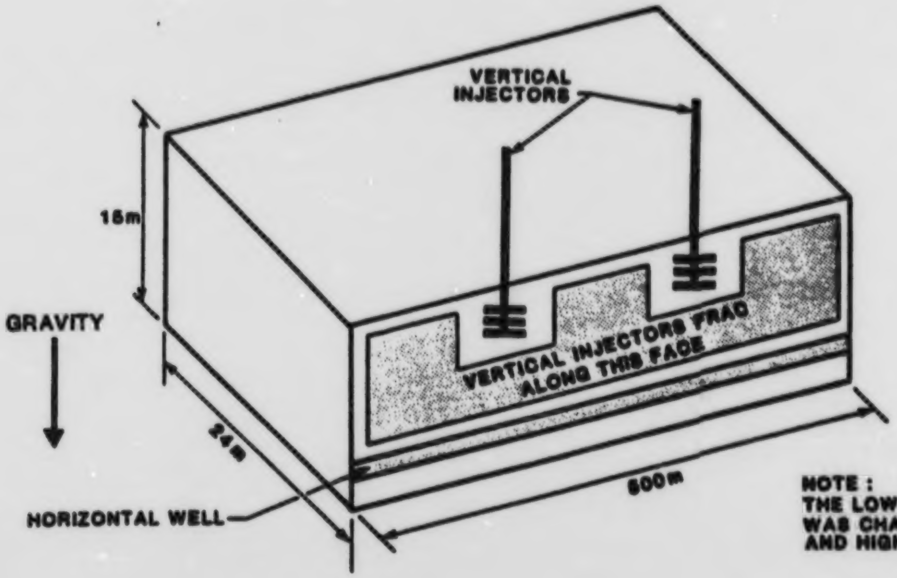
VERTICAL INJECTORS
15m
GRAVITY
VERTICAL INJECTORS FRAC ALONG THIS FACE
24m
500m
HORIZONTAL WELL

OPERATING STRATEGY

VERTICALLY FRAC
BETWEEN ALL WELLS

INJECT AT 9000 kPa
INTO VERTICAL INJECTOR

PRODUCE AT 8950 kPa
FROM 500 m LONG
HORIZONTAL PRODUCER

NOTE :
THE LOWER 6m OF RESERVOIR
WAS CHANGED FOR THE HIGH WATER
AND HIGH BITUMEN CASES STUDIED

Figure 10

HORIZONTAL WELL STEAM DRIVE - COMMERCIAL WELL SPACING CONFIGURATION

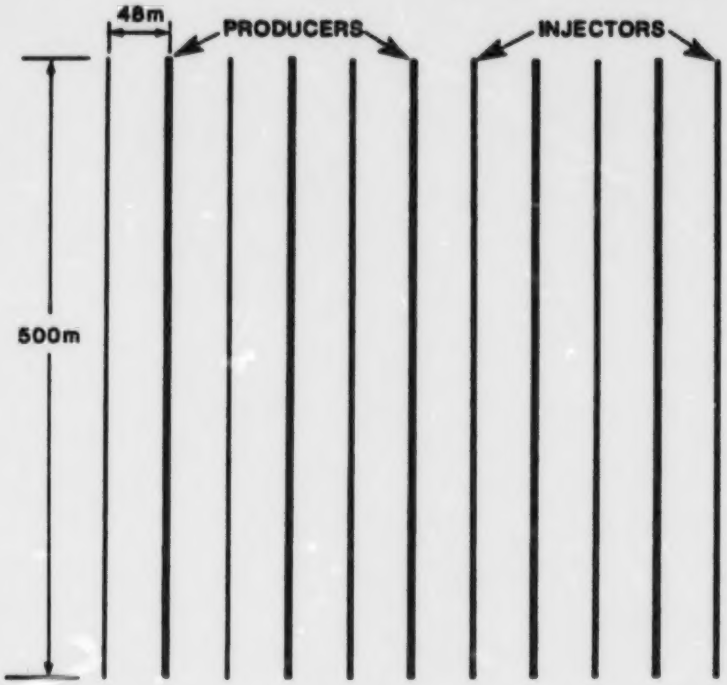
48m
PRODUCERS
INJECTORS
500m

Figure 11

GRAVITY ASSISTED STEAM DRAINAGE INTO HORIZONTAL WELLS COMMERCIAL SPACING

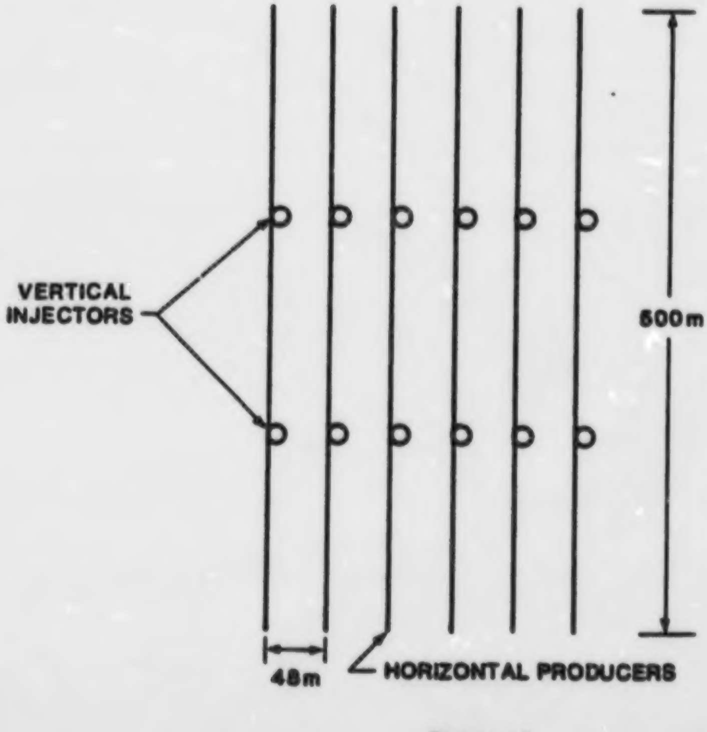
VERTICAL INJECTORS
500m
48m
HORIZONTAL PRODUCERS

Figure 12

5444 H

THIRD INTERNATIONAL CONFERENCE ON HEAVY CRUDE AND TAR SANDS

LONG BEACH,
CALIFORNIA
22-31 JULY 1985

[illegible] OIL SANDS
INFORMATION CENTRE

87

VOLUME II

HCTS/CF.3/8.17
(NOT FOR PRESENTATION)

THIRD INTERNATIONAL CONFERENCE ON HEAVY CRUDE AND TAR SANDS
TERCERA CONFERENCIA INTERNACIONAL SOBRE CRUDOS PESADOS Y ARENAS BITUMINOSAS
TROISIEME CONFERENCE INTERNATIONALE SUR LES PETROLES LOURDS BRUTS ET LES SABLES BITUMINEUX

SIMULATION OF STEAM INJECTION THROUGH HORIZONTAL WELLBORES FOR VISCOUS OIL RECOVERY

BY

G.L. GUSSIS
ARCO OIL AND GAS COMPANY
TEXAS

UNITAR/UNDP INFORMATION CENTRE
FOR HEAVY CRUDE AND TAR SANDS
336 East 45th Street
New York, N.Y. 10017

TEL: (212) 370-1122
TELEX: 662197 infocer

ABSTRACT

Cyclic steam injection and steam drive from 2000 foot (610 m) horizontal wells were numerically simulated and evaluated for viscous oil recovery. Sensitivity studies included consideration of reservoir properties such as relative permeability and layer stratification. Simulated and idealized well patterns included a continuous parallel well configuration, a "spoke" configuration with horizontal wells separated by 45 degrees and a staggered configuration with parallel horizontal wells at different depths. Non-parallel configurations and near horizontal wells with vertical deviations were studied to assess process sensitivity to more realistic well alignments. Continuous parallel was the most promising configuration. Simulated oil recovery was 60% of the oil in place for the most favorable scenario, but was extremely sensitivity to the extent to which wellbores were parallel and horizontal.

INTRODUCTION

Steam injection by steam soak and/or steam drive is the most widely used process for enhanced oil recovery. Potential benefits of steam injection for viscous oil recovery include viscosity reduction, distillation of lighter components, pressure maintenance, and mobility control. To maximize these, high contact efficiency between injected steam and viscous oil should be achieved. One method of increasing contact is by injecting steam from horizontal wells. The length of wellbore contacting a pay zone could be many times larger than with a vertical well in which contact is limited to the pay thickness. Both steam and horizontal wellbore technologies are practiced in oil fields at this time (Meyer et al, 1982). With insulated tubing, steam could be injected at depths up to 3800 feet (1158 m). Horizontal wells have been drilled at lengths as great as 1000 feet (305 m). A simulation study by Rial (1984) discussed potential benefits of this technology for a description typical of the Kern River Field in California.

In this report, steam injection from a horizontal wellbore is simulated as a viscous oil recovery process. Sensitivity studies consider reservoir stratification, well patterns, steam injection schemes, and reservoir properties.

RESULTS AND DISCUSSION

Model Description

The fully implicit THERM steamflood simulator (Scientific Software-Intercomp) developed by Coats (1980) was used for the studies. Simulations were three-dimensional with representative grids as shown in Figure 1.

Reservoir Fluid and Rock Properties

Reservoir temperature for the studies was assumed to be room temperature (75°F or 23.9°C). Reservoir depth was 3500 feet (1067 m) and reservoir pressure was 1600 psi (1.125×10^6 kg/m^2). Three components (water, oil, methane) and three phases (water, oil, and gas) were modeled. Initial oil saturation was 75% and initial water saturation was 25%. The 12°API gravity oil was saturated with methane at reservoir conditions. PVT correlations and associated parameters are listed in Table 1. Relative permeabilities were derived from generalized correlations and are contained in Table 2. The reservoir model was stratified with 5 layers. Permeabilities and porosities of the layers are included in Table 3. Rock compressibility was 3×10^{-5}/psi. Steam quality at the sand face was 80%. Steam was injected at 2500 psi (1.758×10^6 kg/m^2) and fluid was produced against a 700 psi (4.922×10^5 kg/m^2) back pressure. Injection and production rate limits were set at 10,000 STB/D/well (1.84×10^{-2} m^3/s/well). Injection and production were limited by the above-stated pressures, however, and not by the rate constraints.

Horizontal Versus Vertical Wells

Simulations were performed to compare steam soak from a single vertical well with steam soak from a single horizontal well. Results are plotted in Figure 2. The horizontal well section was 840 feet (28.9 m) long and the vertical well section exposed to the pay zone was 100 feet (30.5 m) long. The horizontal section was located at the bottom of the reservoir. For this particular case, the reservoir was assumed to be homogeneous with a horizontal permeability of 1500 md (1.48×10^{-12} m^2) and a vertical permeability of 500 md (4.93×10^{-13} m^2). There were three layers in the model description.

A 90 day steam cycle (7 days production, 17 days injection, 4 days soak, 62 days production) was simulated to determine whether or not a difference between well performances would be apparent in a short time. After 90 days, cumulative production was about 5 times greater for the horizontal well in which 8 times as much well was exposed to the producing interval as with the vertical well. Consequently, 8 times as much water and heat were injected from the horizontal well. Production was not increased 8-fold since the percentage of heat lost to the underburden was greater for the horizontal case. Potential benefits of horizontal wells are indicated by the cumulative production curves in Figure 2. The difference between horizontal and vertical performances is expected to decline with time of operation as a greater percentage of the oil near the vertical well is heated.

Horizontal Well Cases

The base case for the simulations considered an initial 2.2 year period of cyclic steam stimulation to increase injectivity and productivity of wells followed by an extended period of steam drive. Steam cycle lengths are listed in Appendix A. A stratified reservoir description was chosen for the base case as discussed earlier. Results for all of the following simulations are included in Table 4.

Initially, steam soak followed by steam drive was simulated for 20 acre (8.09×10^4 m^2)/well spacing with 2000 foot (610 m) parallel horizontal sections, 2000 foot (610 m) gaps between successive adjacent wellbore sections, and 218 feet (66.5 m) between parallel sections (Figure 3 - 2000' gap parallel case). Results in Table 4 show that cumulative oil recovery after 2.5 years was 9.1% OOIP (original oil in place). The region between adjacent wellbore sections was poorly swept.

To improve sweep, a continuous parallel configuration was modeled for 20 acre (8.09×10^4 m^2)/well spacing with 2000 foot (610 m) horizontal well sections; no gap between adjacent wellbore sections, and 436 feet (132.9 m) between parallel sections (Figure 3 - continuous parallel case). As expected, sweep improved and cumulative oil recovery was 9.9% after 2.2 years.

Since relative permeabilities were derived from generalized correlations, several cases were examined with more optimistic relative permeabilities (Table 5); specifically, increased oil permeability in the presence of gas. For the 2000' gap parallel configuration, simulated oil recovery increased from 9.1% for the generalized relative permeabilities to 10.8% after 2.5 years. The process was stopped at 2.5 years since steam broke through at the wellbore tips and the water/oil ratio increased dramatically within 100 days of converting from steam soak to steam drive at 2.2 years. The oil production rate dropped from 1560 STB/D/pattern (2.87 x 10^{-3} m^3/s/pattern) to less than 100 STB/D/pattern (1.84 x 10^{-4} m^3/s/pattern) (Figure 4). Early breakthrough at wellbore tips probably resulted from a greater percentage of flow out the tips than the rest of the wellbore due to the larger reservoir volume between tips of adjacent wellbore sections. The continuous parallel pattern described above should greatly reduce this effect.

Since steam drive was not attractive for the 2000' gap parallel pattern, continuous steam soak was simulated for this pattern as well as for alternate configurations. Steam cycle lengths are included in Appendix A. All of these simulations used the optimistic relative permeabilities.

For continuous steam soak from the 2000' gap parallel pattern, average oil production rate over 9.3 years was 360 STB/D/well (6.62 x 10^{-4} m^3/s/well) with 27.0% recovery of original oil in place. At 9.3 years, oil rate remained at a reasonable level, although it was beginning to decline (Figure 5). Heat injected from the wellbores at the bottom of the reservoir was reaching the top of the formation and leading to significant oil viscosity reduction at the top of the reservoir (Figure 6). Thus, gravity damage was enhanced by the increased oil mobility.

Several alternate pattern configurations were considered for cyclic steam injection from horizontal wells. These included staggered parallel, continuous parallel, and spokes (Figure 3). With the exception of the staggered parallel configuration, horizontal wells were in the bottom grid layer of the model description to benefit from the oil drainage.

To deliver more heat to the top of the pay zone, a staggered parallel configuration with one wellbore in the top model layer and a second wellbore in the bottom model layer was simulated (Figure 3). Results in Table 4 indicate no significant improvement after 9 years over a configuration with both wellbores placed in the bottom layer. Oil was heated at the top of the reservoir and did drain as in the previous case. However, heat loss to the overburden was greater and the steam traversed less of the pay zone.

As discussed above for the generalized relative permeability cases, sweep was improved with a continuous parallel pattern. A greater portion of the oil was heated with the continuous parallel pattern than with the 2000' gap parallel configuration (Figure 7 and 8) and oil recovery increased almost 20% in 9 years.

A spoke pattern enables many horizontal wells to be drilled from the same drilling pad (Figure 3). Horizontal sections were aligned at 45° to each other. Wells on the pattern diagonals were longer by a factor of the square root of two. Patterns were 80 acres (3.24×10^5 m^2) with 4 wells per pattern. Results in Table 4 show that oil recovery after 9 years was 23% less than the 2000' gap parallel configuration. Figure 9 shows only a slight temperature rise in much of the area between the wellbores since the wellbore tips were separated by such a large distance (933 feet).

Generalized relative permeabilities (Table 2) were used for all of the cases presented below.

As discussed above, cyclic steam stimulation followed by steam drive recovered more oil with the continuous parallel pattern than with the 2000' gap parallel pattern. Simulated oil recovery after 9 years was 41.9% OOIP (Table 4). This was 55% greater than the 2000' gap parallel scheme (with more optimistic relative permeabilities) after 9.3 years. After 9 years, much of the reservoir was heated to over 250°F (121°C) (Figure 10) and live oil viscosity was reduced to approximately 10 cp (0.01 kg/m-s). Simulated oil recovery probably resulted from a combination of gravity drainage and steam drive. Figure 11 shows decreased oil saturation near the top of the reservoir and that oil was driven along the bottom of the reservoir.

Simulated oil recovery for cyclic steam followed by steam drive after 5.6 years was 26.3% OOIP. This represented a 17% increase over the 22.4% OOIP recovery for the continuous parallel case with cyclic steam only (with more optimistic relative permeabilities). Steam drive recovered more oil than continued cyclic steam by heating further into the reservoir (Figures 12 and 13).

A single massive sand description with total reservoir thickness, total kh, and total ϕh the same as those used in the stratified decription above was simulated to examine sensitivity to reservoir stratification. Results for the continuous parallel configuration with the single massive sand description are included in Table 4. After 9 years, oil production increased 49% to 62.6% OOIP from 41.9% OOIP for the same scheme with the stratified description. Comparing Figures 10 and 14, the massive sand case had greater delivery of heat to the upper portions of the reservoir and significant steam override due to greater vertical communication. In the stratified case, the highest permeability layer was at the bottom, vertical communication was less, and steam tended to remain in the lower region of the reservoir.

The advantage of the continuous parallel scheme was the generation of a uniform line drive without early breakthrough between parallel wells. In practice, a perfect line drive and drilling wells aligned continuously would be unlikely. Therefore, simulations were performed for 40 foot (12.2 m) and 150 foot (45.7 m) gaps between adjacent wellbores. Results in Table 4 indicate that simulated oil recovery did decrease as the gap distance increased. For a 150 foot gap (45.7 m), a 12% drop was noted from 41.9% OOIP to 36.8% OOIP. The decline was less for the 40 foot (12.2 m) gap. As the gap increased, the produced water/oil ratio increased sooner, establishing more rapid communication. For horizontal wells at the bottom of the reservoir, establishing communication led to reduced sweep and poorer recovery.

Simulations were run to examine oil production from wells drilled slightly non-parallel to each other. A representative well configuration is shown in Figure 15. Grid dimensions associated with the figure are included in Table 6.

Simulations assumed a deviation from 436 feet (132.9 m) of 106 feet (32.3 m), i.e. a separation at ends of adjacent wellbores of 542 feet (165.2 m). In addition, a case was run considering a separation of 542 feet (165.2 m) plus a 100 foot (30.5 m) gap between ends of adjacent wellbores. For the non-parallel configurations, water breakthrough occurred along the bottom of the reservoir and the water/oil ratio increased above 10.0 approximately 100 days after converting from cyclic steam to steam drive. As discussed above, for horizontal wells establishing a communication path along the bottom of the reservoir resulted in decreased simulated oil recovery. Oil recovery decreased from 41.9% for the parallel case to 24.4% (Table 4). Including a 100 foot (30.5 m) gap between ends of adjacent wellbores did not substantially alter the simulation results from the non-parallel case with no gap. Early breakthrough was induced primarily by the non-parallel configuration of the wells rather than the 100 foot (30.5 m) gap between wellbore ends.

With current drilling technology, maintaining a wellbore completely horizontal along the bottom of the reservoir is unlikely. Therefore, steam injection from a high angle (75°) well and steam injection from a well with some vertical deviation were simulated. Wellbore configurations for these simulations are shown in Figure 16. For high angle wells, parallel, with cyclic steam followed by steam drive, simulated oil recovery was 22.9% OOIP (Table 4). In the simulation, steam channeled across the top of the reservoir reducing sweep. The shorter length of wellbore in the pay zone reduced the contact efficiency.

To simulate a "horizontal" well with vertical deviation, the proximal portion of the wellbore was identical to the high angle well described above. The distal portion of the wellbore was horizontal. Adjacent wellbores were continuous (Figure 16). Simulated oil recovery, at 27.6% OOIP, again was significantly lower than with truly horizontal wells, but was slightly greater than with the high angle well. For the vertical deviation well, there was greater contact between the wellbore and mhe reservoir than with the high angle well.

Assumptions in the simulations included no viscous fingering, constant steam quality along the wellbore, and constant pressure along the wellbore. Sensitivities of the continuous parallel configuration case to these parameters were examined.

To semi-quantitatively simulate early breakthrough due to viscous fingering, a 10 foot wide high permeability streak was included in the reservoir description (Figure 3). The water/oil ratio increased sooner than in the continuous parallel case and oil recovery decreased (Table 4).

To test the assumptions of constant temperature and constant pressure along the wellbore, each was varied independently. Steam quality was decreased from 0.8 to 0.3 along the wellbore. Oil recovery dropped only slightly from 41.9% OOIP to 39.6% OOIP (Table 4). In another simulation, wellbore bottom hole pressure was decreased from 2500 psi (1.76 x 10^6 kg/m^2) to 2490 psi (1.75 x 10^6 kg/m^2) along the wellbore (a 10 psi (0.01 x 10^6 kg/m^2) drop is approximately the drop that would be expected for laminar flow in that length horizontal well). Again, sweep remained fairly uniform and recovery showed almost no decline.

To consider sensitivity to well spacing, a 40 acre (1.62 x 10^5 m^2)/well continuous parallel case was simulated. Figure 17 shows that a much smaller percentage of the reservoir was heated after 9 years than for 20 acre (8.09 x 10^4 m^2)/well spacing (Figure 10). Simulated oil recovery dropped to 27.8% OOIP for the larger spacing. Although this is a significant decrease in cumulative oil recovery, average oil production rate over 9.0 years was higher for the larger spacing (Table 4). For 20 acre (8.09 x 10^4 m^2)/well spacing, water breakthrough occurred sooner and the water/oil ratio thus increased faster. This raises the possibility of beginning with a 40 acre (1.62 x 10^5 m^2) or 80 acre (3.24 x 10^5 m^2) pattern and infill drilling later.

Limitations

Gravity override and reservoir heterogeneities are important factors in determining sweep during a steam injection process. The ability to model these is somewhat restricted in a finite difference model such as used for these studies. In addition, the model cannot adequately simulate viscous fingering. Steam distillation effects and thermal alteration of the oil was not included. Since assumptions remain the same for the different simulation studies, however, comparisons of simulated results could be used to identify key parameters for various recovery processes, rank recovery processes relative to each other, and to establish priorities for additional work.

CONCLUSIONS

On an oil production basis, a single horizontal well is far superior to a single vertical well for cyclic steam recovery of viscous oil. The main benefit derives from greater initial contact of the reservoir by steam with a horizontal well.

The primary recovery mechanism for steam injetion through horizontal wells appears to be a combination of viscosity reduction, gravity drainage, and fluid drive.

Steam drive shows advantages over continued cyclic steam operation. With steam drive from horizontal wells on 20 acre (8.09×10^4 m^2)/well spacing, heat is transferred deeper into the reservoir than with cyclic steam and the oil is driven or dragged to production.

Continuous parallel configurations resulted in the highest oil recovery rates and cumulative oil productions of the configurations simulated. With a continuous parallel arrangement, simulated flow stream lines become linear.

A continuous parallel configuration is highly idealized. Vertical and/or horizontal deviations from the ideal parallel continuous well scheme lead to marked reductions in simulated oil recovery.

Viscous fingering and/or gaps between adjacent wellbores lead to more rapid establishment of communication between parallel wellbores, more rapid breakthrough and reduced benefits from steam drive.

The advantages of steam injection through horizontal wells are more pronounced for a homogeneous reservoir than for a stratified reservoir. Vertical heat transfer and gravity drainage are much more effective in a homogeneous reservoir.

ACKNOWLEDGEMENTS

I would like to thank Gary Charlson, Randy DeRuiter, and Graham Fleming for their useful comments during the course of this work.

REFERENCES

Coats, K. H., In-situ combustion model, Soc. Pet. Eng. J., December 1980.

Meyer, R. F., J. C. Wynn, J. C. Olson, eds. The Future of Heavy Crudes and Tar Sands, Second International Conference, Caracas, Venezuela, February 1982.

Rial, R. M., Third thermal simulation using a horizontal wellbore for steamflooding, SPE Paper No. 13076.

TABLE 1. PVT CORRELATIONS AND PARAMETERS

K-Value Calculation:

$$K_{VIJ} = \left[KV1(I,J) + \frac{KV2(I,J)}{p} + KV3(I,J)_p\right] * EXP\left[- \frac{KV4(I,J)}{T-KV5(I,J)}\right]$$

where

K_{VIJ} = K-value of component I in phase J
p = Pressure, psia
T = Temperature, °R

Gas Phase Viscosity Calculation:

$$\mu_g = \sum_{I=1}^{N_c} X_{Ig} \quad \mu_{Ig}$$

where

$$\mu_{Ig} = AVIS(I,g)T^{BVIS\ (I,g)}$$

and

μ_{Ig} = Component I viscosity in gas phase
X_{Ig} = Mole fraction of component I in gas phase
N_c = Number of components
T = Temperature, °R

Table 1. (Continued)

Liquid Phase Viscosity Calculation:

$$\mu_{\ell} = \prod_{I=1}^{Nc} \mu_{I\ell}^{x_{I\ell}}$$

where,

$$\mu_{I\ell} = \mathrm{EXP}\ \left[\mathrm{AVIS}(I,\ell)\ T^{\mathrm{BVIS}(I,\ell)}\right] - 0.9999$$

and

$\mu_{I\ell}$ = Component I viscosity in liquid phase

COMPONENT	OIL		METHANE	
PHASE	OIL	GAS	OIL	GAS
AVIS	2.395×10^{11}	0	2.997×10^{20}	8.301×10^{-4}
BVIS	-3.802	0	-7.317	0.4751
KV1	1	0	1	0.6693
KV2	0	0	0	4.280×10^{3}
KV3	0	0	0	-2.85×10^{-5}
KV4	0	0	0	6.625
KV5	0	0	0	4.815×10^{2}

TABLE 2. RELATIVE PERMEABILITIES GENERALIZED CORRELATIONS.

Sw	k_{rw}	k_{row}
0.25	0.000	1.00
0.26	0.0003	0.97
0.275	0.0007	0.92
0.29	0.0013	0.87
0.31	0.0024	0.81
0.33	0.0040	0.75
0.35	0.0799	0.6899
0.40	0.01857	0.5548
0.45	0.03378	0.4334
0.55	0.07851	0.2326
0.65	0.1428	0.0904
0.80	0.277	0.00
1.00	1.00	0.00

S_L	k_{rog}	k_{rg}
0.25	0.0	1.00
0.318	0.000001	0.90
0.355	0.000002	0.81
0.429	0.00029	0.62
0.502	0.6028	0.46
0.576	0.013	0.31
0.649	0.039	0.195
0.723	0.097	0.096
0.760	0.14	0.062
0.797	0.20	0.036
0.833	0.28	0.018
0.870	0.39	0.0069
0.900	0.49	0.0021
0.907	0.52	0.0014
0.910	0.53	0.0012
0.922	0.58	0.00043
0.927	0.60	0.00027
0.933	0.63	0.00011
0.944	0.68	0.00
1.00	1.00	0.00

TABLE 3. Layer Description

LAYER	THICKNESS (FEET)	POROSITY	HORIZONTAL PERMEABILITY (MD)	VERTICAL PERMEABILITY (MD)
1	10.5	0.378	2004	1002
2	28.3	0.321	483	242
3	23.5	0.351	1595	798
4	38.8	0.317	247	25
5	19.4	0.378	3385	1692

TABLE 4. RESULTS

CASE	AVERAGE OIL PRODUCTION RATE (STB/D/WELL)	RECOVERY (% OOIP)	DURATION (YEARS)
STRATIFIED DESCRIPTION			
2000' gap parallel, cyclic steam/ steam drive	457	9.1	2.5
Continuous parallel, cyclic steam/ steam drive	580	41.9	9.0
	581	34.9	7.5
	584	26.3	5.6
	560	9.9	2.2
Recovery Process Alternative (Modified Relative Permeabilities)			
2000' gap parallel, cyclic steam/ steam drive	545	10.8	2.5
Pattern Configurations (Modified Relative Permeabilities)			
2000' gap parallel, cyclic steam only	360	27.0	9.3
	413	19.7	5.9
	522	9.2	2.2
Staggered parallel, cyclic steam only	366	26.5	9.0
Continuous parallel, cyclic steam only	429	31.0	9.0
	497	22.4	5.6
	678	12.0	2.2
Spokes, cyclic steam only	288	20.8	9.0

TABLE 4. RESULTS (Continued)

CASE	AVERAGE OIL PRODUCTION RATE (STB/D/WELL)	RECOVERY (% OOIP)	DURATION (YEARS)
Sensitivity to Stratification:			
Continuous parallel, cyclic steam/ steam drive-Homogeneous	865	62.6	9.0
Sensitivity to Drilling Limitations:			
Continuous parallel, cyclic steam/ steam drive - 150' gap	547	36.8	9.0
Continuous parallel, cyclic steam/ steam drive - 40' gap	564	40.0	9.0
Continuous non-parallel, cyclic steam/ steam drive - 542' separation	341	24.4	9.0
Continuous non-parallel, cyclic steam/ steam drive - 542' separation, 100' gap	332	23.7	9.0
Parallel high angle, cyclic steam/ steam drive	317	22.9	9.0
Continuous parallel, cyclic steam/ steam drive - vertical deviation	382	27.6	9.0
Additional Sensitivities:			
Continuous parallel, cyclic steam/ steam drive - high k	531	38.3	9.0
Continuous parallel, cyclic steam/ steam drive - vary steam quality	547	39.6	9.0
Continuous parallel, cyclic steam/ steam drive - vary pressure	575	41.6	9.0
Continuous parallel, cyclic steam/ steam drive - 40 acre	769	27.8	9.0

TABLE 5. RELATIVE PERMEABILITIES MODIFIED

Sw	k_{rw}	k_{row}
0.25	0.000	1.00
0.26	0.0003	0.97
0.275	0.0007	0.92
0.29	0.0013	0.87
0.31	0.0024	0.81
0.33	0.0040	0.75
0.35	0.00799	0.6899
0.40	0.01857	0.5548
0.45	0.03378	0.4334
0.55	0.07851	0.2326
0.65	0.1428	0.0904
0.80	0.277	0.00
1.00	1.00	0.00

S_L	k_{rog}	k_{rg}
0.25	0.00	1.00
0.30	0.021	0.880
0.35	0.055	0.765
0.40	0.090	0.650
0.45	0.130	0.540
0.55	0.235	0.337
0.65	0.360	0.175
0.75	0.540	0.066
0.85	0.745	0.0105
0.90	0.852	0.0016
0.91	0.874	0.00079
0.92	0.896	0.00040
0.93	0.918	0.00011
0.94	0.940	0.000007
0.944	0.9488	0.0
1.0	1.0	0.0

TABLE 6. NON-PARALLEL CONFIGURATION GRID DIMENSIONS.

GRID BLOCK NUMBER	X DIRECTION 100' GAP (FEET)	Y DIRECTION 542' GAP (FEET)
1	20	15.6
2	100	60
3	365	150
4	365	150
5	100	30
6	20	30
7	50	15.6
8		60
9		150
10		150
11		60
12		15.6
13		30
14		30
15		150
16		150
17		60
18		15.6

APPENDIX A

Injection/soak/production cycles (in days) for the simulations are as follows:

For the 2.2 years cyclic steam stimulation,

30 (initial production)
13/2/30
13/2/30
20/4/66
30/5/100
40/5/185
40/5/185

For an additional 6.8 years (9.0 total) cyclic steam, 8 cycles of

50/10/250

For an additional 7.1 years (9.3 total) cyclic steam,

60/10/250
50/10/250
50/10/250
50/10/250
50/10/50
50/10/250
50/10/250
50/10/250
50/10/250

FIGURE 1

REPRESENTATIVE GRIDS

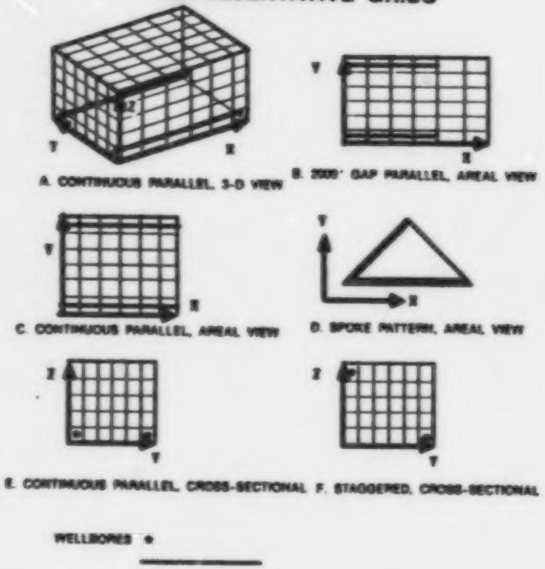

A. CONTINUOUS PARALLEL, 3-D VIEW

B. 2000' GAP PARALLEL, AREAL VIEW

C. CONTINUOUS PARALLEL, AREAL VIEW

D. SPOKE PATTERN, AREAL VIEW

E. CONTINUOUS PARALLEL, CROSS-SECTIONAL

F. STAGGERED, CROSS-SECTIONAL

FIGURE 2

CUMULATIVE OIL PRODUCTION
COMPARISON
VERTICAL VS. HORIZONTAL

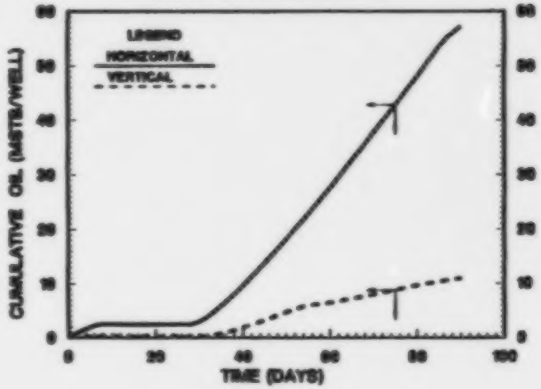

FIGURE 3

WELLBORE CONFIGURATIONS

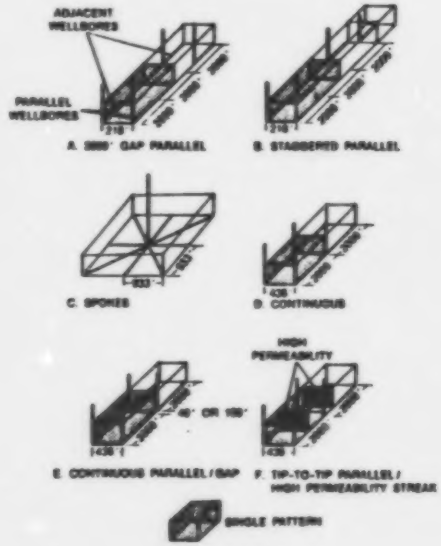
ADJACENT WELLBORES
PARALLEL WELLBORES
210'
2000'
833'
435'
40' OR 100'
HIGH PERMEABILITY

A. 2000' GAP PARALLEL

B. STAGGERED PARALLEL

C. SPOKES

D. CONTINUOUS

E. CONTINUOUS PARALLEL / GAP

F. TIP-TO-TIP PARALLEL / HIGH PERMEABILITY STREAK

SINGLE PATTERN

FIGURE 4

OIL PRODUCTION
2000' GAP PARALLEL
CYCLIC STEAM / STEAM DRIVE

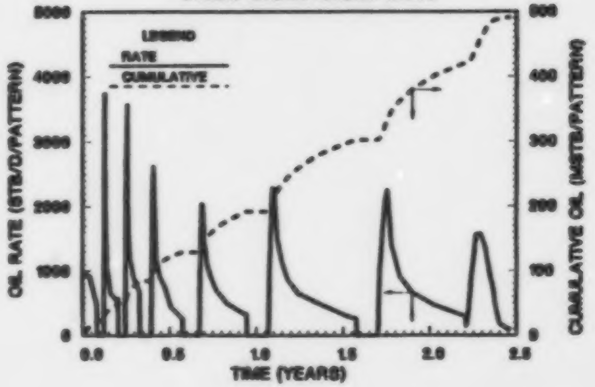

FIGURE 5

OIL PRODUCTION
2000' GAP PARALLEL
CYCLIC STEAM

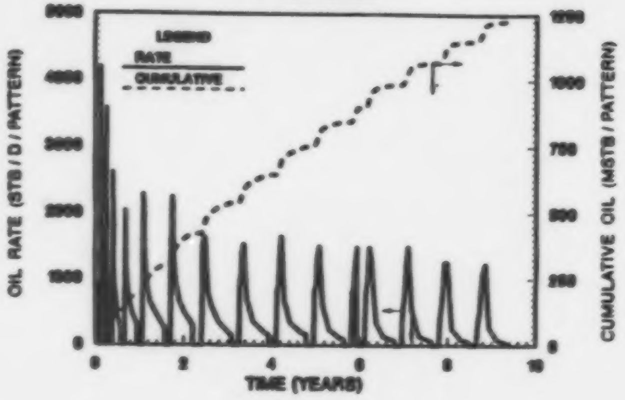

FIGURE 6

OIL VISCOSITY
2000' GAP PARALLEL
CYCLIC STEAM, 9.3 YEARS, TOP LAYER

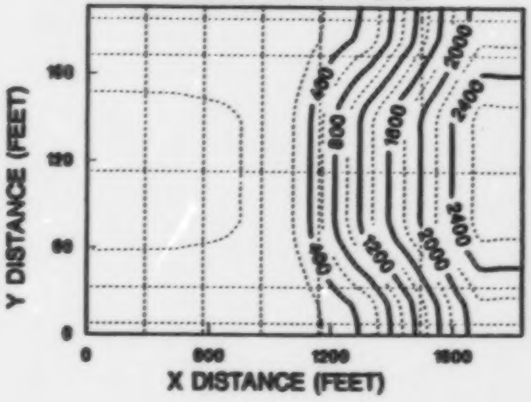

FIGURE 7

TEMPERATURE (°F)
2000' GAP PARALLEL
CYCLIC STEAM, 5.9 YEARS, BOTTOM LAYER

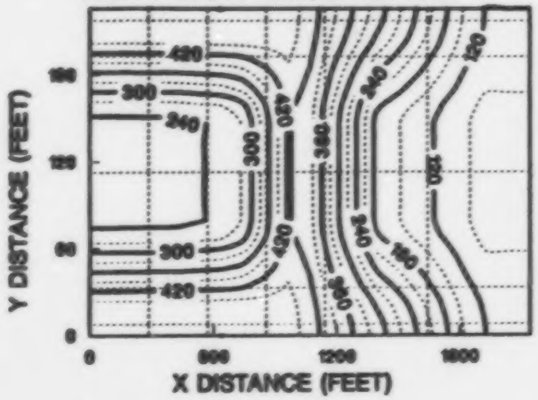

FIGURE 8

TEMPERATURE (°F)
CONTINUOUS PARALLEL
CYCLIC STEAM, 5.6 YEARS, BOTTOM LAYER

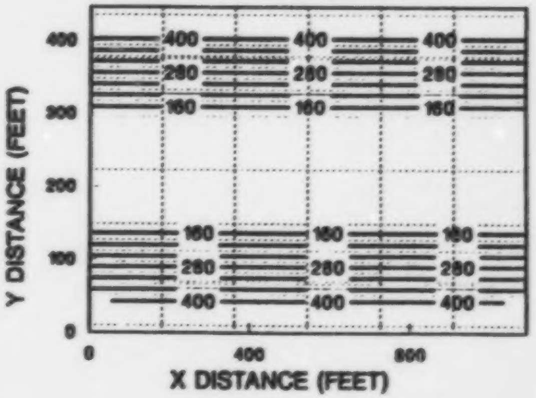

FIGURE 9

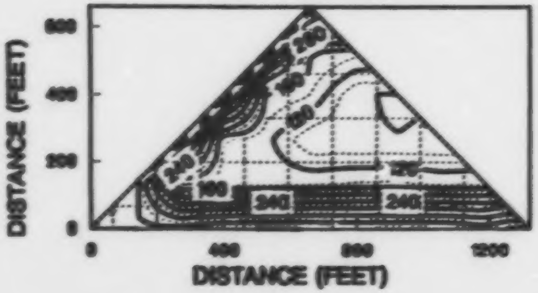
TEMPERATURE (°F)
SPOKES
TIME = 9.0 YEARS-BOTTOM LAYER

FIGURE 10

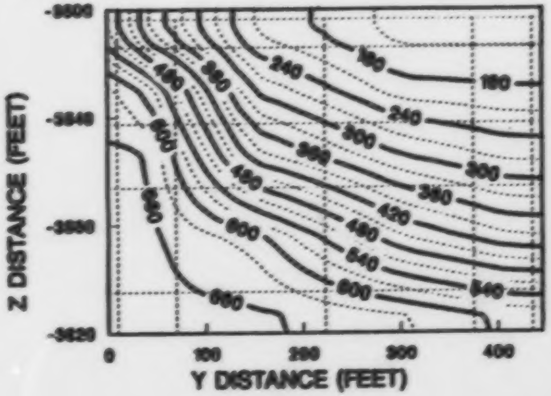
TEMPERATURE (°F)
CONTINUOUS PARALLEL
CYCLIC STEAM / STEAM DRIVE, 9.0 YEARS, YZ PLANE (X = 4)

FIGURE 11

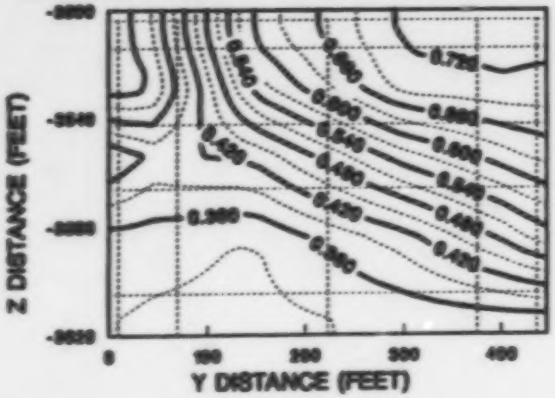
OIL SATURATION
CONTINUOUS PARALLEL / STEAM DRIVE
CYCLIC STEAM / STEAM DRIVE, 9.0 YEARS, YZ PLANE (X = 4)

FIGURE 12

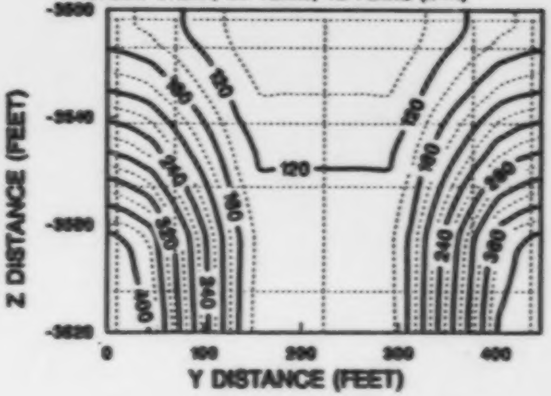
TEMPERATURE (°F)
CONTINUOUS PARALLEL
CYCLIC STEAM, 5.6 YEARS, YZ PLANE (X = 4)

FIGURE 13

TEMPERATURE (°F)
CONTINUOUS PARALLEL
CYCLIC STEAM / STEAM DRIVE, 5.8 YEARS, YZ PLANE (X = 4)

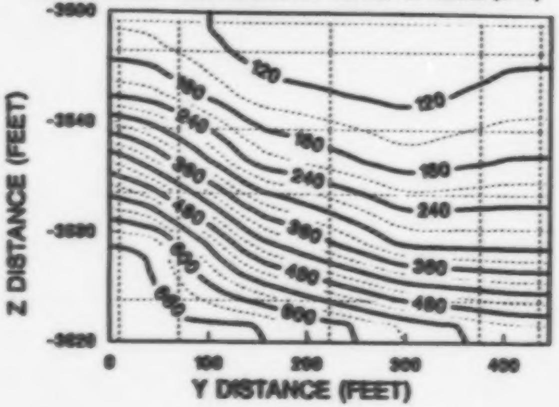

FIGURE 14

TEMPERATURE (°F)
CONTINUOUS PARALLEL, HOMOGENEOUS DESCRIPTION
CYCLIC STEAM / STEAM DRIVE, 9.0 YEARS, YZ PLANE (X = 4)

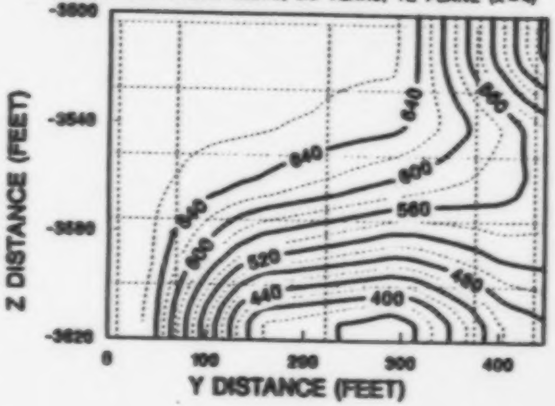

FIGURE 15

NON PARALLEL HORIZONTAL
WELL CONFIGURATION

542' TIP SEPERATION - AERIAL VIEW

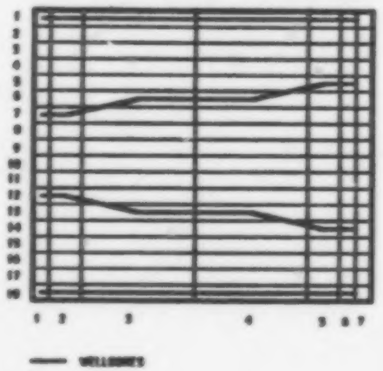
1
2
3
4
5
6
7
8
9
10
11
12
13
14
15
16
17
18
1
2
3
4
5
6
7
WELLBORES

NOTE: NOT DRAWN TO SCALE;
[illegible] LISTED IN TABLE 6

FIGURE 16

HIGH ANGLE AND VERTICAL
DEVIATION SCHEMATIC

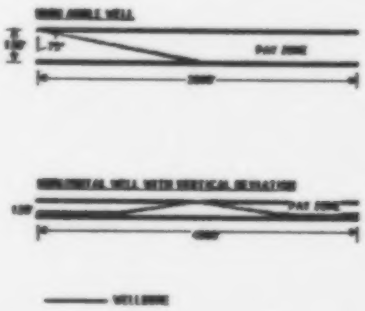
HIGH ANGLE WELL
PAY ZONE
HORIZONTAL WELL WITH VERTICAL DEVIATION
PAY ZONE
WELLBORE

FIGURE 17

TEMPERATURE (°F)
CONTINUOUS PARALLEL, 40 ACRE
CYCLIC STEAM / STEAM DRIVE, 8.0 YEARS, YZ PLANE (X = 4)

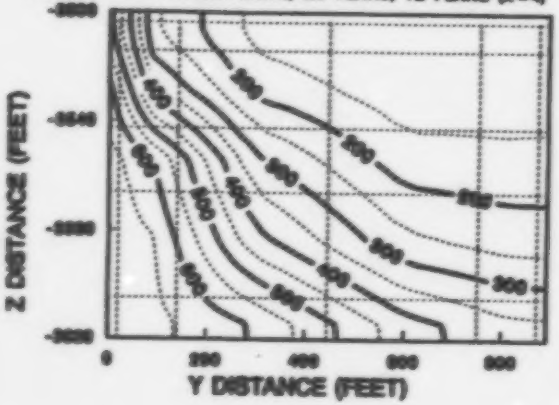

SPE
Society of Petroleum Engineers of AIME

88

SPE 14130

Evaluation of Steamflood Processes Using Horizontal Wells

by W.-S. Huang and M.A. Hight, *Texaco Inc.*
SPE Members

Copyright 1986, Society of Petroleum Engineers

This paper was presented at the SPE 1986 International Meeting on Petroleum Engineering held in Beijing, China March 17-20, 1986. The material is subject to correction by the author. Permission to copy is restricted to an abstract of not more than 300 words. Write SPE, P.O. Box 833836, Richardson, Texas 75083-3836. Telex: 730989 SPE DAL.

ABSTRACT

Steamflood operations commonly encounter problems of steam override. Close well spacing is one method used to reduce this effect. However, blind spot areas still exist in the pattern and leave substantial amounts of unrecovered oil after project termination. This study examines the effect of horizontal wells for improving steamflood conformance. A three-dimensional numerical steamflood simulator was used for the work. The study involves the use of horizontal wells both for 1) mature steamfloods to reduce steam override that has already occurred, and 2) prevention of steam override if used at the start of steamflood operations. The data used were from a typical California heavy oil reservoir.

Simulation indicates that horizontal wells can be effective for reducing or preventing steam override. For a mature 18.5-acre (7.5-ha) pattern, simulated horizontal wells increased ultimate recovery at the end of 11 years from 63.2% to 74.7% OOIP (original oil in place). When used at the start of steamflood, a pattern consisting of vertical and horizontal wells had a predicted recovery of 72.2% OOIP after only seven years.

INTRODUCTION

Application of horizontal wells for mining and oil recovery was practiced by the Russians over 40 years ago.[1] Horizontal wells have been used for exploration in Russia and production in China with limited success in the 1960's.[2] With the improvement in drilling technology, horizontal wells of 4600 feet (1400 m)[2] in Italy and at depths of up to 9500 feet (2900 m) in France have been reported.[3,4] The first modern application of a horizontal well for recovering heavy oil[5] was a 2045-foot (623-m) well drilled to a depth of 1560 feet (475 m) at Cold Lake, Alberta, Canada in 1978. Subsequently, more horizontal wells[6,7,8] for heavy oil recovery were drilled in the Athabasca tar sands at Ft. McMurray, Alberta, Canada.

References and illustrations at end of paper.

Recent interest[1,10-15] in horizontal wells has led to developments which make these wells more feasible. Drilling difficulties such as deviation control, excessive dragging, cuttings removal, and wireline tripping have been at least partially solved. Horizontal wells can be logged[3,16] and completed.[17] As technology in this area improves[18], horizontal well drilling costs decrease which makes horizontal wells more economically feasible.

The purpose of this study is to use reservoir simulation to provide some insight into the possible application of horizontal wells for steamflood. Previous simulation work,[19] indicates that horizontal wellbores can improve oil recovery based on the comparison of a conventional vertical wellbore and a horizontal wellbore model. Other analytical methods[20,21,22] were developed for estimating productivities from horizontal wells.

ADVANTAGES OF HORIZONTAL WELLS

One advantage of horizontal wells as compared to vertical wells is the increase of direct contact between wellbores and pay zones. The perforated interval per vertical well is limited to the pay zone thickness. For a horizontal well, the perforated interval could be more than ten times that of a vertical wellbore, for example, a 400-foot (122-m) horizontal well in a 30-foot (9-m) thick pay zone.

The second advantage is the ability to complete several horizontal wells from a single location and cover a large drainage area. This is essential for drilling in arctic or environmentally sensitive areas or offshore where preparation of drill sites is a major expense.

Thirdly, in the case of very thin pay zone areas, vertical drilling would be uneconomical due to insufficient wellbore openings for production. Properly placed horizontal wells can solve this problem. For certain thin formations with bottom water table, horizontal wells could defer and reduce water coning by providing a low pressure area over a long distance rather than a single point as with vertical wells. This can be achieved as long as the vertical permeability for the zone near the wellbore is uniform, and if uniform withdrawal of produced fluid over the length of the horizontal wellbore can be maintained.

The fourth advantage is the ability to inject and/or produce fluids orthogonal to those from a vertical well. This provides the potential of improving sweep efficiency of a flood and therefore recovery efficiency.

DESCRIPTION

In the steamflooding process, the low density of steam compared with other reservoir fluids causes steam to rise to the top of the formation and create the steam override phenomenon. In the upper portion of the reservoir which was swept by steam, the oil saturation can be reduced to residual oil saturation to steam. However, in the lower portion of the reservoir which was either swept by condensing hot water or bypassed by injection fluid, the oil saturation can still be rather high at the end of the steamflood. These oil pockets, sometimes called blind spots, can be reduced by either drilling infill wells to recover the oil or using limited entry at the producing wells to improve the vertical conformance of a steamflood.

This paper investigates the use of horizontal wells for a mature steamflood project and for an undeveloped reservoir ready for steamflood operation. For the case of a mature steamflood project, the steam override situation is already in existence. Therefore, the investigation centers on the location and effectiveness of the horizontal wells in producing oil and the improvement in oil recovery efficiency. For the case of an undeveloped reservoir, the proper design of a steamflood project to minimize the steam override and obtain maximum oil recovery is the objective of the study.

The scope of this study is therefore to consider some of the ways horizontal wells may be used to provide a better overall sweep efficiency in a steamflood. It is not intended as a recommendation for horizontal wells but to present some potential alternatives for possible steamflood applications. The simulation work is based on the assumption that there are no production or injection problems with horizontal wells. Problems such as sand control and inability to do selective completions still have not been completely solved with horizontal wells and could adversely affect economic considerations.

A commercially available three-dimensional numerical simulator developed for thermal recovery operations was used for the work.[23] The model accounts for 3-phase flow described by the Darcy's flow equation and includes gravity, viscous and capillary forces. Heat transfer is modelled by conduction and convection. Relative permeability curves are temperature dependent. The model is capable of simulating well completions in any direction (vertical, horizontal, inclined or branched).

Reservoir properties used in the study are typical of a California heavy oil reservoir with unconsolidated sand. A dead oil with an API gravity of 13° ($0.98\ g/cm^3$) was used in the simulation.

MATURE STEAMFLOOD RESERVOIRS

Typical steamfloods operate from 2.5-acre (1-ha) to 20-acre (8-ha) patterns. For large injection patterns, infill wells are often used to improve sweep efficiency. For small injection patterns, because of high well densities, the sweep efficiency is usually higher than that of the large patterns. Even with high well densities, blind spots still could be formed. However, there is more target oil in the blind spot of a larger pattern.

Base Case Simulation

An 18.5-acre (7.5-ha) inverted 9-spot pattern (Figure 1a) was used as a basis for this simulation study. Pertinent information used in the study is shown in Table 1. The 125-foot (38-m) formation is divided into five equal layers. All wells were completed in the lower 60% of the oil sand. Steam (at 65% quality) was injected into the central well at a constant rate of 2400 BPD (381 m^3/d) cold water equivalent (Run 1). The project was terminated when the fuel required to generate steam was equivalent to the oil produced from the pattern or instantaneous steam-oil ratio (SOR) of 15. This SOR of 15 was considered to be the economic limit for runs made in this study. A maximum lifting capacity of 1000 BPD (159 m^3/d) was assumed for each producing well. The resulting oil recovery at the end of the project life (15 years) was 64.7% of the OOIP. The predicted oil saturation profile indicates a good steam sweep throughout the upper three layers to S_o less than 0.2 (the upper 60% of the oil zone) but the lower two layers (Figure 2) shows that steam has bypassed most of this area except near the injection well.

Addition of Infill Wells

An infill well was added to the simulation grid midway between center and corner wells (Figure 1b). The well was completed in the lower one-third of the zone only and infill production began after three years of steam injection and continued to the end of the project (Run 2).

Ultimate recovery for Run 2 was 63.2% OOIP after 11 years. Note that the advantage of infill wells is to recover oil sooner. For the 9-spot pattern, the oil recovery at 11 years would have been only 57% at this time. Because of the presence of infill wells, oil production which would otherwise arrive at corner and side wells will be reduced. As a result, the 13-spot pattern would reach economic limit much sooner than a 9-spot pattern unless other operational changes are made.

The oil saturation profile for Run 2 (Figure 3) is about the same as for Run 1 but this stage of the flood is reached four years sooner than in Run 1. There is still a high oil saturation region in the area between the corner and side wells.

Horizontal Well Configurations

Horizontal wells were located in the bottom layer of each simulation grid. Horizontal well producers were assumed to be perforated equally along their entire length of 374 feet (114 m) between side wells and corner wells (Figure 1c).

Run 3 is a repeat of Run 2 except horizontal well production began after six years. The production response on Run 3 is compared with that of Runs 1 and 2 on Figure 4. Please note that the behavior of horizontal well production is similar to that of the infill well production in that both have a rapid increase in production rate and then decline sharply. The peak production rates after three years and six years correspond to the infill production and horizontal well production, respectively. The infill well's production kick was due to drilling into the oil bank, whereas, the horizontal well's production kick was from the increase of direct contact between production wellbores and pay zone in the blind spot area. The first year of horizontal well production affected a 250% increase in the annual oil production rate for the pattern.

Cumulative oil production for Run 3 is plotted in Figure 5 along with the base case, Run 1. Due to the accelerated production from horizontal wells, the life of the project can be reduced to nine years with an ultimate recovery of 65.9% OOIP.

Figure 6 shows the Run 3 oil saturation profiles between center and corner wells at the end of nine years. Comparing this result with those in Figure 3, it is apparent that horizontal wells can effectively reduce the oil saturation in the blind spot from 60% to 30%.

Since one of the advantages of horizontal wells is the ability to handle a large quantity of fluids, an additional study was made to further improve the operation described in Run 3. Run 4 is a repeat of Run 3 except the infill wells were converted to steam injection at a rate of 300 BPD (48 m^3/d) per well and the central injector was converted to hot water injection at a rate of 4800 BPD (763 m^3/d) after six years to coincide with the start of horizontal well production. The simulated horizontal well lifting capacity was 2400 BPD (382 m^3/d). The change of steam injection point, the high water injection rate, and the high production capacity all contribute to improvement in the displacement and sweep efficiencies. As can be seen in Figure 5, the recovery efficiency for Run 4 can reach 74.7% OOIP at 11 years. Figure 7 shows the oil saturation profile of Run 4 at the end of 11 years. The average oil saturation in Layer 5 was reduced to about 25% as compared to 30% in Run 3.

Summary of Mature Steamflood

Table 2 gives a brief summary of Runs 1 through 4. Although Run 1 could recover 64.7% oil in place, the project life is long. Run 2 provides earlier oil production and a shorter project life. However, blind spots still exist. With horizontal wells in place, the blind spots can be eliminated and the ultimate oil recovery can be improved. A comparison of Run 3 with Runs 1 and 2 shows that horizontal wells for a mature 18.5-acre (7.5-ha) pattern would:

1. improve oil recovery to 65.9% OOIP,
2. shorten project life by 2 to 6 years, and
3. reduce oil saturation in the blind spot from 60% to 30%.

The cumulative oil production predicted by Runs 1 to 4 is compared in Figure 8 which shows the incremental oil produced compared to the 9-spot (Run 1). After infill wells are added (Run 2), the cumulative oil production shows a large increase over Run 1 for the first two years. After two years, the oil production rate for Run 2 decreases to a value less than for Run 1 (Figure 4), so the difference in cumulative oil production begins to decrease. If horizontal wells are added (Run 3), there is an additional peak in the oil production rate and the incremental cumulative oil production over the 9-spot is even higher. With the higher injection rates used in Run 4, the horizontal well production rate remains higher longer and the incremental oil production over Run 1 ranges from 664 MSTB (thousand stock-tank barrels),(105,500 m^3) to 501 MSTB (79,650 m^3) from the first year of horizontal well production to the end of the run.

UNDEVELOPED RESERVOIRS

The mature steamflood study has indicated that horizontal wells can be beneficial in producing target oil from blind spots. However, the economics may not be favorable unless target areas are large. An alternative approach is the use of horizontal wells at the start of a steamflood to minimize blind spot formation, rather than correct it, once it has developed. Patterns of parallel horizontal wells as well as combinations of vertical and horizontal wells were simulated. Simulated oil zone thickness was 125 feet (38 m) as in the mature steamflood studies.

Parallel Horizontal Wells

Several patterns composed entirely of horizontal wells were studied. In all patterns, the horizontal injectors were placed near the top of the 125-foot (38-m) thick oil zone and the horizontal producers were placed near the bottom. Simulated horizontal wells ranged in length from 450 feet (137 m) to 680 feet (207 m).

Results for all configurations indicated an even sweep of the oil zone between the parallel wells with blind spots at the ends. Since the length of the wells determines the degree to which end effects will lower recovery, results are dependent on horizontal well lengths and the end-to-end distance between wells. Since there is not an adequate performance history of horizontal wells in unconsolidated sands, there is no maximum practical length known at this time. For the patterns studied, wells were spaced far enough apart so that the drilling costs per acre were approximately the same as for the 18.5-acre (7.5-ha) 13-spot pattern. With this assumption, ultimate recoveries were less than 70% of OOIP for the cases studied. For shorter horizontal wells, the recovery became less because of shorter producing intervals. The optimization of horizontal well's length, spacing, and end-to-end distance would warrant an in-depth investigation for any given reservoir. Since there are more unknown factors in the simulation of parallel horizontal wells there are no further comparisons made with the other patterns investigated at this time.

Vertical and Horizontal Well Combinations

Many vertical and horizontal well combinations were investigated and three promising configurations were identified. Vertical wells were completed in the lower three layers of the simulation grid only and all horizontal wells were completed in the bottom (fifth) layer of the simulation grid. Injection rates were varied with the configurations since the injector to producer ratios were different. Injection was increased as needed to improve results but with a maximum reservoir pressure constraint of 1200 psia (8268 kPa) placed on all runs. This constraint was made in the program to avoid obtaining excessive pressures in a reservoir at a depth of 2400 ft (732 m). A maximum reservoir pressure of 600 psia (4134 kPa) had been observed in the calculation with the optimum injection rates. Injection rates ranged from 0.9 BPD/ac-ft (1.16 m^3/d-ha-m) to 1.7 BPD/ac-ft (2.19 m^3/d-ha-m).

The following configurations (shown in Figures 9 to 11) were studied:

1. Configuration C-1 (Figure 9)

   This configuration has three vertical injection wells and two horizontal producers per pattern. Each pattern is defined by the dashed lines and the shaded area is a symmetrical simulation unit. The advantage of this pattern configuration is the ability of the horizontal wells to draw a large amount of fluid to the bottom of the reservoir and to effectively reduce the steam override phenomenon.

   This run was carried out with an 18.5-acre (7.5-ha) pattern and an injection rate of 3900 BPD (620 m^3/d) or 1.7 BPD/ac-ft (2.19 m^3/d-ha-m). Ultimate recovery was 72.2% OOIP at the end of a 7-year project life and 1.4 pore volumes of steam injection.

   At the end of the project life, the average oil saturation was 15% in the upper 60% of the oil zone and 26% in the lower 40%. The areal and vertical conformance were good and only minimum steam override had occurred.

2. Configuration C-2 (Figure 10)

   Horizontal wells shared by two patterns are placed in the lower portion of the pattern between vertical injectors. One eighth of a pattern was simulated. The number of effective wells per pattern for this configuration is two vertical injectors and two horizontal producers. Injection is in the center and corners of an 18.5-acre (7.5-ha) pattern with a total steam injection rate of 3400 BPD (540 m^3/d) or 1.5 BPD/ac-ft (1.93 m^3/d-ha-m). Ultimate recovery was 73.1% of OOIP after a project life of 14 years. The total steam injected was 1.8 pore volumes. After 14 years a small blind spot area remained along the diagonal midway between the injection wells. Oil saturations in this area range from 35% to 40% in the fifth layer.

3. Configuration C-3 (Figure 11)

   Horizontal wells are placed along the outside edges and diagonally through the center of a square pattern. One fourth of a pattern was simulated. Two vertical injection wells are located on each side of the diagonal horizontal well. There are two vertical injectors and three horizontal producers per pattern in this configuration. To keep the drilling cost per acre similar for all configurations, the pattern size was increased to 26 acres (10.5 ha) for this configuration. Injection rate is 2800 BPD (445 m^3/d) or 0.9 BPD/ac-ft (1.16 m^3/d-ha-m) and the resulting recovery after 14 years, and 1.4 pore volumes of steam injection is 72.9% OOIP. Some steam override occurred in this pattern, leaving a small blind spot area at the ends of the central horizontal well where the distance to the injector is greater. Oil saturations in the blind spot are 50% in Layer 5, but this area only represents 8% of the total pattern area and less than 2% of the pattern volume.

COMPARISON WITH MATURE STEAMFLOOD SIMULATIONS

Cases C-1, C-2, and C-3 were compared with simulations from the mature steamflood study. The best result in the mature steamflood cases (in terms of oil recovery and improvement in vertical steamflood conformance) was obtained with horizontal wells along the pattern boundaries between the corner and side wells (Run 4). This configuration, although effective, would be an expensive alternative. In order to improve the economics, the Run 4 pattern size was increased to 32 acres (13 ha). This run is not meant to recommend or optimize a 32-acre (13-ha) pattern steamflood, rather to form a more equal cost base for comparison. The injection rate was increased to 3000 BPD (477 m^3/d) in the central injector. This was the highest rate possible using the 1200 psia (8268 kPa) limitation with this pattern size. Horizontal wells were placed as shown in Figure 12, (Run 5). The horizontal well length was 787 feet (240 m).

As in the mature steamflood study, the horizontal wells were added after six years of steamflood operation and infill wells were converted to steam injection at this time at a rate of 500 BPD (80 m^3/d) per well. A comparison of oil recovery history from these horizontal well patterns and the inverted 13-spot pattern is shown in Figure 13. The 9-spot pattern has the poorest overall performance. Cases C-2 and C-3 showed 73% OOIP recovery at 14 years. Run 5 showed a poor performance the first eight years due to the localized steam injection in the center of a large pattern but the ultimate recovery was 70.0% of OOIP. Configuration C-1 had a high injection rate and high recovery of 72.2% OOIP and a project life of only seven years.

A conversion to hot water injection after seven years for configuration C-1 was made and the results indicate that the ultimate oil recovery could reach 74.7% at ten years and average oil saturation in the lower 40% of the oil zone could be reduced to 21%. The predicted oil recovery curves for C-1 are contrasted with those of Run 4 in Figure 14. This comparison indicates the advantage of using horizontal wells at the start of a steamflood project because of the earlier response of high oil production rates for Run C-1.

WELL DENSITY AND PERFORATION

One of the advantages of horizontal wells is their longer completion intervals. The well density and total feet of completion per acre are listed in Table 3. For the mature steamflood cases, the addition of infill wells to the 9-spot pattern (comparison of Run 2 with Run 1) doubles the well density and increases the total feet of completion by 67%. For Runs 3 and 4 the addition of infill and horizontal wells triples the well density of the 9-spot pattern but affects a 567% increase in the total feet of completion. Run 5 with its larger pattern size and fewer horizontal wells has a well density in between that of the 9- and 13-spot, but still has several times more feet of perforation than either the 9- or 13-spot. For the undeveloped reservoir (configurations C-1 to C-3), the well densities are similar to that of the 9-spot pattern but the total completion is increased by 250 to 400%.

COMPARISON OF RECOVERY EFFICIENCIES

Table 4 gives a comparison of the results from the 9- and 13-spot vertical well patterns with the combination vertical and horizontal well patterns studied.

Run 5 had the lowest amount of steam injected (1.1 V_p) and the highest flood efficiency (0.372 BO/Bstm). However, the oil recovery (70% OOIP) was not as high as the other vertical and horizontal well combination runs. The larger pattern size of Run 5 with the single injection point resulted in the lowest cumulative production of the runs for the first seven years (Figure 13) and the longest project life (15 years).

The highest oil recovery (73.1% OOIP) at the end of the project life is shown by Run C-2. However, this pattern required the injection of 1.8 pore volumes of steam and reduced the flood efficiency to 0.242 BO/Bstm. Run C-3 also shows a high oil recovery and the lowest development cost per barrel of oil recovered. However, it has a project life of 14 years.

Run C-1 has a good recovery (72.2% OOIP), the shortest project life (seven years) and a high flood efficiency of 0.304 BO/Bstm. The high recovery coupled with the short project life would result in a fast payout for the horizontal wells and provide a good return on investment. Configuration C-1, therefore, is the best of the configurations studied, when economics, oil recovery and steamflood conformance are all considered.

DISCUSSION OF RESULTS

These simulation results indicate that horizontal wells may well be a feasible alternative for improving vertical steamflood conformance. These results should, however, be kept in perspective. The validity of these results is highly dependent on the ability of horizontal wells to perform well in field service. The simulation work is based on a single element of symmetry for a homogeneous reservoir and would not apply to dipping reservoirs or those with significant variations in thickness. Economic comparisons are not shown here because drilling costs for horizontal wells vary greatly from one environment to another and drilling costs are rapidly changing as directional drilling technology improves.

CONCLUSIONS

1. Simulation results indicate that horizontal wells are effective in recovering oil in blind spot areas in a mature steamflood project. Horizontal wells can recover more oil sooner and thus shorten project lives. For example, for the 18.5 acre (7.5-ha) inverted 13-spot pattern studied, if horizontal wells were used six years after the start of steamflood, the oil recovery efficiency can be improved from 63.2% to 65.9% OOIP and the project life can be shortened from 11 to 9 years. Oil saturation in the blind spot can be reduced from 60% to 30%.

2. As significant new technology is available in lifting large amounts of hot fluids from horizontal wells, the use of horizontal wells could allow the reservoir to be operated at higher injection and production throughputs. For example, with the existence of the horizontal wells in the 18.5-acre (7.5-ha) pattern, higher injection rates could be implemented. As a result, the oil recovery efficiency can further be improved from 65.9% to 74.7% OOIP after 11 years.

3. Incorporating horizontal wells at the start of a steamflood project appears to be a feasible approach for alleviating steam override. Several combined vertical and horizontal well configurations have been identified. Through the use of horizontal wells, an 18.5-acre (7.5-ha) pattern in this study can achieve 72.2% OOIP recovery efficiency in seven years. The residual oil saturation in the blind spot can be reduced to 26%. If water injection is incorporated, the recovery efficiency could reach 75% OOIP in 11 years.

4. The well density for the case of combined vertical and horizontal wells (Run C-1) is about 50% of that of the inverted 13-spot with horizontal wells (Run 3). Although the ultimate recovery for both cases are similar, Run C-1 still has a greater advantage in terms of economics, response time and conformance improvement.

5. Computer simulation can be effective for comparing the relative merits of different horizontal and vertical well combinations and operational schemes.

ACKNOWLEDGMENTS

The authors wish to thank the management of Texaco Inc., for permission to publish this paper.

REFERENCES

1. Butler, R.M.: "The Potential of Horizontal Wells", presented at the 5th Annual AOSTRA, "Advances in Petroleum Recovery and Upgrading Technology" Conference , Calgary , Alberta, Canada, June 14 and 15, 1984.

2. "Elf Cites 5 Advantages of Horizontal Drilling", Ocean Industry, V.10, No.6, pp 35-36, June, 1984.

3. Giger, F.M. and Jourdan, A.P.; "The Four Horizontal Wells Producing Oil in Western Europe", presented at the 5th Annual AOSTRA, "Advances in Petroleum Recovery and Upgrading Technology" Conference, Calgary, Alberta, Canada, June 14 and 15, 1984.

4. Jourdan, A.P. and Baron, G.; "Horizontal Well Proves Productivity Advantages", Petroleum Engineer International, October, 1984, pp 23-25.

5. Rezaire, G. E. and Markiw, I. A.; "Esso Resources Horizontal Hole Project at Cold Lake", paper presented at the 30th Annual Technical Meeting of the Petroleum Society of CIM, Banff, Alberta, Canada, May 8-11, 1979.

6. Loxam, D. C.; "Texaco Canada Completes Unique Horizontal Drilling Program", Petroleum Engineer International, September, 1982, pp 40-52.

7. Pugh, G. E.; "A Three Horizontal-Hole Drilling Pattern", The Future of Heavy Crude and Tar Sands, 2nd International Conference, 1982, pp 894-902.

8. Pugh,G.E.; "Drilling of Three Horizontal Hole Pattern, Ft.McMurray,Alberta",presented at the 33rd Annual Technical Meeting of the Petroleum Society of CIM, Calgary,Canada,June 6-9, 1982.

9. Jourdan, A. and Baron, G.; "Horizontal Drilling - Three Field Tests", NOROIL, vol. 10, No. 8, pp 163-167, August 1982.

10. Rosio, J.; "A Fourth Well Successfully Completed by Elf Aquitaine, What is the Next Step?", Petrole Informations No. 1606, pp 4-5, 7, December 20, 1984.

11. Jourdan, A., Reiss, L. H., Baron, G. A. and Wittrich, C.; "One, Two and Three Horizontal Wells in France and Italy", Petrole Informations, No. 1567, pp 17-23, April 15, 1982.

12. "Horizontal Well Boosts Elf's Adriatic Output", Offshore Engineer, pp 73-74, April 1983.

13. Legros, E.; "A Technical Success for Elf Aquitaine: Horizontal Drilling", Ind. Petrol Gaz-Chim No. 554, pp 43-45, April, 1983.

14. Jourdan, A., Reiss, L. H., Baron, G. A., Giger, F., and Wittrisch, C.; "Review of Horizontal Drilling Progress", Petrole Informations No. 1585, pp 27-33, March 25, 1983.

15. Jourdan, A. and Baron, G. A.; "Elf Drills 1000+ Ft. Horizontally", Petroleum Engineer International, pp 51-58, September, 1981.

16. Bleakley, W. B.; "IFP and Elf-Aquitaine Solve Horizontal Well Logging Problem", Petroleum Engineer International, pp 22-24, November 15, 1983.

17. Reiss, L. H. , Jourdan, A. , Giger, F. , Wittrisch, C., and Baron, G.; "Reservoir Development Through Horizontal Drilling", Offshore Northern Seas Advance Project Conference, Stavanger, Norway, November 15-17, 1983.

18. Reiss, L. H., Jourdan, A.P.L., Giger, F. M. and Armessen, P. A.; "Offshore and Onshore European Horizontal Wells", OTC 4791 presented at the 16th Annual OTC in Houston, Texas, May 7-9, 1984.

19. Rial, R. M.; "3D Thermal Simulation Using a Horizontal Wellbore for Steamflooding", SPE 13076, presented at the 59th Annual Technical Conference and Exhibition, Houston, Texas, September 16-19, 1984.

20. Giger, F. M., Reiss, L. H. and Jourdan, A. P.; "The Reservoir Engineering Aspects of Horizontal Drilling", SPE 13024, presented at the 59th Annual Technical Conference and Exhibition, Houston, Texas, September 16-19, 1984.

21. Giger, F. M.; "Horizontal Wells Production Techniques in Heterogeneous Reservoirs", SPE 13710, presented at SPE 1985 Middle East Oil Technical Conference and Exhibition, Bahrain, March 11-14, 1985.

22. Butler, R. M. and Stephens, D. J.; "The Gravity Drainage of Steam-heated Heavy Oil to Parallel Horizontal Wells", paper presented at the 31st Annual Technical Meeting of the Petroleum Society of CIM, Calgary, Canada, May 25-28, 1980.

23. "Combustion and Steamflood Model - THERM", Scientific Software Intercomp, October, 1984.

TABLE 1

RESERVOIR AND FLUID PROPERTIES - HORIZONTAL WELL SIMULATION

Porosity, fraction		0.39
Initial Fluid Saturations, Fraction:	Oil	0.589
	Water	0.411
	Gas	0
Initial Reservoir Temperature, °F (°C)		100 (37.7)
Initial Reservoir Pressure, psi (kPa)		50 (345)
Permeability, md:	Horizontal (μm^2)	3000 (3)
	Vertical (μm^2)	900 (0.9)
Reservoir Thermal Conductivity, Btu/day-ft-°F (W/m-°C)		31.2 (2.25)
Reservoir Heat Capacity, Btu/ft^3-°F (kJ/m^3-°C)		37.0 (2480)
Cap and Base Rock Thermal Conductivity, Btu/day-ft-°F (W/m-°C)		24.0 (1.73)
Cap and Base Rock Heat Capacity, Btu/ft^3-°F (kJ/m^3-°C)		46.0 (3085)

Oil Viscosity,

cp @ °F	Pa-s @ °C
1230 @ 100	1.23 @ 37.7
10 @ 300	0.01 @ 148.9
3.99 @ 400	0.00399 @ 204.4

Quality of Injected Steam, fraction (at sand face) 0.85

Residual Oil Saturation, Fraction
to water: 0.25
to steam: 0.15

TABLE 2

MATURE STEAMFLOOD STUDIES - SUMMARY OF SIMULATION RUNS

RUN	CONFIGURATION	RECOVERY, % of OOIP	PROJECT LIFE YEARS	CUM.OIL PROD. MBbl
1	Inverted 9-spot	64.7	15	2616
2	Inverted 13-spot (infill well prod. only)	63.2	11	2554
3	Inverted 13-spot with Horizontal Wells (infill well prod. only)	65.9	9	2663
4	Inverted 13-spot with Horizontal Wells (infill well prod./inj.)	74.7	11	3021

TABLE 3

SIMULATION OF HORIZONTAL WELL PERFORMANCE WELL DENSITIES AND COMPLETION INTERVALS OF CONFIGURATIONS STUDIED

Run, Description	Well Density Wells/Acre (Wells/ha)	Total Completion Feet/Acre(m/ha)
Run 1, Inverted 9-spot	0.22(0.54)	16.2 (12.2)
Run 2, Inverted 13-spot	0.43(1.06)	27.0 (20.4)
Runs 3 and 4 Inverted 13-spot + Horizontal Wells	0.65(1.60)	108.0 (82.0)
Run 5, Inverted 13-spot + Horizontal Wells	0.31(0.77)	65.3 (49.3)
Configuration C-1	0.27(0.67)	80.8 (61.0)
Configuration C-2	0.22(0.54)	56.8 (42.9)
Configuration C-3	0.20(0.50)	75.6 (57.0)

TABLE 4

SIMULATION OF HORIZONTAL WELL PERFORMANCE COMPARISON OF STEAMFLOOD CONDITIONS AND RECOVERY EFFICIENCIES

Run, Description	Steam Injection Rate/Pattern BPD/ac-ft(m^3/d-ha-m)	Pat.Size, Acres(ha)	Oil Recovery (at end of Proj.Life, % of OOIP)	Proj. Life Years	P.V.Inj. Fraction	BO/Bstm
Run 1, Inverted 9-spot	1.0 (1.29)	18.5(7.5)	64.7	15	1.8	0.200
Run 2, Inverted 13-spot	1.0 (1.29)	18.5(7.5)	63.2	11	1.3	0.286
Run 5, Inverted 13-spot + Horizontal Wells	0.8(1.03)0-6yr. 0.5(0.64)7-15yr.	32 (13)	70.0	15	1.1	0.372
Configuration C-1	1.7 (2.19)	18.5(7.5)	72.2	7	1.4	0.304
Configuration C-2	1.5 (1.93)	18.5(7.5)	73.1	14	1.8	0.242
Configuration C-3	0.9 (1.16)	26.0(10.5)	72.9	14	1.4	0.300

a) 18.6 ACRE (7.5ha) INVERTED 9-SPOT PATTERN - RUN 1

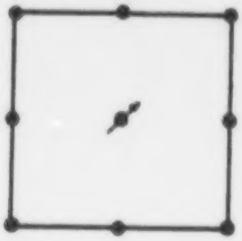

b) 18.6 ACRE (7.5ha) INVERTED 13-SPOT PATTERN - RUN 2

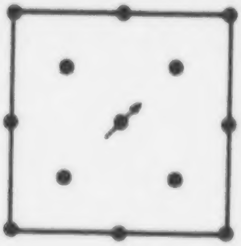

c) 18.6 ACRE (7.5ha) INVERTED 13-SPOT PATTERN WITH HORIZONTAL WELLS - RUNS 3,4

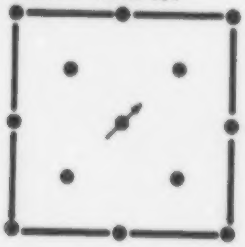

Fig. 1—Well configurations used for mature steamflood study.

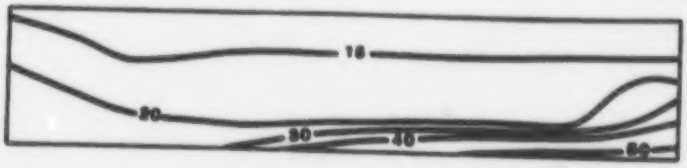

Fig. 2—Run 1 oil saturation profile at end of project life (15 years).

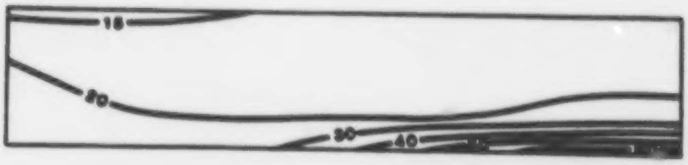

Fig. 3—Run 2 oil saturation profile at end of project life (11 years).

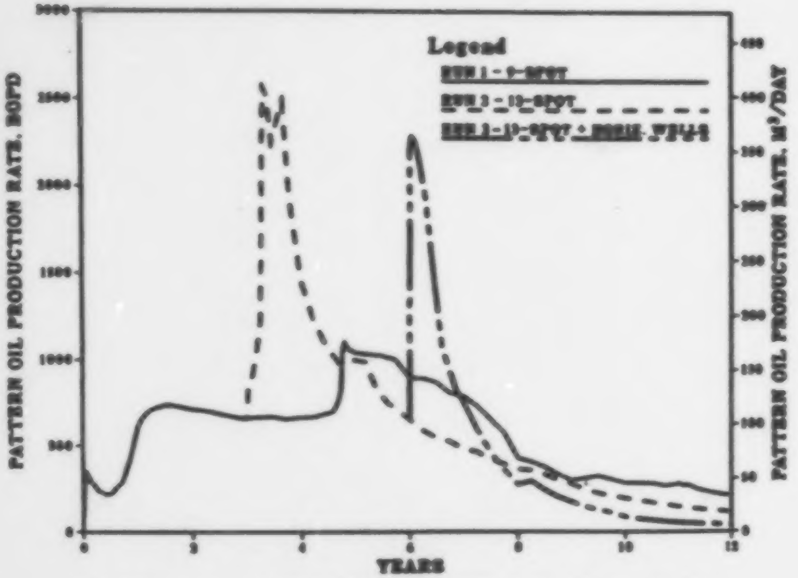

Fig. 4—Comparison of production rates for 18.5-acre (7.5-ha) pattern with and without infill and horizontal wells.

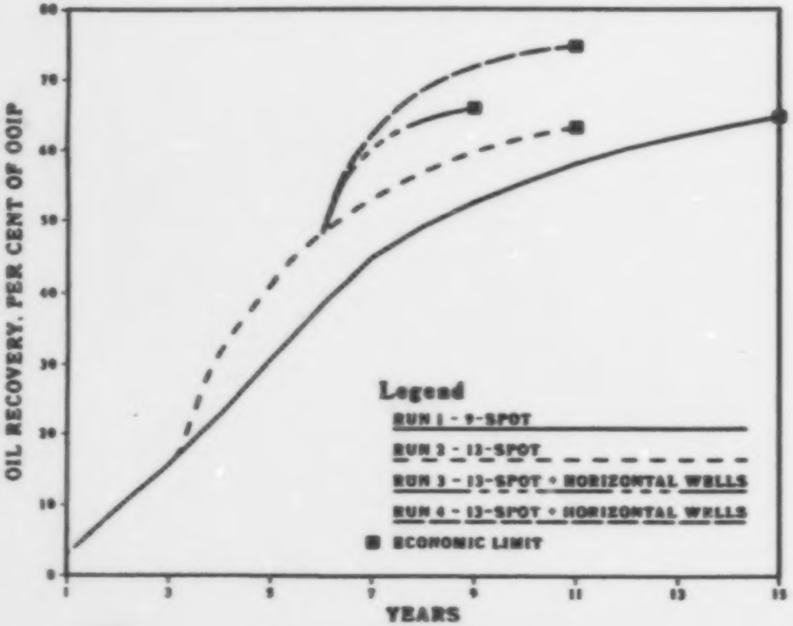

Fig. 5—Comparison of horizontal well oil recoveries.

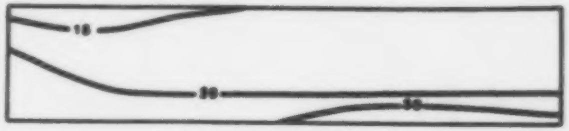

CENTER TO CORNER WELL X-SECTION

Fig. 6—Run 3 oil saturation profile at end of project life (9 years).

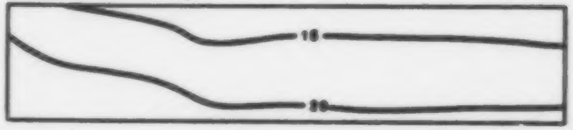

CENTER TO CORNER WELL X-SECTION

Fig. 7—Run 4 oil saturation profile at end of project life (11 years).

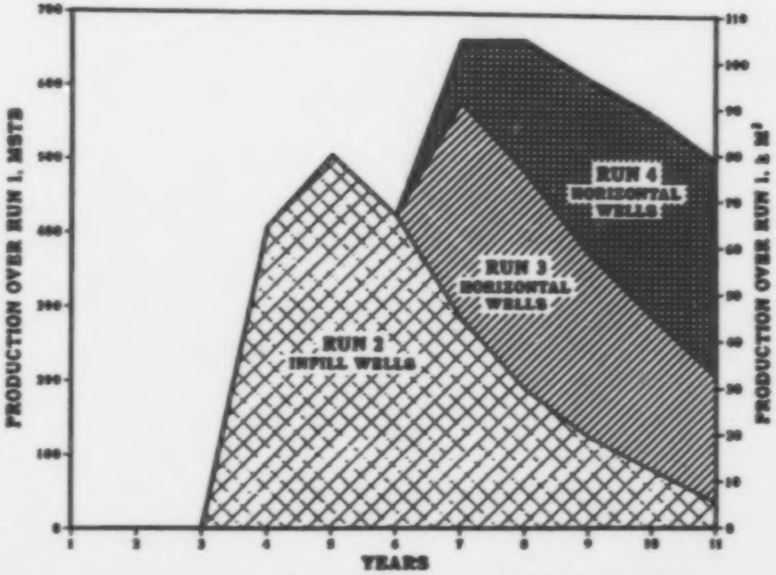

Fig. 8—Additional cumulative oil production over that predicted for an 18.5-acre (7.5-ha) nine-spot pattern.

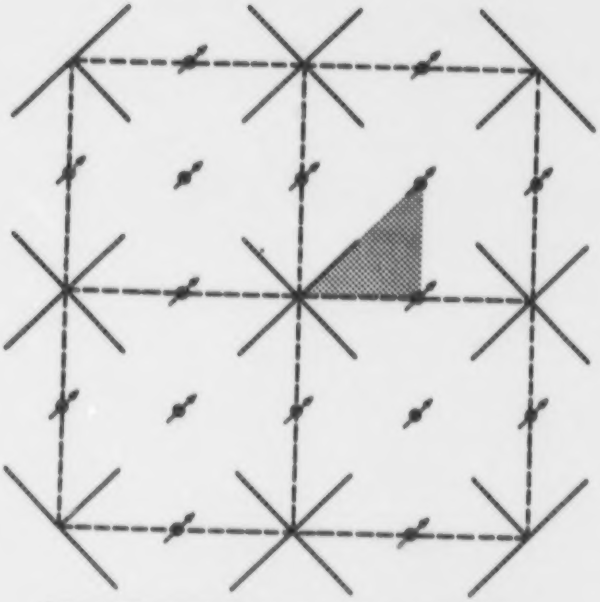

SHADED AREA REPRESENTS 1/8 OF AN 18.5 ACRE (7.5ha) PATTERN

Fig. 9—Combination of vertical and horizontal well patterns: configuration C-1.

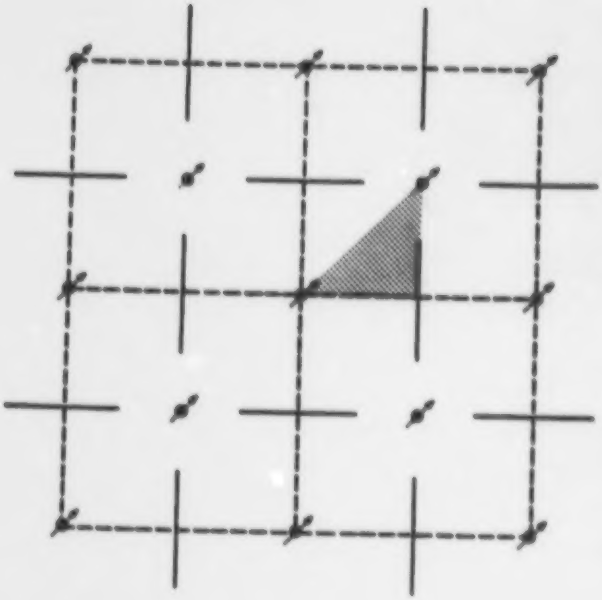

SHADED AREA REPRESENTS 1/8 OF AN 18.5 ACRE (7.5ha) PATTERN

Fig. 10—Combination of vertical and horizontal well patterns: configuration C-2.

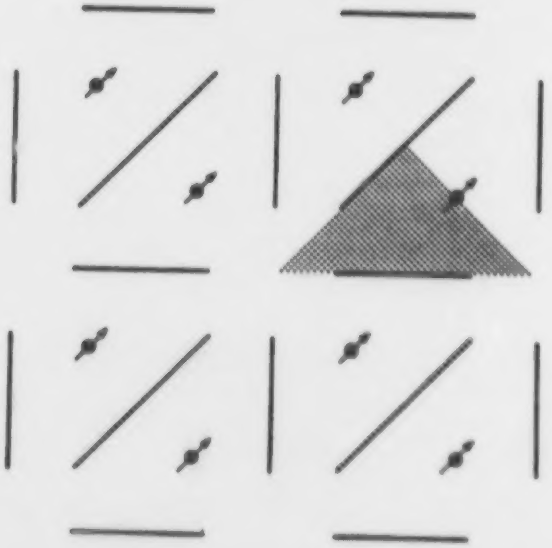

SHADED AREA REPRESENTS 1/4 OF A 26 ACRE (10.5ha) PATTERN

Fig. 11—Combination of vertical and horizontal well patterns: configuration C-3.

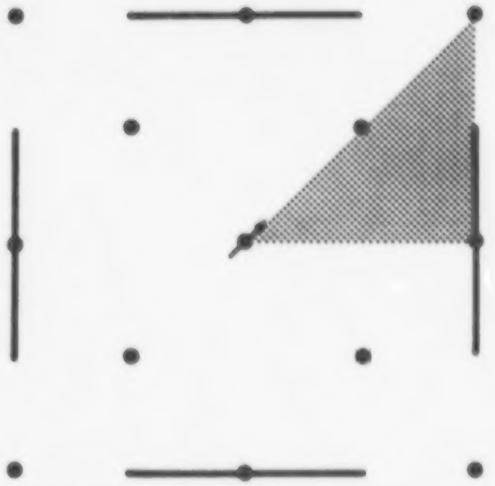

Fig. 12—Combined vertical and horizontal well patterns: Run 5.

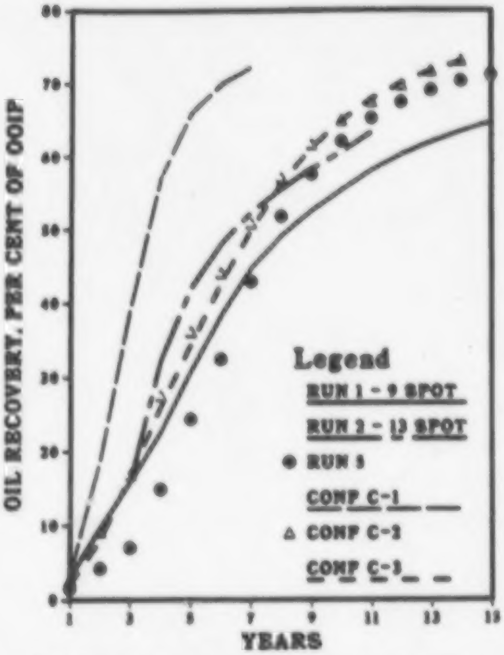

Fig. 13—Simulation of horizontal well performance: comparison of oil recoveries.

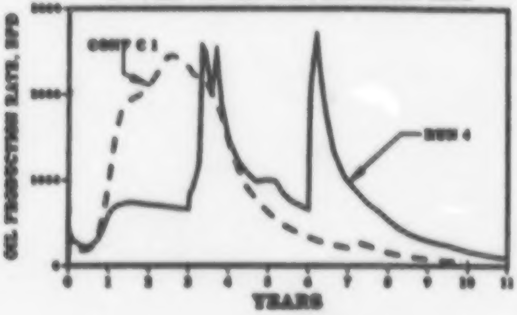

A. TOTAL PATTERN OIL PRODUCTION RATE

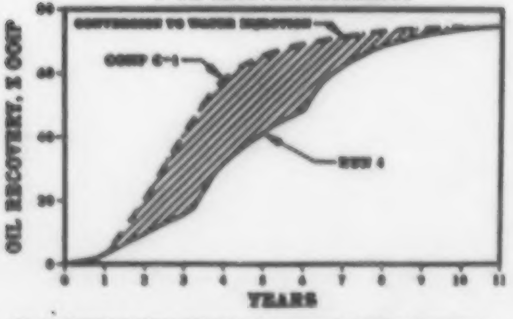

B. OIL RECOVERY EFFICIENCY

Fig. 14—Comparison of horizontal well use for mature and undeveloped reservoirs.

Alberta
OIL SANDS TECHNOLOGY &
RESEARCH AUTHORITY
Library and Information Services

010885

SPE
Society of Petroleum Engineers

(89)

SPE 15088

Numerical Simulation of the HASDrive Process

by L. Hsueh, *Chevron Oil Field Research Co.*

SPE Member

Copyright 1986, Society of Petroleum Engineers

This paper was prepared for presentation at the 56th California Regional Meeting of the Society of Petroleum Engineers held in Oakland, CA, April 2–4, 1986.

This paper was selected for presentation by an SPE Program Committee following review of information contained in an abstract submitted by the author(s). Contents of the paper, as presented, have not been reviewed by the Society of Petroleum Engineers and are subject to correction by the author(s). The material, as presented, does not necessarily reflect any position of the Society of Petroleum Engineers, its officers, or members. Papers presented at SPE meetings are subject to publication review by Editorial Committees of the Society of Petroleum Engineers. Permission to copy is restricted to an abstract of not more than 300 words. Illustrations may not be copied. The abstract should contain conspicuous acknowledgment of where and by whom the paper is presented. Write Publications Manager, SPE, P.O. Box 833836, Richardson, TX 75083-3836. Telex, 730989, SPEDAL.

ABSTRACT

HASDrive (Heated Annulus Steam Drive) is an in-situ thermal process for recovering bitumen from tar sands. This paper presents the results of a numerical simulation of the HASDrive process in repeated, elongated well patterns. Results show that the process can effectively recover bitumen from tar sands. In a basic configuration, the cumulative recovery in ten years is predicted to be high, but the rate of production is low during the early steam-injection period. Several well configurations and operating procedures were investigated to accelerate the early year production. The recovery mechanisms and the sensitivity of the process to various parameters are also discussed in this paper.

INTRODUCTION

Bitumen is a naturally occurring mixture of viscous hydrocarbons. The total reserves of bitumen in the world are estimated to be over four trillion barrels.[1] Bitumen is characterized by its low gravity (6 to 13°API) and extremely high viscosity (approximately 0.1 to 10 million centipoise at reservoir conditions).

In its naturally occurring state, bitumen is not recoverable at a commercial rate through a well. Conventional steamflooding cannot work satisfactorily because bitumen ahead of the heated zone does not have sufficient mobility to flow to the production well.

HASDrive[2] is an in-situ thermal process for recovering bitumen from tar sands. The process utilizes a horizontal, cased, unperforated pipe running between a vertical steam-injection well and a vertical production well (see Fig. 1). High pressure, high temperature steam is first circulated through the HAS pipe which heats the surrounding tar sand by conduction. In time, a heated annulus is formed around the HAS pipe. Continuous steam injection and production at the vertical wells begin when sufficient mobility around the HAS pipe has been established. The heated annulus acts as a communication path between the injection and production wells.

As the injected steam contacts the bitumen, the bitumen is mobilized. Both the bitumen and steam condensates drain to the HAS pipe where they are swept to the vertical production well by the pressure gradient maintained between the production and injection wells. Steam circulation in the HAS pipe is maintained at a sufficient rate to keep the communication path between production and injection wells open throughout the life of the project.

SIMULATION

Reservoir Properties

The reservoir descriptions used in this simulation study are hypothetical; they are intended to be representative of a homogeneous Athabasca oil sand. The bitumen is assumed to be a non-volatile, single-component oil. The reservoir porosity is assumed to be 35% and the initial oil saturation is 65%. The total original oil in place (OOIP) is 1765 bbl per acre-foot. Table 1 lists reservoir properties used as input.

The viscosity of bitumen[3] is shown as a function of temperature in Figure 2. At reservoir conditions, the bitumen viscosity is 0.1 million cp. It decreases to 30 cp at 260°F. Thermal conductivity of the tar sand is assumed to be 31 BTU/(ft-day-F).

Relative permeability curves for water-oil and oil-gas systems are shown in Figure 3. Relative

---

References and illustrations at end of paper.

permeability and end-point saturations are assumed to be independent of temperature. Three-phase relative permeabilities are calculated by the modified Stone equation.[4,5] Capillary pressure was assumed to be negligible.

Model Description

The ISCOM simulator[6] version 2.2 was used in this study. The program was developed by the Computer Modelling Group of Calgary, Alberta. The simulator is a multicomponent, multiphase model accounting for gravity and heat transfer by convection and conduction. The simulation equations are solved with a fully implicit method.

Figure 4 is a schematic layout of the HASDrive pattern used in the base case study. It is a repeated, elongated well pattern, 1600 ft long and 136 ft wide, having a total area of 5 acres.

For a repeated well pattern, the lines of symmetry are usually the no-flow boundaries or streamlines. In the base case HASDrive simulation, the well pattern was divided into four symmetric elements, each having dimensions of 800 x 85 x 68 feet. A model grid of 7 x 7 x 4 (see Fig. 5) was used for most cases studied in this work. The HAS pipe is shown in the first vertical section, third layer from bottom. The HAS pipe is 17.0 ft above the bottom of the tar sand to minimize the heat loss to underlying strata.

In the simulation, the rate of heat transfer, Q, from the HAS pipe to the adjacent blocks is proportional to the temperature difference between the HAS pipe and adjacent block.

$$Q = h\,A\,\Delta t \qquad (1)$$

To minimize numerical dispersion, variable grid block sizes were used. The block size is smallest for the blocks containing the injection and production wells and the HAS pipe. The block dimensions in the Y and Z direction are smaller than in the X direction because of the rapid saturation changes in these directions resulting from steam override and bitumen drainage. The block size in the X direction is large because of the elongated geometry.

RESULTS

Base Case

Prior to the steamflood, steam is circulated into the HAS pipe to heat and maintain the pipe surface at 500°F. Heat is transferred from the pipe surface to the tar sand, bitumen, and water that surround the pipe. With time, a heated annulus is developed around the HAS pipe. This becomes the communication path between the injection and production wells.

Based on the analytical solution given in Carslaw and Jaeger,[7] the time required to heat a 5-foot diameter communication channel above 260°F is estimated to be approximately 40 days. Within the 5-foot diameter communication channel, the temperature of tar sand and bitumen are above 260°F. At this temperature, bitumen mobility is sufficiently high to allow practical steam drive.

Continuous steam injection starts after the 5-foot communication path has been established. As the steam heats the reservoir, bitumen is mobilized and drains toward the HAS pipe where it forms a bank of high oil saturation. The bitumen bank is then effectively displaced toward the production well.

Because of the elongated well pattern (800 ft long), no steam breakthrough at the production well occurs before 6-1/2 years of steam injection. The delayed steam breakthrough makes it possible to heat a sufficiently large portion of the reservoir to achieve high volumetric sweep and high overall recovery.

1. Cumulative Production

The cumulative bitumen production for the base case is shown in Figure 6. Bitumen production curves have a shape characteristic of that for a heavy oil. In the early years, the production rate is low and then increases rapidly with continual reservoir heating. The production rate reaches a peak before steam breakthrough and declines thereafter.

The cumulative bitumen production is about 35% OOIP at steam breakthrough and more than 70% OOIP at the end of the tenth year of injection. The high ultimate oil recovery may be attributed to the following factors:

1. The reservoir is thoroughly heated prior to steam breakthrough.
2. Gravity causes bitumen drainage to the HAS pipe where it is effectively displaced.
3. A high volumetric sweep efficiency for a well pattern with a length-to-width ratio of twelve to one.

2. Steam Injection Rate

Early in the steam-injection period, the injection rate is limited by the injection pressure. As the reservoir warms up, the injection rate increases and reaches a maximum rate of 1.5 BPD/acre-ft, set in the model as a limit.

Steam must also be circulated through the HAS pipe to keep it hot. The heat consumed in the HAS pipe was calculated from a heat balance. The amount of heat consumed in the HAS pipe was then converted to an equivalent number of barrels of 50% quality steam at 445°F.

The annual steam consumption in the injection well and the HAS pipe are shown in Figure 7. Steam used in the HAS pipe increases as the production rate increases in the early years. Later, the consumption drops to zero as the injected steam breaks through.

3. Steam-Oil Ratio

Annual oil production for the 5-acre pattern and annual steam-oil ratio are summarized in Table 2 [illegible] the base case configuration. The annual [illegible]-oil ratios are the sum of the annual steam consumption in the injection well and the HAS pipe, divided by the annual oil production. The annual steam-oil ratio decreases from 14 in the first year to a low of 2.5 at the time of steam breakthrough, and increases to 6.4 at the end of ten years of injection.

Effect of Input Variables

1. Grid Block Size

The effect of grid block size on cumulative oil production is illustrated in Figure 8. The block sizes in the X direction were refined to 10, 15, 25, 40, 60, 100, 150, 150, 100, 60, 40, 25, 15, and 10 feet, for a total of 800 ft. Doubling the number of grid blocks from 7 x 7 x 4 to 14 x 7 x 4 caused a slight increase in oil production. This effect is considered to be negligible.

However, doubling the number of grid blocks caused an almost four-fold increase in computation time (from 26.7 to 98.1 CPU minutes for a ten-year run on a Cray 2 computer) and a four-fold increase in memory storage space requirement (from 1099 to 4525 megaword-sec). The average CPU time per time step increased from 4.98 to 13.16 seconds. Since the difference in the results was negligible, all remaining simulations shown in this paper were made [illegible] the 7 x 7 x 4 grid.

2. Relative Permeability

The relative permeabilities to oil, water, and gas are the most uncertain variables in a numerical simulation. Their uncertainty is a result of the difficulty in measuring and reproducing the permeability values in the laboratory.

To study the sensitivity of the calculated results to relative permeabilities, a different set of curves from Reddy[8] was used. The calculated cumulative oil production curve is shown in Figure 9. The base case results are also plotted in this figure as dashed curves for comparison. The shape of cumulative production curves is very similar to the base case, but it is shifted to the right. Thus, it appears that the timing was changed, but the recovery mechanism was not affected by the new set of relative permeability curves.

3. Heat Transfer Coefficient

Since the HAS pipe is hotter than its surroundings, heat is transferred from the pipe to the tar sand by conduction as well as by convection. The overall heat transfer rate is proportional to the interfacial area and the temperature difference [illegible]oss the HAS pipe and tar sand interface.

The proportionality constant h in Equation (1) is the heat transfer coefficient. It is usually a function of fluid velocity, flow geometry, viscosity, and thermal conductivity of the fluid. In most cases, it is a strong function of the flow geometry. For a viscous fluid in the presence of convection, the heat transfer coefficient is in the range of 10-100 BTU/(ft^2-hr-F).[9,10] Because of the high viscosity bitumen and the convective flow outside the horizontal HAS pipe, the heat transfer coefficient was assumed to be 15 BTU/(ft^2-hr-F) for the base case.

Figure 10 shows the sensitivity of cumulative oil production to heat transfer coefficients varying from 3 to 30 BTU/(ft^2-hr-F). As expected, the higher the heat transfer from the HAS pipe, the faster the recovery.

Effect of HAS Pipe Diameter

The low oil production in the early years of the HASDrive base case is caused by the limited size of the communication path.

The communication path prior to steam drive was established by thermal conduction from the HAS pipe. The rate of heat conduction decreases rapidly as the diameter of the communication channel grows. For example, it takes 40 days to heat a 5-foot diameter channel to 260°F or higher with a 6-inch HAS pipe and 500°F steam; it would take a year to increase this channel diameter to 10 feet.

Using a larger size HAS pipe and higher temperature steam are effective ways to increase the rate of growth of the communication channel. For example, the time required to create a 10-foot diameter channel is 77 days when a 12-inch diameter HAS pipe and 600°F steam are used.

Figure 11 shows the cumulative oil production with a 10-foot diameter communication channel. The bitumen production is significantly higher in the early years for this case.

Effect of Pattern Width

The cost of drilling a horizontal HAS pipe is high. As an alternative, increasing the pattern width can reduce the horizontal drilling cost per unit area. However, as the pattern width increases, the areal sweep efficiency decreases.

A numerical simulation was performed to evaluate drilling an additional HAS pipe in the direction perpendicular to the original HAS pipe. Results of this simulation indicated that this configuration was not an effective method to improve the areal sweep. However, drilling additional offset production wells can effectively improve the areal sweep efficiency. This approach, in essence, trades off the high cost of a horizontal well with multiple conventional production wells.

Figure 12 shows the preferred method of improving areal sweep in a 200-foot wide well pattern. Bitumen is first produced from the production well which is located 7 feet off-set from the HAS pipe and 190 feet away from the injection well. After steam breakthrough occurs in two years, the producer is shut-in.

A second production well is then drilled 17.5 feet from the HAS pipe and 550 feet away from the injection well. This producer is also shut-in after steam breakthrough. A third production well is then drilled 40 feet from the HAS pipe and 800 feet away from the injection well. It is produced until the end of the project's life.

Figure 13 shows the cumulative bitumen production from one-fourth of a pattern having a width of 200 feet (increased from 136 feet in the base case) and a reservoir thickness of 85 feet. The stepwise increase in the off-set distance of the production well induces steam to flow away from the HAS pipe; therefore, it effectively improves sweep efficiency. Furthermore, the use of closer-spaced off-set production wells also accelerates the early year production. This greatly improves the economics of this process.

Effect of Well Configuration

Several well configurations were simulated, but none of these configurations improved the areal sweep efficiency and production rate significantly. Examples of well configurations that were examined include (1) combining the steam injection well and the HAS pipe into one horizontal well; (2) using a horizontal injection well; and (3) reversing the injection and production wells in every other location. Only the first configuration is discussed here. Figure 14 shows that steam is injected into the reservoir through a perforated HAS pipe.

The cumulative oil productions for this case (solid curve) and the base case (dashed curve) are compared in Figure 15. The initial bitumen production is slightly higher for the perforated HAS pipe case. But the ultimate recovery is only 45% OOIP at the end of the tenth year of injection, which is much lower than the base case HASDrive.

The low recovery is a result of short-circuiting of steam between injection and production wells. Because of the short distance from the tip of the horizontal injection well to the bottom of the production well, bitumen near the production well is first mobilized, creating a short flow path. Water and steam are short-circuited through this path, which makes bitumen recovery very inefficient.

To minimize the short-circuit effect, moving the injection well away from the production well was simulated. However, as the injection well is pulled back, control of the heated flow path is impaired. A slight cooling of the bitumen in this zone would cause a rapid increase in viscosity and hence a rapid decrease in mobility. Bitumen and water could no longer flow along a well-controlled communication path as in the base case HASDrive.

Advantages of the HASDrive Process

Effective steamflooding of tar sands requires fluid communication between injection and production wells. Such a communication path can be developed through use of a steam-heated horizontal well, such as the HAS pipe. This provides a well-controlled fluid communication path.

Because the HAS pipe provides a controlled communication path, the direction of fluid flow can b[illegible] designed according to the geology of a reservoir. The fluid flow is not limited by the direction of horizontal fractures or high-water-saturation strata. These natural communication paths can become plugged when hot bitumen is cooled by contacting unheated formation. On the other hand, the communication path generated by the HAS pipe can be kept open throughout the life of the project. It can also be reopened after a major shut down of steam injection.

Furthermore, steam conformance of the HASDrive process is high; heat loss is low in comparison with other processes[11-17] using induced or naturally occurring fractures or high-water-saturation zones.

Several other advantages of the HASDrive process are:

1. Directional control in drilling of a HAS pipe is not as critical as in other horizontal well processes.[18,19]

2. Because HASDrive does not use the horizontal well as a production well, sand control problems would be less severe.

3. Because the HAS pipe is an unperforated pipe, steam distribution along its length would not be a problem.

CONCLUSIONS

1. Numerical simulation studies show that bitumen can be effectively recovered from tar sands by the HASDrive process.

2. Using elongated well patterns, it is possible to improve areal sweep efficiency while avoiding premature steam breakthrough.

3. For the base case well configuration, it is possible to recover more than 70% OOIP in ten years with a cumulative steam-oil ratio of 4.6.

4. A potential drawback of the HASDrive process may be the low initial oil-production rate. However, increasing the diameter and temperature of the heated communication path or using off-set production wells can effectively accelerate production.

5. It is essential to heat the HAS pipe with steam to maintain an effective communication path between production and injection wells.

6. The dominant recovery mechanism in the HASDrive process is gravity drainage, assisted by a steam drive.

ACKNOWLEDGEMENTS

I thank J. H. Duerksen, K. C. Hong, and D. J. Anderson of Chevron Oil Field Research Company for their helpful comments.

REFERENCES

Phizackerley, P. H. and Scott, L. O., "Major Tar Sand Deposits of the World", Proceedings of the 7th World Petroleum Congress, Elsevier Pub., Vol. 3, pp. 551-571 (1967).

2. Anderson, D. J., Kirkvold, C. F., and Pisio, P., "Method of Recovering Viscous Petroleum from Tar Sand", U. S. Patent 3,994,340, November 30, 1976, U. S. Patent 3,994,341, November 30, 1976, and U. S. Patent 4,008,765, February 22, 1977.

3. Carrigy, M. A., "The Physical and Chemical Nature of a Typical Tar Sand: Bulk Properties and Behavior", Proceedings of the 7th World Petroleum Congress, Elsevier Pub., Vol. 3, pp. 573-581 (1967).

4. Stone, H. L., "Estimation of Three-Phase Relative Permeability and Residual Oil Data", J. Can. Petro. Tech. 12, 53-61, No. 4, October-December 1973.

5. Aziz, K. and Settari, A., Petroleum Reservoir Simulation, Ch. 2, Applied Science Publishers, London, 1979.

6. Rubin, B. and Buchanan, W. L., "A General Purpose Thermal Model", SPE 11713 presented at the 53rd Annual California Regional Meeting of SPE, March 23-25, 1983, Ventura, CA.

Carslaw, H. S. and Jaeger, J. C., Conduction of Heat in Solids, Oxford, 2nd Edition (1959).

8. Reddy, G. S., Prowse, D. R., and Redford, D. A., "Physical Modeling and Numerical Simulation of In Situ Recovery of Bitumen from Oil Sand by Steam Injection", Paper No. 80-31-10, presented at the 31st Annual Technical Meeting of the Petroleum Society of CIM in Calgary, May 25-28, 1980.

9. Bird, R. B., Stewart, W. E., and Lightfoot, E. N., Transport Phenomena, Wiley, New York (1960), Chapter 13.

10. White, P. D. and Moss, J. T., Thermal Recovery Methods Penn Well, Tulsa (1983), Chapter 6.

11. Volkenborn, A., et al., "Discussion, Recovery of Extra Heavy Oil and Bitumen by Non-Mining Methods", Proceedings of the 11th World Petroleum Congress, London, Vol. III, pp. 273-279 (1983).

12. Doscher, T. M., "Technical Problems in In Situ Methods for Recovery of Bitumen from Tar Sands", 7th World Petroleum Congress, Mexico City, Vol. III, pp. 625-632.

13. Britton, M. W., Martin, W. L., Leibrecht, R. J., and Harmon, R. A., "The Street Ranch Pilot Test of Fracture-Assisted Steamflood Technology", paper presented at the 1982 California Regional Meeting of the SPE, San Francisco, California, March 24-26, 1982, SPE 10707.

14. Redford, D. A., "In-Situ Recovery from the Athabasca Oil Sands - Past Experience and Future Potential", Paper No. 84-35-123, paper presented at the 35th Annual Technical Meeting of the Petroleum Society of CIM, Calgary, June 10-13, 1984.

15. Waxman, M. H., Closmann, P. J., and Deeds, C. T., "Peace River Tar Flow Experiments under In-Situ Conditions", SPE 9511, Preprint presented at the 55th SPE Fall Meeting, Dallas, September 21-24, 1980.

16. Gorrill, R. G., Henderson, I. C., and Myhill, N. A., "Operational Progress of the Peace River In Situ Project", Proceedings of the 11th World Petroleum Congress, London, Vol. III, pp. 243-250, (1983).

17. Tam, E. S., Edmunds, N. R., and Redford, D. A., "Methods of Enhancing Fluid Communication in Oil Sands", paper presented at the 4th Symposium on Enhanced Oil Recovery, Tulsa, OK, April 15-18, 1984.

18. Butler, R. M., "Method for Continuously Producing Viscous Hydrocarbons by Gravity Drainage While Injecting Heated Fluids", U. S. Patent 4,344,485, August 17, 1982.

19. Butler, R. M., "The Potential of Horizontal Wells - Some Introductory Comments", paper presented at 5th Annual Advances in Petroleum Recovery and Upgrading Technology Conference, June 14-15, 1984, Calgary, Alberta.

TABLE 1

RESERVOIR DATA USED in THE SIMULATION

Pattern area, acres	5.0
Distance between injector and producer, ft	800
Sand thickness, ft	85
Porosity, % bulk volume	35
Permeability	
Horizontal, darcy	3.0
Vertical, darcy	1.5
Initial reservoir pressure, psia	350
Initial reservoir temperature, °F	60
Initial water saturation, % pore volume	35
Initial oil saturation, % pore volume	65
Injected steam temperature, °F	445
Pressure, psia	400
Max. rate BPD/Ac-ft (CWE)	1.5
Compressibility of oil, psi^{-1}	1.03×10^{-4}
Water, psi^{-1}	3.23×10^{-6}
Formation, psi^{-1}	5.0×10^{-5}
Thermal conductivity, BTU/(ft-day-°F)	
Rock	31.5
Water	8.6
Oil	1.85
Gas	0.70
Volumetric heat capacity, BTU (ft^3-°F)	35.0
Thermal expansion coefficient	
Oil, 1/°F	0.33×10^{-3}
Water, 1/°F	0.44×10^{-3}

TABLE 2

PREDICTED YEARLY STEAM CONSUMPTION
AND OIL PRODUCTION IN BASE CASE
WITH A 6" HAS PIPE

	Steam Consumption				
Time Yrs	Inj. Well BBL/Yr	HAS Pipe BBL/Yr	Oil Production BBL/Yr	Annual Steam/Oil Ratio	Cumulative Steam/Oil Ratio
Pre*		13,200			
1	48,100	69,800	8,720	13.5	15.0
2	99,500	85,800	15,300	12.1	13.2
3	127,100	98,800	21,200	10.6	12.0
4	153,000	116,000	39,100	6.88	9.62
5	193,000	127,500	64,800	4.95	7.59
6	231,000	127,800	95,400	3.76	6.10
7	231,000	77,000	125,000	2.46	4.87
8	231,000	1,000	93,200	2.50	4.39
9	231,000	0	49,100	4.71	4.41
10	231,000	0	36,150	6.39	4.55
Total	1,776,000	724,000	548,000		

*Steam consumed in the warm-up period, pre-steamflood.

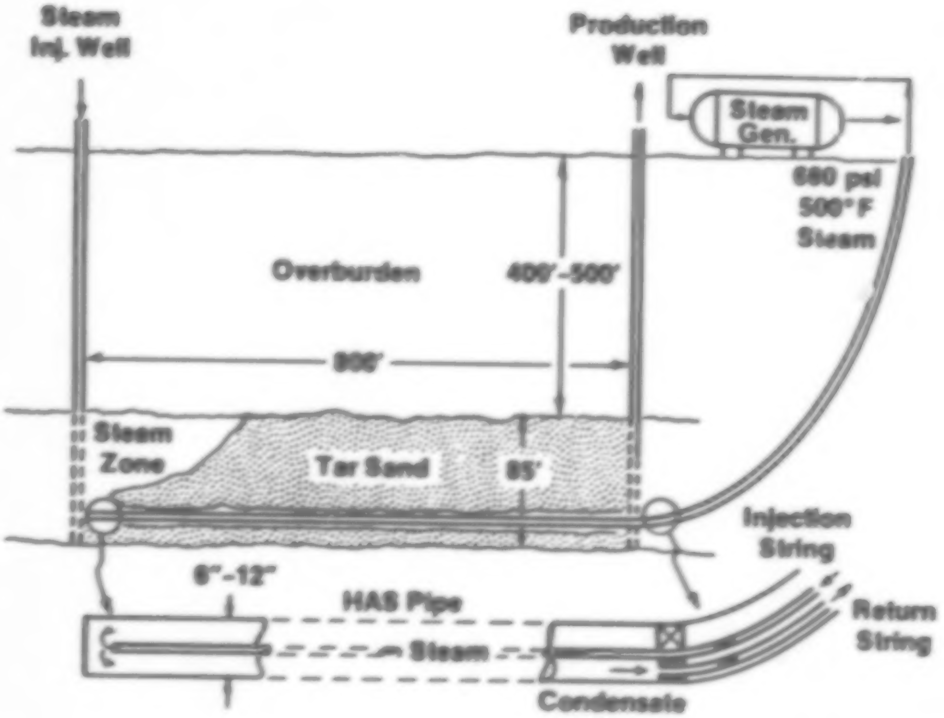
Steam
Inj. Well
Production
Well
Steam
Gen.
680 psi
500°F
Steam
Overburden
400'-500'
800'
Steam
Zone
Tar Sand
85'
Injection
String
6"-12"
HAS Pipe
Steam
Return
String
Condensate

Figure 1
HASDrive (Heated Annulus Steam Drive)

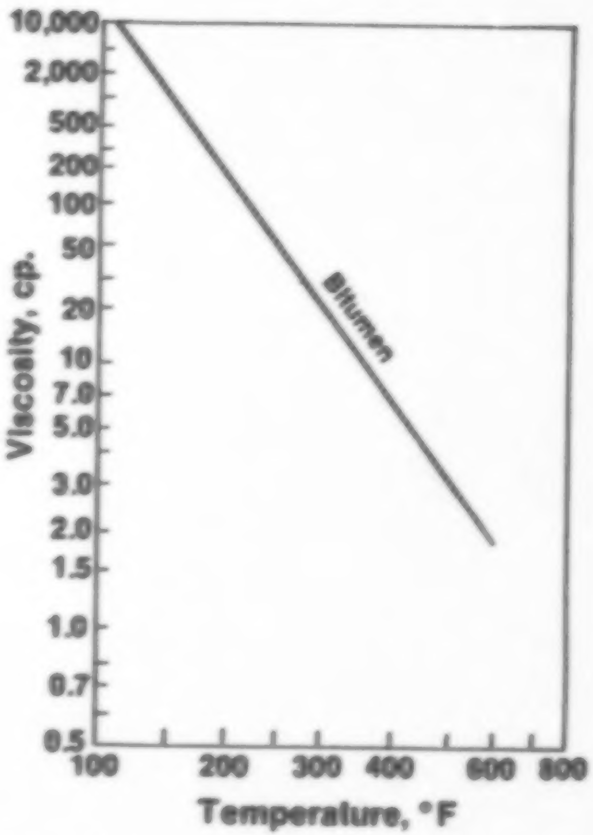

Figure 2
Viscosities of Bitumen

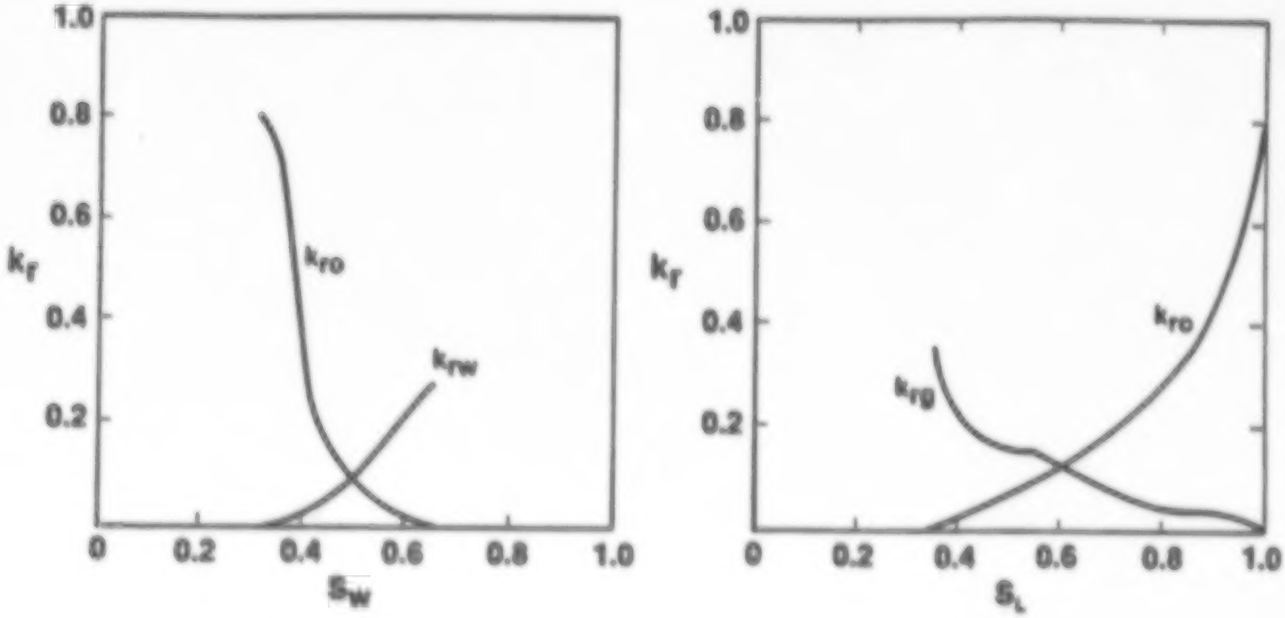

Water-Oil

Gas-Oil

Figure 3
Relative Permeability Curves

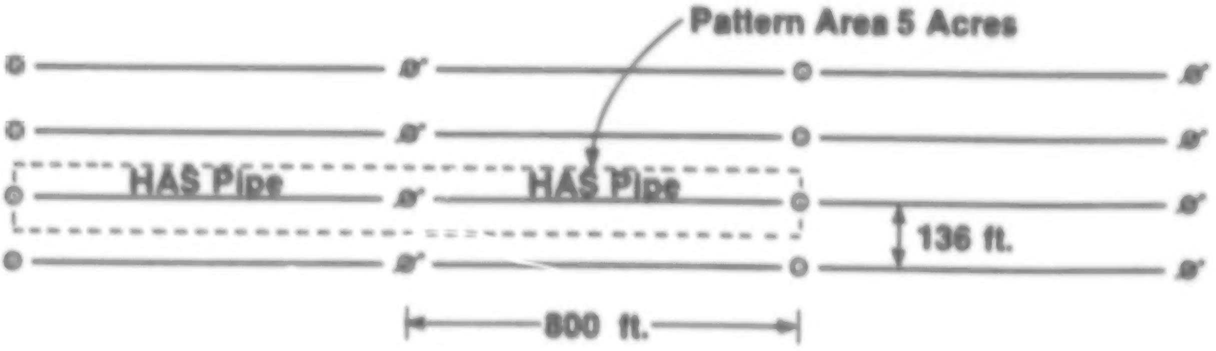
Pattern Area 5 Acres
HAS Pipe
HAS Pipe
136 ft.
800 ft.

Figure 4
Base Case Well Pattern

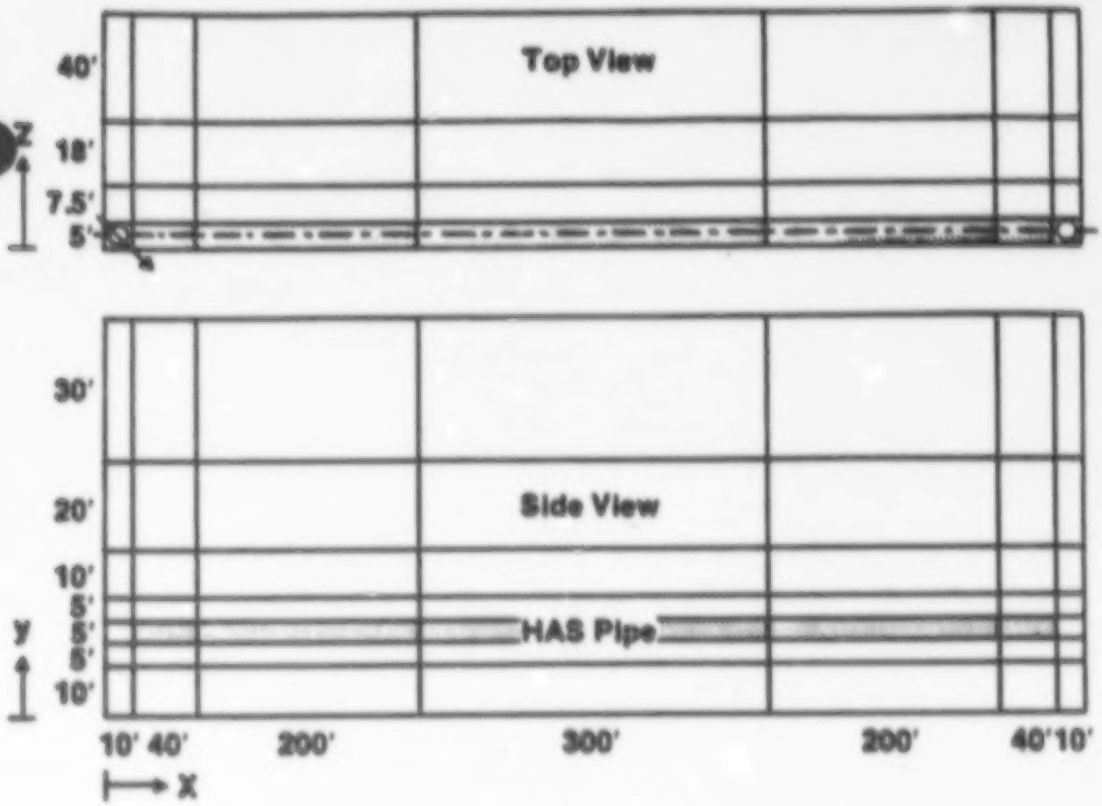
Top View
40'
Z
18'
7.5'
5'
30'
Side View
20'
10'
5'
y
5'
HAS Pipe
5'
10'
10' 40'
200'
300'
200'
40'10'
X

Figure 5
ase Case Grid Blocks, 1/4 HASDrive Pattern, 7 x 7 x 4 Blocks

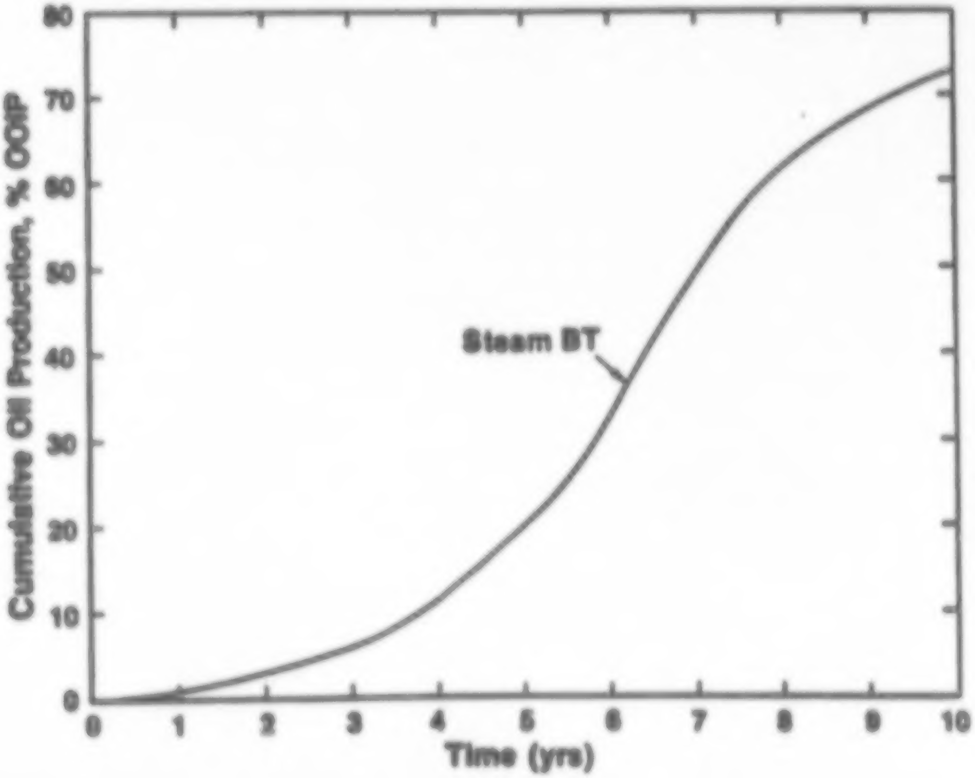

Figure 6

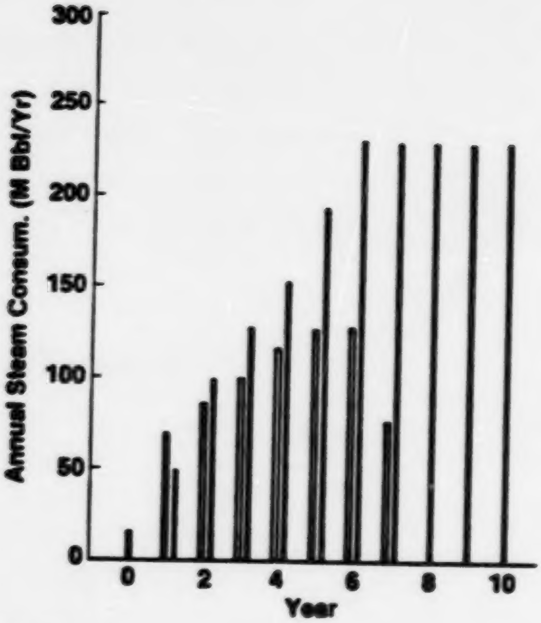

Figure 7
Annual Steam Consumption in Pattern HAS Pipes (Open Bars), and in Injection Well (Solid Bars)

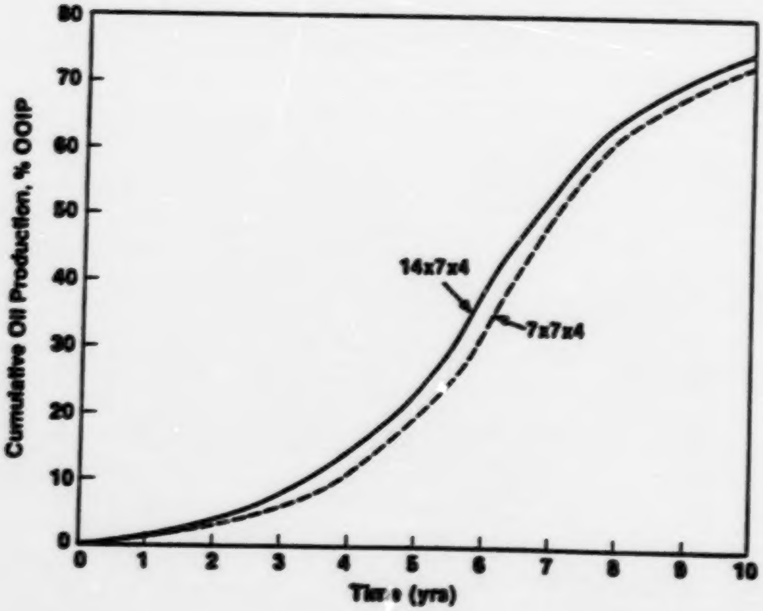

Figure 8
Effect of Grid Blocks on the Cumulative Oil Production, Base Case HASDrive

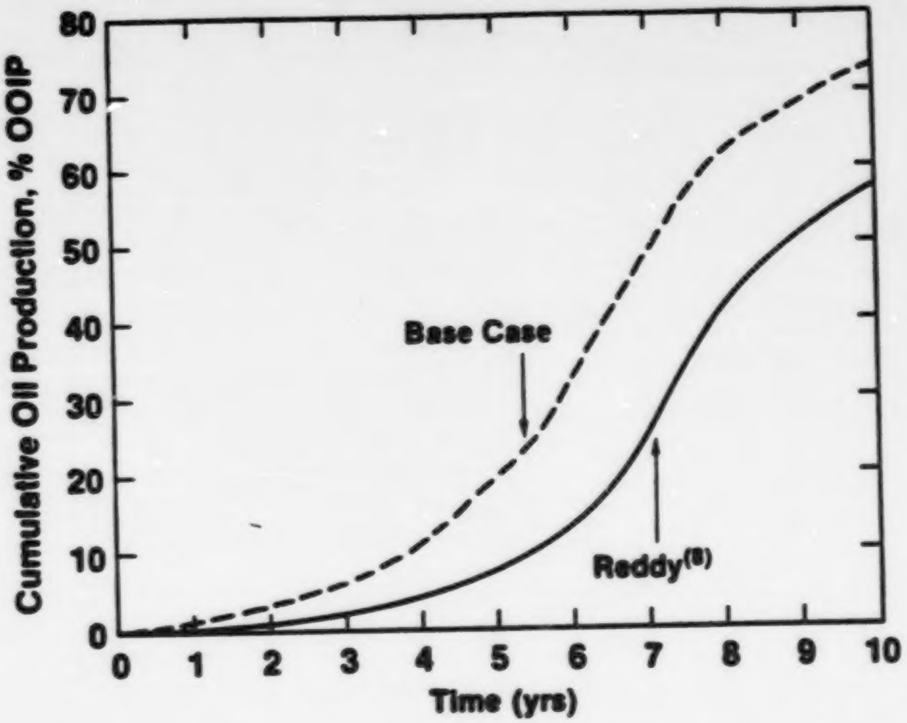

Figure 9
Predicted Cumulative Oil Producing Using Relative Permeability Curves from Reddy[8]

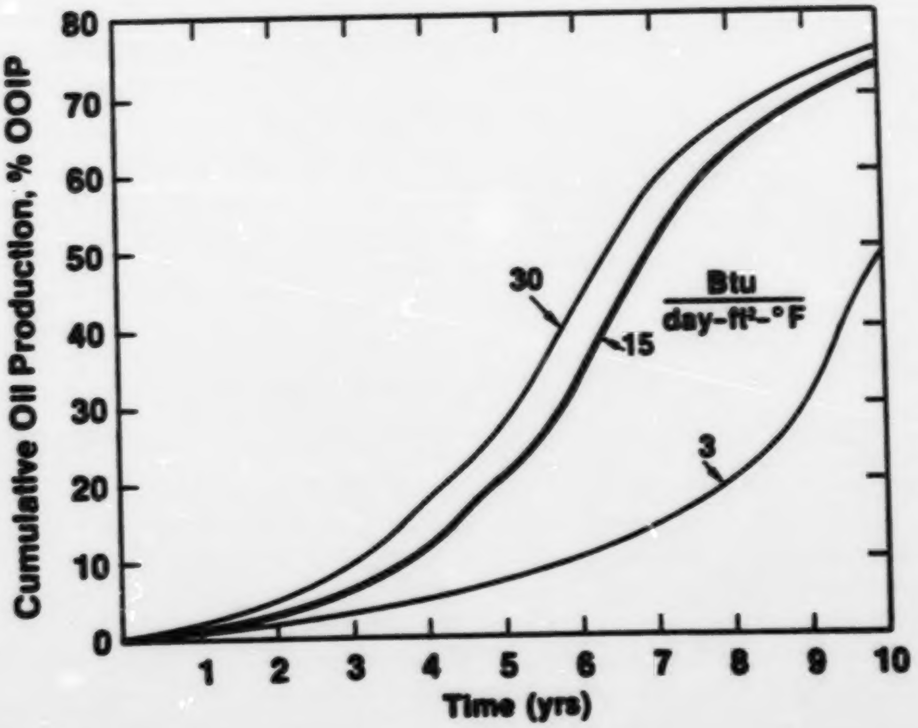

Figure 10
Effect of Heat Transfer Coefficients on the Cumulative Oil Production

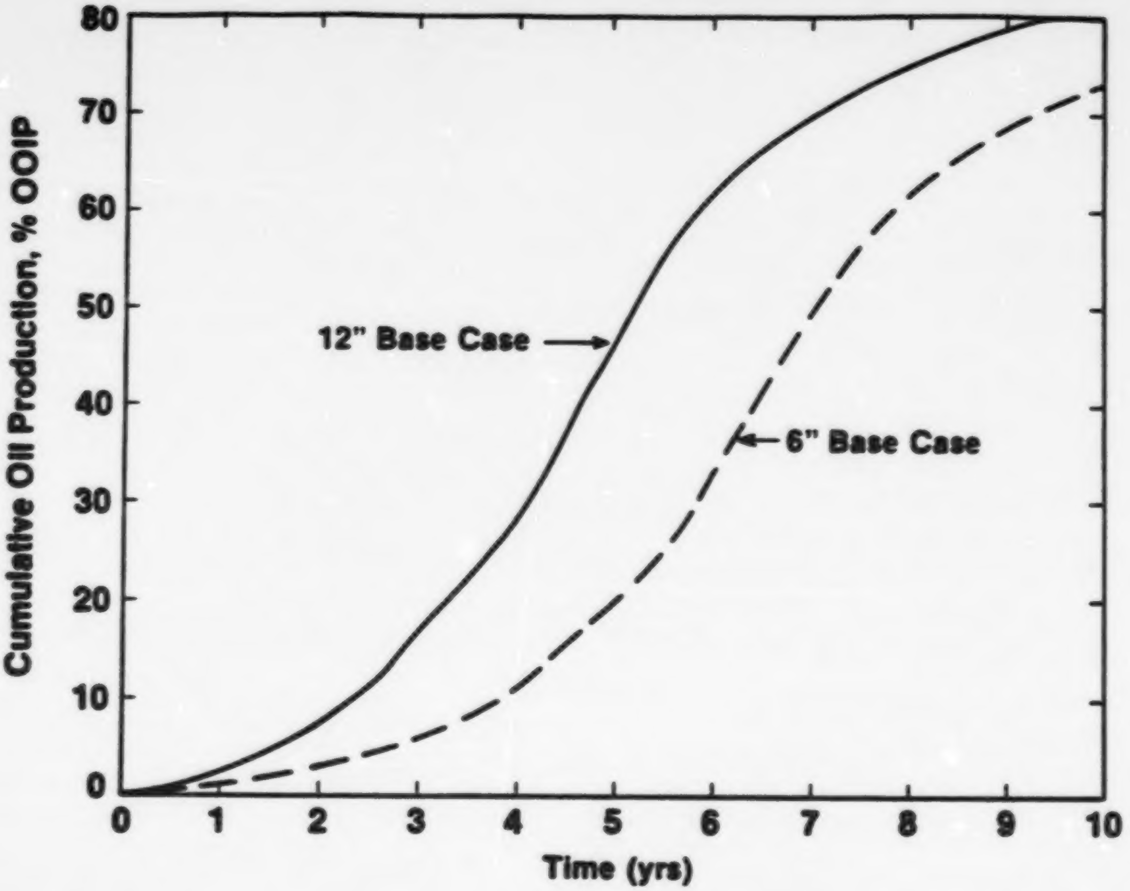

Figure 11
Cumulative Oil Production, Effect of HAS Pipe Diameter

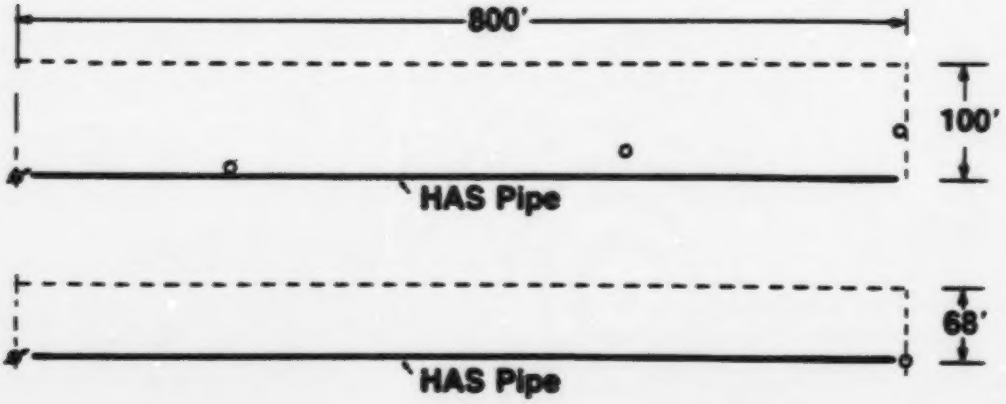
800'
100'
HAS Pipe
68'
HAS Pipe

Figure 12
1/4 HASDrive Pattern, Aerial Views, with and without Offset Wells

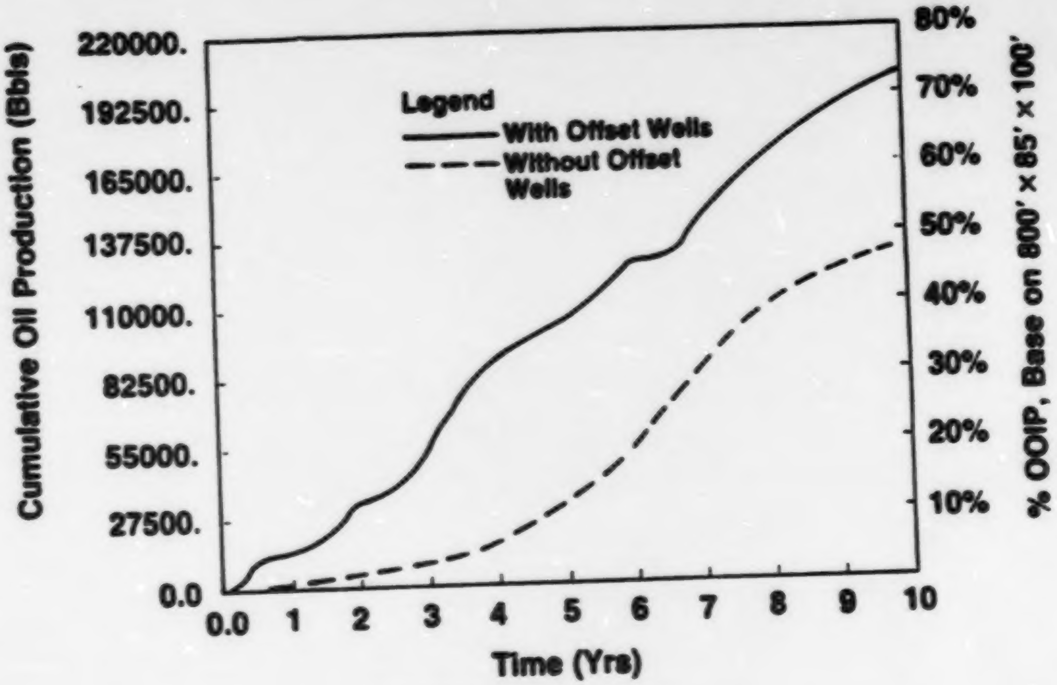

Figure 13
Cumulative Oil Production for Multiple Offset Production Wells in the HASDrive Process

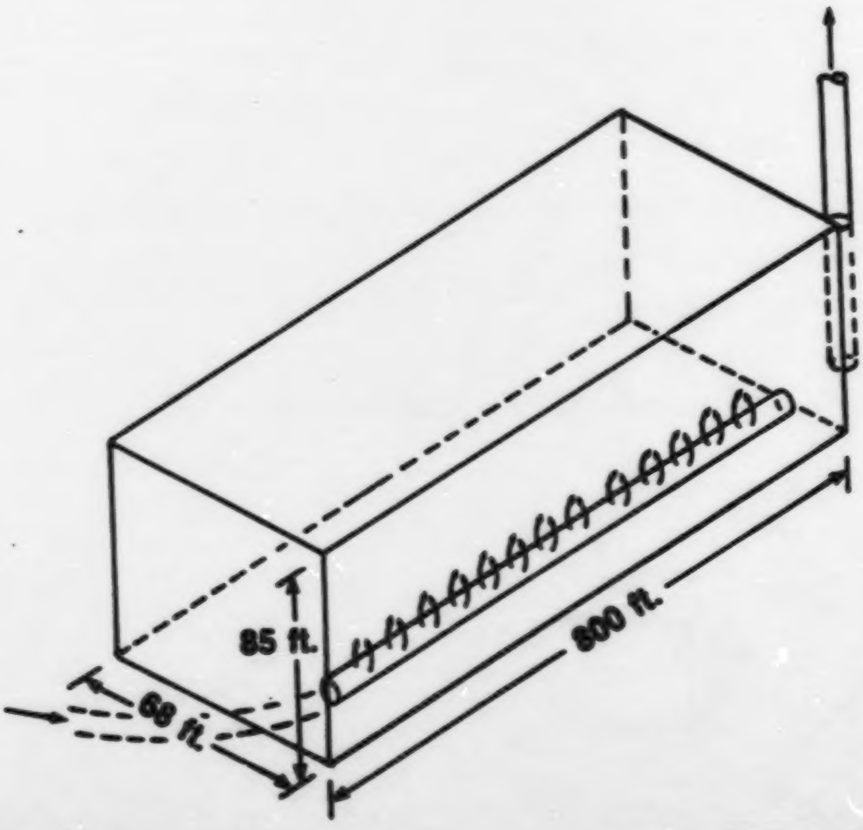
85 ft.
68 ft.
800 ft.

Figure 14
A HAS Injection well pattern

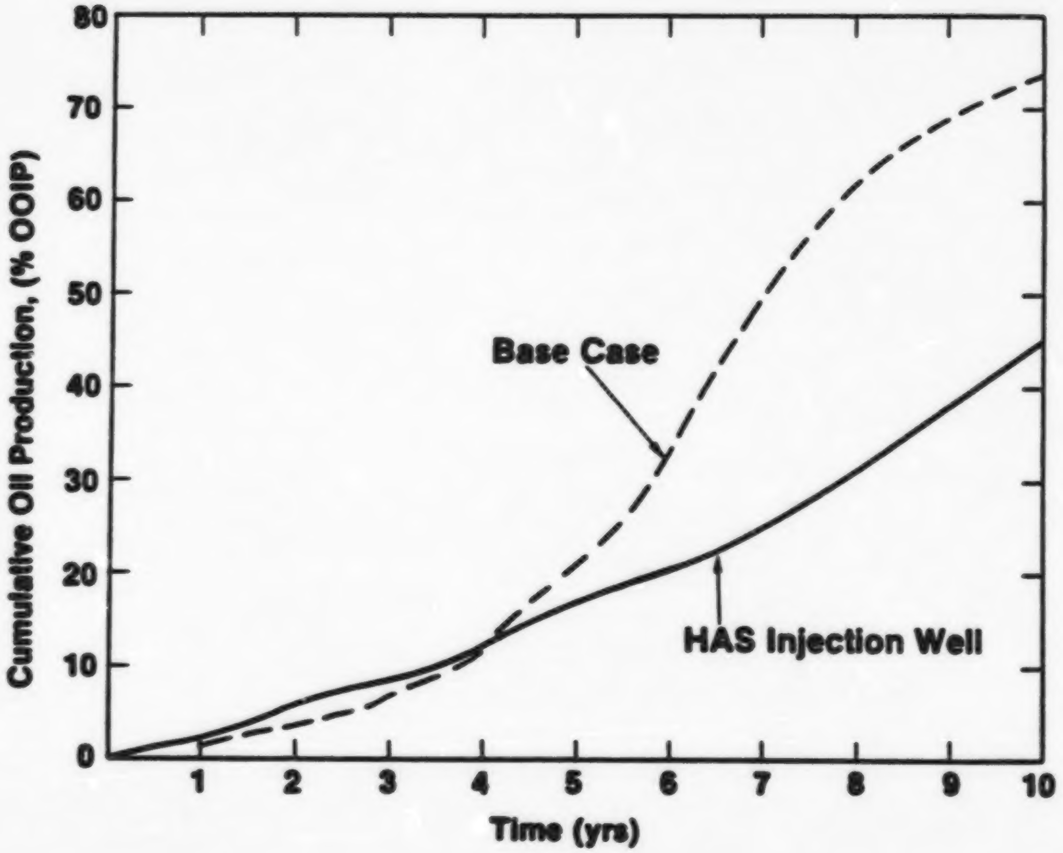

Figure 15
Cumulative Oil Production For a HAS Injection Well

5129 E

90

PREPRINTS
VOLUME II

PAPERS PRESENTED AT THE

36TH ANNUAL TECHNICAL MEETING
OF THE
PETROLEUM SOCIETY OF CIM

HELD JOINTLY WITH

THE CANADIAN SOCIETY OF PETROLEUM GEOLOGISTS

CONVENTION CENTRE
EDMONTON, ALBERTA, CANADA
JUNE 2 - 5, 1985

Preprints have been arranged in two volumes. Volume I contains papers presented on Monday June 3, and Tuesday June 4, 1985. Volume II contains papers presented on Wednesday June 5, 1985.

PETROLEUM SOCIETY OF CIM

PAPER NO. 85-36-62

THIS IS A PREPRINT — SUBJECT TO CORRECTION

SWEEP EFFICIENCY IMPROVEMENT USING HORIZONTAL WELLS OR TILTED HORIZONTAL WELLS IN MISCIBLE FLOODS

by
S.M. Chen
J. Olynyk
Gulf Canada Resources Inc.

PUBLICATION RIGHTS RESERVED

THIS PAPER IS TO BE PRESENTED AT THE 36TH ANNUAL TECHNICAL MEETING OF THE PETROLEUM SOCIETY OF CIM HELD JOINTLY WITH THE CANADIAN SOCIETY OF PETROLEUM GEOLOGISTS IN EDMONTON JUNE 2-5, 1985. DISCUSSION OF THIS PAPER IS INVITED. SUCH DISCUSSION MAY BE PRESENTED AT THE TECHNICAL MEETING AND WILL BE CONSIDERED FOR PUBLICATION IN CIM JOURNALS IF FILED IN WRITING WITH THE TECHNICAL PROGRAM CHAIRMAN PRIOR TO THE CONCLUSION OF THE MEETING.

ABSTRACT

Two factors determine oil recovery:

i) displacement efficiency
ii) sweep efficiency

For a miscible flood, high displacement efficiencies may be obtained. However, field performance (i.e. early solvent breakthrough) shows that sweep efficiencies are generally low, and may be attributed to the vastly different properties between the miscible and reservoir fluids.

This paper discusses the improvement in performance that may be expected if horizontal injectors and producers are used in a miscible flood scheme.

A numerical simulation model was used to quantify the increase in areal sweep efficiency that will result from using horizontal wells of various lengths at different mobility ratios in a 5-spot or staggered line-drive pattern. The study showed that the greatest percentage increase in areal sweep efficiency occurred at conditions with the most adverse mobility ratios.

The increase in productivity at various wellbore lengths was also calculated and displayed in graphical form, showing that the productivity index may increase by nearly 5 times as the wellbore length is extended.

The improvement in flood front stability, effect on solvent dilution, and the potential uses of tilted horizontal wells in layered reservoirs, as well as some of the disadvantages and limitations involved with using horizontal wells have also been reviewed.

INTRODUCTION

There are two factors that determine the recovery from an oil reservoir: 1) displacement efficiency and 2) sweep efficiency.

The use of miscible fluids to displace reservoir oil results in very high displacement efficiencies, reducing residual oil saturations to a small fraction of the original hydrocarbon pore volume.

However, the differences in mobilities between the reservoir and the injected fluids has led to very poor sweep efficiencies, as evidenced by field performance. The more mobile solvent sweeps only a small portion of the project pattern before breaking through at the producing wells. It would seem that the generally poor sweep efficiencies that can be expected by using a fluid of such vastly different properties to displace oil Ts one of the prime factors preventing field scale projects from being technically and economically successful.

The purpose of this paper is to investigate the improvement in areal sweep efficiency and general field performance that may be expected if horizontal wells, rather than vertical wells, are used in a miscible flood scheme.

The concept of using horizontal wellbores, so-called 'horizontal wells', as a means of improving recovery and productivity dates back to the 1950's(1,2), but the most recent applications have generally been confined to the field of heavy oil. Little attention has been paid to the potential advantages to be gained by utilizing horizontal wellbores in miscible flooding schemes.

This paper presents the results of a simulation study that was done to quantify the improvement in areal sweep efficiency that may be achieved by using horizontal wells instead of vertical wells. The potential uses of tilted horizontal wells, and the effect of horizontal wells on flood front stability and solvent dilution will also be discussed. The increase in productivity has been calculated and results are shown in graphical form. Some of the limitations and disadvantages in using horizontal wellbores have also been pointed out.

NUMERICAL SIMULATION STUDY

To simulate the areal sweep efficiencies in a 5-spot (or staggered line-drive) quarter pattern (as shown in Figure 1), a 2 dimensional, Cartesian-Coordinate, homogeneous model was set up using a Vectorized Implicit Program (VIP) developed by J.S. Nolen and Associates. To represent ideal miscible displacement, water and gas were used as injection fluids, acting as solvents to reduce the residual oil saturation down to 5% of the original pore volume.

Cases Studies

The cases studied were:

1) Point source injector with point source producer (i.e. conventional vertical wellbores).

2) Horizontal injectors with horizontal producers, varying the length of the wellbores so that the wellbore at the injector and at the producer extended over a) 25%, b) 50%, c) 75% and d) 100% of the 1/4 pattern length.

3) Vertical injector with horizontal producer, where the producing wellbore length is equal to the length of the side of the quarter pattern.

4) Vertical producer with horizontal injector, where the wellbore length at the injector is equal to the length of the side of the 1/4 pattern.

For cases 1 through 2(d), the areal sweep efficiencies were obtained for mobility ratios between 1 and 200. The sweep efficiencies for cases 3 and 4 were studied only at mobility ratios ranging from 10 to 200.

Grid System Design

For each case examined, the grid system was designed in a different way due to several factors that had to be considered to achieve realistic results and to keep the cases on an equal basis for comparison purposes. The general criteria for setting up grid systems for each case were:

a) use a parallel grid (3,4) to simulate miscible displacement process,
b) use the same or similar number of active grid blocks for each grid system,
c) keep the number of grid blocks directly between wellbores the same.

Since it is considered to be more realistic to simulate flow using a parallel grid for each configuration studied, the grid system was designed such that the area directly between wellbores of any length was covered by a parallel grid system, and the area towards the edges of the 1/4 pattern, away from the ends of the wellbores, was covered with a diagonal grid. This type of grid system should, therefore, more accurately model the miscible displacement behaviour (3,4) between a horizontal producer and injector, and result in more realistic recoveries. The grid systems used to simulate the behaviour of the horizontal wells is shown in Figure 2 through Figure 5.

For the point source (vertical well) case, the width of the grid blocks containing the injector and producer were reduced to 2% of the 1/4 pattern length to better represent the actual 'point source' behaviour. The point grid system is shown in Figure 6.

For the situation with a vertical/horizontal well combination, the grid shown in Figure 7 was used. In this grid, the grid block containing the vertical well was reduced in width to 2% of the quarter pattern length to better represent the actual 'point source' behaviour. The grid system also adhered to the criteria listed in points a, b, and c above.

Definition of 'Mobility Ratio' and Areal Sweep Efficiency

For the purpose of this study, the 'mobility ratio' was defined as:

$$M = \frac{(k_{absolute}/\mu)_{solvent}}{(k_{absolute}/\mu)_{oil}}$$

which reduced to:

$$M = \frac{\mu_{oil}}{\mu_{solvent}}$$

The effect of relative permeability will be discussed in the next section.

The areal sweep efficiency (E_S) at solvent breakthrough was then defined in the following manner:

$$E_S = \frac{R_f}{E_D}$$

where R_f = percent of original oil-in-place produced at breakthrough,
and E_D = displacement efficiency

$$= \frac{Soi - Sor}{Soi}$$

where Soi = initial oil saturation
and Sor = residual oil saturation as defined by the endpoint on the relative permeability curve.

Relative Permeability and Cutoffs Defining Solvent Breakthrough

It was found that the areal sweep efficiencies from the simulator were a strong function of the shape of the relative permeability curves that were used. Therefore, in this study, the relative permeability curves were used as a matching parameter and adjusted so that at solvent breakthrough, the areal sweep efficiencies for mobility ratios ranging from 1 to 200 for the vertical producer/injector case matched the published data. The relative permeability curves for water/oil and gas/oil systems are shown in Figures 8 and 9.

For mobility ratios between 1 and 10, water was used as the injected solvent. Breakthrough was defined as the point when the water-cut at the producer reached 1%.

Gas was used as the miscible fluid for mobility ratios between 10 and 200, with breakthrough being reached when the producing GOR increased by 1/2 percent. To ensure the continuity of the results when switching from water to gas, the relative permeability curve for gas was adjusted such that the areal sweep efficiencies at a mobility ratio of 10 were equal for both water and gas injection.

Simulation Results

A) Vertical Wells - Effect of Relative Permeability and Cut-Off, and Comparison With the Published Results

Using the point source grid for vertical wells, the areal sweep efficiencies at breakthrough for cases where the mobility ratios varied between 1 and 200 were obtained, with fair agreement with published results (5,6). The relative permeability curves, GOR and water-cut cutoffs selected to define solvent breakthrough were adjusted to achieve the best match possible with the data of Habermannand Claridge.

The sweep efficiencies from this simulation study versus those published in the literature are shown in Figure 10. The effect of varying the shape of the gas relative permeability curve and GOR cutoff is shown in Figure 11, using the relative permeability curve B shown in Figure 9, and defining breakthrough when the GOR increased by 10%.

B) Horizontal Producers Paired with Horizontal Injectors

Cases were then run for the same range of mobility ratios with both the injector and producer as horizontal wells, with wellbore lengths of 25%, 50%, 75% and 100% of the length of the quarter pattern. The calculated areal sweep efficiencies obtained from these runs were then plotted against mobility ratio for each set of wellbore lengths. Results are shown in Figure 12, with the results from the vertical well cases for comparison. Figure 12 shows that using horizontal wells improved areal sweep efficiencies significantly, with the greatest percentage increase occurring at the more adverse mobility ratios. The increase in efficiency over the vertical well scenario for each set of wellbore lengths for the range of mobility ratios from 1 to 200 is plotted in Figure 13.

C) Combination of Horizontal Injector with Vertical Producer and Vertical Injector with Horizontal Producer

The effect of using a horizontal injector paired with a vertical producer, or a vertical injector paired with a horizontal producer was examined for a mobility ratios of 10 through 200, with the wellbore of the horizontal well in either case extending the entire length of the quarter pattern. The resulting areal sweep efficiencies are plotted in Figure 14, (along with the previously discussed data for comparison), which shows that the increase in sweep efficiency over using 2 vertical wellbores is disappointing.

The case with a horizontal producer and a vertical injector showed virtually no change over the vertical well case for the range of mobility ratios investigated. The best configuration, using a horizontal injector with a vertical producer, increased the sweep efficiency by only 4% at a mobility ratio of 10, and closely followed the trend for the horizontal well case where L/r_e = 25% as the mobility ratio approached 200.

It would appear that combining linear and radial flow patterns in a reservoir establishes pressure gradients such that little additional pattern area is swept compared to when 2 point sources (vertical wells) are used.

In addition to this result, it should be noted that even if full length horizontal injectors were drilled to increase the sweep efficiency and injectivity index, the productivity index of the vertical producer would remain unchanged. Therefore, the production rates from the vertical wells would still be a limiting factor deciding project life and payout period.

It is therefore concluded that using a combination of vertical and horizontal wells as a means of improving the project performance in a miscible flood scheme is inadviseable.

Tilted Horizontal Wells

The use of tilted horizontal wells would be considered in a situation where the reservoir is layered, with poor communication between the layers. Each layer would then be completed with a horizontal wellbore with some effective length which could be expressed as a percentage of the total length of the pattern in that layer. The sweep efficiency per layer could then be evaluated using the curves in Figure 12, and compared to the sweep efficiency that could be expected by using vertical injectors and producers.

Figure 15 is a schematic diagram of one possible situation and is used to illustrate the following example:

eg: Tilted horizontal wells in a reservoir with 2 layers

The effective wellbore length in both layer 1 and 2 would be 50% of the pattern length. Therefore, the areal sweep efficiency for each layer would be 38% for a mobility ratio of 10. In contrast, if vertical wells were used, the areal sweep efficiency per layer would be 28%. Therefore, in this example, a higher recovery would be achieved with the use of tilted horizontal wells.

It should be noted that when there are more than 2 layers contacted by a tilted horizontal well, an estimate of the recovery factor in the middle layer becomes more subjective, as the sweep efficiency becomes a function of the location of the wellbore in those layers. For example, consider the 3-layer reservoir illustrated in Figure 16. For the middle layer, there is no curve in Figure 12 which would be applicable to this completion configuration and flow geometry. Therefore, the areal sweep efficiency for the middle layers in a multi-layer system must be estimated independently.

INCREASE IN PRODUCTIVITY INDEX USING HORIZONTAL WELLS

By completing a reservoir with a horizontal wellbore, the area contacted by the wellbore is greatly increased, and the productivity index of the producer should, therefore, also increase.

In Appendix I, the increase in productivity that will result from using a horizontal well was calculated. First, the flow equations for the flow geometry in the following systems were derived:

a) vertical producer (point source), radial flow,
b) partial horizontal well - where the equation is valid for wellbores extending up to 20% of the pattern length (i.e, $L/r_e \leq 0.2$)
c) full length horizontal well (line drive), linear flow for a full 5 spot pattern.

The equations were then written in the form

$Q/\Delta p = f(k, A, \mu, B, r_e, r_w, L)$

which is the expression for the productivity index in a system at steady-state or pseudo steady-state conditions. The ratio of the productivity indices, PR = J(horizontal)/J(vertical) , could then be obtained directly from an analytical solution for the above three cases. The detail calculations are shown in Appendix I.

Using these data, a curve of PR vs L/r_e was generated using a least squares curve fitting technique with the criteria that the curve must increase monotonically. This curve, displayed in Figure 17 shows that the productivity index will increase by almost 5 fold if the wellbore extends the entire length of the project pattern. These results are similar to those reported in the literature$^{(7,8)}$.

It should be noted that an increase in productivity index will have a significant impact on the project life and economics. As the productivity index increases, the production rates increase, therefore, project life and payout time decrease and project economics are enhanced.

EFFECT OF HORIZONTAL WELLS ON FLOOD FRONT STABILITY AND MIXING

In miscible displacements, the initiation and propagation of viscous fingers, and the co-efficient of dispersive mixing, are related to the velocity of the solvent flood front$^{(3)}$. The more slowly the flood front advances, the fewer losses there will be due to viscous fingering, and the less the solvent will be diluted due to dispersive mixing.

A horizontal wellbore introduces linear flow into a scheme and reduces the flood front velocity for a given injection rate, therefore, a more stable flood front and less dilution of the solvent may be expected. Velocities for radial and linear flow for a fixed injection rate may be calculated as shown below:

(Please refer to the illustration in Figure 18.)

- Vertical injector - radial flow

$V_{radial} = Qinj/(2\pi rh)$

where: r = distance of the solvent front from the wellbore
h = formation thickness

- Horizontal injector - linear flow; wellbore length = 100% of pattern length.

$V_{linear} = Qinj/(4Lh)$

where: L = length of a horizontal wellbore in a quarter pattern

Therefore, the ratio of the velocities is:

$$\frac{V_{linear}}{V_{radial}} = \frac{\pi r}{2L}$$

and $V_{linear} < V_{radial}$ for $r < 0.64L$

That is, the velocity of the solvent front from a horizontal injector will be less than the velocity of the solvent front flowing radially away from a vertical injector, until the distance of the front from the injector is equal to 64% of the length of the pattern. Therefore, horizontal wells may be used to avoid the severe viscous-fingering and solvent dilution which may occur in the vicinity of a vertical wellbore.

Horizontal Wells in a Fractured System

In a reservoir with either natural or induced fractures, the use of horizontal wells must be carefully evaluated. Once the solvent front reaches a highly permeable channel, the miscible fluid will flow preferentially through this channel. Since the areal sweep efficiency will be a function of the fracture distribution and orientation, there may be an improvement or a reduction in areal sweep efficiency. This topic requires further study but is beyond the scope of this paper.

Drilling and Completions

Horizontal wells have successfully been drilled, cored, logged, completed and stimulated although the technology is in the early stages of development, especially for completion and stimulation.

The average cost of drilling a horizontal well is approximately three times that of drilling a vertical well(8). As drilling techniques improve and become more sophisticated, the cost/well will decrease.

Another consideration for miscible flooding is that when the ability to kick off a number of laterals from the same wellbore becomes more developed, there should be a significant reduction in the number of wells that need to be spudded for a project and project economics will be enhanced accordingly.

Conclusions

1. Using a horizontal injector with a horizontal producer in a miscible flood scheme can improve the areal sweep efficiency significantly. Results from a simulation study have been presented in this paper.
2. The largest percentage increase in areal sweep efficiency occurs at the most adverse mobility ratios.
3. Using a combination of vertical and horizontal wells in a flood pattern is not recommended. The optimum configuration, a full length horizontal injector paired with a vertical producer, increases the areal sweep efficiency in a manner similar to the case with 2 horizontal wells of lengths extending 25% of the pattern length. However, since the productivity index of the vertical producer will remain unchanged, production rates, and therefore, project economics, will not improve.
4. Tilted horizontal wells may be used in a layered reservoir with poor communication between layers.
5. By extending the length of the wellbore, productivity may be increased by nearly 5 fold. As productivity index increases, production rates increase, and project payout times and economics improve accordingly.
6. Using horizontal wells decreases the velocity of the solvent flood front, resulting in a more stable flood front due to the reduction in viscous fingering and less dilution of the solvent due to dispersive mixing.
7. Although this study was restricted to a homogeneous reservoir, the use of horizontal wells in fractured systems must be carefully evaluated, since the areal sweep efficiency may be dominated by the fracture distribution and orientation.
8. Horizontal wells have been drilled, cored, logged, completed, and stimulated. As this technology becomes more advanced, horizontal wells should become more cost effective.

NOMENCLATURE

A - Cross sectional area to flow

D - distance from the external boundary to the center of the wellbore

E_D - displacement efficiency

E_s - areal sweep efficiency

h - formation thickness

J - productivity index

J_{LP} - productivity index for a partial horizontal well

J_R - productivity index for a vertical well, radial flow

J_{100} - productivity index for a horizontal well where $L/r_e = 100\%$

k - permeability

$k_{absolute}$ - absolute permeability

L - length of horizontal wellbore

M - mobility ratio

P_e - pressure at boundary of drainage radius

PR - ratio of productivity index for a horizontal well to the productivity index for a vertical well

PR_{20} - ratio of productivity indices for horizontal wells where $L/r_e < 20\%$

PR_{100} - ratio of productivity indices for horizontal wells where $L/r_e = 100\%$

P_w - pressure at the wellbore

Q - flowrate

Q_L - flow rate - linear flow

Q_{LP} - flow rate - partial horizontal well

NOMENCLATURE (Cont'd)

Q_R - flow rate - radial flow

Q_{100} - flow rate - horizontal well where $L/r_e = 100\%$

r_e - reservoir or drainage radius

R_f - recovery factor

r_w - wellbore radius

S_{oi} - initial oil saturation

S_{or} - residual oil saturation, as defined by the endpoint on the relative permeability curve

v - flood front velocity

B - formation volume factor

μ - viscosity

L/r_e - length of horizontal well in proportion to the drainage radius, or pattern size

REFERENCES

1. Joshi, S.D., and Threlkeld, C.B., "Laboratory Studies of Thermally Aided Gravity Drainage Using Horizontal Wells", presented at the fifth Annual Advances in Petroleum Recovery and Upgrading Technology Conference, Calgary, Alberta (June 14 & 15, 1984).
2. Butler, R.M., "The Potential of Horizontal Wells", presented at the fifth Annual Advances in Petroleum Recovery and Upgrading Technology Conference, Calgary, Alberta (June 14&15, 1984).
3. Stalkup Jr., Fred I., "Miscible Displacement", SPE Monograph Volume 8. (1983).
4. Settari, A., Price, H.S. and Dupont, T., "Development and Testing of Variational Methods for Simulation of Miscible Displacement in Porous Media", Soc. Pet. Eng. J. (June 1977), 228-44.
5. Habermann, B., "The Efficiency of Miscible Displacement as a Function of Mobility Ratio", Trans. AIME (1960), 219, 264; Miscible Processes, Reprint Series, SPE, Dallas (1965) 8, 205-14.
6. Claridge, E.L. "Prediction of Recovery in Unstable Miscible Flooding", Soc. of Pet. Eng. J. (April 1972) 143-155.
7. Craft, Holden & Graves, "Well Design, Drilling & Production", Prentice-Hall Inc., New Jersey, (1962), 494.
8. Diger, F.M. and Jourdan, A.P., "The Four Horizontal Wells Producing Oil in Western Europe", presented at the fifth Annual Advances in Petroleum Recovery and Upgrading Technology Conference, Calgary, Alberta (June 14&15, 1984).
9. Churchill, Ruel V., Brown, James W., and Verhey, Roger F., "Complex Variables and Applications", McGraw-Hill Book Co., 3rd ed.
10. Craft and Hawkins, "Applied Petroleum Engineering", Prentice-Hall, Inc., 1959.

Appendix 1: Improvement In Productivity Using Horizontal Wells

Definition of 'Productivity Index'

The 'productivity Index' may be defined as the ratio of the production rate over the pressure drawdown when the system is at steady-state (i.e. an external source exists) or speudo-steady-state conditions, that is:

$$\text{Productivity Index, } J = \frac{Q}{Pe-Pw}$$

Derivation of flow equations

(a) Horizontal wells (L = 100%), and vertical wells

The production rate, Q, may be obtained from steady-state flow equations:(10)

Linear flow:

$$Q_L = \frac{1.127\ kA(Pe-Pw)}{\mu \cdot B \cdot D} \qquad \text{.... (2)}$$

Radial flow:

$$Q_R = \frac{7.08\ kh(Pe-Pw)}{\mu \cdot B(\ln r_e/r_w)} \qquad \text{.... (3)}$$

When considering the flow geometry in the case of a horizontal or vertical producer (as illustrated in Fig. A1), Equation (2) and (3) can be expressed as:

(i) Full length horizontal well (wellbore extends over the entire length of a 5-spot pattern)

$$\frac{Q_{100}}{2} = \frac{1.127\ k(2Lh)(Pe-Pw)}{\mu \cdot B \cdot L} \qquad \text{.... (4)}$$

(ii) Vertical well - full pattern

$$Q_R = \frac{7.08\ kh(Pe-Pw)}{\mu\ B(\ln r_e/r_w)} \qquad \text{.... (5)}$$

where: L = the half length of a horizontal wellbore

r_e = reservoir radius

D = distance from the external boundary to the center of the wellbore

h = formation thickness

(b) Partial horizontal wellbore

The equation applicable to flow into a horizontal well that does not extend over the entire length of the full pattern (i.e., partial length horizontal wells), can be derived using the following coordinate transformation(9) as illustrated in Fig. A2.

$$x = L(\cosh u)(\cos v) \qquad \text{.... (6-a)}$$

$$y = L(\sinh u)(\sin v) \qquad \text{.... (6-b)}$$

It should be noted that this transformation does not exactly represent a circular boundary when transferring from the u-v plane back to the x-y plane. As the ratio of L/r_e increases (the length of the horizontal wellbore increases with respect to the pattern length), the circular boundary becomes more elliptual in shape, this deviation being due to the different values of the hyperbolic sine and hyperbolic cosine. However, for a horizontal wellbore with a length of less than 20% of the pattern width (i.e. $L/r_e \leq 0.2$), the error in this transformation is less than 2%.

The use of this transformation results in the following equation to describe flow:

Partial horizontal well - quarter pattern

$$Q_{LP} = \frac{1.127\ kA(Pe-Pw)}{\mu\ B\ D}$$

$$= \frac{1.127\ k(h\ \pi/2)(Pe-Pw)}{\mu \cdot B \cdot Ue} \qquad \text{....(7-a)}$$

where $U_e = \cosh^{-1}(r_e/L)$

Therefore:

$$Q_{LP} = \frac{1.127\ k(h\ \pi/2)(Pe-Pw)}{\mu \cdot B \cdot \cosh^{-1}(r_e/L)} \qquad \text{.... (7-b)}$$

Since the definition of the inverse hyperbolic cosine is:

$$\cosh^{-1} u = \ln(u+\sqrt{u^2-1}),\ \text{for } u \geq 1 \qquad \text{..... (8-a)}$$

the $\cosh^{-1}(r_e/L)$ term in the denominator of Equation (7-b) may be re-written as:

$$\cosh^{-1}(r_e/L) = \ln\left(\frac{r_e}{L} + \sqrt{\left(\frac{r_e}{L}\right)^2 - 1}\right) \qquad \text{.. (8-b)}$$

For $r_e/L \gg 1$,

$$\cosh^{-1}(r_e/L) = \ln(2 \cdot r_e/L)$$

$$= \ln\ (r_e/(L/2)) \qquad \text{.... (8-c)}$$

Substituting into Equation (7-b), for flow into a partial horizontal well in a quarter pattern,

$$Q_{LP} = \frac{1.127(h\ \pi/2)k(Pe-Pw)}{\mu \cdot B \cdot \cosh^{-1}(r_e/L)} \qquad \text{.... (9-a)}$$

$$= \frac{1.77\ kh(Pe-Pw)}{\mu \cdot B \cdot \ln(r_e/(L/2))} \qquad \text{.... (9-b)}$$

For a full pattern:

$$Q_{LP} = \frac{7.08\ kh(Pe-Pw)}{\mu \cdot B \cdot \ln\ (r_e/(L/2))} \qquad \text{.... (10)}$$

Productivity Indices

To this point, 3 equations, (4), (5) and (10) have been derived to represent flow from 3 different types of wellbores: vertical, partial horizontal, and full length horizontal. These equations may be re-written in the form $Q/\Delta p$ to express the productivity index in each case:

i) Vertical well - point source, full pattern

$$J_R = \frac{Q_R}{(Pe-Pw)}$$

$$= \frac{7.08\ kh}{\mu B \cdot \ln(r_e/r_w)} \qquad \text{.... (11)}$$

ii) Partial horizontal well (for $L \leq 0.2\ r_e$)

$$J_{LP} = \frac{Q_{LP}}{(Pe-Pw)}$$

$$= \frac{7.08\ kh}{\mu B \cdot \ln(r_e/(L/2))} \qquad \text{.... (12)}$$

iii) Full length horizontal well ($L = 1.0\ r_e$)

$$J_{100} = \frac{Q_{100}}{(Pe-Pw)}$$

$$= \frac{4.508\ kLh}{\mu \cdot B \cdot L} \qquad \text{.... (13)}$$

The improvement in productivity index that may be expected by using a horizontal wellbore of some length may be denoted by the ratio of the productivity indices for horizontal and vertical wells. That is:

Productivity Ratio = PR

$$= \frac{J_{horizontal}}{J_{vertical}}$$

For horizontal wellbores with lengths of up to 20% of the pattern length, the ratio may be expressed as:

$$PR_{20} = \frac{7.08\ kh/[\mu B \cdot \ln(r_e/(L/2))]}{7.08\ kh/(\mu B \cdot \ln(r_e/r_w))}$$

$$= \frac{\ln(r_e/r_w)}{\ln(2 \cdot r_e/L)} \quad .... \ (14)$$

For horizontal wellbores extending over 100% of the pattern length,

$$PR_{100} = \frac{(4.508\ kLh)/(\mu B \cdot L)}{(7.08\ kh)/(\mu B \cdot \ln(r_e/r_w))}$$

$$= 0.6367 \ln(r_e/r_w) \quad .... \ (15)$$

Equations (14) and (15) may be used to produce a plot of

$$PR*1/(\ln r_e/r_w) \quad \text{vs.} \quad L/r_e$$

However, since the value of $1/\ln(r_e/r_w)$ is very close to 7.6 for 40 acre spacing, it is simpler to plot $7.6 * PR \cdot 1/\ln(r_e/r_w)$. This plot is shown in Fig. 17.

The points for $L/r_e \leq 0.2$ and $L/r_e = 1.0$ may be calculated directly from Equations (14) and (15) and the remainder of the curve was produced using a least squares curve- fitting technique with the criteria that the curve must increase monotonically. The equations used to produce the curve are:

For $L/r_e \leq 20\%$,

$$PR\left(\frac{1}{\ln(r_e/r_w)}\right) = \frac{1}{\ln(2 \cdot r_e/L)} \quad ... \ (16)$$

For $L/r_e > 20\%$,

$$PR\left(\frac{1}{\ln(r_e/r_w)}\right) = 0.1954 + 1.5963\left(\frac{L}{r_e}\right) - 2.2421\left(\frac{L}{r_e}\right)^2 + 1.4332\left(\frac{L}{r_e}\right)^3 - 0.34625\left(\frac{L}{r_e}\right)^4 \quad .... \ (17)$$

The assumptions inherent in these calculations is that the formation is relatively thin, or has a high vertical permeability. Otherwise, the use of the PR curve shown here may give optimistic estimates of the increase in productivity ratio that may be expected using a horizontal wellbore.

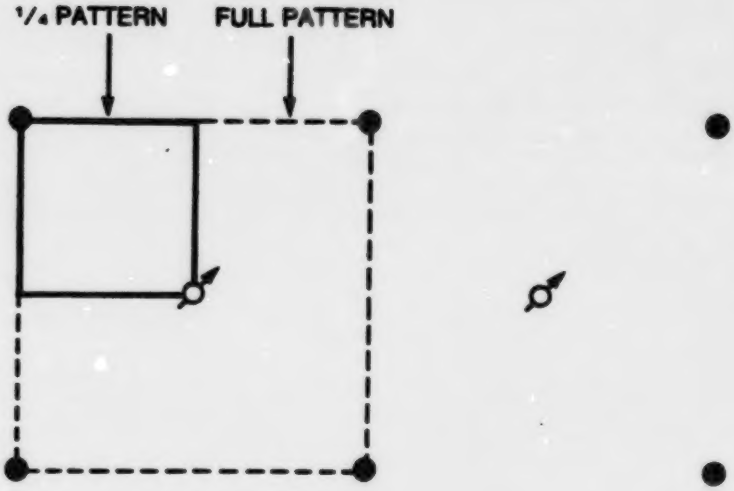
1/4 PATTERN
FULL PATTERN

FIGURE 1
5 – SPOT OR STAGGERED LINE DRIVE PATTERN

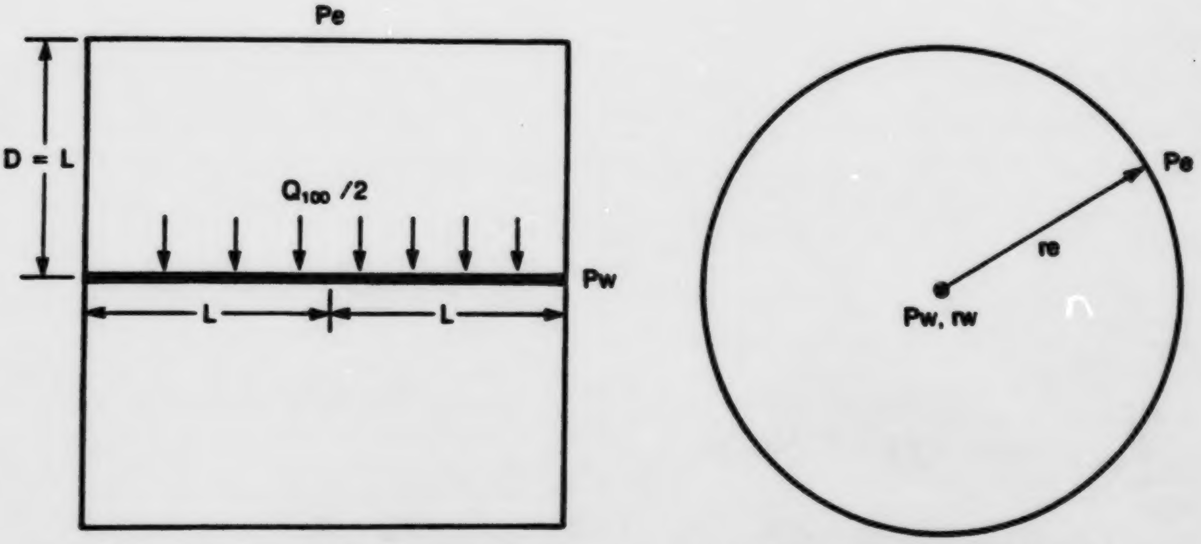
Pe
D = L
Q_{100} /2
Pw
L
L
Pe
re
Pw, rw

(a) FULL LENGTH HORIZONTAL PRODUCER (LINEAR FLOW)

(b) VERTICAL PRODUCER (RADIAL FLOW)

FIGURE A1
LINEAR & RADIAL FLOW CASES

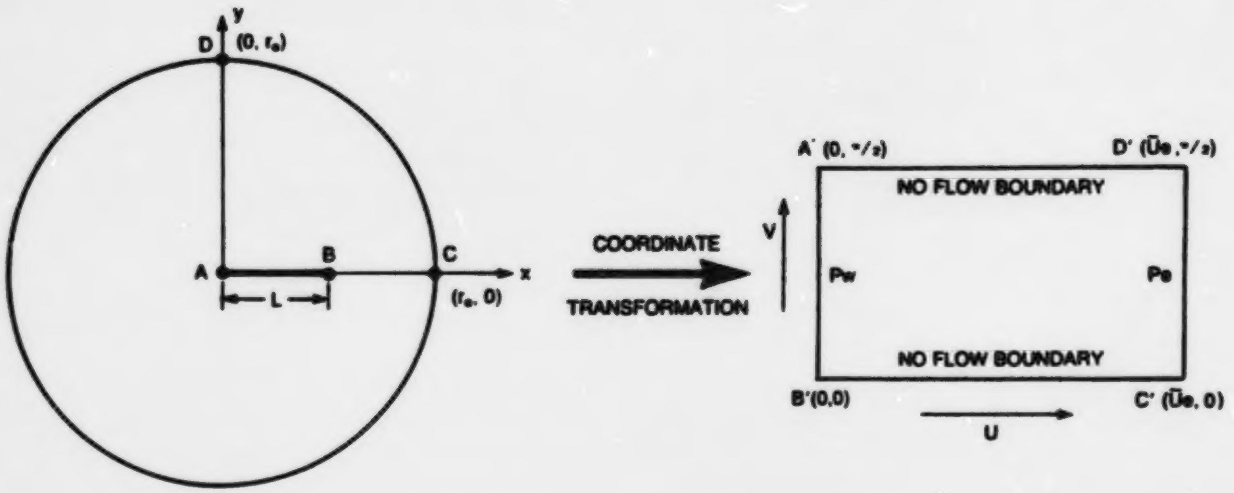
y
D
(0, r_e)
A
B
C
x
L
(r_e, 0)
COORDINATE
TRANSFORMATION
A' (0, $\pi/2$)
D' ($\bar{U}e$, $\pi/2$)
NO FLOW BOUNDARY
V
Pw
Pe
NO FLOW BOUNDARY
B'(0,0)
C' ($\bar{U}e$, 0)
U

FIGURE A2
COORDINATE TRANSFORMATION

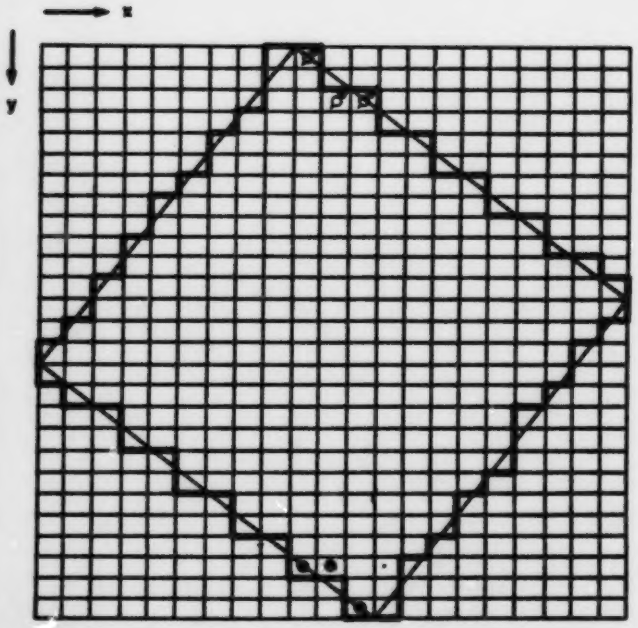

21 × 27
● - PRODUCER
ϭ - INJECTOR

FIGURE 2
GRID USED FOR L/r_e = 25 %

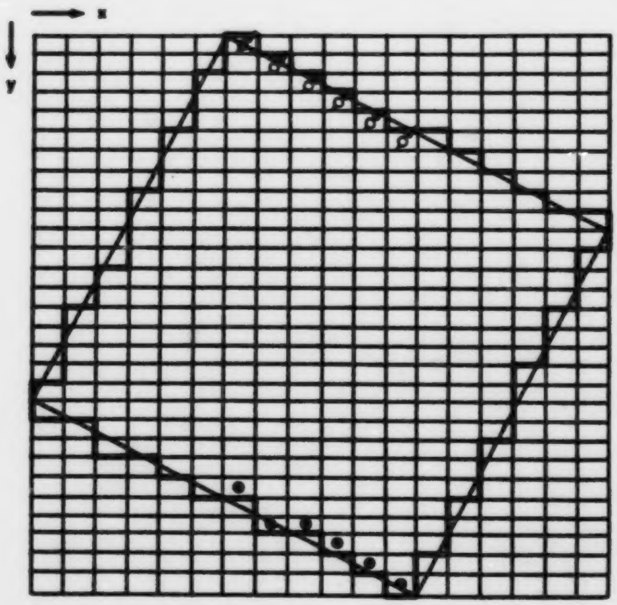

18 × 29
● - PRODUCER
ϭ - INJECTOR

FIGURE 3
GRID USED FOR L/r_e = 50 %

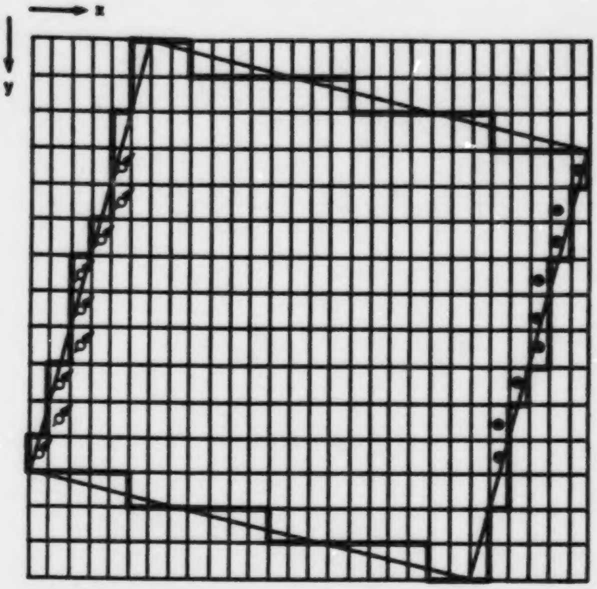

28 × 15
● – PRODUCER
ø – INJECTOR

FIGURE 4
GRID USED FOR $^{L}/r_e$ = 75 %

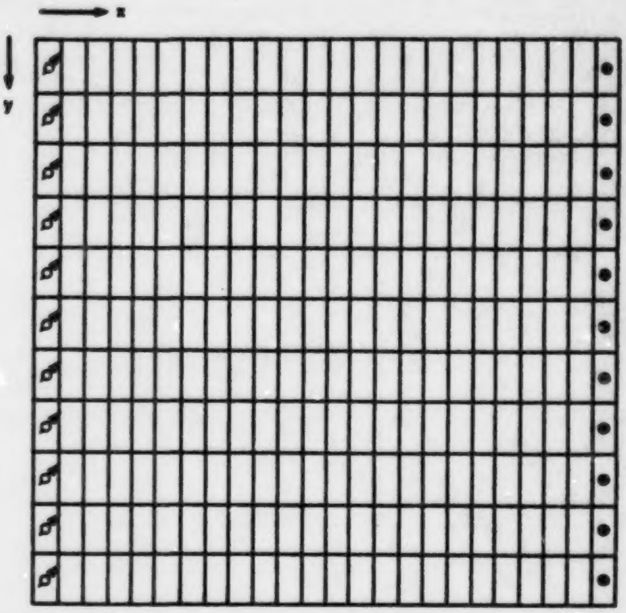

24 × 11
● – PRODUCER
ø – INJECTOR

FIGURE 5
GRID USED FOR $^{L}/r_e$ = 100 %

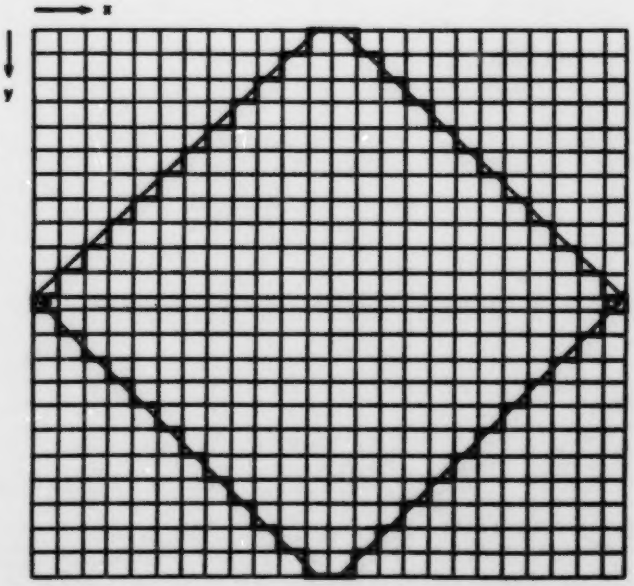

24 × 23
● – PRODUCER
ø – INJECTOR

FIGURE 6
POINT SOURCE GRID

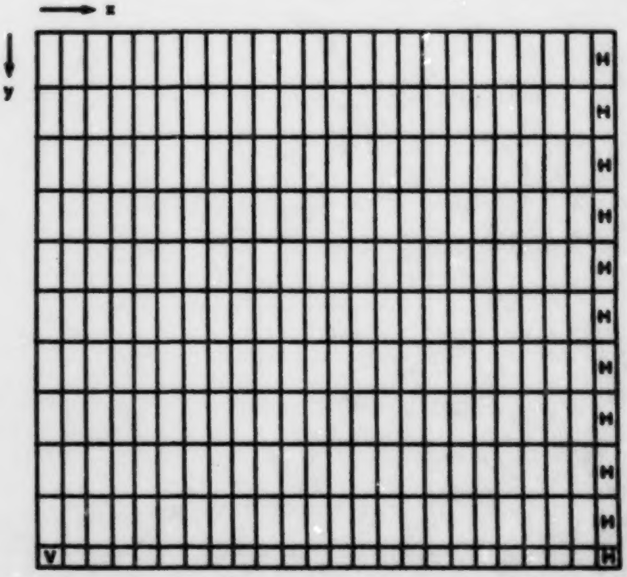

24 × 11
V – VERTICAL WELL
H – HORIZONTAL WELL

FIGURE 7
GRID USED FOR HORIZONTAL/
VERTICAL WELL COMBINATION

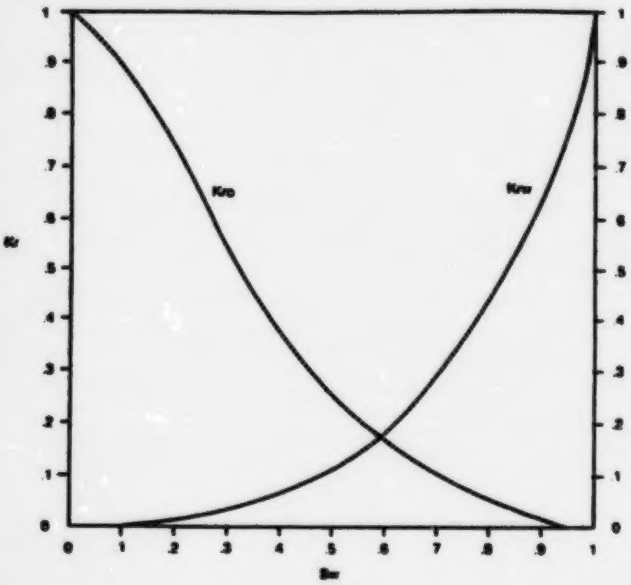

FIGURE 8

WATER-OIL RELATIVE PERMEABILITY CURVES

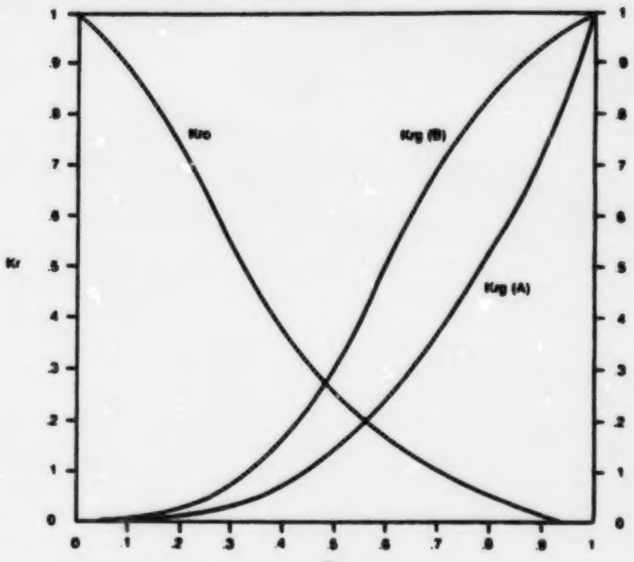

krg (A) - Used in this study to match published results

krg (B) - Sensitivity case curve

FIGURE 9

GAS-OIL RELATIVE PERMEABILITY CURVES

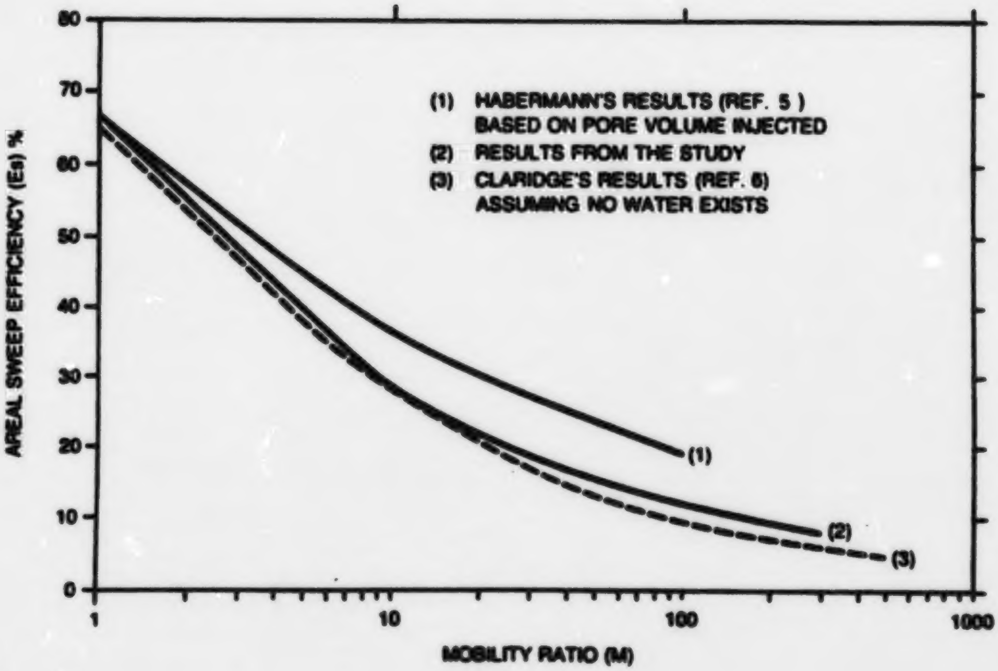

FIGURE 10

AREAL SWEEP EFFICIENCY VS MOBILITY RATIO
VERTICAL WELLS ONLY
RESULTS FROM THIS STUDY VS PUBLISHED DATA

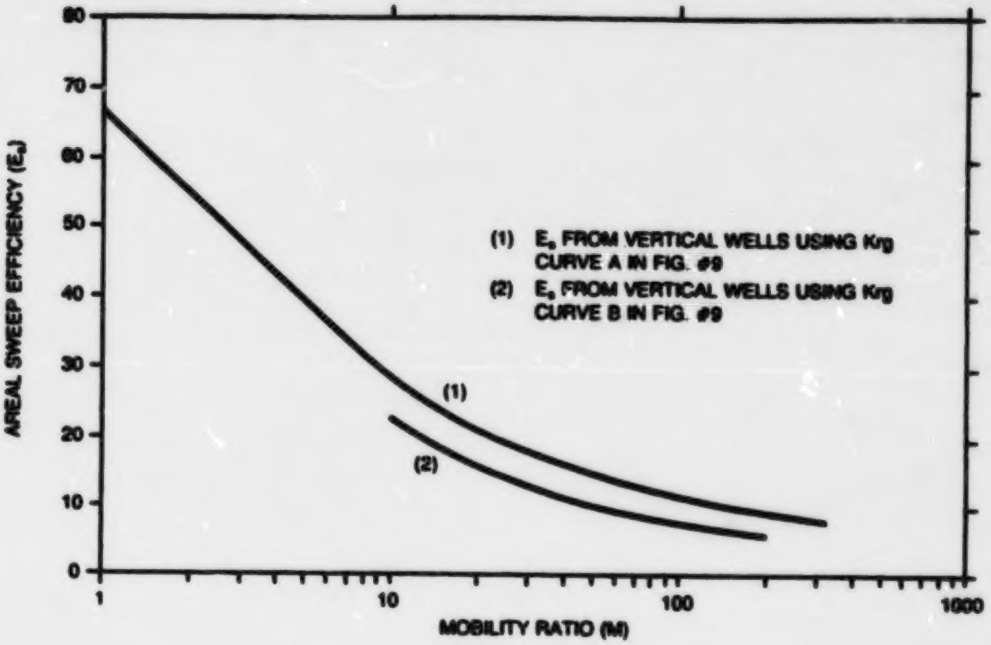

FIGURE 11
AREAL SWEEP EFFICIENCY SENSITIVITY TO SHAPE OF REL. PERM. CURVE

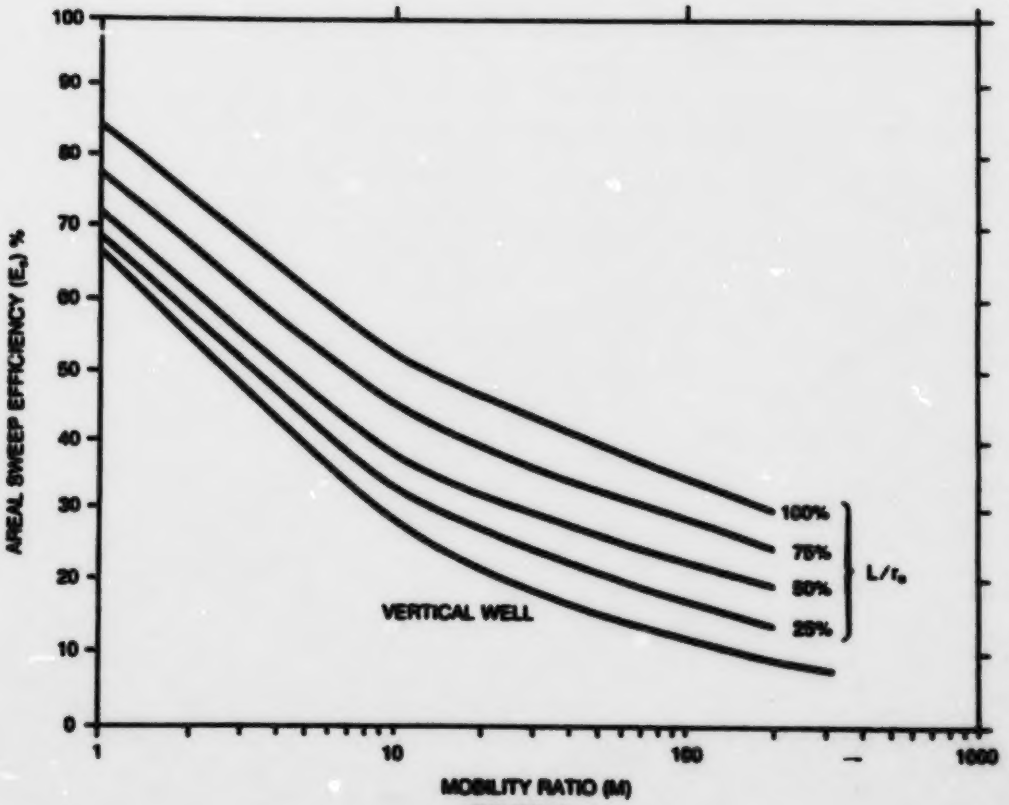

FIGURE 12
E_a VS M FOR VARIOUS WELLBORE LENGTHS

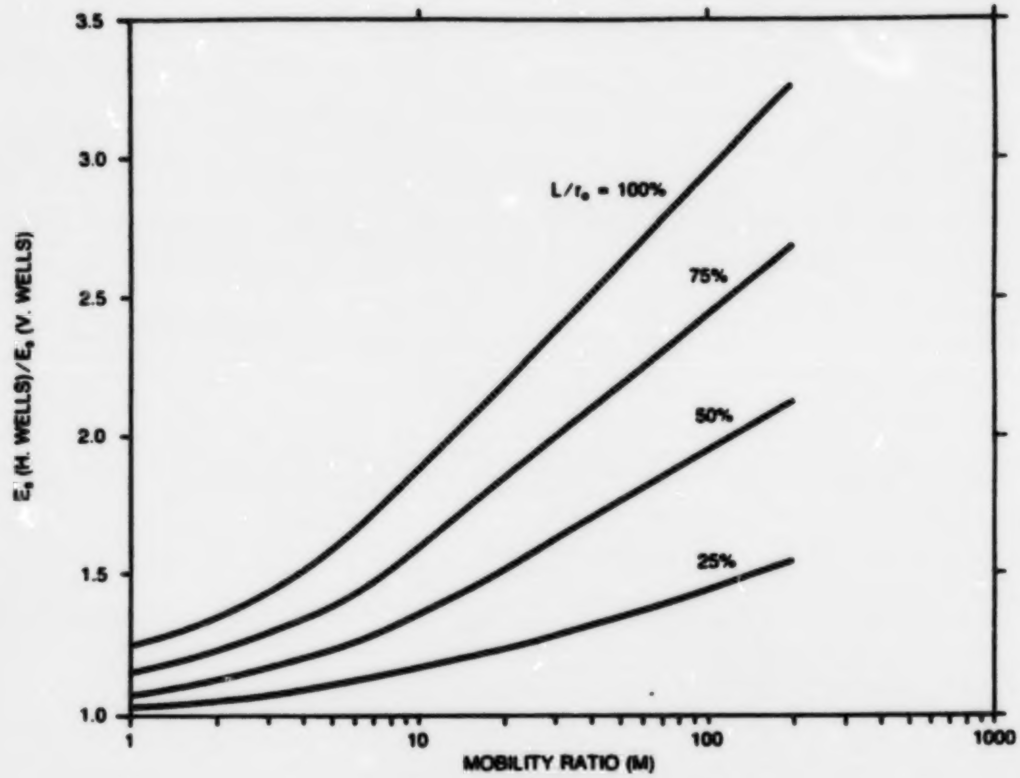

FIGURE 13

E_a HORIZONTAL/E_a VERTICAL VS M FOR VARIOUS WELLBORE LENGTHS

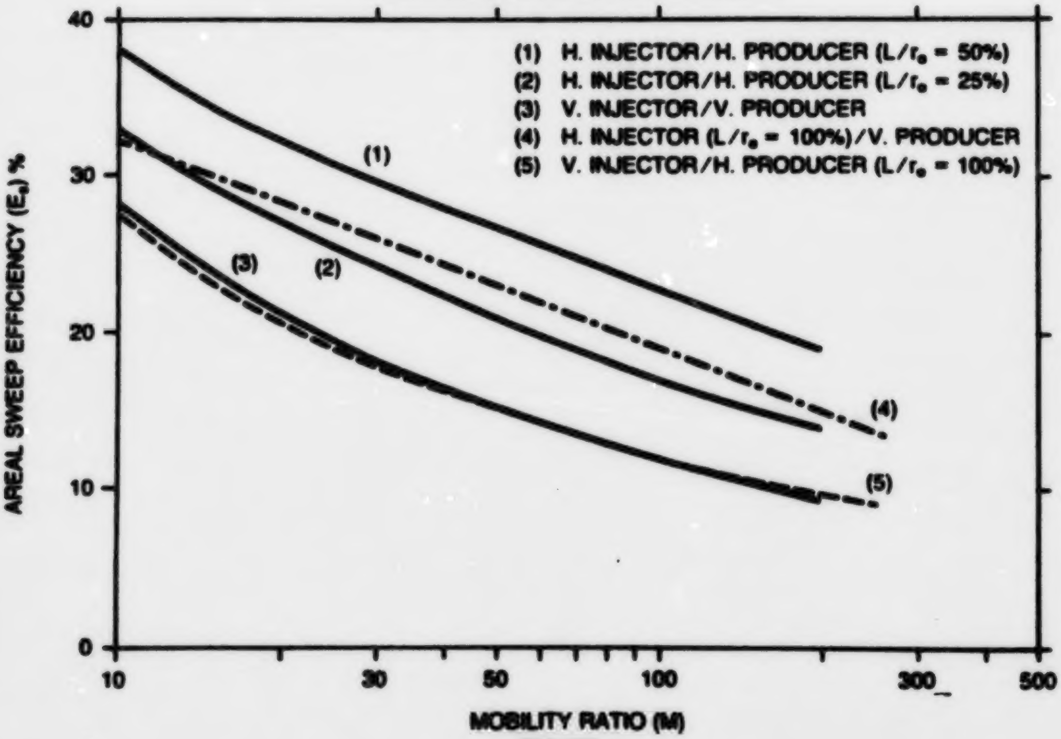

FIGURE 14

E_a VS M FOR HORIZONTAL/ VERTICAL WELL COMBINATIONS

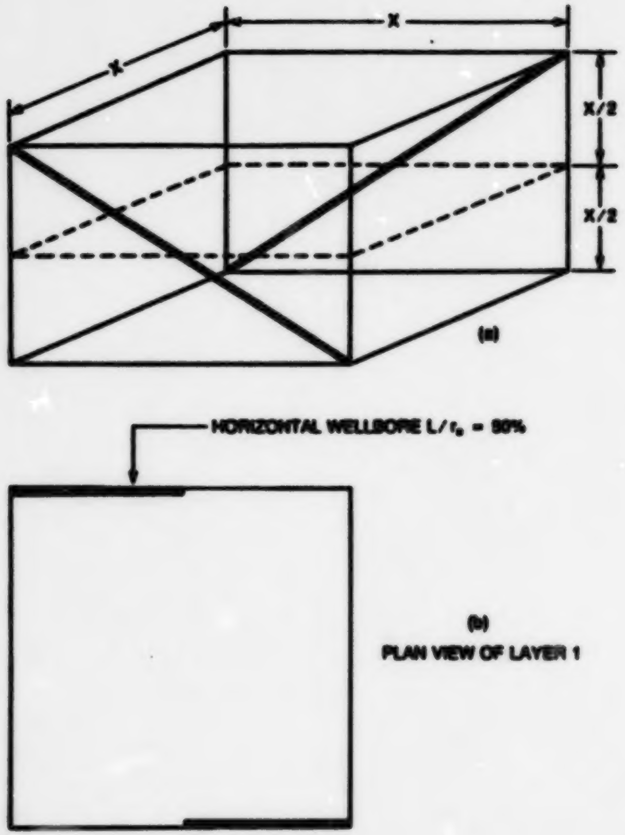

X
X
X/2
X/2
(a)
HORIZONTAL WELLBORE L/r_e = 90%

(b)
PLAN VIEW OF LAYER 1

FIGURE 15
TILTED HORIZONTAL WELLS IN
A 2 – LAYER RESERVOIR

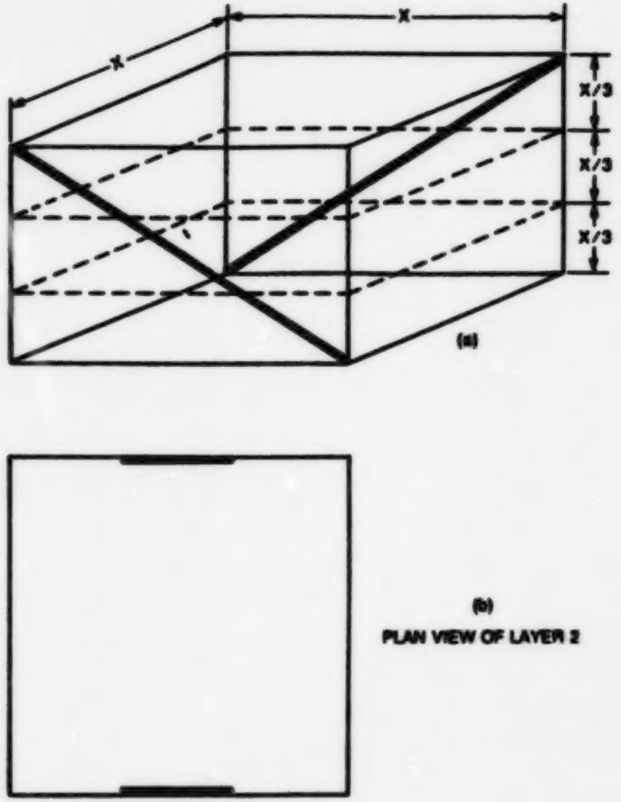

(b)
PLAN VIEW OF LAYER 2

FIGURE 16
TILTED HORIZONTAL WELL IN
A 3 – LAYER RESERVOIR

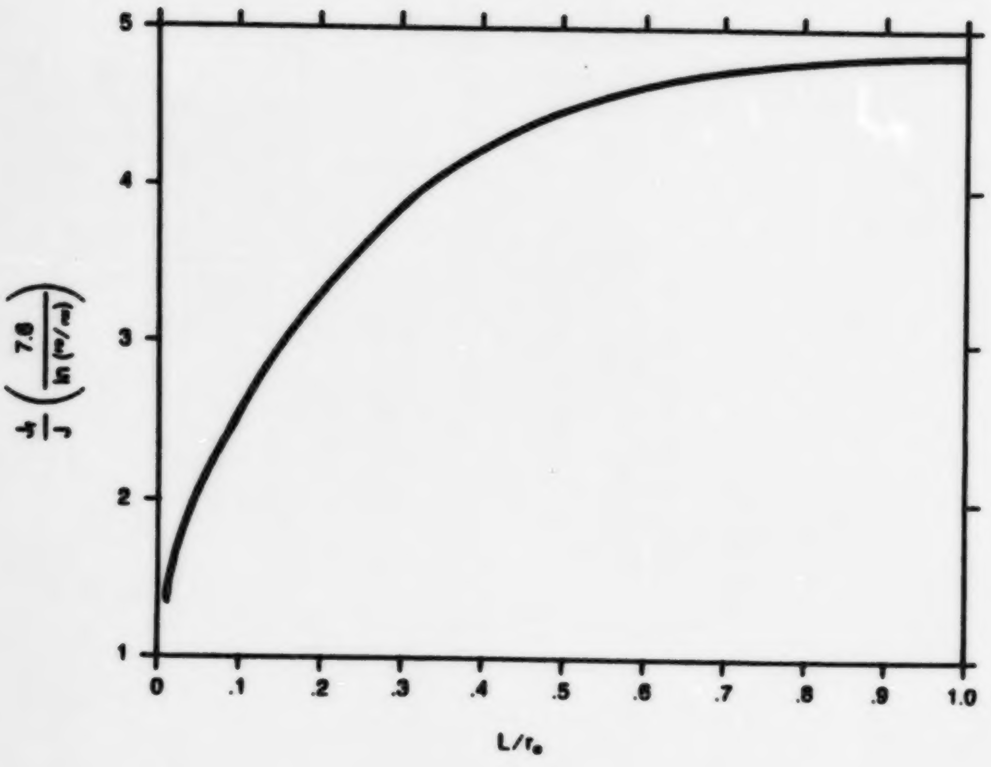

FIGURE 17

PRODUCTIVITY INDEX INCREASE Vs. WELLBORE LENGTH

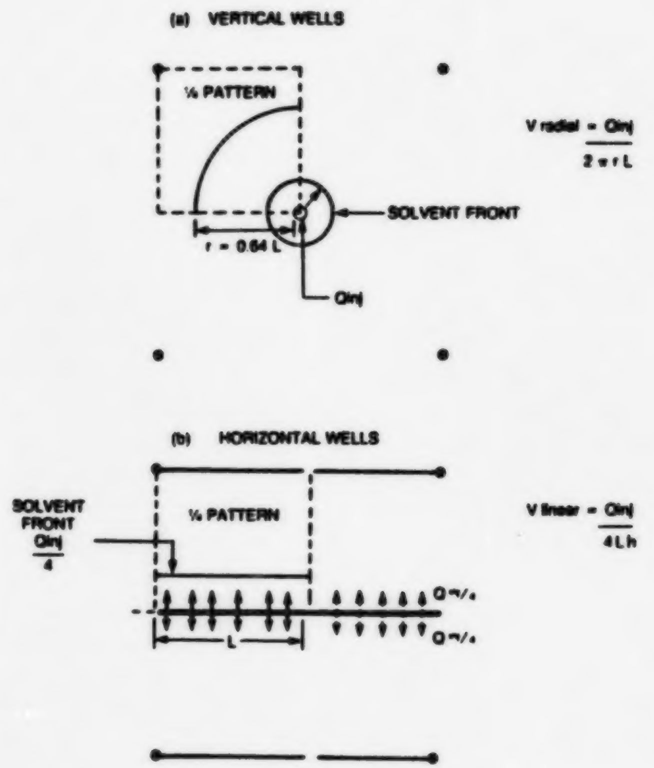
(a) VERTICAL WELLS
¼ PATTERN
r = 0.64 L
SOLVENT FRONT
Qinj
$V_{radial} = \frac{Qinj}{2 \pi r L}$
(b) HORIZONTAL WELLS
¼ PATTERN
SOLVENT FRONT
$\frac{Qinj}{4}$
L
$Q_{inj/4}$
$Q_{inj/4}$
$V_{linear} = \frac{Qinj}{4 L h}$

FIGURE 18
RADIAL & LINEAR FLOW IN
A 5 – SPOT QUARTER PATTERN

SPE
Society of Petroleum Engineers of AIME

91

SPE 13091

A Comparative Evaluation of Vertical and Horizontal Drainage Wells for the Degasification of Coal Seams

by G.R. King and T. Ertekin, *Pennsylvania State U.*

SPE Members

Copyright 1984 Society of Petroleum Engineers of AIME

This paper was presented at the 59th Annual Technical Conference and Exhibition held in Houston, Texas, September 16–19, 1984. The material is subject to correction by the author. Permission to copy is restricted to an abstract of not more than 300 words. Write SPE, 6200 North Central Expressway, Drawer 64706, Dallas, Texas 75206 USA. Telex 730989 SPEDAL.

ABSTRACT

A two-phase, single well numerical simulator capable of modeling the performance of either vertical wells, or horizontal wellbores drilled from a vertical shaft, has been developed. For the vertical wells, the model allows for the prediction of post-fracture performance. The hydraulically induced fractures can be specified as either infinite conductivity or finite (constant) conductivity, so that conventional, as well as massive treatments, can be modeled.

For the horizontal boreholes the problem is idealized as N infinite conductivity boreholes distributed uniformly around a vertical shaft and extending radially outward. The problem is then reduced by considering a symmetric element defined by θ_{sym}. The value of θ_{sym} is solely dependent on the value of N. This symmetric element can then be modeled in radial coordinates by placing a single horizontal borehole along $\theta=0$, and a no flow boundary along $\theta=\theta_{sym}$.

For coal seams, the formation to be modeled is a dual porosity reservoir. The natural fracture network of the coal seam (the butt and face cleat) has been assigned an effective porosity and permeability. A time dependent, quasi-steady state sorption term has been included to describe the phenomenon of gas desorbing from the formation matrix to the fracture network.

All the equations generated by the model are solved simultaneously by the fully implicit, Newton-Raphson procedure. Both the numerical and mathematical developments are presented in detail.

The model has been used to sift through the many parameters associated with the two production schemes in order to determine those which most significantly affect production. Where possible these parameters, along with their effects, are put into dimensionless form, and type curves for predicting recovery, based on these dimensionless groups are presented. Finally, a comparison between the performance of vertical drainage wells and horizontal boreholes, using field data, is made.

References and illustrations at end of paper.

INTRODUCTION

The use of vertical wells for the drainage of methane from coal seams prior to mining operations was suggested by Rice[1] in 1928. In the ensuing years, many methods of methane production have been employed with varying degrees of success. Two of the more promising methods are:

1. Methane drainage via vertical boreholes from the surface.
2. Methane drainage via horizontal boreholes from shaft bottoms.

Of these two methods, the use of vertically oriented wells is more common.[2-10] In this technique, degasification wells are drilled and completed several years prior to mining. Vertical wells are generally hydraulically stimulated to increase the permeability of the coal seam in the vicinity of the wellbore.

The hydraulic stimulation process consists of the high pressure injection of a fluid (commonly water, gelled water, or foam) and a propant down the wellbore and into the formation. The fluid is used to widen and extend the coal seam cleat (the natural fractures inherent to all coal seams), while the propant is used to keep the fractures open once pressure is released. This differs from a conventional hydraulic fracturing treatment, in that, the fluid does not mechanically fracture the formation but simply opens pre-existing fractures.

Vertical wells are also used to drain methane from previously mined areas, when a gas bearing overburden is present.[3,11,12] In this technique wells are drilled into the porous, but not necessarily permeable, roof rock. After pillaring, the unsupported roof collapses into the mine, creating a highly permeable rubble (gob). Gas is released during the collapse of the roof and travels through the gob to the drainage wells. Hydraulic stimulation of these gob degasification wells has also been attempted[13], however unsatisfactory results were obtained.

Although the use of vertical drainage wells has the advantages of simplicity, low drilling costs, and low maintenance costs, there are several disadvantages associated with this technique. Due to the permeability anisotropy which exists in virgin coal masses, some operators[14] believe that only a long narrow volume, parallel to the direction of greatest permeability, will be drained. For vertical wells to be successful, therefore, the hydraulically induced fracture must be oriented perpendicular to the direction of greatest permeability. Also, if the seam to be produced is minable, the hydraulic fracture must remain contained within the formation.[5] A poorly designed stimulation treatment could cause irreparable damage to the roof rock, rendering the seam unminable in the vicinity of the well.

When producing methane from a shaft bottom, several 100 to 2000 ft, horizontal boreholes are drilled radially outward.[3,5,15,16] Gas production from these horizontal boreholes ranges from 100 to 450 SCF/day per linear foot of hole.[3,5] The major advantage of this technique is that the direction of the boreholes can be controlled, so that at least one borehole is guaranteed to be oriented perpendicular to the direction of greatest permeability.

There are also several operational problems associated with this production scheme. In order to use horizontal boreholes, the seam must be thick and free of faults, to ensure that the boreholes remain in the seam.[17] Also, underground tubing, drilling, and gathering systems often interfere with mining activity.

COAL SEAMS AS NATURAL GAS RESERVOIRS

The reservoir engineering aspects of coal seams have previously been reported,[12,18-20] however, a brief description will be given here.

Coal seams are characterized by a dual porosity nature, in which they contain both a micropore (primary porosity) and a macropore (fracture porosity) system. The micropore system in coal seams has the same role as the matrix (primary) porosity in "conventional" dual porosity reservoirs, that is, it has a large storage capacity but contributes very little to the long distance transportation of reservoir fluids.

Although the role of the primary porosity is the same in coal seams and "conventional" dual porosity reservoirs, there are two major differences. The first is that while the gas stored in the matrix of "conventional" dual porosity reservoirs is free gas, which obeys the real gas law, the gas stored in the micropores of a coal seam is in an adsorbed state, and thus, obeys an entirely different set of laws. The second difference is that due to the size of the micropores (generally, the average diameter is less than 20 Å[21]), the principle transport mechanism through the primary porosity is a diffusion process.

The macropore system of a coal seam is made up of the volume occupied by natural fractures (cleat). The fracture spacing is very uniform, ranging from a fraction of an inch to several inches. Two distinct fracture types exist in coal seams. The face cleat is continuous throughout the seam, while the butt cleat is generally discontinuous, ending at [illegible] intersection with the face cleat. Figure 1 is a schematic representation of the macropore system in a coal seam.

Homogeneous, unfractured coal is relatively impermeable to gas and water. The in-situ permeability of large coal masses; therefore, is due to the macropores. The dependence of the permeability on the cleat leads to the anisotropy exhibited by most coal seams, with the direction of greatest permeability oriented parallel to the continuous face cleat.

DESCRIPTION OF THE NUMERICAL MODEL

The numerical model used in this study has been discussed and validated in previous papers[20,22], and it is similar to those used by Boyer et al.[23] and Pavone and Schwerer.[24]

The equations used in the model are:

$$\nabla_a \cdot \left(\frac{k_{rg} k_a}{\mu_g} \frac{P_{ag}}{z} \nabla_a P_{ag}\right) = \frac{\partial V_i}{\partial t} + \frac{\partial}{\partial t}\left(\frac{\phi_a S_{ag} P_{ag}}{z}\right) \quad (1)$$

$$\nabla_a \cdot \left(\frac{k_{rw} k_a}{\mu_w B_w} \nabla_a P_{aw}\right) = \frac{\partial}{\partial t}\left(\frac{\phi_a S_{aw}}{B_w}\right) \quad (2)$$

$$\frac{\partial V_i}{\partial t} = -D_i a(V_i - V_E(P_{ag})) \quad (3)$$

$$V_E(P_{ag}) = \frac{V_L P_{ag}}{P_L + P_{ag}} \quad (4a)$$

or

$$V_E(P_{ag}) = HP_{ag} \quad (4b)$$

$$P_{cgw}(S_{ag}) = P_{ag} - P_{aw} \quad (5)$$

$$S_{ag} + S_{aw} = 1.0 \quad (6)$$

In these equations, the subscripts "a" and "i" refer to the macropores and micropores, respectively. All variables are defined in the nomenclature. The development of these equations is presented in detail in reference (20), while theoretical considerations are given in Appendices A, B, and C of this paper.

The finite difference approximations to Equations (1) through (6) are obtained by a conventional seven point, mesh centered formulation. The resulting approximations are reduced to two nonlinear algebraic equations in two principle unknowns, P_{ag} and S_{ag}. The two nonlinear equations are then solved simultaneously using the fully implicit, Newton-Raphson procedure.

Hydraulic Fracture Formulations

The differential operator in Equations (1) and (2), ∇_a, acts on the macropore pressure and is dependent on the coordinate geometry being used in the simulation. The model described in this paper allows for elliptical, rectangular, and radial coordinate systems.

The use of elliptical coordinates for reservoir flow problems has been discussed in detail in the petroleum literature.[25,25] For an anisotropic coal seam containing a vertical well or for an isotropic coal seam containing an infinite conductivity fracture, the isopotential and streamlines lie on constant values of the elliptical coordinates ξ and η. Thus, for the situations listed above, the use of elliptical geometry reduces the flow problem to one spatial dimension, with the wellbore or fracture treated as an internal boundary. Figure 2 shows the elliptical geometry in the presence of an infinite conductivity fracture.

For finite conductivity fractures, a convenient coordinate system does not exist. The use of rectangular coordinates for finite conductivity fracture models has been discussed extensively.[27-29] In this approach, a quarter of the drainage volume is modeled, with a long, narrow row of mesh points representing the hydraulic fracture. These fracture nodes are assigned the permeability and porosity values of the propant. The wellbore boundary condition is imposed along the width of the first fracture node. Figure 3 shows a finite conductivity fracture in a rectangular grid model.

The method described above is not directly applicable in radial coordinates, due to the divergent nature of the radii. Figure 4 shows the fracture representation in radial coordinates. To compensate for the increasing width of the fracture, Murtha and Ertekin[30] made the following development for finite conductivity fractures in radial coordinate geometry.

Starting with the definition of dimensionless conductivity[31]:

$$C_{Df} = \frac{k_f\, w_f}{k_a\, x_f} \qquad (7)$$

Keeping the conductivity constant along the divergent fracture wedge leads to the following expression:

$$k_{f_j}\, w_{f_j} = k_f\, w_f \qquad j=1,2,\ldots NJFRAC \qquad (8)$$

The "width" of the j^{th} node can be defined as the arclength at the node's radius:

$$w_{f_j} = 2r_j\Delta\theta_1 \qquad j=1,2,\ldots NJFRAC \qquad (9)$$

The factor 2 in Equation (9) is due to the symmetry across the boundary at $\theta=0$. Substituting Equation (9) into Equation (8) and rearranging:

$$k_{f_j} = \frac{k_f\, w_f}{2r_j\Delta\theta_j} \qquad j=1,2,\ldots NJFRAC \qquad (10)$$

Equation (10) gives the expression for the permeability of the j^{th} node of the wedge representing the finite conductivity fracture.

Infinite conductivity fractures can also be modeled in cartesian and radial geometries by the use of sources and sinks, as suggested by Nghiem.[32] A comparison of the results of simulation runs for the three coordinate geometries is presented in Figure 5. The reservoir data for these simulations are presented in Table 1.

The simulation geometry is chosen by the user and is dependent on the problem to be solved. For example, in anisotropic coal seams, the rectangular geometry would be most appropriate, while for multiple fractures (such as those generated by explosive fracturing or tailored-pulse loading) the radial geometry would be used.

Horizontal Borehole Formulation

The horizontal boreholes considered in this study are infinite conductivity boreholes. The formulation for this type of borehole is similar to that for conventional, infinite conductivity fractures, with two essential differences. The first difference is due to the borehole not completely penetrating the entire width of the coal seam. This leads to cylindrical flow in the vicinity of the wellbores and must be accounted for in the model. Figure 6 shows the streamlines for flow to a fully penetrating fracture, a partially penetrating fracture, and a horizontal borehole. In order to represent flow to either a partially penetrating fracture or a horizontal borehole, a three dimensional simulation is required. Figures 7 and 8 show an actual borehole and its model representation in three dimensional rectangular and radial grids. Since the boreholes in the model are assumed to have infinite conductivity, the method of sources and sinks is still applicable.

Figure 8 illustrates the second major difference between the horizontal boreholes and conventional fractures, that is, more than two multiple boreholes may extend radially outward. If the coal seam is homogeneous (but not necessarily isotropic), and equal length wellbores are distributed uniformly about the perimeter of the vertical shaft, then a plane of symmetry exists at an angle of:

$$\theta_{sym} = \frac{\pi}{N}$$

from a borehole situated at $\theta=0$. In this equation N is the number of multiple boreholes to be simulated. The condition of homogeneity, which was stated above, implies that all the boreholes are opened to production simultaneously.

To model the symmetric element defined by θ_{sym}, a partially penetrating, infinite conductivity borehole is placed along $\theta=0$, while a no-flow boundary is placed across the entire width of $\theta=\theta_{sym}$. The borehole is nominally set midway between the topmost and bottommost bedding planes of the seam, however this can be overridden by the user. Finally, production into the shaft may or may not be permitted, at the user's discretion.

RESULTS

Single-Phase, Unstimulated Vertical Wells

For single-phase, conventional (single-porosity) gas wells the equations solved by the model, Equations (1) through (6), reduce to the standard equations used in well test analysis. The analytical solutions to these equations are well known,[33] however, Figure 9 is presented so that comparisons can be made between conventional gas wells and coal seam degasification wells. Since most coal seams are either produced into a pipeline or vented into the atmosphere, only the constant well pressure case will be considered in this study.

Figure 9 is a plot of the dimensionless flow rate, q_D, versus dimensionless time, t_{DR}, for various ratios of r_e/r_w. The curves in this figure were generated numerically using the model described in the previous sections. These curves indicate that the dimensionless flow rate, at a given dimensionless time, is solely dependent on the value of r_e/r_w.

For unstimulated degasification wells, Equations (1) through (6) reduce to:

$$\frac{1}{r_D}\frac{\partial}{\partial r_D}\left(r_D\frac{\partial m_D(P_a)}{\partial r_D}\right) = (1-\omega')\frac{\partial V_{1D}}{\partial t'_{DR}} + \omega'\frac{\partial m_D(P_a)}{\partial t'_{DR}} \qquad (11)$$

$$(1-\omega')\frac{\partial V_{1D}}{\partial t'_{DR}} = -\lambda'_R\,(V_{1D}-V_{ED}) \qquad (12)$$

where:

$$r_D = \frac{r}{r_w} \qquad (13)$$

$$t'_{DR} = \frac{2.636\times10^{-4}\,k_a t}{\left(\frac{2P_{sc}\,T\,V^*_E}{T_{sc}[m(P^*_a)-m(P_{wf})]} + \phi_a c^*_g \mu^*_g\right) r_w^2} \qquad (14)$$

$$m_D(P_a) = \frac{m(P^*_a) - m(P_a)}{m(P^*_a) - m(P_{wf})} \qquad (15)$$

$$\omega' = \frac{\phi_a c^*_g \mu^*_g}{\frac{2P_{sc}\,T V^*_E}{T_{sc}[m(P^*_a) - m(P_{wf})]} + \phi_a c^*_g \mu^*_g} \qquad (16)$$

$$\lambda'_R = \frac{316.14\,D_1 a P_{sc} T V^*_E r_w^2}{T_{sc}[m(P^*_a) - m(P_{wf})]\,k_a} \qquad (17)$$

Equations (11) and (12) are similar to the equations developed by Warren and Root[34] for "conventional" dual porosity reservoirs. The prime variables are parameters whose definitions are different than those presented in Warren and Root's original paper. These different definitions are necessary because of the differences in the micropore storage and transport as discussed in previous sections and in Appendices A and B.

In Equations (11) and (12), the variables containing the subscript "R" are variables whose definitions depend on radial geometry. For example, in the sections dealing with stimulated wells, the definition of dimensionless time, t'_D, will change. To distinguish between the dimensionless groups for unstimulated and stimulated wells, the subscripts "R" and "f" will be used, respectively.

The solutions to Equations (11) and (12) are much more complicated than those for conventional gas wells. These solutions depend on the parameters r_e/r_w, ω', and λ'_R, as well as the characteristics of the dimensionless sorption isotherm, V_{ED}. In order to keep the number of parameters manageable, only infinite acting ($r_e/r_w \to \infty$) coal seams will be considered. A typical solution for a seam of this type is presented in Figure 10.

Figure 10 shows the dimensionless flow rate into a vertical drainage well from an infinite acting coal seam. Plotted along with the production rate is the average dimensionless diffusion/desorption rate in the vicinity of the degasification well. From the results presented in this figure, three distinct time periods can be observed. In the first time period, the diffusion/desorption rate is low while the production rate is high. Thus, in this period the production rate is dominated by the depletion of the natural fractures. This period is then followed by a transitional period, in which, the diffusion/desorption rate becomes increasingly more significant. In the last period, the production rate and the diffusion/desorption rate are essentially the same. In the third time period, therefore, the production rate is dominated by the depletion of the micropores.

The parameters ω' and λ' in Equations (11) and (12) are, respectively, the dimensionless storage capacity and dimensionless transfer coefficient. Although the definitions of these two parameters are different than those of their counterparts for "conventional" dual porosity reservoirs, their functions are the same. A great deal of the dual porosity literature[34,35,36] is concerned with the effects of ω and λ on reservoir performance, however, a brief discussion (in the context of the coal seam parameters ω' and λ'_R) will be given here.

Figure 11 is a type curve for solutions of Equations (11) and (12) for various values of the parameters ω' and λ'_R. For a constant λ'_R, the initial production decreases with decreasing values of ω'. Thus, the production rate during the natural fracture dominated period is governed by the parameter ω'.

For constant ω', a unique initial gas rate exists, however, as time continues the rates diverge. The divergence of these solutions occurs during the transitional period and is governed by the parameter λ'_R. Two important effects of λ'_R are illustrated in Figure 11. The first is that the onset of the transitional period occurs earlier with increased values of λ'_R. The second consequence of an increased value of λ'_R is that the production rates during this period are greater.

q_{sc} = Flow rate at standard conditions MSCF/day

R = Gas constant

$R = 10.73 \frac{\text{psia ft}^3}{\text{lb-moles }^{\circ}\text{R}}$

r = Radial coordinate ft

r_w = Well radius ft

r_e = External radius ft

S = Phase saturation fraction

S_{ag}^{*} = Initial gas saturation fraction

T = Reservoir temperature °R

T_{sc} = Temperature at standard conditions °R

t = Time Hours

t_{DR} = Dimensionless time for conventional reservoirs

$$t_{DR} = \frac{2.636\text{x}10^{-4}\, k_a t}{(\phi_i c_i + \phi_a c_a)\mu\, r_w^2}$$

t'_{DR} = Dimensionless time for unstimulated coal seams

$$t'_{DR} = \frac{2.636\text{x}10^{-4}\, k_a t}{\left(\frac{2P_{sc}\, T\, V_E^{*}}{T_{sc}[m(P_a^{*}) - m(P_{wf})]} + \phi_a c_g^{*} \mu_g^{*}\right) r_w^2}$$

t'_{Df} = Dimensionless time for stimulated coal seams

$$t'_{Df} = \frac{2.636\text{x}10^{-4}\, k_a t}{\left(\frac{2P_{sc}\, T\, V_E^{*}}{T_{sc}[m(P_a^{*}) - m(P_{wf})]} + \phi_a c_g^{*} \mu_g^{*}\right) x_f^2}$$

$V_E(P_a)$ = Equilibrium sorption isotherm SCF/ft³

V_{ED} = Dimensionless isotherm

$$V_{ED} = \frac{V_E^{*} - V_E(P_a)}{V_E^{*}}$$

V_E^{*} = Initial gas content (adsorbed gas) SCF/ft³

V_i = Volumetric gas concentration SCF/ft³

V_{iD} = Dimensionless concentration

$$V_{iD} = \frac{V_E^{*} - V_i}{V_E^{*}}$$

V_L = Langmuir volume constant SCF/ft³

w_f = Fracture width ft

X = Transformed rectangular coordinate ft

$\ _i$ [illegible] in a multiple porous media

x = Rectangular coordinate ft

x_f = Actual fracture half length ft

Y = Transformed rectangular coordinate ft

y = Rectangular coordinate ft

z = Gas super compressibility factor

Greek

$\alpha = 2.636\text{x}10^{-4} \frac{\text{ft}^2 \text{ cp}}{\text{hr md psi}}$

$\beta = 4.167\text{x}10^{-2} \frac{\text{day}}{\text{hr}}$

η = Elliptical coordinate

θ = Radial coordinate

θ_{sym} = Boundary of symmetric element

λ = Dimensionless transfer coefficient for "conventional" dual porosity reservoirs

λ'_R = Dimensionless transfer coefficient for unstimulated coal seams

λ'_f = Dimensionless transfer coefficient for stimulated coal seams

μ = Dynamic viscosity cp

ξ = Elliptical coordinate

π = 3.14159...

ρ = Density lb/ft³

ϕ = Porosity fraction

ω = Dimensionless storage capacity for "conventional" dual porosity reservoirs

ω' = Dimensionless storage capacity for coal seams

$\nabla\cdot$ = Divergence operator

∇ = Gradient operator

Subscripts

a = Macropore

c = Capillary

D = Dimensionless

E = Equilibrium

e = External

f = Fracture

g = Gas

Superscripts

In Equation (12), the term V_{ED} is the dimensionless sorption isotherm and is a function of the macropore pressure. For coal seams in which a Langmuir isotherm can be used to describe the sorption characteristics, the dimensionless isotherm can be defined by:

$$V_{ED}(P_a) = \frac{1}{V_E^*}\left(\frac{V_L P_a}{P_L + P_a}\right) \tag{18}$$

where V_E^* is the initial gas content of the seam, and V_L and P_L are Langmuir constants. In cases where $P_L >> P_a^*$, Equation (13) reduces to:

$$V_{ED}(P_a) = \frac{1}{V_E^*}\left(\frac{V_L P_a}{P_L}\right) \tag{19a}$$

or

$$V_{ED}(P_a) = \frac{H}{V_E^*} P_{ag} \tag{19b}$$

which is Henry's Law.

Figure 11 was generated using a Henry's Law isotherm. The initial gas content and Henry's Law coefficient were 19.19 SCF/ft^3 (14.11 cc/gm) and 0.0385 SCF/ft^3 psi, respectively. To show the influence of the sorption isotherm on the production rate, a series of computer simulations was conducted using a Langmuir isotherm. In these runs the Langmuir coefficients, V_L=28.78 SCF/ft^3 and P_L=250 psia ($P_a^*/2$), were chosen so that the initial gas content was kept at 19.19 SCF/ft^3. Figure 12 is a comparison of the production rates for the Henry's Law isotherm and the Langmuir isotherm. As expected, the rates during the early, fracture dominated period were not affected, while those in the transitional and diffusion/desorption dominated periods were significantly altered.

Single-Phase, Stimulated Vertical Wells

For single-phase degasification wells stimulated with an infinite conductivity fracture, Equations (1) through (6) reduce to:

$$\frac{\partial^2 m_D(P_a)}{\partial \xi^2} + \frac{\partial^2 m_D(P_a)}{\partial \eta^2} = \frac{1}{2}\,[\cosh(2\xi) - \cos(2\eta)]$$

$$[(1-\omega')\frac{\partial V_{1D}}{\partial t'_{Df}} + \omega'\frac{\partial m_D(P_a)}{\partial t'_{Df}}] \tag{20}$$

$$(1-\omega')\frac{\partial V_{1D}}{\partial t'_{Df}} = -\lambda'_f\,(V_{1D} - V_{ED}) \tag{21}$$

where:

$$t'_{Df} = \frac{2.636\times10^{-4}\,k_a t}{\frac{2P_{sc}TV_E^*}{[illegible](P_a^*) - m(P_{wf})]} + [illegible]\,x_f^2} \tag{22}$$

$$\lambda'_f = \frac{316.14\,D_1 a P_{sc} T V_E^*\,x_f^2}{T_{sc}[m(P_a^*) - m(P_{wf})]\,k_a} \tag{23}$$

and Equation (20) is written in elliptical coordinates.

Type curves for solutions of Equations (20) and (21) were also numerically generated and are presented in Figure 13. In this figure, the three production periods are again apparent. Two important observations can be made in Figure 13. The first is that the dimensionless production rate has been increased by a factor of three, which directly corresponds to a threefold increase in the actual degasification rate.

The second observation is that the dimensionless transfer coefficient, λ', increases by as much as five orders of magnitude for hydraulically stimulated wells. For the typical coal seam properties used in this study, unstimulated wells yielded values of λ'_R in the range of 10^{-9} to 10^{-6}. For the same coal seam properties hydraulically stimulated degasification wells yielded values of λ'_f between 10^{-4} to 10^{-1}. This is due to the fracture half length term, x_f^2, which appears in the definition of λ'_f. It is interesting to note that doubling the fracture half length effectively quadruples the diffusion coefficient.

Figure 13 was generated for a homogeneous, isotropic coal seam. Its use, however, can be extended to anisotropic coal seams by considering an effective fracture half length.[25] For anisotropic reservoirs, the geometric mean permeability:

$$\bar{k}_a = \sqrt{k_{||}\,k_{\perp}} \tag{24}$$

should be used in the definitions of the dimensionless variables (Equations (22) and (23)). In Equation (24), $k_{||}$ is the permeability in the direction parallel to the $||$ hydraulic fracture and $k_{\perp}$ is the permeability in the direction perpendicular to $\perp$ the hydraulic fracture. Also, the effective fracture half length:

$$\bar{x}_f = \sqrt{\bar{k}_a/k_{||}}\;x_f \tag{25}$$

should replace the actual fracture half length. The mathematical basis for using this definition of effective fracture half length is presented in Appendix C. Equations (24) and (25) indicate that if the fracture is oriented parallel to the face cleat ($k_{||} > k_{\perp}$) the effective half length is less than the actual half length.

In Figure 13, only infinite conductivity fractures were considered. There are many instances, however, when the hydraulically induced fracture would have a finite conductivity. These instances include the use of unpropped fractures, production of coal fines adversely affecting fracture permeability, precipitation of solids from reservoir brine adversely affecting fracture permeability, etc. A series of simulations was conducted to investigate the effects of fracture conductivity on reservoir performance. These simulation runs are summarized in Figure 14.

In conventional gas reservoirs, fractures with conductivities (as defined by Equation (7)) greater than [illegible] are [illegible] infinite.

conductivity fractures. The production performances presented in Figure 14 show the same to be true for coal seams. Also, for the cases studied, it appears that coal seams are less sensitive than conventional gas reservoirs to fracture permeability damage. This is indicated by the smaller relative changes in flow rate when the fracture conductivity is reduced in Figure 14.

Two-Phase Vertical Wells

Figures 15 and 16 are history matches of degasification wells from the Mary Lee coal seam in the Warrior Basin. The input data used in the matches are presented in Table 2. For the discussion of two phase reservoirs, unless otherwise specified, this data will be used.

The fracture properties which were found to most significantly affect the well performance were the fracture length, fracture permeability, and orientation of the fracture with respect to the face cleat. Several simulations were conducted to determine the sensitivity of the fracture treatment on these key parameters.

Figure 17 summarizes the effects of the fracture length on the gas and water rates from this coal seam. The fracture permeability and orientation are the same as those stated in Table 2. The behavior illustrated in this figure is to be expected, that is, as the fracture length increased, the gas rate increased.

The production histories exhibited in Figure 17 are very typical for coal seams.[37] The production rate is initially high, but decreases rapidly with the depletion of the natural fractures. After reaching a minimum, the production rate steadily increases. This is the "negative decline" period[38] and is caused by methane desorption increasing the relative permeability to gas. Finally, the production rate reaches a maximum and begins to decrease. This period corresponds to the depletion of the micropores.

Figure 18 shows the effects of fracture permeability on the gas and water production rates. Again, the expected behavior, production rates increasing with increasing permeability, were observed. From the results presented in Figures 17 and 18, it appears that the success of the stimulation treatment is more sensitive to fracture permeability than to fracture length.

The two parameters, fracture permeability and fracture length, are, to some extent, controllable and may be optimized in the design of the stimulation treatment. The orientation of the fracture with respect to the face cleat, in most cases, cannot be controlled. Figure 19 shows two possible gas production histories from the same fracture design, in the coal seam being considered in this study. The only difference in the curves presented in this figure is the orientation of the fracture. Figures of this type are instrumental in determining the optimistic and pessimistic rates which can be expected after stimulation.

Two-Phase Horizontal Boreholes

The coal seam properties listed in Table 2 were used as input for the simulation of hypothetical horizontal borehole projects. The vertical shaft in all cases was 14 feet in diameter and closed to production. Several six-inch diameter boreholes were assumed to have been drilled from the shaft bottom. The parameters which were found to influence the production most significantly were the length and number of the boreholes. The depth of the boreholes, in relation to the top of the seam, was also investigated. For the thin seam considered in this study, this parameter was found to be relatively unimportant. For thick seams, however, such as those in the Western United States, this parameter may be very important and future studies in this area should be conducted.

The effects of borehole length are summarized in Figure 20. In this figure, the total gas production rate (the cumulative rate into the shaft from all boreholes) is plotted versus time. Four boreholes were used to generate these comparisons. As expected, as the length of the boreholes increased, the gas production increased. Comparing Figure 17 to Figure 20, it can be observed that length is a more important parameter for the horizontal boreholes than it is for the vertical fractures.

Figure 21 is a comparison of the performance of the multiple boreholes. The production rates for two through six, 200 ft boreholes are presented. Figures 20 and 21 indicate that the production from horizontal boreholes is more sensitive to the length of the borehole than to the number of boreholes.

Finally, a 200 ft (half length) infinite conductivity fracture; two, 200 ft boreholes; and six, 200 ft boreholes are compared in Figure 22. Since the total length of the two fracture wings is equal to the total length of the two boreholes, it would be expected that the flow rate into the fracture would be greater because it fully penetrates the coal seam. This behavior is observed in Figure 22. A more interesting comparison can be made between the fractured well and the six horizontal boreholes.

The flow into the six boreholes is initially greater than that into the fractured well. After approximately 200 days the flow rates cross over, so that the flow into the boreholes is less. These flow rates then stabilize towards the end of the two year simulation with the flow rate into the fractured well approximately 1 MSCF/day greater.

The total inner surface area of six 200 ft boreholes is 3770 ft^2 while the surface area exhibited by the fractured well is 4000 ft^2. Although the surface area is less for the boreholes, it is positioned in such a way that for early times, the gas will travel shorter distances to reach the boreholes. This would account for the greater production rate during the early time period. At later times, during the pseudo-radial flow period, gas has to travel further to both the boreholes or the fracture. During this period, the effect of the reduced surface area is responsible for the lower production rate.

SUMMARY AND CONCLUSIONS

A two-phase, single well simulator, which can be used to model two of the major coal seam degasification schemes, has been developed. For vertical degasification wells, the model allows for either infinite or finite conductivity hydraulic fractures. For production into horizontal boreholes, a single borehole is modeled, with a no-flow boundary placed on the plane of symmetry defined by $\theta_{sym} = \frac{\pi}{N}$ (where N is the number of boreholes). This model was then used to evaluate these two production schemes.

From the material presented in this paper, the following conclusions are drawn:

1. The production of methane from coal seams can be divided into three time periods. The first period is the fracture flow dominated period. The production rates during this period are governed by the dimensionless storage capacity, ω'. The second period is the transitional period. The arrival of this period, and the production rates associated with it, are governed by the dimensionless transfer coefficient, λ'. The third period is the diffusion/desorption period. The production rates during this period are controlled by the sorption isotherm.
2. For typical coal seam properties, the range of the unstimulated transfer coefficient, λ_R', is approximately 10^{-9} to 10^{-6}, while for the stimulated transfer coefficient, the range is approximately 10^{-4} to 10^{-1}.
3. Unlike "conventional" dual porosity reservoirs, the parameters ω' and λ' do not uniquely determine the production rates into a well. The characteristics of the sorption isotherm must also be considered. The effects of the isotherm occur during the transitional period and govern flow during the diffusion/sorption dominated period.
4. Coal seams are less sensitive than conventional gas wells to reductions in the hydraulic fracture permeability.
5. In coal seams the success of the stimulation treatment appears to be more sensitive to fracture permeability than to fracture length.
6. The effects of permeability anisotropy are very important in the production from hydraulically stimulated, vertical wells. When considering the economics of the stimulation treatment, the orientation of the fracture with respect to the face cleat must be considered.
7. In horizontal borehole projects, the length of the boreholes appears to be more important than the number of boreholes.
8. The length of a horizontal borehole is more critical than the penetration length of a vertical fracture.
9. For the thin seam considered, the vertical positioning of the boreholes was not important. For thicker coal seams the depth [illegible]

NOMENCLATURE

Roman

a = Warren and Root shape factor ft^{-2}

B_w = Water formation volume factor bbl/STB

C_{Df} = Dimensionless fracture conductivity

c = Compressibility psi^{-1}

c_g^* = Initial gas compressibility psi^{-1}

D_i = Micropore diffusion coefficient ft^2/day

H = Henry's Law coefficient SCF/ft^3/psi

h = Coal seam height ft

j = Series index integer

k_a = Macropore permeability md

$\bar{k}_a$ = Geometric mean permeability md

k_f = Hydraulic fracture permeability md

k_r = Relative permeability fraction

k_x = Macropore permeability in x-direction md

k_y = Macropore permeability in y-direction md

$k_{||}$ = Macropore permeability parallel to hydraulic fracture md

$k_{\perp}$ = Macropore permeability perpendicular to hydraulic fracture md

MW = Molecular weight lb/lb mole

$m(P_a)$ = Real gas potential psi^2/cp

$m_D(P_a)$ = Dimensionless gas potential

$$m_D(P_a) = \frac{m(P_a^*) - m(P_a)}{m(P_a^*) - m(P_{wf})}$$

N = Number of horizontal boreholes integer

P_a = Macropore pressure psia

P_a^* = Initial macropore pressure psia

P_c = Capillary pressure psia

P_L = Langmuir pressure constant psia

P_{sc} = Pressure at standard conditions psia

P_{wf} = Flowing bottomhole pressure psia

q_D = Dimensionless flow rate

$$q_D = \frac{5.03\times10^4\, q_{sc}\, P_{sc}\, T}{k_a h [m(P_a^*) - m(P_{wf})]\, T_{sc}}$$

q_{sc} = Flow rate at standard conditions MSCF/day

R = Gas constant

$$R = 10.73 \frac{\text{psia ft}^3}{\text{lb-moles °R}}$$

r = Radial coordinate ft

r_w = Well radius ft

r_e = External radius ft

S = Phase saturation fraction

S^*_{ag} = Initial gas saturation fraction

T = Reservoir temperature °R

T_{sc} = Temperature at standard conditions °R

t = Time Hours

t_{DR} = Dimensionless time for conventional reservoirs

$$t_{DR} = \frac{2.636\text{x}10^{-4}\, k_a t}{(\phi_i c_i + \phi_a c_a)\mu\, r_w^2}$$

t'_{DR} = Dimensionless time for unstimulated coal seams

$$t'_{DR} = \frac{2.636\text{x}10^{-4}\, k_a t}{\left\{\frac{2P_{sc}\, T\, V^*_E}{T_{sc}[m(P^*_a) - m(P_{wf})]} + \phi_a c^*_g \mu^*_g\right\} r_w^2}$$

t'_{Df} = Dimensionless time for stimulated coal seams

$$t'_{Df} = \frac{2.636\text{x}10^{-4}\, k_a t}{\left\{\frac{2P_{sc}\, T\, V^*_E}{T_{sc}[m(P^*_a) - m(P_{wf})]} + \phi_a c^*_g \mu^*_g\right\} x_f^2}$$

$V_E(P_a)$ = Equilibrium sorption isotherm SCF/ft^3

V_{ED} = Dimensionless isotherm

$$V_{ED} = \frac{V^*_E - V_E(P_a)}{V^*_E}$$

V^*_E = Initial gas content (adsorbed gas) SCF/ft^3

V_i = Volumetric gas concentration SCF/ft^3

V_{iD} = Dimensionless concentration

$$V_{iD} = \frac{V^*_E - V_i}{V^*_E}$$

V_L = Langmuir volume constant SCF/ft^3

w_f = Fracture width ft

X = Transformed rectangular coordinate ft

x_i = Effective fracture half length in anisotropic porous medium ft

x = Rectangular coordinate ft

x_f = Actual fracture half length ft

Y = Transformed rectangular coordinate ft

y = Rectangular coordinate ft

z = Gas super compressibility factor

Greek

$$\alpha = 2.636\text{x}10^{-4} \frac{\text{ft}^2\ \text{cp}}{\text{hr md psi}}$$

$$\beta = 4.167\text{x}10^{-2} \frac{\text{day}}{\text{hr}}$$

η = Elliptical coordinate

θ = Radial coordinate

θ_{sym} = Boundary of symmetric element

λ = Dimensionless transfer coefficient for "conventional" dual porosity reservoirs

λ'_R = Dimensionless transfer coefficient for unstimulated coal seams

λ'_f = Dimensionless transfer coefficient for stimulated coal seams

μ = Dynamic viscosity cp

ξ = Elliptical coordinate

π = 3.14159...

ρ = Density lb/ft^3

ϕ = Porosity fraction

ω = Dimensionless storage capacity for "conventional" dual porosity reservoirs

ω' = Dimensionless storage capacity for coal seams

$\nabla\cdot$ = Divergence operator

∇ = Gradient operator

Subscripts

a = Macropore

c = Capillary

D = Dimensionless

E = Equilibrium

e = External

f = Fracture

g = Gas

i = Micropore

R = Radial

r = Relative

sc = Standard conditions

sym = Symmetry

w = Water

wf = Flowing well

x = X-direction

y = Y-direction

REFERENCES

1. Rice, G. S.: "Safety in Coal Mining," U.S. Bureau of Mines, RI 277, (1928).

2. Elder, C. H. and Duel, M.: "Hydraulic Stimulation Increases Degasification Rate of Coalbeds," U.S. Bureau of Mines, RI 8047 (1975).

3. Kim, A. G.: "Methane Drainage from Coalbeds: Research and Utilization," Methane Gas from Coalbeds - Development, Production, and Utilization, MERC/SP-78/1 (January 18, 1978), 12-17.

4. Lambert, S. W. and Trevits, M. A.: "Methane Drainage: Experience with Hydraulic Stimulation through Slotted Casing," U.S. Bureau of Mines, RI 8295 (1978).

5. Unconventional Natural Gas: Resources, Potential, and Technology, Satriana, M., Noyes Data Corporation (1980), 148-182.

6. Chase, R. W.: "Degasification of Coal Seams via Vertical Boreholes: A Field and Computer Simulation Study," Ph.D. Dissertation, The Pennsylvania State University (March 1980).

7. Mahoney, J. V., Stubbs, P. B., Schwerer, F. C., and Dobscha, E. X.: "Effects of a No-Proppant Foam Stimulation Treatment on a Coal Seam Degasification Borehole," paper SPE/DOE 8931 presented at the SPE/DOE Symposium on Unconventional Gas Recovery, Pittsburgh, PA (May 18-21, 1980).

8. Gilles, A., Snygg, A. J., Dickehuth, P., and Howarth, S. M.: "Utilization and Recovery Economics for Vertical Wells in Coalbed Methane," paper SPE/DOE 8946 presented at the SPE/DOE Symposium on Unconventional Gas Recovery, Pittsburgh, PA (May 18-21, 1980).

9. Steidl, P. F., Trevits, M. A., and Diamond, W. P.: "Completion Techniques and Production Data from Vertical Methane Drainage Boreholes, Jawbone Coalbed, Dickenson County, Virginia," paper SPE/DOE 8965 presented at the SPE/DOE Symposium on Unconventional Gas Recovery, Pittsburgh, PA (May 18-21, 1980).

10. Trevits, M. A., Richards, W. L., and von Schonfeldt, H. A. G.: "Determining the Feasibility of Using Vertical Boreholes to Drain Gas from the Pocahontas No. 3 Coalbed, Buchanan County, VA," paper SPE/DOE 8966 presented at the SPE/DOE Symposium on Unconventional Gas Recovery, Pittsburgh, PA (May 18-21, 1980).

11. Moore, T. D. and Zabetakis, M. G.: "Effect of a Surface Borehole on Longwall Gob Degasification (Pocahontas No. 3 Coalbed)," U.S. Bureau of Mines, RI 7657 (1972).

12. Enhanced Recovery of Unconventional Gas, Kuuskraa, V. A., Brashear, J. P., Doscher, T. M., and Elkins, L. E. (under contract to Levin and Associates), DOE Contract No. EF-77-C-01-2705 (October 1978).

13. Maksimovic, S. D., Elder, C. H., and Kissell, F. N.: "Hydraulic Stimulation of a Surface Borehole for Gob Degasification," U.S. Bureau of Mines, RI 8228 (1977).

14. Davis, J. G.: "An Outline of Consol's Research Program on Methane Control as Related to the Pittsburgh Seam," Proceedings of the West Virginia Coal Mining Institute (1971), 61-68.

15. Fields, H. H., Krickovic, S., Sainato, A. and Zabetakis, M. G.: "Degasification of Virgin Pittsburgh Coalbed through a Large Borehole," U.S. Bureau of Mines, RI 7800 (1973).

16. Fields, H. H., Perry, J. H., and Duel, M.: "Commercial-Quality Gas from a Multipurpose Borehole Located in the Pittsburgh Coalbed," U.S. Bureau of Mines, RI 8025 (1975).

17. Oyler, D. C., Diamond, W. P., and Jeran, P. W.: "Directional Drilling for Coalbed Degasification - Program Goals and Progress in 1978," U.S. Bureau of Mines, RI 8380 (1979).

18. Cervik, J.: "Behavior of Coal-Gas Reservoirs," paper SPE 1973 presented at the Fourth Annual Eastern Regional Meeting of the Society of Petroleum Engineers of AIME, Pittsburgh, PA (November 2-3, 1967).

19. Ancell, K. L. and Lambert, S.: "Analysis of the Coalbed Degasification Process at a Seventeen Well Pattern in the Warrior Basin of Alabama," paper SPE/DOE 8971 presented at the SPE/DOE Symposium on Unconventional Gas Recovery, Pittsburgh, PA (May 18-21, 1980).

20. King, G. R., Ertekin, T., and Schwerer, F. C.: "Numerical Simulation of the Transient Behavior of Coal Seam Degasification Wells," paper SPE 12258 presented at the Seventh SPE Symposium on Reservoir Simulation, San Francisco, CA (November 16-18, 1983).

21. Kim, A. G. and Douglas, L. J.: "Gases Desorbed from Five Coals of Low Gas Content," U.S. Bure[illegible] of Mines, RI 7768 (1973).

22. Ertekin, T., King, G. R., and Schwerer, F. C.: "Development of Coal-Gas Simulators and Mathematical Models for Well Test Strategies (Computer Models for Single- and Two-Phase Flow in Heterogeneous Coal Seams to a Well with a Finite-Conductivity Fracture)," *Topical Report*, Report No. GRI-81/0173, Gas Research Institute (1983).

23. Boyer, C. M., Morrison, H. L., Pavone, A. M., and Schwerer, F. C.: "Methane Modeling - Predicting the Inflow of Methane Gas into Coal Mines," *Annual Report* DOE/PC/30123-T4 (February 16, 1982).

24. Pavone, A. M. and Schwerer, F. C.: "Development of Coal-Gas Production Simulators and Mathematical Models for Well Test Strategies (Computer Model for an Array of Vertical Wells and Overview of Contract Results)," *Final Report*, Contract No. 5081-321-0457, Gas Research Institute (1984).

25. Kücük, F.: "Transient Flow in Elliptical Systems," Ph.D. Dissertation, Stanford University (May 1978).

26. Obüt, T. and Ertekin, T.: "A Composite System Solution in Elliptical Flow Geometry," paper SPE 13078 presented at the SPE Annual Technical Conference and Exhibition, Houston, TX (September 16-19, 1984).

27. Holditch, S. A. and Morse, R. A.: "The Effects of Non-Darcy Flow on the Behavior of Hydraulically Fractured Gas Wells," *Journal of Petroleum Technology* (October 1976), 1169-1179.

28. Holditch, S. A.: "Factors Affecting Water Blocking and Gas Flow from Hydraulically Fractured Gas Wells, "*Journal of Petroleum Technology* (December 1979), 1515-1524.

29. Lee, W. J. and Holditch, S. A.: "Fracture Evaluation with Pressure Transient Testing in Low-Permeability Gas Reservoirs," *Journal of Petroleum Technology* (September 1981), 1776-1792.

30. Murtha, J. A. and Ertekin, T.: "Numerical Simulation of Power Law Fluid Flow in a Vertically Fractured Reservoir," paper SPE 12011 presented at the 58th Annual Technical Conference and Exhibition, San Francisco, CA (October 5-8, 1983).

31. Cinco-L., H., Samaniego-V., F., and Dominguez-A., N.: "Transient Pressure Behavior for a Well with a Finite-Conductivity Vertical Fracture," *Society of Petroleum Engineers Journal* (August 1978), 253-264.

32. Nghiem, L. X.: "Modeling Infinite-Conductivity Vertical Fractures Using Source and Sink Terms," paper SPE 10507 presented at the Sixth SPE Symposium on Reservoir Simulation, New Orleans, LA (February 1-3, 1982).

33. Theory and Practice of the Testing of Gas Wells, [illegible] (19[illegible]).

34. Warren, J. E. and Root, P. J.: "The Behavior of Naturally Fractured Reservoirs," *Society of Petroleum Engineers Journal* (September, 1963), 245-255.

35. de Swaan, A.: "Analytical Solutions for Determining Naturally Fractured Reservoir Properties by Well Testing," *Society of Petroleum Engineers Journal* (June 1976), 117-122.

36. Serra, K., Reynolds, A. C., and Raghavan, R.: "New Pressure Transient Analysis Methods for Naturally Fractured Reservoirs," *Journal of Petroleum Technology* (December 1983), 2271-2283.

37. *Economic Analysis of Vertical Wells for Coalbed Methane Recovery, TRW Energy Systems Group*, DOE Contract No. DE-AC21-78MC08089 (April 1981).

38. Harrison, G. C. and Gordon, R. B.: "Negative Decline Curves of Coalbed Degasification Wells," paper SPE/DOE/GRI 12874 presented at the SPE/DOE/GRI Symposium on Unconventional Gas Recovery, Pittsburgh, PA (May 13-15, 1984).

39. Al-Hussainy, R. and Ramey, H. J., and Crawford, P. B.: "The Flow of Real Gases through Porous Media," *Journal of Petroleum Technology* (May 1966), 624-636.

APPENDIX A

Theory

Warren and Root[34] formulated the following set of coupled equations which describes the flow of homogeneous, slightly compressible fluids through dual porosity reservoirs.

$$\frac{k_a}{\mu} \nabla^2 P_a = \phi_i c_i \frac{\partial P_i}{\partial t} + \phi_a c_a \frac{\partial P_a}{\partial t} \tag{26a}$$

$$\phi_i c_i \frac{\partial P_i}{\partial t} = \frac{-k_i a}{\mu} (P_i - P_a) \tag{26b}$$

These equations were derived by assuming pseudo-steady state fluid transfer between the micropore and macropore systems. Written in terms of dimensionless quantities, the radial forms of Equations (26a) and (26b) become:

$$\frac{1}{r_D} \frac{\partial}{\partial r_D} (r_D \frac{\partial P_{aD}}{\partial r_D}) = (1-\omega) \frac{\partial P_{iD}}{\partial t_{DR}} + \omega \frac{\partial P_{aD}}{\partial t_{DR}} \tag{27a}$$

$$(1-\omega) \frac{\partial P_{iD}}{\partial t_{DR}} = -\lambda (P_{iD} - P_{aD}) \tag{27b}$$

The parameters, ω and λ, are defined by:

$$\omega = \frac{\phi_a c_a}{(\phi_a c_a + \phi_i c_i)} \tag{28}$$

$$\lambda = \frac{k_i a r_w^2}{k_a} \tag{29}$$

Equations (27) through (29), when subjected to appropriate initial and boundary conditions, uniquely determine the pressure distribution in those dual porosity reservoirs which are consistent with the assumptions used in their (Equations (27) through (29)) derivation.

Unfortunately, several differences between coal seams and "conventional" dual porosity reservoirs make Equations (27) through (29) inappropriate for coal seams. These are:

1. In coal seams the reservoir fluid, methane, is highly compressible.
2. In the micropores of coal seams, the methane is stored in an adsorbed state rather than a free state.
3. Methane transport through the micropores is a diffusion process.

The equations, similar to Equations (26a) and (26b), which are applicable to coal seams are:

$$\nabla\cdot\left(\frac{\alpha k_a}{\mu_g}\frac{P_a}{z}\nabla P_a\right) = \frac{\partial V_i}{\partial t} + \frac{\phi_a c_g P_a}{z}\frac{\partial P_a}{\partial t} \qquad (30a)$$

$$\frac{\partial V_i}{\partial t} = -\beta D_i a[V_i - V_E(P_a)] \qquad (30b)$$

In Equations (30a) and (30b) the following entries are identified:

V_i is the volumetric methane concentration in SCF/ft^3.

$V_E(P_a)$ is an equilibrium isotherm in SCF/ft^3.

D_i is the micropore diffusion coefficient in ft^2/day.

a is the shape factor discussed by Warren and Root in ft^{-2}.

α and β are unit conversion constants.

The dimensionless forms of Equations (30a) and (30b) in radial coordinates become (see Appendix B):

$$\frac{1}{r_D}\frac{\partial}{\partial r_D}\left[r_D\frac{\partial m_D(P_a)}{\partial r_D}\right] = (1-\omega')\frac{\partial V_{iD}}{\partial t'_{DR}} + \omega'\frac{\partial m_D(P_a)}{\partial t'_{DR}} \qquad (31a)$$

$$(1-\omega')\frac{\partial V_{iD}}{\partial t'_{DR}} = -\lambda'_R\,[V_{iD} - V_{ED}(P_a)] \qquad (31b)$$

where:

$$m(P_a) = 2\int_{P_{sc}}^{P_a}\frac{P_a}{\mu_g(P_a)\,z(P_a)}\,dP_a \qquad (32)$$

$$m_D(P_a) = \frac{m(P_a^*) - m(P_a)}{m(P_a^*) - m(P_{wf})} \qquad (33)$$

$$t'_{DR} = \frac{\alpha k_a t}{\left(\frac{2P_{sc}\,T\,V_E^*}{T_{sc}[m(P_a^*) - m(P_{wf})]} + \phi_a c_g^* \mu_g^*\right) r_w^2} \qquad (34)$$

$$\omega' = \frac{\phi_a c_g^* \mu_g^*}{\left(\frac{2P_{sc}\,T\,V_E^*}{T_{sc}[m(P_a^*) - m(P_{wf})]} + \phi_a c_g^* \mu_g^*\right) r_w^2} \qquad (35)$$

$$\lambda'_R = \frac{2\beta\,D_i\,a\,P_{sc}\,T\,V_E^*\,r_w^2}{\alpha T_{sc}[m(P_a^*) - m(P_{wf})]k_a} \qquad (36)$$

It should be noted that if the initial gas content V_E^* is zero, the aforementioned definitions collapse into those of conventional gas reservoirs.

In elliptical coordinates the dimensionless equations become (see Appendix C):

$$\frac{\partial^2 m_D(P_a)}{\partial \xi^2} + \frac{\partial^2 m_D(P_a)}{\partial \eta^2} = \frac{1}{2}[\cosh(2\xi) - \cos(2\eta)]\left[(1-\omega')\frac{\partial V_{iD}}{\partial t'_{Df}} + \omega'\frac{\partial m_D(P_a)}{\partial t'_{Df}}\right] \qquad (37a)$$

$$(1-\omega')\frac{\partial V_{iD}}{\partial t'_{Df}} = -\lambda'_f\,(V_{iD} - V_{ED}) \qquad (37b)$$

where:

$$t'_{Df} = \frac{\alpha k_a t}{\left(\frac{2P_{sc}\,T\,V_E^*}{T_{sc}[m(P_a^*) - m(P_{wf})]} + \phi_a c_g^* \mu_g^*\right) x_f^2} \qquad (38)$$

$$\lambda'_f = \frac{2\beta\,D_i\,a\,P_{sc}\,T\,V_E^*\,x_f^2}{\alpha T_{sc}[m(P_a^*) - m(P_{wf})]k_a} \qquad (39)$$

APPENDIX B

Radial Coordinates

Starting with the radial form of the diffusivity equation for fissured porous media:

$$\frac{1}{r}\frac{\partial}{\partial r}\left(\frac{\alpha r k_a}{\mu_g}\rho\frac{\partial P_a}{\partial r}\right) = \rho_{sc}\frac{\partial V_i}{\partial t} + \phi_a\frac{\partial \rho}{\partial t} \qquad (40a)$$

$$\frac{\partial V_i}{\partial t} = -D_i a[V_i - V_E(P_a)] \qquad (40b)$$

For a compressible fluid:

$$\rho = \frac{MW\ P}{ZRT} \tag{41}$$

Substituting in Equation (40a):

$$\frac{1}{r}\frac{\partial}{\partial r}\left(\frac{\alpha r k_a}{\mu_g}\frac{P_a}{z}\frac{\partial P_a}{\partial r}\right) = \frac{P_{sc}\ T}{T_{sc}}\frac{\partial V}{\partial t} + \frac{\phi_a c_g P_a}{z}\frac{\partial P_a}{\partial t} \tag{42a}$$

$$\frac{\partial V_1}{\partial t} = -\ \beta D_1 a\ [V_1 - V_E(P_a)] \tag{42b}$$

Defining the dimensionless methane concentration and equilibrium isotherm as:

$$V_{1D} = \frac{V_E^{\circ} - V_1}{V_E^{\circ}} \tag{43}$$

$$V_{ED} = \frac{V_E^{\circ} - V_E(P_a)}{V_E^{\circ}} \tag{44}$$

and substituting into Equations (42a) and (42b) one obtains:

$$\frac{1}{r}\frac{\partial}{\partial r}\left(\frac{\alpha r k_a}{\mu_g}\frac{P_a}{z}\frac{\partial P_a}{\partial r}\right) = \frac{-P_{sc}\ T\ V_E^{\circ}}{T_{sc}}\frac{\partial V_{1D}}{\partial t} + \frac{\phi_a c_g P_a}{z}\frac{\partial P_a}{\partial t} \tag{45a}$$

$$\frac{\partial V_{1D}}{\partial t} = -\ \beta D_1 a\ [V_{1D} - V_{ED}(P_a)] \tag{45b}$$

Defining the dimensionless radius as:

$$r_D = \frac{r}{r_w} \tag{46}$$

and substituting into Equations (45a) and (45b) yields:

$$\frac{1}{r_D}\frac{\partial}{\partial r_D}\left(\frac{\alpha r_D k_a}{\mu_g}\frac{P_a}{z}\frac{\partial P_a}{\partial r_D}\right) = \frac{-P_{sc}\ T\ V_E^{\circ}\ r_w^2}{T_{sc}}\frac{\partial V_{1D}}{\partial t} + \frac{\phi_a c_g P_a r_w^2}{z}\frac{\partial P_a}{\partial t} \tag{47a}$$

$$\frac{\partial V_{1D}}{\partial t} = -\ \beta D_1 a\ [V_{1D} - V_{ED}(P_a)] \tag{47b}$$

Substituting Equations (47a) and [illegible] one obtains:

$$\frac{1}{r_D}\frac{\partial}{\partial r_D}\left[r_D\frac{\partial m(P_a)}{\partial r_D}\right] = \frac{-2P_{sc}\ T\ V_E^{\circ}\ r_w^2}{\alpha T_{sc} k_a}\frac{\partial V_{1D}}{\partial t} + \frac{\phi_a c_g \mu_g r_w^2}{\alpha k_a}\frac{\partial m(P_a)}{\partial r_D} \tag{48a}$$

$$\frac{\partial V_{1D}}{\partial t} = -\ \beta D_1 a\ [V_{1D} - V_{ED}(P_a)] \tag{48b}$$

where $m(P_a)$ is the real gas potential, i.e.:

$$m(P_a) = 2\int_{P_{sc}}^{P_a}\frac{\hat{P}_a}{\mu_g(\hat{P}_a)\ z(\hat{P}_a)}\,d\hat{P}_a \tag{49}$$

Defining the dimensionless potential as:

$$m_D(P_a) = \frac{m(P_a^{\circ}) - m(P_a)}{m(P_a^{\circ}) - m(P_{wf})} \tag{50}$$

and substituting into Equations (48a) and (48b) the following expressions are obtained:

$$\frac{1}{r_D}\frac{\partial}{\partial r_D}\left[r_D\frac{\partial m_D(P_a)}{\partial r_D}\right] = \frac{2P_{sc}\ T\ V_E^{\circ}\ r_w^2}{\alpha T_{sc}[m(P_a^{\circ}) - m(P_{wf})]k_a}\frac{\partial V_{1D}}{\partial t} + \frac{\phi_a c_g \mu_g r_w^2}{\alpha k_a}\frac{\partial m_D(P_a)}{\partial t} \tag{51a}$$

$$\frac{\partial V_{1D}}{\partial t} = -\ \beta D_1 a\ [V_{1D} - V_{ED}(P_{ag})] \tag{51b}$$

The dimensionless storage capacity is defined as:

$$\omega' = \frac{\phi_a c_g \mu_g}{\left\{\frac{2P_{sc}\ T\ V_E^{\circ}}{T_{sc}[m(P_a^{\circ}) - m(P_{wf})]} + \phi_a c_g \mu_g\right\}} \tag{52}$$

Substituting Equation (52) into Equation (51) one obtains:

$$\frac{1}{r_D}\frac{\partial}{\partial r_D}\left[r_D\frac{\partial m_D(P_a)}{\partial r_D}\right] = \left\{\frac{2P_{sc}\ T\ V_E^{\circ}}{T_{sc}[m(P_a^{\circ}) - m(P_{wf})]} + \phi_a c_g \mu_g\right\}(1-\omega')\frac{r_w^2}{\alpha k_a}\frac{\partial V_{1D}}{\partial t}$$

$$+ \left\{\frac{2P_{sc}\ T\ V_E^{\circ}}{T_{sc}[m(P_a^{\circ}) - m(P_{wf})]} + \phi_a c_g \mu_g\right\}$$

$$\frac{r_w^2}{\alpha k_a}\frac{\partial m_D(P_a)}{\partial t}$$ [illegible]

$$\frac{\left(\frac{2P_{sc}\,T\,V_E^*}{T_{sc}[m(P_a) - m(P_{wf})]} + \phi_a c_g \mu_g\right)}{\frac{2P_{sc}\,T\,V_E^*}{T_{sc}[m(P_a^*) - m(P_{wf})]}} (1-\omega') \frac{\partial V_{iD}}{\partial t}$$

$$= - \beta D_i a\,[V_{iD} - V_{ED}(P_a)] \qquad (53b)$$

Using the definition of dimensionless time:

$$t'_{DR} = \frac{\alpha k_a t}{\left(\frac{2P_{sc}\,T\,V_E^*}{T_{sc}[m(P_a) - m(P_{wf})]} + \phi_a c_g \mu_g\right) r_w^2} \qquad (54)$$

and substituting into Equations (53a) and (53b) the following equations are obtained:

$$\frac{1}{r_D}\frac{\partial}{\partial r_D}\left[r_D \frac{\partial m_D(P_a)}{\partial r_D}\right] = (1-\omega')\frac{\partial V_{iD}}{\partial t'_{DR}}$$

$$+ \omega' \frac{\partial m_D(P_a)}{\partial t'_{DR}} \qquad (55a)$$

$$(1-\omega')\frac{\partial V_{iD}}{\partial t'_{DR}}$$

$$= \frac{-2\beta\, D_i\, a\, P_{sc}\, T\, V_E^*\, r_w^2}{\alpha T_{sc}[m(P_a^*) - m(P_{wf})]k_a}[V_{iD} - V_{ED}(P_a)] \qquad (55b)$$

Now, defining the dimensionless transfer coefficient as:

$$\lambda'_R = \frac{2\beta\, D_i\, a\, P_{sc}\, T\, V_E^*\, r_w^2}{\alpha T_{sc}[m(P_a^*) - m(P_{wf})]k_a} \qquad (56)$$

and substituting into Equations (55) yields:

$$\frac{1}{r_D}\frac{\partial}{\partial r_D}\left[r_D \frac{\partial m_D(P_a)}{\partial r_D}\right] = (1-\omega')\frac{\partial V_{iD}}{\partial t'_{DR}}$$

$$+ \omega' \frac{\partial m_D(P_a)}{\partial t'_{DR}} \qquad (57a)$$

$$(1-\omega')\frac{\partial V_{iD}}{\partial t'_{DR}} = -\lambda\,(V_{iD} - V_{ED}) \qquad (57b)$$

The term $(c_g \mu_g)$ in the definitions of ω' and t'_{DR} represents a weak nonlinearity and is generally evaluated at the initial coal seam conditions.

APPENDIX C

Elliptical Coordinates

[illegible] (26a) and (26b) one obtains:

$$\frac{\partial}{\partial x}\left(\frac{\alpha k_x}{\mu_g}\frac{P_a}{z}\frac{\partial P_a}{\partial x}\right) + \frac{\partial}{\partial y}\left(\frac{\alpha k_y}{\mu_g}\frac{P_a}{z}\frac{\partial P_a}{\partial y}\right)$$

$$= \frac{P_{sc}\,T}{T_{sc}}\frac{\partial V_i}{\partial t} + \frac{\phi_a c_g P_a}{z}\frac{\partial P_a}{\partial t} \qquad (58a)$$

$$\frac{\partial V_i}{\partial t} = - \beta D_i a\,[V_i - V_E(P_a)] \qquad (58b)$$

If an infinite conductivity fracture is oriented along the x-axis, then:

$$k_{||} = k_x \qquad (59a)$$

$$k_{\perp} = k_y \qquad (59b)$$

Substitution into Equations (58a) and (58b) gives:

$$\frac{\partial}{\partial x}\left(\frac{\alpha k_{||}}{\mu_g}\frac{P_a}{z}\frac{\partial P_a}{\partial x}\right) + \frac{\partial}{\partial y}\left(\frac{\alpha k_{\perp}}{\mu_g}\frac{P_a}{z}\frac{\partial P_a}{\partial y}\right)$$

$$\frac{P_{sc}\,T}{T_{sc}}\frac{\partial V_i}{\partial t} + \frac{\phi_a c_g P_a}{z}\frac{\partial P_a}{\partial t} \qquad (60a)$$

$$\frac{\partial V_i}{\partial t} = - \beta D_i a\,[V_i - V_E(P_a)] \qquad (60b)$$

For an anisotropic medium, the following transformations can be made on the spatial coordinates:

$$X = \sqrt{\bar{k}_a/k_{||}}\;x \qquad (61a)$$

$$Y = \sqrt{\bar{k}_a/k_{\perp}}\;y \qquad (61b)$$

where:

$$\bar{k}_a = \sqrt{k_{||}k_{\perp}} \qquad (62)$$

Equations (61a), (61b) and (62) transform Equations (26a) and (26b) to:

$$\frac{\partial}{\partial X}\left(\frac{\alpha \bar{k}_a}{\mu_g}\frac{P_a}{z}\frac{\partial P_a}{\partial X}\right) + \frac{\partial}{\partial Y}\left(\frac{\alpha \bar{k}_a}{\mu_g}\frac{P_a}{z}\frac{\partial P_a}{\partial Y}\right)$$

$$= \frac{P_{sc}\,T}{T_{sc}}\frac{\partial V_i}{\partial t} + \frac{\phi_a c_g P_a}{z}\frac{\partial P_a}{\partial t} \qquad (63a)$$

$$\frac{\partial V_i}{\partial t} = - \beta D_i a\,[V_i - V_E(P_a)] \qquad (63b)$$

Thus, a fracture of length x_f in the original coordinate system will have a length

$$X_f = \sqrt{\bar{k}_a/k_{||}}\ x_f \tag{64}$$

in the transformed system.

Using the definition of elliptical coordinates,

$$X = X_f \cosh(\xi) \cos(\eta) \tag{65a}$$

$$Y = X_f \sinh(\xi) \sin(\eta) \tag{65b}$$

and the definition of real gas potential, Equations (63a) and (63b), can be transformed to

$$\frac{\partial^2 m(P_a)}{\partial \xi^2} + \frac{\partial^2 m(P_a)}{\partial \eta^2} = \frac{X_f^2}{2} [\cosh(2\xi) - \cos(\eta)]$$

$$[\frac{2P_{sc}\ T}{\alpha T_{sc}\bar{k}_a} \frac{\partial V_i}{\partial t} + \frac{\phi_a c_g \mu_g}{\alpha \bar{k}_a} \frac{\partial m(P_a)}{\partial t}] \tag{66a}$$

$$\frac{\partial V_i}{\partial t} = -\ BD_i a\ [V_i - V_E(P_a)] \tag{66b}$$

Following the procedure outlined in Appendix B, Equations (66a) and (66b) reduce to:

$$\frac{\partial^2 m_D(P_a)}{\partial \xi^2} + \frac{\partial^2 m_D(P_a)}{\partial \eta^2} = \frac{1}{2} [\cosh(2\xi) - \cos(2\eta)]$$

$$[(1-\omega') \frac{\partial V_{iD}}{\partial t'_{Df}} + \omega' \frac{\partial m_D(P_a)}{\partial t'_{Df}}] \tag{67a}$$

$$(1-\omega') \frac{\partial V_{iD}}{\partial t'_{Df}} = -\lambda'_f [V_{iD} - V_{ED}(P_a)] \tag{67b}$$

which are the elliptical forms of the flow equations for fissured media.

TABLE 1

INPUT DATA FOR COMPARISON OF ELLIPTICAL RECTANGULAR AND RADIAL FRACTURE FORMULATIONS

Variable Name	Symbol Used in Text	Numerical Value
External Radius	r_e	500.0 ft
Well Radius	r_w	2.0 ft
Seam Thickness	h	5.0 ft
Initial Gas Saturation	S°_{ag}	13.0 percent
Initial Seam Pressure	P°_{ag}	450.0 psi
Well Pressure (at coal face)	P_{wf}	20.0 psi
Seam Temperature	T	70.0 F
Permeability Perpendicular to Fracture	$k_{\perp}$	3.15 md
Permeability Parallel to Fracture	$k_{\|\|}$	3.15 md
Porosity	ϕ_a	5.0 percent
Relative Permeability to Water at Critical Gas Saturation	$k_{rw}(S_{gc})$	0.24 percent
Diffusion Constant	$D_i a$	10^{-7} sec
Initial Gas Content	V°_E	27.5 SCF/ft^3 (20.2 cc/gm)
Langmuir Volume Constant	V_L	34.3 SCF/ft^3
Langmuir Pressure Constant	P_L	111.7 psia
Fracture Half Length	x_f	200.0 ft
Fracture Width	w_f	0.05 inch
Fracture Permeability	k_f	∞ md

TABLE 2

INPUT DATA FOR HISTORY MATCHES PRESENTED IN FIGURES 15 AND 16

Variable Name	Symbol Used in Text	Unstimulated Well	Stimulated Well
External Radius (Closed)	r_e	500.0 ft	500.0 ft
Well Radius	r_w	2.0 ft	2.0 ft
Seam Thickness	h	5.0 ft	5.0 ft
Initial Gas Saturation	S°_{ag}	5.0 percent	13.0 percent
Initial Seam Pressure	P°_{ag}	450.0 psi	450.0 psi
Well Pressure (at coal face)	P_{wf}	20.0 psi	20.0 psi
Seam Temperature	T	70.0°F	70.0°F
Average Permeability	$\bar{k}_a$	3.40 md	5.61 md
Permeability Perpendicular to Fracture	$k_{\perp}$	-	3.15 md
Permeability Parallel to Fracture	$k_{\|\|}$	-	10.0 md
Porosity	ϕ_a	3.5 percent	5.0 percent
Relative Permeability to Water at Critical Gas Saturation	$k_{rw}(S_{gc})$	0.826	0.24
Diffusion Constant	$D_i a$	5.36×10^{-8} sec	9.99×10^{-8} sec
Initial Gas Content	V°_E	27.5 SCF/ft^3 (20.2 cc/gm)	27.5 SCF/ft^3
Langmuir Volume Constant	V_L	34.3 SCF/ft^3	34.3 SCF/ft^3
Langmuir Pressure Constant	P_L	111.7 psia	111.7 psia
Fracture Half Length	x_f	-	200.0 ft
Fracture Width	w_f	-	0.05 inch
Fracture Permeability	k_f	-	5.5×10^{4} md

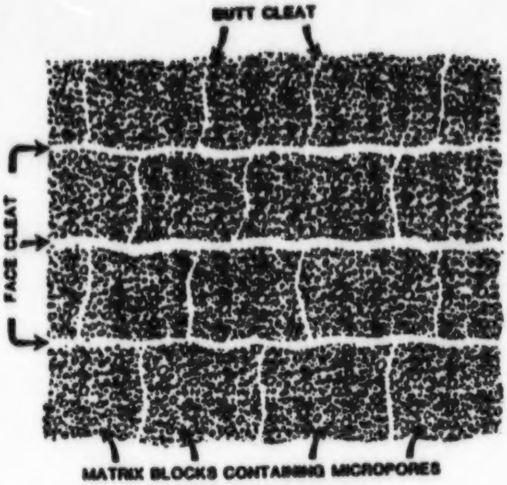
BUTT CLEAT
FACE CLEAT
MATRIX BLOCKS CONTAINING MICROPORES

Fig. 1—Plan view of dual porosity coal seam

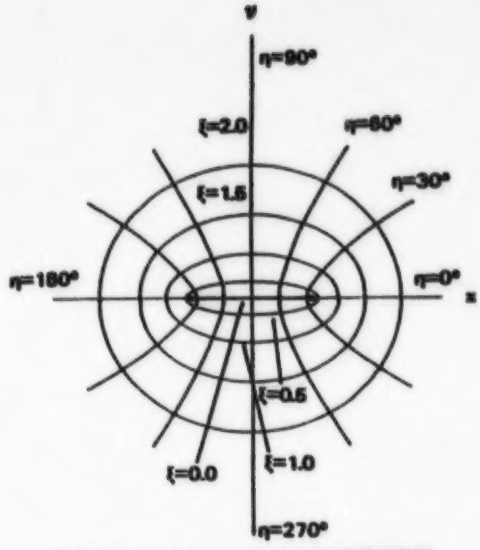
y
η=90°
ξ=2.0
η=60°
ξ=1.5
η=30°
η=180°
η=0°
x
ξ=0.5
ξ=0.0
ξ=1.0
η=270°

Fig. 2—Representation of infinite conductivity fracture in elliptical coordinates

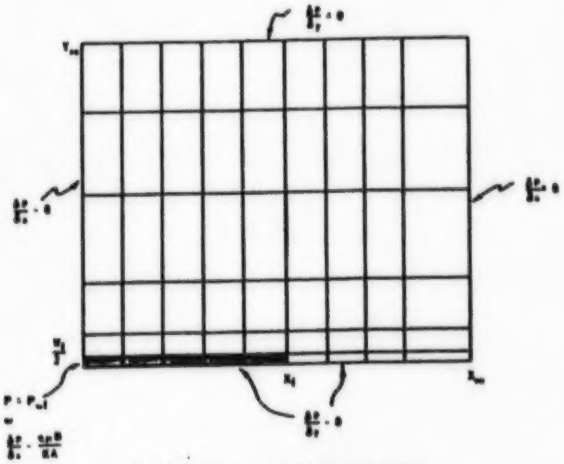
$\frac{\partial p}{\partial y} = 0$
y_m
$\frac{\partial p}{\partial x} = 0$
$\frac{\partial p}{\partial x} = 0$
$\frac{w}{2}$
$P = P_{wf}$
or
$\frac{\partial p}{\partial x} = \frac{q \mu B}{kA}$
x_f
$\frac{\partial p}{\partial y} = 0$
x_m

Fig. 3—Representation of fracture in rectangular coordinates

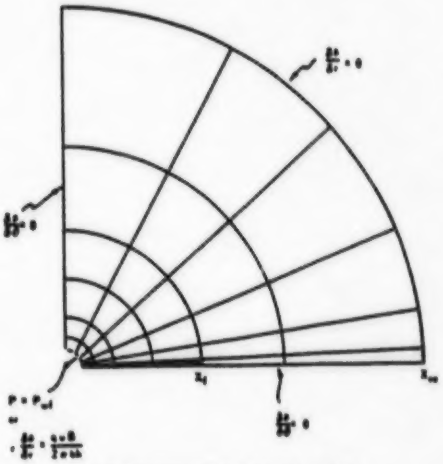
$\frac{\partial p}{\partial r} = 0$
$\frac{\partial p}{\partial \theta} = 0$
$P = P_{wf}$
or
$r\frac{\partial p}{\partial r} = \frac{q \mu B}{2 \pi kh}$
x_f
$\frac{\partial p}{\partial \theta} = 0$
x_m

Fig. 4—Representation of fracture in radial coordinates

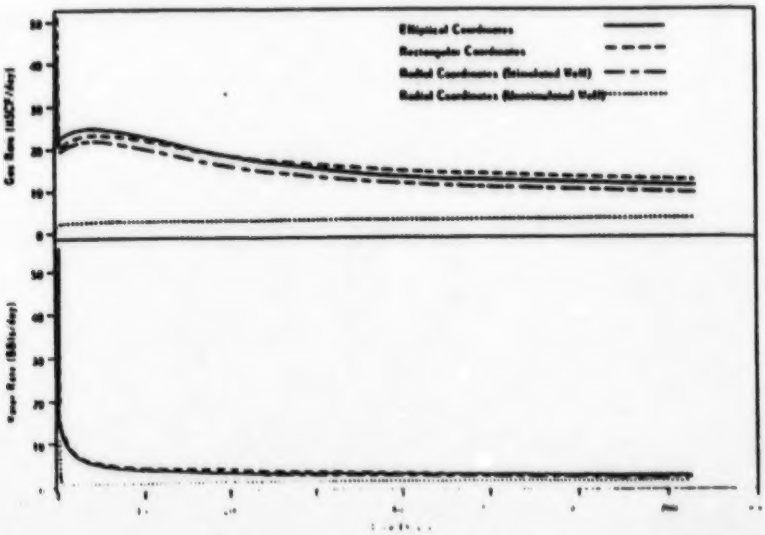

Fig. 5

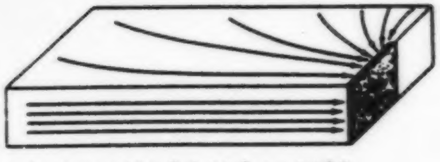

A. Streamlines to an Infinite Conductivity Fracture which Fully Penetrates the Coal Seam

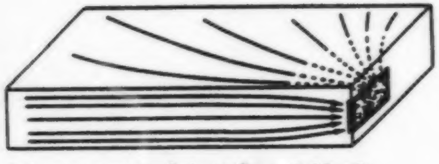

B. Streamlines to an Infinite Conductivity Fracture which Partially Penetrates the Coal Seam

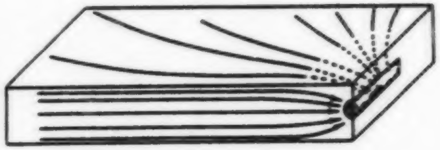

C. Streamlines to an Infinite Capacity Horizontal Borehole

Fig. 6—Schematic representation of flow toward low potential areas

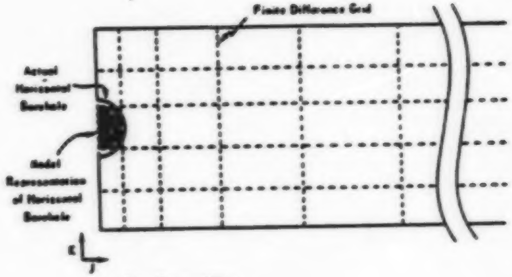
Finite Difference Grid
Actual Horizontal Borehole
Model Representation of Horizontal Borehole
k
j

A. Cross Sectional View

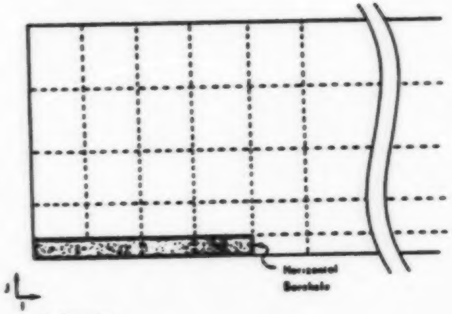
Horizontal Borehole
j
i

B. Plan View

Fig. 7—Model representation of a horizontal borehole in a 2D rectangular grid

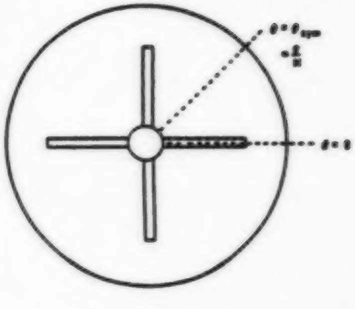

A. Plan View of Multiple Boreholes (N = 4)

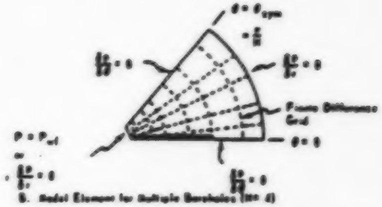
θ = θ_sym
= π/N
∂p/∂θ = 0
∂p/∂r = 0
Finite Difference Grid
θ = 0
p = p_wf
or
∂p/∂r = 0
∂p/∂θ = 0

B. Radial Element for Multiple Boreholes (N = 4)

Fig. 8—Model representation of multiple boreholes in a radial grid

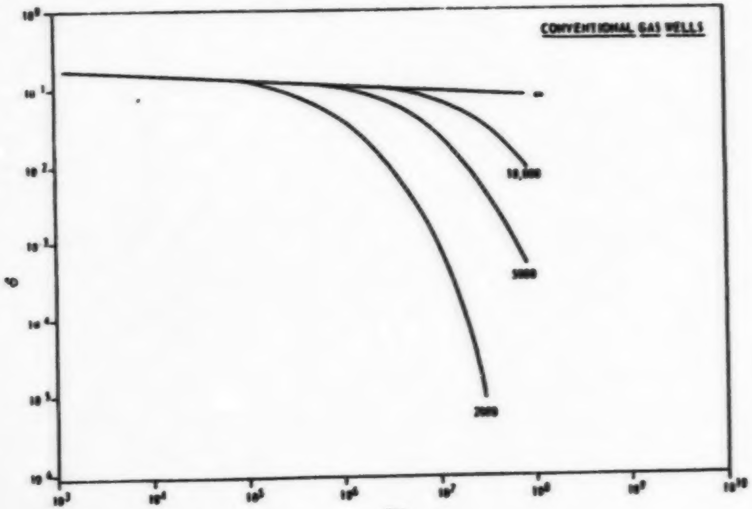

Fig. 9—Dimensionless flow rate vs. dimensionless time for a conventional gas well

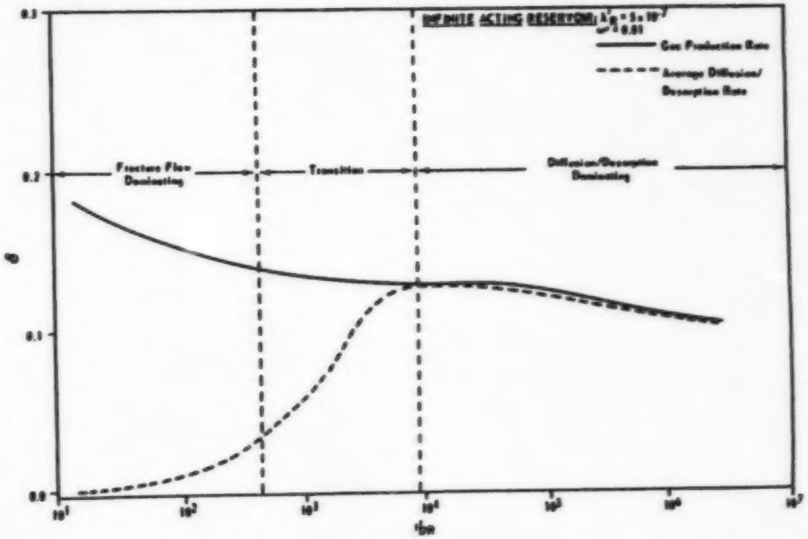

Fig. 10—Typical model solution for a coal degasification well

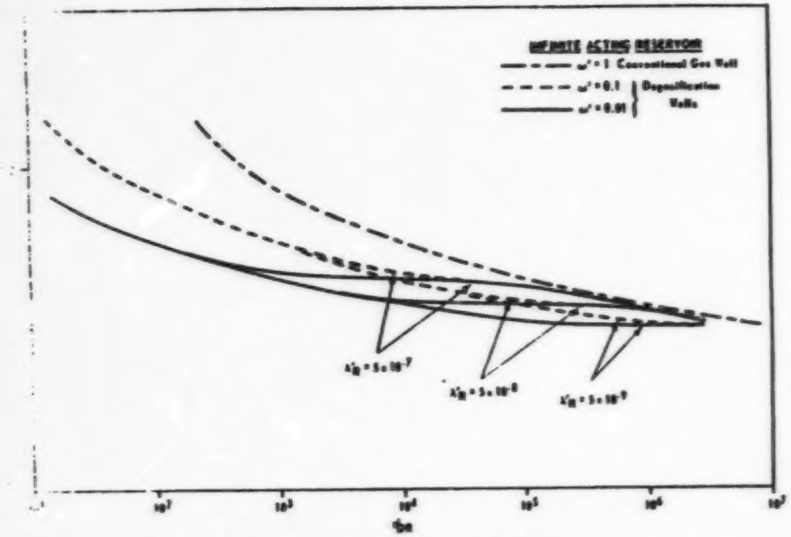

Fig. 11—Type curve for constant pressure, unstimulated vertical well

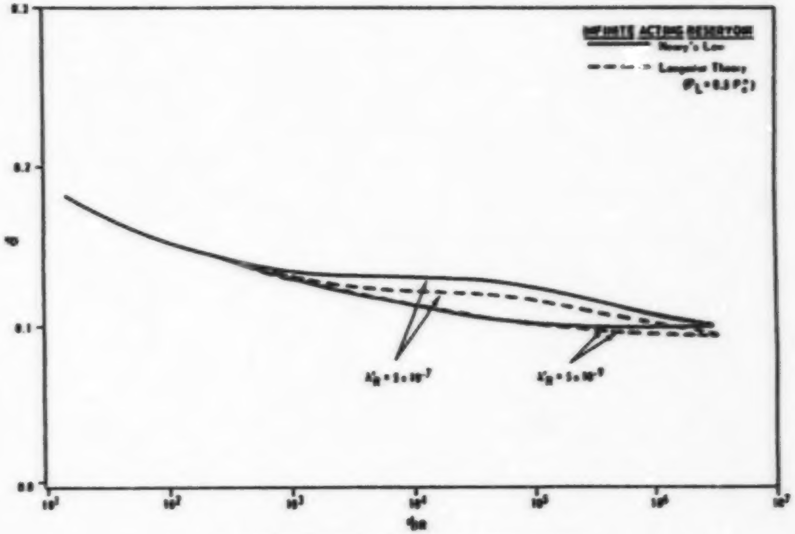

Fig. 12—Comparison of a Henry's law isotherm and a Langmuir isotherm

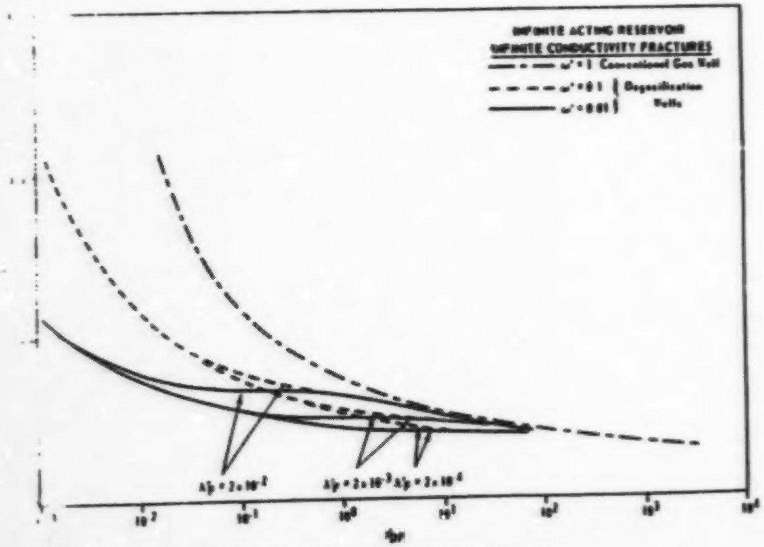

Fig. 13—Type curve for a constant-pressure, stimulated vertical well

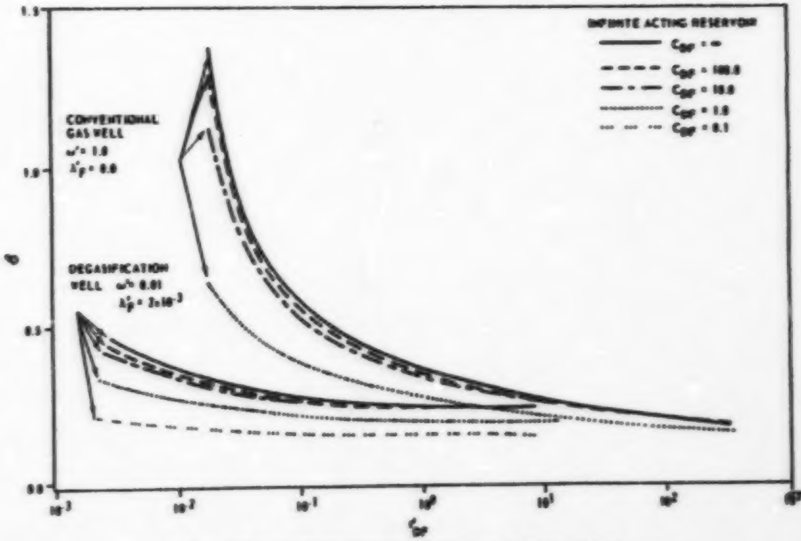

Fig. 14—Comparison of fracture conductivities for conventional and degasification wells

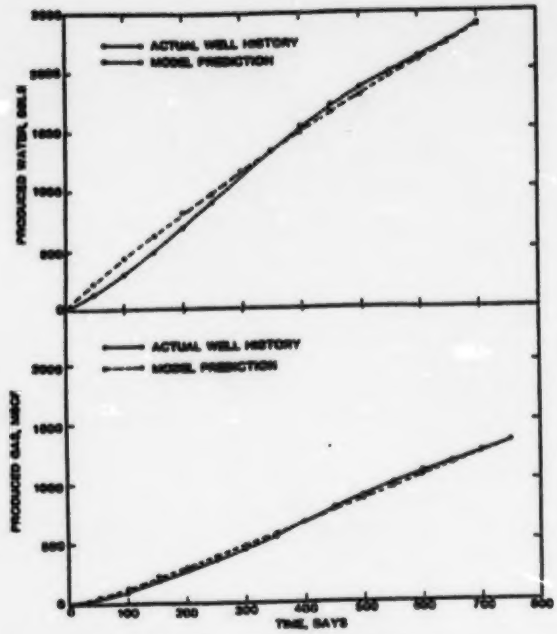

Fig. 15—History match of an unstimulated degasification well.

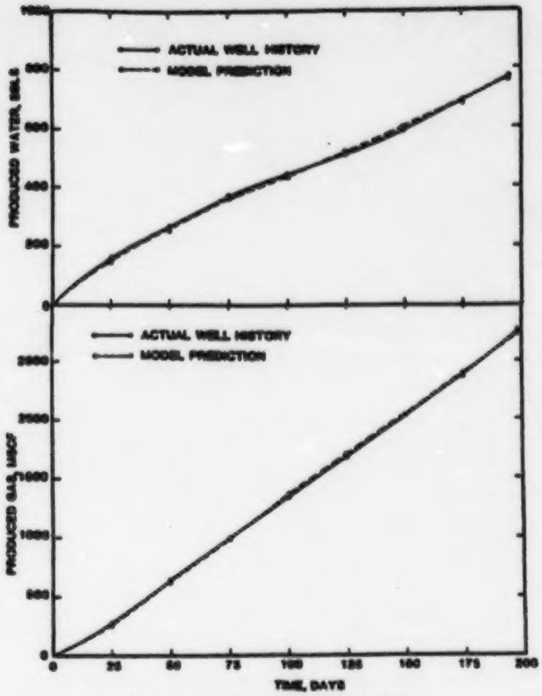

Fig. 16—History match of a stimulated degasification well

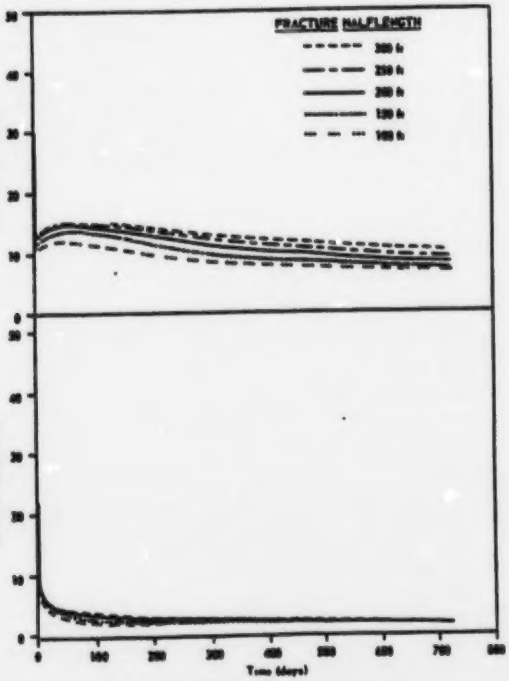

Fig. 17—Effects of fracture length on degasification rate

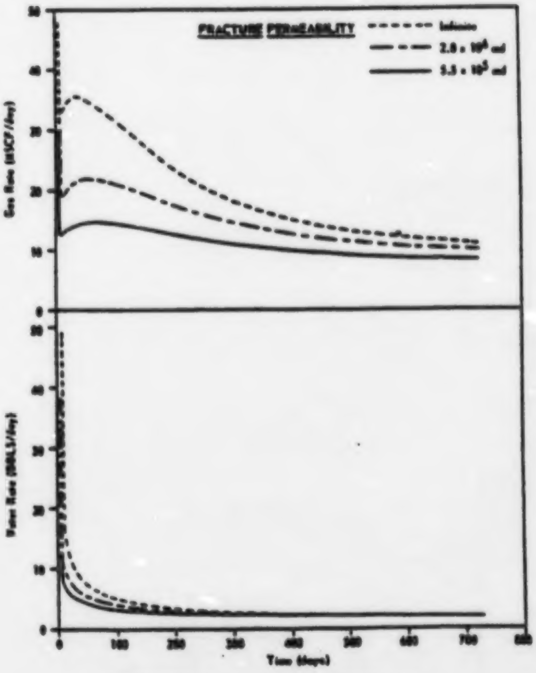

Fig. 18—Effects of fracture permeability on degasification rate

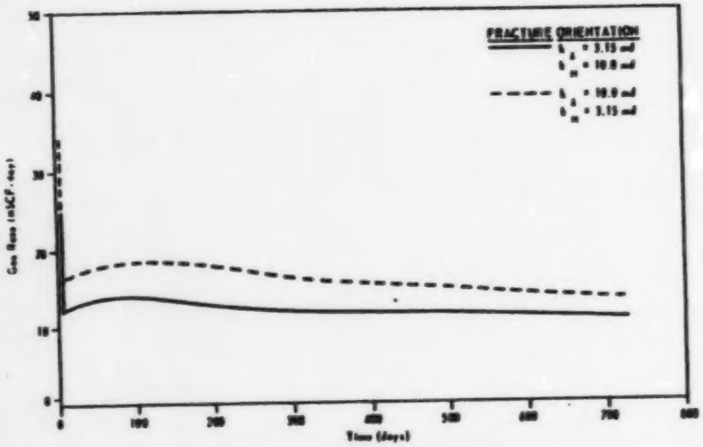

Fig. 19—Effects of fracture orientation on degasification rate

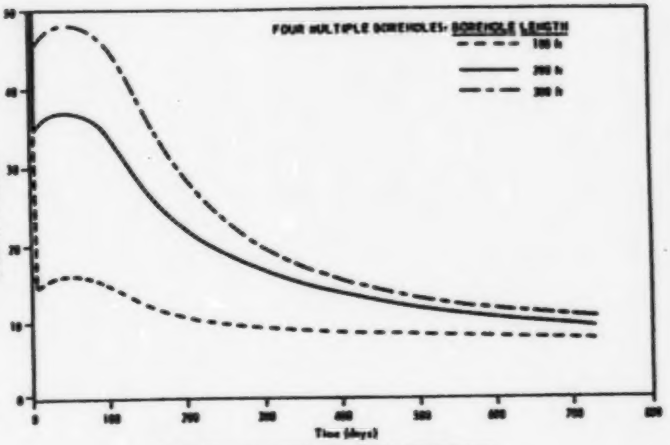

Fig. 20—Effects of horizontal borehole length on degasification rate

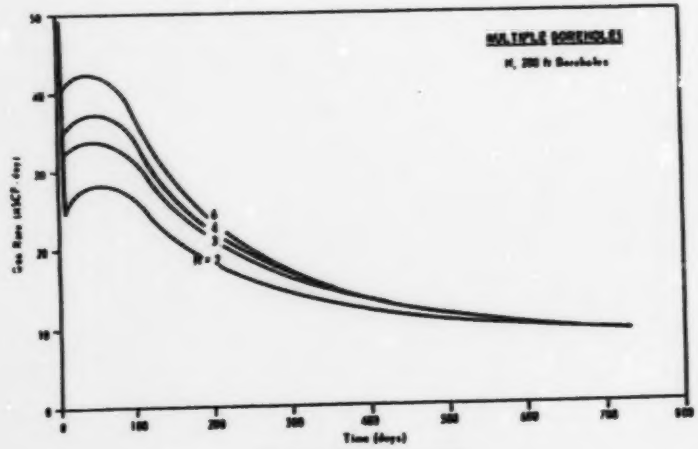

Fig. 21—Comparison of multiple boreholes

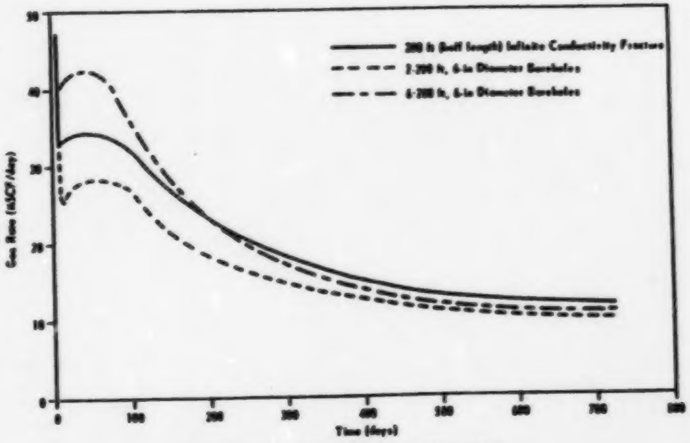

Fig. 22—Comparison of horizontal boreholes vs. a fractured well